Dissertation zur Erlangung des Doktorgrades der Fakultät für Chemie und Pharmazie der Ludwig-Maximilians-Universität München

Exploiting NAD^+ co-factor interactions and mimetics in the rational design of potent Sirt2 and Sirt5 inhibitors

Ricky Wirawan

aus

Jakarta, Indonesien

2026

Erklärung

Diese Dissertation wurde im Sinne von § 7 der Promotionsordnung vom 28. November 2011 von Herrn Prof. Dr. Franz Bracher betreut.

Eidesstattliche Versicherung

Diese Dissertation wurde eigenständig und ohne unerlaubte Hilfe erarbeitet.

München, den 08.01.2026 _____

Ricky Wirawan

Dissertation eingereicht am: 08.01.2026

1. Gutachter: Prof. Dr. Franz Bracher
2. Gutachter: Prof. Dr. Ivan Huc

Mündliche Prüfung am: 23.02.2026

Acknowledgements

I would like to express my sincere gratitude to my supervisor, Prof. Dr. Franz Bracher, for the opportunity he provided me to be a part of an amazing team to pursue my PhD studies. I am extremely grateful for his constant guidance, dedicated leadership and the intellectual freedom he provided me to pursue my ideas in every challenge that I faced.

I would also like to thank Prof. Dr. Ivan Huc for his assessment and pivotal role as my second examiner. My sincere appreciation also extends to the other members of my examination committee - Prof. Dr. Franz Paintner, Prof. Dr. Oliver Scherf-Clavel, Prof. Dr. Wolfgang Frieß and Prof. Dr. Ernst Wagner.

This work would not be possible without the proper financial resources. I would like to acknowledge SFB1309 for funding and collaborative purposes.

I deeply appreciate all the collaborative efforts from my colleagues and research partners that made this work possible. I would like to thank Dr. Lars Allmendinger, Claudia Glas and Brigitte Breitenstein for NMR measurements, Dr. Werner Spahl for MS measurements, Dr. Peter Mayer for X-ray crystallographic measurements, Anna Niedrig for HPLC purity determinations, Martina Stadler for performing MTT assays, Prof. Dr. Michael Groll, PD Dr. Eva Huber and Anna Heider from the Technische Universität München for their expertise in X-ray crystallography; Dr. Thomas Wein for molecular docking experiments and *in silico* calculations; Prof. Dr. Manfred Jung, Niklas Papenkordt and Florian Friedrich from the Albert-Ludwigs-Universität Freiburg for performing Sirt2 cell-based assays and Reaction Biology Corp., PA, USA for performing various *in vitro* assays.

I gratefully acknowledge my colleagues - Dr. Vasilii Morozov, Dr. Tulika Chakrabortty, Dr. Artheswari Gunanithi, Ashley Roby and Nikolas Schneider - who worked alongside me in the teaching and supervision of the inorganic chemistry practical courses. I wish to acknowledge Dr. Marco Keller for his leadership and unwavering support, Martina Stadler for chemicals and reagents preparations, Dr. Can Zenger, Dr. Ilya Jourjine, Dr. Mathieu Denis and Niklas Böcher for their positive and uncomplicated attitude, and their invaluable support and teamwork. Special thanks to Dr. Mathieu Denis as well for the lengthy and insightful discussions regarding boronic acid chemistry.

I would like to thank my colleagues from the Bracher group - Dr. Jürgen Krauss, Dr. Marco Keller, PD Dr. Christoph Müller, Dr. Thomas Klaßmüller, Dr. Philipp Rühl, Dr. Francesca Dona, Dr. Miriam Hollweck, Karl Sauvageot-Witzku, Melanie Pfoser, Anna Niedrig, Dr. Ilya Jourjine, Dr. Maximilian Liebl, Ludwig Huber, Michelle Peter, Stefan Frei, Ina Kunz, Irene Cid, Ferdinand

Breu, Pavlos Pelagias, Dr. Can Zenger and Dr. Matthias Frei - for the positive, supportive and encouraging working environment. My sincere gratitude further goes out to Dr. Matthias Frei for the many fruitful discussions and our seamless collaborative works.

I would also like to acknowledge several of my students - Carolina Almeida, Nour Shoeir, Florian Ungar, Simon Huber and Paula Schober - for the support in the laboratory benchwork.

To my loved ones, for whom I am dearly grateful, thank you for the constant support and encouragement from the beginning that made this amazing journey possible.

Publications

Frei, M.*; **Wirawan, R.***; Wein, T.; Bracher, F. Lead Structure-Based Hybridization Strategy Reveals Major Potency Enhancement of SirReal-type Sirt2 Inhibitors. *Int. J. Mol. Sci.* **2025**, *26*, 9855.

Wirawan, R.; Huber, S. A.; Wein, T.; Bracher, F. Balsalazide-Derived Heterotriaryls as Sirtuin 5 Inhibitors: A Case Study of a Reversible Covalent Inhibition Strategy. *Molecules* **2025**, *30*, 3821.

Wirawan, R.*; Frei, M.*; Heider, A.; Papenkordt, N.; Friedrich, F.; Wein, T.; Jung, M.; Groll, M.; Huber, E. M.; Bracher, F. Tailored SirReal-type inhibitors enhance SIRT2 inhibition through ligand stabilization and disruption of NAD^+ co-factor binding. *RSC Med. Chem.* **2025**, *16*, 5419-5440.

Glas, C.; **Wirawan, R.**; Bracher, F. A Short Approach to *N*-aryl-1,2,3,4-tetrahydroisoquinolines from *N*-(2-bromobenzyl)anilines *via* a Reductive Amination/Palladium-Catalyzed Ethoxyvinylation/Reductive *N*-alkylation Sequence. *Synthesis* **2021,** *53*, 1943-1954.

---

*Equal contribution as first author.

Table of Contents

1. Introduction

The epigenetic state of an organism, which is regulated by meticulous orchestration of diverse biological processes, plays an essential role in genome function and integrity. Several major pathological conditions such as cancer have been associated with the disruption of the balance of the epigenome. Although the intricate relationship between epigenetics and diseases has been thoroughly investigated over the past few years, there still exists a vast void of knowledge that needs to be addressed. The development of novel chemical entities as practical diagnostic tools and effective pharmaceutical drugs may offer a solid framework for epigenetic research and therapy.[1-3]

1.1. Epigenetic regulation

The field of epigenetics encompasses the study of complex regulatory networks that control heritable changes in gene expression through inducible epigenetic mechanisms without any alterations in the DNA sequence[4, 5]. Influenced by internal and external environmental stimuli, dynamic epigenetic changes can occur through responses from epigenetic regulators[6]. Such changes translate to acquired phenotypic traits that can be established and propagated during cell division and is necessary for growth and healthy development of an individual[6]. However, irregular expression or silencing of genes due to aberrant epigenetic changes can lead to the progression of various pathological conditions[7] such as cancer[8-10], type 2 diabetes[11, 12], cardiovascular diseases[13-15] and neurological disorders[16, 17]. In cells, the negatively charged DNA is densely packed as chromatin with 147 base pairs wrapped around an octamer of four basic, positively charged core proteins called histones that each exists as duplicates to form a nucleosome[18, 19] (Figure 1). Three distinct major mechanisms involved in epigenetic regulation have been identified which include DNA methylation, covalent post-translational modifications of histones and gene silencing by non-coding RNAs[20, 21]. Non-coding RNAs are strands of RNA that constitute about 1% of the entire genome and can interfere with transcription or translation[21]. In contrast, epigenetic regulation *via* DNA methylation and post-translational modifications of histones are performed by epigenetic tools which are classified into three different subgroups called writers, readers and erasers (Figure 1). Writers are enzymes that attach various chemical modifications such as methyl and acetyl groups on the DNA and histones. These attained modifications can then be recognised by specialised domain-containing proteins called readers which can recruit further protein machineries associated with transcriptional constraint. Erasers, on the contrary, balances this process by catalysing the removal of the chemical modifications carried out by the writers.[22]

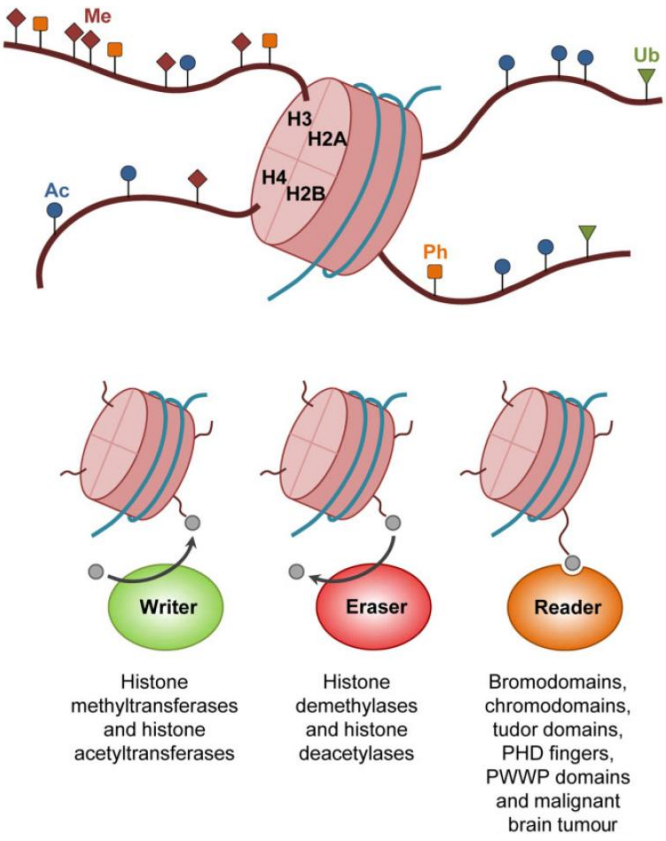

Figure 1: A nucleosome constitutes an octamer of four different histone proteins (H3, H4, H2A and H3B) that is enveloped by 147 DNA base pairs (top). Histone tails are subject to post-translational modifications that include methylation (Me), acetylation (Ac), phosphorylation (Ph) and ubiquitination (Ub). Epigenetic tools are classified into three different subgroups - writers, readers and erasers (bottom). Image taken from Simó-Riudalbas and Esteller[23] with permission from John Wiley and Sons and Copyright Clearance Center.

DNA methyltransferase-catalysed methylations occur at the pyrimidine ring of cytosines that leads to the formation of 5-methylcytosines[7]. Regions in the DNA with high occurrence of cytosine-guanine dinucleotides (CpG) often exist in promotor regions[7, 24]. Methylation of CpG sites has been shown to hinder the binding of transcription factors and RNA polymerase and thus gene expression[7, 24]. Equally important, post-translational modifications of histones can regulate DNA packaging and gene expression through various mechanisms. These covalent modifications are typically observed at the basic lysine and arginine sites of *N*-terminal histone tails that protrude out of the nucleosomes[18]. However, core modifications at the interface between the histones and at the lateral surface in contact with the DNA have also been discovered more recently[25-27]. Although several post-translational modifications of histones were identified, histone methylation, acetylation and phosphorylation represent a more profound area in this landscape[19, 28]. While methyl groups on histones function mostly as markers for readers[29], acetylation and phosphorylation can additionally mediate DNA packaging and transcription accessibility *via* charge modulation that disrupts electrostatic interactions between positively charged histones and negatively charged DNA[19]. This process

can naturally be reversed by erasers such as histone deacetylases and is instrumental in maintaining the balance of epigenetic regulation.

1.2. Histone deacylases and Sirtuins

Acyl moieties on histones play an essential role in epigenetic regulation not only through their function as markers for readers such as bromodomains, but also as regulators in DNA packaging. This process relies on the neutralisation and regeneration of the positive charges present on lysine residues of histones that serve as the complementary partners to the negatively charged phosphate groups of the DNA backbone. Facilitated by histone acetyltransferases, acetyl residues from acetyl CoA can be introduced onto lysine residues. At physiological pH, this nullifies the positive charges of the histones and thereby attenuates the electrostatic interactions between the DNA and histones. Consequently, the DNA disentangles away from histones to form the open form of chromatin called euchromatin that is more accessible to transcription. Conversely, the cleavage of the acetyl moieties from the lysine residues of histones catalysed by histone deacetylases regenerates the positive charges. This leads to the reassembly of the DNA around the histones to form the densely, packed closed form of chromatin called heterochromatin that is less accessible to transcription (Figure 2).[30-32]

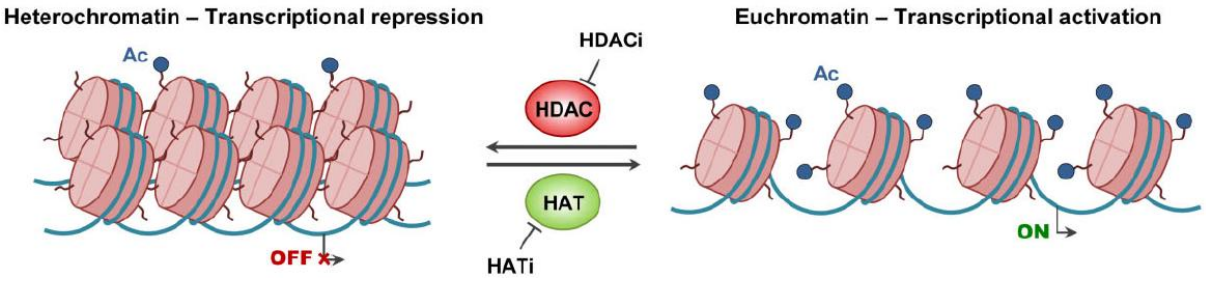

Figure 2: Histone acetyltransferases (HATs) catalyse the attachment of acetyl moieties to the lysine residues of histones that leads to the formation of euchromatin. Histone deacetylases (HDACs) revert this process through cleavage of the acetyl moieties that leads to the formation of tightly packed heterochromatin. Image taken from Simó-Riudalbas and Esteller[23] with permission from John Wiley and Sons and Copyright Clearance Center.

Although the term “histone deacetylases” suggests that their enzymatic activity is restricted to solely histones, the broader spectrum of natural substrates for histone deacetylases should be acknowledged. Non-histone proteins such as transcription factors, DNA repair proteins, nuclear import factors, alpha-tubulin and cytoskeleton proteins were additionally identified as targets for histone deacetylases[33]. Moreover, an array of biological processes that extend beyond deacetylation were observed in the activity of histone deacetylases which includes desuccinylation[34], demalonylation[35], demyristoylation[36] and ADP-ribosylation[37]. Thus, instead of histone deacetylase the more modern and accurate term to describe this family of enzymes

is perhaps protein or lysine deacylase. Nevertheless, most reports still stick to the historical term since most major phenotypic responses stem from histone deacetylation[32].

Histone deacetylases are subdivided into four different classes based on their homology to yeast orthologs as shown in Figure 3. Class I, II and IV histone deacetylases catalyse the cleavage of acetyl groups utilising a zinc ion as their co-factor that provides activation of the lysine acetamide bond that promotes the nucleophilic attack of a water molecule. Accordingly, class I, II and IV histone deacetylases are susceptible to potent inhibition by potent zinc chelators, in particular hydroxamic acids such as the approved histone deacetylase inhibitors vorinostat, belinostat and trichostatin A.[32, 38]

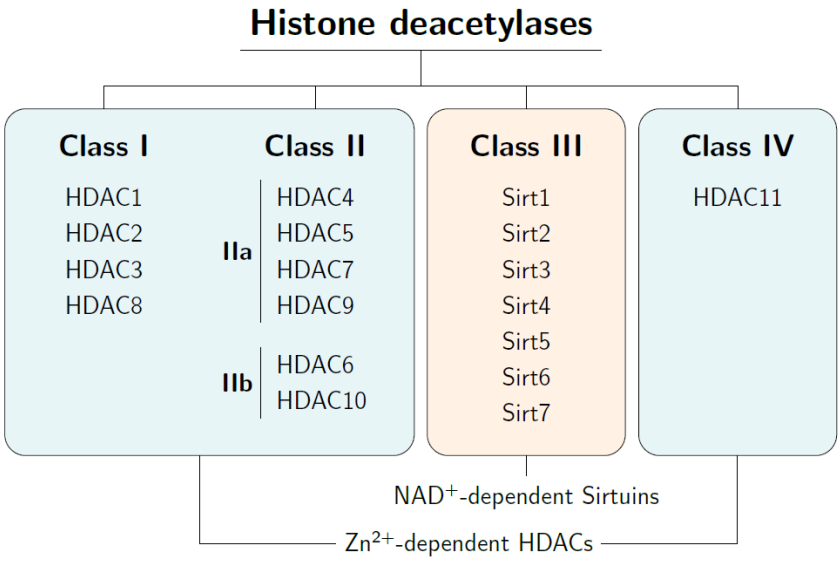

Figure 3: The family of histone deacetylases is categorised into four different classes. Class I, II and IV represent classical zinc-dependent histone deacetylases. Class III histone deacetylases represent NAD^+-dependent sirtuins. Image taken from Behnisch-Cornwell *et al.*[38] with permission from Creative Commons Attribution.

In contrast, class III histone deacetylases represent a unique class of highly conserved NAD^+-dependent enzymes known as sirtuins (Sirt)[38]. This family of proteins was first identified in the budding yeast *Saccharomyces cerevisiae*, where the silent information regulator 2 (Sir2) gene product was characterised as an NAD^+-dependent deacetylase[39-41]. The term sirtuin was later introduced to reflect the broader family of Sir2-related homologous proteins discovered across a wide range of species[40, 42]. Thus far, seven different subtypes of sirtuins were identified in humans, each with its own distinct function and subcellular localisation[43] (Figure 4). Sirt1, Sirt6 and Sirt7 are predominantly found in the nucleus, whereas Sirt3, Sirt4 and Sirt5 are primarily found in the mitochondria[43]. Sirt2 is a cytoplasmic protein but can shuttle into the nucleus during the G2/M transition of the cell cycle to perform its pivotal role in the deacetylation of microtubules necessary for cell division[43].

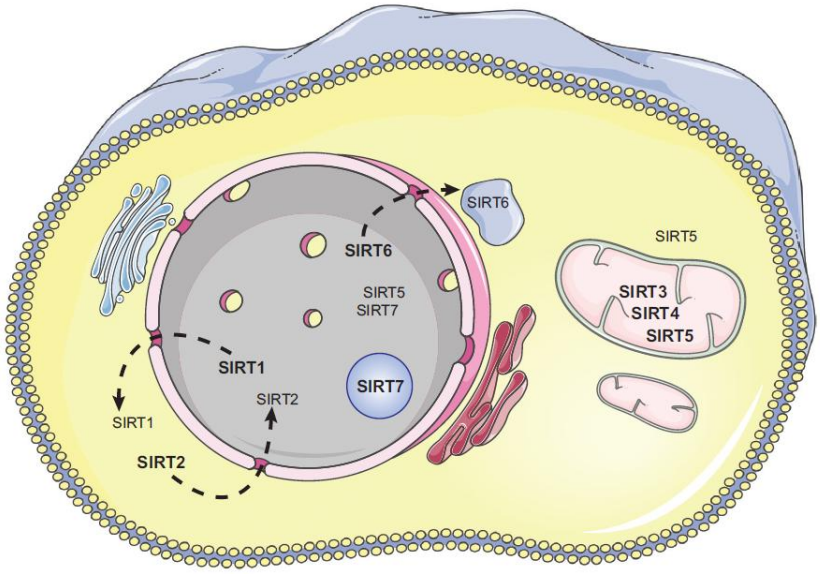

Figure 4: Subcellular localisation of the seven human sirtuin subtypes. Image taken from Giblin and Lombard[43] with permission from Elsevier and Copyright Clearance Center.

Notably, sirtuins do not exhibit any sequence homology to the other classical histone deacetylases[44]. Yet, among the sirtuin proteins a high degree of sequence conservation was observed, albeit with variations present in the *N*-terminal and *C*-terminal flanks[44]. Consequently, sirtuins share a similar overall three-dimensional protein structure as exemplified by Sirt2 and Sirt5 in Figure 5[44].

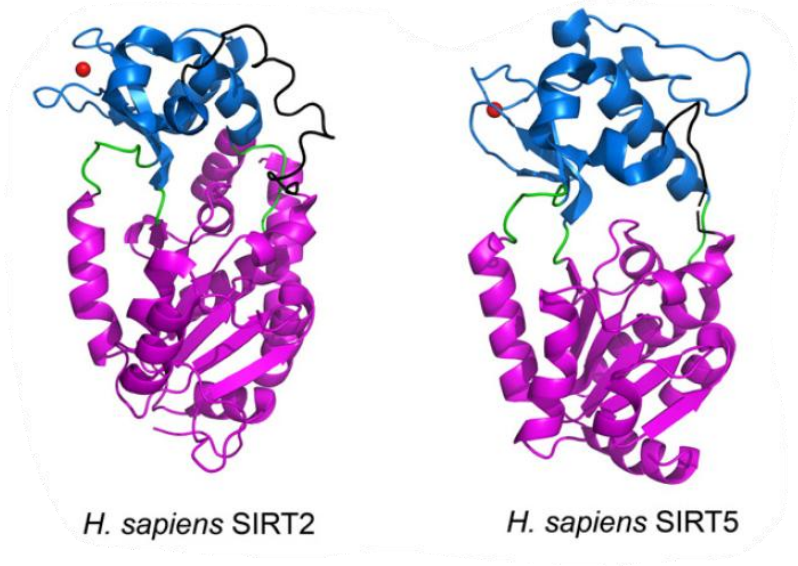

Figure 5: Crystal structure of human Sirt2 (PDB ID: 1J8F[45]) and Sirt5 (PDB ID: 2B4Y[46]). The catalytic core represents the cavity that is enclosed by a small zinc-binding domain (blue) and the larger Rossman-fold domain (magenta) that are connected by loops (green) and the cofactor binding loop region (black). The Zn^{2+} ion (red) helps maintain the structural integrity of the small domain through interactions with β strands. Image taken from Sanders *et al.*[44] with permission from Elsevier and Copyright Clearance Center.

Approximately 275 amino acids account for the conserved catalytic core region of sirtuins[44, 47]. This active site cavity is surrounded by a small zinc-binding domain and a larger domain that adopts a classical open α/β Rossmann-fold structure[44, 47]. The smaller domain shows the most structural variability among the sirtuin proteins, allowing discrimination between a plethora of protein substrates for subtype specific binding at the underlying active site[44, 48]. Nevertheless, the zinc-binding motif in the small domain is constructed from highly conserved cysteine-containing sequences[44]. Unlike the classical histone deacetylases, the zinc ion in sirtuins is not directly involved in their enzymatic activity but rather serves to maintain the structural integrity of the small domain through interactions with the β strands[44]. Connected with the small domain by a series of loops, the larger and more conserved Rossmann-fold domain constitutes a central β sheet made up of six parallel β strands that is sandwiched between several α helices to form a motif typical for nucleotide binding[44, 47]. Thus, the co-factor NAD^+ of sirtuins is befittingly bounded in the Rossman-fold domain but stretches all the way to the active site where the NAD^+-mediated enzymatic deacetylation of protein substrates take place[44, 47]. This process is initiated by the formation of *O*-alkylimidate intermediate (**I**) *via* an S_N2 reaction involving the nucleophilic attack of the acetamide oxygen atom of the acetylated lysine at the ribose C-1' of the co-factor NAD^+ (Figure 6)[49, 50]. Subsequent intramolecular nucleophilic attack of the neighbouring 2'-hydroxy group at the activated imidate bond generates the cyclic acetal intermediate **II**[49, 50]. The generally accepted mechanism then proceeds through the release of the deacetylated lysine with the formation of a bicyclic acetoxonium ion **IIIa**[49, 50]. However, a recent work reported a slightly different mechanistic pathway, through which the imidate intermediate **IIIb** is formed from the cyclic acetal intermediate **II**[51]. Hydrolysis of both intermediates **IIIa** and **IIIb** *via* the tetrahedral hydroxy acetal intermediate **IVa** and hemiacetal intermediate **IVb**, respectively, leads to the formation of the mutual product 2'-*O*-Acetyl-ADP-ribose (**V**)[49-51]. As opposed to the original route *via* intermediates **IIIa** and **IVa**, this newly proposed mechanistic route *via* intermediates **IIIb** and **IVb** delivers the deacetylated lysine in the final step[51].

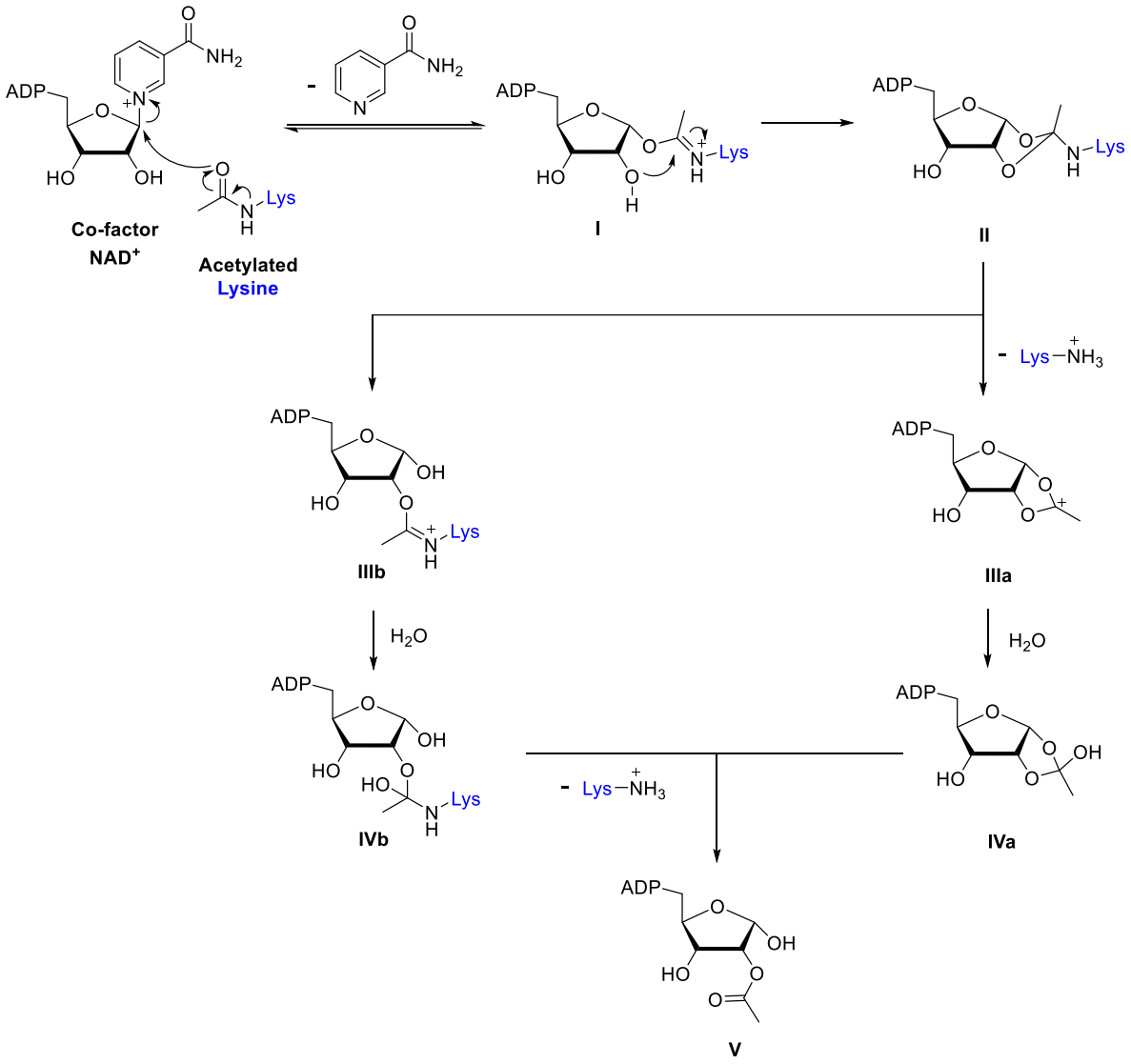

Figure 6: Proposed general mechanism of the NAD^+-dependent deacetylation of lysine substrates in sirtuins. The widely accepted mechanism involves the formation of a a bicyclic acetoxonium ion **IIIa** and subsequent hydrolysis to form 2'-O-acetyl-ADP-ribose (**V**)[49, 50]. However, an alternative mechanistic route has been proposed with the identification of intermediate **IIIb**[51]. Subsequent hydrolysis of **IIIb** leads to the mutual product **V**[51].

1.3. Sirt2

Sirt2 is one of the seven sirtuin subtypes that emerged as a key target due to its broad catalytic scope and diverse substrates and thus its involvement in the pathogenesis of various diseases. As the most abundantly expressed sirtuin subtype and one that exhibits an age-dependent accumulation in the brain, Sirt2 plays a central role in the pathology of neurodegenerative disorders[52, 53]. For example, Sirt2-mediated deacetylation of alpha-synuclein promotes its aggregation and the formation of toxic aggregates, a typical hallmark in the progression of Parkinson's disease[54]. Consequently, Sirt2 inhibition proved to have neuroprotective effects and may serve as a potential therapeutical option[54]. Moreover, in the progression of cancer, a correlation between Sirt2 inhibition and a decrease in the concentration of the oncoprotein c-Myc was observed[55]. Since the oncoprotein c-Myc is upregulated in around 50% of human tumours, Sirt2 inhibition may serve as a promising therapeutic approach against c-Myc-driven cancers[55]. In addition, the implication of Sirt2 in various viral and bacterial infections has been shown in recent years[56-58]. Through the inhibition of Sirt2, supressed growth and replication of several pathogens including HIV-1 and *Mycobacterium tuberculosis* was demonstrated, displaying the potential of Sirt2 as a novel target in the treatment of infectious diseases[56-58].

Despite all the evidence of Sirt2 as a prospective biological target for various pharmaceutical interventions, no Sirt2 inhibitor has yet received regulatory approval for clinical applications. Numerous efforts have been undertaken over the past few years to develop potent and subtype selective Sirt2 inhibitors with satisfactory physicochemical properties. However, these laborious efforts still pose a significant challenge. Several Sirt2 inhibitors with drug-like properties were developed, employing various binding mechanisms with the aim of increasing potency and subtype selectivity (Figure 7). As such, certain potent Sirt2 inhibitors were specifically developed to form stable covalent intermediates with the co-factor NAD^+ by incorporating reactive functional groups such as thioamide (**TM**[55] and **KPM-2**[59]) or thiourea (**AF8**[60]). Additionally, oxadiazole- and chroman-4-one-based Sirt2 inhibitors were developed and optimised that led to the generation of **Moniot compound 39**[61] and compound **6f**[62], respectively, both exhibiting low micromolar IC_{50} values. Moreover, natural product derived Sirt2 inhibitors were identified such as **NPD11033**[63], a synthetic compound derived from the plant-based alkaloid cytisine that is medically used for smoking cessation[64]. By means of high-throughput screening, further Sirt2 inhibitors such as **AGK2**[65] with an IC_{50} of 3.5 µM was identified.

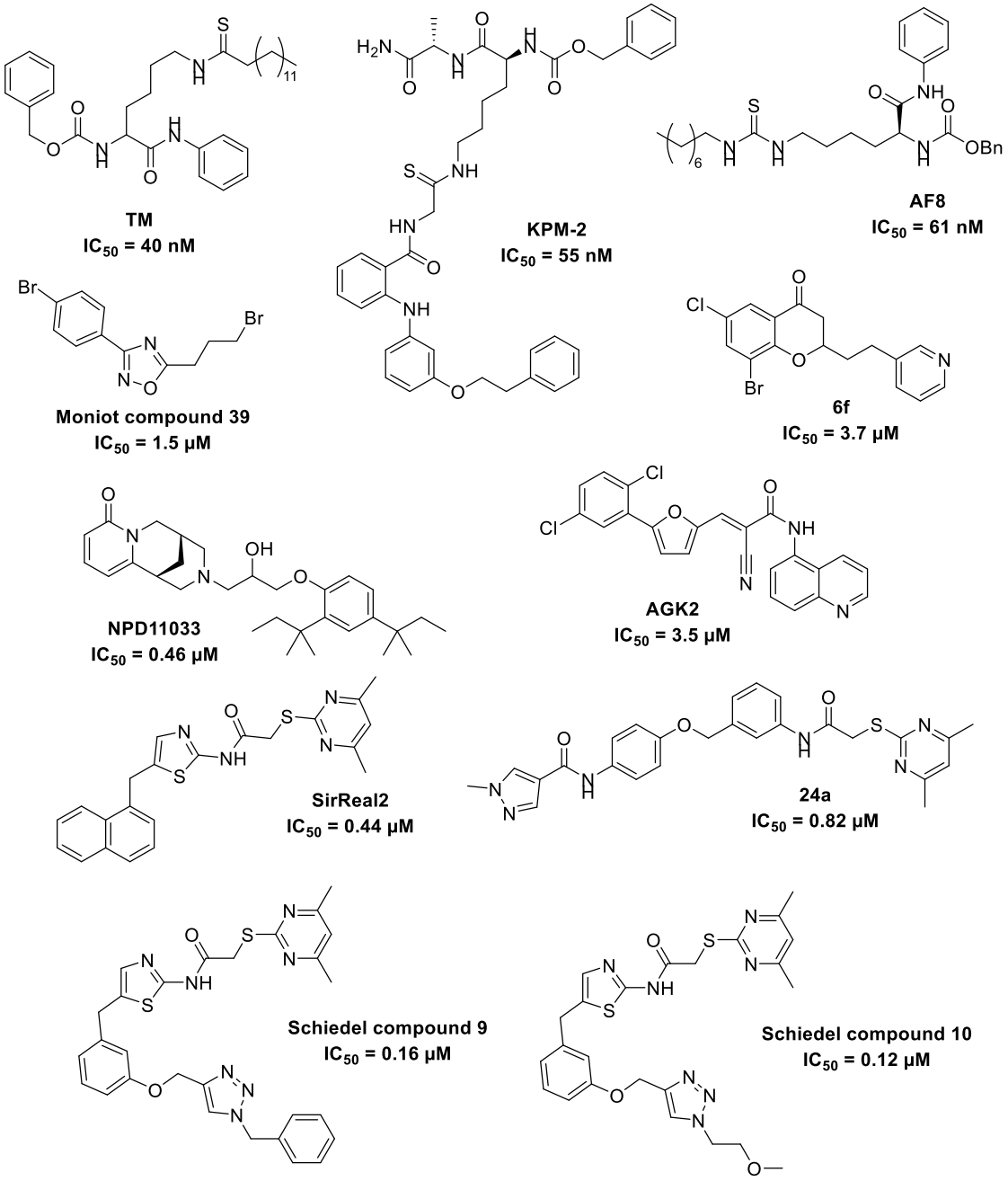

Figure 7: Selected examples of published Sirt2 inhibitors. Image adapted from Wirawan *et al.*[66] with permission from Creative Commons Attribution.

Substantial advancement in the field of Sirt2 was made by the group of Prof. Dr. Manfred Jung, who identified a series of aminothiazoles as potent Sirt2 inhibitors and provided a mechanistic insight into their binding mode, in which the term sirtuin rearranging ligands (SirReals) was coined[67, 68]. Among these aminothiazoles, **SirReal2**[67, 68] showed promising inhibitory effects with an IC_{50} of 0.44 µM. X-ray co-crystallographic studies of Sirt2-SirReal2-NAD^+ complex unveiled a ligand-induced rearrangement of the active site of Sirt2 that exposes a yet-unexploited selectivity pocket, in which the 4,6-dimethylmercaptopyrimidine scaffold occupies (Figure 8)[68].

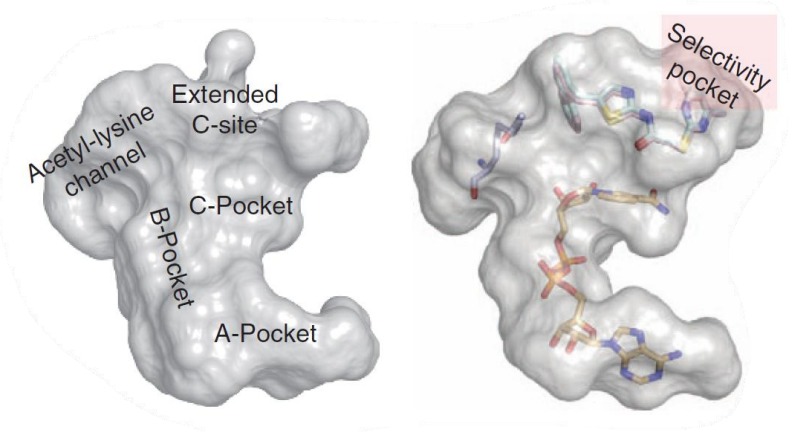

Figure 8: Surface representation of the substrate- and the co-factor NAD^+ binding pockets, divided into their subsites (left). Upon binding of **SirReal2** at the active site, a ligand-induced rearrangement of the active site results in the emergence of a selectivity pocket. The co-factor NAD^+ binds nearby at the A-, B- and C-Pocket (right). Image taken from Rumpf *et al*.[68] with permission from Creative Commons Attribution.

Extending their efforts within the framework of developing Sirt2 affinity probes, two further triazole-based SirReals with improved potency (**Schiedel compound 9**[69] and **10**[69]) were identified by the Jung group. Since its discovery, related studies[70, 71] exploiting the selectivity pocket of Sirt2 were independently conducted which led to the identification of the potent and subtype selective Sirt2 inhibitor **24a**[70] by Yang and colleagues.

1.4. Sirt5

Sirt5 is another sirtuin subtype that gained significant interest in recent years. As a predominantly mitochondrial enzyme, Sirt5 serves as a fundamental regulator in various metabolic processes that is necessary for healthy cellular homeostasis[72]. Through the deacylation, in particular desuccinylation, of various protein substrates, Sirt5 takes a governing position in numerous metabolic processes such as ammonia detoxification[73], ROS elimination[74], ß-oxidation of fatty acids[75], glycolysis[76] and ketogenesis[77]. Thus, dysregulation of Sirt5 has been implicated with the progression and exacerbation of several diseases including metabolic disorders[72], neurodegeneration[78, 79] and cancer[80-82]. Multiple endeavours for the development of drug-like Sirt5 inhibitors were pursued, however most of them still suffer from subpar potency, lack of subtype selectivity and poor pharmacokinetic properties (Figure 9). For example, the indolinone compound **GW5074**[83, 84], the ß-naphthol-based **cambinol**[85] and **Maurer compound 2**[85] demonstrated micro-molar inhibitory activities against both Sirt5 and Sirt2. In addition, these compounds as well as **Liu compound 37**[86] may show promiscuity towards other biological targets due to highly reactive motifs such as Michael acceptors and alkylidene thiobarbiturates that are typical in false-positive pan assay interference compounds (PAINS)[87].

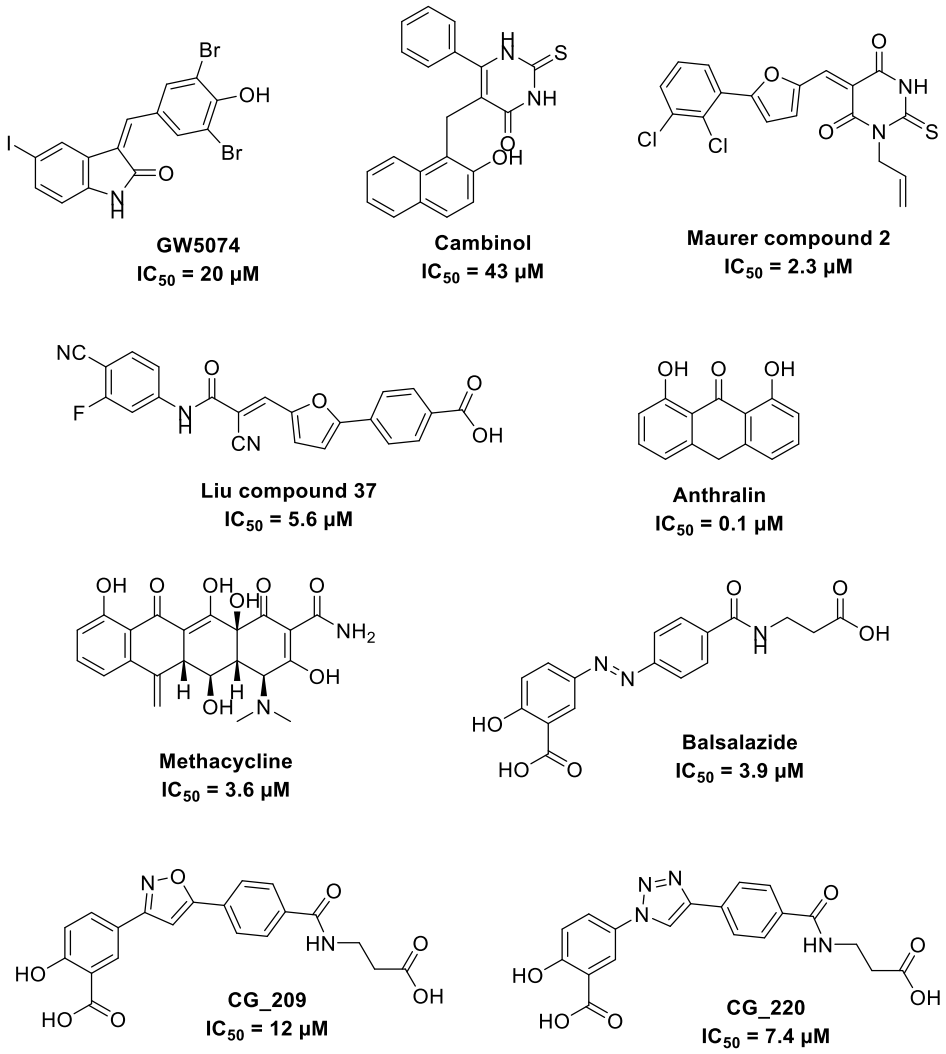

Figure 9: Selected examples of compounds that exhibit inhibitory effects against Sirt5. Image taken from Wirawan *et al.*[88] with permission from Creative Commons Attribution.

Approved drugs such as **anthralin**[89], **methacycline**[89] and **balsalazide**[89] that were identified in a high-throughput screening as Sirt5 inhibitors deem unsuitable for drug repurposing due to various reasons such as toxicity (anthralin), stability issues (anthralin), undesired antimicrobial effects (methacycline) or poor pharmacokinetic properties (balsalazide)[90]. **Balsalazide** is an oral prodrug for the treatment of local inflammatory bowel disease[91]. Upon reductive cleavage of the azo moiety of **balsalazide** by the gut bacteria, the anti-inflammatory active pharmaceutical ingredient 5-aminosalicylic acid is released[91]. Thus, optimisation efforts were necessary, if **balsalazide** should be designated as a promising oral drug candidate targeting Sirt5. Conducted by Carina Glas in the group of Prof. Dr. Franz Bracher, the development of **CG_209**[90, 92] and **CG_220**[90, 92] involves the substitution of the azo bond of **balsalazide** with an isoxazole and a triazole ring, respectively, which naturally improves their stability against enzymatic degradation by the gut bacteria and thus their oral bioavailability.

2. Objectives

This presented work focuses on the design, chemical synthesis and biological evaluation of inhibitors targeting two different sirtuin subtypes, namely Sirt2 and Sirt5. The development of these inhibitors from literature-published lead structures will be performed with various drug design techniques with the aim of enhancing their potency, whilst still retaining their subtype selectivity. In parallel to the work by Frei *et al.*[93] on the optimisation of **SirReal2** and derivatives thereof targeting Sirt2 by the group of Prof. Dr. Franz Bracher, this thesis will cover the study of the advanced SirReal2 derivative **24a**. Moreover, potency improvement of the pharmacokinetically optimised **balsalazide**-derived Sirt5 inhibitors **CG_209** and **CG_220** will be pursued. Initial insight of the actual or theoretical binding poses of these lead structures was obtained from the co-crystal structure of **24a** (PDB ID: 5YQO[70]) with Sirt2 and the docking calculations[90] of **balsalazide** in Sirt5, which were derived from the co-crystal structure of a Sirt5-succinyl-lysine-peptide complex (PDB ID: 3RIY[94]). Bounded at the active site in spatial proximity to the co-factor NAD^+, the hypothesis was postulated, in which significant increase in the binding affinity and thus potency of these lead structures could be achieved through the exploitation of the co-factor NAD^+. The rationale behind this perspective can be dissected into two distinct drug optimisation techniques, that is firstly, strong, targeted interactions of inhibitors with the vicinal hydroxy groups of the NAD^+ ribose moiety through appropriate electrophilic functional groups capable of reversible covalent bonding or halogen bonding, and secondly, the development of bisubstrate analogues that simultaneously mimic the natural substrate and the essential co-factor NAD^+. For the former, the selection process of appropriate functional groups involves careful consideration and evaluation of established inhibitors that mediate through this proposed mode of action. Although reactive warheads such as Michael acceptors, ß-lactones and ß-lactams, epoxides and sulfonyl fluorides have been implemented in the development of irreversible covalent binders, the risks of immunogenic reactions and off-target toxicity are almost inevitable[95-97]. In contrast, reversible covalent inhibition offers the opportunity of dissociation from off-targets, reducing the potential of undesired side effects while still retaining extended binding at the intended target protein[98]. Approved therapeutical drugs such as the 20S proteasome inhibitor bortezomib for the treatment of multiple myeloma relies on reversible covalent binding between its boronic acid moiety and the Thr1 oxygen atom of the proteasome[99, 100]. In addition, the antidiabetic agent saxagliptin utilises its nitrile moiety for reversible covalent bonding with the Ser630 oxygen atom of DPP4 for potent inhibition[101]. Moreover, the treatment of sickle cell anaemia with the aldehyde-bearing voxelotor mediates through a reversible Schiff base formation between the aldehyde moiety of voxelotor and the Val1 primary amine of haemoglobin[102]. As such, these functional groups may present promising opportunities in the design of potent Sirt2 and Sirt5 inhibitors through their

engagement in reversible covalent bonding with the ribose hydroxy groups of the co-factor NAD^+ (Figure 10A-C). Additionally, these functional groups have the capability to participate in strong non-covalent interactions in the form of hydrogen bonding with the ribose hydroxy groups of the co-factor NAD^+. Often regarded as the hydrophobic equivalent of hydrogen bonding[103], halogen bonding has also seen notable success in medicinal chemistry, exemplified by the optimisation of PDE5[104] and HIV-1 reverse transcriptase[105, 106] inhibitors. These strong non-covalent interactions stem from the anisotropic distribution of electrons within halogens, resulting in the formation an electron-deficient σ-hole that enables strong bonding with a variety of nucleophiles[107-110], for example the hydroxy groups of the co-factor NAD^+ (Figure 10D). Thus, the application of halogen bonding within this investigation may present a promising complementary approach in the design of potent sirtuin inhibitors.

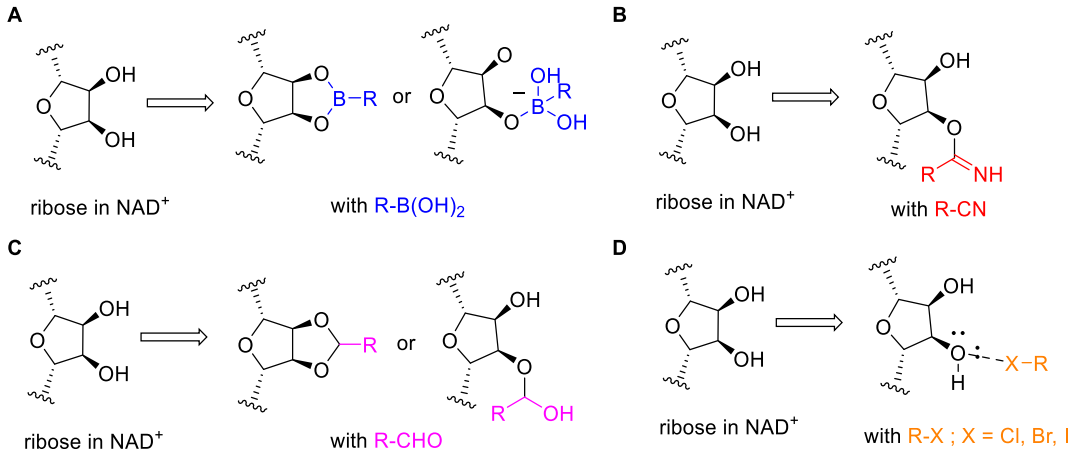

Figure 10: (**A**) Boronic acids can react reversibly with one or both hydroxy groups of the NAD^+ ribose unit to form (cyclic) boronic acid esters. (**B**) Nitriles can react reversibly with one of both hydroxy groups to form iminoethers. (**C**) Aldehydes can form reversible hemiacetals or cyclic acetals. (**D**) Halogen bonds can form between chlorine, bromine or iodine and the lone pair of electrons of the hydroxy groups. Image taken from Wirawan *et al.*[66] with permission from Creative Commons Attribution.

Initial docking experiments with the envisaged boronic acid derivatives of the Sirt2 inhibitor lead structure **24a** provided an insight into the optimal positions for the introduction of various functional groups that enable reversible covalent bonding and halogen bonding to the hydroxy groups of the ribose unit of the co-factor NAD^+ (Figure 11A). These envisaged derivatives containing aromatic boronic acids, nitriles, aldehydes and halogens at two distinct neighbouring positions on the inhibitor scaffold will be systematically synthesised and biologically evaluated.

Similarly, the synthesis and biological evaluation of the envisaged derivatives of the Sirt5 inhibitors **CG_209** and **CG_220** bearing these selected reversible covalent warheads will be carried out through guidance from docking experiments. Notably, the docking studies of these

envisaged Sirt5 inhibitors suggested the need of an additional methylene group for optimal spacing and interactions of the desired functional groups with the ribose hydroxy groups of NAD^+ (Figure 11B and C). Challenges concerning the synthesis of enantiomerically pure derivatives of **CG_209** and **CG_220** will additionally be addressed and navigated within the scope of this study.

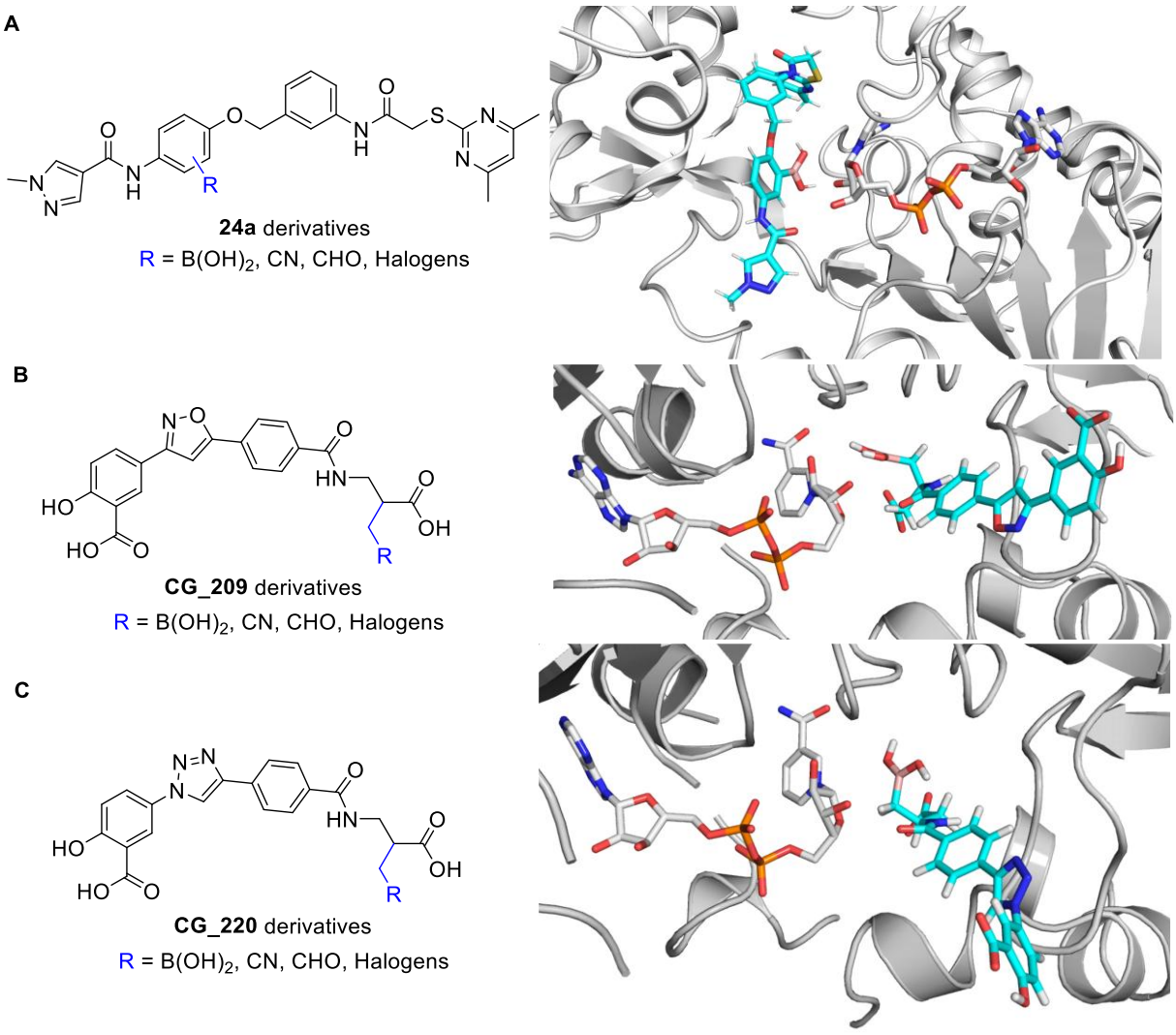

Figure 11: Envisaged derivatives of the Sirt2 inhibitor (**A**) **24a** and the Sirt5 inhibitors (**B**) **CG_209** and (C) **CG_220**. Initial docking experiments of the corresponding envisaged boronic acid derivatives of these lead structures (cyan) revealed the optimal positioning of functional group modifications for reversible covalent bonding and halogen bonding with the the co-factor NAD^+ (grey). Image adapted from Wirawan *et al.*[66, 88] with permission from Creative Commons Attribution.

In the third objective, the focus lies on the development of Sirt2 bisubstrate analogues that mimic both the natural peptide substrate and the essential co-factor NAD^+. These preformed bisubstrate analogues consist of two fragments that are tethered to one another *via* a suitable linker, each targeting a different binding site in the enzyme. Thus, bisubstrate analogues hold the potential of establishing further inhibitor-enzyme interactions that could create a positive

synergistic effect and thus enhancement in the binding affinity as well as improved selectivity, when compared to their monosubstrate counterparts[111]. This concept can be well defined using thermodynamic models that describe the binding of ligands at their intended target. The change in the Gibbs free energy (ΔG) is a widely accepted parameter that describes the spontaneity of inhibitor binding and is correlated with enthalpic (ΔH) and entropic (ΔS) changes of the system in accordance with equation 1[112], and with the dissociation constant (K_d) of the inhibitor-enzyme complex in accordance with equation 2[111]. An exergonic process that is represented by a negative ΔG value conveys a spontaneous binding event[112]. This can be achieved through either negative enthalpic changes (ΔH), which is associated with energy release from favourable inhibitor-enzyme interactions, or positive entropic changes (ΔS), which is associated with a decrease in the order of the system[112]. In bisubstrate analogues, the total change in the Gibbs free energy (ΔG) is comprised of the changes in the Gibbs free energy of the first substrate analogue (ΔG_1), the co-substrate analogue (ΔG_2) and the linker (ΔG_3) as indicated by equation 3[111]. Thus, following equation 4, which is derived from equation 2 and equation 3, a minimal linear decrease in the total Gibbs free energy through additional favourable binding of a co-substrate can result in an exponential decrease in the dissociation of the inhibitor-enzyme complex, potentially turning micromolar-potent fragments into nanomolar-potent bisubstrate inhibitors[111].

$$\Delta G = \Delta H - T\Delta S \quad (1)$$

$$\Delta G = RT \ln K_d \quad (2)$$

$$\Delta G = \Delta G_1 + \Delta G_2 + \Delta G_3 \quad (3)$$

$$\Delta G_1 + \Delta G_2 + \Delta G_3 = RT \ln K_d \quad (4)$$

However, the conformational constraint that is associated from the covalent linkage of two substrate analogues should be acknowledged, as this may restrict their mobility and thus hinder their optimal fit in the binding site[111]. Paradoxically, the utilisation of a flexible linker, in particular longer linkers for spatially distant binding sites, may introduce additional entropic loss that disfavours binding[111]. This conundrum represents one of the main challenges and complications in the development of drug-like bisubstrate analogues. Nevertheless, several bisubstrate analogues have been successfully established as protein methyltransferase inhibitors[113], DNA methyltransferase inhibitors[114], glycosyltransferase inhibitors[115] and kinase inhibitors[116-118]. Although several sirtuin inhibitors have been developed that target the substrate binding pocket, or the NAD^+ co-factor binding pocket[65, 84, 119, 120], there have been, to the best of current knowledge, no reports of bisubstrate analogues that simultaneously mimic the natural substrate and the essential co-factor NAD^+ of sirtuins. Perhaps the only relevant and comparable work is the recent development of nicotinamide-based Sirt2 inhibitors for example by Cui and colleagues that were shown by docking calculation experiments to

simultaneously bind to the C-pocket of the NAD^+ binding site and an arylamide motif that stretches and binds presumably either to the acetyl-lysine channel or the extended C-site for further interactions[121-123] (Figure 12).

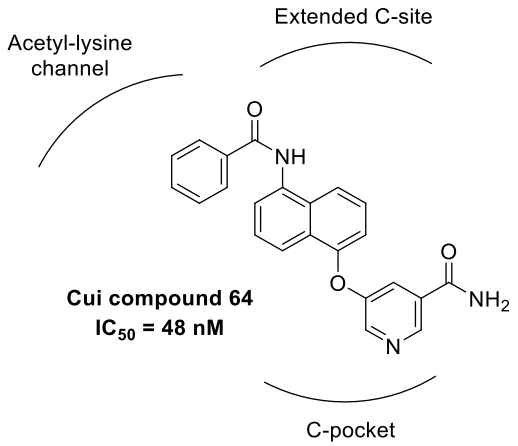

Figure 12: Visual representation of a possible binding pose of Cui compound 64 that simultaneously binds to the C-pocket of NAD^+ binding site and the extended C-site or the acetyl-lysine channel.

For the rational design of Sirt2 bisubstrate analogues within the work investigated in this thesis, both the extended C-site and the selectivity pocket, will be targeted in addition to the C-pocket of the NAD^+ binding site. The structurally minor complex SirReal-type Sirt2 inhibitor **28a** was selected as a suitable lead structure to provide an initial proof of concept (Figure 13A). The selection for a suitable linker with optimal length, flexibility and stability to connect **28a** with an NAD^+ co-factor mimetic was inspired by the reversible covalent moieties of the first two projects such as cyclic boronates or acetals. In addition, the determination of a suitable NAD^+ co-factor mimetic with drug-like properties is of paramount importance to ensure optimal efficacy of the bisubstrate analogue. A reasonable consideration for this purpose would be to use the endogenous co-factor NAD^+ itself. However, given the substantial size of NAD^+ and the instability of the pyrophosphates[124], only the essential part of the co-factor involved in the enzymatic reaction, nicotinamide riboside, will be taken into consideration. A low-molecular, drug-like mimetic that captures structural similarities to nicotinamide riboside without the possession of a pharmacokinetically unfavourable permanent positive charge that hampers cell penetration should be selected. Although the removal of the permanent positive charge of nicotinamide could be accomplished *via* the reduction of the pyridinium ring, the 1,4-dihydronicotinamide product is notoriously unstable und could not only isomerise to the 1,2- and the 1,6-dihydronicotineamide by-products, but also decompose or oxidise, even upon storage at -80 °C[125]. Alternatively, the commercially available IMP dehydrogenase inhibitor[126] Ribavirin presents itself as a promising substitute (Figure 13B).

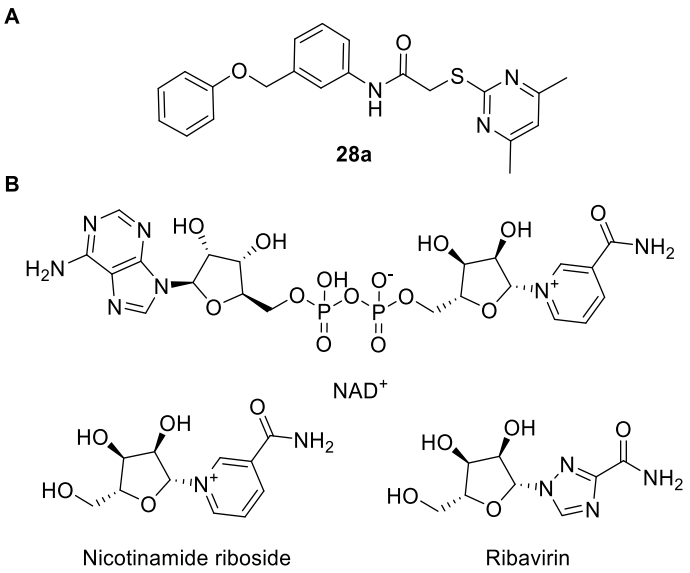

Figure 13: (**A**) Chemical structure of the SirReal type Sirt2 inhibitor 28a and (**B**) NAD^+, nicotinamide riboside and ribavirin.

Ribavirin is an antiviral agent used to treat various viral infections such as hepatitis C virus and Lassa fever[127, 128]. Sharing the ribosyl scaffold with nicotinamide riboside, ribavirin additionally features an heteroarylamide that is structurally aligned with that of nicotinamide riboside. Furthermore, the nitrogen-containing, aromatic triazole ring of ribavirin that lacks a positive charge even under physiological conditions conveniently offers a more drug-like motif compared to the pyridinium ring of nicotinamide riboside. Connecting **28a** (substrate mimetic) to ribavirin (nicotinamide riboside mimetic) with a suitable linker (Figure 14) will be attempted by utilising **28a** derivatives equipped with appropriate electrophilic functional groups such as boronic acids or aldehydes that allow cyclisations with the diol unit of ribavirin. This third project aims to investigate the potential benefits of bisubstrate analogues in drug design, and in doing so potentially advancing the repertoire of potent and subtype selective Sirt2 inhibitors.

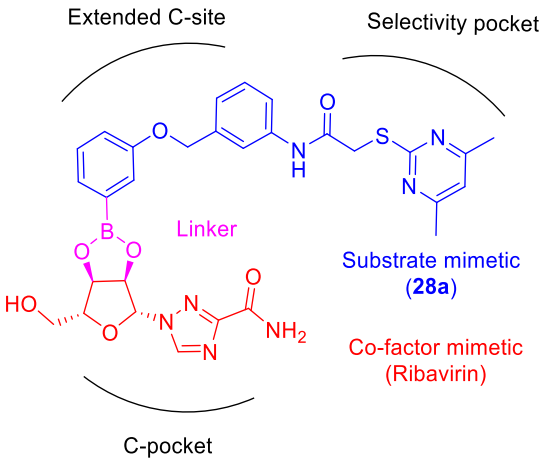

Figure 14: Envisaged Sirt2 bisubstrate analogue that features a substrate mimetic (**28a**) binding to the extended C-site and the selectivity pocket of the active site and a nicotinamide riboside mimetic (ribavirin) that binds to the C-pocket of the NAD^+ binding site, exemplified with a boronate linker.

3. Results & Discussions

This section outlines and summarizes the results obtained over the course of this thesis and these results are presented in the form of four individual projects. Three of these projects have been published in peer-reviewed scientific journals, while the fourth has been prepared as a manuscript and is awaiting additional results from collaborative partners prior to submission for peer-reviewed publication.

3.1. Project I: Tailored SirReal-type inhibitors as highly potent Sirt2 inhibitors

Wirawan, R.*; Frei, M.*; Heider, A.; Papenkordt, N.; Friedrich, F.; Wein, T.; Jung, M.; Groll, M.; Huber, E. M.; Bracher, F. Tailored SirReal-type inhibitors enhance SIRT2 inhibition through ligand stabilization and disruption of NAD^+ co-factor binding. *RSC Med. Chem.* **2025**, *16*, 5419-5440.

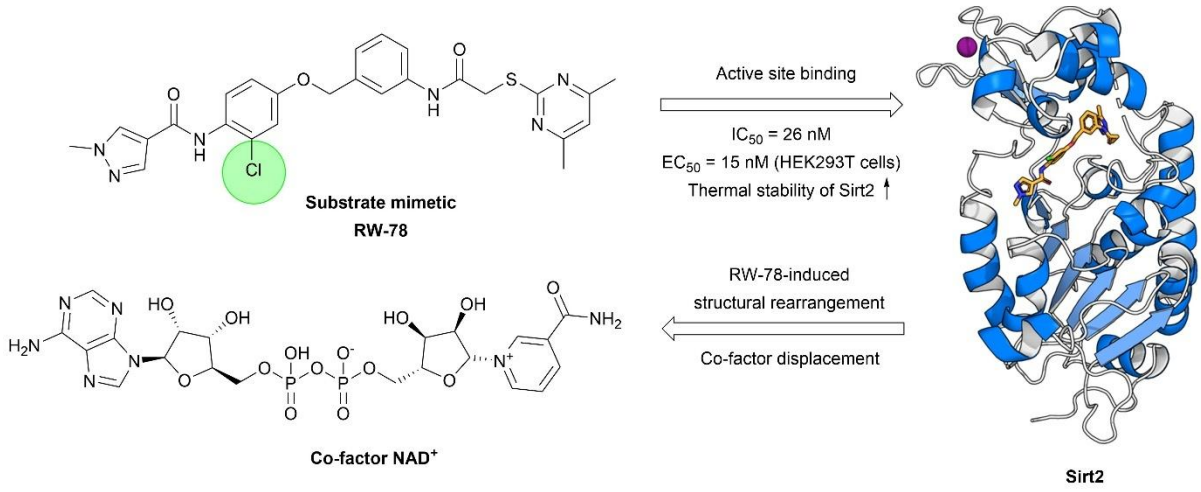

3.1.1. Summary

A systematic investigation on the inhibitory effects of functionalized Sirt2 inhibitors was performed by employing diverse electrophilic functional groups, which were designed to target the ribose vicinal diol unit of the essential co-factor NAD^+ to potentially enhance Sirt2 inhibition. Appropriate functional groups such as boronic acids, nitriles and aldehydes that can undergo reversible covalent bonding with the ribose vicinal diol unit of NAD^+ were carefully selected through evaluation of established inhibitors that mediate through this proposed mode of action. In addition, halogen bonding has also seen notable success as a tool to significantly increase the potency of inhibitors and were thus investigated complementary to reversible covalent inhibition. Guided by initial docking studies, 15 Sirt2 inhibitors were synthesized based on **SirReal2** and **24a**. The chloro-containing derivative **29** (**RW-78**) emerged as a highly potent

and subtype-selective Sirt2 inhibitor with an IC_{50} of 26 nM, which significantly outperforms **SirReal2** (IC_{50} = 240 nM) and its lead structure **24a** (IC_{50} = 79 nM). Fluorescence-based thermal shift assays were initially performed to investigate the potential role of the co-factor NAD^+ in the potency enhancement of **RW-78**. Results revealed a significant increase of the melting point of **RW-78**-Sirt2 complex (ΔT = 6.5 °C) at 30 µM inhibitor concentration but showed no dependence on NAD^+. Co-crystallization experiments were then carried out to elucidate the exact binding mode of **RW-78**. X-ray visualizations unveiled inhibitor stabilization in the active site *via* newly formed halogen bonds with the π-system of F235. Furthermore, unique structural rearrangement of residues at the active site was induced upon binding of **RW-78** that led to the displacement of the co-factor NAD^+, highlighting co-factor displacement as a viable strategy in the development of Sirt2 inhibitors. In addition, Sirt2 target engagement of **RW-78** in HEK293T cells were investigated *via* NanoBRET assays and results showed high target engagement with an EC_{50} value of 15 nM.

3.1.2. Personal Contributions

My personal contributions to this journal article include the synthesis and the characterization of the SirReal-type inhibitor **24a** and all derivatives thereof, the management and coordination of this project, the writing of the original draft, the reviewing and editing of the final manuscript, and the preparation of the graphical abstract and supplementary information.

Matthias Frei synthesised and characterized all **SirReal2** derivatives, provided support in the writing of the original draft, reviewed and edited the final manuscript, and prepared the supplementary information. Anna Heider expressed Sirt2 proteins and performed X-ray co-crystallization experiments and provided support both in the writing of the original draft and the preparation of the supplementary information. Niklas Papenkordt performed the NanoBRET assays. Florian Friedrich performed the fluorescence-based thermal shift assays. Thomas Wein performed molecular docking experiments. Manfred Jung supervised the NanoBRET and fluorescence-based thermal shift assays and reviewed and edited the final manuscript. Michael Groll supervised the expression of Sirt2 proteins and X-ray co-crystallization experiments and reviewed and edited the final manuscript. Eva Maria Huber supervised the expression of Sirt2 proteins and X-ray co-crystallization experiments, provided support in the writing of the original draft and reviewed and edited the final manuscript. Franz Bracher conceptualized and designed the study, managed and coordinated the project, supervised all synthetic work, provided funding and resources, and reviewed and edited the final manuscript.

3.1.3. Article

All materials from this article were reproduced with permission from Creative Commons Attribution in accordance with the Royal Society of Chemistry. This article is printed in the original wording. Formatting may vary slightly compared to the original article.

RSC
Medicinal Chemistry

ROYAL SOCIETY OF CHEMISTRY

RESEARCH ARTICLE

View Article Online
View Journal

Cite this: DOI: 10.1039/d5md00144g

Tailored SirReal-type inhibitors enhance SIRT2 inhibition through ligand stabilization and disruption of NAD$^+$ co-factor binding

Ricky Wirawan, †[a] Matthias Frei, †[a] Anna Heider, [b] Niklas Papenkordt, [c] Florian Friedrich, [c] Thomas Wein, [a] Manfred Jung, [c] Michael Groll, [b] Eva M. Huber [b] and Franz Bracher *[a]

Received 14th February 2025,
Accepted 6th August 2025

DOI: 10.1039/d5md00144g

rsc.li/medchem

Human sirtuin 2 (SIRT2) is an NAD$^+$ dependant enzyme that has been linked to the pathogenesis of various diseases, making it a promising target for pharmaceutical intervention. This study presents a systematic investigation on the inhibitory effects of SIRT2 inhibitors functionalized with diverse electrophilic functional groups. Guided by initial docking studies, we designed and synthesised 14 derivatives of two published potent lead structures **24a** and **SirReal2**. The most potent and subtype selective SIRT2 inhibitor **29** (**RW-78**) exhibits an IC_{50} of 26 nM, which outperforms its lead structure **24a** (IC_{50} = 79 nM) by a factor of 3. The increased potency of **29** is explained by halogen–π interactions with SIRT2 residues as visualized by X-ray crystallography. Furthermore, **29** interferes with NAD$^+$ binding, highlighting co-factor displacement as a valid strategy to inhibit SIRT2. Additionally, we showed cellular target engagement *via* NanoBRET assays in HEK293T cells (EC_{50} = 15 nM). Altogether our findings provide a deeper insight into the structure–activity relationships of these SirReal-type inhibitors and offer new avenues for optimisation of SIRT2 inhibitors.

Introduction

Sirtuins, belonging to class III histone deacetylases, constitute a family of highly conservative NAD$^+$-dependant proteins that are involved in the regulation of various biological processes such as metabolism, aging, inflammation and oxidative stress.[1] Although sirtuins were initially recognised solely for their deacetylation activity,[2] recent studies unveiled a broader catalytic scope that includes desuccinylation,[3] demalonylation,[3] demyristoylation[4] and ADP-ribosylation.[5] Furthermore, sirtuin substrates extend beyond histones to include other proteins, such as α-tubulin,[6] p53 (ref. 7) and NF-κB.[8] Of the seven sirtuin subtypes, SIRT2 emerged as a key target, particularly due to its involvement in the pathogenesis of cancer,[9] viral infections[10] and neurodegenerative diseases.[11,12] Despite numerous efforts over the past few years, the development of potent and subtype selective SIRT2 inhibitors with satisfactory physicochemical properties still poses a significant challenge. Published SIRT2 inhibitors with drug-like properties have been shown to possess a wide range of structural diversity with various binding mechanisms (Fig. 1). SIRT2 inhibitors with greater potency tend to incorporate thioamide (**KPM-2** (ref. 13) and **TM**[9]) and thiourea (**AF8**)[14] scaffolds that can form stable covalent intermediates with the essential co-factor NAD$^+$. Additionally, SIRT2 inhibitors with other structural motifs such as oxadiazole (**Moniot_39**)[15] and chroman-4-one (**6f**)[16] were identified with IC_{50} values covering low micromolar ranges. The alkaloid cytisine derived compound **NPD11033** was shown by Kudo *et al.* to likewise be a potent SIRT2 inhibitor.[17] Further potent SIRT2 inhibitors such as **AGK2** were detected by means of high-throughput screening.[18] Similarly, a series of aminothiazoles were discovered through library screening, in which the term sirtuin rearranging ligands (SirReals) was coined.[19,20] Among these aminothiazoles, **SirReal2** displayed high inhibitory potency with an IC_{50} value of 0.44 μM.[19] X-ray crystallographic studies on a SIRT2–**SirReal2**–NAD$^+$ complex unveiled a ligand-induced structural rearrangement of the active site that generates the emergence of a selectivity pocket that is occupied by the 4,6-dimethyl-2-mercaptopyrimidine motif. Further optimisations employing triazole motifs led to SIRT2 inhibitors with improved potency (**Vogelmann_12** (**SH10**)[21] and **Schiedel_9** and **Schiedel_10**[22]). Extending efforts for the development of alternative SIRT2 inhibitors exploiting this selectivity pocket, Yang *et al.* synthesised a library of

[a] *Department of Pharmacy, Ludwig-Maximilians University Munich, Butenandtstraße 5-13, 81377 Munich, Germany. E-mail: franz.bracher@cup.uni-muenchen.de*
[b] *Center for Protein Assemblies, Technical University of Munich, Ernst-Otto-Fischer Straße 8, 85748 Garching, Germany*
[c] *Institute of Pharmaceutical Sciences, Albert-Ludwigs-Universität Freiburg, Albertstraße 25, 79104 Freiburg im Breisgau, Germany*
† Equal contribution as first author to this work.

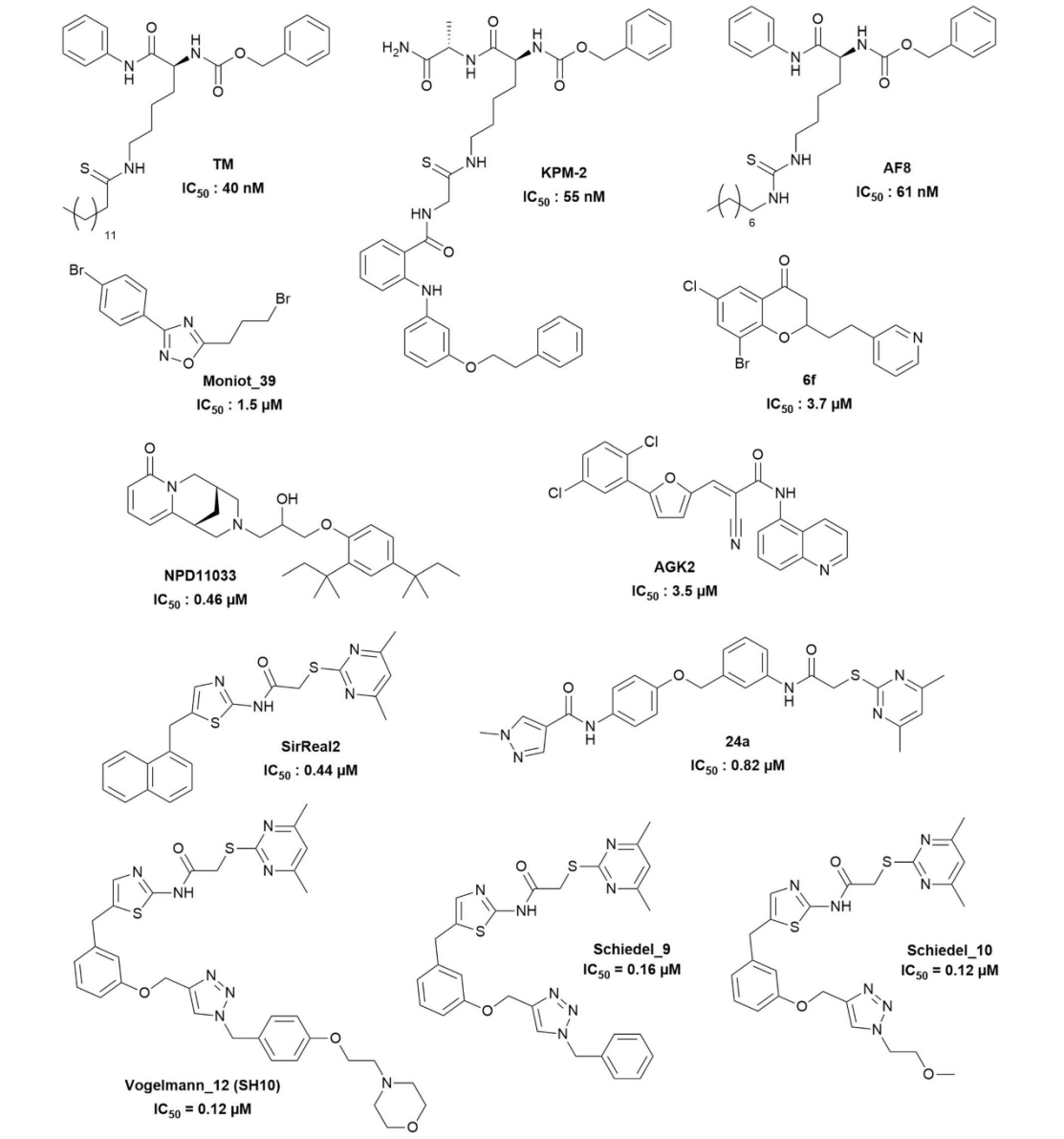

Fig. 1 Examples of published SIRT2 inhibitors.

N-acylaniline derivatives that identified **24a** as a potent and selective SIRT2 inhibitor with an IC_{50} value of 0.82 µM.[23,24]

Design rationale

Based on the published co-crystal structures of SIRT2 with either **24a** (PDB ID: 5YQO)[23] or **SirReal2** and NAD^+ (PDB ID: 4RMG),[19] we hypothesised that significant increase in the potency of these lead structures can be achieved through strong, targeted interactions with the vicinal hydroxy groups of the ribose unit of NAD^+ by utilizing appropriate functional groups that enable reversible covalent binding or halogen bonding. Although reactive warheads such as Michael acceptors, β-lactones and β-lactams, epoxides and sulfonyl

View Article Online
RSC Medicinal Chemistry Research Article

fluorides have seen application in drug development and present themselves as attractive irreversible covalent binders, the potential for immunogenic reactions and off-target toxicity is almost inevitable.[25–27] In contrast, reversible covalent inhibitors can dissociate from off-targets, reducing the potential of unwanted side effects while retaining extended binding at the intended target protein.[28] Several reversible covalent inhibitors have been successfully approved as therapeutic drugs, such as the boronic acid bortezomib that inhibits the 20S proteasome for the treatment of multiple myeloma,[29,30] the nitrile-based dipeptidylpeptidase 4 (DPP4) inhibitor saxagliptin for the treatment of type 2 diabetes mellitus,[31] and the aldehyde-bearing voxelotor for the treatment of sickle cell anaemia.[32] Functional groups such as boronic acids, nitriles and aldehydes do not only possess the capability to undergo reversible covalent bonding, but can also form strong non-covalent interactions in the form of hydrogen bonding, *e.g.* with the ribose hydroxy groups of the co-factor NAD^+. Comparably, non-covalent interactions *via* halogen bonding, which is sometimes referred to as the hydrophobic equivalent of hydrogen bonding,[33] represent an area of interest in current rational drug design approaches as demonstrated by the optimisation of PDE5 (ref. 34) and HIV-1 reverse transcriptase inhibitors[35,36] and offer, as such, a promising drug optimisation technique. This non-covalent interaction arises from the anisotropic electron distribution in halogen residues, creating a σ-hole with depleted electron density that enables strong bonding with diverse nucleophiles.[37–40] By tailoring lead structures **24a** and **SirReal2** with such functional groups, we aimed to achieve, in a (to our knowledge) unprecedented manner in the sirtuin field, reversible covalent binding and strong halogen bonding with the co-factor NAD^+ of SIRT2 that strives for significant enhancement in potency (Fig. 2).

Encouraged by initial docking studies of the envisaged boronic acid derivatives of **24a** and **SirReal2** that showed poses of the boronic acid moiety in proximity to the vicinal diol unit of NAD^+ (Fig. 3), we continued our efforts[41] in developing highly potent and sub-type selective SIRT2 inhibitors through systematic investigation of the effects of such functional groups on these two selected lead structures.

Results and discussion

Chemistry

The lead structure **24a** (here **10**) was synthesised according to literature with slight modifications in the chronology.[23,24] Syntheses of functionalised **24a** derivatives **11–14** were initiated by the amide coupling of 4-amino-2-bromophenol (**2**) and 1-methyl-1*H*-pyrazole-4-carboxylic acid to give amide **4** (Scheme 1). Williamson ether synthesis of **4** with 3-nitrobenzyl bromide gave bromobenzene intermediate **6**, which afforded nitrile **9** with zinc(II) cyanide following published procedures,[42] and boronic acid **8** following Miyaura borylation protocols[43] and subsequent oxidative cleavage of boronic acid pinacol ester **7**. In the final step, reduction of the nitrobenzene derivatives **6**, **8** and **9** followed by amide coupling with 2-((4,6-dimethylpyrimidin-2-yl)thio)acetic acid gave bromobenzene derivative **11**, boronic acid **13** and nitrile **14**, respectively. In contrast, the introduction of the aldehyde functional group was performed in the final step due to its instability. Here, bromobenzene derivative **11** was formylated to aldehyde **12** with *in situ* generated carbon monoxide from *N*-formylsaccharin following protocols from Ueda *et al.*[44] A liquid–liquid extraction protocol[45] utilising sodium bisulfite to form a charged bisulfite adduct with subsequent regeneration of the aldehyde *via* basification was necessary, since purification with flash column chromatography alone did not afford the desired aldehyde **12** with sufficient purity. However, the obtained 3% yield was rather unsatisfactory, owing to stability issues. Nevertheless, the amount of product **12** obtained sufficed for chemical analysis and biological testing. Analogously, the preparation of the isomeric functionalised **24a** derivatives **29–34** followed a

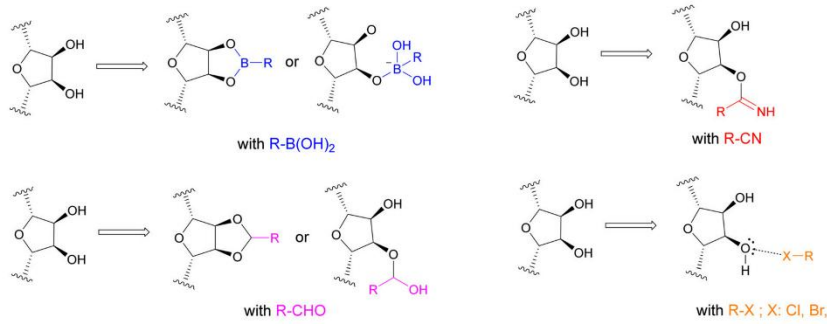

Fig. 2 Proposed binding mechanisms and interactions of the selected functional groups with the ribose unit of the co-factor NAD^+. Boronic acids can undergo reversible covalent bonding with one or both hydroxy groups to form (cyclic) boronates. Nitriles can form iminoethers, and aldehydes can form hemiacetals or cyclic acetals. Halogen residues such as chlorine, bromine and iodine can form halogen bonds with the ribose hydroxy groups.

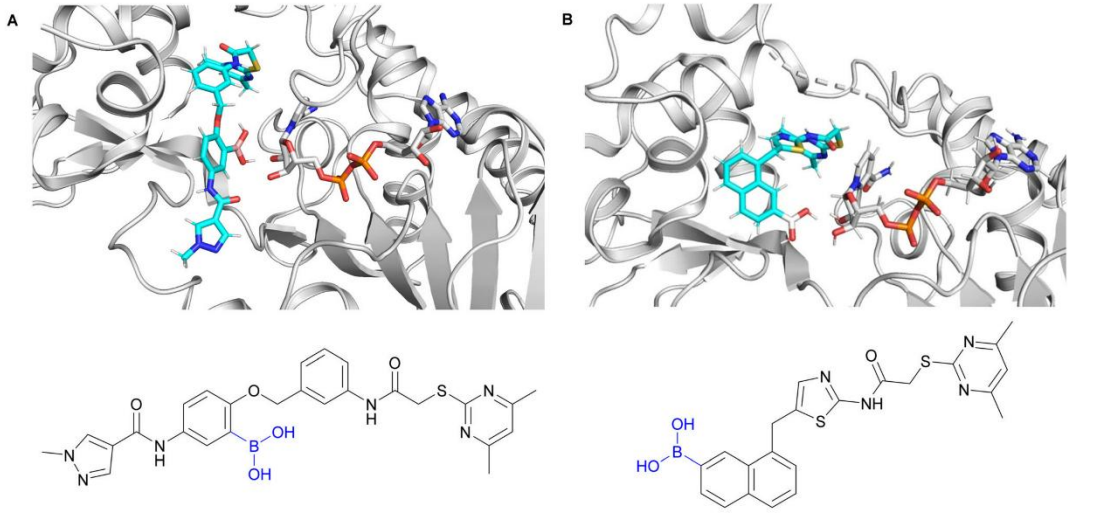

Fig. 3 (A) Docking poses of the envisaged **24a** boronic acid derivative (cyan) based on PDB ID: 5YQO[23] (NAD^+ shown was extracted separately from PDB ID: 4RMG[19]) and (B) **SirReal2** boronic acid derivative (cyan) based on PDB ID: 4RMG[19] in the presence of NAD^+ showing the boronic acids in proximity to the vicinal diol unit of ribose of NAD^+ for reversible covalent bonding.

similar synthetic route. Building blocks 4-amino-3-bromophenol (**18**) and 4-amino-3-iodophenol (**19**) were obtained from the reduction of 3-bromo-4-nitrophenol (**15**) and 3-iodo-4-nitrophenol (**16**), respectively. These phenols and the commercially available 4-amino-3-chlorophenol (**17**) were then subjected to Williamson ether synthesis prior to amide coupling with 1-methyl-1*H*-pyrazole-4-carboxylic acid as we noticed a significantly higher reactivity of the phenols compared to the aromatic amines. Similar to the previous synthetic route, bromobenzene intermediate **24** served as a key intermediate for the preparation of boronic acid **27** and nitrile **28**. Reduction of the nitrobenzene derivatives **23**–**25** and **28** and subsequent amide coupling with 2-((4,6-dimethylpyrimidin-2-yl)thio)acetic acid in the final step afforded halogenated derivatives **29**–**31** and nitrile **34**, respectively. It is noteworthy that the amide coupling with 2-((4,6-dimethylpyrimidin-2-yl)thio)acetic acid after the reduction of the boronic acid-bearing nitrobenzene **27** failed with various amide coupling reagents. To overcome this problem, the highly reactive bromoacetyl bromide was instead implemented, thereby generating a α-bromoacetamide intermediate that underwent nucleophilic substitution with 4,6-dimethylpyrimidine-2-thiol to give boronic acid **33**. Aldehyde **32** was obtained from bromobenzene derivative **30** with the same formylation[44] and bisulfite-mediated purification[45] protocol that was developed for the synthesis of aldehyde **12**.

The synthesis of functionalised **SirReal2** derivatives was initiated by the preparation of aminothiazole **38** mainly according to literature (Scheme 2).[20] In deviation therefrom, intermediate 7-bromonaphtalene-1-amine (**37**) was prepared in a two-step process according to a patented method.[46] Starting from 7-bromo-1-tetralone (**35**), oxime **36** was prepared and then converted to 7-bromonaphtalene-1-amine (**37**) *via* Semmler–Wolff aromatisation. Subsequently, a modified Meerwein arylation afforded aminothiazole **38** that served as a key intermediate for further functional group modifications, such as the palladium-catalysed synthesis[42,47] of nitrile **39** and cyanomethyl derivative **40**. Notably, the introduction of the boronic acid necessitated the protection of the amine. *N*-Boc protection of aminothiazole **38** gave bromobenzene intermediate **41**, which underwent Miyaura borylation[43] to give boronic acid pinacol ester **42**. Oxidative cleavage of **42** and subsequent *N*-Boc cleavage with TFA gave boronic acid **44**. The functionalised **SirReal2** derivatives **45**–**48** were then obtained in the final step from **38**–**40** and **44** *via* amide coupling with 2-((4,6-dimethylpyrimidin-2-yl)thio)acetic acid. Formylation of **45** was again performed in the final step of the synthesis, in this case using a protocol from Konishi *et al.*[48] that utilises a different phosphine ligand, which generated a better yield for the preparation of aldehyde **49**. Laborious purification of aldehyde **49** with the aforementioned liquid–liquid extraction protocol[45] *via* a bisulfite adduct was not necessary in this case.

In vitro sirtuin inhibitory activities

The determination of SIRT2 inhibitory activity was performed by Reaction Biology Corporation (Malvern, USA) with a fluorescence-based assay utilizing the fluorogenic peptide of p53 residues 379–382 (RHKK(Ac)-Fl). In general, the determined IC_{50} values of literature-known lead

View Article Online
RSC Medicinal Chemistry Research Article

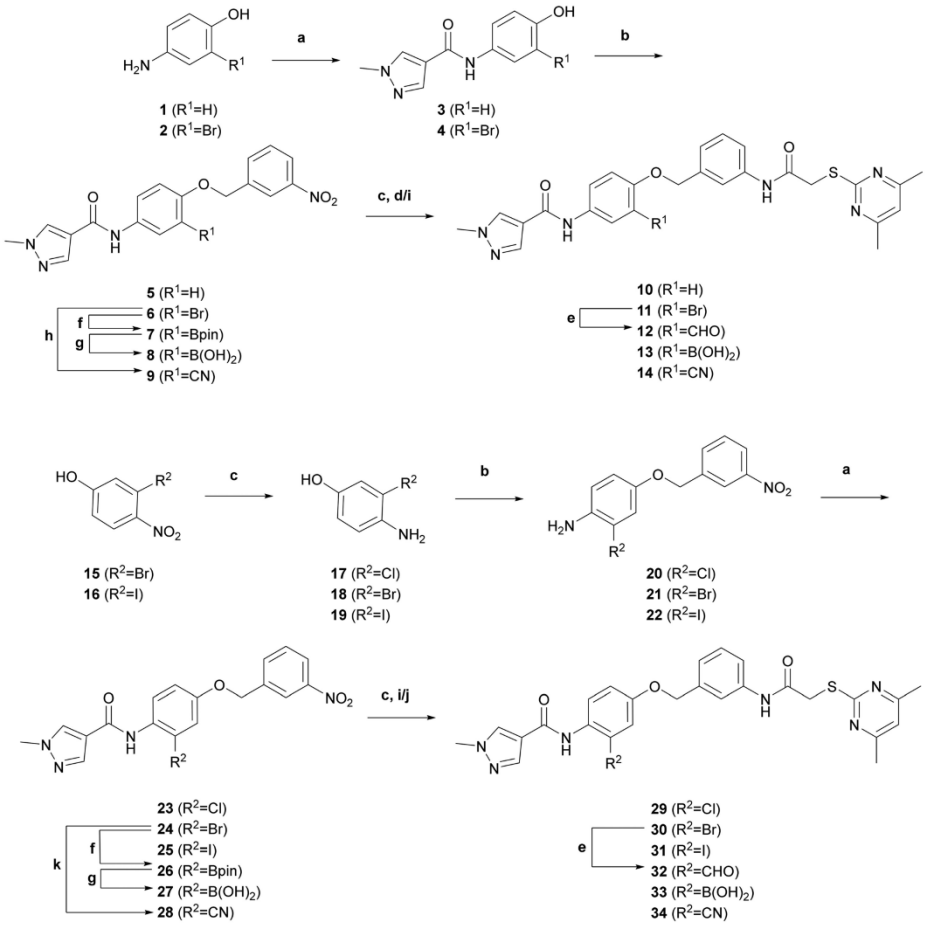

Scheme 1 Reagents and conditions: (a) 1-methyl-1*H*-pyrazole-4-carboxylic acid, HATU, DIPEA, THF, rt–65 °C, 3 h–6 d, 21–71%; (b) 3-nitrobenzyl bromide, K_2CO_3, DMF, 0 °C–rt, 5 h–16 h, 38% quant.; (c) Fe, NH_4Cl, EtOH, 90 °C, 2 h, 86–89%; (d) 2-((4,6-dimethylpyrimidin-2-yl)thio)acetic acid, EDC, HOBt, DIPEA, DCM, rt, 18 h, 62% (over 2 steps); (e) $Pd(OAc)_2$, dppb, *N*-formylsaccharin, Na_2CO_3, Et_3SiH, DMF, 75 °C, 19 h, 3%; (f) B_2pin_2, $PdCl_2$(dppf)·DCM, KOAc, 1,4-dioxane, 95 °C, 19 h, 26–45%; (g) $NaIO_4$, NH_4OAc or HCl, acetone/H_2O or THF/H_2O, rt, 2 h–15 h; 45% quant. (h) $Zn(CN)_2$, $Pd(PPh_3)_4$, DMF, 150 °C, 22 h, 7%; (i) 2-((4,6-dimethylpyrimidin-2-yl)thio)acetic acid, EDC·HCl, 4-DMAP, DMF, rt, 18 h–7 d, 40–69% (over 2 steps); (j) bromoacetyl bromide, DMF, rt, 30 min; then 4,6-dimethylpyrimidine-2-thiol, *t*-BuOK, DMF, rt, 19 h, 26% (over 3 steps); (k) CuCN, DMF, 150 °C, 22 h, 46%.

structures **24a** (here **10**)[23] and **SirReal2** (ref. 20) in this assay are in accordance with their published values. Furthermore, all **24a** derivatives showed potent and subtype selective inhibition of SIRT2 in the nanomolar range (Table 1). However, the introduction of the boronic acid, nitrile and aldehyde moieties in both positions R^1 and R^2 (**12–14**, **32–34**) showed no improvement, and to some extent a decrease in the potency compared to the lead structure **24a** (**10**). Similarly, halogen modifications with bromine at the R^1 position (**11**) showed no significant improvement in potency. On the contrary, we observed a significant increase in potency by the introduction of halogens at the R^2 position (compounds **29–31**), highlighting the importance of the position of the functional group modifications. In particular, chlorobenzene derivative **29** displayed a 3-fold increase in potency, exhibiting an IC_{50} value of 26 nM, but also the iodine (compound **31**, IC_{50} = 29 nM) and bromine derivatives (compound **30**, IC_{50} = 54 nM) were highly potent. These results lead to the following ranking in descending order of potency: Cl > I > Br. Although in theory the chlorine atom should form the weakest halogen bond with the ribose hydroxy groups of NAD^+,[37] the observation that the chlorobenzene derivative **29**

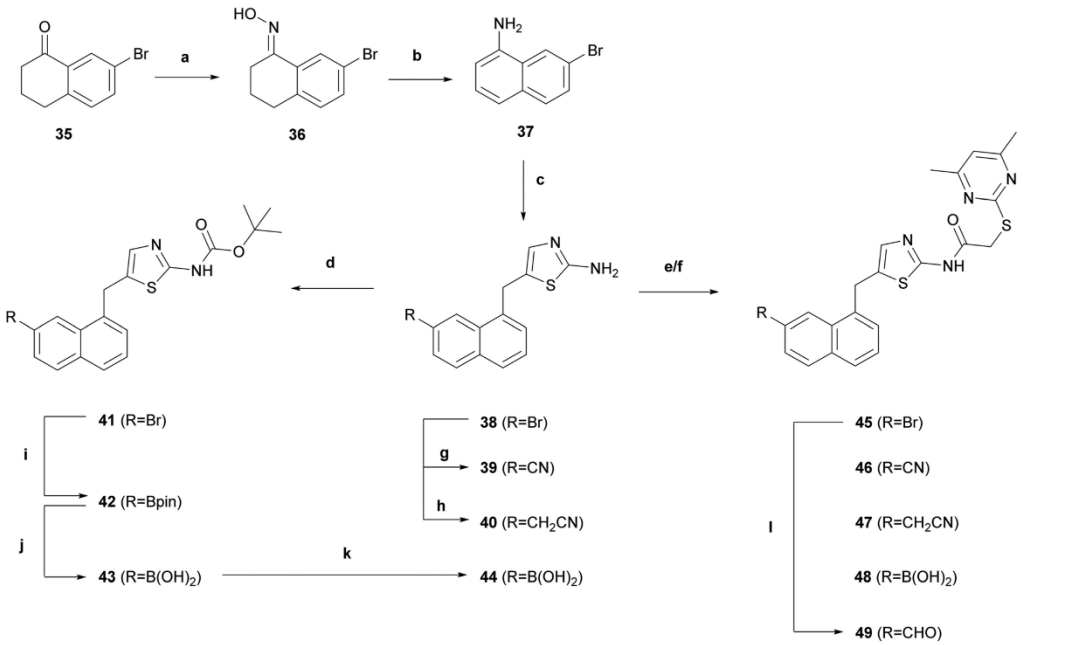

Scheme 2 Reagents and conditions: (a) $NH_2OH{\cdot}HCl$, pyridine, $EtOH/H_2O$, rt, 24 h, quant.; (b) Ac_2O, H_2SO_4, AcOH, 120 °C, 24 h, 25%. (c) $NaNO_2$, HCl; then $FeCl_3{\cdot}6H_2O$, HCl, H_2O, 0 °C, 10 min; then $CuCl_2{\cdot}2H_2O$, HCl, acetone/EtOH, 0 °C, 10 min; then acrolein, acetone/H_2O, rt, 4 h; then thiourea, EtOH, 80 °C, 30 h, 41% (over 4 steps); (d) Boc_2O, toluene, 100 °C, 4.5 h, 85%; (e) 2-((4,6-dimethylpyrimidin-2-yl)thio)acetic acid, HATU, DIPEA, DMF, rt, 18 h, 29–40%; (f) 2-((4,6-dimethylpyrimidin-2-yl)thio)acetic acid, EDC·HCl, 4-DMAP, DMF, rt, 16 h, 17–52%; (g) $Zn(CN)_2$, $Pd(PPh_3)_4$, DMF, 80 °C, 18 h, 61%; (h) 4-(4,4,5,5-tetramethyl-1,3,2-dioxaborolan-2-yl)isoxazole, $PdCl_2$(dppf)·DCM, DMF, 90 °C, 20 h, 26% (i) B_2pin_2, $PdCl_2$(dppf)·DCM, KOAc, 1,4-dioxane, 80 °C, 1 h; then rt, 2 h, 51%; (j) $NaIO_4$, HCl, THF/H_2O, rt, 4 h, 84%; (k) TFA, $CHCl_3$, rt, 17 h, quant.; (l) $Pd(OAc)_2$, dppf, *N*-formylsaccharin, Na_2CO_3, Et_3SiH, DMF, 75 °C, 19 h, 11%.

outperformed both bromobenzene and iodobenzene derivatives **30** and **31** suggests a much more complex mechanism than mere halogen bonding for the underlying increase in potency. Additional factors such as the atomic radius and thus steric requirements of these halogens may also play a significant role in the increase in potency, where the smaller chlorine atom may experience less steric effects upon binding at the active site compared to the larger bromine and iodine atoms. Halogen modification of **SirReal2** with bromine (compound **45**) pointed similarly to an increase in potency. This is consistent with the published IC_{50} values of **SirReal2** and 7-bromo-**SirReal2** (**45**).[20] Although the introduction of boronic acid and aldehyde groups (compounds **48**, **49**) did not display any significant improvement in potency, the **SirReal2** derivative **46** bearing a nitrile group showed a 2-fold increase in SIRT2 inhibition with an IC_{50} value of 122 nM. In comparison, the homologous cyanomethyl derivative **47** only had similar potency to **SirReal2** (Table 1).

The determination of subtype selectivity against SIRT1, 3 and 5 was performed by measuring the residual enzyme activity after treatment with the corresponding inhibitor at a fixed concentration of 50 μM and subsequent calculation of the percentage inhibition. All target compounds tested showed selectivity towards SIRT2, as corresponding inhibition values of SIRT1, 3 and 5 indicate IC_{50} values of over 50 μM with an exception for compound **33** that showed 71% inhibition at 50 μM. Nevertheless, considering the low IC_{50} value of 202 nM for the desired target SIRT2, selectivity is considered as sufficient.

Thermal stability of SIRT2–inhibitor complexes

To investigate the potential role of the co-factor NAD^+ in the potency enhancement of the chloro-derivate **29** (**RW-78**) and nitrile **46** (**FM295**) compared to their corresponding lead structures **24a** and **SirReal2**, we performed fluorescence thermal shift assays (Fig. 4). The thermal stability of SIRT2 was determined in the presence of 10 μM and 30 μM inhibitor and in the presence and absence of 2.5 mM co-factor NAD^+. The presence of 30 μM of compound **29** resulted in a significant increase in the melting temperature of SIRT2 (ΔT = 6.5 °C) compared to its lead structure **24a** (ΔT = 3 °C). However, results showed that the inhibitor-induced SIRT2 stabilization was

View Article Online
RSC Medicinal Chemistry Research Article

Table 1 *In vitro* inhibition of human SIRT1, 2, 3 and 5 by functionalised derivatives of **24a** and **SirReal2**. IC_{50} values against SIRT2 are given as mean with standard deviations (n = 3). Inhibition percentages at 50 μM for SIRT1, 3 and 5 are given as mean without standard deviations (n = 2)

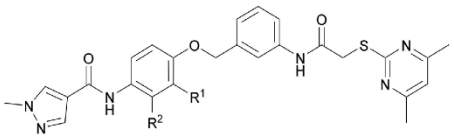

Compound ID	R^1	R^2	IC_{50} (nM) SIRT2	Inhibition of SIRT1/3/5 in %@50 μM SIRT1	SIRT3	SIRT5
10 (**24a**[a])	H	H	79 ± 4	n.d.	n.d.	n.d.
11	Br	H	81 ± 10	n.i.	24	13
12	CHO	H	147 ± 13	2	24	16
13	$B(OH)_2$	H	294 ± 17	29	5	10
14	CN	H	125 ± 18	6	35	2
29	H	Cl	26 ± 2	12	26	7
30	H	Br	54 ± 7	4	43	1
31	H	I	29 ± 2	5	22	12
32	H	CHO	184 ± 9	n.i.	7	6
33	H	$B(OH)_2$	202 ± 6	71	24	14
34	H	CN	91 ± 7	23	31	4

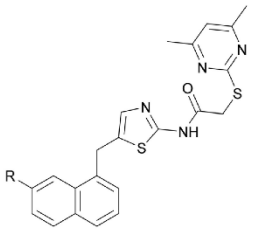

Compound ID	R	IC_{50} (nM) SIRT2	Inhibition of SIRT1/3/5 in %@50 μM SIRT1	SIRT3	SIRT5
SirReal2[b]	H	235 ± 10	n.d.	n.d.	n.d.
45[c]	Br	196 ± 17	n.d.	n.d.	n.d.
46	CN	122 ± 8	6	9	8
47	CH_2CN	235 ± 19	n.i.	15	2
48	$B(OH)_2$	235 ± 36	19	12	23
49	CHO	356 ± 42	11	13	21

[a] Literature-known compound **24a** by Yang *et al.* with a published IC_{50} of 0.82 μM for SIRT2.[23] [b] Literature-known compound **SirReal2** by Rumpf *et al.* with a published IC_{50} of 0.44 μM for SIRT2.[19] [c] Literature-known compound **45** by Schiedel *et al.* with a published IC_{50} of 0.21 μM for SIRT2 (ref. 20).

independent from NAD^+, contradicting our initial proposed binding mode. Similar results were obtained with the nitrile **46**.

Co-crystal structure of SIRT2 with compounds 29 (RW-78) and 31 (RW-80)

To clarify the binding mode of the most potent inhibitors we aimed for co-crystal structures with human SIRT2. To this end, we expressed human SIRT2 56-356 as a N-terminal His_6-SUMO fusion in *Escherichia coli* and purified the protein *via* affinity and size exclusion chromatography with tag removal in between (Fig. S1). Crystallization trials finally yielded an apo structure of SIRT2 (2.15 Å resolution, Table S1, PDB ID: 9S44) and two complex structures with **29** (**RW-78**) (1.45 Å, Table S2, Fig. 5, PDB ID: 9S46) and **31** (**RW-80**, Fig. S2A) (1.45 Å, Table S3, PDB ID: 9S48) in the same space group.

Both **29** and **31** occupy a pocket located slightly below the NAD^+-binding cleft, previously exploited by other potent and selective SIRT2 inhibitors like **SirReal2** and **24a** (Fig. 5A and S2A and B).[19,23] Compared to our SIRT2 apo structure, the ligand bound structures adopt the "open-locked-state" reported first in the SIRT2:**SirReal2** co-crystal structure (PDB ID: 4RMG; root mean square deviation ≤0.223 Å over 218 C^α atoms).[19,49] Both **29** and **31** are coordinated by the same protein residues and only differ by their halogen atom (Fig. 5B and S2B). In the binding pocket, the inhibitor is stabilized by multiple interactions previously described for the lead structure **24a** (PDB: 5YQO, Fig. S2B).[23] Most

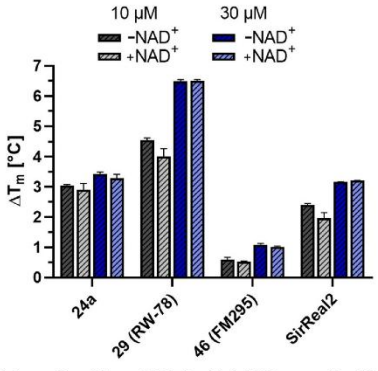

Fig. 4 Melting point shifts of SIRT2 with inhibitors at 10 μM and 30 μM in the presence and absence of 2.5 mM co-factor NAD^+ with no dependency on the co-factor observed. All melting temperature shifts measured were referenced to the melting temperature of SIRT2 without inhibitor, also in the presence and absence of the co-factor. Under both these conditions, the reference melting temperatures showed no significant change, each yielding a melting temperature of 53 °C.

importantly, the amide next to the methyl pyrazole hydrogen bonds to the carbonyl oxygen of V^{233} and R^{97}. Additionally, the chlorine (**29**) or iodine (**31**) atom engages in halogen–π-interactions with F^{235} (Fig. 5B and S2A and B). The spacing between the chlorine atom of **29** and the centroid of the π-system of F^{235} (3.6 Å) matches the average distance of C–Cl···π-bonds (3.854 Å),[50] explaining the high potency of **29**. Contrary to our design, **29** and **31** do not engage in interactions with the SIRT2 co-factor NAD^+ but stabilize the enzyme in an inactive state. This state is established by rearrangements of residues near the active site (Fig. 5B and S2C). For instance, the catalytic histidine H^{187} is slightly shifted compared to SIRT2 apo structures (PDB ID: 1J8F,[49] PDB ID: 9S44). In addition, by interacting with the inhibitor, F^{96} and R^{97} move into the NAD^+-binding pocket, displacing the co-factor and prohibiting NAD^+-binding. Therefore, the determined structures do not show electron densities for the co-factor, although 5 mM NAD^+ was included in the crystallization screens. Instead of the co-factor, the NAD^+-binding site contains many water molecules. Considering the high affinity of **29** and **31** (Table 1), the entropic barrier that is associated with the displacement of NAD^+ and the binding of water molecules must be counteracted by an enormous enthalpic stabilization of the inhibitors in the SIRT2 pocket. Notably, the NAD^+ displacement is supported by thermal shift assays (Fig. 4), which revealed that **29** increases the melting temperature of SIRT2 independently of NAD^+.

Cellular target engagement in HEK293T cells *via* NanoBRET assay

Cellular SIRT2 target engagement of chloro-derivative **29** was assessed in HEK293T cells *via* NanoBRET assay that was developed by Vogelmann *et al.*[21] The NanoBRET tracer pre-treated cells were incubated with increasing concentrations of chloro-derivative **29**, reflecting its intracellular binding to SIRT2. Compound **29** showed high target engagement with an EC_{50} value of 15 nM (Fig. 6), validating our data obtained from *in vitro* inhibition studies. For comparison, the highly potent triazole-based SirReal inhibitor **Vogelmann_12** (**SH10**) was used as a reference and showed an EC_{50} value of 99 nM.

Conclusions

Based on the rationale to target the essential co-factor NAD^+ of SIRT2 *via* reversible covalent binding or halogen bonding with appropriate functional groups, a total of 14 potent and subtype selective SIRT2 inhibitors were synthesised. While lead structure modifications of **SirReal2** and **24a** with polar,

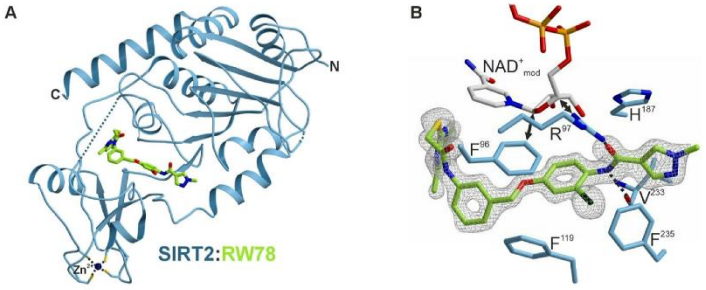

Fig. 5 (A) Co-crystal structure of human SIRT2 (blue) with its inhibitor **29** (**RW-78**, green) (PDB ID: 9S46). Residues 104–106 and 303 are disordered and indicated by blue dotted lines. The zinc ion bound to SIRT2 is shown as a dark blue sphere and coordinating cysteines are depicted as sticks. (B) Close-up view of **29** (green) bound to SIRT2. The experimental F_O–F_C omit electron density is shown as a gray mesh contoured to 3σ. Coordinating amino acid side chains (blue) are shown as sticks and labelled by the one-letter code. **29** is stabilized by hydrogen bonds to R^{97} and the V^{233} carbonyl oxygen (black dotted lines). The chlorine atom of **29** interacts with F^{235} *via* halogen–π-bonding. Binding of **29** induces movements of F^{96} and R^{97} into the NAD^+-binding site (see also Fig. S2C). Modelling of the NAD^+ co-factor (extracted from the SIRT2:**SirReal2** coordinates (PDB ID: 4RMG))[19] into the SIRT2:**RW-78** structure by superposition illustrates that F^{96} and R^{97} clash with NAD^+ (black double arrows) and hence displace the co-factor.

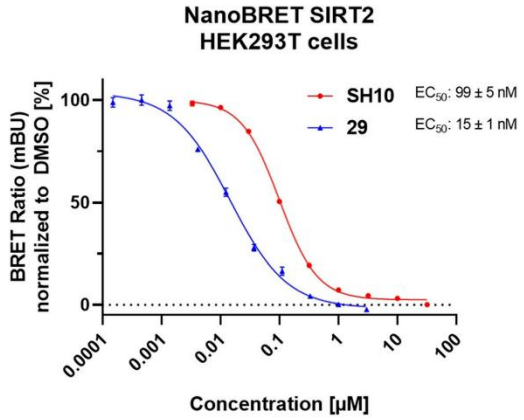

Fig. 6 NanoBRET-based cellular target engagement of the SIRT2 inhibitor **29**. Cellular binding of **29** was evaluated using a NanoBRET target engagement assay in live HEK293T cells. Cells were incubated with 2 μM NanoBRET tracer and treated with increasing concentrations **29** for 2 hours at 37 °C. Binding for **SH10** is plotted as a reference. For compound **29**, a stable HEK293T cell line expressing NanoLuc-SIRT2 fusion construct was used, whereas for **SH10** HEK293T cells were transiently transfected with the NanoLuc-SIRT2 fusion construct.

potential reversible covalent binding warheads showed ambiguous results, nitrile **46** (**FM295**; IC_{50} = 122 nM) demonstrated significant potency enhancement compared to its lead structure **SirReal2** (IC_{50} = 235 nM). Among the halogenated derivatives of **24a** (**10**), compounds **30** (IC_{50} = 54 nM) and **31** (IC_{50} = 29 nM) outperformed the lead structure **24a** (IC_{50} = 79 nM). In addition, ligand **29** (**RW-78**) emerged as the best member of the whole series and as one of the most potent SIRT2 inhibitors known to date (IC_{50} = 26 nM) while maintaining high subtype selectivity. X-ray crystallographic data visualized that compound **29** (**RW-78**) undergoes halogen–π interactions with SIRT2 and induces structural changes that interfere with co-factor binding. These results are in agreement with thermal shift assays indicating that the inhibition of compound **29** (**RW-78**) is NAD^+ independent. In addition, the utility of compound **29** (**RW-78**) in the cellular context was validated *via* NanoBRET assay in HEK293T cells that showed high target engagement to SIRT2 (EC_{50} = 15 nM). In conclusion, our findings provide a valuable contribution to a deeper understanding of the structure–activity relationships of SIRT2 inhibitors and a foundation for further optimisation of SIRT2-selective inhibitors.

Experimental

Chemistry

Materials and instruments. All solvents and reagents were purchased from commercial sources and used without further purification. Standard vacuum line techniques were applied. Reactions were monitored *via* thin layer silica gel chromatography (TLC) using polyester sheets POLYGRAM SIL G/UV254 coated with 0.2 mm silica gel (Macherey-Nagel). Plates were visualised using UV light (254 nm or 365 nm) or staining with $KMnO_4$, CAM (ceric ammonium molybdate) or DNPH (dinitrophenylhydrazine). Products were purified by flash column chromatography (normal-phase silica gel chromatography) using SiO_2 60 (0.040–0.063 mm, 230–400 mesh ASTM) from Merck. NMR spectra were recorded with Avance III HD 400 MHz Bruker BioSpin and Avance III HD 500 MHz Bruker BioSpin (^{1}H-NMR: 400 MHz and 500 MHz, ^{13}C-NMR: 101 MHz and 126 MHz) using the deuterated solvent stated. Chemical shifts (δ) are quoted in parts per million (ppm) and referenced to the residual solvent peak. Multiplicities are denoted as s-singlet, d-doublet, t-triplet, q-quartet and quin-quintet. Coupling constants J are given in Hz and round to the nearest 0.1 Hz. Infrared spectra were recorded from 4000 to 650 cm^{-1} on a PERKIN ELMER Spectrum BX-59343 FT-IR instrument. A Smiths Detection DuraSamp IR II Diamond ATR sensor was used for detection. The absorption bands are reported in wavenumbers [cm^{-1}]. High resolution mass spectra (HR-MS) were recorded using a Jeol Mstation 700 or JMS GCmate II Jeol instrument for electron impact ionisation (EI). Thermo Finnigan LTQ was used for electrospray ionisation (ESI). Melting points were measured with a Büchi Schmelzpunktapparatur B-540. HPLC analytical measurements at 210 nm and 254 nm for purities determination was performed with the following methods:

Method 1:
Zorbax SB C18 3.5 μm (4.6 × 100 mm), injection volume 5 μL.
a) MeCN/water (35 : 65); flow rate 1.0 mL min^{-1}; temp. 35 °C.
b) MeCN/water (50 : 50); flow rate 1.2 mL min^{-1}; temp. 35 °C.
c) MeCN/water (50 : 50); flow rate 1.2 mL min^{-1}; temp. 50 °C.

Method 2:
Raptor C18 5 μm (4.6 × 150 mm), injection volume 5 μL.
a) MeCN/water (35 : 65); flow rate 0.7 mL min^{-1}; temp. 35 °C.

Method 3:
Zorbax Eclipse Plus® C18 5 μm (4.6 × 150 mm), injection volume 5 μL.
a) MeCN/water (70 : 30); flow rate 1.0–1.5 mL min^{-1}; temp. 30–50 °C.
b) MeCN/water (50 : 50); flow rate 1.0–1.5 mL min^{-1}; temp. 30–50 °C.
c) MeCN/phosphate buffer pH = 5 (70 : 30); flow rate 1.0–1.2 mL min^{-1}; temp. 30–50 °C.

Synthetic procedures

General procedure A – amide coupling (I) with HATU and DIPEA. To a stirred solution of the appropriate carboxylic acid (1.0 equivalent) in THF with a concentration of 0.20 M were added DIPEA (3.0 equivalents) and HATU (1.5 equivalents). The reaction mixture was stirred at room temperature for 1 h. The appropriate amine (1.0 equivalent) was then added and unless stated otherwise, the reaction mixture was further stirred at room temperature for 3 h.

DCM and water were then added, the resulting two phases were separated, and the aqueous phase was extracted with DCM (3×). The combined organic phases were dried using a phase separation paper and the solvent was removed *in vacuo*. Unless stated otherwise, the crude product was then purified by FCC using the indicated eluent.

General procedure B – amide coupling (II) with EDC, HOBt and DIPEA. To a stirred solution of the appropriate amine (1.0 equivalent) in DCM with a concentration of 0.10 M were added HOBt (1.5 equivalents), EDC (2.0 equivalents), DIPEA (2.0 equivalents) and the appropriate carboxylic acid (2.0 equivalents). The reaction mixture was stirred at room temperature for 18 h. DCM and water were then added, the resulting two phases were separated, and the aqueous phase was extracted with DCM (3×). The combined organic phases were dried using a phase separation paper and the solvent was removed *in vacuo*. The crude product was then purified by FCC using the indicated eluent.

General procedure C – amide coupling (III) with EDC·HCl and 4-DMAP. To a stirred solution of the appropriate carboxylic acid (2.0 equivalents) in DMF with a concentration of 0.40 M were added EDC·HCl (2.0 equivalents) and 4-DMAP (2.0 equivalents). The reaction mixture was stirred at room temperature for 15 minutes. Afterwards, the appropriate amine (1.0 equivalent) was added and the solution was stirred at the stated temperature for the stated time. The solution was then diluted with EtOAc and the organic phase was washed with brine (3×). The organic phase was dried using a phase separation paper and the solvent was removed *in vacuo*. The crude product was then purified by FCC using the indicated eluent.

General procedure D – Williamson ether synthesis. To a stirred solution of the appropriate phenol (1.0 equivalent) in DMF with a concentration of 0.10 M was added K_2CO_3 (3.0 equivalents). The reaction mixture was stirred at room temperature for 30 minutes. Afterwards, the appropriate alkyl halide (1.2 equivalents) was added and the mixture was stirred at room temperature for 16 h. The solution was then diluted with EtOAc and the organic phase was washed with brine (3×). The organic phase was dried using a phase separation paper and the solvent was removed *in vacuo*. The crude product was then purified by the stated procedure.

General procedure E – nitrobenzene reduction. To a stirred solution of the appropriate nitrobenzene derivative (1.0 equivalent) in EtOH with a concentration of 0.010 M were added iron powder (5.0 equivalents) and 0.30 M aq. NH_4Cl (5.0 equivalents) at 50 °C. The reaction mixture was then refluxed at 90 °C for 2 h. Afterwards, the iron powder was filtered off from the still hot mixture, and the filtrate was concentrated *in vacuo*. Unless stated otherwise, the crude product was used for the next step without further purification.

***N*-(4-Hydroxyphenyl)-1-methyl-1*H*-pyrazole-4-carboxamide (3).** Prepared according to General procedure A from 1-methyl-1*H*-pyrazole-4-carboxylic acid (500 mg, 3.96 mmol) and aminophenol **1** (433 mg, 3.96 mmol). The crude product was purified by FCC (DCM/MeOH 96 : 4) to give **3** (179 mg, 3.96 mmol, 21%) as a white solid; m.p. 225 °C; IR (ATR) $\tilde{\nu}$/cm^{-1} 3347, 3020, 1641, 1602, 1558, 1530, 1510, 1430, 1351, 1202, 1099, 1006, 860, 813, 749; δ_H (400 MHz; $(CD_3)_2SO$) 9.57 (s, 1H, CONH), 9.18 (s, 1H, OH), 8.24 (s, 1H, 5-H), 7.96 (s, 1H, 3-H), 7.47–7.41 (m, 2H, 2′-H and 6′-H), 6.74–6.68 (m, 2H, 3′-H and 5′-H), 3.87 (s, 3H, CH_3). δ_C (101 MHz; $(CD_3)_2SO$) 160.00 (CONH), 153.40 (C-4′), 138.62 (C-3), 132.34 (C-5), 130.63 (C-1′), 121.92 (C-2′ and C-6′), 118.72 (C-4), 114.96 (C-3′ and C-5′), 38.79 (CH_3); HRMS (ESI): calcd.: 218.0924; found: {*m*/*z*: $[M + H]^+$ 218.0928}.

***N*-(3-Bromo-4-hydroxyphenyl)-1-methyl-1*H*-pyrazole-4-carboxamide (4).** Prepared according to General procedure A from 1-methyl-1*H*-pyrazole-4-carboxylic acid (500 mg, 3.96 mmol) and aminophenol **2** (761 mg, 3.96 mmol). The crude product was purified by FCC (DCM/MeOH 98 : 2) to give amide **4** (649 mg, 2.19 mmol, 55%) as a light pink solid; m.p. 218 °C; IR (ATR) $\tilde{\nu}$/cm^{-1} 3108, 1637, 1596, 1558, 1410, 1268, 1227, 1197, 1008, 852, 801, 753, 657; δ_H (400 MHz; $(CD_3)_2SO$) 9.98 (s, 1H, OH), 9.69 (s, 1H, CONH), 8.25 (s, 1H, 5-H), 7.96 (s, 1H, 3-H), 7.89 (d, J = 2.5 Hz, 1H, 2′-H), 7.45 (dd, J = 8.8, 2.5 Hz, 1H, 6′-H), 6.90 (d, 1H, 5′-H), 3.88 (s, 3H, CH_3). δ_C (101 MHz; $(CD_3)_2SO$) 160.14 (CONH), 150.02 (C-4′), 138.65 (C-3), 132.50 (C-5), 131.83 (C-1′), 124.45 (C-2′), 120.73 (C-6′), 118.37 (C-4), 116.01 (C-5′), 108.52 (C-3′), 38.83 (CH_3); HRMS (ESI): calcd.: 296.0029; found: {*m*/*z*: $[M + H]^+$ 296.0033}.

1-Methyl-*N*-(4-((3-nitrobenzyl)oxy)phenyl)-1*H*-pyrazole-4-carboxamide (5). Prepared according to General procedure D from phenol **3** (165 mg, 0.760 mmol) and 1-(bromomethyl)-3-nitrobenzene (197 mg, 0.911 mmol). The crude product was purified by FCC (DCM/MeOH 95 : 5) to give ether **5** (221 mg, 0.626 mmol, 82%) as a yellow solid. Analytical data are in alignment with literature.[23]

***N*-(3-Bromo-4-((3-nitrobenzyl)oxy)phenyl)-1-methyl-1*H*-pyrazole-4-carboxamide (6).** Prepared according to General procedure D from phenol **4** (3.10 g, 10.5 mmol) and 1-(bromomethyl)-3-nitrobenzene (2.71 g, 12.6 mmol). The crude product was resuspended in hexanes, vacuum filtered, and the residue washed sequentially with hexanes (2×), EtOAc (2×) and DCM (1×). The filtrate was discarded and the solid residue collected to give ether **6** (4.52 g, 10.5 mmol, quant.) as a beige solid; m.p. 226 °C; IR (ATR) $\tilde{\nu}$/cm^{-1} 3394, 3114, 1649, 1593, 1550, 1520, 1499, 1397, 1357, 1275, 1229, 1057, 1001, 881, 853, 790, 728.; δ_H (400 MHz; $(CD_3)_2SO$) 9.82 (s, 1H, CONH), 8.38–8.36 (m, 1H, 2″-H), 8.27 (s, 1H, 5-H), 8.22–8.19 (m, 1H, 4″-H), 8.04 (d, J = 2.5 Hz, 1H, 2′-H), 8.00–7.97 (m, 1H, 3-H), 7.96–7.91 (m, 1H, 6″-H), 7.73 (t, J = 7.9 Hz, 1H, 5″-H), 7.65 (dd, J = 8.9, 2.6 Hz, 1H, 6′-H), 7.22 (d, J = 9.0 Hz, 1H, 5′-H), 5.34 (s, 2H, CH_2), 3.89 (s, 3H, CH_3). δ_C (101 MHz; $(CD_3)_2SO$) 160.31 (CONH), 149.96 (C-4′), 147.86 (C-3″), 139.16 (C-1″), 138.71 (C-3), 133.87 (C-1′), 133.74 (C-6″), 132.63 (C-5), 130.10 (C-5″), 124.42 (C-2′), 122.78 (C-4″), 121.78 (C-2″), 120.29 (C-6′), 118.20 (C-4), 114.43 (C-5′), 110.77 (C-3′), 69.05 (CH_2), 38.85 (CH_3); HRMS (ESI): calcd.: 431.0349; found: {*m*/*z*: $[M + H]^+$ 431.0355}.

1-Methyl-*N*-(4-((3-nitrobenzyl)oxy)-3-(4,4,5,5-tetramethyl-1,3,2-dioxaborolan-2-yl)phenyl)-1*H*-pyrazole-4-carboxamide (7). $PdCl_2$(dppf)·DCM (93.3 mg, 0.128 mmol), bis(pinacolato) diboron (648 mg, 2.55 mmol), bromo derivative **6** (550 mg, 1.28 mmol) and KOAc (501 mg, 5.10 mmol) were dissolved in degassed 1,4-dioxane (40 mL) under N_2 atmosphere and stirred at 95 °C for 19 h. The reaction mixture was cooled to room temperature and then filtered. The filtrate was then diluted with EtOAc (50 mL). Water (50 mL) was added, the resulting two phases were separated, and the aqueous phase was extracted with EtOAc (3 × 60 mL). The combined organic phases were then dried using a phase separation paper and concentrated *in vacuo.* The crude product was purified by FCC (hexanes/EtOAc 20 : 80) to give boronic acid pinacol ester **7** (277 mg, 0.579 mmol, 45%) as a yellow solid; m.p. 254 °C; IR (ATR) $\tilde{\nu}$/cm^{-1} 3339, 2982, 1640, 1557, 1530, 1495, 1344, 1318, 1239, 1140, 1068, 1008, 812, 731; δ_H (400 MHz; $(CD_3)_2SO$) 9.75 (s, 1H, CONH), 8.55 (s, 1H, 2″-H), 8.28 (s, 1H, 5-H), 8.21–8.16 (m, 1H, 4″-H), 8.03–7.99 (m, 2H, 3-H and 6″-H), 7.97 (dd, J = 9.0, 2.7 Hz, 1H, 6′-H), 7.83 (d, J = 2.8 Hz, 1H, 2′-H), 7.71 (t, J = 8.0 Hz, 1H, 5″-H), 7.09 (d, J = 9.0 Hz, 1H, 5′-H), 5.25 (s, 2H, CH_2), 3.89 (s, 3H, NCH_3), 1.33 (s, 12H, $(CH_3)_4$). δ_C (101 MHz; $(CD_3)_2SO$) 160.14 (CONH), 158.47 (C-4′), 147.97 (C-3″), 140.25 (C-1″), 138.72 (C-3), 133.04 (C-6″), 132.48 (C-5 and C-1′), 129.59 (C-5″), 128.41 (C-2′), 124.72 (C-6′), 122.23 (C-4″), 120.94 (C-2″), 118.52 (C-4), 117.15 (C-3′), 112.48 (C-5′), 83.30 ($(C(CH_3)_2)_2$), 68.07 (CH_2), 38.83 (NCH_3), 24.63 ($(CH_3)_4$); HRMS (ESI): calcd.: 479.2096; found: {m/z: $[M + H]^+$ 479.2114}.

(5-(1-Methyl-1*H*-pyrazole-4-carboxamido)-2-((3-nitrobenzyl)oxy)phenyl)boronic acid (8). To a stirred solution of boronic acid pinacol ester **7** (80.0 mg, 0.167 mmol) in acetone (20 mL) were added sodium periodate (107 mg, 0.502 mmol), ammonium acetate (38.7 mg, 0.502 mmol) and water (7 mL). The reaction mixture was stirred vigorously at room temperature for 2 h. Afterwards, acetone was removed *in vacuo* and the reaction mixture was diluted with DCM (20 mL). Water (25 mL) was added, the resulting two phases were separated, and the aqueous phase was extracted with DCM (3 × 25 mL). The combined organic phases were then dried with Na_2SO_4 and then concentrated *in vacuo.* The crude product was then purified by FCC (DCM/MeOH 97 : 3) to give boronic acid **8** (30.0 mg, 75.7 μmol, 45%) as an off-white solid; m.p. 190 °C (decomposition); IR (ATR) $\tilde{\nu}$/cm^{-1} 3292, 2919, 1638, 1557, 1528, 1492, 1417, 1351, 1316, 1227, 1157, 1008, 861, 808, 759, 733, 673; δ_H (400 MHz; $(CD_3)_2SO$) 9.68 (s, 1H, CONH), 8.40–8.38 (m, 1H, 2′-H), 8.27 (s, 1H, 5″-H), 8.21–8.17 (m, 1H, 4′-H), 7.99 (s, 1H, 3″-H), 7.95 (d, J = 7.4 Hz, 1H, 6′-H), 7.86 (s, 2H, $B(OH)_2$), 7.81–7.76 (m, 1H, 4-H), 7.74–7.70 (m, 2H, 6-H and 5′-H), 7.01 (d, J = 8.9 Hz, 1H, 3-H), 5.30 (s, 2H, CH_2), 3.88 (s, 3H, CH_3). δ_C (101 MHz; $(CD_3)_2SO$) 160.11 (CONH), 157.64 (C-2), 147.88 (C-3′), 139.80 (C-1′), 138.70 (C-3″), 133.96 (C-6′), 132.44 (C-5 and C-5″), 129.99 (C-5′), 127.17 (C-6), 123.02 (C-4), 122.65 (C-4′), 122.04 (C-2′), 118.59 (C-4″), 111.88 (C-3), 68.30 (CH_2), 38.81 (CH_3); HRMS (ESI): calcd.: 419.1133; found: {m/z: $[M + Na]^+$ 419.1140}.

***N*-(3-Cyano-4-((3-nitrobenzyl)oxy)phenyl)-1-methyl-1*H*-pyrazole-4-carboxamide (9).** Bromo derivative **6** (200 mg, 0.464 mmol), $Pd(PPh_3)_4$ (53.6 mg, 46.4 μmol) and $Zn(CN)_2$ (32.7 mg, 0.278 mmol) were dissolved in dry DMF (1 mL) under N_2 atmosphere and stirred at 150 °C for 22 h. The reaction mixture was cooled to room temperature and then diluted with EtOAc (25 mL). The organic phase was washed with brine (4 × 30 mL) and then dried with Na_2SO_4 and concentrated *in vacuo.* The crude product was purified by FCC (DCM/MeOH 98 : 2) to give nitrile **9** (11.6 mg, 30.7 μmol, 7%) as a beige solid; m.p. 251 °C; IR (ATR) $\tilde{\nu}$/cm^{-1} 3397, 2226, 1668, 1593, 1553, 1528, 1510, 1351, 1319, 1287, 1247, 1207, 1011, 870, 861, 814, 748, 731; δ_H (400 MHz; $(CD_3)_2SO$) 9.97 (s, 1H, CONH), 8.37 (s, 1H, 2″-H), 8.29 (s, 1H, 5-H), 8.23 (d, J = 8.3 Hz, 1H, 4″-H), 8.08 (s, 1H, 2′-H), 7.99 (s, 1H, 3-H), 7.95–7.88 (m, 2H, 6′-H and 6″-H), 7.75 (t, J = 7.9 Hz, 1H, 5″-H), 7.37 (d, J = 9.2 Hz, 1H, 5′-H), 5.43 (s, 2H, CH_2), 3.89 (s, 3H, CH_3). δ_C (101 MHz; $(CD_3)_2SO$) 160.50 (CONH), 155.32 (C-4′), 147.89 (C-3″), 138.75 (C-3), 138.51 (C-1″), 133.96 (C-6″), 133.11 (C-1′), 132.75 (C-5), 130.24 (C-5″), 126.68 (C-6′), 124.31 (C-2′), 123.04 (C-4″), 122.06 (C-2″), 117.98 (C-4), 116.15 (CN), 114.17 (C-5′), 100.54 (C-3′), 69.01 (CH_2), 38.87 (CH_3); HRMS (ESI): calcd.: 378.1197; found: {m/z: $[M + H]^+$ 378.1195}.

***N*-(4-((3-(2-((4,6-Dimethylpyrimidin-2-yl)thio)acetamido)-benzyl)oxy)phenyl)-1-methyl-1*H*-pyrazole-4-carboxamide (10).** Prepared according to literature.[23]

***N*-(3-Bromo-4-((3-(2-((4,6-dimethylpyrimidin-2-yl)thio)-acetamido)benzyl)oxy)phenyl)-1-methyl-1*H*-pyrazole-4-carboxamide (11).** Prepared according to General procedure E from nitrobenzene **6** (1.00 g, 2.32 mmol). The obtained crude amine was reacted with 2-((4,6-dimethylpyrimidin-2-yl)thio)acetic acid (924 mg, 4.66 mmol) according to General procedure C. The reaction mixture was stirred at room temperature for 4 days. The crude product was purified by FCC (DCM/MeOH 98 : 2) to give **11** (610 mg, 1.05 mmol, 45% over two steps) as a pale-yellow solid; m.p. 96 °C; IR (ATR) $\tilde{\nu}$/cm^{-1} 3284, 1646, 1582, 1551, 1526, 1490, 1441, 1339, 1264, 1223, 1048, 1005, 873, 755, 690; δ_H (400 MHz; $(CD_3)_2SO$) 10.29 (s, 1H, 3″-NHCO), 9.79 (s, 1H, 4-CONH), 8.27 (s, 1H, 5-H), 8.02 (d, J = 2.5 Hz, 1H, 2′-H), 7.98 (s, 1H, 3-H), 7.69 (t, J = 1.9 Hz, 1H, 2″-H), 7.60 (dd, J = 9.0, 2.5 Hz, 1H, 6′-H), 7.57–7.53 (m, 1H, 4″-H), 7.34 (t, J = 7.8 Hz, 1H, 5″-H), 7.18–7.17 (m, 1H, 5′-H or 6″-H), 7.16–7.14 (m, 1H, 5′-H or 6″-H), 6.96 (s, 1H, 5‴-H), 5.15 (s, 2H, OCH_2), 4.04 (s, 2H, SCH_2), 3.89 (s, 3H, NCH_3), 2.32 (s, 6H, 4‴-CH_3 and 6‴-CH_3). δ_C (101 MHz; $(CD_3)_2SO$) 169.32 (C-2‴), 166.95 (C-4‴ and C-6‴), 166.62 (3″-NHCO), 160.27 (4-CONH), 150.34 (C-4′), 139.19 (C-3″), 138.71 (C-3), 137.39 (C-1″), 133.53 (C-1′), 132.61 (C-5), 128.89 (C-5″), 124.41 (C-2′), 122.26 (C-6″), 120.22 (C-6′), 118.65 (C-4″), 118.24 (C-4), 117.95 (C-2″), 116.05 (C-5″), 114.29 (C-5′), 110.68 (C-3′), 70.27 (OCH_2), 38.84 (NCH_3), 35.47 (SCH_2), 23.33 (4″-CH_3 and 6″-CH_3); HRMS (ESI): calcd.: 581.0965; found: {m/z: $[M + H]^+$ 581.0973}; purity (HPLC): 210 nm: >95%; 254 nm: >95% (method 1a).

***N*-(4-((3-(2-((4,6-Dimethylpyrimidin-2-yl)thio)acetamido)-benzyl)oxy)-3-formylphenyl)-1-methyl-1*H*-pyrazole-4-carboxamide (12).** Bromoarene **11** (250 mg, 0.430 mmol), $Pd(OAc)_2$ (2.90 mg, 12.9 μmol, 3 mol%), dppb (8.25 mg, 19.3 μmol, 4.5 mol%), *N*-formylsaccharin (287 mg, 1.29 mmol) and Na_2CO_3 (137 mg, 1.29 mmol) were added to a 30 mL glass tube, which was then evacuated and backfilled three times with N_2. A degassed solution of Et_3SiH (90.3 μL, 0.560 mmol) in DMF (1 mL) was added to the glass tube under N_2 atmosphere. The mixture was stirred for 15 min at room temperature and subsequently warmed to 75 °C and stirred for another 19 h. The reaction mixture was cooled to room temperature, then diluted with EtOAc (15 mL) and washed with brine (3 × 15 mL). The organic phase was dried with a phase separation paper and concentrated *in vacuo*. The crude product was redissolved in MeOH (5 mL), sat. aq. $NaHSO_3$ (25 mL) was added, stirred for approximately 30 s, diluted with H_2O (25 mL), and then extracted with EtOAc (3 × 25 mL). The collected aqueous phase was basified with 50% NaOH (10 mL) and extracted with DCM (3 × 25 mL). The combined organic layers were dried with Na_2SO_4 and concentrated *in vacuo*. The obtained crude residue was purified by FCC (DCM/MeOH 98 : 2) to give **13** (7.0 mg, 13 μmol, 3%) as an off-white solid; m.p. 92 °C; IR (ATR) $\tilde{\nu}$/cm^{-1} 3284, 2921, 2852, 1667, 1582, 1553, 1532, 1442, 1308, 1264, 1223, 1168, 1005, 873, 755, 690; δ_H (400 MHz; $(CD_3)_2SO$) 10.48 (s, 1H, CHO), 9.59 (s, 1H, 3″-NHCO), 7.97 (dd, *J* = 9.0, 2.9 Hz, 1H, 6′-H), 7.90 (s, 1H, 5-H), 7.83–7.80 (m, 2H, 3-H and 2′-H), 7.63 (t, 1H, 2″-H), 7.59 (s, 1H, 4-CONH), 7.38 (dt, 1H, 4″-H), 7.33 (t, *J* = 7.7 Hz, 1H, 5″-H), 7.17 (dt, *J* = 7.5 Hz, 1H, 6″-H), 7.05 (d, *J* = 9.0 Hz, 1H, 5′-H), 6.85 (s, 1H, 5‴-H), 5.18 (s, 2H, OCH_2), 3.92 (s, 3H, NCH_3), 3.85 (s, 2H, SCH_2), 2.46 (s, 6H, 4‴-CH_3 and 6‴-CH_3). δ_C (101 MHz; $(CD_3)_2SO$) 189.29 (CHO), 170.40 (C-2‴), 168.40 (3″-NHCO), 168.11 (C-4‴ and C-6‴), 160.89 (4-CONH), 157.95 (C-4′), 139.17 (C-3″), 138.30 (C-3), 137.70 (C-1″), 132.25 (C-1′ or C-3′), 132.23 (C-5), 129.66 (C-5″), 128.70 (C-6′), 125.49 (C-1′ or C-3′), 123.13 (C-6″), 119.83 (C-2′), 119.61 (C-4″), 119.04 (C-4), 118.68 (C-2″), 117.09 (C-5‴), 114.35 (C-5′), 70.98 (OCH_2), 39.71 (NCH_3), 35.90 (SCH_2), 24.09 (4‴-CH_3 and 6‴-CH_3).; HRMS (ESI): calcd.: 529.1658; found: {*m*/*z*: $[M-H]^-$ 529.1665}; purity (HPLC): 210 nm: >95%; 254 nm: >95% (method 1a).

(2-((3-(2-((4,6-Dimethylpyrimidin-2-yl)thio)acetamido)-benzyl)oxy)-5-(1-methyl-1*H*-pyrazole-4-carboxamido)phenyl)-boronic acid (13). Prepared according to General procedure E from nitrobenzene **8** (15.0 mg, 37.9 μmol). The obtained crude amine was reacted with 2-((4,6-dimethylpyrimidin-2-yl) thio)acetic acid (15.2 mg, 76.5 μmol) according to General procedure B. The crude product was purified by FCC (DCM/MeOH 96 : 4) to give **13** (13.0 mg, 23.8 μmol, 62% over two steps) as a white solid; m.p. 193 °C; IR (ATR) $\tilde{\nu}$/cm^{-1} 3435, 3325, 1683, 1625, 1581, 1550, 1530, 1495, 1443, 1374, 1322, 1265, 1225, 1166, 1043, 1017, 885, 815, 750; δ_H (400 MHz; $(CD_3)_2SO$) 10.30 (s, 1H, 3″-NHCO), 9.69 (s, 1H, 4′-CONH), 8.27 (s, 1H, 5′-H), 7.99 (s, 1H, 3′-H), 7.83–7.76 (m, 2H, 4-H and 6-H), 7.74 (s, 2H, $B(OH)_2$), 7.67 (s, 1H, 2″-H), 7.55 (d, *J* = 8.1 Hz, 1H, 4″-H), 7.34 (t, *J* = 7.8 Hz, 1H, 5″-H), 7.18 (d, *J* = 7.6 Hz, 1H, 6″-H), 7.01 (d, *J* = 8.9 Hz, 1H, 3-H), 6.95 (s, 1H, 5‴-H), 5.13 (s, 2H, OCH_2), 4.04 (s, 2H, SCH_2), 3.88 (s, 3H, NCH_3), 2.32 (s, 6H, 4‴-CH_3 and 6‴-CH_3). δ_C (101 MHz; $(CD_3)_2SO$) 169.31 (C-2‴), 166.96 (C-4‴ and C-6‴), 166.62 (3″-NHCO), 160.12 (4′-CONH), 158.53 (C-2), 139.23 (C-3‴), 138.71 (C-3′), 137.76 (C-1″), 132.44 (C-5), 132.33 (C-5′), 129.01 (C-5″), 127.56 (C-4 or C-6), 123.46 (C-4 or C-6), 122.53 (C-6″), 121.82 (C-1), 118.68 (C-4′), 118.61 (C-4″), 118.13 (C-2″), 116.06 (C-5‴), 111.89 (C-5″), 69.79 (OCH_2), 38.82 (NCH_3), 35.47 (SCH_2), 23.33 (4‴-CH_3 and 6‴-CH_3); HRMS (ESI): calcd.: 545.1784; found: {*m*/*z*: $[M-H]^-$ 545.1788}; purity (HPLC): 210 nm: 92%; 254 nm: >95% (method 1a).

***N*-(3-Cyano-4-((3-(2-((4,6-dimethylpyrimidin-2-yl)thio)-acetamido)benzyl)oxy)phenyl)-1-methyl-1*H*-pyrazole-4-carboxamide (14).** Prepared according to General procedure E from nitrobenzene **9** (90.0 mg, 0.238 mmol). The obtained crude amine was reacted with 2-((4,6-dimethylpyrimidin-2-yl) thio)acetic acid (100 mg, 0.507 mmol) according to General procedure B. The crude product was purified by FCC (DCM/MeOH 96 : 4) to give **14** (82.5 mg, 0.156 mmol, 62% over two steps) as a yellow solid; m.p. 165 °C; IR (ATR) $\tilde{\nu}$/cm^{-1} 3353, 2227, 1661, 1587, 1555, 1535, 1503, 1446, 1410, 1263, 1232, 1004, 860, 817, 752, 688; δ_H (400 MHz; $(CD_3)_2SO$) 10.31 (s, 1H, 3″-NHCO), 9.94 (s, 1H, 4-CONH), 8.29 (s, 1H, 5-H), 8.07 (s, 1H, 2′-H), 7.99 (s, 1H, 3-H), 7.85 (d, *J* = 9.1 Hz, 1H, 6′-H), 7.67 (s, 1H, 2″-H), 7.57 (d, *J* = 8.1 Hz, 1H, 4″-H), 7.39–7.33 (m, 1H, 5″-H), 7.33–7.28 (m, 1H, 5′-H), 7.17 (d, *J* = 7.6 Hz, 1H, 6″-H), 6.94 (s, 1H, 5‴-H), 5.25 (s, 2H, OCH_2), 4.04 (s, 2H, SCH_2), 3.89 (s, 3H, NCH_3), 2.31 (s, 6H, 4‴-CH_3 and 6‴-CH_3). δ_C (101 MHz; $(CD_3)_2SO$) 169.31 (C-2‴), 166.95 (C-4‴ and C-6‴), 166.66 (3″-NHCO), 160.47 (4-CONH), 155.68 (C-4′), 139.28 (C-3″), 138.74 (C-3), 136.78 (C-1″), 132.78 (C-1′), 132.72 (C-5), 129.03 (C-5″), 126.61 (C-6′), 124.30 (C-2′), 122.43 (C-6″), 118.87 (C-4″), 118.02 (C-2′), 116.28 (CN), 116.04 (C-5‴), 114.08 (C-5′), 100.36 (C-3′), 70.20 (OCH_2), 38.86 (NCH_3), 35.48 (SCH_2), 23.32 (4‴-CH_3 and 6‴-CH_3); HRMS (ESI): calcd.: 550.1637; found: {*m*/*z*: $[M + Na]^+$ 550.1633}; purity (HPLC): 210 nm: >95%; 254 nm: >95% (method 1a).

4-Amino-3-bromophenol (18). Prepared according to General procedure E from nitroarene **15** (5.00 g, 22.9 mmol). The crude product was purified by FCC (DCM/MeOH 97 : 3) to give 4-amino-3-bromophenol (**18**) (3.85 g, 20.5 mmol, 89%) as a light pink solid. Analytical data are in alignment with literature.[51]

4-Amino-3-iodophenol (19). Prepared according to General procedure E from nitroarene **16** (1.00 g, 3.66 mmol). The crude product was purified by FCC (DCM/MeOH 97 : 3) to give aniline **19** (738 mg, 3.14 mmol, 86%) as a grey-white solid. Analytical data are in alignment with literature.[51]

2-Chloro-4-((3-nitrobenzyl)oxy)aniline (20). To a stirred solution of phenol **17** (500 mg, 3.41 mmol) in DMF (25 mL) was added K_2CO_3 (1.42 g, 10.2 mmol) and the reaction mixture was stirred for 30 minutes. 1-(Bromomethyl)-3-nitrobenzene (885 mg, 4.10 mmol) was then added and the reaction mixture was stirred at 0 °C for another 5 h. The

reaction mixture was diluted with EtOAc and washed with brine (3 × 200 mL). The organic phase was dried using a phase separation paper and concentrated *in vacuo*. The crude product was purified by FCC (DCM) to give ether **20** (475 mg, 1.70 mmol, 50%) as an orange solid; m.p. 102 °C; IR (ATR) $\tilde{\nu}$/cm^{-1} 3443, 3361, 3090, 2866, 1607, 1572, 1527, 1500, 1480, 1467, 1387, 1350, 1231, 1093, 1041, 901, 887, 823, 808, 796, 732; δ_H (400 MHz; $(CD_3)_2SO$) 8.27 (dt, J = 2.3, 0.6 Hz, 1H; 2′-H), 8.18 (ddd, J = 8.2, 2.4, 1.0 Hz, 1H, 4′-H), 7.87 (ddd, J = 7.7, 1.7, 1.0 Hz, 1H, 6′-H), 7.69 (t, J = 7.9 Hz, 1H, 5′-H), 6.97 (d, J = 2.7 Hz, 1H, 3-H), 6.81 (dd, J = 8.8, 2.8 Hz, 1H, 5-H), 6.75 (d, J = 8.8 Hz, 1H, 6-H), 5.15 (d, J = 0.8 Hz, 2H, CH_2), 4.91 (s, 2H, NH_2). δ_C (101 MHz; $(CD_3)_2SO$) 149.24 (C-4), 147.81 (C-3′), 139.75 (C-1′), 139.16 (C-1), 133.99 (C-6′), 130.00 (C-5′), 122.62 (C-4′), 121.88 (C-2′), 117.28 (C-2), 116.21 (C-6), 115.63 (C-3 or C-5), 115.53 (C-3 or C-5), 68.72 (CH_2); HRMS (ESI): calcd.: 279.0531; found: {m/z: $[M + H]^+$ 279.0532}.

2-Bromo-4-((3-nitrobenzyl)oxy)aniline (21). Prepared according to General procedure D from phenol **18** (3.85 g, 20.5 mmol) and 1-(bromomethyl)-3-nitrobenzene (5.31 g, 24.6 mmol). The crude product was purified by FCC (DCM + 0.5% MeOH) to give ether **21** (3.15 g, 9.75 mmol, 48%) as an orange solid; m.p. 84 °C; IR (ATR) $\tilde{\nu}$/cm^{-1} 3417, 3340, 3073, 1707, 1601, 1581, 1525, 1499, 1387, 1343, 1318, 1228, 1094, 1050, 1030, 811, 729, 667; δ_H (400 MHz; $(CD_3)_2SO$) 8.28–8.25 (m, 1H, 2′-H), 8.18 (ddd, J = 8.2, 2.4, 1.0 Hz, 1H, 4′-H), 7.87 (ddd, 1H, 6′-H), 7.69 (t, J = 7.9 Hz, 1H, 5′-H), 7.11 (d, J = 2.8 Hz, 1H, 3-H), 6.85 (dd, J = 8.8, 2.8 Hz, 1H, 5-H), 6.76 (d, J = 8.8 Hz, 1H, 6-H), 5.15 (s, 2H, CH_2), 4.88 (s, 2H, NH_2). δ_C (101 MHz; $(CD_3)_2SO$) 149.41 (C-4), 147.81 (C-3′), 140.34 (C-1), 139.74 (C-1′), 133.99 (C-6′), 130.00 (C-5′), 122.62 (C-4′), 121.88 (C-2′), 118.37 (C-3), 116.30 (C-5 or C-6), 116.10 (C-5 or C-6), 107.43 (C-2), 68.75 (CH_2); HRMS (EI): calcd.: 321.9953; found: {m/z: $[M]^{\cdot+}$ 321.9940}.

2-Iodo-4-((3-nitrobenzyl)oxy)aniline (22). Prepared according to General procedure D from phenol **19** (682 mg, 2.90 mmol) and 1-(bromomethyl)-3-nitrobenzene (752 mg, 3.48 mmol). The crude product was purified by FCC (DCM/hexanes 90 : 10) to give ether **22** (405 mg, 1.09 mmol, 38%) as a brown solid; m.p. 109 °C; IR (ATR) $\tilde{\nu}$/cm^{-1} 3420, 3345, 3050, 2856, 1615, 1599, 1569, 1519, 1493, 1452, 1346, 1317, 1230, 1091, 1043, 930, 869, 802, 729, 665; δ_H (500 MHz; $(CD_3)_2SO$) 8.27 (td, J = 1.7, 0.8 Hz, 1H, 2′-H), 8.18 (ddd, J = 8.3, 2.4, 1.1 Hz, 1H, 4′-H), 7.87 (ddd, J = 7.6, 1.7, 1.0 Hz, 1H, 6′-H), 7.69 (t, J = 7.9 Hz, 1H, 5′-H), 7.28 (d, J = 2.8 Hz, 1H, 3-H), 6.87 (dd, J = 8.8, 2.9 Hz, 1H, 5-H), 6.72 (d, J = 8.8 Hz, 1H, 6-H), 5.13 (s, 2H, CH_2), 4.81 (s, 2H, NH_2). δ_C (126 MHz; $(CD_3)_2SO$) 149.63 (C-4), 147.81 (C-3′), 143.22 (C-1), 139.80 (C-1′), 133.99 (C-6′), 129.99 (C-5′), 124.28 (C-3), 122.61 (C-4′), 121.88 (C-2′), 117.04 (C-5), 114.88 (C-6), 83.11 (C-2), 68.73 (CH_2); HRMS (ESI): calcd.: 370.9887; found: {m/z: $[M + H]^+$ 370.9886}.

***N*-(2-Chloro-4-((3-nitrobenzyl)oxy)phenyl)-1-methyl-1*H*-pyrazole-4-carboxamide (23).** Prepared according to General procedure A from 1-methyl-1*H*-pyrazole-4-carboxylic acid (195 mg, 1.55 mmol) and aniline **20** (440 mg, 1.55 mmol). The reaction mixture was stirred at 65 °C for 3 days. The crude product was purified by recrystallisation from DCM to give amide **23** (363 mg, 0.938 mmol, 61%) as an off-white solid; m.p. 191 °C; IR (ATR) $\tilde{\nu}$/cm^{-1} 3413, 3119, 1671, 1584, 1552, 1527, 1477, 1349, 1279, 1248, 1216, 1093, 1050, 1003, 876, 850, 807, 800, 750, 731, 708; δ_H (400 MHz; $(CD_3)_2SO$) 9.53 (s, 1H, CONH), 8.33 (t, J = 2.0 Hz, 1H, 2″-H), 8.27 (s, 1H, 5-H), 8.21 (ddd, J = 8.2, 2.4, 1.1 Hz, 1H, 4″-H), 7.97 (s, 1H, 3-H), 7.93 (ddd, J = 7.7, 1.7, 1.0 Hz, 1H, 6″-H), 7.72 (t, J = 7.9 Hz, 1H, 5″-H), 7.41 (d, J = 8.8 Hz, 1H, 6′-H), 7.26 (d, J = 2.8 Hz, 1H, 3′-H), 7.06 (dd, J = 8.8, 2.9 Hz, 1H, 5′-H), 5.32 (s, 2H, CH_2), 3.88 (s, 3H, CH_3). δ_C (101 MHz; $(CD_3)_2SO$) 160.71 (CONH), 156.35 (C-4′), 147.87 (C-3″), 139.04 (C-1″), 138.83 (C-3), 134.14 (C-6″), 132.61 (C-5), 130.53 (C-2′), 130.13 (C-5″), 129.70 (C-6′), 128.13 (C-1′), 122.88 (C-4″), 122.11 (C-2″), 117.82 (C-4), 115.47 (C-3′), 114.23 (C-5′), 68.41 (CH_2), 38.83 (CH_3); HRMS (ESI): calcd.: 387.0855; found: {m/z: $[M + H]^+$ 387.0854}.

***N*-(2-Bromo-4-((3-nitrobenzyl)oxy)phenyl)-1-methyl-1*H*-pyrazole-4-carboxamide (24).** Prepared according to General procedure A from 1-methyl-1*H*-pyrazole-4-carboxylic acid (1.23 g, 9.75 mmol) and aniline **21** (3.15 g, 9.75 mmol). The reaction mixture was stirred at 65 °C for 6 days. The crude product was purified by recrystallisation from DCM to give amide **24** (2.97 g, 6.89 mmol, 71%) as a white solid; m.p. 192 °C; IR (ATR) $\tilde{\nu}$/cm^{-1} 3399, 3116, 2992, 1674, 1605, 1587, 1523, 1475, 1410, 1385, 1342, 1279, 1217, 1046, 1028, 852, 811, 749, 732.; δ_H (400 MHz; $(CD_3)_2SO$) 9.52 (s, 1H, CONH), 8.33 (t, J = 2.0 Hz, 1H, 2″-H), 8.26 (s, 1H, 5-H), 8.21 (dt, J = 8.2, 1.6 Hz, 1H, 4″-H), 7.97 (s, 1H, 3-H), 7.93 (d, J = 7.7 Hz, 1H, 6″-H), 7.72 (t, J = 7.9 Hz, 1H, 5″-H), 7.41 (d, J = 2.8 Hz, 1H, 3′-H), 7.38 (d, J = 8.8 Hz, 1H, 6′-H), 7.10 (dd, J = 8.8, 2.8 Hz, 1H, 5′-H), 5.32 (s, 2H, CH_2), 3.88 (s, 3H, CH_3). δ_C (101 MHz; $(CD_3)_2SO$) 160.45 (CONH), 156.24 (C-4′), 147.61 (C-3″), 138.79 (C-1″), 138.55 (C-3), 133.88 (C-6″), 132.31 (C-5), 129.87 (C-6′ or C-5″), 129.70 (C-6′ or C-5″), 129.37 (C-1′), 122.61 (C-4″), 121.84 (C-2″), 121.24 (C-2′), 118.14 (C-3′), 117.62 (C-4), 114.54 (C-5′), 68.16 (CH_2), 38.57 (CH_3); HRMS (ESI): calcd.: 429.0204; found: {m/z: $[M–H]^-$ 429.0203}.

***N*-(2-Iodo-4-((3-nitrobenzyl)oxy)phenyl)-1-methyl-1*H*-pyrazole-4-carboxamide (25).** Prepared according to General procedure A from 1-methyl-1*H*-pyrazole-4-carboxylic acid (122 mg, 0.964 mmol) and aniline **22** (357 mg, 0.964 mmol). The reaction mixture was stirred at 65 °C for 16 h. The crude product was purified by FCC (DCM/MeOH 98 : 2) to give amide **25** (216 mg, 0.452 mmol, 47%) as a brown solid; m.p. 213 °C; IR (ATR) $\tilde{\nu}$/cm^{-1} 3378, 3125, 1657, 1579, 1553, 1520, 1440, 1399, 1347, 1299, 1273, 1218, 1095, 1057, 998, 866, 846, 808, 752, 727, 697; δ_H (500 MHz; $(CD_3)_2SO$) 9.51 (s, 1H, CONH), 8.33 (t, J = 2.0 Hz, 1H, 2″-H), 8.25 (s, 1H, 6-H), 8.21 (ddd, J = 8.3, 2.4, 1.1 Hz, 1H, 4″-H), 7.97 (s, 1H, 4-H), 7.94–7.91 (m, 1H, 6″-H), 7.72 (t, J = 7.9 Hz, 1H, 5″-H), 7.58 (d, J = 2.8 Hz, 1H, 3′-H), 7.28 (d, J = 8.7 Hz, 1H, 6′-H), 7.11 (dd, J = 8.7, 2.8 Hz, 1H, 5′-H), 5.30 (s, 2H, CH_2), 3.89 (s, 3H, CH_3). δ_C (126 MHz; $(CD_3)_2SO$) 160.69 (CONH), 156.46 (C-4′), 147.86 (C-3″), 139.13 (C-1″), 138.78 (C-4), 134.12 (C-6″), 133.10 (C-1′), 132.52 (C-6), 130.12 (C-5″), 129.26 (C-6′), 124.29 (C-3′), 122.84

(C-4″), 122.07 (C-2″), 118.08 (C-5), 115.41 (C-5′), 99.74 (C-2′), 68.33 (CH_2), 38.24 (CH_3); HRMS (ESI): calcd.: 479.0211; found: {*m*/*z*: $[M + H]^+$ 479.0208}.

1-Methyl-*N*-(4-((3-nitrobenzyl)oxy)-2-(4,4,5,5-tetramethyl-1,3,2-dioxaborolan-2-yl)phenyl)-1*H*-pyrazole-4-carboxamide (26). $PdCl_2$(dppf)·DCM (20.4 mg, 27.8 μmol), bis(pinacolato) diboron (141 mg, 0.557 mmol), bromoarene **24** (120 mg, 0.278 mmol), and KOAc (109 mg, 1.11 mmol) were dissolved in degassed 1,4-dioxane (15 mL) under N_2 atmosphere and stirred at 95 °C for 20 h. The reaction mixture was cooled to room temperature and then filtered. The filtrate was diluted with EtOAc (50 mL). Water (50 mL) was added, the resulting two phases were separated, and the aqueous phase was extracted with EtOAc (3 × 60 mL). The combined organic phases were dried using a phase separation paper and concentrated *in vacuo*. The crude product was purified by FCC (hexanes/EtOAc 4 : 96 + 3% MeOH) to give boronic acid pinacol ester **26** (34.5 mg, 72.1 μmol, 26%) as a pale-yellow solid; m.p. 199 °C; IR (ATR) $\tilde{\nu}$/cm^{-1} 2967, 1641, 1606, 1530, 1482, 1349, 1315, 1266, 1157, 1129, 1013, 876, 802, 726; δ_H (400 MHz; $(CD_3)_2SO$) 11.67 (s, 1H, CONH), 8.42 (s, 1H, 5-H), 8.31 (t, *J* = 2.0 Hz, 1H, 2″-H), 8.19 (ddd, *J* = 8.2, 2.4, 1.0 Hz, 1H, 4″-H), 8.13 (s, 1H, 3-H), 7.93–7.90 (m, 1H, 6″-H), 7.70 (t, *J* = 7.9 Hz, 1H, 5″-H), 7.16 (d, 1H, 6′-H), 6.98–6.94 (m, 2H, 5′-H), 5.26 (s, 2H, CH_2), 3.95 (s, 3H, NCH_3), 1.16 (s, 12H, $(CH_3)_4$). δ_C (101 MHz; $(CD_3)_2SO$) 159.77 (CONH), 155.40 (C-4′), 147.83 (C-3″), 139.95 (C-1″), 139.05 (C-3), 133.89 (C-6″), 133.72 (C-5), 132.37 (C-1′), 130.07 (C-5″), 122.58 (C-4″), 121.85 (C-2″), 117.34 (C-3′ and C-6′), 114.48 (C-5′), 113.92 (C-4), 79.44 ($(\mathbf{C}(CH_3)_2)_2$), 67.98 (CH_2), 38.89 (NCH_3), 26.05 ($(CH_3)_4$); HRMS (ESI): calcd.: 479.2096; found: {*m*/*z*: $[M + H]^+$ 479.2092}.

(2-(1-Methyl-1*H*-pyrazole-4-carboxamido)-5-((3-nitrobenzyl)oxy)phenyl)boronic acid (27). To a stirred solution of boronic acid pinacol ester **26** (330 mg, 0.690 mmol) in THF/water 4 : 1 v/v (25 mL) was added sodium periodate (738 mg, 3.45 mmol) and the reaction mixture was stirred vigorously at room temperature for 45 minutes. 1 M HCl (0.828 mmol, 0.828 mL) was then added, and the mixture stirred for 15 h. The milky suspension was diluted with DCM (15 mL), filtered and the residue washed with DCM (1×) and MeOH (1×). The filtrate was discarded and the solid residue collected to give boronic acid **27** (274 mg, 0.692 mmol, quant.) as an off-white solid; m.p. 260 °C (decomposition); IR (ATR) $\tilde{\nu}$/cm^{-1} 3545, 3295, 3107, 2858, 1640, 1602, 1532, 1476, 1346, 1206, 1098, 1015, 882, 805, 739; δ_H (400 MHz; CF_3COOD) 9.00 (s, 1H, 3″-H), 8.65 (s, 1H, 5″-H), 8.46 (s, 1H, 2′-H), 8.34 (d, *J* = 8.8 Hz, 1H, 4′-H), 7.92 (d, *J* = 7.6 Hz, 1H, 6′-H), 7.69 (t, *J* = 8.0 Hz, 1H, 5′-H), 7.38–7.33 (m, 2H, 3-H and 6-H), 7.25 (dd, *J* = 8.7, 2.8 Hz, 1H, 4-H), 5.38 (s, 2H, CH_2), 4.29 (s, 3H, CH_3). δ_C (101 MHz; CF_3COOD) 160.53 (C-5), 159.44 (CONH), 149.88 (C-3′), 140.65 (C-1′), 139.87 (C-3″), 139.00 (C-5″), 136.12 (C-6′), 132.11 (C-2), 131.70 (C-5′), 125.19 (C-4′), 124.13 (C-2′), 120.57 (C-3), 119.89 (C-4), 117.07 (C-6), 114.82 (C-4″), 71.13 (CH_2), 40.45 (CH_3); HRMS (ESI): calcd.: 379.1208; found: {*m*/*z*: $[M–H_2O + H]^+$ 379.1205}.

***N*-(2-Cyano-4-((3-nitrobenzyl)oxy)phenyl)-1-methyl-1*H*-pyrazole-4-carboxamide (28).** To a stirred solution of bromoarene **24** (350 mg, 0.812 mmol) in dry DMF (4 mL) was added CuCN (147 mg, 1.62 mmol). The reaction mixture was stirred at 150 °C for 22 h. Afterwards, the reaction mixture was concentrated *in vacuo* and the crude residue was resuspended in 20 mL aq. NH_4OH. The resulting suspension was vacuum filtered, and the residue was washed with aq. NH_4OH until the filtrate was no longer blue. The filtrate was discarded, and the filter residue was further washed sequentially with water (3 × 25 mL), DCM (4 × 25 mL), EtOAc (2 × 25 mL) and MeOH (2 × 25 mL). The filter residue was collected to give nitrile **28** (142 mg, 0.376 mmol, 46%) as a brownish-yellow solid; m.p. 197 °C; IR (ATR) $\tilde{\nu}$/cm^{-1} 3293, 3117, 3074, 2922, 2229, 1651, 1615, 1587, 1518, 1483, 1419, 1387, 1348, 1286, 1227, 1161, 1101, 1048, 1003, 977, 886, 875, 823, 730; δ_H (400 MHz; $(CD_3)_2SO$) 10.06 (s, 1H, CONH), 8.34 (t, *J* = 2.0 Hz, 1H, 2″-H), 8.29 (s, 1H, 5-H), 8.24–8.20 (m, 1H, 4″-H), 7.99 (s, 1H, 3-H), 7.95–7.91 (m, 1H, 6″-H), 7.72 (t, *J* = 8.0 Hz, 1H, 5″-H), 7.57 (d, *J* = 2.6 Hz, 1H, 3′-H), 7.44–7.40 (m, 2H, 5′-H and 6′-H), 5.35 (s, 2H, OCH_2), 3.90 (s, 3H, CH_3). δ_C (101 MHz; $(CD_3)_2SO$) 160.77 (CONH), 155.43 (C-4′), 147.88 (C-3″), 138.90 (C-1″), 138.77 (C-3), 134.23 (C-6″), 133.61 (C-1′), 132.86 (C-5), 130.16 (C-5″), 128.68 (C-6′), 122.97 (C-4″), 122.22 (C-2″), 121.10 (C-5′), 117.98 (C-3′), 117.45 (C-4), 116.72 (CN), 110.38 (C-2′), 68.58 (OCH_2), 38.89 (CH_3); HRMS (ESI): calcd.: 376.1046; found: $\{m/z: [M–H]^-$ 376.1053}.

***N*-(2-Chloro-4-((3-(2-((4,6-dimethylpyrimidin-2-yl)thio)-acetamido)benzyl)oxy)phenyl)-1-methyl-1*H*-pyrazole-4-carboxamide (29).** Prepared according to General procedure E from nitroarene **23** (150 mg, 0.388 mmol). The obtained crude amine was reacted with 2-((4,6-dimethylpyrimidin-2-yl) thio)acetic acid (154 mg, 0.779 mmol) according to General procedure C. The reaction mixture was stirred at room temperature for 2 days. The crude product was purified by FCC (DCM/MeOH 98 : 2) to give **29** (145 mg, 0.269 mmol, 69% over two steps) as a pale-yellow solid; m.p. 86 °C; IR (ATR) $\tilde{\nu}$/cm^{-1} 3270, 3081, 1651, 1580, 1552, 1514, 1490, 1440, 1264, 1203, 1045, 1004, 874, 784, 755, 690; δ_H (400 MHz; $(CD_3)_2SO$) 10.29 (s, 1H, 3″-NHCO), 9.51 (s, 1H, 4-CONH), 8.26 (s, 1H, 5-H), 7.97 (s, 1H, 3-H), 7.69 (t, *J* = 1.9 Hz, 1H, 2″-H), 7.54 (ddd, *J* = 8.2, 2.2, 1.1 Hz, 1H, 4″-H), 7.38 (d, *J* = 8.9 Hz, 1H, 6′-H), 7.33 (t, *J* = 7.8 Hz, 1H, 5″-H), 7.18 (d, *J* = 2.8 Hz, 1H, 3′-H), 7.16–7.12 (m, 1H, 6″-H), 6.99 (dd, *J* = 8.8, 2.8 Hz, 1H, 5′-H), 6.96 (s, 1H, 5‴-H), 5.13 (s, 2H, OCH_2), 4.04 (s, 2H, SCH_2), 3.88 (s, 3H, NCH_3), 2.32 (d, *J* = 0.5 Hz, 6H, 4‴-CH_3 and 6‴-CH_3). δ_C (101 MHz; $(CD_3)_2SO$) 169.31 (C-2‴), 166.96 (C-4‴ and C-6‴), 166.63 (3″-NHCO), 160.71 (4-CONH), 156.70 (C-4′), 139.23 (C-3″), 138.82 (C-3), 137.33 (C-1″), 132.59 (C-5), 130.48 (C-2′), 129.64 (C-6′), 128.92 (C-5″), 127.81 (C-1′), 122.48 (C-6″), 118.65 (C-4″), 118.08 (C-2″), 117.85 (C-4), 116.06 (C-5‴), 115.32 (C-3′), 114.18 (C-5′), 69.65 (OCH_2), 38.82 (NCH_3), 35.47 (SCH_2), 23.32 (4‴-CH_3 and 6‴-CH_3); HRMS (ESI): calcd.: 537.1470; found: {*m*/*z*: $[M + H]^+$ 537.1466}; purity (HPLC): 210 nm: >95%; 254 nm: 89% (method 1a).

***N*-(2-Bromo-4-((3-(2-((4,6-dimethylpyrimidin-2-yl)thio)acetamido)benzyl)oxy)phenyl)-1-methyl-1*H*-pyrazole-4-carboxamide (30).** Prepared according to General procedure E from nitroarene **24** (1.36 g, 3.14 mmol). The obtained crude amine was reacted with 2-((4,6-dimethylpyrimidin-2-yl)thio) acetic acid (1.25 g, 6.31 mmol) according to General procedure C. The reaction mixture was stirred at room temperature for 4 days. The crude product was purified by FCC (DCM/MeOH 98 : 2) to give **30** (1.18 g, 2.03 mmol, 64% over two steps) as a yellow solid; m.p. 83 °C; IR (ATR) $\tilde{\nu}$/cm^{-1} 3269, 2923, 1651, 1581, 1553, 1514, 1490, 1441, 1265, 1219, 1203, 1032, 1004, 872, 785, 757, 692; δ_H (500 MHz; $(CD_3)_2SO$) 10.29 (s, 1H, 3″-NHCO), 9.50 (s, 1H, 4-CONH), 8.26 (s, 1H, 5-H), 7.96 (s, 1H, 3-H), 7.68 (t, J = 1.8 Hz, 1H, 2″-H), 7.54 (dt, J = 8.0, 1.7 Hz, 1H, 4″-H), 7.37–7.31 (m, 3H, 3′-H, 6′-H and 5″-H), 7.14 (dt, J = 7.7 Hz, 1H, 6″-H), 7.04 (dd, J = 8.8, 2.8 Hz, 1H, 5′-H), 6.96 (s, 1H, 5‴-H), 5.13 (s, 2H, OCH_2), 4.04 (s, 2H, SCH_2), 3.88 (s, 3H, NCH_3), 2.32 (s, 6H, 4‴-CH_3 and 6‴-CH_3). δ_C (126 MHz; $(CD_3)_2SO$) 169.31 (C-2‴), 166.96 (C-4‴ and C-6‴), 166.63 (3″-NHCO), 160.71 (4-CONH), 156.85 (C-4′), 139.23 (C-3″), 138.81 (C-3), 137.34 (C-1″), 132.57 (C-5), 129.90 (C-6′), 129.31 (C-1′), 128.93 (C-5″), 122.47 (C-6″), 121.47 (C-2′), 118.64 (C-4″), 118.26 (C-3′), 118.06 (C-2″), 117.91 (C-4), 116.06 (C-5‴), 114.73 (C-5′), 69.65 (OCH_2), 38.83 (NCH_3), 35.47 (SCH_2), 23.33 (4‴-CH_3 and 6‴-CH_3); HRMS (ESI): calcd.: 581.0965; found: {m/z: $[M + H]^+$ 581.0967}; purity (HPLC): 210 nm: >95%; 254 nm: >95% (method 1a).

***N*-(4-((3-(2-((4,6-Dimethylpyrimidin-2-yl)thio)acetamido)benzyl)oxy)-2-iodophenyl)-1-methyl-1*H*-pyrazole-4-carboxamide (31).** Prepared according to General procedure E from nitroarene **25** (100 mg, 0.209 mmol). The obtained crude amine was reacted with 2-((4,6-dimethylpyrimidin-2-yl)thio)acetic acid (83.1 mg, 0.419 mmol) according to General procedure C. The reaction mixture was stirred at room temperature for 18 h. The crude product was purified by FCC (DCM/MeOH 98 : 2) to give **31** (83.7 mg, 0.133 mmol, 64% over two steps) as a beige solid; m.p. 107 °C; IR (ATR) $\tilde{\nu}$/cm^{-1} 3269, 2919, 1649, 1581, 1552, 1511, 1487, 1441, 1265, 1205, 1004, 978, 867, 784, 756, 691; δ_H (500 MHz; $(CD_3)_2SO$) 10.29 (s, 1H, 3″-NHCO), 9.49 (s, 1H, 4-CONH), 8.25 (s, 1H, 5-H), 7.97 (s, 1H, 3-H), 7.68 (t, J = 1.9 Hz, 1H, 2″-H), 7.54 (dt, J = 8.3, 1.5 Hz, 1H, 4″-H), 7.51 (d, J = 2.8 Hz, 1H, 3′-H), 7.33 (t, J = 7.8 Hz, 1H, 5″-H), 7.25 (d, J = 8.7 Hz, 1H, 6′-H), 7.13 (d, J = 7.6 Hz, 1H, 6″-H), 7.05 (dd, J = 8.7, 2.9 Hz, 1H, 5′-H), 6.97 (s, 1H, 5‴-H), 5.11 (s, 2H, OCH_2), 4.04 (s, 2H, SCH_2), 3.88 (s, 3H, NCH_3), 2.32 (s, 6H, 4‴-CH_3 and 6‴-CH_3). δ_C (126 MHz; $(CD_3)_2SO$) 169.31 (C-2‴), 166.96 (C-4‴ and C-6‴), 166.62 (3″-NHCO), 160.69 (4-CONH), 156.81 (C-4′), 139.22 (C-3″), 138.78 (C-3), 137.42 (C-1″), 132.78 (C-1′), 132.51 (C-5), 129.20 (C-6′), 128.91 (C-5″), 124.20 (C-3′), 122.44 (C-6″), 118.62 (C-4″), 118.10 (C-4), 118.02 (C-2″), 116.06 (C-5‴), 115.31 (C-5′), 99.71 (C-2′), 69.56 (OCH_2), 38.83 (NCH_3), 35.47 (SCH_2), 23.33 (4‴-CH_3 and 6‴-CH_3); HRMS (ESI): calcd.: 629.0826; found: {m/z: $[M + H]^+$ 629.0822}; purity (HPLC): 210 nm: >95%; 254 nm: >95% (method 1c).

***N*-(4-((3-(2-((4,6-Dimethylpyrimidin-2-yl)thio)acetamido)benzyl)oxy)-2-formylphenyl)-1-methyl-1*H*-pyrazole-4-carboxamide (32).** **30** (150 mg, 0.258 mmol), $Pd(OAc)_2$ (1.74 mg, 7.74 μmol, 3 mol%), dppb (4.95 mg, 11.6 μmol, 4.5 mol%), *N*-formylsaccharin (172 mg, 0.774 mmol), and Na_2CO_3 (82.0 mg, 0.774 mmol) were added to a 30 mL glass tube, which was then evacuated and backfilled three times with N_2. A degassed solution of Et_3SiH (54.2 μL, 0.335 mmol) in DMF (0.6 mL) was added to the glass tube under N_2 atmosphere. The mixture was stirred for 15 min at room temperature and subsequently warmed to 75 °C and stirred for another 19 h. The reaction mixture was cooled to room temperature, then diluted with EtOAc (15 mL) and washed with brine (3 × 15 mL). The organic phase was dried with a phase separation paper and concentrated *in vacuo*. The crude product was redissolved in MeOH (5 mL), sat. aq. $NaHSO_3$ (25 mL) was added, stirred for approximately 30 seconds, diluted with H_2O (25 mL), and then extracted with EtOAc (3 × 25 mL). The aqueous phase was basified with 50% NaOH (10 mL) and extracted with DCM (3 × 25 mL). The combined organic layers were dried with Na_2SO_4 and concentrated *in vacuo*. The obtained crude residue was purified by FCC (DCM/MeOH 98 : 2) to give **32** (3.8 mg, 7.2 μmol, 3%) as a yellow solid; m.p. 87 °C; IR (ATR) $\tilde{\nu}$/cm^{-1} 3232, 2921, 2852, 1727, 1654, 1582, 1553, 1529, 1487, 1435, 1286, 1264, 1220, 1154, 1031, 893, 785, 696; δ_H (500 MHz; $(CD_3)_2SO$) 11.45 (s, 1H, 4-CONH), 9.91 (s, 1H, CHO), 9.58 (s, 1H, 3″-NHCO), 8.76 (d, J = 10.1 Hz, 1H, 6′-H), 7.96 (s, 2H, 3-H and 5-H), 7.63 (t, 1H, 2″-H), 7.38 (dt, J = 8.0, 1.6 Hz, 1H, 4″-H), 7.32 (t, J = 7.8 Hz, 1H, 5″-H), 7.28–7.25 (m, 2H, 3′-H and 5′-H), 7.16 (d, J = 7.4 Hz, 1H, 6″-H), 6.85 (s, 1H, 5‴-H), 5.11 (s, 2H, OCH_2), 3.95 (s, 3H, NCH_3), 3.85 (s, 2H, SCH_2), 2.47 (s, 6H, 4‴-CH_3 and 6‴-CH_3). δ_C (126 MHz; $(CD_3)_2SO$) 195.98 (CHO), 170.43 (C-2‴), 168.31 (3″-NHCO), 168.11 (4‴-CH_3 and 6‴-CH_3), 161.20 (4-CONH), 154.24 (C-4′), 139.16 (C-3″), 139.03 (C-3), 138.00 (C-1″), 135.85 (C-1′), 131.99 (C-5), 129.60 (C-5″), 123.70 (C-5′), 123.20 (C-6″), 122.70 (C-2′), 121.61 (C-6′), 121.03 (C-3′), 119.76 (C-4), 119.46 (C-4″), 118.76 (C-2″), 117.06 (C-5‴), 70.71 (OCH_2), 39.73 (NCH_3), 35.90 (SCH_2), 30.09 (4‴-CH_3 and 6‴-CH_3); HRMS (ESI): calcd.: 553.1633; found: {m/z: $[M + Na]^+$ 553.1633}; purity (HPLC): 210 nm: >95%; 254 nm: >95% (method 1b).

(5-((3-(2-((4,6-Dimethylpyrimidin-2-yl)thio)acetamido)benzyl)oxy)-2-(1-methyl-1*H*-pyrazole-4-carboxamido)phenyl)boronic acid (33). Prepared according to General procedure F from nitroarene **27** (90.0 mg, 0.227 mmol). The obtained crude amine was dissolved in dry DMF (3 mL) and bromoacetyl bromide (23.8 μL, 0.274 mmol) was added. The reaction mixture was stirred at room temperature for 30 minutes. The solution was then diluted with EtOAc (50 mL) and washed with brine (3 × 20 mL). The organic phase was dried using a phase separation paper and concentrated *in vacuo*. The brown oily crude product was redissolved in dry DMF (8 mL), 4,6-dimethylpyrimidine-2-thiol (64.5 mg, 0.46 mmol) and *t*-BuOK (51.6 mg, 0.46 mmol) were added, and the reaction mixture was stirred at room temperature for 19 h. The solution was then diluted with EtOAc (150 mL) and

washed with brine (3 × 100 mL). The organic phase was dried using a phase separation paper and concentrated *in vacuo*. The crude product was purified by FCC (DCM/10% NH_3 in MeOH 88 : 12) to give product **33** (32.1 mg, 58.7 μmol, 26% over three steps) as a pale-yellow solid; m.p. 165 °C; IR (ATR) $\tilde{\nu}$/cm^{-1} 3271, 2922, 2853, 1667, 1633, 1601, 1581, 1553, 1532, 1480, 1441, 1312, 1264, 1205, 1009, 874, 787, 749, 690; δ_H (400 MHz; $(CD_3)_2SO$) 11.78 (s, 1H, 4′-CONH), 10.20 (s, 1H, 3″-NHCO), 8.25 (s, 1H, 5′-H), 7.96 (s, 1H, 3′-H), 7.62 (d, J = 8.3 Hz, 1H, 3-H), 7.58 (s, 1H, 2″-H), 7.53 (d, J = 8.2 Hz, 1H, 4″-H), 7.30 (d, J = 3.0 Hz, 1H, 6-H), 7.21 (t, J = 7.8 Hz, 1H, 5″-H), 7.04 (d, J = 7.6 Hz, 1H, 6″-H), 6.94 (dd, J = 8.9, 3.0 Hz, 1H, 4-H), 6.86 (s, 1H, 5‴-H), 5.00 (s, 2H, OCH_2), 3.98 (s, 2H, SCH_2), 3.71 (s, 3H, NCH_3), 2.28 (s, 6H, 4‴-CH_3 and 6‴-CH_3). δ_C (101 MHz; $(CD_3)_2SO$) 169.29 (C-2‴), 166.90 (C-4‴ and C-6‴), 166.57 (3″-NHCO), 159.32 (4′-CONH), 155.13 (C-5) 139.07 (C-3″), 138.65 (C-3′), 137.98 (C-1″), 133.14 (C-2 and C-5′), 128.68 (C-5″), 122.30 (C-6″), 119.01 (C-6), 118.40 (C-4″), 117.91 (C-2″), 117.72 (C-3), 115.98 (C-4′ and C-5‴), 114.14 (C-4), 69.07 (OCH_2), 38.75 (NCH_3), 35.41 (SCH_2), 23.28 (4‴-CH_3 and 6‴-CH_3); HRMS (ESI): calcd.: 527.1673; found: {m/z: $[M–H_2O–H]^-$ 527.1680}; purity (HPLC): 210 nm: >95%; 254 nm: >95% (method 2a).

***N*-(2-Cyano-4-((3-(2-((4,6-dimethylpyrimidin-2-yl)thio)-acetamido)benzyl)oxy)phenyl)-1-methyl-1*H*-pyrazole-4-carboxamide (34).** Prepared according to General procedure E from nitroarene **28** (130 mg, 0.344 mmol). The obtained crude amine was reacted with 2-((4,6-dimethylpyrimidin-2-yl) thio)acetic acid (103 mg, 0.520 mmol) according to General procedure C. The reaction mixture was stirred at room temperature for 7 days. The crude product was purified by FCC (DCM/10% NH_3 in MeOH 99 : 1) to give **34** (73.4 mg, 0.139 mmol, 40% over two steps) as a yellow solid; m.p. 93 °C; IR (ATR) $\tilde{\nu}$/cm^{-1} 3271, 2922, 2853, 2229, 1652, 1581, 1552, 1490, 1441, 1265, 1226, 1161, 1003, 873, 785, 756, 691; δ_H (500 MHz; $(CD_3)_2SO$) 10.30 (s, 1H, 3″-NHCO), 10.04 (s, 1H, 4-CONH), 8.29 (s, 1H, 5-H), 7.98 (s, 1H, 3-H), 7.70 (t, J = 2.0 Hz, 1H, 2″-H), 7.54 (dt, J = 8.1, 1.9 Hz, 1H, 4″-H), 7.50 (d, J = 2.9 Hz, 1H, 3′-H or 5′-H), 7.41 (d, J = 8.9 Hz, 1H, 6′-H), 7.36–7.35 (m, 1H, 5″-H), 7.34–7.32 (m, 1H, 3′-H or 5′-H), 7.14 (d, J = 7.5 Hz, 1H, 6″-H), 6.96 (s, 1H, 5‴-H), 5.16 (s, 2H, OCH_2), 4.04 (s, 2H, SCH_2), 3.90 (s, 3H, NCH_3), 2.32 (s, 6H, 4‴-CH_3 and 6‴-CH_3). δ_C (126 MHz; $(CD_3)_2SO$) 169.31 (C-2‴), 166.96 (C-4‴ and C-6‴), 166.64 (3″-NHCO), 160.76 (4-CONH), 155.75 (C-4′), 139.25 (C-3″), 138.89 (C-3), 137.08 (C-1″), 133.30 (C-1′), 132.85 (C-5), 128.96 (C-3′ or C-5′), 128.63 (C-6′), 122.59 (C-6″), 121.03 (C-5″), 118.73 (C-4″), 118.17 (C-2″), 117.82 (C-3′ or C-5′), 117.47 (C-4), 116.77 (CN), 116.06 (C-5‴), 110.36 (C-2′), 69.80 (OCH_2), 38.87 (NCH_3), 35.48 (SCH_2), 23.32 (4‴-CH_3 and 6‴-CH_3); HRMS (ESI): calcd.: 528.1812; found: {m/z: $[M + H]^+$ 528.1814}; purity (HPLC): 210 nm: >95%; 254 nm: >95% (method 1a).

8-((2-Aminothiazol-5-yl)methyl)-2-naphthonitrile (39). To a stirred solution of bromo derivative **38** (500 mg, 1.57 mmol) in dry DMF (5 mL) were added zinc cyanide (110 mg, 0.940 mmol) and $Pd(PPh_3)_4$ (181 mg, 0.157 mmol). The reaction mixture was stirred at 80 °C for 18 h under N_2 atmosphere, then was diluted with water (50 mL) and extracted with EtOAc (3 × 100 mL). The combined organic layers were dried over sodium sulfate, the solvent was evaporated *in vacuo* and the crude product was purified by FCC (hexanes/EtOAc/NEt_3 30 : 70 : 1) to give **39** (254 mg, 0.957 mmol, 61%) as a light-yellow solid; m.p. 216 °C; IR (ATR) $\tilde{\nu}$/cm^{-1} 3397, 3283, 3116, 2221, 1629, 1517, 1438, 1377, 1326, 1310, 1270, 1204, 1160, 1120, 1052, 889, 861, 835, 794, 749, 721, 688; δ_H (500 MHz; $(CD_3)_2SO$) 8.75 (d, J = 1.6 Hz 1H, 8-H), 8.13 (d, J = 8.4 Hz, 1H, 5-H), 7.95 (d, J = 8.2 Hz, 1H, 4-H), 7.80 (dd, J = 8.5, 1.5 Hz, 1H, 6-H), 7.67 (dd, J = 8.2, 7.0 Hz, 1H, 3-H), 7.57 (dd, J = 7.2, 1.2 Hz, 1H, 2-H), 6.77 (s, 1H, 4′-H), 6.69 (s, 2H, NH_2), 4.46 (s, 2H, CH_2). δ_C (126 MHz; $(CD_3)_2SO$) 167.80 (C-2′), 137.86 (C-1), 135.88 (C-4′), 134.94 (C-4a), 130.64 (C-8), 130.14 (C-8a), 130.13 (C-5), 129.10 (C-3), 127.99 (C-2), 127.25 (C-4), 126.23 (C-6), 124.03 (C-5′), 119.37 (CN), 108.50 (C-7), 29.46 (CH_2); HRMS (ESI): calcd.: 266.0746; found: {m/z: $[M + H]^+$ 266.0745}.

2-(8-((2-Aminothiazol-5-yl)methyl)naphthalen-2-yl)acetonitrile (40). To a stirred solution of bromoarene **38** (323 mg, 1.01 mmol) in DMF (1.21 mL) was added 4-(4,4,5,5-tetramethyl-1,3,2-dioxaborolan-2-yl)isoxazole (237 mg, 1.22 mmol) and 1 M KF solution (513 μL, 513 μmol). The mixture was degassed in an ultrasonic bath under nitrogen atmosphere. $PdCl_2$(dppf)·DCM (12.5 mg, 0.0171 mmol) was then added under nitrogen counterflow and the reaction mixture was stirred at 90 °C for 20 h. The mixture was allowed to cool to room temperature, diluted with water (50 mL) and brine (50 mL), and extracted with EtOAc (3 × 50 mL). The combined organic layers were dried over sodium sulfate. After evaporating the solvent *in vacuo*, the crude product was purified by FCC (hexanes/EtOAc 50 : 50) to give cyanomethyl derivative **40** (74.4 mg, 0.266 mmol, 26%) as a light brown solid; m.p. 203 °C; IR (ATR) $\tilde{\nu}$/cm^{-1} 3463, 3112, 1613, 1519, 1403, 1354, 1301, 1195, 1035, 930, 844, 825, 794, 770, 754, 673; δ_H (400 MHz; $(CD_3)_2SO$) 8.14 (d, J = 1.6 Hz, 1H, 8-H), 7.98 (d, J = 8.4 Hz, 1H, 5-H), 7.84 (dd, J = 8.1,1.6 Hz 1H, 4-H), 7.52–7.41 (m, 3H, 2-H, 3-H, 6-H), 6.77 (s, 1H, 4′-H), 6.66 (s, 2H, NH_2), 4.37 (s, 2H, CH_2), 4.23 (s, 2H, CH_2CN). δ_C (101 MHz; $(CD_3)_2SO$) 167.69 (C-2′), 136.37 (C-1), 135.67 (C-4′), 132.58 (C-4a), 131.01 (C-8a), 129.46 (C-5), 128.98 (C-7), 126.95 (C-4), 126.89 (C-2), 125.99 (C-3), 135.87 (C-6), 124.19 (C-5′), 122.85 (C-8), 119.21 (CN), 29.74 (CH_2), 22.89 (CH_2CN); HRMS (ESI): calcd.: 280.0903; found: {m/z: $[M + H]^+$ 280.0902}.

***tert*-Butyl (5-((7-bromonaphthalen-1-yl)methyl)thiazol-2-yl) carbamate (41).** To a stirred solution of aminothiazole **38** (0.738 g, 2.31 mmol) in toluene (75 mL) was added di-*tert*-butyl dicarbonate (1.98 mL, 9.24 mmol) dropwise at room temperature. The reaction mixture was stirred at 100 °C for 4.5 h and then the solvent was evaporated *in vacuo*. The crude product was purified by FCC (hexanes/EtOAc 80 : 20) to give **41** (828 mg, 1.98 mmol, 85%) as a beige solid; m.p. 296 °C; IR (ATR) $\tilde{\nu}$/cm^{-1} 2726, 1710, 1579, 1546, 1495, 1447, 1391, 1368, 1321, 1297, 1251, 1236, 1080, 1056, 1028, 880, 860, 844, 825, 809, 763, 750, 683; δ_H (400 MHz; $(CD_3)_2SO$) 11.25 (s, 1H, NHCO), 8.32 (d, J = 2.0 Hz, 1H, 8-H), 7.93 (d, J = 8.8 Hz, 1H,

5-H), 7.87 (m, 1H, 4-H), 7.65 (dd, J = 8.8, 1.9 Hz, 1H, 6-H), 7.56–7.48 (m, 2H, 2-H, 3-H), 7.19 (s, 1H, 4′-H), 4.52 (s, 2H, CH_2), 1.41 (s, 9H, $C(CH_3)_3$). δ_C (126 MHz; $(CD_3)_2SO$) 158.38 (C-2′), 152.70 (NHCO), 135.65 (C-1), 134.90 (C-4′), 132.28 (C-8a), 132.08 (C-4a), 130.91 (C-5), 130.39 (C-5′), 128.88 (C-6), 127.75 (C-2), 127.37 (C-4), 126.40 (C-3), 126.02 (C-8), 119.78 (C-7), 80.88 ($\underline{C}(CH_3)_3$), 29.29 (CH_2), 27.84 ($C(CH_3)_3$); HRMS (ESI): calcd.: 417.0278; found: {m/z: $[M–H]^-$ 417.0285}.

***tert*-Butyl (5-((7-(4,4,5,5-tetramethyl-1,3,2-dioxaborolan-2-yl)naphthalen-1-yl)methyl)thiazol-2-yl)carbamate (42).** $PdCl_2$(dppf)·DCM (281 mg, 0.383 mmol), bis(pinacolato) diboron (1.46 g, 5.75 mmol), bromoarene derivative **41** (804 mg, 1.92 mmol) and KOAc (753 mg, 7.67 mmol) were dissolved in degassed anhydrous 1,4-dioxane (15 mL) under N_2 atmosphere and stirred at 80 °C for 1 h and then at room temperature for another 2 h. Subsequently the mixture was diluted with water (100 mL) and brine (100 mL) and extracted with EtOAc (3 × 100 mL). The combined organic layers were dried over sodium sulfate. After evaporating the solvent *in vacuo*, the crude product was purified by FCC (hexanes/EtOAc 100 : 0 → 100 : 20) to give boronic acid pinacol ester **42** (456 mg, 0.978 mmol, 51%) as a beige solid; m.p. 203 °C; IR (ATR) $\tilde{\nu}$/cm^{-1} 2975, 1719, 1624, 1568, 1457, 1369, 1341, 1309, 1251, 1240, 1142, 1090, 1059, 1009, 982, 962, 836, 804, 768, 755, 690; δ_H (400 MHz; $(CD_3)_2SO$) 11.24 (s, 1H, NHCO), 8.49 (s, 1H, 8-H), 7.93 (d, J = 8.2 Hz, 1H, 5-H), 7.85 (d, J = 8.1 Hz, 1H, 4-H), 7.73 (dd, J = 8.2, 1.0 Hz, 1H, 6-H), 7.53 (dd, J = 8.2, 7.0 Hz, 1H, 3-H), 7.45 (d, J = 7.0 Hz 1H, 2-H), 7.13 (s, 1H, 4′-H), 4.55 (s, 2H, CH_2), 1.41 (s, 9H, $C(CH_3)_3$), 1.33 (s, 12H, $O_2C_2(CH_3)_4$). δ_C (101 MHz; $(CD_3)_2SO$) 158.35 (C-2′), 152.69 (NHCO), 136.82 (C-1), 135.08 (C-4a), 134.86 (C-4), 131.27 (C-8), 130.34 (C-5′), 130.31 (C-8a), 130.00 (C-6), 127.95 (C-5), 127.23 (C-4), 126.76 (C-3), 126.70 (C-2), 125.41 (C-7), 83.83 ($O_2\underline{C}_2(CH_3)_4$), 80.86 ($\underline{C}(CH_3)_3$), 29.25 ($CH_2$), 27.82 ($C(CH_3)_3$), 24.71 ($O_2C_2(CH_3)_4$); HRMS (ESI): calcd.: 465.2025; found: {m/z: $[M–H]^-$ 465.2033}.

(8-((2-({*tert*-Butoxycarbonyl)amino)thiazol-5-yl)methyl)-naphthalen-2-yl)boronic acid (43). To a stirred solution of **42** (541 mg, 1.16 mmol) in THF/water 3 : 1 v/v (6 mL), was added sodium periodate (744 mg, 3.48 mmol) and the reaction mixture was stirred at room temperature for 1 h. Then, 1 M HCl (1.16 mL) was added and the mixture was stirred for another 3 h, then the mixture was extracted with EtOAc (3 × 50 mL). The combined organic layers were dried over sodium sulfate. After evaporating the solvent *in vacuo*, the crude product was purified by FCC (DCM/MeOH 100 : 2) to give boronic acid **43** (376 mg, 0.978 mmol, 84%) as a white solid; m.p. 194 °C (decomposition); IR (ATR) $\tilde{\nu}$/cm^{-1} 2976, 1716, 1624, 1558, 1458, 1368, 1346, 1306, 1250, 1151, 1094, 1061, 1024, 837, 755, 697; δ_H (400 MHz; $(CD_3)_2SO$) 11.21 (s, 1H, NHCO), 8.68 (s, 1H, 8-H), 8.23 (s, 2H, $B(OH)_2$), 7.88–7.86 (m, 2H, 5-H, 6-H), 7.80 (d, J = 8.1 Hz, 1H, 4-H), 7.48 (dd, J = 8.1, 7.0 Hz, 1H, 3-H), 7.42 (dd, J = 7.0, 1.3 Hz, 1H, 2-H), 7.19 (s, 1H, 4′-H), 4.54 (s, 2H, CH_2), 1.41 (s, 9H, $C(CH_3)_3$). δ_C (126 MHz; $(CD_3)_2SO$) 158.33 (C-2′), 152.73 (NHCO), 136.95 (C-1), 134.82 (C-4), 134.57 (C-4a), 131.72 (C-7), 130.74 (C-6, C-8a), 130.55 (C-8), 130.46 (C-5′), 127.28 (C-5), 127.02 (C-4), 126.41 (C-3), 126.32 (C-2), 80.90 ($\underline{C}(CH_3)_3$), 29.23 (CH_2), 27.88 ($C(CH_3)_3$); HRMS (ESI): calcd.: 385.1388; found: {m/z: $[M + H]^+$ 358.1388}.

(8-((2-Aminothiazol-5-yl)methyl)naphthalen-2-yl)boronic acid (44). To a stirred solution of *N*-Boc-derivative **43** (407 mg, 1.06 mmol) in chloroform (10 mL) was added TFA (3.98 mL, 53.0 mmol) at room temperature. The reaction mixture was stirred at room temperature for 17 h. Subsequently brine (15 mL) was added, and the solution was basified with NaOH (2.33 g, 58.3 mmol). After collecting the organic phase, the aqueous phase was extracted with DCM/2-propanol (3 × 30 mL, 4 : 1 v/v) and then EtOAc/2-propanol (3 × 30 mL, 4 : 1). The combined organic layers were dried over sodium sulfate and the solvent was evaporated *in vacuo* to give **44** (302 mg, 1.06 mmol, quant.) as a light greyish-white solid; m.p. 281 °C (decomposition); IR (ATR) $\tilde{\nu}$/cm^{-1} 2929, 1599, 1554, 1515, 1456, 1379, 1315, 1256, 1157, 1051, 834, 754, 699; δ_H (500 MHz; $(CD_3)_2SO$) 8.69 (d, J = 1.1 Hz, 1H, 8-H), 8.21 (s, 2H, $B(OH)_2$), 7.90–7.82 (m, 2H, 5-H, 6-H), 7.77 (d, J = 8.1 Hz, 1H, 4-H), 7.46 (dd, J = 8.2, 7.0 Hz, 1H, 3-H), 7.37 (dd, J = 7.0, 1.2 Hz, 1H, 2-H), 6.74 (s, 1H, 4′-H), 6.64 (s, 2H, NH_2), 4.40 (s, 2H, CH_2). δ_C (126 MHz; $(CD_3)_2SO$) 167.70 (C-2′), 137.26 (C-1), 135.59 (C-4′), 134.46 (C-4a), 131.55 (C-7) 130.78 (C-8), 130.49 (C-8a), 130.44 (C-6), 127.16 (C-5), 126.74 (C-4), 126.30 (C-3), 125.94 (C-2), 124.49 (C-5′), 29.58 (CH_2); HRMS (ESI): calcd.: 285.0864; found: {m/z: $[M + H]^+$ 285.0863}.

***N*-(5-((7-Bromonaphthalen-1-yl)methyl)thiazol-2-yl)-2-((4,6-dimethylpyrimidin-2-yl)thio)acetamide (45).** To a stirred solution of aminothiazole **38** (627 mg, 1.96 mmol) in dry DMF (5 mL) were added DMAP (120 mg, 0.982 mmol), EDC···HCl (461 mg, 2.36 mmol) and a solution of 2-((4,6-dimethylpyrimidin-2-yl)thio)acetic acid (389 mg, 1.96 mmol) in dry DMF (1 mL) at room temperature. The reaction mixture was stirred at room temperature for 16 h. Water (50 mL) and brine (50 mL) were added, and the mixture was extracted with DCM (3 × 100 mL). The combined organic layers were dried over sodium sulfate, the solvent was evaporated *in vacuo* and the crude product was purified by FCC (DCM/EtOAc 90 : 10) to give **45** (509 mg, 1.02 mmol, 52%) as a white solid. Analytical data are in alignment with literature.[20]

***N*-(5-((7-Cyanonaphthalen-1-yl)methyl)thiazol-2-yl)-2-((4,6-dimethylpyrimidin-2-yl)thio)acetamide (46).** To a stirred solution of 2-((4,6-dimethylpyrimidin-2-yl)thio)acetic acid (194 mg, 0.976 mmol) in dry DMF (3 mL) were added DIPEA (429 µL, 2.44 mmol) and HATU (371 mg, 0.976 mmol) and the reaction mixture was stirred at room temperature for 1 h. Aminothiazole **39** (216 mg, 0.814 mmol) was added and the reaction mixture was stirred at room temperature for another 18 h. Then the mixture was diluted with water (150 mL) and extracted with EtOAc (4 × 100 mL). The combined organic layers were dried over sodium sulfate. After evaporating the solvent *in vacuo*, the crude product was purified by FCC (hexanes/EtOAc 40 : 60) to give amide **46**

(105 mg, 0.235 mmol, 29%) as a white solid; m.p. 218 °C; IR (ATR) $\tilde{\nu}$/cm^{-1} 2897, 2221, 1687, 1581, 1530, 1429, 1374, 1322, 1258, 1243, 1161, 966, 876, 841, 819, 755, 715; δ_H (500 MHz; $(CD_3)_2SO$) 12.20 (s, 1H, CONH), 8.75 (d, J = 1.6 Hz, 1H, 8-H), 8.13 (d, J = 8.4 Hz, 1H, 5-H), 7.97 (d, J = 8.2 Hz, 1H, 4-H), 7.80 (dd, J = 8.5, 1.5 Hz, 1H, 6-H), 7.68 (dd, J = 8.2, 7.0 Hz, 1H, 3-H), 7.61 (dd, J = 7.1, 1.3 Hz, 1H, 2-H), 7.33 (s, 1H, 4′-H), 6.92 (s, 1H, CH_2), 4.64 (s, 2H, CH_2S), 4.05 (s, 2H, CH_2S), 2.25 (s, 6H, 4-CH_3, 6-CH_3). δ_C (126 MHz; $(CD_3)_2SO$) 168.86 (C-2″), 166.96 (C-4″, C-6″), 166.85 (NHCO), 156.77 (C-2′), 137.45 (C-1), 135.07 (C-4′), 134.99 (C-4a), 130.74 (C-5′), 130.58 (C-8), 130.19 (C-5), 130.09 (C-8a), 129.12 (C-3), 128.31 (C-2), 127.49 (C-4), 126.32 (C-6), 119.32 (CN), 116.08 (C-5″), 108.65 (C-7), 34.01 (CH_2S), 28.95 (CH_2), 23.19 (4-CH_3, 6-CH_3); HRMS (ESI): calcd.: 444.0958; found: {m/z: $[M–H]^-$ 444.0956}; purity (HPLC): 210 nm: >95%; 254 nm: >95% (method 3c).

***N*-(5-((7-(Cyanomethyl)naphthalen-1-yl)methyl)thiazol-2-yl)-2-((4,6-dimethylpyrimidin-2-yl)thio)acetamide (47).** To a stirred solution of 2-((4,6-dimethylpyrimidin-2-yl)thio)acetic acid (73.4 mg, 0.370 mmol) in dry DMF (0.5 mL) were added DIPEA (130 µL, 0.741 mmol) and HATU (141 mg, 0.370 mmol) and the reaction mixture was stirred at room temperature for 1 h. Aminothiazole **40** (69.0 mg, 0.247 mmol) was added and the reaction mixture was stirred at room temperature for another 18 h. Then the mixture was diluted with water (50 mL) and extracted with EtOAc (4 × 50 mL). The combined organic layers were dried over sodium sulfate. After evaporating the solvent *in vacuo*, the crude product was purified by FCC (hexanes/EtOAc 50 : 50) to give amide **47** (45.5 mg, 0.0990 mmol, 40%) as a white solid; m.p. 179 °C; IR (ATR) $\tilde{\nu}$/cm^{-1} 2925, 1687, 1580, 1549, 1524, 1505, 1434, 1403, 1340, 1280, 1260, 1229, 1177, 1155, 1121, 1035, 951, 932, 891, 845, 823, 792, 757, 717; δ_H (500 MHz; $(CD_3)_2SO$) 12.18 (s, 1H, NHCO), 8.13 (s, 1H, 8-H), 7.98 (d, J = 8.4 Hz, 1H, 5-H), 7.85 (dd, J = 6.5, 3.0 Hz, 1H, 4-H), 7.51–7.45 (m, 3H, 2-H, 3-H, 6-H), 7.31 (s, 1H, 4′-H), 6.92 (s, 1H, 5″-H), 4.54 (s, 2H, CH_2), 4.21 (s, 2H, CH_2CN), 4.05 (s, 2H, CH_2S), 2.26 (s, 6H, 4-CH_3, 6-CH_3). δ_C (126 MHz; $(CD_3)_2SO$) 168.85 (C-2″), 166.98 (C-4″, C-6″), 166.77 (NHCO), 156.62 (C-2′), 135.98 (C-1), 134.87 (C-4′), 132.64 (C-4a), 130.97 (C-8a), 130.91 (C-5′), 129.52 (C-5), 129.15 (C-7), 127.20 (C-2, C-4), 126.03 (C-3), 125.95 (C-6), 122.86 (C-8), 119.18 (CN), 116.09 (C-5″), 34.00 (CH_2S), 29.28 (CH_2), 23.21 (4-CH_3, 6-CH_3), 22.89 (CH_2CN); HRMS (ESI): calcd.: 458.1115; found: {m/z: $[M–H]^-$ 458.1113}; purity (HPLC): 210 nm: >95%; 254 nm: >95% (method 3c).

(8-((2-(2-((4,6-Dimethylpyrimidin-2-yl)thio)acetamido)-thiazol-5-yl)methyl)naphthalen-2-yl)boronic acid (48). To a stirred solution of amine **44** (304 mg, 1,07 mmol) in dry DMF (5 mL) were added DMAP (65.4 mg, 0.535 mmol), EDC···HCl (251 mg, 1.28 mmol) and a solution of 2-((4,6-dimethylpyrimidin-2-yl)thio)acetic acid (212 mg, 1.07 mmol) in dry DMF (1 mL) at room temperature. The reaction mixture was stirred at room temperature for 16 h. Water (100 mL) and brine (50 mL) were added, and the mixture was extracted with EtOAc (3 × 100 mL). The combined organic layers were dried over sodium sulfate, the solvent was evaporated *in vacuo*, and the crude product was purified by FCC (DCM/MeOH/NH_3 (aq., 25%) 100 : 5 : 0.05) to give amide **48** (82.5 mg, 0.178 mmol, 17%) as a white solid; m.p. 153 °C (decomposition); IR (ATR) $\tilde{\nu}$/cm^{-1} 2928, 1691, 1623, 1583, 1533, 1438, 1385, 1313, 1265, 1163, 1030, 972, 893, 837, 758, 668; δ_H (500 MHz; $(CD_3)_2SO$) 12.17 (s, 1H, NHCO), 8.68 (s, 1H, 8-H), 8.20 (s, 2H, $B(OH)_2$), 7.88–7.84 (m, 2H, 5-H, 6-H), 7.79 (d, J = 8.1 Hz, 1H, 4-H), 7.47 (dd, J = 8.2, 7.0 Hz, 1H, 3-H), 7.41 (dd, J = 7.0, 1.3 Hz, 1H, 2-H), 7.27 (s, 1H, 4′-H), 6.92 (s, 1H, 5″-H), 4.57 (s, 2H, CH_2), 4.05 (s, 2H, CH_2S), 2.26 (s, 6H, 4-CH_3, 6-CH_3). δ_C (126 MHz; $(CD_3)_2SO$) 168.87 (C-2″), 166.99 (C-4″, C-6″), 166.76 (NHCO), 156.58 (C-2′), 136.80 (C-1), 134.80 (C-4′), 134.51 (C-4a), 131.73 (C-7), 131.21 (C-5′), 130.70 (C-8), 130.51 (C-6), 130.43 (C-8a), 127.23 (C-5), 127.00 (C-4), 126.33 (C-3), 126.27 (C-2), 116.11 (C-5″), 34.01 (CH_2S), 29.10 (CH_2), 23.23 (4-CH_3, 6-CH_3); HRMS (ESI): calcd.: 465.1221; found: {m/z: $[M + H]^+$ 465.1220}; purity (HPLC): 210 nm: >95%; 254 nm: >95% (method 3a).

2-((4,6-Dimethylpyrimidin-2-yl)thio)-*N*-(5-((7-formylnaphthalen-1-yl)methyl)thiazol-2-yl)acetamide (49). Bromoarene **45** (200 mg, 0.400 mmol), $Pd(OAc)_2$ (2.70 mg, 0.0120 mmol, 3 mol%), dppf (9.99 mg, 0.0180 mmol, 4.5 mol%), *N*-formylsaccharin (134 mg, 0.601 mmol) and Na_2CO_3 (63.7 mg, 0.601 mmol) were added to a 30 mL glass tube, which was then evacuated and backfilled three times with N_2. A degassed solution of Et_3SiH (84.1 µL, 0.521 mmol) in DMF (2 mL) was added to the glass tube under N_2 atmosphere. The mixture was stirred for 10 min at room temperature and subsequently warmed to 80 °C and stirred for another 16 h. After cooling to room temperature, the mixture was diluted with water (100 mL) and extracted with DCM (3 × 50 mL). After the combined organic layers were dried over sodium sulfate, the solvent was evaporated *in vacuo* and the crude product was purified using two consecutive PTLCs (hexanes/EtOAc/NEt_3 50 : 50 : 1 and DCM/EtOAc 70 : 30) to give **49** (18.8 mg, 0.0419 mmol, 11%) as a white solid; m.p. 219 °C; IR (ATR) $\tilde{\nu}$/cm^{-1} 2961, 1921, 2852, 1691, 1580, 1533, 1434, 1368, 1341, 1297, 1259, 1231, 1168, 1187, 1168, 1134, 1014, 972, 886, 860, 794, 762, 751, 711; δ_H (500 MHz; $CDCl_3$) 11.43 (bs, 1H, NHCO), 10.02 (s, 1H, CHO), 8.45 (s, 1H, 8-H), 7.90 (d, J = 8.5 Hz, 1H, 5-H), 7.84 (dd, J = 8.5, 1.5 Hz, 1H, 6-H), 7.78 (d, J = 8.2 Hz, 1H, 4-H), 7.52 (dd, J = 8.3, 7.0 Hz, 1H, 3-H), 7.44 (d, J = 7.1 Hz, 1H, 2-H), 7.01 (s, 1H, 4′-H), 6.76 (s, 1H, 5″-H), 4.53 (s, 2H, CH_2), 3.76 (s, 2H, CH_2S), 2.40 (s, 6H, 4-CH_3, 6-CH_3). δ_C (126 MHz; $CDCl_3$) 192.53 (CHO), 170.05 (C-2″), 168.49 (C-4″, C-6″), 167.65 (NHCO), 157.19 (C-2′), 137.92 (C-1), 137.47 (C-4a), 135.61 (C-4′), 134.64 (C-7), 131.92 (C-5′), 131.41 (C-8a), 130.54 (C-8), 130.35 (C-5), 129.29 (C-3), 128.39 (C-4), 128.17 (C-2), 123.02 (C-6), 117.24 (C-5″), 34.71 (CH_2S), 30.74 (CH_2), 23.94 (4-CH_3, 6-CH_3); HRMS (ESI): calcd.: 417.0920; found: {m/z: $[M + Na]^+$ 417.0919}; purity (HPLC): 210 nm: >95%; 254 nm: >95% (method 3b).

Biology

Sirtuin assays. The determination of inhibitory activity on the corresponding sirtuin enzymes was carried out based on

View Article Online
RSC Medicinal Chemistry Research Article

a fluorescence-based assay commissioned by Reaction Biology Corporation (Malvern, USA) following an internal experimental protocol. Test substances were prepared in DMSO, delivered into the respective enzyme mixture (prepared with reaction buffer: Tris-HCl, pH = 8) and incubated for 10 minutes at 30 °C. Subsequently the substrate mixture (NAD^+ and a 7-amino-4-methylcoumarin-based fluorogenic peptide substrate) was added to initiate the deacetylation reaction. After 2 hours incubation at 30 °C, 2 mM nicotinamide (universal sirtuin inhibitor, to stop the reaction) and protease-based developer (to generate fluorescence by the cleavage of 7-amino-4-methylcoumarin) was added. At 30 °C 1 hour later, the respective fluorescence was measured (extinction/emission = 360 nm/460 nm). The inhibitory effect of the test compounds is indirectly proportional to the amount of converted fluorescent substrate standardized as 100% activity of the control without inhibitor. The test substances were tested in 10-dose IC_{50} triplicate mode, with 3-fold serial dilution starting at 50 μM final reaction concentration and if necessary, starting at 100 μM. For each serially diluted replicate of the triplicate, an IC_{50} value was determined by sigmoidal curve fitting, resulting in three IC_{50} values, from which the mean and corresponding standard deviation were subsequently calculated. Data processing was performed based on Prism 8.0.2 software (GraphPad Software, Boston, USA). Subtype selectivity on SIRT1, SIRT3 and SIRT5 was evaluated in a single dose duplicate mode at 50 μM final test compound concentration according to previous outlined internal protocol of Reaction Biology Corporation by determining the enzyme activity of the respective sirtuins in % (no inhibitor control as 100% activity).

Fluorescence thermal shift assays. Fluorescence thermal shift assays were performed in white 96-well plates (Hard-Shell PCR Plates, BioRad, USA) with a total volume of 20 μL per well and a final DMSO concentration of 5% (v/v), following a published protocol.[19,21] Briefly, 10 μL SIRT2 (final concentration of 6.0 μM, purified according to published protocol[21]) and SYPRO Orange (5× final concentration, Sigma-Aldrich, Germany) in assay buffer (25 mM Tris-HCl, 150 mM NaCl, 1 mM DTT, pH 8.0) were mixed with 10 μL of compound (final concentration of 30 μM and 10 μM) and incubated at 25 °C and 350 rpm for 5 min. The compounds were prepared as 10 mM stock solutions in DMSO and diluted in the assay such that a final DMSO concentration of 5% (v/v) was achieved. If necessary, NAD^+ was added to a final concentration of 2.5 mM. Fluorescence intensity was recorded during a temperature gradient of 1 °C per 20 s from 25 to 95 °C using a real-time PCR machine (C1000 Touch™ Thermal Cycler, CFX96™ Real-Time System, BioRad, USA). Melting temperatures were determined using GraphPad Prism, following a published procedure.[52]

Cloning and expression of SIRT2 56-356. The human *SIRT2* 2-389 gene (Table S4) was synthesized and cloned in a pETDuet based vector encoding an N-terminal His_6-SUMO tag by Eurofins Genomics. This construct served for Q5 mutagenesis with primers A-D (Table S5) to yield His_6-SUMO-Ser-SIRT2 56-356. All plasmids were controlled by sequencing. *SIRT2* 56-356 was expressed as an N-terminal His_6-SUMO fusion in Rosetta(DE3) cells. Overnight cultures were grown in LB with ampicillin (180 mg L^{-1}) and chloramphenicol (50 mg L^{-1}) at 37 °C, 130 rpm. Expression cultures were inoculated with 25 mL overnight culture per liter autoinduction medium from Studier[53] (adapted according to Table 2) with the antibiotics ampicillin (90 mg L^{-1}) and chloramphenicol (25 mg L^{-1}) added. After 18 h at 37 °C, 130 rpm, the cells were cultured for 24 h at 16 °C, 130 rpm for protein expression. Cells were harvested by centrifugation for 20 min at 5000 × *g*, 20 °C, and washed with 0.9% (w/v) NaCl. The supernatant was removed by centrifugation for 20 min at 5000 × *g*, 4 °C, and the cell pellets were stored at −20 °C.

Protein purification of SIRT2 56-356. Cell pellets were resuspended on ice in 100 mM HEPES pH 7.0, 300 mM NaCl, 20 mM imidazole, 2 mM β-mercaptoethanol, 1 mg of DNAse I, and Pefabloc® SC. After lysis by sonication, the cell debris was removed by centrifugation for 20 min at 41 000 × *g*, 4 °C. The lysate was loaded onto a NiSepharose column (HisTrap™ HP 5 mL, Cytiva) previously equilibrated with buffer A (100 mM HEPES pH 7.0, 300 mM NaCl, 20 mM imidazole, 2 mM β-mercaptoethanol) by an Äkta pure™ System (GE Healthcare) at 4 °C. The column was washed with 10 CV of buffer A, and SIRT2 was eluted by a continuous gradient from 0 to 100% buffer B (100 mM HEPES pH 7.0, 300 mM NaCl, 500 mM imidazole, 2 mM β-mercaptoethanol). All purification steps were monitored by UV absorption at 280 nm and SDS-PAGE. To remove the His_6-SUMO-tag, the fractions containing SIRT2 were dialyzed overnight at 4 °C with His_6-SUMO-protease against 2 L of 50 mM HEPES pH 7.0, 150 mM NaCl, 2 mM β-mercaptoethanol. Precipitated protein was removed by centrifugation, and the supernatant was subjected to a second Ni^{2+} affinity chromatography. The flow-through containing cleaved SIRT2 was collected and concentrated to a volume of 2 mL using an Amicon® centrifugal filter (Merck) with 10 000 MWCO. The protein solution was loaded on a HiLoad® 16/600 Superdex® 200 pg column (Cytiva) at 4 °C using 25 mM HEPES pH 7.0, 100 mM NaCl, 2 mM DTT as running buffer. Fractions containing SIRT2 were pooled and concentrated using Amicon® 10 000

Table 2 Composition of autoinduction medium

Content [g L^{-1}]		Compound
5.0	g L^{-1}	Yeast extract
10	g L^{-1}	Peptone
0.5	g L^{-1}	Glucose
1.9	g L^{-1}	Lactose
5.0	g L^{-1}	Glycerol
0.2	g L^{-1}	Magnesium sulfate
3.4	g L^{-1}	Potassium dihydrogen phosphate
3.5	g L^{-1}	Disodium hydrogen phosphate
2.8	g L^{-1}	Ammonium chloride
pH adjusted to		pH 6.8

MWCO centrifugal filters (Merck). The protein was frozen in liquid nitrogen and stored at −80 °C until further use.

Crystallisation and X-ray structure determination of SIRT2 56-356. SIRT2 56-356 (23.7 mg mL^{-1}) was crystallized without ligand by sitting drop vapor diffusion at 20 °C. A 2 : 1 ratio of protein and reservoir solution containing 0.2 M ammonium formate, 20% (w/v) PEG3350 led to crystals within two months. Crystals were cryoprotected with 35% (v/v) glycerol and flash frozen in liquid nitrogen.

Crystal structures of SIRT2 56-356 with ligands were obtained from hanging drop crystallization experiments at 20 °C. The SIRT2 56-356 protein was diluted to 7.3 mg mL^{-1} in 25 mM HEPES pH 7.0, 100 mM NaCl, 2 mM DTT, and mixed with 5 mM NAD^+ and 500 μM of **29** (**RW-78**)/**31** (**RW-80**) dissolved in DMSO, respectively. The solution was incubated for 1 h on ice, and any precipitate was removed by centrifugation for 10 min at 16 000 × *g*. Crystals grew after 5 days in 24-well, with 300 μL of 0.1 M sodium acetate, 17% (w/v) PEG3350 as reservoir, and a drop ratio of 1 μL protein to 1 μL reservoir solution. The crystals were soaked with 10 μL of 30% (v/v) ethylene glycol and vitrified in liquid nitrogen. Diffraction images of SIRT2 56-356:**RW-78**, and SIRT2 56-356:**RW-80** were recorded using synchrotron radiation of λ = 1.060 Å at the P13 beamline from PETRAIII at DESY (Deutsches Elektronen-Synchrotron, EMBL, Hamburg, Germany). Recorded reflections were processed using the XDS suite, and data reduction was performed with XSCALE.[54,55] Phasing of the SIRT2 56-356 apo structure was performed by molecular replacement with PHASER[56] and the coordinates of SIRT2:**SirReal2** (PDB ID: 4RMG[19]). The solution was refined by restrained refinement with REFMAC5 (ref. 57) and iteratively rebuilt with COOT (v. 0.9).[58] The resulting model was used to phase the SIRT2 56-356:**RW-78** data set, followed by iterating model building in COOT[58] with restrained refinements in REFMAC5.[57] The ligand was prepared in AceDRG.[59] Water molecules were positioned with ARP/wARP 8.0.[60] The apo structure was completed by TLS refinement, whereas the SIRT2 56-356:**RW-78** structure was refined with anisotropic restraints to satisfactory R_{work} and R_{free} values. The SIRT2 56-356:**RW-80** structure was phased with the SIRT2:**RW-78** structure in REFMAC5 (ref. 57) and built as described for SIRT2 56-356:**RW-78**. The geometry of the final structures was analyzed by the MOLPROBITY[61] online tool, and the structures were deposited in the RCSB Protein Data Bank (Tables S1–S3).

NanoBRET assay. The NanoBRET target engagement assay was performed as previously described by Vogelmann *et al.*,[21] with the modification that stably transfected HEK293T cells expressing the NanoLuc-tagged SIRT2(50-356) fusion protein were used instead of transient transfection. HEK293T-NLuc-Sirt250-356 cells were cultured under standard conditions (37 °C, 5% CO_2) in DMEM supplemented with 10% fetal bovine serum, 2 mM glutamine, and 300 μg mL^{-1} hygromycin as a selection marker. For the assay, cells were trypsinized, resuspended in Opti-MEM® reduced serum medium, and adjusted to a concentration of 2 × 10^5 cells per mL. To determine the affinities of the inhibitors, a final tracer concentration of 2 μM was used. Serially diluted inhibitor and tracer were added to the cell suspension, and 100 μL were seeded into 96-well white, sterile, nonbinding surface plates. Plates were incubated at 37 °C with 5% CO_2 for 2 hours. For BRET measurements, NanoBRET NanoGlo Substrate (Promega cat. #N1571) was added to the wells according to the manufacturer's protocol. All measurements were performed using the 2102 EnVision™ Multilabel Reader (PerkinElmer), equipped with a 460 nm filter (donor) and a 615 nm filter (acceptor). The BRET ratio was calculated as the ratio of acceptor to donor signal, and data were normalized to vehicle-treated controls. Apparent intracellular binding affinities (EC_{50} values) were determined by fitting dose–response curves using nonlinear regression analysis in GraphPad Prism. All experiments were conducted in triplicate unless otherwise noted, and results are presented as mean ± standard deviation.

Computational methods

Docking simulations. Docking simulations were carried out with Schrödinger software suite (Schrödinger Inc., New York City, USA, version 2020-3).[62] Crystal structures of SIRT2 and respective lead structures were imported from the Protein Data Bank (PDB)[63] (**SirReal2**: PDB ID: 4RMG;[19] **24a**: PDB ID: 5YQO[23]) and prepared with the Protein Preparation Wizard (Schrödinger Inc. New York City, USA). All ligands were prepared with the Ligand Preparation Wizard using Epik for protonation and charge calculations.[64] Docking was performed using Glide in standard precision mode SP (all docking parameters left to their default values). Results were inspected and visualized with PyMOL 2.5.8 (Schrödinger Inc., New York city, USA). The top-ranking poses were analysed, considering the favourable spatial orientation in relation to the crystal structures of the corresponding lead compounds.

Author contributions

This study was conceptualised and supervised by F. B. Investigation, methodology, experimental execution and data curation were performed by R. W., M. F., A. H., N. P., F. F., T. W., M. J., M. G. and E. M. H. Original manuscript draft was written and edited by R. W. and M. F. with inputs from A. H., E. M. H. and F. B. All authors partook in the discussion of the findings and thoroughly reviewed the final manuscript for publication.

Conflicts of interest

There are no conflicts to declare.

Data availability

Supplementary information is available: 1H and ^{13}C NMR spectra of compounds, HPLC chromatograms of tested compounds, Tables S1–S5: Crystallographic data, Fig. S1: Purification of human SIRT2 56-356 and Fig. S2: Close-up view of the SIRT2 ligand binding site can be found in the SI. See DOI: **https://doi.org/10.1039/D5MD00144G**.

The data supporting this article have been included as part of the SI. X-ray coordinates have been deposited in the RCSB Protein Data Bank under the accession codes 9S44 (SIRT2 56-356), 9S46 (SIRT2 56-356:**RW-78**) and 9S48 (SIRT2 56-356:**RW-80**).

Acknowledgements

This research was funded by the Deutsche Forschungsgemeinschaft (DFG, German Research Foundation), Ju295/18-1 to M. Jung (project number 503267011) and SFB1309 (Chemical Biology of Epigenetic Modifications, project ID: 325871075–SFB1309) to F. Bracher, M. Groll and E. M. Huber. A. Heider acknowledges financial support by the Stiftung der Deutschen Wirtschaft (sdw, Foundation of German Business). The synchrotron data was collected at beamline P13 operated by EMBL Hamburg at the PETRA III storage ring (DESY, Hamburg, Germany) under grant no. MX-1019. We thank the staff of beamline P13 for assistance during data collection. We thank Lars Allmendinger and Claudia Glas for NMR measurements, Werner Spahl and Sonja Kosak for MS measurements and Anna Niedrig for HPLC purity determinations.

References

1 Q. J. Wu, T. N. Zhang, H. H. Chen, X. F. Yu, J. L. Lv, Y. Y. Liu, Y. S. Liu, G. Zheng, J. Q. Zhao, Y. F. Wei, J. Y. Guo, F. H. Liu, Q. Chang, Y. X. Zhang, C. G. Liu and Y. H. Zhao, *Signal Transduction Targeted Ther.*, 2022, **7**, 402.
2 A. A. Sauve, C. Wolberger, V. L. Schramm and J. D. Boeke, *Annu. Rev. Biochem.*, 2006, **75**, 435–465.
3 J. Du, Y. Zhou, X. Su, J. J. Yu, S. Khan, H. Jiang, J. Kim, J. Woo, J. H. Kim, B. H. Choi, B. He, W. Chen, S. Zhang, R. A. Cerione, J. Auwerx, Q. Hao and H. Lin, *Science*, 2011, **334**, 806–809.
4 X. Zhang, S. Khan, H. Jiang, M. A. Antonyak, X. Chen, N. A. Spiegelman, J. H. Shrimp, R. A. Cerione and H. Lin, *Nat. Chem. Biol.*, 2016, **12**, 614–620.
5 G. Liszt, E. Ford, M. Kurtev and L. Guarente, *J. Biol. Chem.*, 2005, **280**, 21313–21320.
6 M. M. Maxwell, E. M. Tomkinson, J. Nobles, J. W. Wizeman, A. M. Amore, L. Quinti, V. Chopra, S. M. Hersch and A. G. Kazantsev, *Hum. Mol. Genet.*, 2011, **20**, 3986–3996.
7 H. Vaziri, S. K. Dessain, E. Ng Eaton, S. I. Imai, R. A. Frye, T. K. Pandita, L. Guarente and R. A. Weinberg, *Cell*, 2001, **107**, 149–159.
8 F. Yeung, J. E. Hoberg, C. S. Ramsey, M. D. Keller, D. R. Jones, R. A. Frye and M. W. Mayo, *EMBO J.*, 2004, **23**, 2369–2380.
9 H. Jing, J. Hu, B. He, Y. L. Negrón Abril, J. Stupinski, K. Weiser, M. Carbonaro, Y. L. Chiang, T. Southard, P. Giannakakou, R. S. Weiss and H. Lin, *Cancer Cell*, 2016, **29**, 297–310.
10 C. Duran-Castells, A. Llano, A. Kawana-Tachikawa, A. Prats, I. Martinez-Zalacain, M. Kobayashi-Ishihara, B. Oriol-Tordera, R. Peña, C. Gálvez, S. Silva-Arrieta, B. Clotet, E. Riveira-Muñoz, E. Ballana, J. G. Prado, J. Martinez-Picado, J. Sanchez, B. Mothe, D. Hartigan-O'Connor, T. Wyss-Coray, A. Meyerhans, M. Gisslén, R. W. Price, C. Soriano-Mas, J. A. Muñoz-Moreno, C. Brander and M. Ruiz-Riol, *J. Virol.*, 2023, **97**, e0165522.
11 R. M. de Oliveira, H. Vicente Miranda, L. Francelle, R. Pinho, É. M. Szegö, R. Martinho, F. Munari, D. F. Lázaro, S. Moniot, P. Guerreiro, L. Fonseca-Ornelas, Z. Marijanovic, P. Antas, E. Gerhardt, F. J. Enguita, B. Fauvet, D. Penque, T. F. Pais, Q. Tong, S. Becker, S. Kügler, H. A. Lashuel, C. Steegborn, M. Zweckstetter and T. F. Outeiro, *PLoS Biol.*, 2017, **15**, e2000374.
12 N. Sola-Sevilla, A. Mesa-Lombardo, M. Aleixo, S. Expósito, T. Diaz-Perdigón, A. Azqueta, F. Zamani, T. Suzuki, S. Maioli, F. Eroli, A. Matton, M. J. Ramírez, M. Solas, R. M. Tordera, E. D. Martín and E. Puerta, *J. Neuroimmune Pharmacol.*, 2023, **18**, 529–550.
13 P. Mellini, Y. Itoh, H. Tsumoto, Y. Li, M. Suzuki, N. Tokuda, T. Kakizawa, Y. Miura, J. Takeuchi, M. Lahtela-Kakkonen and T. Suzuki, *Chem. Sci.*, 2017, **8**, 6400–6408.
14 A. S. Farooqi, J. Y. Hong, J. Cao, X. Lu, I. R. Price, Q. Zhao, T. Kosciuk, M. Yang, J. J. Bai and H. Lin, *J. Med. Chem.*, 2019, **62**, 4131–4141.
15 S. Moniot, M. Forgione, A. Lucidi, G. S. Hailu, A. Nebbioso, V. Carafa, F. Baratta, L. Altucci, N. Giacché, D. Passeri, R. Pellicciari, A. Mai, C. Steegborn and D. Rotili, *J. Med. Chem.*, 2017, **60**, 2344–2360.
16 T. Seifert, M. Malo, T. Kokkola, K. Engen, M. Fridén-Saxin, E. A. Wallén, M. Lahtela-Kakkonen, E. M. Jarho and K. Luthman, *J. Med. Chem.*, 2014, **57**, 9870–9888.
17 N. Kudo, A. Ito, M. Arata, A. Nakata and M. Yoshida, *Philos. Trans. R. Soc., B*, 2018, **373**, 20170070.
18 T. F. Outeiro, E. Kontopoulos, S. M. Altmann, I. Kufareva, K. E. Strathearn, A. M. Amore, C. B. Volk, M. M. Maxwell, J. C. Rochet, P. J. McLean, A. B. Young, R. Abagyan, M. B. Feany, B. T. Hyman and A. G. Kazantsev, *Science*, 2007, **317**, 516–519.
19 T. Rumpf, M. Schiedel, B. Karaman, C. Roessler, B. J. North, A. Lehotzky, J. Oláh, K. I. Ladwein, K. Schmidtkunz, M. Gajer, M. Pannek, C. Steegborn, D. A. Sinclair, S. Gerhardt, J. Ovádi, M. Schutkowski, W. Sippl, O. Einsle and M. Jung, *Nat. Commun.*, 2015, **6**, 6263.
20 M. Schiedel, T. Rumpf, B. Karaman, A. Lehotzky, J. Oláh, S. Gerhardt, J. Ovádi, W. Sippl, O. Einsle and M. Jung, *J. Med. Chem.*, 2016, **59**, 1599–1612.
21 A. Vogelmann, M. Schiedel, N. Wössner, A. Merz, D. Herp, S. Hammelmann, A. Colcerasa, G. Komaniecki, J. Y. Hong, M. Sum, E. Metzger, E. Neuwirt, L. Zhang, O. Einsle, O. Groß, R. Schüle, H. Lin, W. Sippl and M. Jung, *RSC Chem. Biol.*, 2022, **3**, 468–485.

22 M. Schiedel, T. Rumpf, B. Karaman, A. Lehotzky, S. Gerhardt, J. Ovádi, W. Sippl, O. Einsle and M. Jung, *Angew. Chem., Int. Ed.*, 2016, **55**, 2252–2256.
23 L. L. Yang, H. L. Wang, L. Zhong, C. Yuan, S. Y. Liu, Z. J. Yu, S. Liu, Y. H. Yan, C. Wu, Y. Wang, Z. Wang, Y. Yu, Q. Chen and G. B. Li, *Eur. J. Med. Chem.*, 2018, **155**, 806–823.
24 L. Yang, X. Ma, C. Yuan, Y. He, L. Li, S. Fang, W. Xia, T. He, S. Qian, Z. Xu, G. Li and Z. Wang, *Eur. J. Med. Chem.*, 2017, **134**, 230–241.
25 M. Gehringer and S. A. Laufer, *J. Med. Chem.*, 2019, **62**, 5673–5724.
26 R. A. M. Serafim, L. Haarer, J. G. B. Pedreira and M. Gehringer, *Curr. Res. Chem. Biol.*, 2023, **3**, 100040.
27 L. Zheng, Y. Li, D. Wu, H. Xiao, S. Zheng, G. Wang and Q. Sun, *MedComm: Oncol.*, 2023, **2**, e56.
28 L. Boike, N. J. Henning and D. K. Nomura, *Nat. Rev. Drug Discovery*, 2022, **21**, 881–898.
29 M. Groll, C. R. Berkers, H. L. Ploegh and H. Ovaa, *Structure*, 2006, **14**, 451–456.
30 P. Beck, C. Dubiella and M. Groll, *Biol. Chem.*, 2012, **393**, 1101–1120.
31 Y.-H. Wang, F. Zhang, H. Diao and R. Wu, *ACS Catal.*, 2019, **9**, 2292–2302.
32 D. Oksenberg, K. Dufu, M. P. Patel, C. Chuang, Z. Li, Q. Xu, A. Silva-Garcia, C. Zhou, A. Hutchaleelaha, L. Patskovska, Y. Patskovsky, S. C. Almo, U. Sinha, B. W. Metcalf and D. R. Archer, *Br. J. Haematol.*, 2016, **175**, 141–153.
33 A. Priimagi, G. Cavallo, P. Metrangolo and G. Resnati, *Acc. Chem. Res.*, 2013, **46**, 2686–2695.
34 Z. Xu, Z. Liu, T. Chen, T. Chen, Z. Wang, G. Tian, J. Shi, X. Wang, Y. Lu, X. Yan, G. Wang, H. Jiang, K. Chen, S. Wang, Y. Xu, J. Shen and W. Zhu, *J. Med. Chem.*, 2011, **54**, 5607–5611.
35 D. M. Himmel, K. Das, A. D. Clark, S. H. Hughes, A. Benjahad, S. Oumouch, J. Guillemont, S. Coupa, A. Poncelet, I. Csoka, C. Meyer, K. Andries, C. H. Nguyen, D. S. Grierson and E. Arnold, *J. Med. Chem.*, 2005, **48**, 7582–7591.
36 A. Benjahad, J. Guillemont, K. Andries, C. H. Nguyen and D. S. Grierson, *Bioorg. Med. Chem. Lett.*, 2003, **13**, 4309–4312.
37 G. Cavallo, P. Metrangolo, R. Milani, T. Pilati, A. Priimagi, G. Resnati and G. Terraneo, *Chem. Rev.*, 2016, **116**, 2478–2601.
38 Y. Lu, Y. Liu, Z. Xu, H. Li, H. Liu and W. Zhu, *Expert Opin. Drug Discovery*, 2012, **7**, 375–383.
39 Z. Xu, Z. Yang, Y. Liu, Y. Lu, K. Chen and W. Zhu, *J. Chem. Inf. Model.*, 2014, **54**, 69–78.
40 R. Wilcken, M. O. Zimmermann, A. Lange, A. C. Joerger and F. M. Boeckler, *J. Med. Chem.*, 2013, **56**, 1363–1388.
41 M. Frei, T. Wein and F. Bracher, *Molecules*, 2025, **30**, 1728.
42 I. Heisler, B. Buchmann, A. Cleve, M. Heroult, R. Neuhaus, H. Petrul, M. Quanz-Schöffel and C. C. Kopitz, WO2016202935A1, 2016.
43 F. Zhou, X. Xu, L. Zhang, Z. Liu, G. Hu, Q. Ding, F. Xie, B. Zheng, Q. LV and J. Lan, US2022177462A1, 2022.
44 T. Ueda, H. Konishi and K. Manabe, *Angew. Chem., Int. Ed.*, 2013, **52**, 8611–8615.
45 M. Boucher, M. Furigay, P. Quach and C. Brindle, *Org. Process Res. Dev.*, 2017, **21**, 1394–1403.
46 S. Müller, R. Schohe-Loop, N. Ortega Henandez, F. Süssmeier, E. J. Nunez, T. Brumby, N. Lindner, C. Gerdes, E. Pook, A. Buchmüller, F. Z. Gaugaz, D. Lang, S. Zimmermann, A. H. M. Ehrmann, M. Gerisch, L. Lehmann, A. Timmermann, M. Schäfer, G. Schmidt, K.-H. Schlemmer, M. Follmann, E. Kersten, V. Wang, X. Gao and Y. Wang, WO2019219517A1, 2019.
47 J. Velcicky, A. Soicke, R. Steiner and H.-G. Schmalz, *J. Am. Chem. Soc.*, 2011, **133**, 6948–6951.
48 H. Konishi, M. Kumon, M. Yamaguchi and K. Manabe, *Tetrahedron*, 2020, **76**, 131639.
49 M. S. Finnin, J. R. Donigian and N. P. Pavletich, *Nat. Struct. Biol.*, 2001, **8**, 621–625.
50 Y. Lu, Y. Wang and W. Zhu, *Phys. Chem. Chem. Phys.*, 2010, **12**, 4543–4551.
51 L. R. Smith, N. Mahoney and R. J. Molyneux, *J. Nat. Prod.*, 2003, **66**, 169–176.
52 F. H. Niesen, H. Berglund and M. Vedadi, *Nat. Protoc.*, 2007, **2**, 2212–2221.
53 F. W. Studier, *Protein Expression Purif.*, 2005, **41**, 207–234.
54 W. Kabsch, *J. Appl. Crystallogr.*, 1993, **26**, 795–800.
55 W. Kabsch, *Acta Crystallogr., Sect. D: Biol. Crystallogr.*, 2010, **66**, 125–132.
56 A. J. McCoy, R. W. Grosse-Kunstleve, P. D. Adams, M. D. Winn, L. C. Storoni and R. J. Read, *J. Appl. Crystallogr.*, 2007, **40**, 658–674.
57 G. N. Murshudov, P. Skubak, A. A. Lebedev, N. S. Pannu, R. A. Steiner, R. A. Nicholls, M. D. Winn, F. Long and A. A. Vagin, *Acta Crystallogr., Sect. D: Biol. Crystallogr.*, 2011, **67**, 355–367.
58 P. Emsley, B. Lohkamp, W. G. Scott and K. Cowtan, *Acta Crystallogr., Sect. D: Biol. Crystallogr.*, 2010, **66**, 486–501.
59 F. Long, R. A. Nicholls, P. Emsley, S. Graaeulis, A. Merkys, A. Vaitkus and G. N. Murshudov, *Acta Crystallogr., Sect. D: Biol. Crystallogr.*, 2017, **73**, 112–122.
60 R. J. Morris, A. Perrakis and V. S. Lamzin, *Methods Enzymol.*, 2003, **374**, 229–244.
61 C. J. Williams, J. J. Headd, N. W. Moriarty, M. G. Prisant, L. L. Videau, L. N. Deis, V. Verma, D. A. Keedy, B. J. Hintze, V. B. Chen, S. Jain, S. M. Lewis, W. B. Arendall, 3rd, J. Snoeyink, P. D. Adams, S. C. Lovell, J. S. Richardson and D. C. Richardson, *Protein Sci.*, 2018, **27**, 293–315.
62 R. A. Friesner, J. L. Banks, R. B. Murphy, T. A. Halgren, J. J. Klicic, D. T. Mainz, M. P. Repasky, E. H. Knoll, M. Shelley, J. K. Perry, D. E. Shaw, P. Francis and P. S. Shenkin, *J. Med. Chem.*, 2004, **47**, 1739–1749.
63 H. M. Berman, J. Westbrook, Z. Feng, G. Gilliland, T. N. Bhat, H. Weissig, I. N. Shindyalov and P. E. Bourne, *Nucleic Acids Res.*, 2000, **28**, 235–242.
64 J. C. Shelley, A. Cholleti, L. L. Frye, J. R. Greenwood, M. R. Timlin and M. Uchimaya, *J. Comput.-Aided Mol. Des.*, 2007, **21**, 681–691.

Supplementary Information (SI) for RSC Medicinal Chemistry.

Supplementary Information

Tailored SirReal-type inhibitors enhance SIRT2 inhibition through ligand stabilization and disruption of NAD^+ co-factor binding

Ricky Wirawan[†a] Matthias Frei[†a], Anna Heider[b], Niklas Papenkordt[c], Florian Friedrich[c], Thomas Wein[a], Manfred Jung[c], Michael Groll[b], Eva M. Huber[b] and Franz Bracher*[a]

[a]Department of Pharmacy, Ludwig-Maximilians University Munich, Butenandtstraße 5-13, 81377 Munich, Germany. *E-mail: franz.bracher@cup.uni-muenchen.de
[b]Center for Protein Assemblies, Technical University of Munich, Ernst-Otto-Fischer-Straße 8, 85748 Garching, Germany.
[c]Institute of Pharmaceutical Sciences, Albert-Ludwigs-Universität Freiburg, Albertstraße 25, 79104 Freiburg im Breisgau, Germany.

[†]Equal contribution as first author to this work.

Table of Contents:

^{1}H and ^{13}C NMR spectra of compound **3**

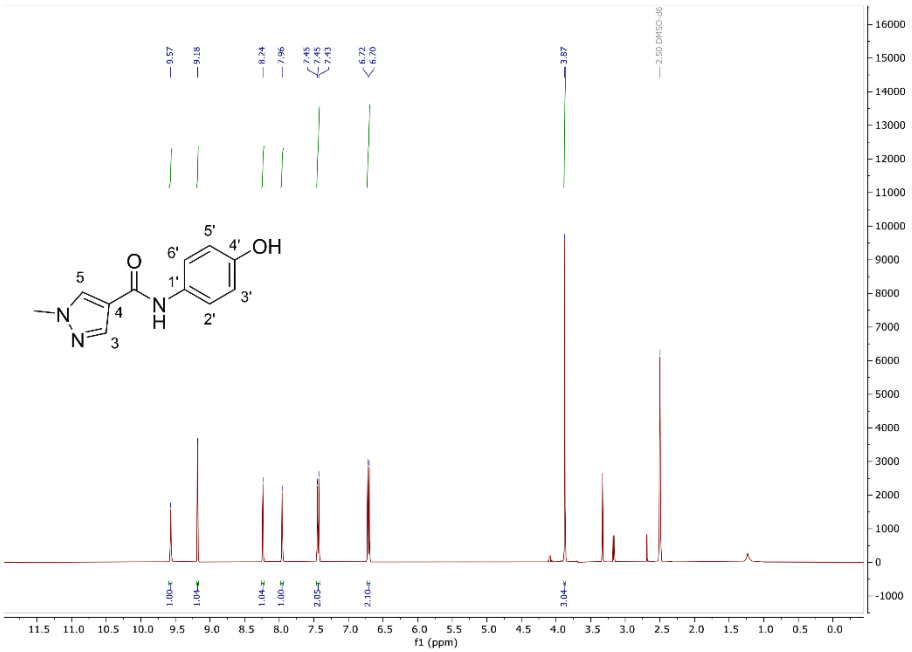

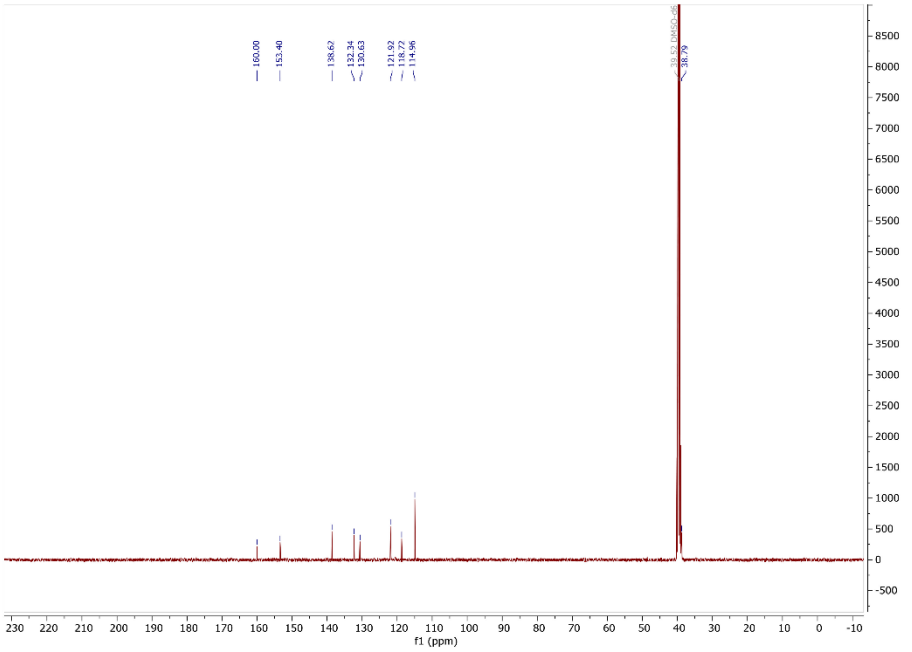

2

^{1}H and ^{13}C NMR spectra of compound **4**

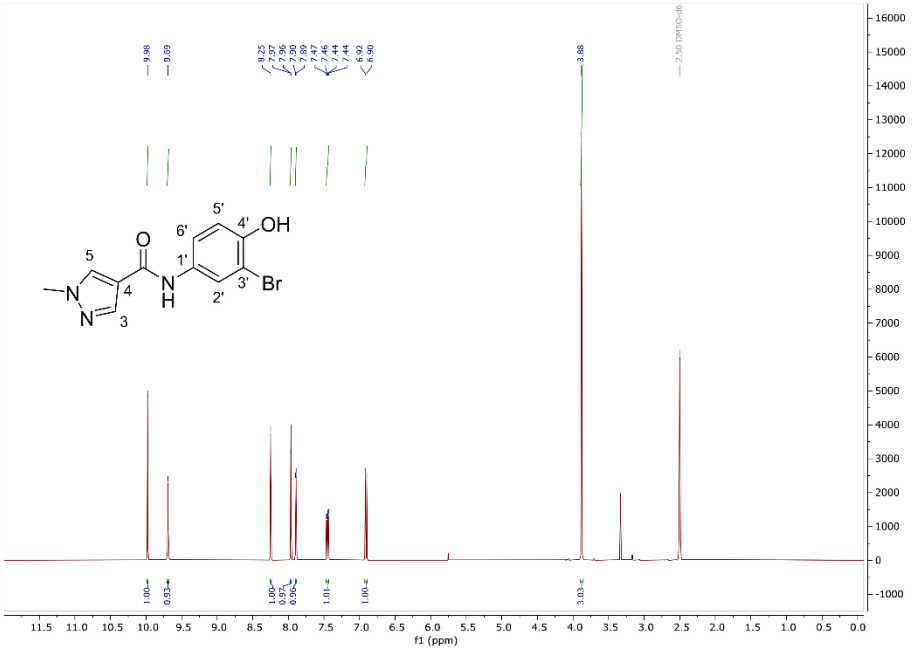

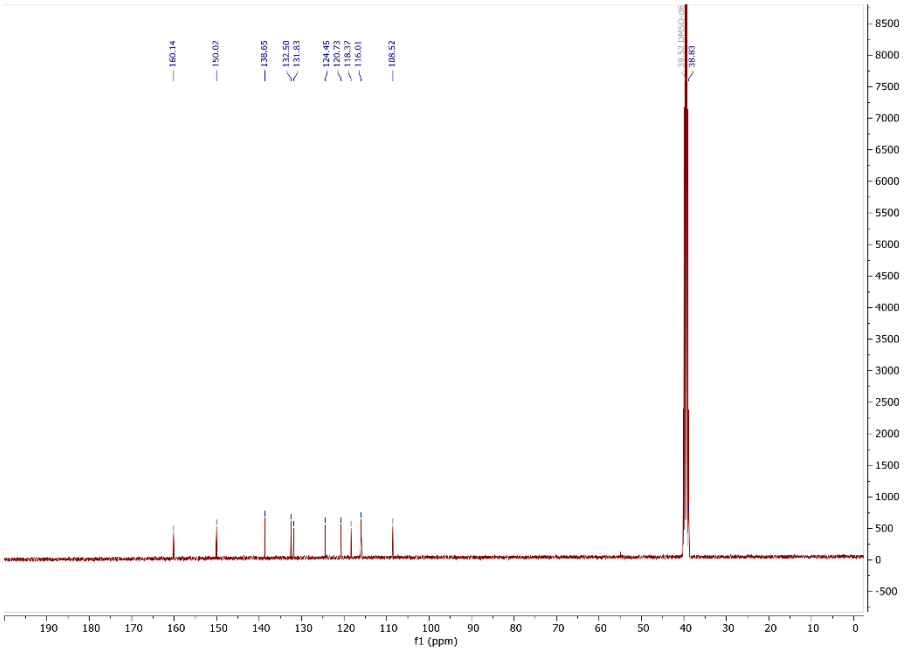

3

^{1}H and ^{13}C NMR spectra of compound **6**

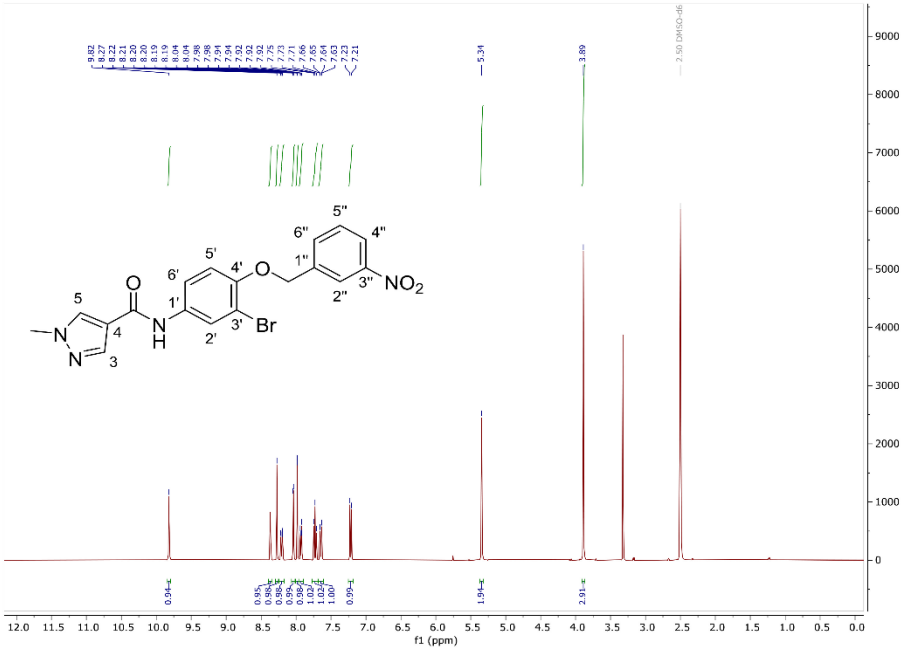

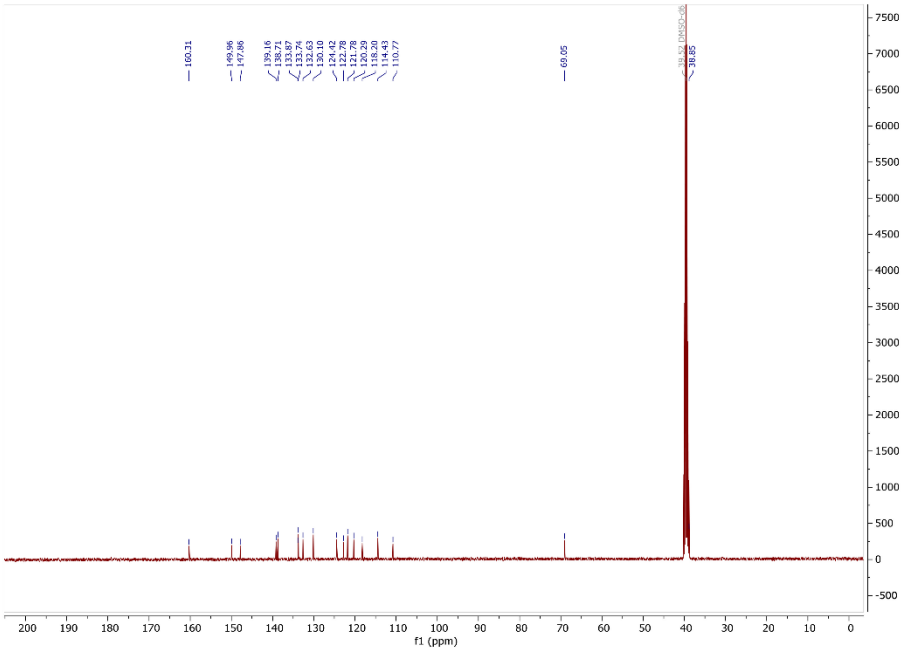

^{1}H and ^{13}C NMR spectra of compound **7**

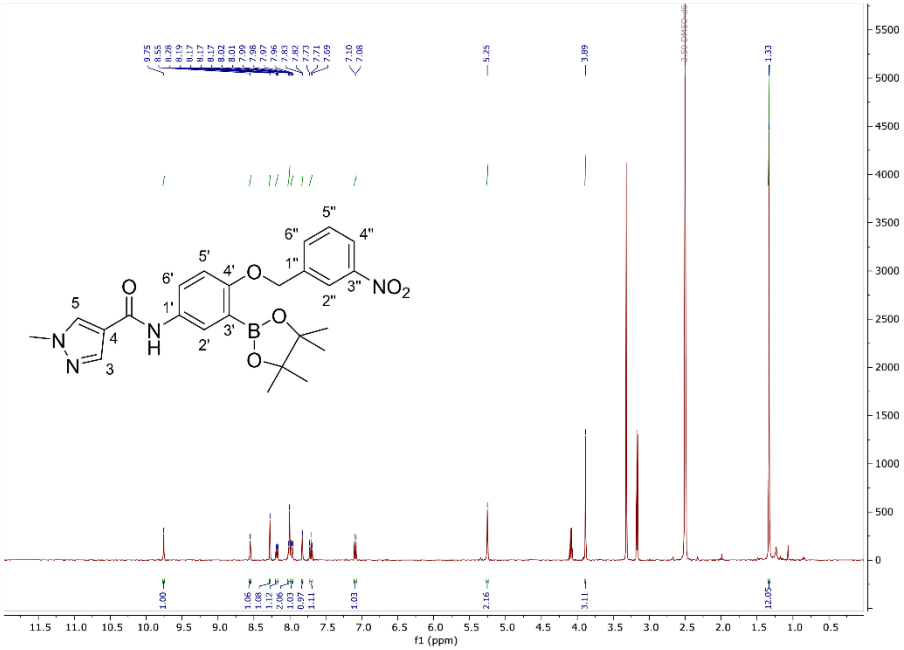

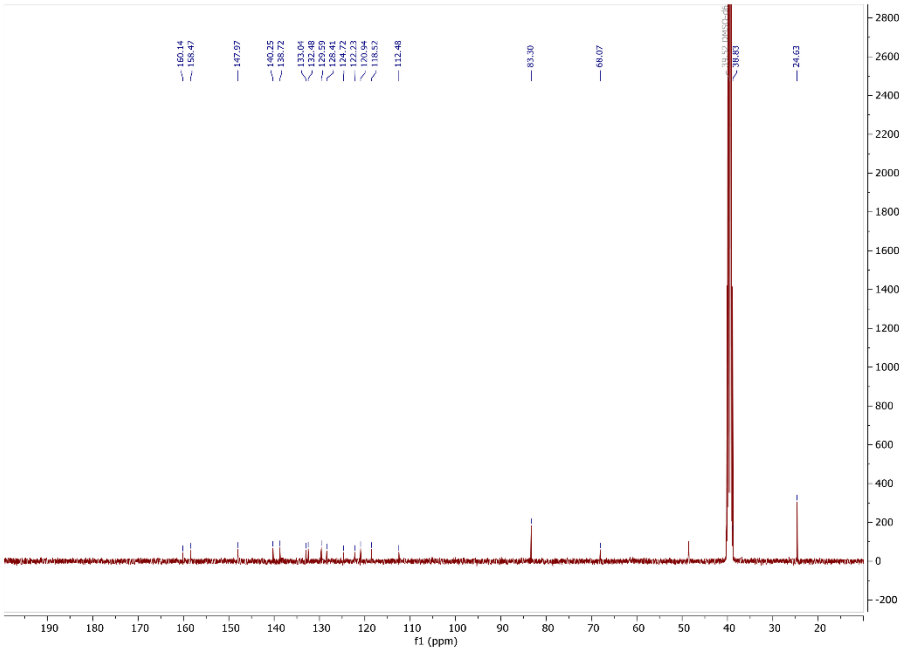

^{1}H and ^{13}C NMR spectra of compound **8**

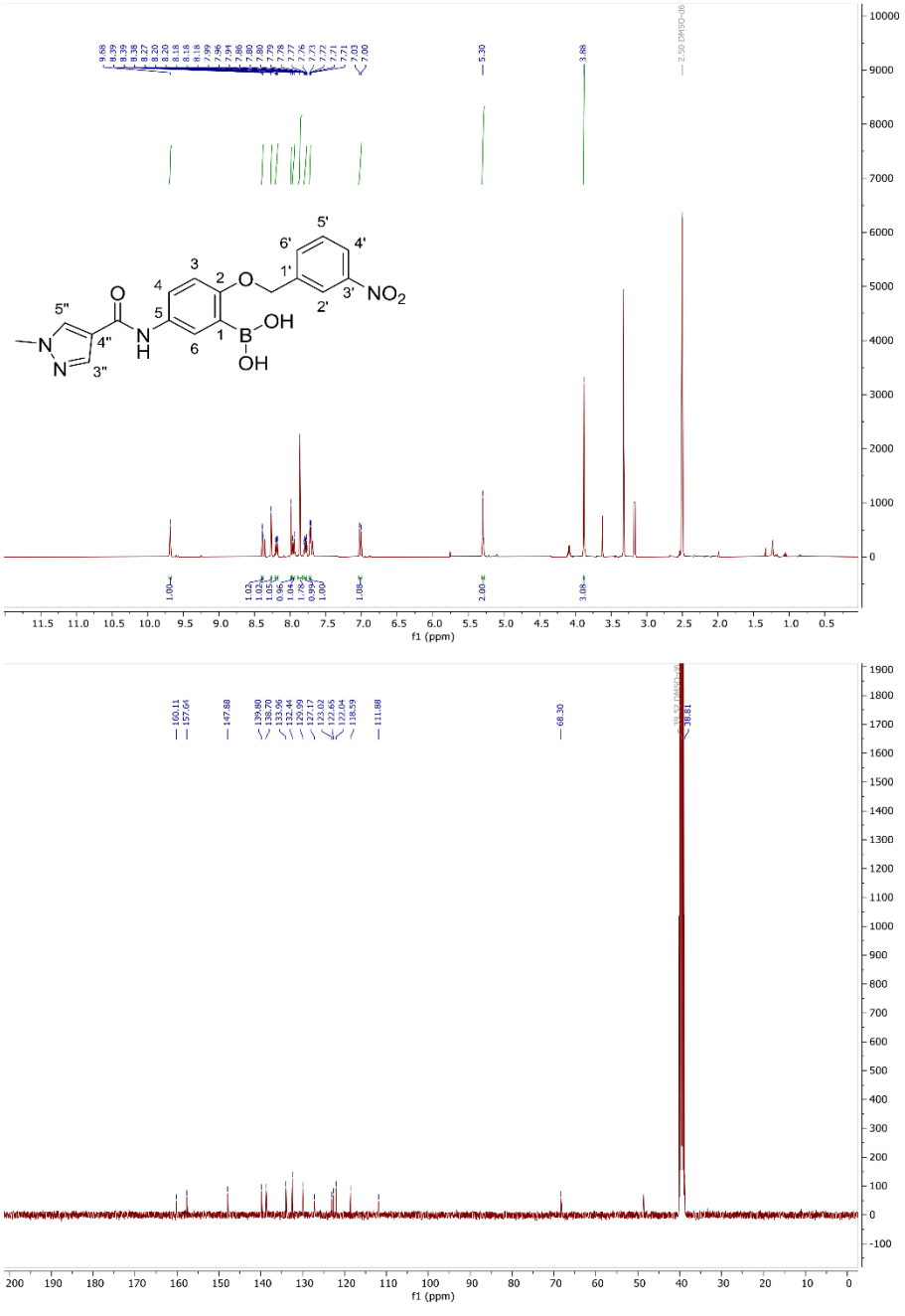

^{1}H and ^{13}C NMR spectra of compound **9**

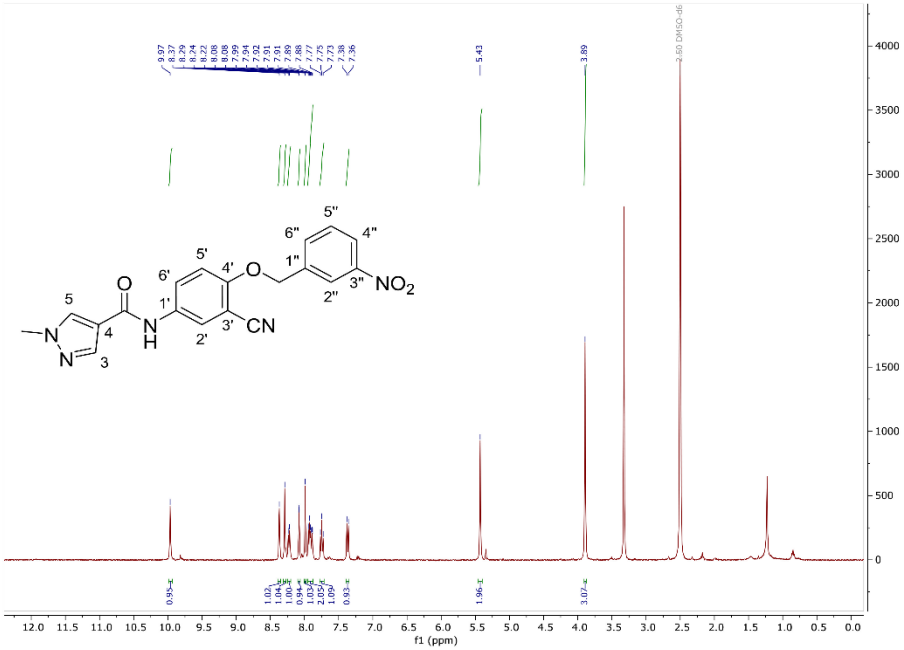

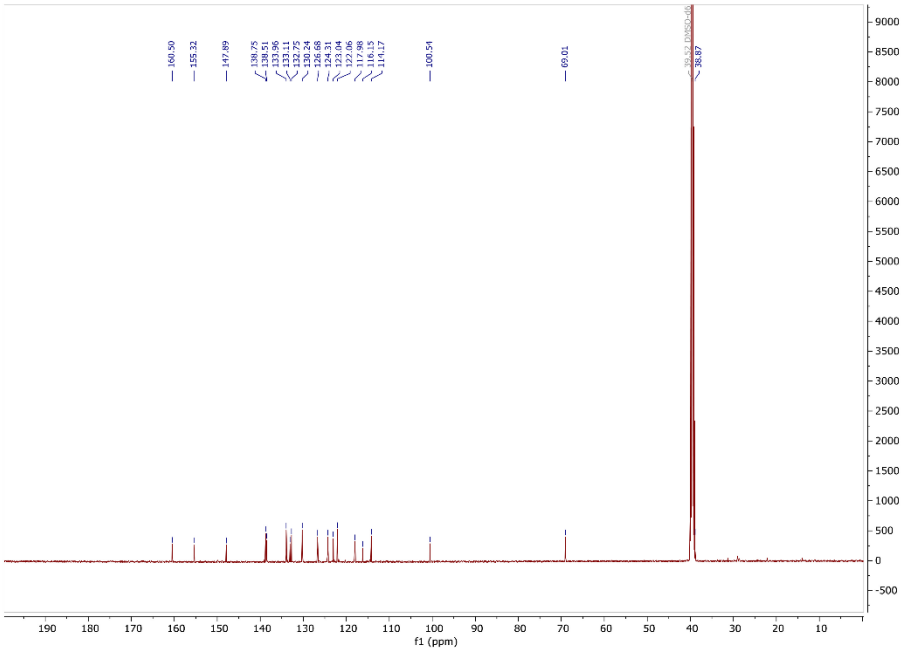

^{1}H and ^{13}C NMR spectra of compound **11**

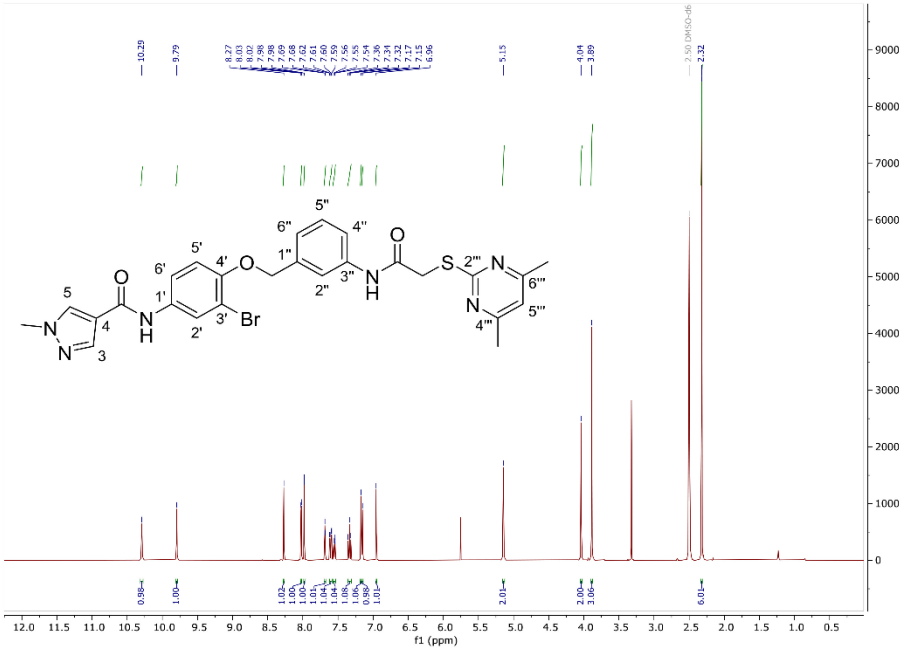

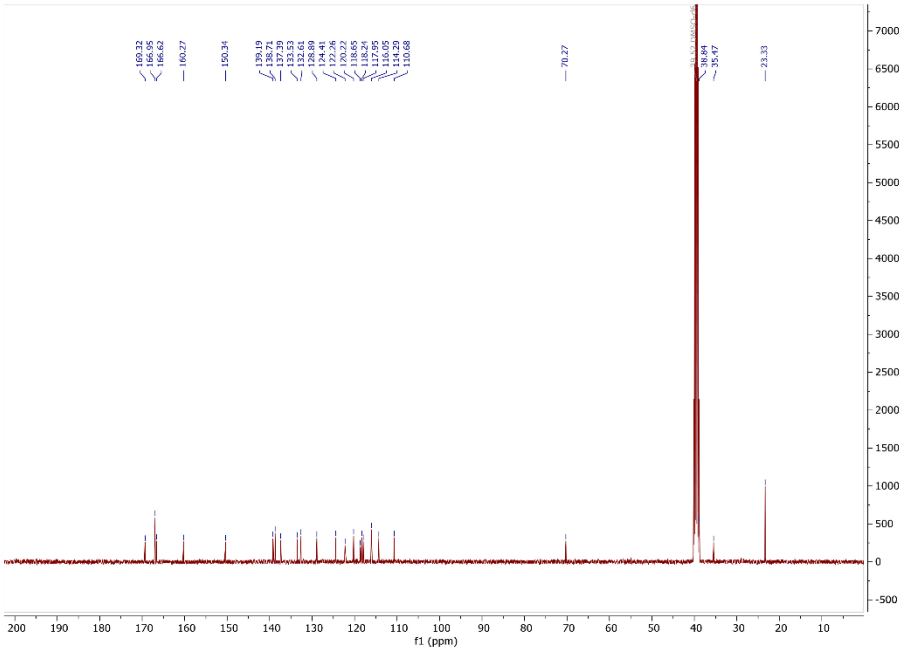

^{1}H and ^{13}C NMR spectra of compound **12**

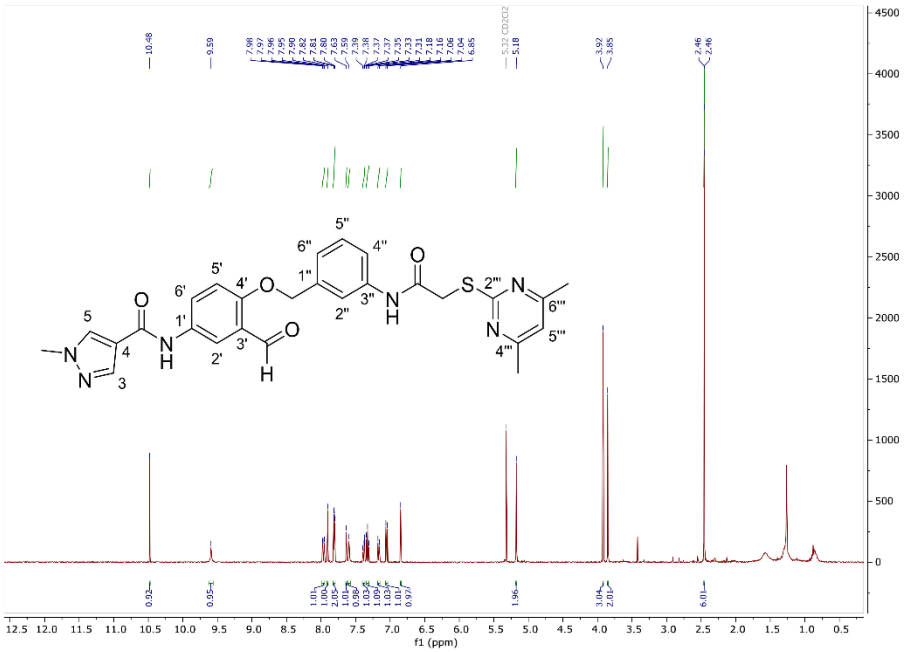

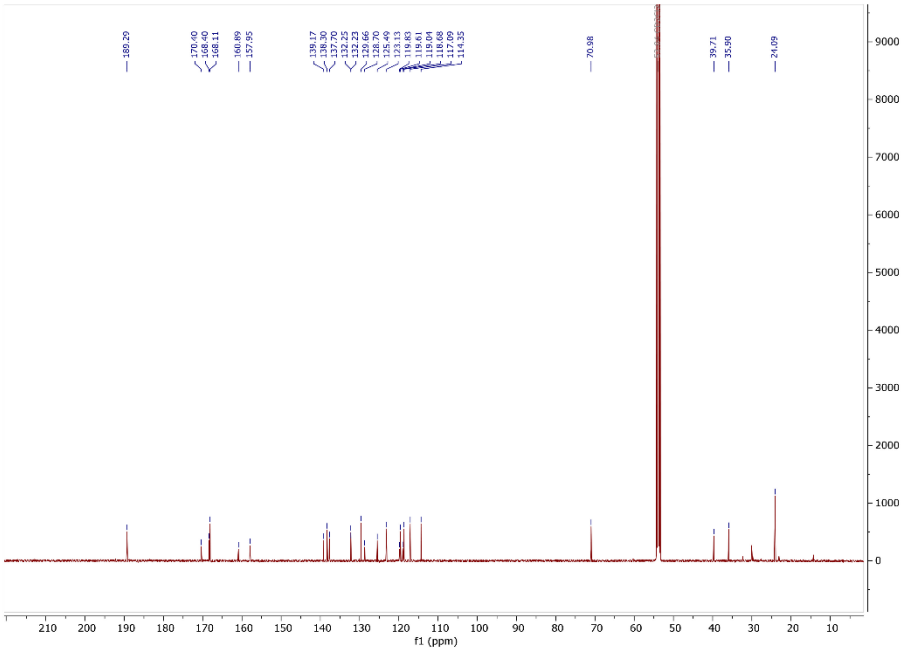

^{1}H and ^{13}C NMR spectra of compound **13**

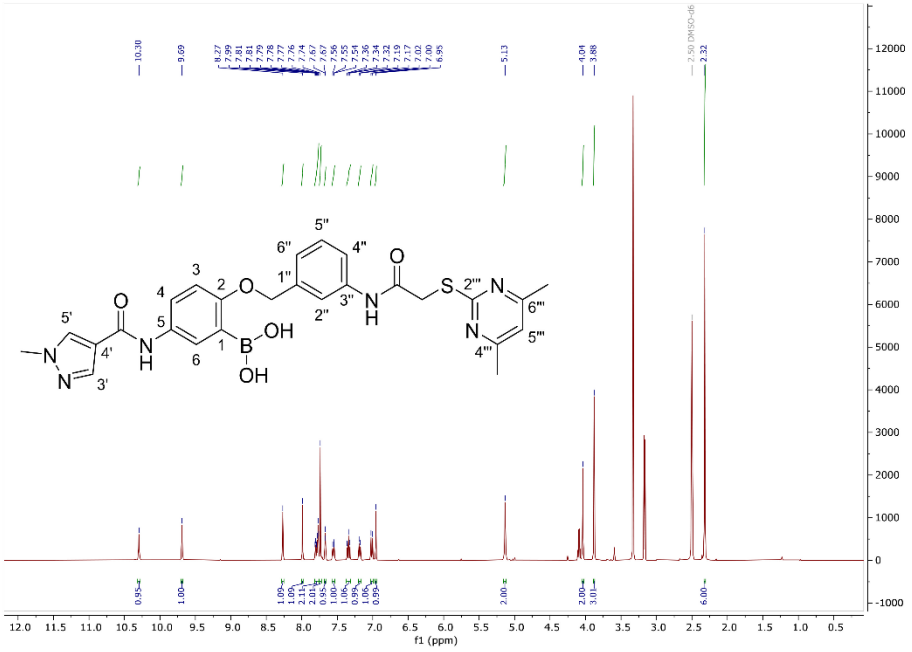

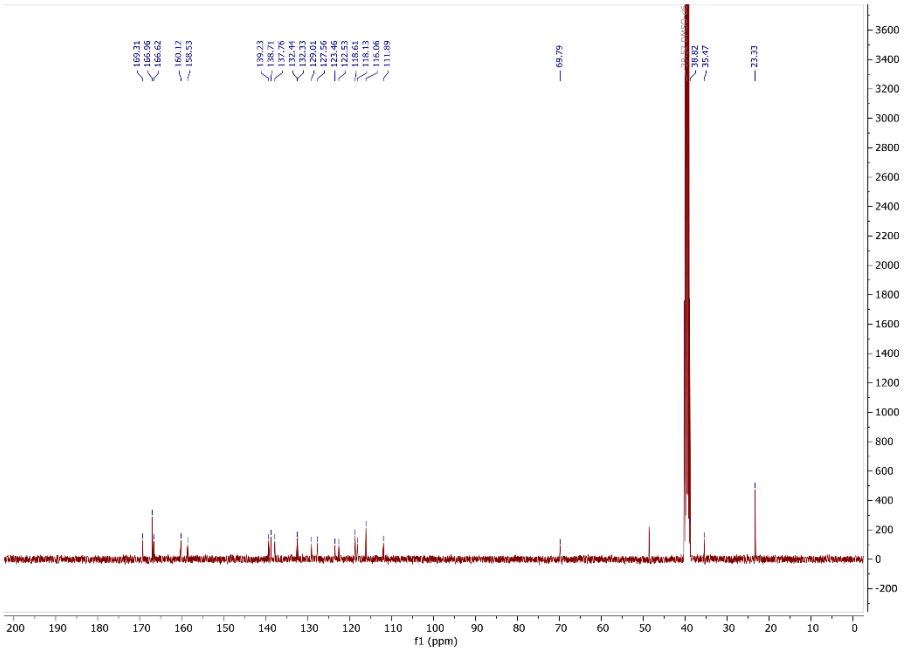

^{1}H and ^{13}C NMR spectra of compound **14**

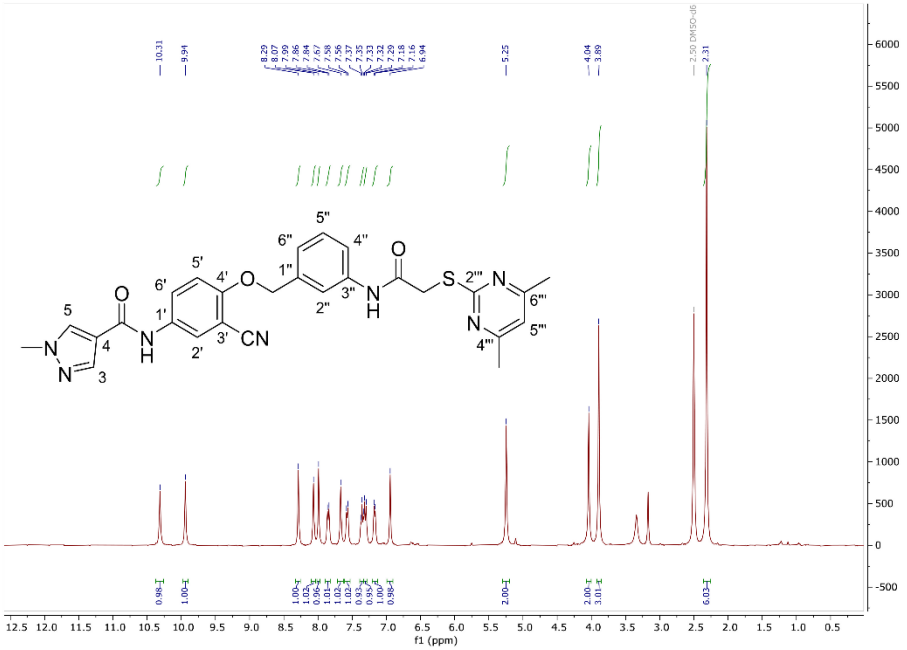

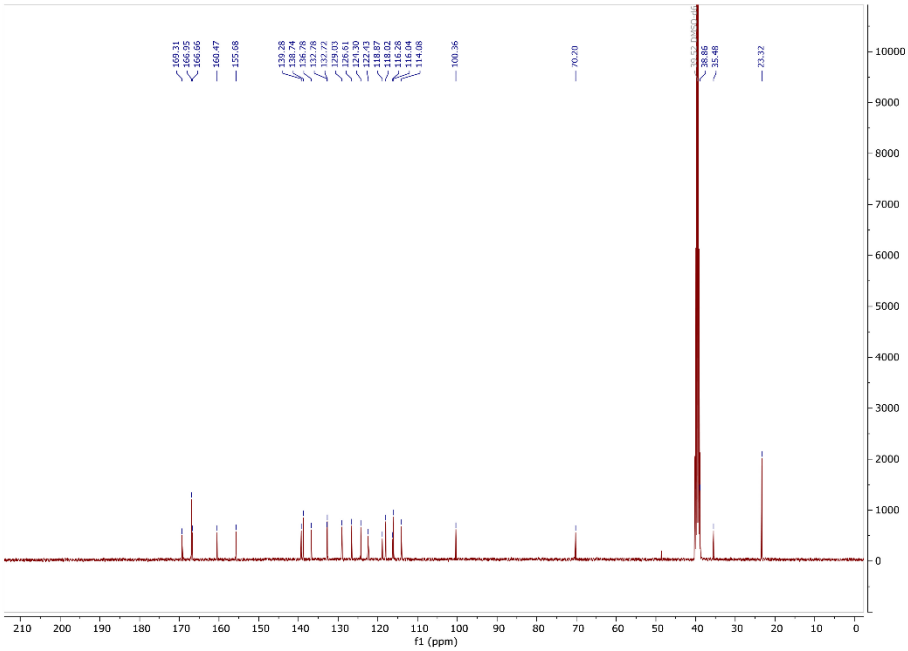

^{1}H and ^{13}C NMR spectra of compound **20**

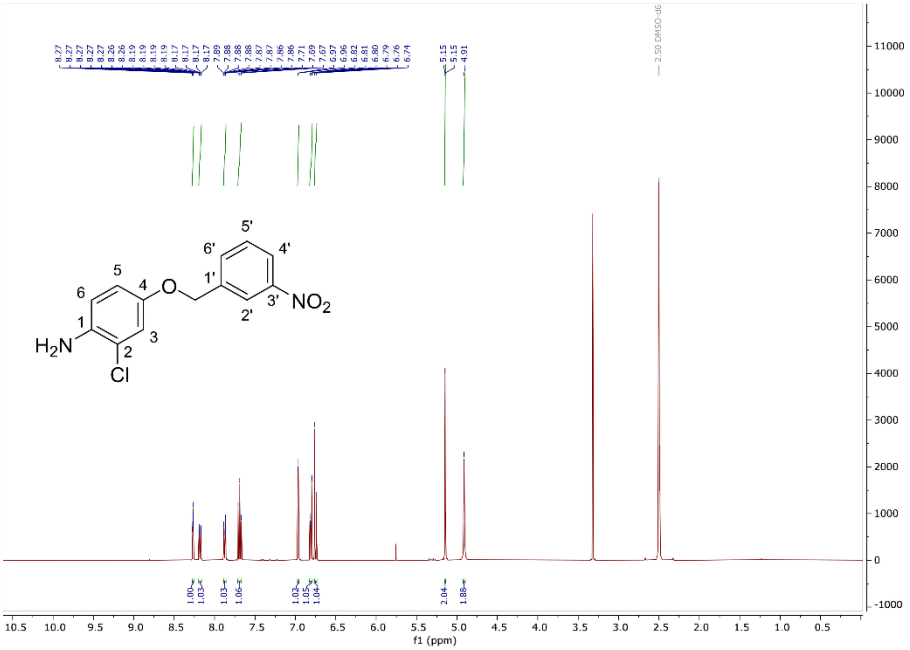

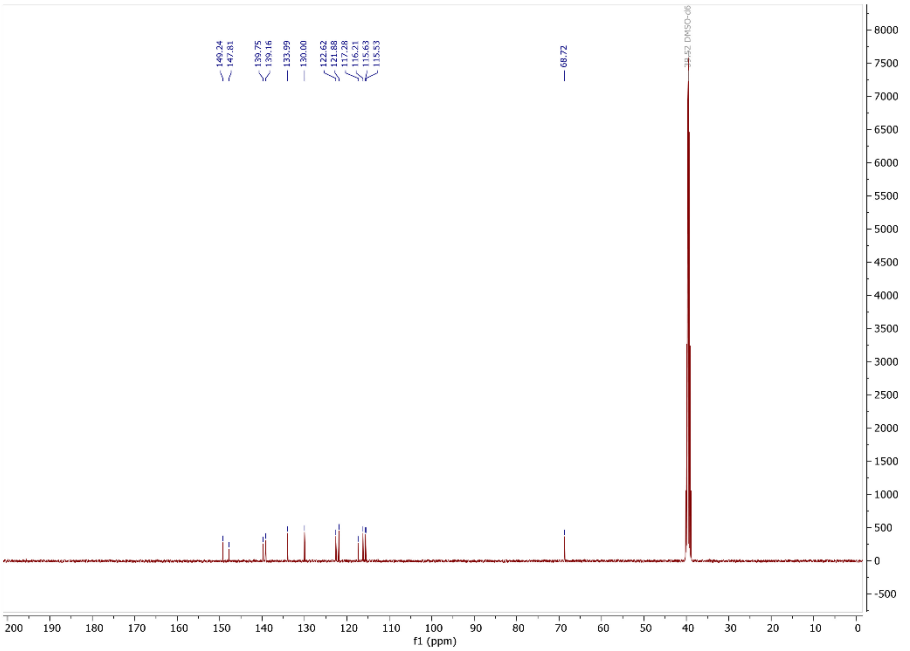

^{1}H and ^{13}C NMR spectra of compound **21**

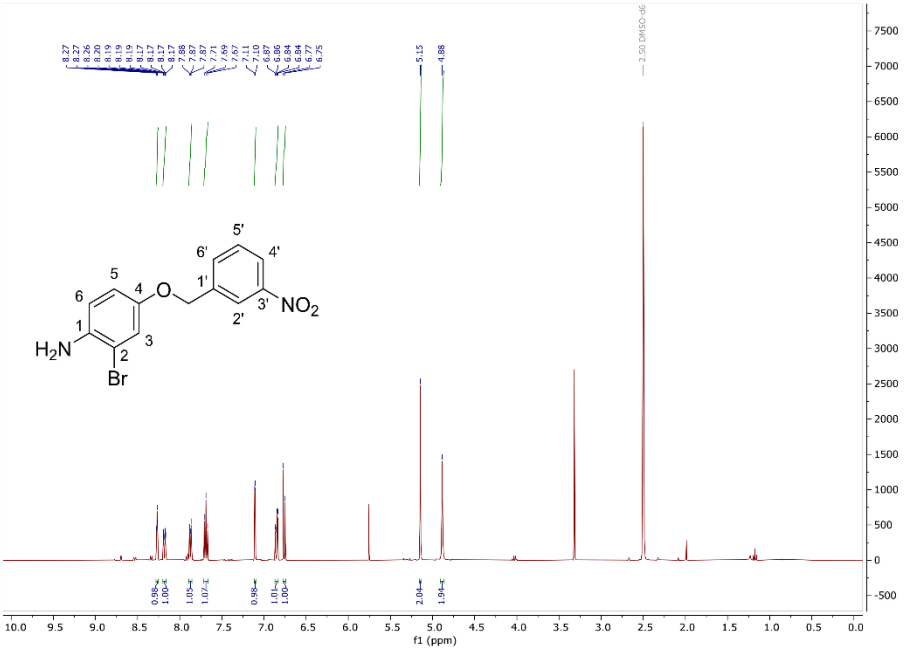

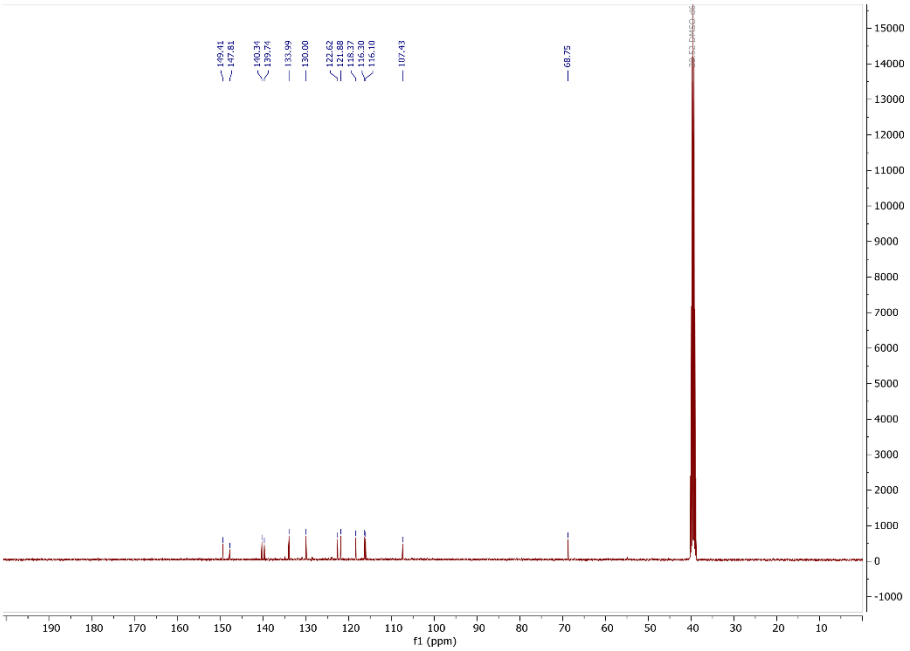

^{1}H and ^{13}C NMR spectra of compound **22**

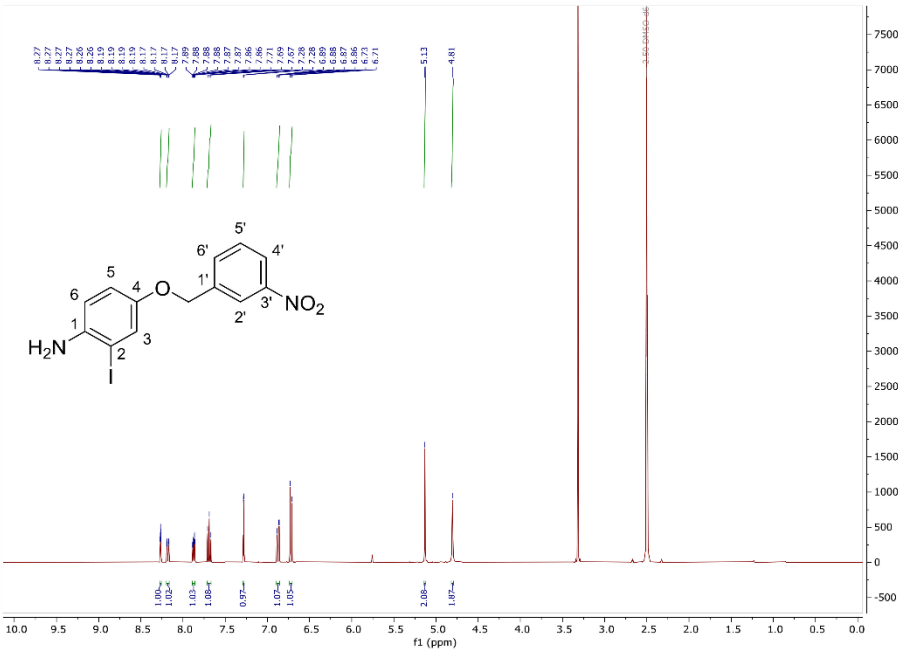

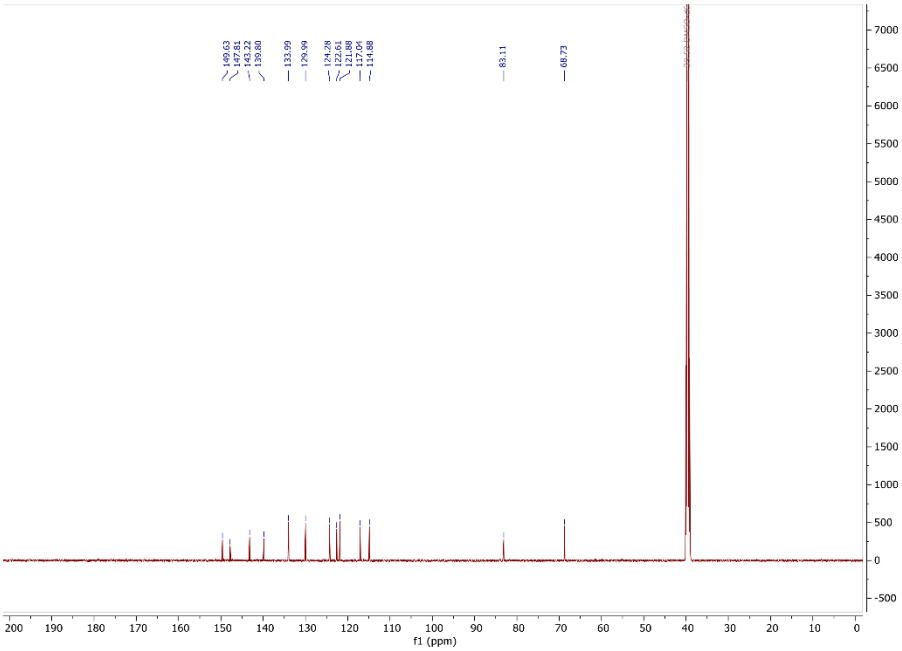

^{1}H and ^{13}C NMR spectra of compound **23**

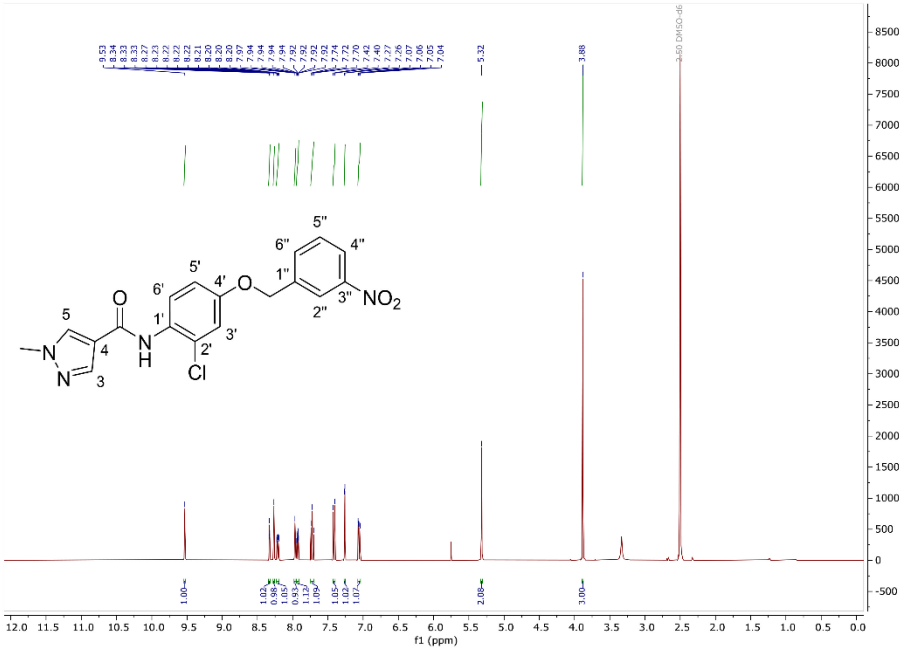

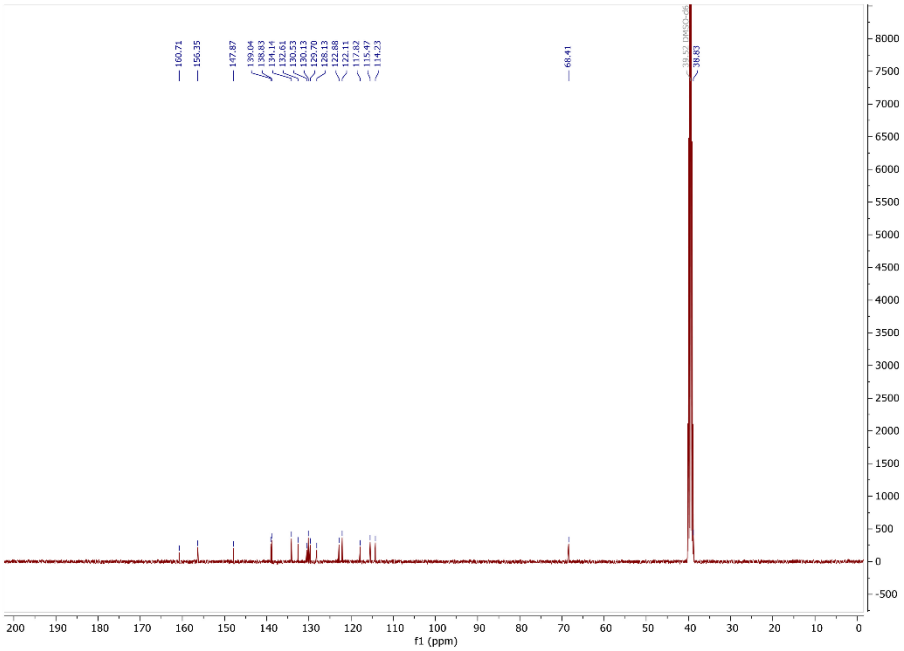

^{1}H and ^{13}C NMR spectra of compound **24**

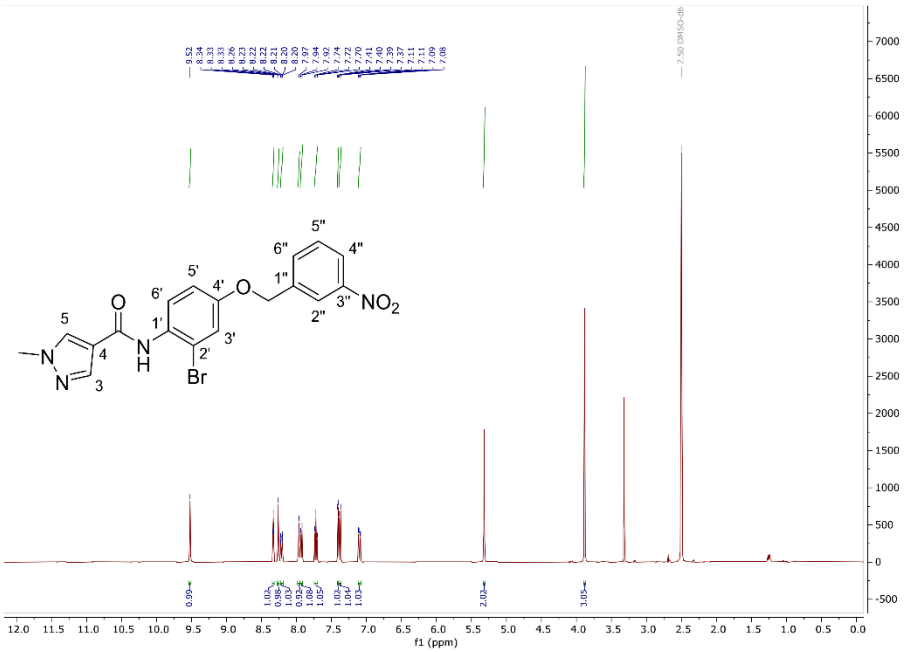

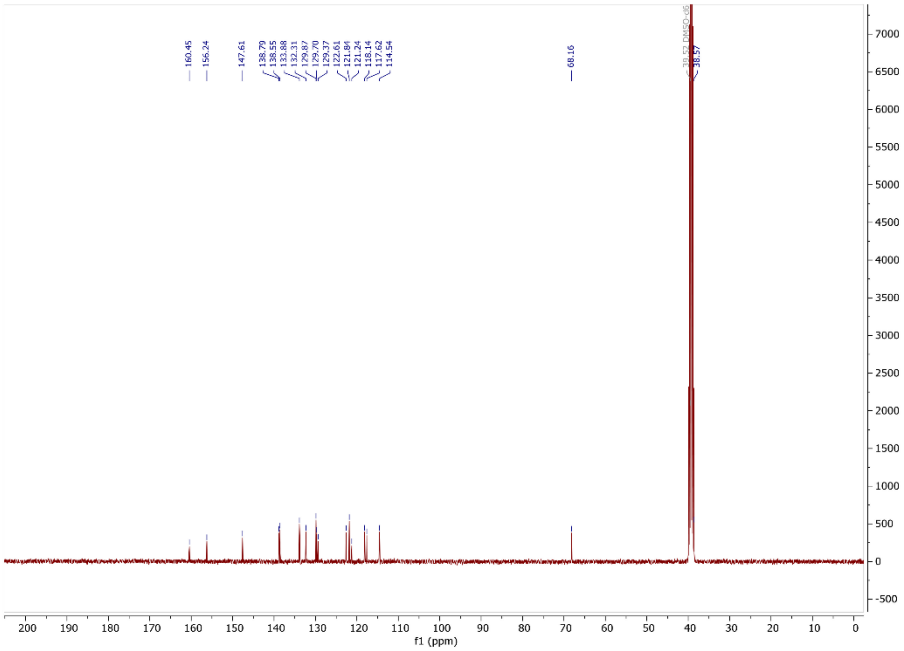

^{1}H and ^{13}C NMR spectra of compound **25**

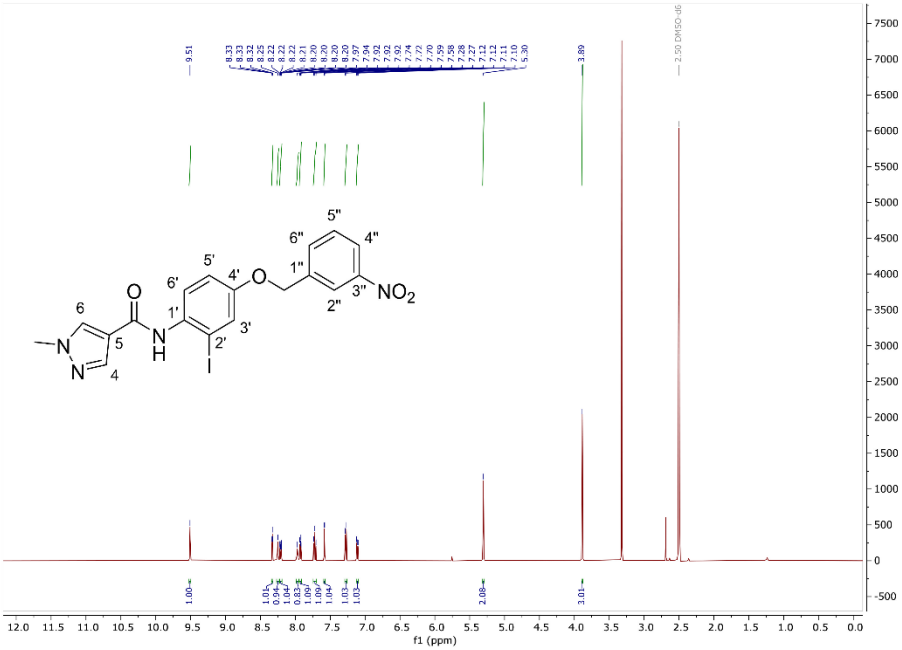

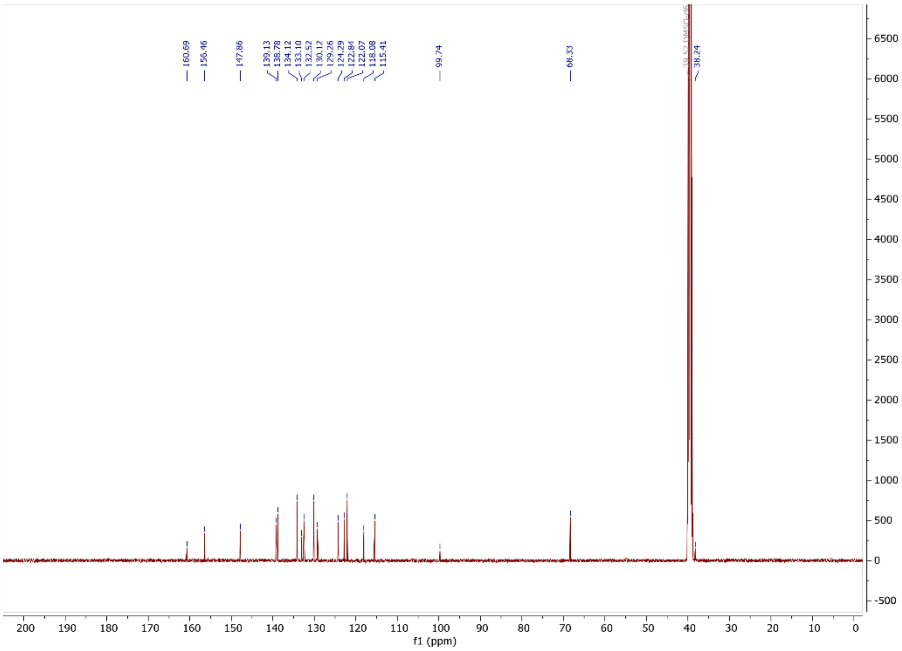

^{1}H and ^{13}C NMR spectra of compound **26**

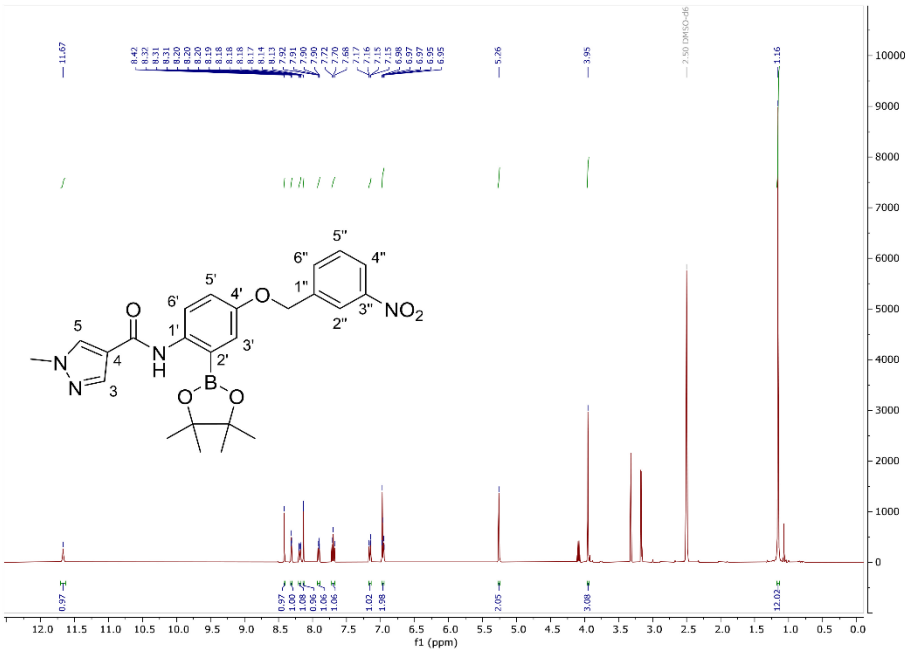

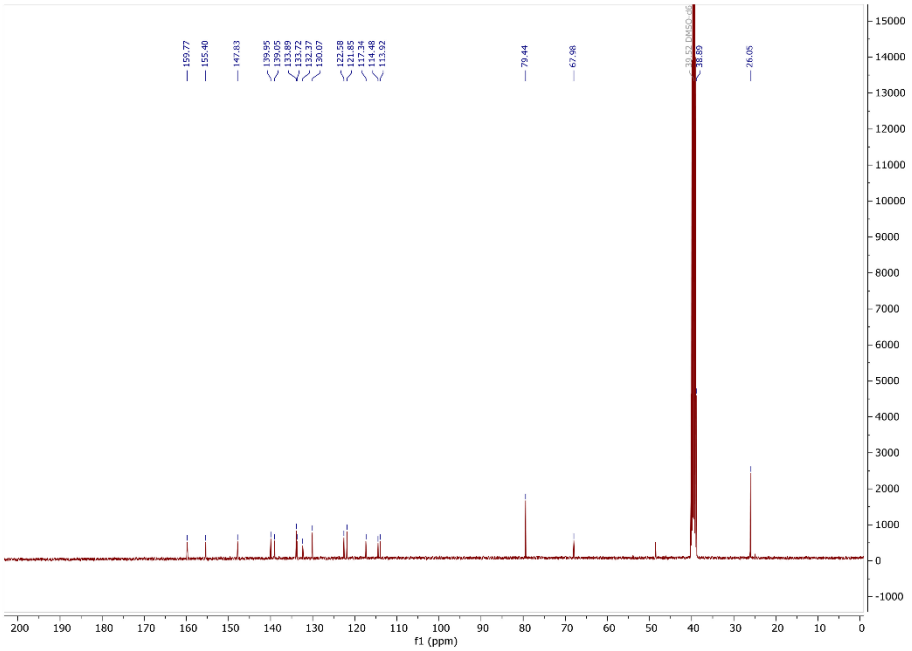

^{1}H and ^{13}C NMR spectra of compound **27**

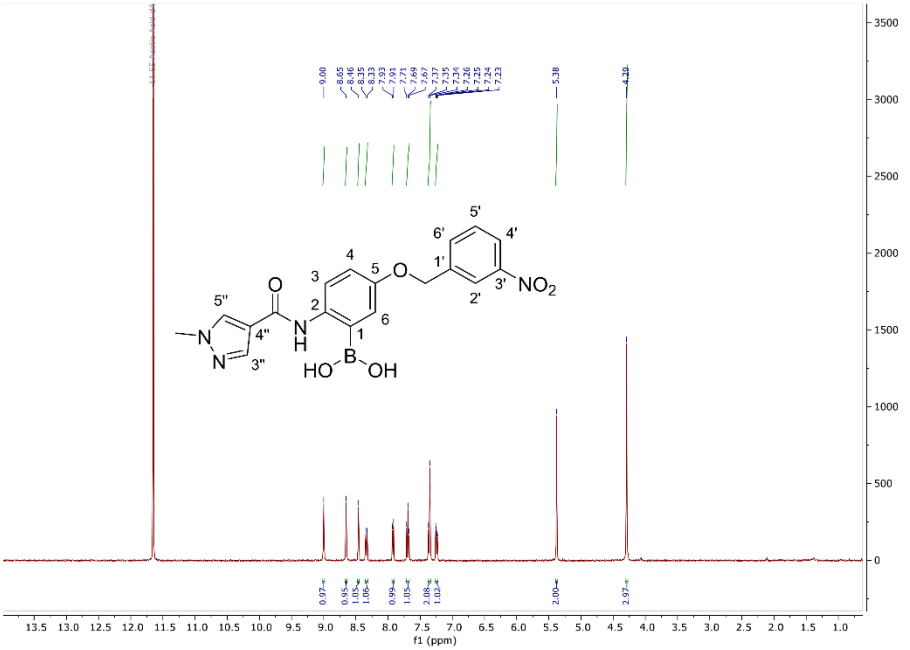

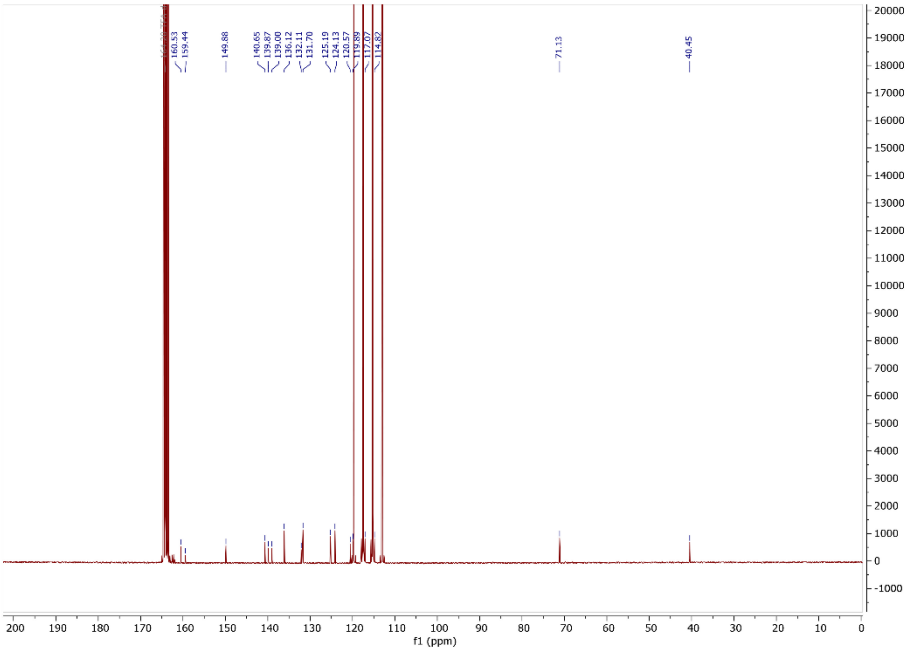

^{1}H and ^{13}C NMR spectra of compound **28**

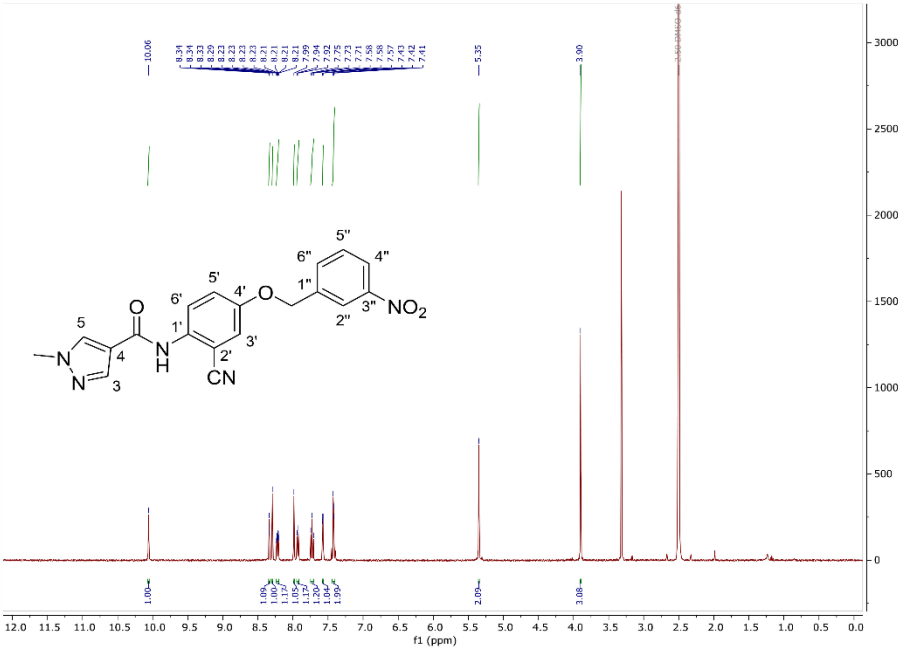

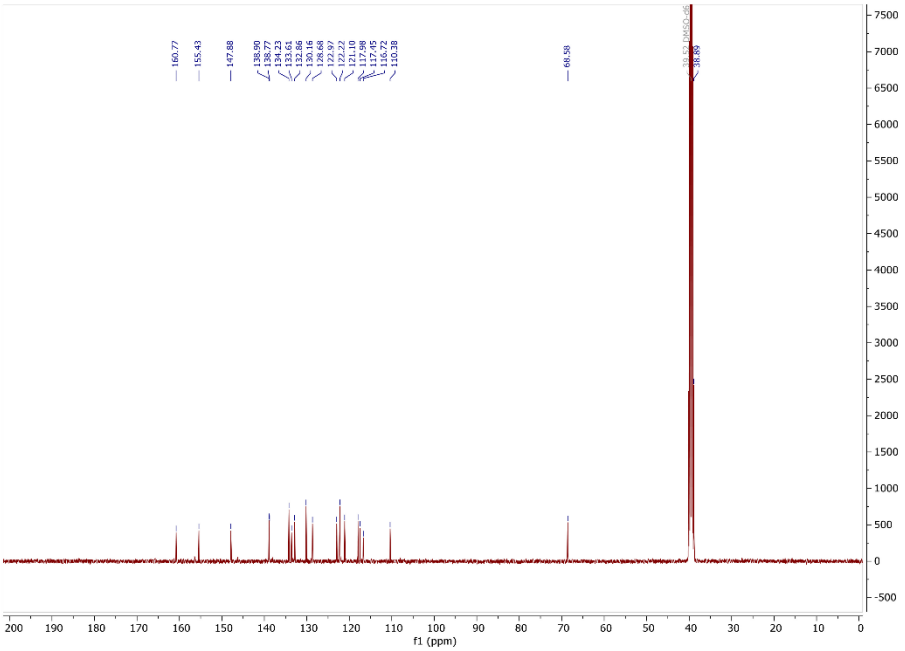

^{1}H and ^{13}C NMR spectra of compound **29**

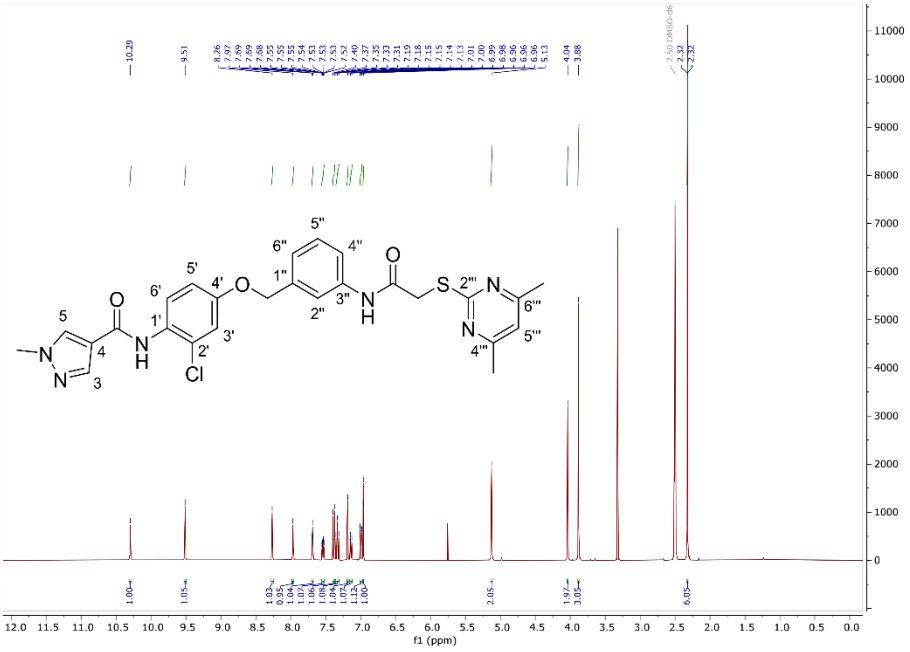

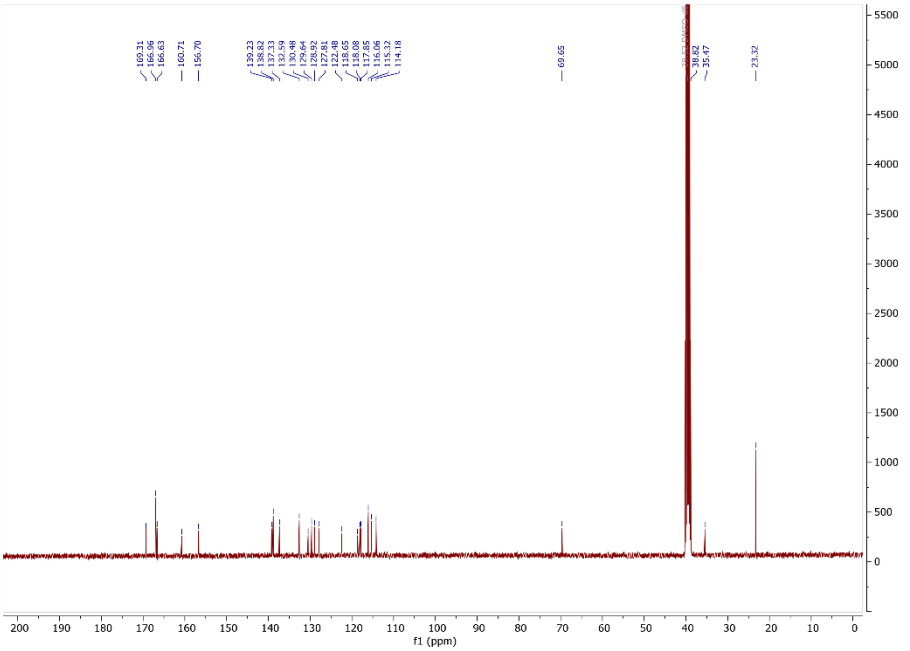

^{1}H and ^{13}C NMR spectra of compound **30**

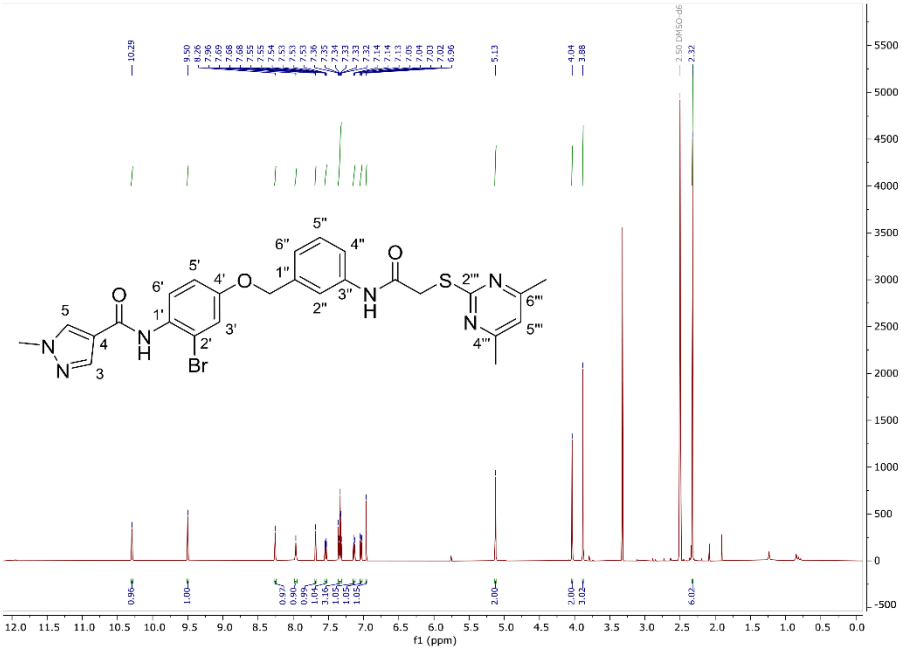

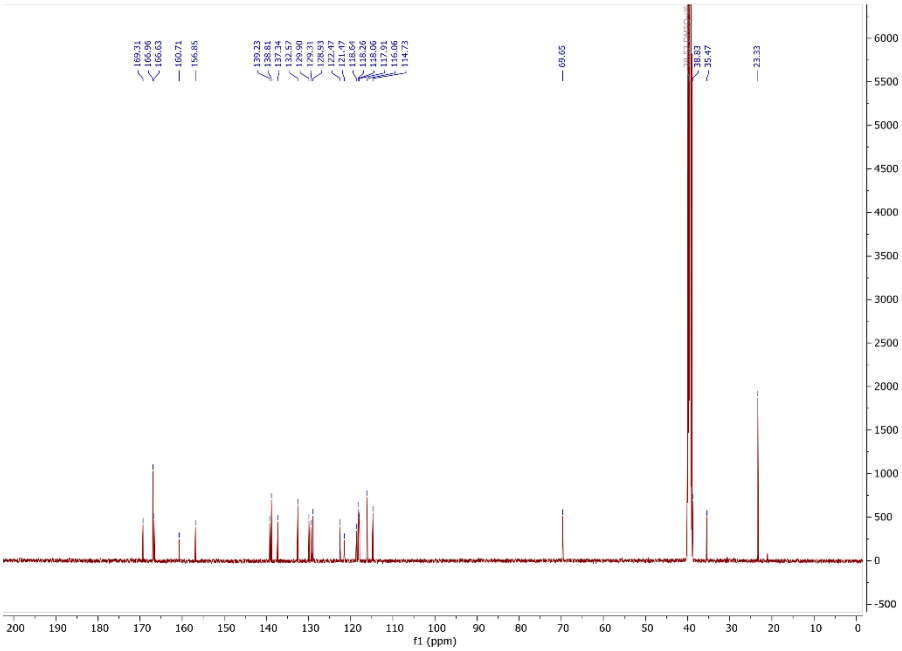

^{1}H and ^{13}C NMR spectra of compound **31**

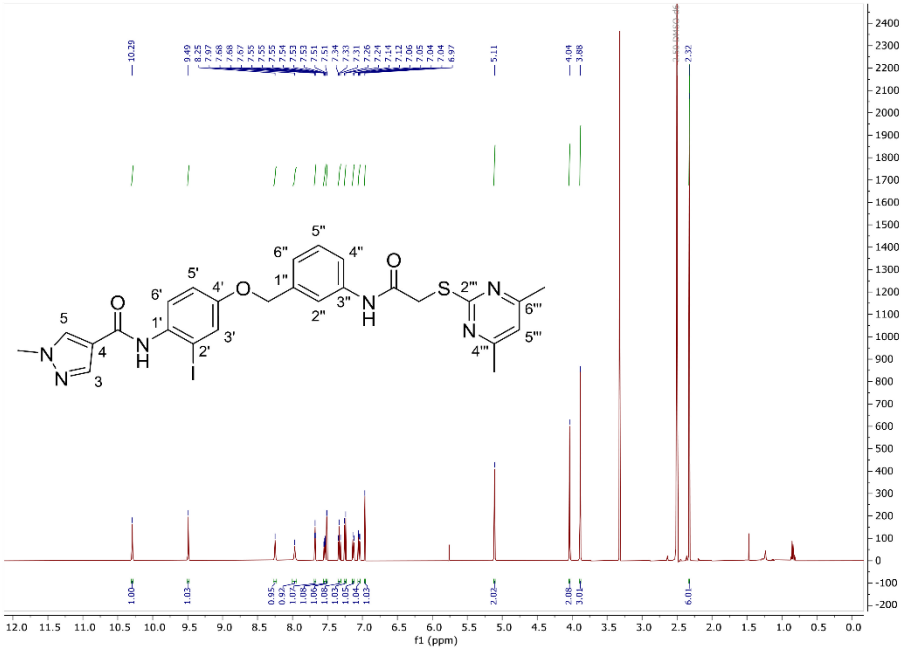

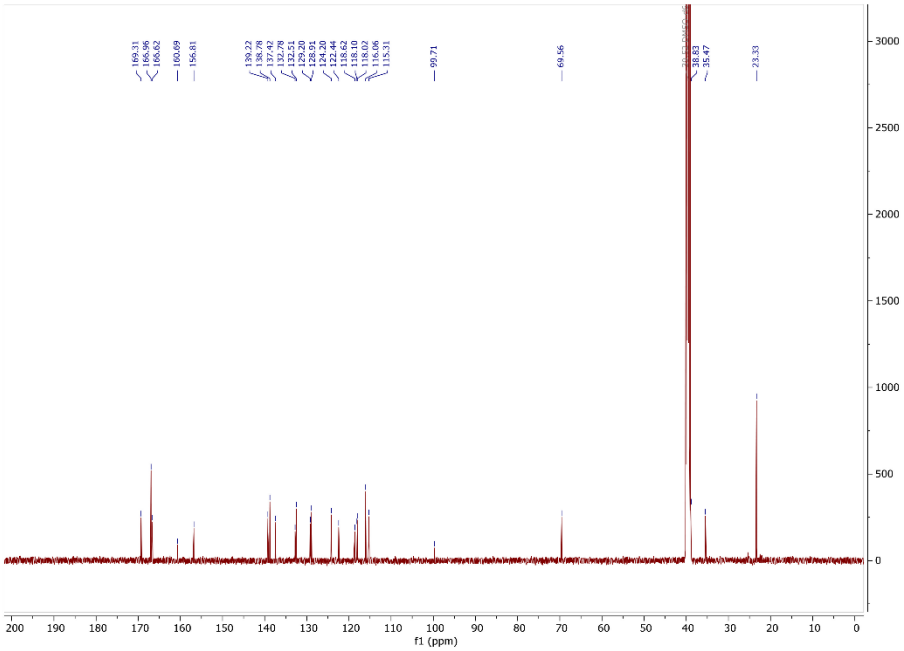

^{1}H and ^{13}C NMR spectra of compound **32**

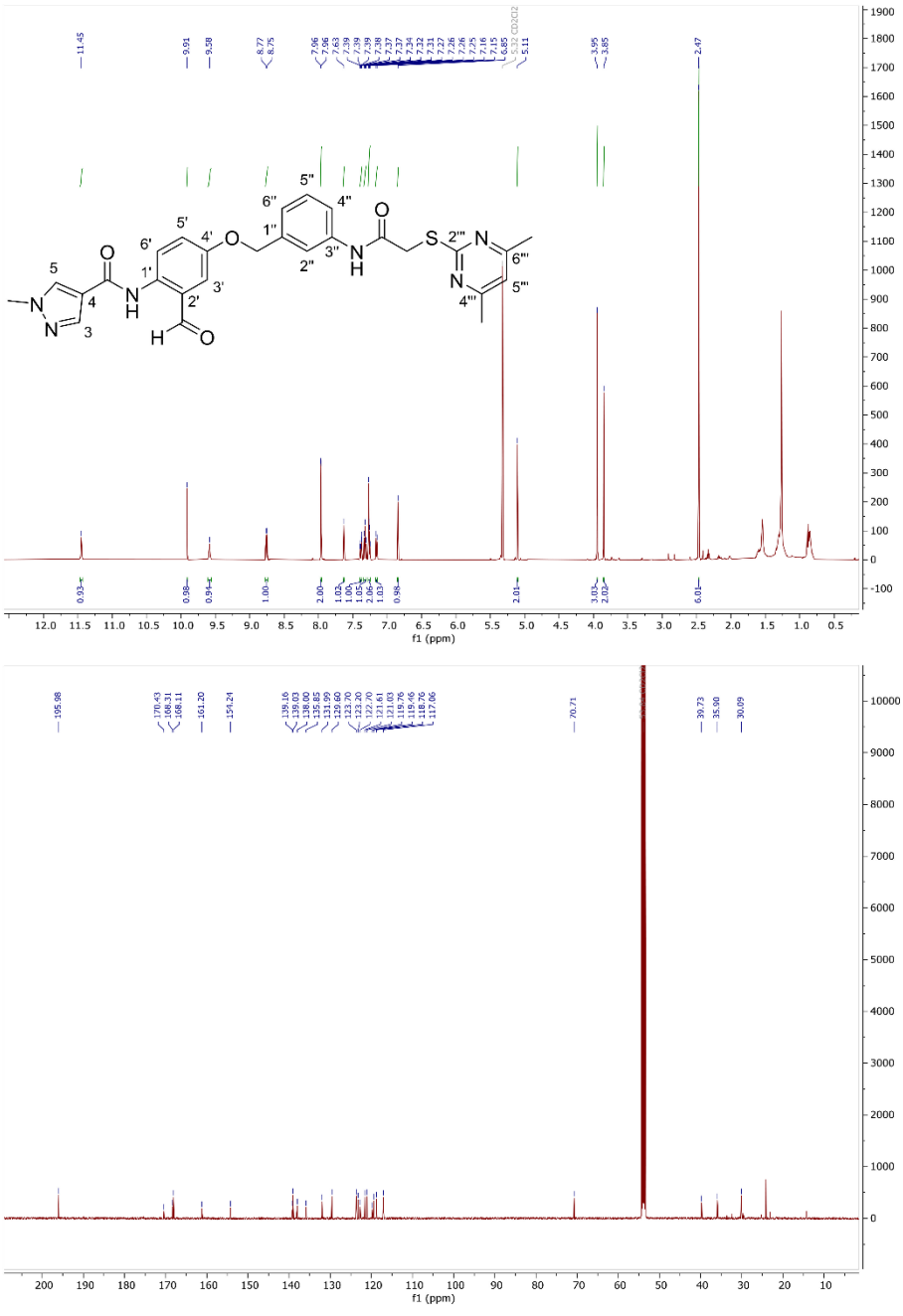

^{1}H and ^{13}C NMR spectra of compound **33**

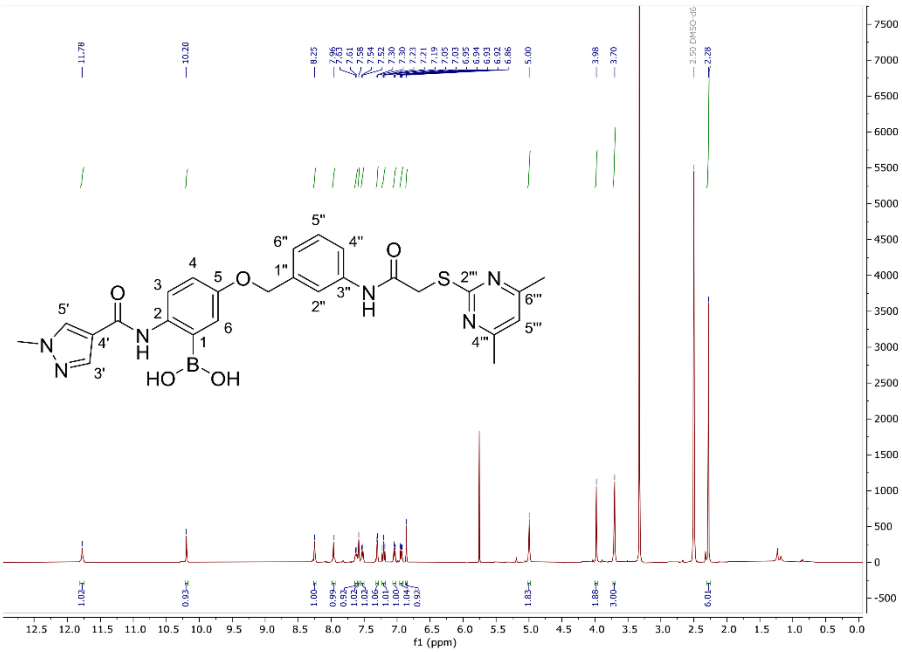

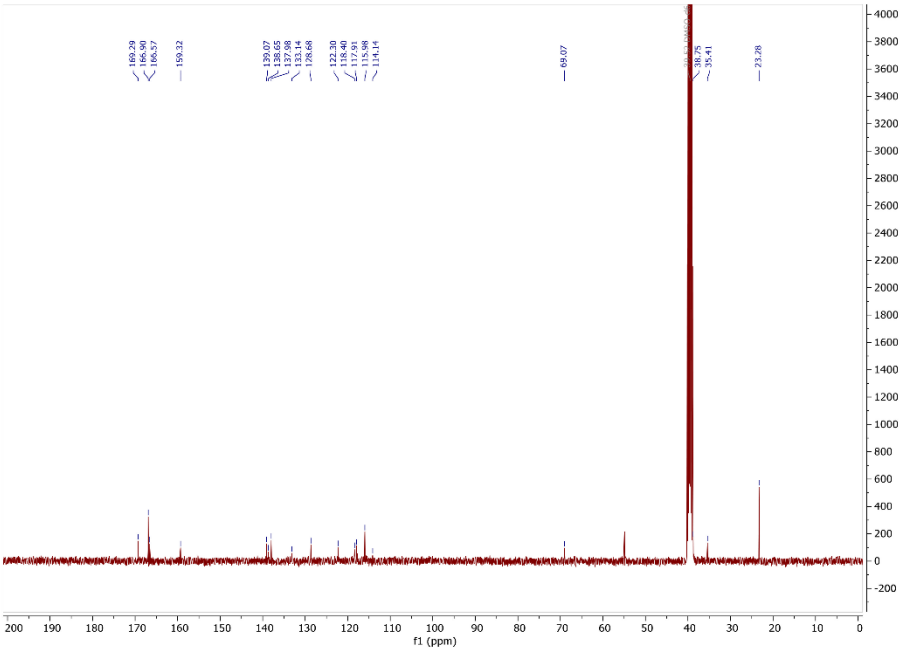

^{1}H and ^{13}C NMR spectra of compound **34**

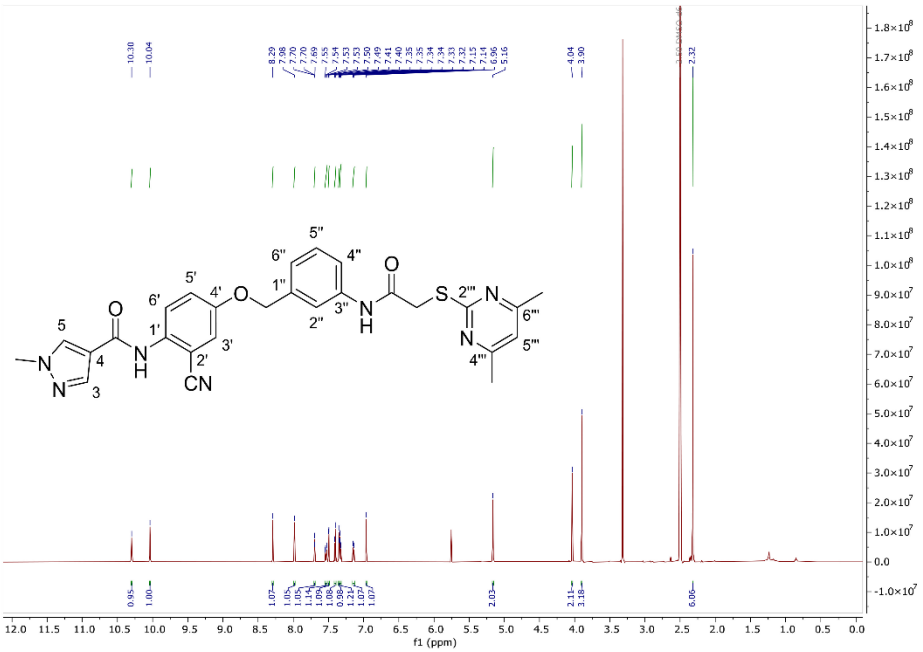

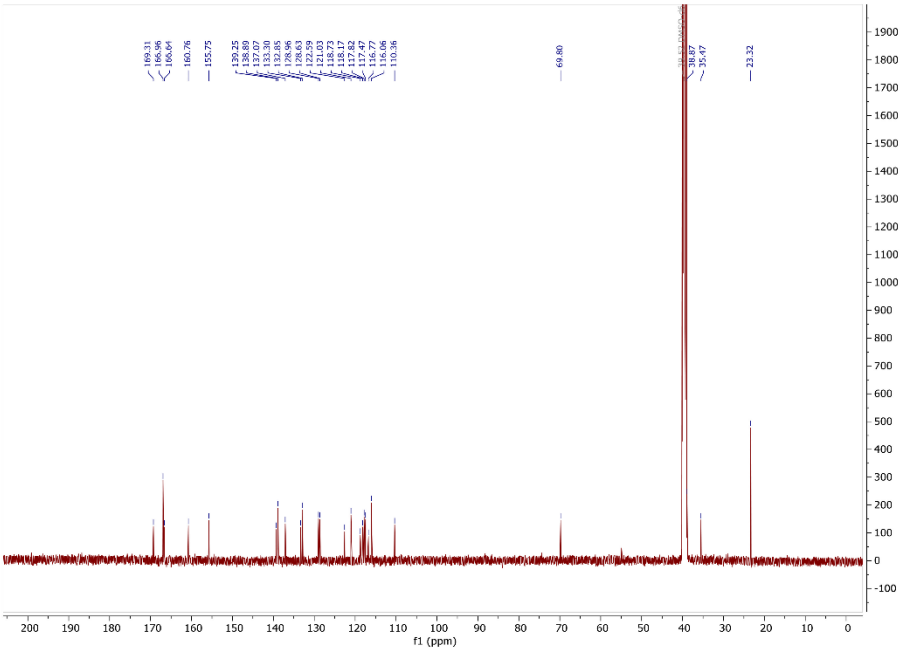

^{1}H and ^{13}C NMR spectra of compound **39**

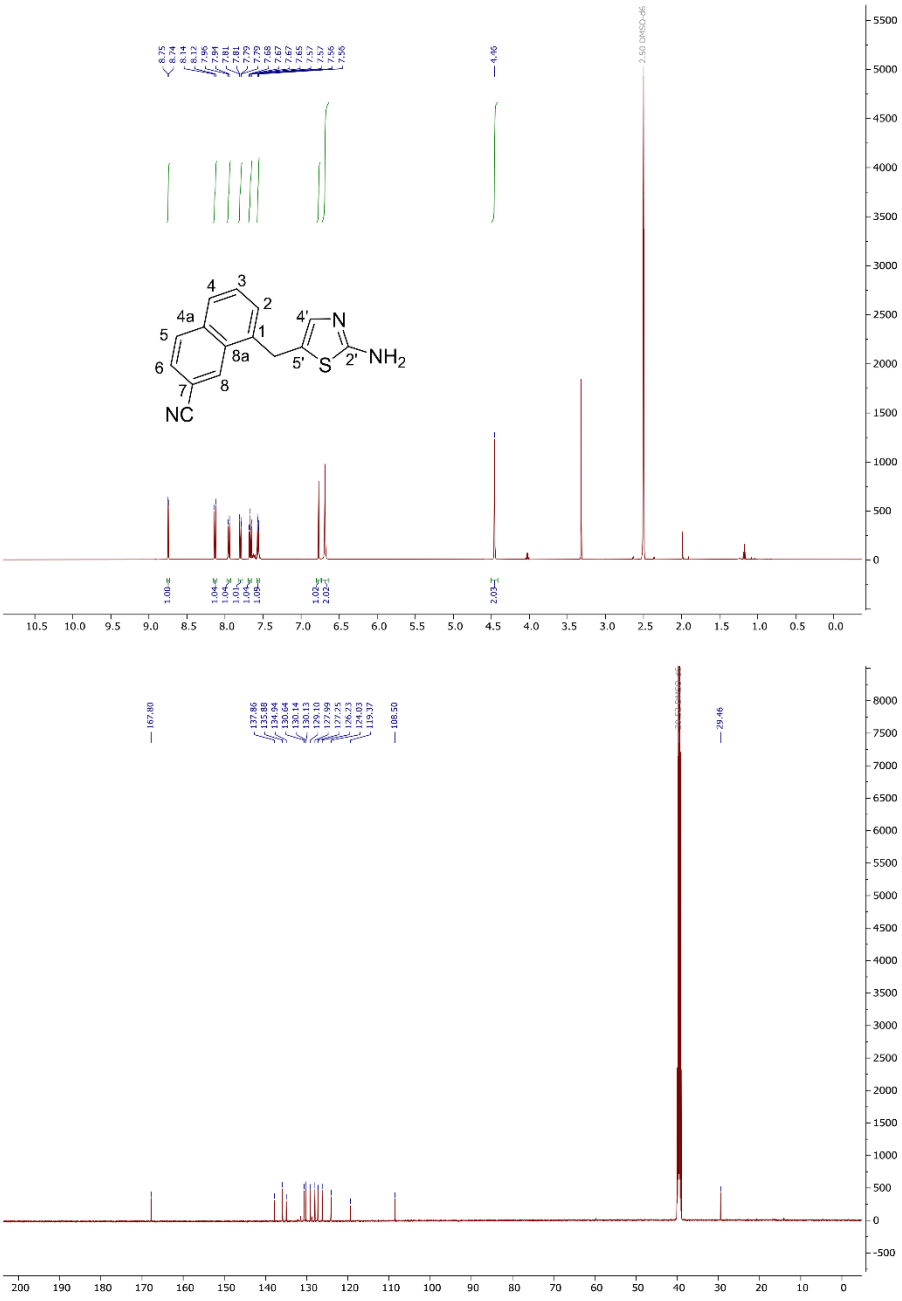

^{1}H and ^{13}C NMR spectra of compound **40**

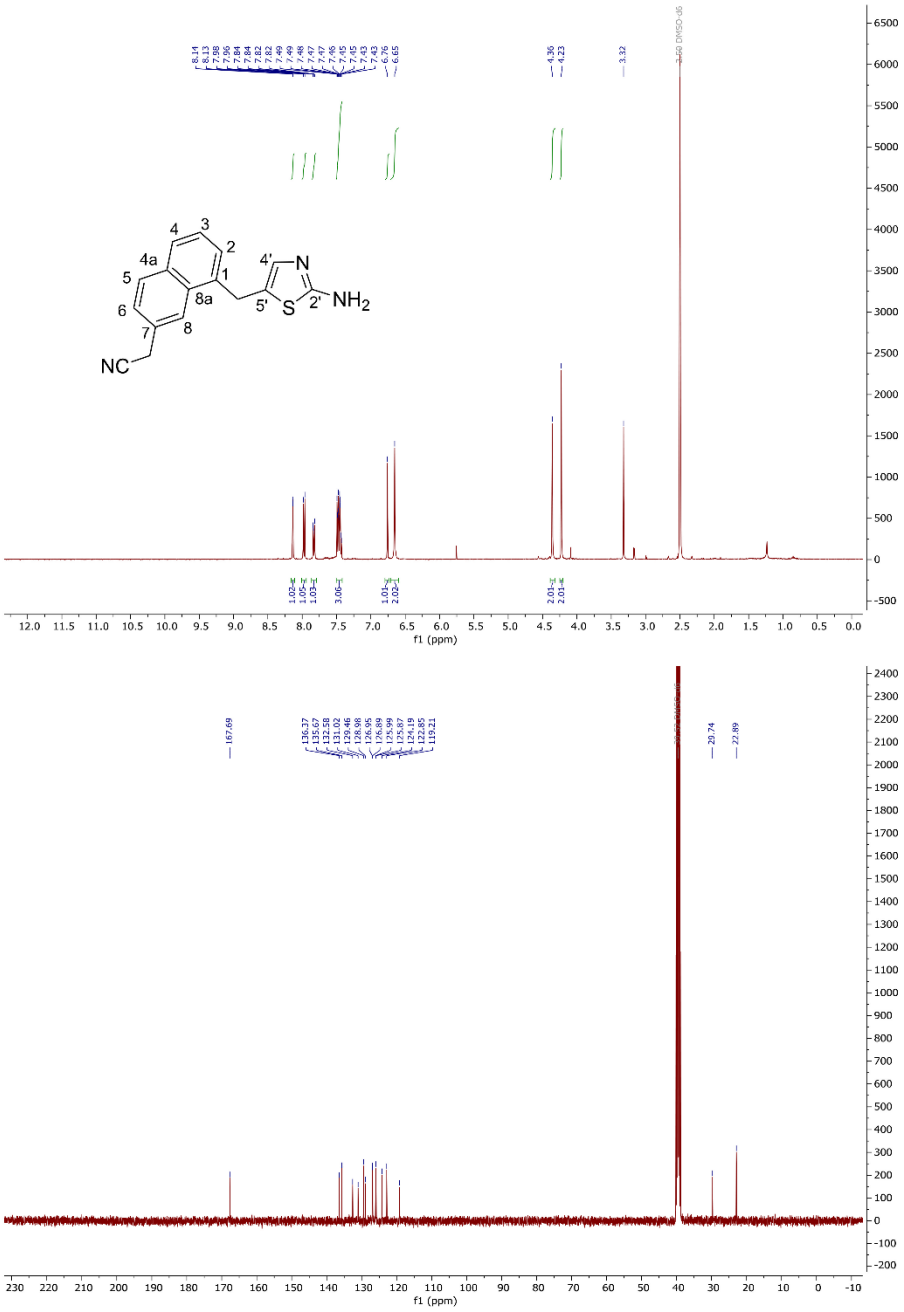

^{1}H and ^{13}C NMR spectra of compound **41**

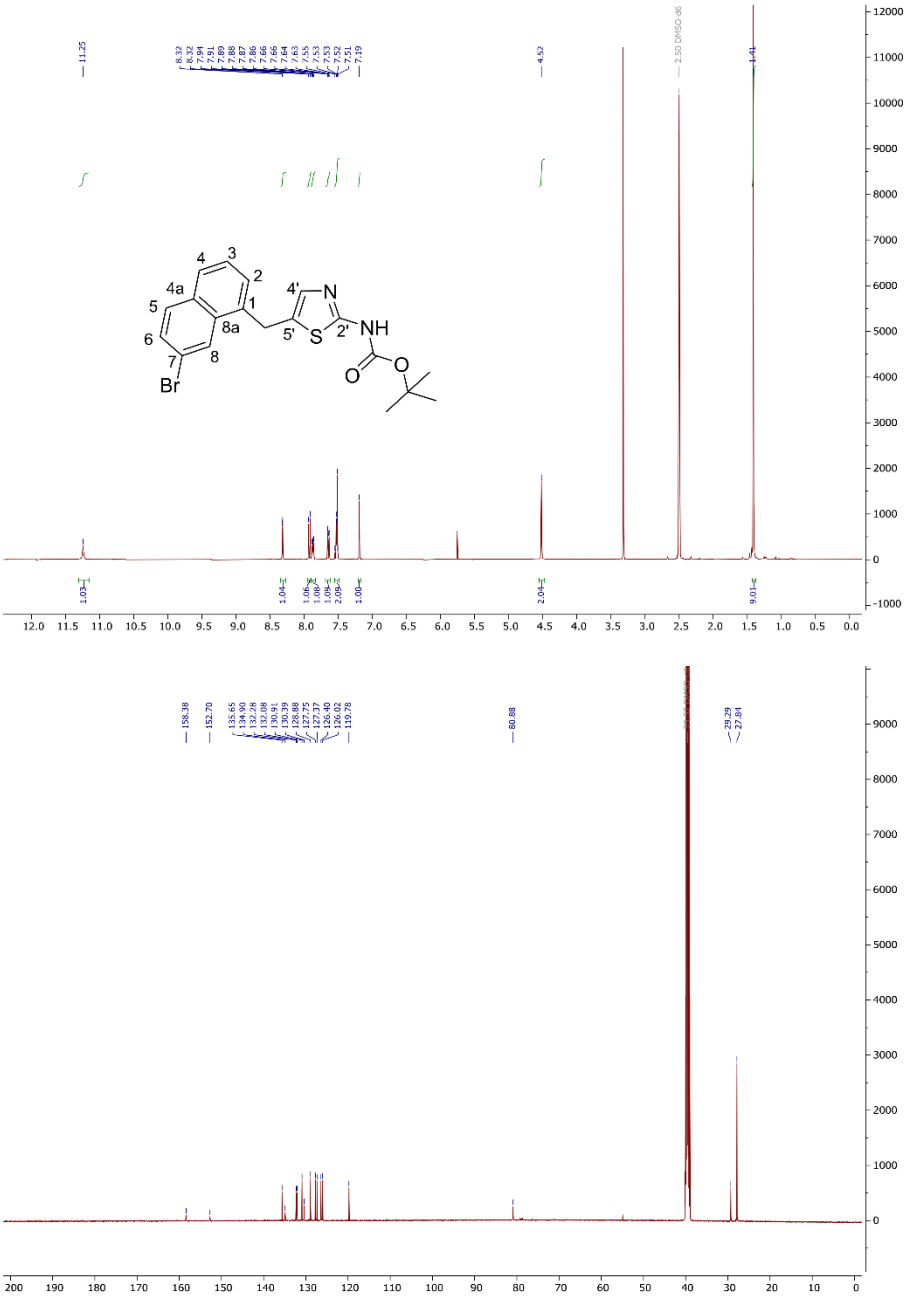

^{1}H and ^{13}C NMR spectra of compound **42**

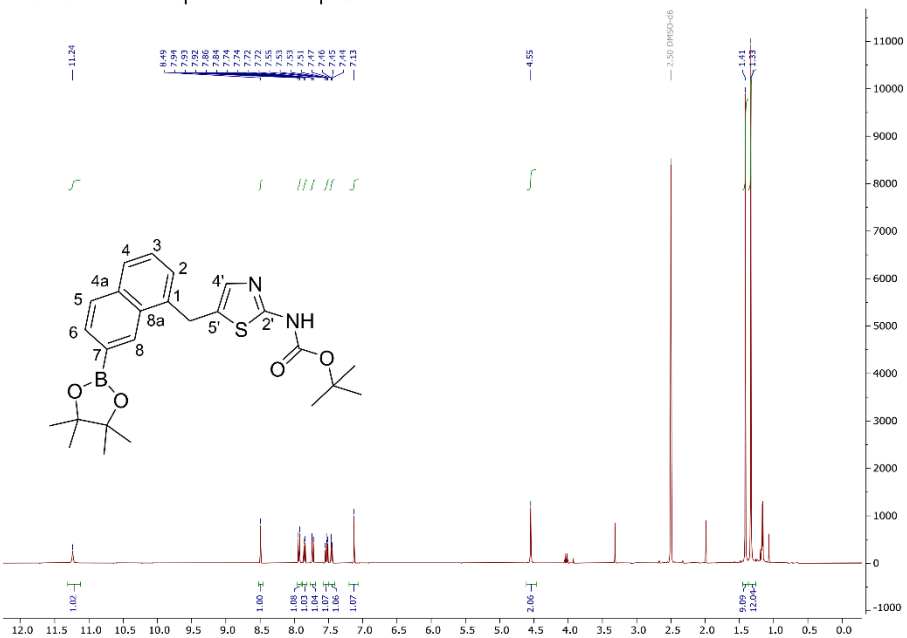

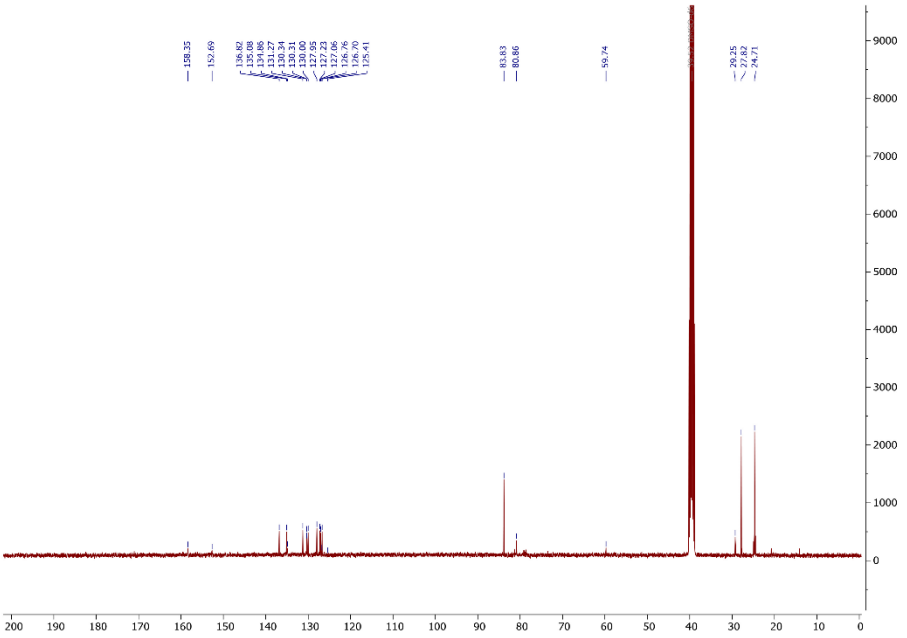

^{1}H and ^{13}C NMR spectra of compound **43**

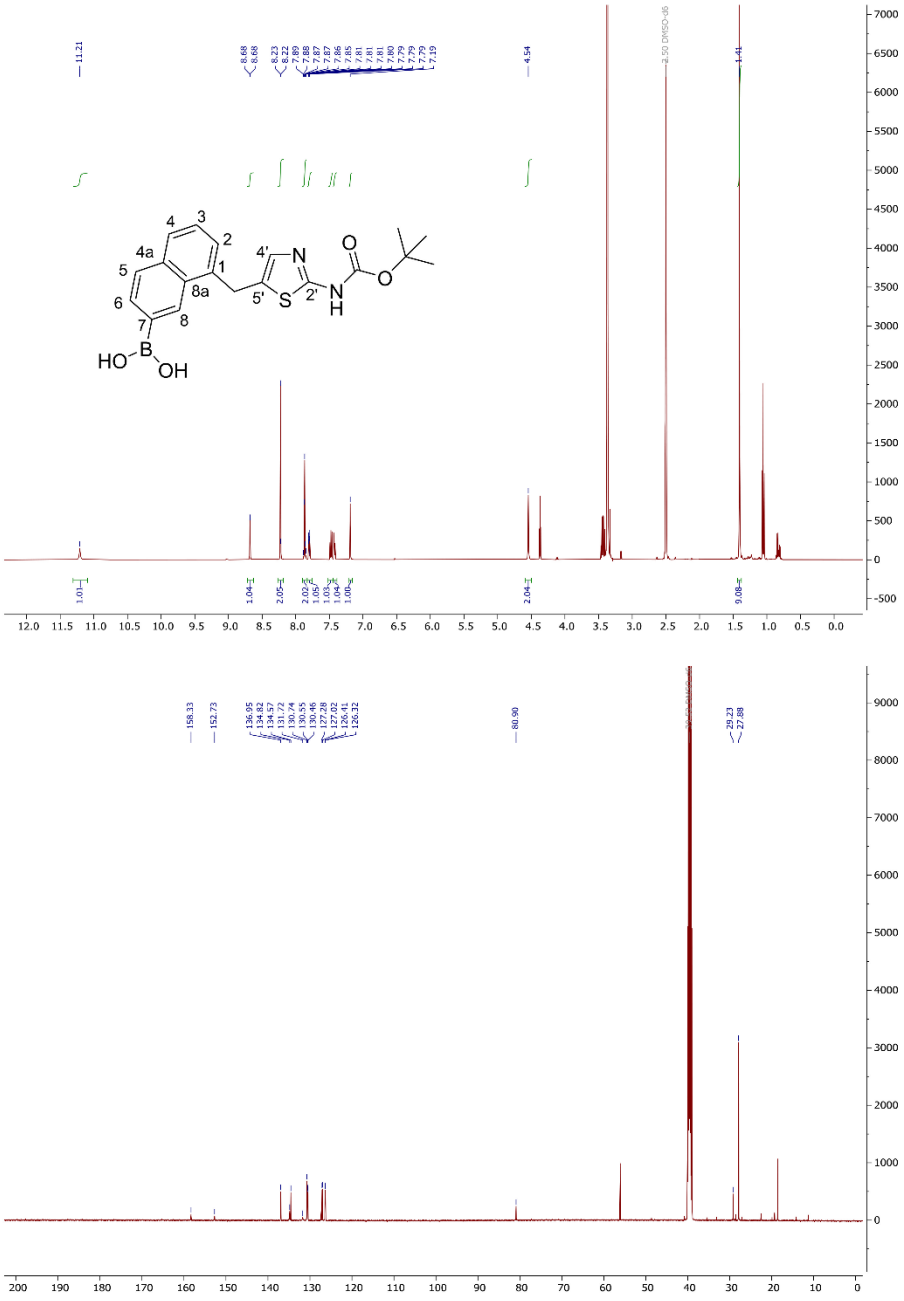

^{1}H and ^{13}C NMR spectra of compound **44**

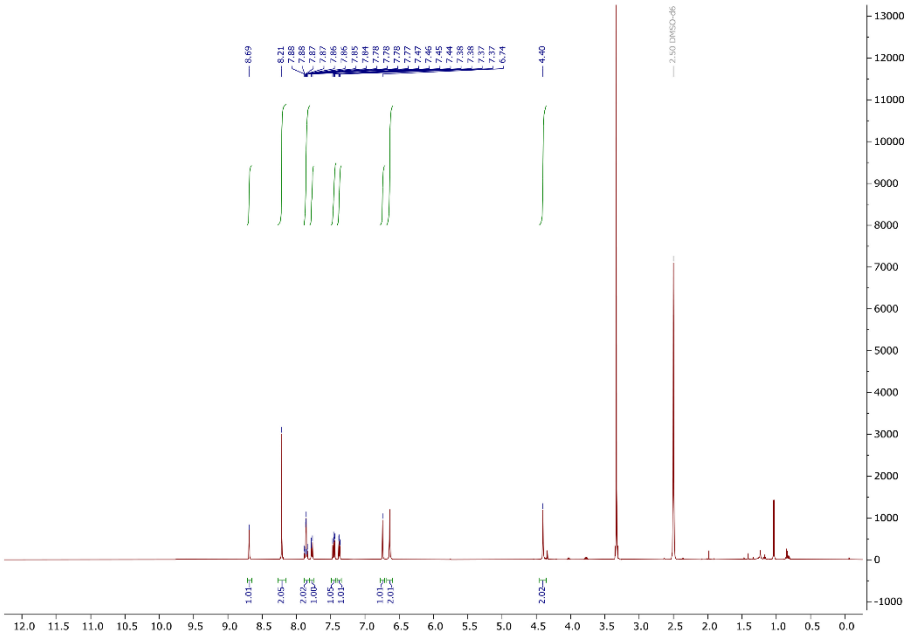

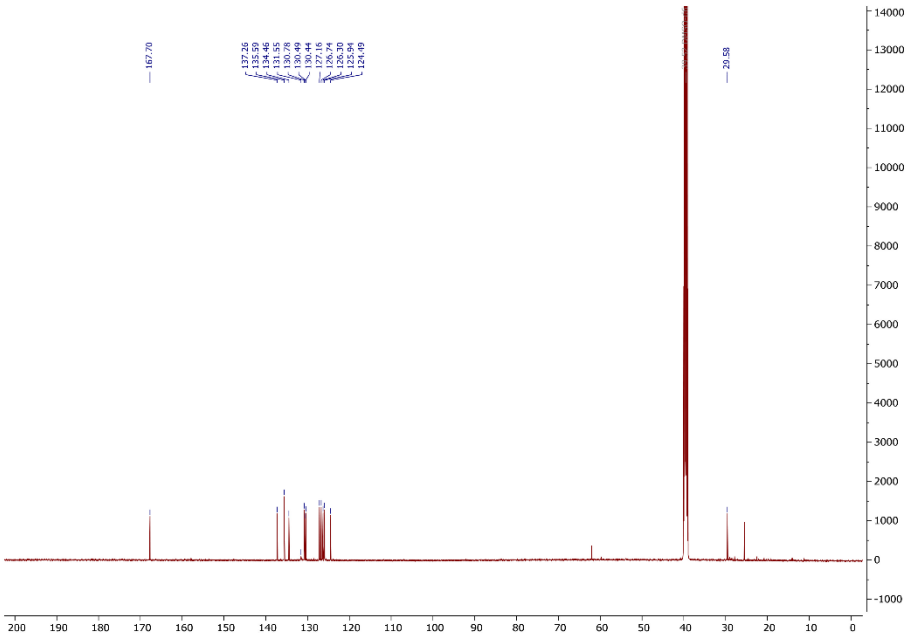

^{1}H and ^{13}C NMR spectra of compound **46**

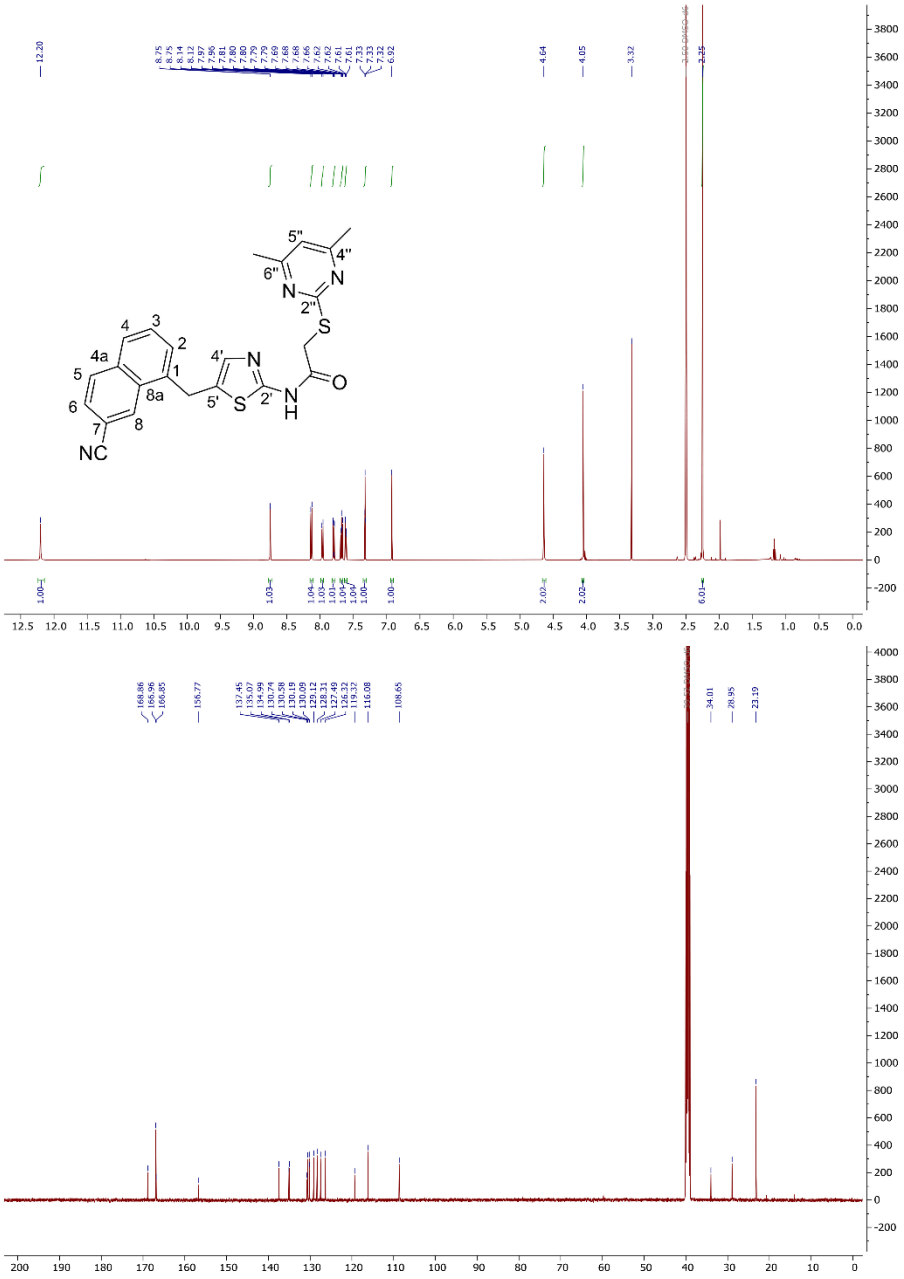

^{1}H and ^{13}C NMR spectra of compound **47**

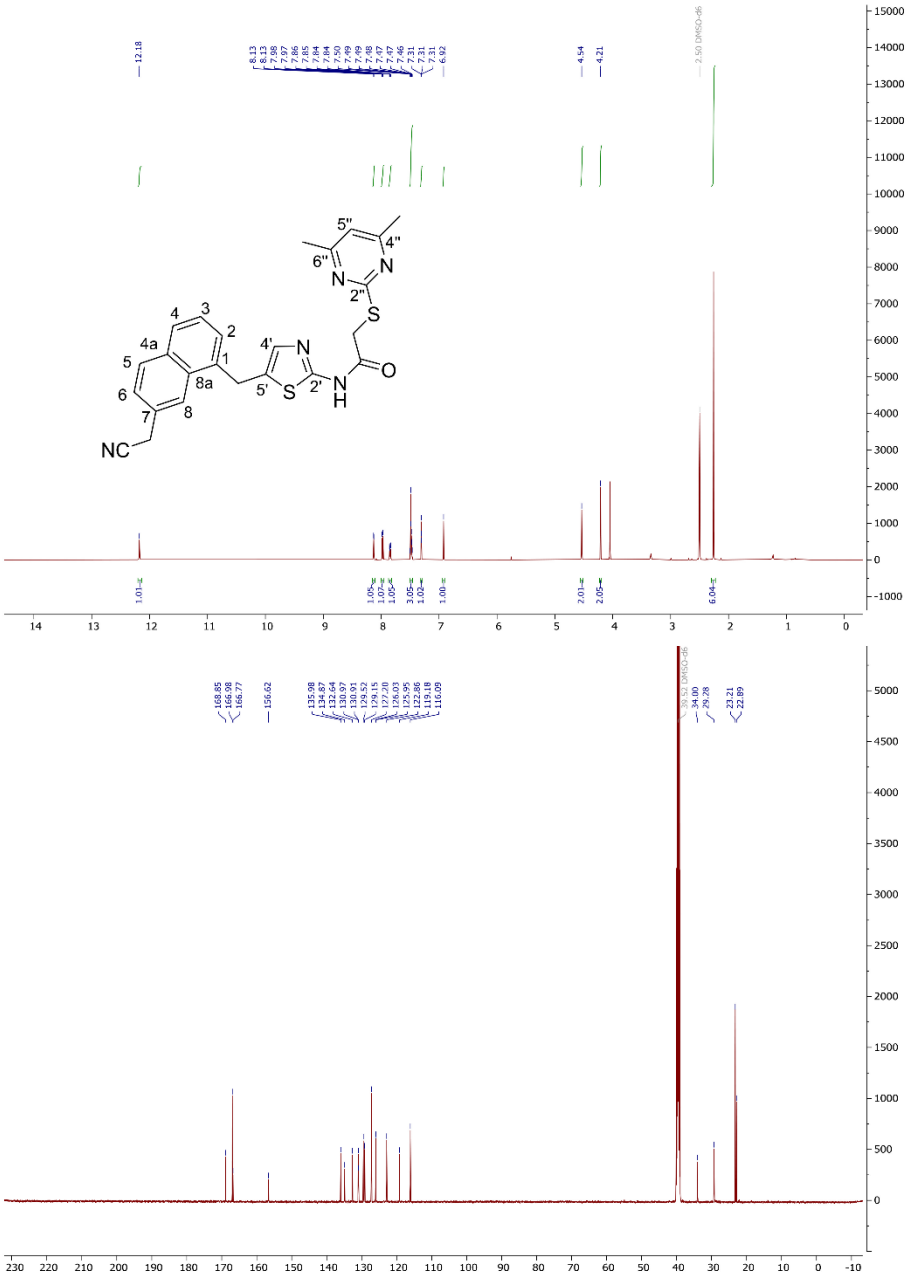

^{1}H and ^{13}C NMR spectra of compound **48**

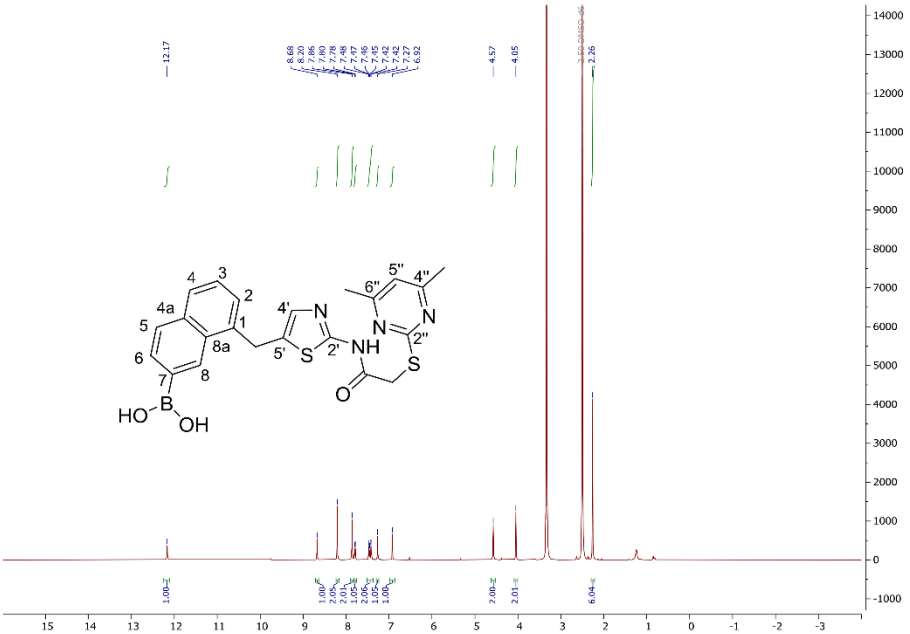

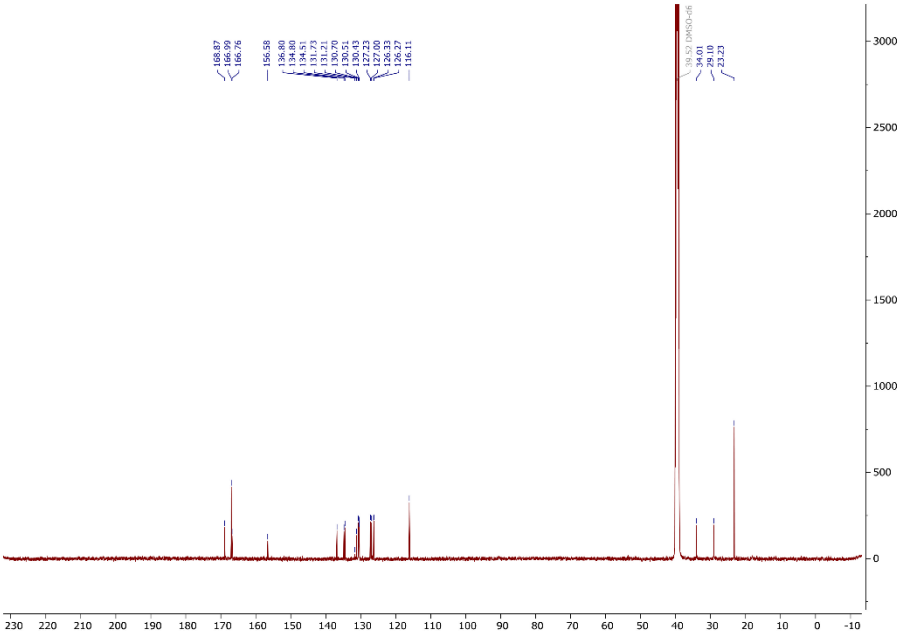

^{1}H and ^{13}C NMR spectra of compound **49**

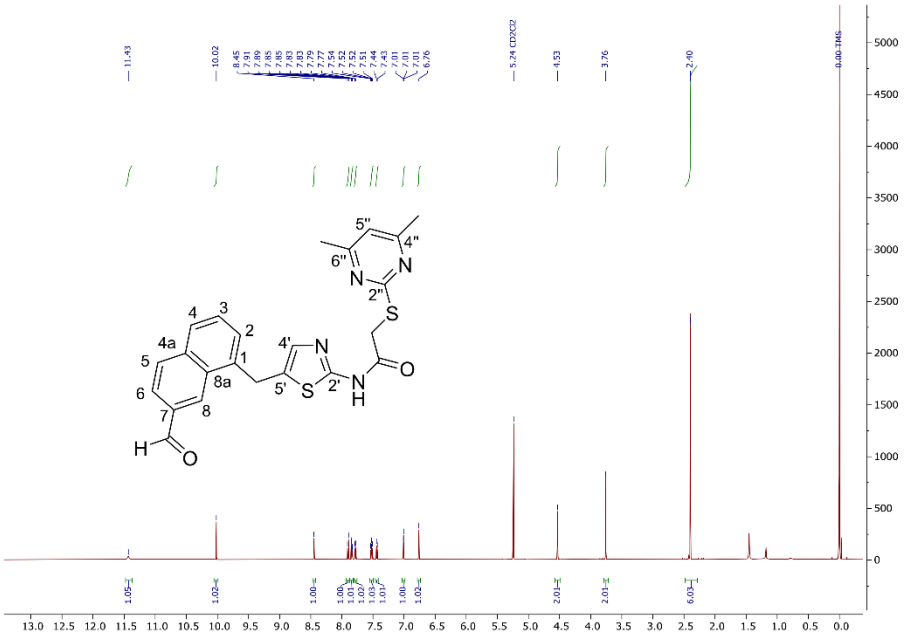

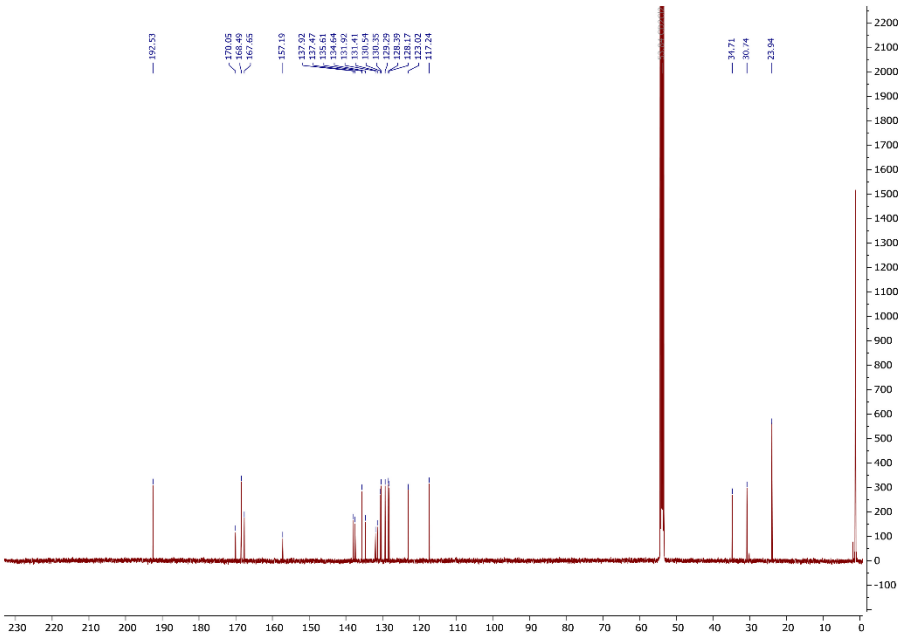

HPLC chromatogram of compound **11**

Chromatogram and Results

Injection Details

Injection Name:	**RW-50**	*Run Time (min):*	**24,99**	
Vial Number:	**Vial:3**	*Injection Volume:*	**5,00**	
Injection Type:	**Unknown**	*Wavelength A:*	**210**	
Column:	**Zorbax SB C18 3,5µm 4,6x100mm 861953-902**	*Wavelength B:*	**254**	
Instrument Method:	**35 AcN 65 Wasser**			
Processing Method:	**SG-094**	*Flow rate:*	**1,000**	**mL/min**
Injection Date/Time:	**18.Jul.23 19:11**	*Column Temperat:*	**35,0**	**°C**
Pump Channel A:	**35,00** AcN			
Pump Channel B:				
Pump ChannelC:				
Pump Channel D:	**65** Wasser			

Chromatogram

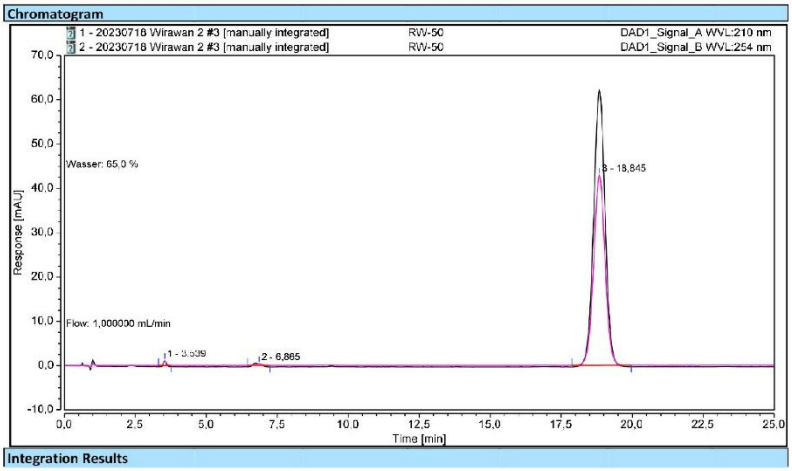

Integration Results

210nm

No.	Peak Name	Retention Time min	Area mAU*min	Relative Area %
1		3,539	0,161	0,54
2		6,725	0,247	0,82
3		18,845	29,514	98,64
Total:			**29,921**	**100,00**

254mn

No.	Peak Name	Retention Time min	Area mAU*min	Relative Area %
1		3,539	0,140	0,68
2		6,865	0,123	0,60
3		18,845	20,237	98,72
Total:			**20,499**	**100,00**

HPLC chromatogram of compound **12**

Chromatogram and Results

Injection Details

Injection Name:	**RW-57**	*Run Time (min):*	**24,99**	
Vial Number:	**Vial:4**	*Injection Volume:*	**5,00**	
Injection Type:	**Unknown**	*Wavelength A:*	**210**	
Column:	**Zorbax SB C18 3,5µm 4,6x100mm 861953-902**	*Wavelength B:*	**254**	
Instrument Method:	**35 AcN 65 Wasser**			
Processing Method:	**SG-094**	*Flow rate:*	**1,000**	**mL/min**
Injection Date/Time:	**18.Jul.23 19:37**	*Column Temperat:*	**35,0**	**°C**
Pump Channel A:	**35,00** AcN			
Pump Channel B:				
Pump ChannelC:				
Pump Channel D:	**65** Wasser			

Chromatogram

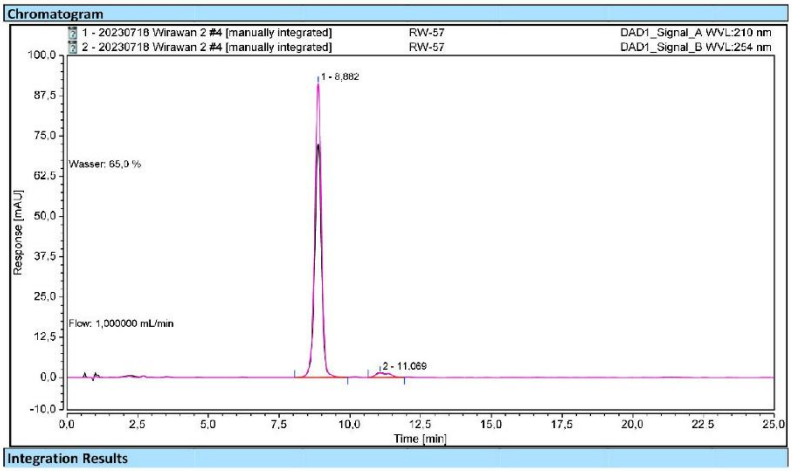

Integration Results

210nm

No.	Peak Name	Retention Time min	Area mAU*min	Relative Area %
1		8,882	20,044	96,45
2		11,069	0,738	3,55
Total:			**20,782**	**100,00**

254mn

No.	Peak Name	Retention Time min	Area mAU*min	Relative Area %
1		8,882	25,106	97,27
2		11,069	0,705	2,73
Total:			**25,811**	**100,00**

HPLC chromatogram of compound **13**

InstrumentLNanni/Honey Sequence:20230718 Wirawan 2 Page 1 of 2

Chromatogram and Results

Injection Details

Injection Name:	**RW-22 in MeOH**	*Run Time (min):*	**15,31**	
Vial Number:	**Vial:12**	*Injection Volume:*	**5,00**	
Injection Type:	**Unknown**	*Wavelength A:*	**210**	
Column:	**Zorbax SB C18 3,5µm 4,6x100mm 861953-902**	*Wavelength B:*	**254**	
Instrument Method:	**35 AcN 65 Wasser**			
Processing Method:	**SG-094**	*Flow rate:*	**1,000**	**mL/min**
Injection Date/Time:	**19.Jul.23 09:00**	*Column Temperatt*	**35,0**	**°C**
Pump Channel A:	**35,00** AcN			
Pump Channel B:				
Pump ChannelC:				
Pump Channel D:	**65** Wasser			

Chromatogram

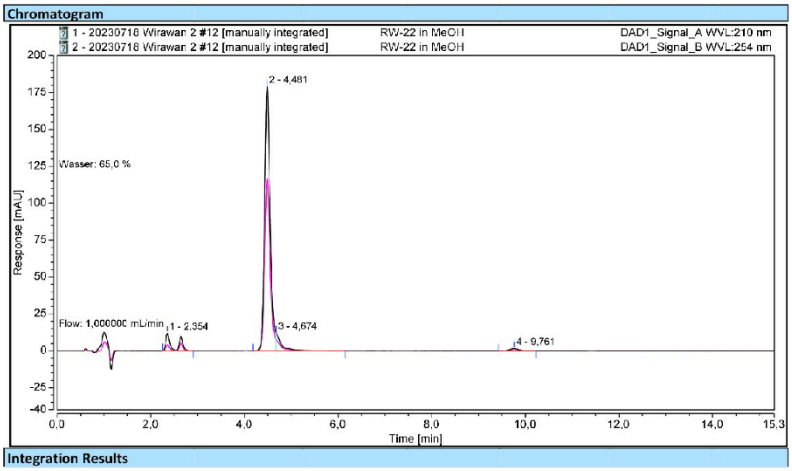

Integration Results

210nm

No.	Peak Name	Retention Time min	Area mAU*min	Relative Area %
1		2,354	1,944	6,76
2		4,481	24,817	86,26
3		4,674	1,652	5,74
4		9,761	0,356	1,24
Total:			**28,769**	**100,00**

254mn

No.	Peak Name	Retention Time min	Area mAU*min	Relative Area %
1		2,354	0,359	2,00
3		4,481	16,320	90,58
4		4,694	0,924	5,13
n.a.	n.a.	n.a.	n.a.	n.a.
Total:			**17,604**	**97,70**

Reinheit Honey/Integration

Chromeleon (c) Dionex
Version 7.2.9.11323

HPLC chromatogram of compound **14**

Instrument:NanniHoney Sequence:20231123 Wirawan Page 1 of 1

Chromatogram and Results

Injection Details

Injection Name:	**RW-41**	*Run Time (min):*	**9,99**	
Vial Number:	**Vial:3**	*Injection Volume:*	**5,00**	
Injection Type:	**Unknown**	*Wavelength A:*	**210**	
Column:	**Zorbax SB C18 3,5µm 4,6x100mm 861953-902**	*Wavelength B:*	**254**	
Instrument Method:	**35 AcN 65 Wasser**			
Processing Method:	**SG-094**	*Flow rate:*	**1,000**	**mL/min**
Injection Date/Time:	**23.Nov.23 14:52**	*Column Temperatu*	**35,0**	**°C**
Pump Channel A:	**35,00** AcN			
Pump Channel B:				
Pump ChannelC:				
Pump Channel D:	**65** Wasser			

Chromatogram

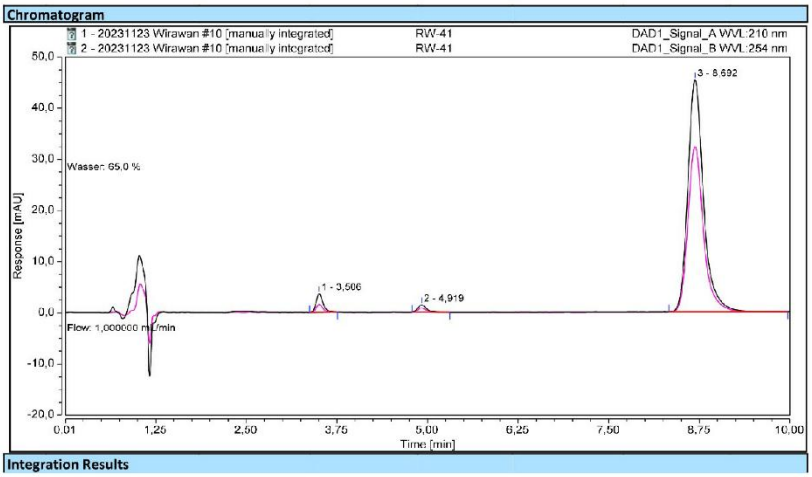

Integration Results

210nm

No.	Peak Name	Retention Time min	Area mAU*min	Relative Area %
1		3,506	0,401	3,34
2		4,919	0,198	1,65
3		8,692	11,417	95,02
Total:			**12,016**	**100,00**

254nm

No.	Peak Name	Retention Time min	Area mAU*min	Relative Area %
1		3,506	0,168	2,01
2		4,919	0,127	1,52
3		8,692	8,068	96,47
Total:			**8,363**	**100,00**

Reinheit Honey/Integration

Chromeleon (c) Dionex Version 7.2.9.11323

HPLC chromatogram of compound **29**

Instrument:NanniHoney Sequence:20231123 Wirawan Page 1 of 1

Chromatogram and Results

Injection Details

Injection Name:	**RW-78**	*Run Time (min):*	**9,99**	
Vial Number:	**Vial:4**	*Injection Volume:*	**5,00**	
Injection Type:	**Unknown**	*Wavelength A:*	**210**	
Column:	**Zorbax SB C18 3,5µm 4,6x100mm 861953-902**	*Wavelength B:*	**254**	
Instrument Method:	**35 AcN 65 Wasser**			
Processing Method:	**SG-094**	*Flow rate:*	**1,000**	**mL/min**
Injection Date/Time:	**23.Nov.23 15:02**	*Column Temperatu*	**35,0**	**°C**
Pump Channel A:	**35,00** AcN			
Pump Channel B:				
Pump ChannelC:				
Pump Channel D:	**65** Wasser			

Chromatogram

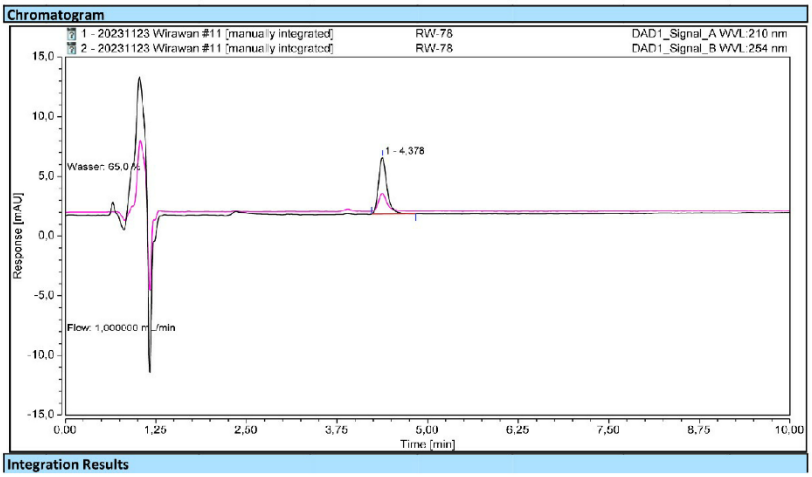

Integration Results

210nm

No.	Peak Name	Retention Time min	Area mAU*min	Relative Area %
1		4,378	0,626	100,00
Total:			**0,626**	**100,00**

254nm

No.	Peak Name	Retention Time min	Area mAU*min	Relative Area %
2		4,378	0,193	89,04
Total:			**0,193**	**89,04**

Reinheit Honey/Integration

Chromeleon (c) Dionex Version 7.2.9.11323

HPLC chromatogram of compound **30**

Chromatogram and Results

Injection Details

Injection Name:	**RW-63**	*Run Time (min):*	**24,99**	
Vial Number:	**Vial:6**	*Injection Volume:*	**5,00**	
Injection Type:	**Unknown**	*Wavelength A:*	**210**	
Column:	**Zorbax SB C18 3,5µm 4,6x100mm 861953-902**	*Wavelength B:*	**254**	
Instrument Method:	**35 AcN 65 Wasser**			
Processing Method:	**SG-094**	*Flow rate:*	**1,000**	**mL/min**
Injection Date/Time:	**18.Jul.23 20:28**	*Column Temperat:*	**35,0**	**°C**
Pump Channel A:	**35,00** AcN			
Pump Channel B:				
Pump ChannelC:				
Pump Channel D:	**65** Wasser			

Chromatogram

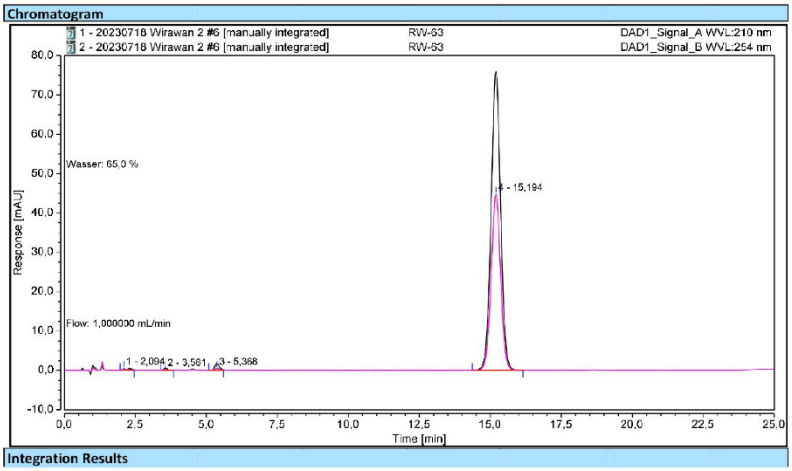

Integration Results

210nm

No.	Peak Name	Retention Time min	Area mAU*min	Relative Area %
n.a.	n.a.	n.a.	n.a.	n.a.
1		3,561	0,066	0,22
2		5,368	0,323	1,07
3		15,194	29,702	98,71
Total:			**30,091**	**100,00**

254mn

No.	Peak Name	Retention Time min	Area mAU*min	Relative Area %
1		2,094	0,061	0,35
2		3,561	0,025	0,14
3		5,368	0,084	0,48
4		15,194	17,534	99,04
Total:			**17,704**	**100,00**

Reinheit Honey/Integration

Chromeleon (c) Dionex
Version 7.2.9.11323

HPLC chromatogram of compound **31**

Instrument:NanniHoney Sequence:20231123 Wirawan Page 1 of 1

Chromatogram and Results

Injection Details

Injection Name:	**RW-80**		*Run Time (min):*	**14,99**	
Vial Number:	**Vial:5**		*Injection Volume:*	**5,00**	
Injection Type:	**Unknown**		*Wavelength A:*	**210**	
Column:	**Zorbax SB C18 3,5µm 4,6x100mm 861953-902**		*Wavelength B:*	**254**	
Instrument Method:	**50 Acetonitril 50 Wasser Honey**				
Processing Method:	**SG-094**		*Flow rate:*	**1,200**	**mL/min**
Injection Date/Time:	**24.Nov.23 09:31**		*Column Temperatu*	**50,0**	**°C**
Pump Channel A:	**50,00**	Acetonitril			
Pump Channel B:		Methanol			
Pump ChannelC:					
Pump Channel D:	**50**	Wasser			

Chromatogram

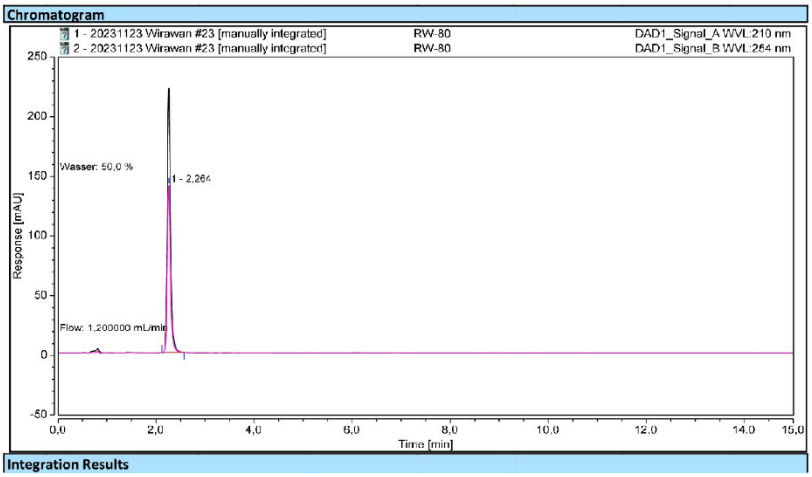

Integration Results

210nm

No.	Peak Name	Retention Time min	Area mAU*min	Relative Area %
1		2,264	17,110	100,00
Total:			**17,110**	**100,00**

254nm

No.	Peak Name	Retention Time min	Area mAU*min	Relative Area %
1		2,264	10,756	100,00
Total:			**10,756**	**100,00**

Reinheit Honey/Integration

Chromeleon (c) Dionex Version 7.2.9.11323

HPLC chromatogram of compound **32**

Chromatogram and Results

Injection Details

Injection Name:	**RW-64 DMSO /ACN**	*Run Time (min):*	**9,99**	
Vial Number:	**Vial:23**	*Injection Volume:*	**5,00**	
Injection Type:	**Unknown**	*Wavelength A:*	**210**	
Column:	**Zorbax SB C18 3,5µm 4,6x100mm 861953-902**	*Wavelength B:*	**254**	
Instrument Method:	**50 AcN 50 Wasser**			
Processing Method:	**SG-094**	*Flow rate:*	**1,200**	**mL/min**
Injection Date/Time:	**19.Jul.23 11:03**	*Column Temperat:*	**35,0**	**°C**
Pump Channel A:	**50,00** AcN			
Pump Channel B:				
Pump ChannelC:				
Pump Channel D:	**50** Wasser			

Chromatogram

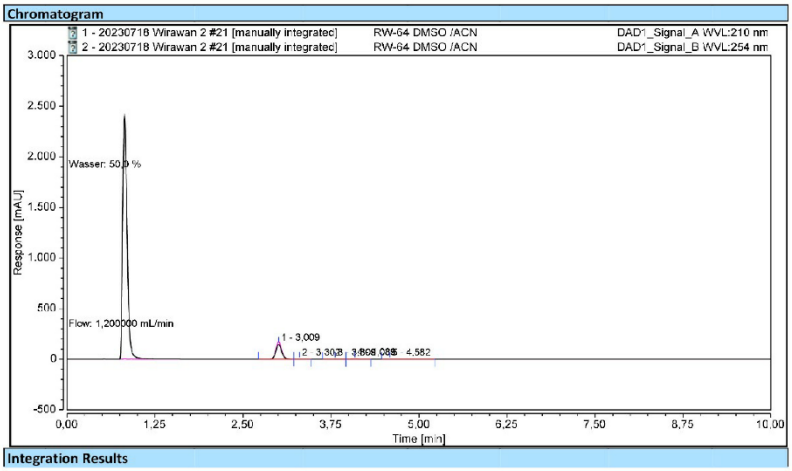

Integration Results

210nm

No.	Peak Name	Retention Time min	Area mAU*min	Relative Area %
1		3,009	13,767	96,39
2		3,302	0,071	0,50
3		3,809	0,122	0,85
4		4,089	0,233	1,63
5		4,582	0,090	0,63
Total:			**14,282**	**100,00**

254nm

No.	Peak Name	Retention Time min	Area mAU*min	Relative Area %
1		3,009	16,108	98,63
n.a.	n.a.	n.a.	n.a.	n.a.
2		3,816	0,072	0,44
3		4,089	0,151	0,93

HPLC chromatogram of compound **33**

Chromatogram and Results

Injection Details

Injection Name:	**RW-46 in MeOH + Wasser**	*Run Time (min):*	**9,99**	
Vial Number:	**Vial:13**	*Injection Volume:*	**5,00**	
Injection Type:	**Unknown**	*Wavelength A:*	**210**	
Column:	**Raptor C18 5µm 4,6x150mm**	*Wavelength B:*	**254**	
Instrument Method:	**35 AcN 65 Wasser**			
Processing Method:	**SG-094**	*Flow rate:*	**0,700**	**mL/min**
Injection Date/Time:	**25.Jul.23 12:13**	*Column Temperat:*	**35,0**	**°C**
Pump Channel A:	**35,00** AcN			
Pump Channel B:				
Pump ChannelC:				
Pump Channel D:	**65** Wasser			

Chromatogram

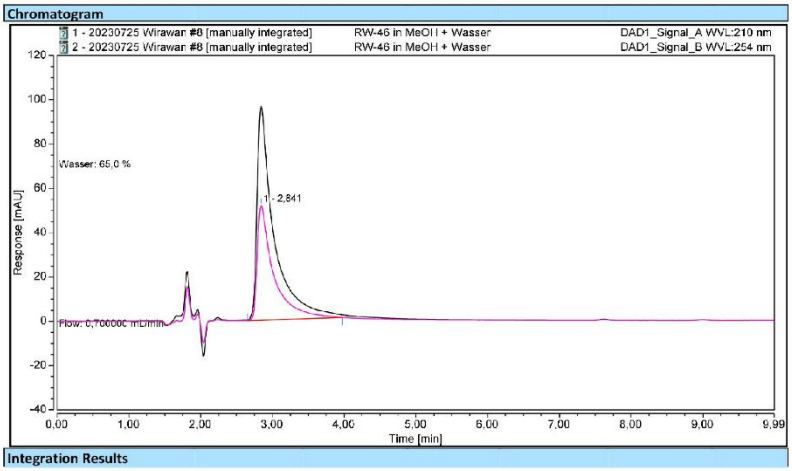

Integration Results

210nm

No.	Peak Name	Retention Time min	Area mAU*min	Relative Area %
1		2,841	25,538	100,00
Total:			**25,538**	**100,00**

254mn

No.	Peak Name	Retention Time min	Area mAU*min	Relative Area %
1		2,841	13,799	100,00
Total:			**13,799**	**100,00**

HPLC chromatogram of compound **34**

Chromatogram and Results

Injection Details

Injection Name:	**RW-61**	*Run Time (min):*	**24,99**	
Vial Number:	**Vial:5**	*Injection Volume:*	**5,00**	
Injection Type:	**Unknown**	*Wavelength A:*	**210**	
Column:	**Zorbax SB C18 3,5µm 4,6x100mm 861953-902**	*Wavelength B:*	**254**	
Instrument Method:	**35 AcN 65 Wasser**			
Processing Method:	**SG-094**	*Flow rate:*	**1,000**	**mL/min**
Injection Date/Time:	**18.Jul.23 20:03**	*Column Temperat:*	**35,0**	**°C**
Pump Channel A:	**35,00** AcN			
Pump Channel B:				
Pump ChannelC:				
Pump Channel D:	**65** Wasser			

Chromatogram

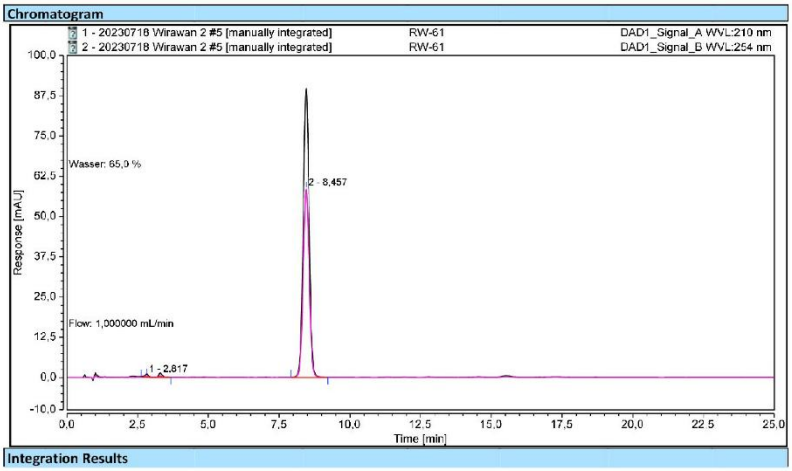

Integration Results

210nm

No.	Peak Name	Retention Time min	Area mAU*min	Relative Area %
1		2,817	0,103	0,47
3		8,457	21,893	98,73
Total:			**21,996**	**99,19**

254mn

No.	Peak Name	Retention Time min	Area mAU*min	Relative Area %
1		2,817	0,081	0,56
2		8,457	14,282	99,44
Total:			**14,363**	**100,00**

HPLC chromatogram of compound **46**

Instrument:NanniHoney Sequence:20230324 Frei Page 1 of 2

Chromatogram and Results

Injection Details

Injection Name:	**fm 295**		*Run Time (min):*	**14,99**	
Vial Number:	**Vial:4**		*Injection Volume:*	**10,00**	
Injection Type:	**Unknown**		*Wavelength A:*	**210**	
Column:	**Eclipse Plus C18 5µm 4,6x 150mm USUXB17231**		*Wavelength B:*	**254**	
Instrument Method:	**50 AcN 50 Wassser**				
Processing Method:	**SG-094**		*Flow rate:*	**1,200**	**mL/min**
Injection Date/Time:	**24.Mrz.23 16:30**		*Column Temperatu*	**50,0**	**°C**
Pump Channel A:	**50,00**	Acetonitril			
Pump Channel B:					
Pump ChannelC:		Phosphatpuffer pH 5			
Pump Channel D:	**50**	Wasser			

Chromatogram

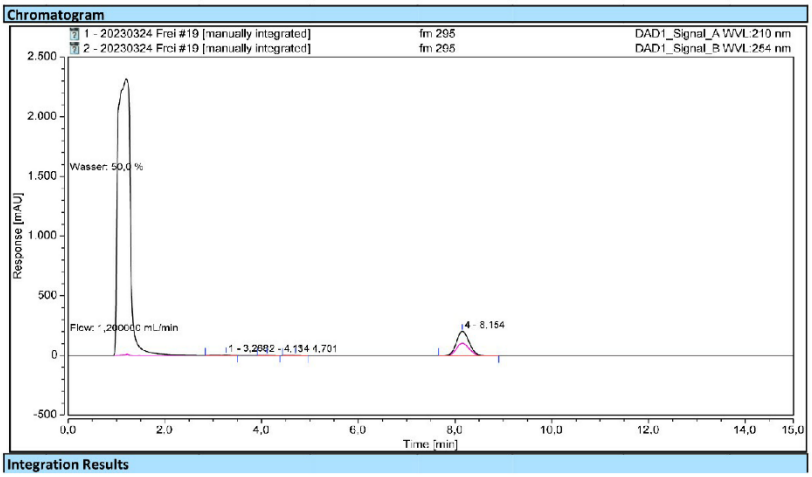

Integration Results

210nm

No.	Peak Name	Retention Time min	Area mAU*min	Relative Area %
1		3,268	0,675	1,10
2		4,114	0,229	0,37
3		4,701	0,073	0,12
4		8,154	60,603	98,41
Total:			**61,579**	**100,00**

254nm

No.	Peak Name	Retention Time min	Area mAU*min	Relative Area %
1		3,268	0,247	0,79
2		4,114	0,060	0,19
n.a.	n.a.	n.a.	n.a.	n.a.
4		8,154	31,011	98,91

Reinheit Honey/Integration

Chromeleon (c) Dionex
Version 7.2.9.11323

HPLC chromatogram of compound **47**

Instrument:NanniHoney Sequence:20230324 Frei Page 1 of 2

Chromatogram and Results

Injection Details

Injection Name:	**fm 302**		*Run Time (min):*	**9,99**	
Vial Number:	**Vial:6**		*Injection Volume:*	**10,00**	
Injection Type:	**Unknown**		*Wavelength A:*	**210**	
Column:	**Eclipse Plus C18 5µm 4,6x 150mm USUXB17231**		*Wavelength B:*	**254**	
Instrument Method:	**50 AcN 50 Wassser**				
Processing Method:	**SG-094**		*Flow rate:*	**1,200**	**mL/min**
Injection Date/Time:	**24.Mrz.23 14:34**		*Column Temperatu*	**50,0**	**°C**
Pump Channel A:	**50,00**	Acetonitril			
Pump Channel B:					
Pump ChannelC:		Phosphatpuffer pH 5			
Pump Channel D:	**50**	Wasser			

Chromatogram

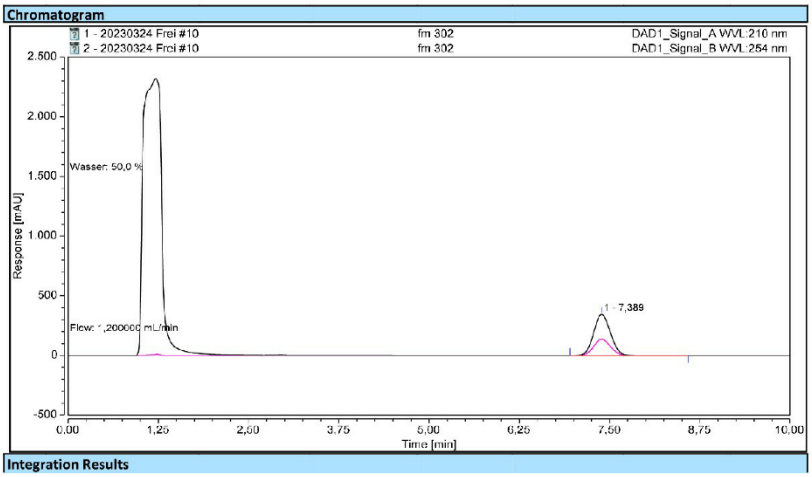

Integration Results

210nm

No.	Peak Name	Retention Time min	Area mAU*min	Relative Area %
1		7,389	91,840	100,00
Total:			**91,840**	**100,00**

254nm

No.	Peak Name	Retention Time min	Area mAU*min	Relative Area %
1		7,389	36,535	100,00
Total:			**36,535**	**100,00**

Reinheit Honey/Integration Chromeleon (c) Dionex Version 7.2.9.11323

HPLC chromatogram of compound **48**

Instrument:Nanni/Honey Sequence:20230324 Frei Page 1 of 1

Chromatogram and Results

Injection Details

Injection Name:	**fm 320 Acn**		*Run Time (min):*	**9,99**	
Vial Number:	**Vial:11**		*Injection Volume:*	**10,00**	
Injection Type:	**Unknown**		*Wavelength A:*	**210**	
Column:	**Eclipse Plus C18 5µm 4,6x 150mm USUXB17231**		*Wavelength B:*	**254**	
Instrument Method:	**50 AcN 50 Wassser**				
Processing Method:	**SG-094**		*Flow rate:*	**1,200**	**mL/min**
Injection Date/Time:	**24.Mrz.23 13:19**		*Column Temperat:*	**50,0**	**°C**
Pump Channel A:	**50,00**	Acetonitril			
Pump Channel B:					
Pump ChannelC:		Phosphatpuffer pH 5			
Pump Channel D:	**50**	Wasser			

Chromatogram

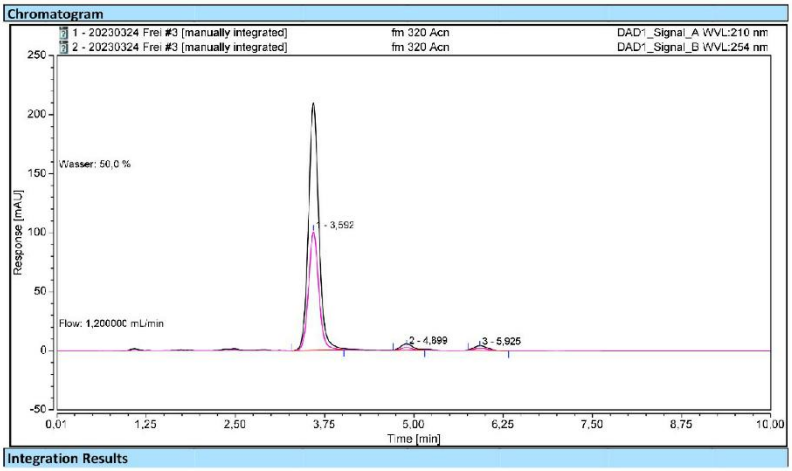

Integration Results

210nm

No.	Peak Name	Retention Time min	Area mAU*min	Relative Area %
1		3,592	34,769	94,75
2		4,899	0,988	2,69
3		5,925	0,939	2,56
Total:			**36,696**	**100,00**

254mn

No.	Peak Name	Retention Time min	Area mAU*min	Relative Area %
1		3,592	16,757	95,42
2		4,899	0,407	2,32
3		5,925	0,398	2,26
Total:			**17,562**	**100,00**

Reinheit Honey/Integration

Chromeleon (c) Dionex
Version 7.2.9.11323

HPLC chromatogram of compound **49**

Instrument:NanniHoney Sequence:20230324 Frei Page 1 of 2

Chromatogram and Results

Injection Details

Injection Name:	**fm 316**		*Run Time (min):*	**14,99**	
Vial Number:	**Vial:10**		*Injection Volume:*	**10,00**	
Injection Type:	**Unknown**		*Wavelength A:*	**210**	
Column:	**Eclipse Plus C18 5µm 4,6x 150mm USUXB17231**		*Wavelength B:*	**254**	
Instrument Method:	**50 AcN 50 Wassser**				
Processing Method:	**SG-094**		*Flow rate:*	**1,200**	**mL/min**
Injection Date/Time:	**24.Mrz.23 18:04**		*Column Temperatu*	**50,0**	**°C**
Pump Channel A:	**50,00**	Acetonitril			
Pump Channel B:					
Pump ChannelC:		Phosphatpuffer pH 5			
Pump Channel D:	**50**	Wasser			

Chromatogram

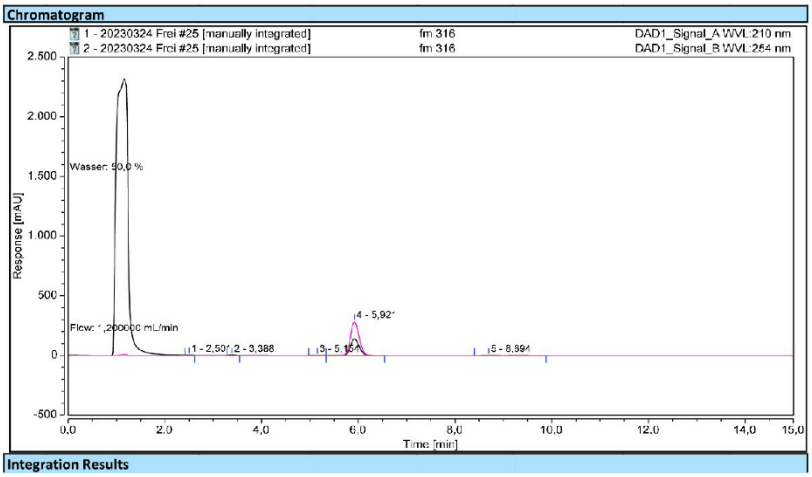

Integration Results

210nm

No.	Peak Name	Retention Time min	Area mAU*min	Relative Area %
1		2,494	0,172	0,57
2		3,388	0,512	1,69
3		5,147	0,173	0,57
4		5,921	28,811	94,83
5		8,694	0,712	2,34
Total:			**30,380**	**100,00**

254nm

No.	Peak Name	Retention Time min	Area mAU*min	Relative Area %
1		2,501	0,205	0,35
2		3,388	0,064	0,11
3		5,154	0,041	0,07

Reinheit Honey/Integration

Chromeleon (c) Dionex
Version 7.2.9.11323

4		5,921	58,581	98,84
5		8,694	0,375	0,63
Total:			**59,267**	**100,00**

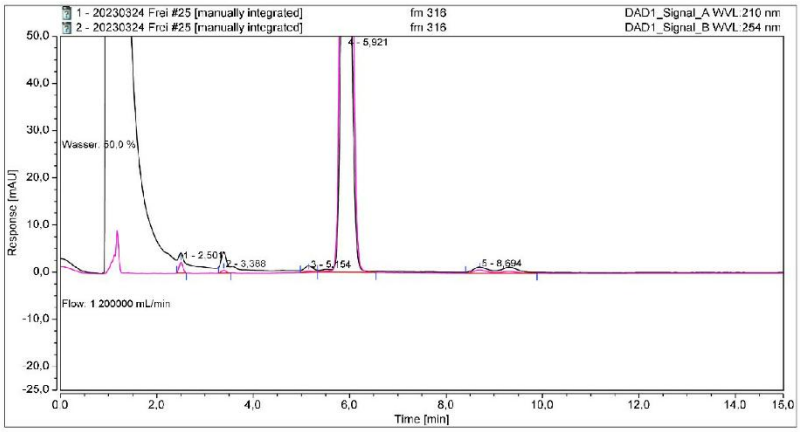

Table S1. Crystallographic data collection and refinement statistics.

	SIRT2
Crystal parameters	
Space group	$P2_1$
Cell constants	a = 35.8 Å
	b = 73.5 Å
	c = 55.0 Å
	β = 95.3°
Data collection	
Beam line	P13, PETRA III, DESY
Wavelength (Å)	1.060
Resolution range (Å)[b]	30.0-2.15
	(2.25-2.15)
No. observations	51,769
No. unique reflections[c]	15,167
Completeness (%)[b]	97.8 (98.6)
R_{merge} (%)[b,d]	8.7 (68.8)
I/σ (I)[b]	9.2 (2.6)
Refinement (REFMAC5)	
Resolution range (Å)	30-1.25
No. refl. working set	14,404
No. refl. test set	758
No. non hydrogen	2251
No. of ligand atoms	1
Solvent	39
R_{work}/R_{free} (%)[e]	22.8 / 27.4
r.m.s.d. bond (Å) / angle (°)[f]	0.002 / 1.2
Average B-factor (Å^2)	47.4
Ramachandran Plot (%)[g]	97.8 / 2.2 / 0
PDB accession code	**9S44**

[a] Asymmetric unit

[b] The values in parentheses for resolution range, completeness, R_{merge} and I/σ (I) correspond to the highest resolution shell

[c] Data reduction was carried out with XDS and from a single crystal. Friedel pairs were treated as identical reflections

[d] $R_{merge}(I) = \Sigma_{hkl}\Sigma_j \mid I(hkl)_j - \langle I(hkl)\rangle \mid / \Sigma_{hkl} \Sigma_j I(hkl)_j$, where $I(hkl)_j$ is the j^{th} measurement of the intensity of reflection hkl and $\langle I(hkl)\rangle$ is the average intensity

[e] $R = \Sigma_{hkl} \mid |F_{obs}| - |F_{calc}| \mid / \Sigma_{hkl} |Fobs|$, where R_{free} is calculated without a sigma cut off for a randomly chosen 5% of reflections, which were not used for structure refinement, and R_{work} is calculated for the remaining reflections

[f] Deviations from ideal bond lengths/angles

[g] Percentage of residues in favored region / allowed region / outlier region

Table S2. Crystallographic data collection and refinement statistics.

	SIRT2:RW-78
Crystal parameters	
Space group	$P2_1$
Cell constants	a = 35.8 Å
	b = 73.7 Å
	c = 55.9 Å
	β = 94.8°
Data collection	
Beam line	P13, PETRA III, DESY
Wavelength (Å)	1.060
Resolution range (Å)[b]	30.0-1.45
	(1.55-1.45)
No. observations	175,238
No. unique reflections[c]	50,844
Completeness (%)[b]	99.1 (99.0)
R_{merge} (%)[b,d]	8.8 (67.2)
I/σ (I)[b]	7.9 (1.9)
Refinement (REFMAC5)	
Resolution range (Å)	30-1.45
No. refl. working set	48,299
No. refl. test set	2,542
No. non hydrogen	2,653
No. of ligand atoms	62
Solvent	215
R_{work}/R_{free} (%)[e]	15.7 / 19.0
r.m.s.d. bond (Å) / angle (°)[f]	0.003 / 1.2
Average B-factor (Å^2)	19.3
Ramachandran Plot (%)[g]	98.6 / 1.4 / 0
PDB accession code	**9S46**

[a] Asymmetric unit

[b] The values in parentheses for resolution range, completeness, R_{merge} and I/σ (I) correspond to the highest resolution shell

[c] Data reduction was carried out with XDS and from a single crystal. Friedel pairs were treated as identical reflections

[d] $R_{merge}(I) = \Sigma_{hkl}\Sigma_j \mid I(hkl)_j - \langle I(hkl)\rangle \mid / \Sigma_{hkl} \Sigma_j I(hkl)_j$, where $I(hkl)_j$ is the j^{th} measurement of the intensity of reflection hkl and $\langle I(hkl)\rangle$ is the average intensity

[e] $R = \Sigma_{hkl} \mid |F_{obs}| - |F_{calc}| \mid / \Sigma_{hkl} |Fobs|$, where R_{free} is calculated without a sigma cut off for a randomly chosen 5% of reflections, which were not used for structure refinement, and R_{work} is calculated for the remaining reflections

[f] Deviations from ideal bond lengths/angles

[g] Percentage of residues in favored region / allowed region / outlier region

Table S3. Crystallographic data collection and refinement statistics.

	SIRT2:RW-80
Crystal parameters	
Space group	$P2_1$
Cell constants	a = 35.9 Å
	b = 73.7 Å
	c = 55.9 Å
	β = 94.8 °
Data collection	
Beam line	P13, PETRA III, DESY
Wavelength (Å)	1.060
Resolution range (Å)[b]	30.0-1.45
	(1.55-1.45)
No. observations	176,079
No. unique reflections[c]	49,669
Completeness (%)[b]	96.7 (95.0)
R_{merge} (%)[b,d]	7.9 (78.8)
I/σ (I)[b]	9.5 (2.0)
Refinement (REFMAC5)	
Resolution range (Å)	30-1.45
No. refl. working set	47,182
No. refl. test set	2,483
No. non hydrogen	2,621
No. of ligand atoms	70
Solvent	241
R_{work}/R_{free} (%)[e]	15.6 / 18.7
r.m.s.d. bond (Å) / angle (°)[f]	0.003 / 1.2
Average B-factor (Å^2)	18.6
Ramachandran Plot (%)[g]	98.2 / 1.8 / 0
PDB accession code	**9S48**

[a] Asymmetric unit

[b] The values in parentheses for resolution range, completeness, R_{merge} and I/σ (I) correspond to the highest resolution shell

[c] Data reduction was carried out with XDS and from a single crystal. Friedel pairs were treated as identical reflections

[d] $R_{merge}(I) = \Sigma_{hkl}\Sigma_j \mid I(hkl)_j - \langle I(hkl)\rangle \mid / \Sigma_{hkl} \Sigma_j I(hkl)_j$, where $I(hkl)_j$ is the j^{th} measurement of the intensity of reflection hkl and $\langle I(hkl)\rangle$ is the average intensity

[e] $R = \Sigma_{hkl} \mid |F_{obs}| - |F_{calc}| \mid / \Sigma_{hkl} |Fobs|$, where R_{free} is calculated without a sigma cut off for a randomly chosen 5% of reflections, which were not used for structure refinement, and R_{work} is calculated for the remaining reflections

[f] Deviations from ideal bond lengths/angles

[g] Percentage of residues in favored region / allowed region / outlier region

Table S4. DNA sequence of *SIRT2* 2-389 as ordered and subcloned by Eurofins Genomics.

Construct	DNA sequence
SIRT2 2-389	GCAGAGCCAGACCCCTCTCACCCTCTGGAGACCCAGGCAGGGAAG GTGCAGGAGGCTCAGGACTCAGATTCAGACTCTGAGGGAGGAGCC GCTGGTGGAGAAGCAGACATGGACTTCCTGCGGAACTTATTCTCCC AGACGCTCAGCCTGGGCAGCCAGAAGGAGCGTCTGCTGGACGAGC TGACCTTGGAAGGGGTGGCCCGGTACATGCAGAGCGAACGCTGTC GCAGAGTCATCTGTTTGGTGGGAGCTGGAATCTCCACATCCGCAGG CATCCCCGACTTTCGCTCTCCATCCACCGGCCTCTATGACAACCTA GAGAAGTACCATCTTCCCTACCCAGAGGCCATCTTTGAGATCAGCTA TTTCAAGAAACATCCGGAACCCTTCTTCGCCCTCGCCAAGGAACTCT ATCCTGGGCAGTTCAAGCCAACCATCTGTCACTACTTCATGCGCCT GCTGAAGGACAAGGGGCTACTCCTGCGCTGCTACACGCAGAACATA GATACCCTGGAGCGAATAGCCGGGCTGGAACAGGAGGACTTGGTG GAGGCGCACGGCACCTTCTACACATCACACTGCGTCAGCGCCAGCT GCCGGCACGAATACCCGCTAAGCTGGATGAAAGAGAAGATCTTCTC TGAGGTGACGCCCAAGTGTGAAGACTGTCAGAGCCTGGTGAAGCCT GATATCGTCTTTTTTGGTGAGAGCCTCCCAGCGCGTTTCTTCTCCTG TATGCAGTCAGACTTCCTGAAGGTGGACCTCCTCCTGGTCATGGGT ACCTCCTTGCAGGTGCAGCCCTTTGCCTCCCTCATCAGCAAGGCAC CCCTCTCCACCCCTCGCCTGCTCATCAACAAGGAGAAAGCTGGCCA GTCGGACCCTTTCCTGGGGATGATTATGGGCCTCGGAGGAGGCAT GGACTTTGACTCCAAGAAGGCCTACAGGGACGTGGCCTGGCTGGG TGAATGCGACCAGGGCTGCCTGGCCCTTGCTGAGCTCCTTGGATG GAAGAAGGAGCTGGAGGACCTTGTCCGGAGGGAGCACGCCAGCAT AGATGCCCAGTCGGGGGCGGGGGTCCCCAACCCCAGCACTTCAGC TTCCCCCAAGAAGTCCCCGCCACCTGCCAAGGACGAGGCCAGGAC AACAGAGAGGGAGAAACCCCAGTGA

Table S5. Primers used to generate His_6-SUMO-Ser-*SIRT2* 56-356 by Q5-mutagenesis.

ID	Primer name	DNA-sequence
A	SIRT2_2-356_fw	TGACTGCAGGTCGAC
B	SIRT2_2-356_rv	CGACTGGGCATCTATG
C	SIRT2 _56-356_fw	GAGCGTCTGCTGGAC
D	SIRT2_56-356_rv	GGATCCACCGATCTG

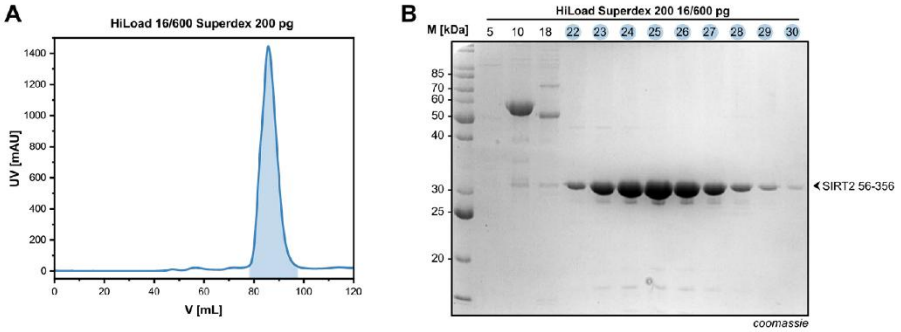

Fig. S1. Purification of human SIRT2 56-356. (**A**) Size exclusion chromatography profile of SIRT2 56-356 on a HiLoad® 16/600 Superdex® 200 pg column. (**B**) SDS-PAGE of fractions from the size exclusion chromatography. Blue fractions correspond to blue shaded peak area in panel A.

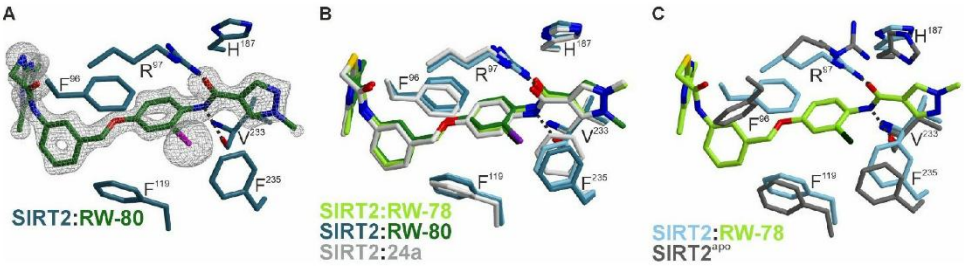

Fig. S2. Close-up view of the SIRT2 ligand binding site. Hydrogen bonds are shown as black dotted lines. Key amino acids are visualised as sticks and labelled by the one-letter code. (**A**) F_O-F_C omit electron density (grey mesh contoured to 3 σ) of **31** (**RW-80**, dark green) bound to SIRT2 (PDB ID: 9S48; blue-green). (**B**) Superposition of inhibitors **10** (**24a** (PDB ID: 5YQO)[1], white), **29** (**RW-78**, green, PDB ID: 9S46), and **31** (**RW-80**, dark green, PDB ID: 9S48) in their respective SIRT2 binding pocket. All three inhibitors are located similarly in the binding cleft. (**C**) Comparison of the inhibitor binding site in the SIRT2:**29** complex (**RW-78**, green) and the SIRT2 apo structure (grey residues, PDB ID: 9S44). Depicted residues undergo rearrangements upon ligand binding.

1. L. L. Yang, H. L. Wang, L. Zhong, C. Yuan, S. Y. Liu, Z. J. Yu, S. Liu, Y. H. Yan, C. Wu, Y. Wang, Z. Wang, Y. Yu, Q. Chen and G. B. Li, *Eur J Med Chem*, 2018, **155**, 806-823.

3.2. Project II: Lead structure-based hybridization strategy in the development of Sirt2 inhibitors

Frei, M.*; **Wirawan, R.***; Wein, T.; Bracher, F. Lead structure-based hybridization strategy reveals major potency enhancement of SirReal-type Sirt2 inhibitors. *Int. J. Mol. Sci.* **2025**, *26*, 9855.

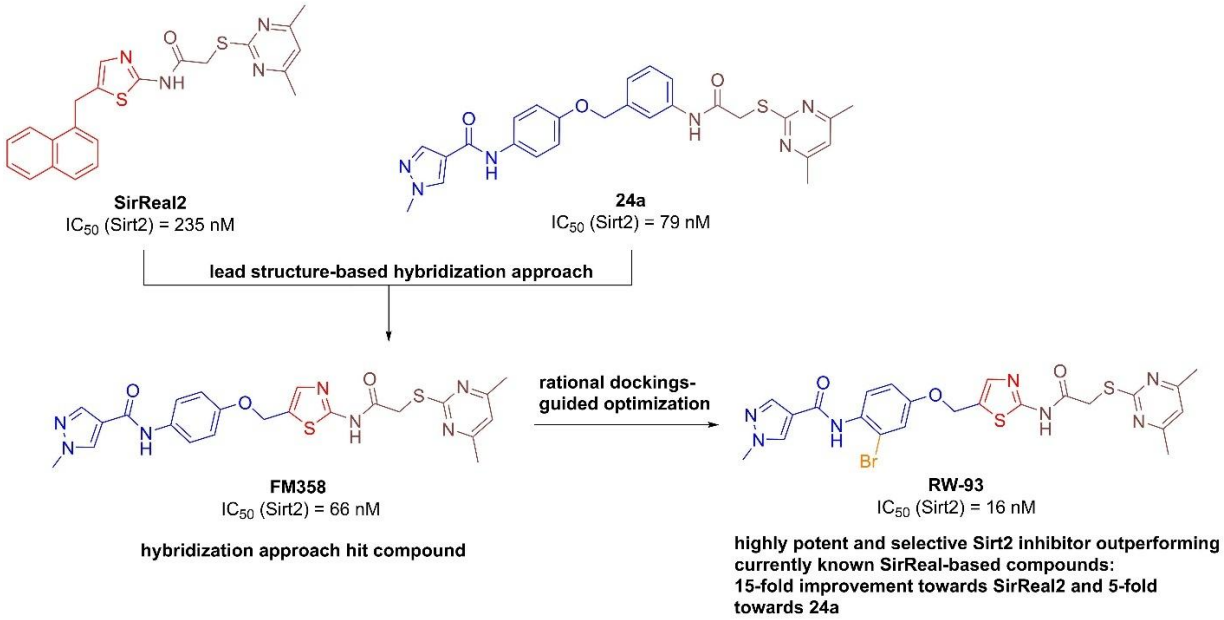

3.2.1. Summary

The hybridization of relevant pharmacophoric features of lead compounds represents a viable methodology in drug development and optimisation. This approach was implemented utilising the Sirt2 inhibitors **SirReal2** and **24a** as lead compounds to develop highly potent and subtype selective Sirt2 hybrid inhibitors. Guided by molecular docking experiments, a series of seven hybrid inhibitors was rationally designed and synthesised. The bromo-derivative hybrid inhibitor **RW-93** emerged from this study as the most potent low-molecular subtype-selective Sirt2 inhibitor known to date, displaying an IC_{50} of 16 nM, highlighting this approach as an effective strategy in the development of highly potent and subtype-selective Sirt2 inhibitors. The *in vitro* data were validated *via* MM-GBSA calculations which showed a good correlation between the two datasets. In addition, *in silico* ADME profiling of the Sirt2 hybrid inhibitors was performed by assessing their physicochemical and pharmacokinetic parameters, which demonstrated promising drug-like properties for further development.

3.2.2. Personal Contributions

My personal contributions to this journal article include the synthesis and the characterization of the optimised halogen derivatives of the Sirt2 hybrid inhibitors in the second optimization

series, the management and coordination of this project, the support in the writing of the original draft, the reviewing and editing of the final manuscript and the preparation of the supplementary information.

Matthias Frei synthesised, characterized and investigated the initial Sirt2 hybrid inhibitors, managed and coordinated the project, wrote the original draft, reviewed and edited the final manuscript, and prepared the graphical abstract and supplementary information. Thomas Wein performed molecular docking experiments, MM-GBSA calculations and ADME profiling. Franz Bracher conceptualized and designed the study, managed and coordinated the project, supervised all synthetic work, provided funding and resources, and reviewed and edited the final manuscript.

3.2.3. Article

International Journal of *Molecular Sciences*

MDPI

Article

Lead Structure-Based Hybridization Strategy Reveals Major Potency Enhancement of SirReal-Type Sirt2 Inhibitors

Matthias Frei †, Ricky Wirawan †, Thomas Wein and Franz Bracher *

Department of Pharmacy, Center for Drug Research, Ludwig-Maximilians University, Butenandtstr. 5–13, 81377 Munich, Germany; ricky.wirawan@cup.uni-muenchen.de (R.W.)

* Correspondence: franz.bracher@cup.uni-muenchen.de; Tel.: +49-89-218077301

† These authors contributed equally to this work.

Abstract

Selective and potent inhibitors of the NAD^+-dependent deacetylase Sirt2 represent a valuable epigenetic strategy for the treatment of currently incurable diseases such as Parkinson's disease, Huntington's disease, Alzheimer's disease, and multiple sclerosis. Guided by molecular docking and MM/GBSA validation studies, a lead structure-based hybridization strategy was developed, resulting in a series of very effective Sirt2 inhibitors. With **RW-93,** we present a highly potent and subtype selective Sirt2 inhibitor (IC_{50} = 16 nM), which as a next generation SirReal-type inhibitor significantly surpasses established Sirt2 inhibitors and contributes to the extension of the current SAR profile. The structural modification strategy employed in this study proved to be highly promising, resulting in the identification of the most potent low-molecular-weight Sirt2 inhibitor reported to date, providing a promising target for further medicinal chemistry-driven SAR studies.

Keywords: sirtuin 2 inhibitor; Sirt2 inhibitor; SirReal2; structure–activity relationship; hybridization strategy; highly potent and selective Sirt2 inhibitor; structural optimization

Academic Editor: Kota V. Ramana

Received: 3 September 2025
Revised: 5 October 2025
Accepted: 8 October 2025
Published: 10 October 2025

Citation: Frei, M.; Wirawan, R.; Wein, T.; Bracher, F. Lead Structure-Based Hybridization Strategy Reveals Major Potency Enhancement of SirReal-Type Sirt2 Inhibitors. *Int. J. Mol. Sci.* **2025**, *26*, 9855. https://doi.org/10.3390/ijms26209855

1. Introduction

Histone modifications take a key position in epigenetic regulation processes, essentially controlled by acetylation and deacetylation of lysine on *N*-terminal histone tails catalyzed by histone acetyltransferases (HATs) and histone deacetylases (HDACs) [1–3]. HDACs are generally categorized into 4 classes (class I-IV), with class III being referred to as sirtuins. Sirtuins are divided into 7 subtypes (Sirt1-7) based on different cell function and localization and, in contrast to the other HDACs, are not zinc-dependent but require NAD^+ as a cofactor for catalytic activity [4,5].

Sirtuins play a fundamental role in pathophysiological mechanisms, making them a significant therapeutic target of ongoing intensive research. Selective inhibition of Sirt2 is associated with numerous positive effects such as anti-angiogenesis, neuroprotection and anti-inflammation, and represents a valuable tool in understanding and treating related diseases [6–10]. Selective Sirt2 inhibitors, which are chemically and structurally diverse, display various binding modes and mechanisms that target the C-pocket, the extended C-site including the selectivity pocket, the substrate channel, or the cofactor NAD^+ [11]. The development of sirtuin rearranging ligands (SirReals) as potent inhibitors that selectively inhibit Sirt2 by inducing a hydrophobic selectivity pocket during binding, laid the

foundation for extensive structure–activity relationship studies and inspired further development of corresponding inhibitors (Figure 1) [12,13].

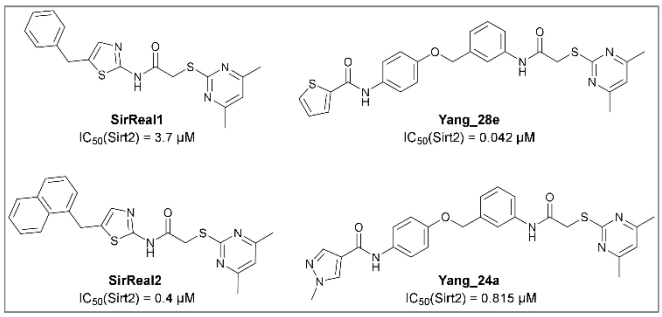

Figure 1. Chemical structures and inhibitory activities of selected Sirt2 inhibitors based on the SirReal feature. The originally reported IC_{50} values were determined under differing assay conditions, precluding direct comparability. Compound **Yang_28e** was reported to exhibit greater potency than **SirReal2**, while compound **Yang_24a** constitutes a further variation of **Yang_28e**.

SirReal-type inhibitors share a 2-((4,6-dimethylpyrimidin-2-yl)thio)acetamide moiety as characteristic structural feature, which occupies the hydrophobic selectivity pocket induced after binding of the inhibitor in the active site and thus significantly determines Sirt2 selectivity and enables corresponding potency. First generation benchmark **SirReal2** developed by Rumpf et al. shows intense van der Waals interactions within the substrate channel based on the corresponding naphthalene residue. Various aromatic (Phe131, Phe234) and aliphatic amino acids (Leu134, Ile169, Ile232, Val233) as well as the nicotinamide moiety of NAD^+ are being addressed [14]. Subsequently Schiedel et al. developed further optimized compounds based on the initial SirReal-type inhibitors, providing valuable structure–activity relationships [15,16]. With Sirt2 inhibitors **Yang_28e** [17] and **Yang_24a** [18], Yang et al. presented advanced SirReal-derivatives that demonstrate an even stronger inhibitory effect and high selectivity, providing a comprehensive contribution and solid foundation for enabling profounded SAR studies. The recurring 2-((4,6-dimethylpyrimidin-2-yl)thio)acetamide moiety guarantees high Sirt2 selectivity by binding into the in situ induced selectivity pocket and ensures a comparable general alignment of the SirReal-type inhibitors within the binding pocket. The *N*-phenylthiophene-2-carboxamide moiety in **Yang_28e** and the 1-methyl-*N*-phenyl-1*H*-pyrazole-4-carboxamide moiety in **Yang_24a**, which are linked by a benzyl ether structure, enable further and more intense π-π interactions (e.g., with Phe235) and hydrophilic interactions (H-bond with Val233) within the substrate channel of Sirt2 [17,19].

Initial analysis of the superposition (Figure 2) of the crystal structures of the lead compounds **SirReal2** and **Yang_24a** revealed structural similarities and several characteristic elements, forming the fundament for the development of the envisaged hybridization strategy. In continuation of our work in the synthesis and biological evaluation of Sirt2 inhibitors [20], the fundamental approach was to integrate the amide-based channel binding residue of **Yang_24a** into the thiazole structure of **SirReal2** and link it via a benzyl ether bridge instead of the methylene bridge, generating hybrid candidate **FM358**. Further structural features such as the benzene (**SirReal1**) and naphthalene rings (**SirReal2**) and the *N*-phenylthiophene-2-carboxamide moiety (**Yang_28e**) of other lead structures were selected to generate hybrid candidates **FM345**, **FM368** and **FM352** (Scheme 1).

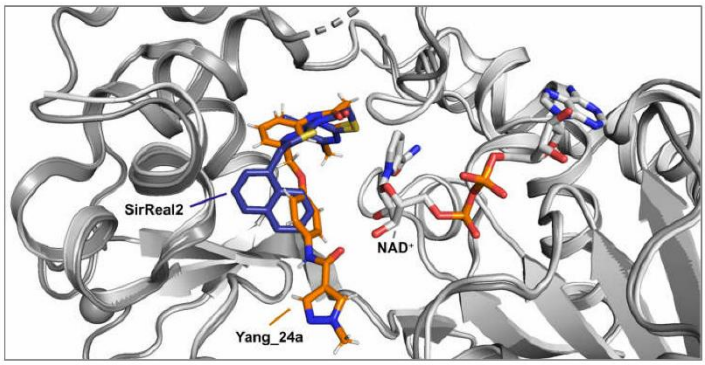

Figure 2. Crystal structure superimposition of **SirReal2** (purple) and cofactor NAD^+ (grey, PDB ID: 4RMG) with compound **Yang_24a** (orange, taken from PDB ID: 5YQO).

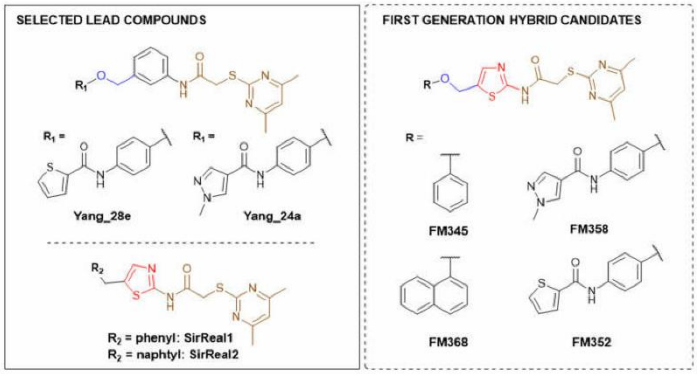

Scheme 1. General hybridization approach based on lead compounds **SirReal2** and **Yang_28e** generating four first round (aryloxymethyl)thiazole candidates **FM345**, **FM358**, **FM368** and **FM352**.

The novel (aryloxymethyl)thiazolamide structure thus considered should be able to orient the 1-methyl-*N*-phenyl-1*H*-pyrazole-4-carboxamide residue of the pharmacophore more favourably by changing the spatial angle and increasing the structural flexibility, thereby blocking the function of cofactor NAD^+ more effectively and therefore increasing the inhibitory activity. The most promising hybrid candidate **FM358** derived from this hybridization approach of **SirReal2** and **Yang_24a** was to be extended by the design of further variations to enable a more comprehensive structure–activity relationship study.

2. Results

2.1. Initial Docking Experiments for the Validation of the Hybridization Concept

Guided by docking experiments, the resulting library of four hybridized target compounds (Scheme 1) was evaluated for its inhibitory potential and the predicted spatial arrangement was analysed in relation to the orientation of the respective substrate channel residues. The docking study carried out with the envisaged hybrid candidates shows encouraging results (Figure 3).

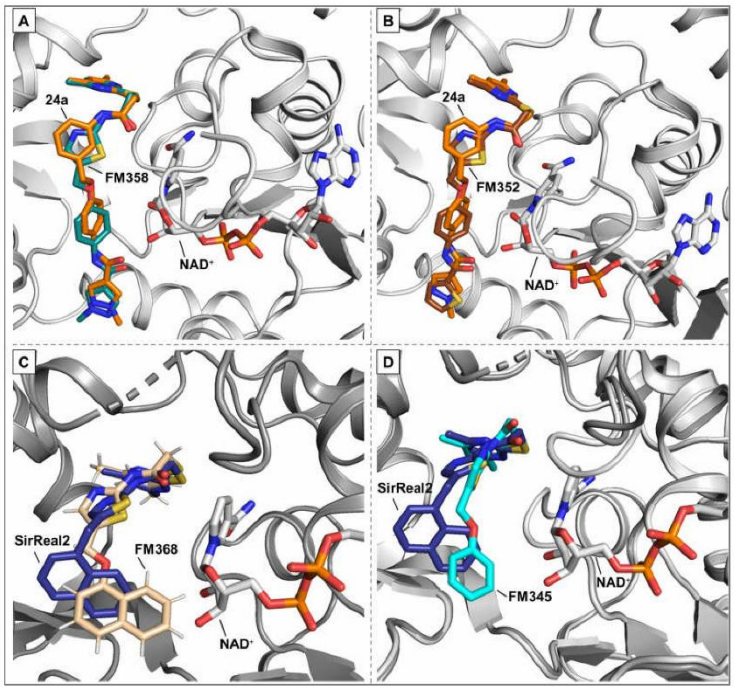

Figure 3. (**A**) Docking pose of hybrid **FM358** (green) based on the co-crystal structure of lead compound **Yang_24a** (orange, PDB ID: 5YQO). The position of cofactor NAD^+ (grey) was copied from PDB ID: 4RMG for visualization, as not included in the crystal structure of **Yang_24a** (PDB ID: 5YQO). (**B**) Docking pose of hybrid **FM352** (brown) based on co-crystal structure of lead compound **Yang_24a** (orange, PDB ID: 5YQO). The position of cofactor NAD^+ (grey) was copied from PDB ID: 4RMG for visualization, as not included in the crystal structure of **Yang_24a** (PDB ID: 5YQO). (**C**) Docking pose of hybrid **FM368** (cream) based on co-crystal structure of lead compound **SirReal2** (blue, PDB ID: 4RMG) and cofactor NAD^+ (grey). (**D**) Docking pose of hybrid **FM345** (cyan) based on the co-crystal structure of lead compound **SirReal2** (blue, PDB ID: 4RMG) and NAD^+ (grey).

All predicted poses show a principal correlation with the co-crystal structures of the lead compounds including a high overlap of the selectivity pocket binder motif, an essential prerequisite for the Sirt2 selectivity of the featured SirReal-based inhibitors. The calculated spatial orientations of **FM358** and **FM352** are very similar to each other and to the co-crystal structure of **Yang_24a**, only the amide-based substrate channel residue of both hybrid candidates is slightly shifted. **FM345** and **FM368** differ mainly in the position of benzene and naphthalene rings, which in the prediction occupy a more central position in the substrate channel, closer to cofactor NAD^+, compared to **SirReal2**, which is mainly mediated by the higher flexibility of the benzyl ether.

Consequently, the docking experiments show promising predictions indicating high potency, therefore a strategy for the synthesis of these hybrid target compounds was developed.

2.2. Synthesis of First Generation Hybrid Candidates

The preparation of the desired hybrid target compounds **FM345**, **FM358**, **FM368** and **FM352** was achieved in five steps each, requiring the establishment of a general synthesis approach to the previously unknown structural class of 2-acylamino-5-(aryloxymethyl)thiazoles (see Scheme 2). 2-((4,6-Dimethylpyrimidin-2-yl)thio)acetic acid (**2**) was obtained by base-mediated thioether synthesis of 4,6-dimethylpyrimidine-2-thiol (**1**) and 2-chloroacetic acid, with subsequent EDC·HCl mediated amidation with 2-aminothiazole-5-carbaldehyde to amide **3**. Reduction of the aldehyde group in compound **3** using sodium borohydride gave the primary alcohol **4**, which was subsequently converted to the corresponding alkyl chloride **5** using thionyl chloride. The Williamson ether synthesis to the previously unknown 5-(aryloxymethyl)thiazoles failed under a standard setup with conventional reaction conditions due to C-alkylation tendencies at the electron-rich phenolates, which is why after extensive experimentation a protocol using preformed sodium phenolates was established, allowing the preparation of the target compounds **FM345**, **FM352**, **FM358** and **FM368**.

Phenyl ether **FM345** was synthesized using alkyl chloride **5** and commercially available sodium phenoxide in dichloromethane. Sodium 1-naphtholate was prepared from 1-naphthol and sodium methanolate, which subsequently allowed the synthesis of **FM368** with alkyl chloride **5** in acetone instead of dichloromethane to reduce unwanted C-alkylation. The phenolates required for the preparation of **FM352** and **FM358** each had to be synthesized in two steps. 4-Aminophenol (**6**) was reacted with thiophene-2-carbonyl chloride and pyridine to form amide **7**, which was then transformed with sodium methanolate to the corresponding phenolate, finally yielding **FM352** with alkyl chloride **5** in dichloromethane. In a HATU-mediated amidation of 4-aminophenol (**6**) and 1-methyl-1*H*-pyrazole-4-carboxylic acid, product **8** was obtained. Notably, undesired side reactions involving the formation of ester and the amide-ester side products were also generated due to similar reactivities of both the aromatic amine and phenol groups of 4-aminophenol (**6**) towards 1-methyl-1*H*-pyrazole-4-carboxylic acid. Fortunately, the desired amide **8** could be isolated in a reasonable yield. The corresponding phenolate was then synthesized upon treatment with sodium methanolate, which was finally subjected to a Williamson ether synthesis with alkyl chloride **5** in dichloromethane yielding **FM358**.

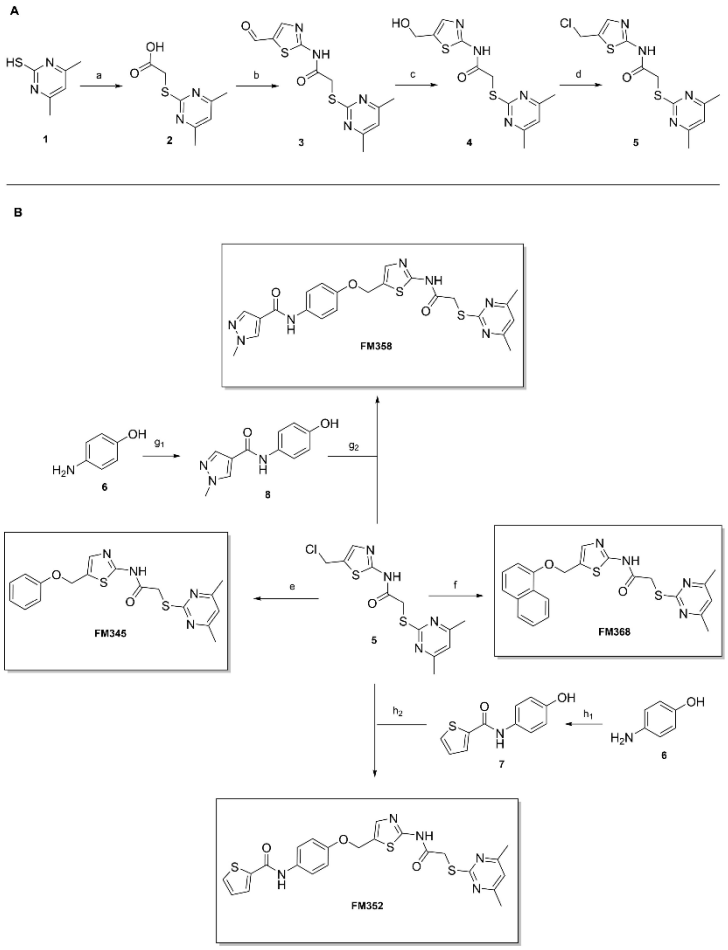

Scheme 2. (**A**) (a) 2-chloroacetic acid, NEt_3, acetonitrile, rt, 24 h, 81% for **2**; (b) 2-aminothiazole-5-carbaldehyde, DMAP, EDC·HCl, DMF, rt, 16 h, 46% for **3**; (c) $NaBH_4$, MeOH, 3 h, 0 °C, quantitative for **4**; (d) $SOCl_2$, DCM, 18 h, rt, quantitative for **5**. (**B**) (e) sodium phenoxide, rt, 24 h, DCM, 18% for **FM345**; (f) 1-naphthol, NaOMe 25% (*w*/*w*) in MeOH, rt, 2 min, DCM, crude for ; then **5**, acetone, rt, 5 h, 14% for **FM368**; (g_1) 1-methyl-1*H*-pyrazole-4-carboxylic acid, DIPEA, HATU, THF, 3 h, rt, 21% for **8**; (g_2) NaOMe 25% (*w*/*w*) in MeOH, rt, 2 min, DCM, crude; then **5**, DCM, rt, 17% for **FM358**; (h_1) thiophene-2-carbonyl chloride, pyridine, DMF, 1.5 h, rt, 69% for **7**; (h_2) NaOMe 25% (*w*/*w*) in MeOH, rt, 2 min, DCM, crude; then **5**, DCM, rt, 38% for **FM352**.

2.3. *Biological Evaluation of First-Generation Hybrid Candidates, Assessment of the Concept Strategy, and Refinement and Approach to Second-Generation Hybrid Candidates*

The determination of the inhibitory potency and corresponding subtype selectivity of the synthesized hybrid candidates was performed by Reaction Biology Cooperation (Malvern, PA, USA) using a fluorescence-based assay (Table 1).

Table 1. Inhibitory activity on Sirt2 and corresponding subtype selectivity towards Sirt1, Sirt3 and Sirt5 of respective inhibitors was determined by Reaction Biology Corporation (Malvern, PA, USA) using fluorescence-based assays. IC_{50} values were obtained for each serial dilution within the triplicate set through sigmoidal curve fitting, and the mean with standard deviation (SD) was calculated from these three values. Residual enzyme activity of Sirt1, Sirt3, and Sirt5 was measured as a percentage at a final inhibitor concentration of 50 µM, based on duplicate samples, and the mean with standard deviation (SD) was calculated thereof. Abbreviation: n.d.: not determined.

ID	Chemical Structure	IC_{50} [µM] ± SD Sirt2	Residual Enzyme Activity [%] ± SD		
			Sirt1	Sirt3	Sirt5
SirReal2	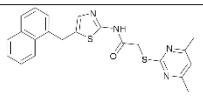	0.235 ± 0.008	n.d.	n.d.	n.d.
Yang_24a	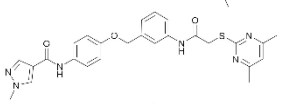	0.0790 ± 0.0030	n.d.	n.d.	n.d.
Yang_28e	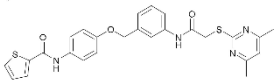	0.0867 ± 0.0085	n.d.	n.d.	n.d.
FM358	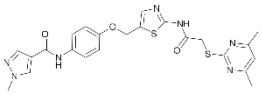	0.0656 ± 0.0044	71.9 ± 0.6	62.5 ± 0.1	79.8 ± 0.6
FM352	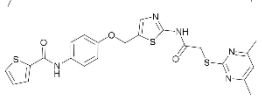	0.0935 ± 0.0064	101 ± 1	75.8 ± 5.3	75.6 ± 1.1
FM345	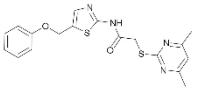	5.29 ± 0.73	95.6 ± 2.3	78.8 ± 0.8	94.6 ± 2.3
FM368	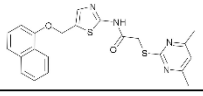	6.51 ± 0.84	88.5 ± 2.7	85.0 ± 0.5	89.1 ± 1.4

Due to different assay conditions used in the original publications, corresponding lead compounds were resynthesized according to literature (**Yang_28e** [17] and **Yang_24a** [19]) or acquired from commercial suppliers **(SirReal2**, Sigma-Aldrich) and included in the screening performed in order to ensure comparability of the values. **SirReal2** was published with an IC_{50} value of 0.4 µM on Sirt2 and achieved a comparable IC_{50} value of 235 nM in the assay system used. The more potent optimizations based on **SirReal2**, **Yang_28e** (published IC_{50} = 41 nM, here IC_{50} = 87 nM) and **Yang_24a** (published IC_{50} = 0.815 µM, here 79 nM), represent a significant improvement of **SirReal2**, as reported. Of the four first target compounds synthesized, **FM358** (IC_{50} = 66 nM) shows the strongest inhibitory activity on Sirt2 and thus outperforms the corresponding lead compounds **SirReal2** (IC_{50} = 235 nM) and **Yang_24a** (IC_{50} = 79 nM). **FM352** (IC_{50} = 94 nM) is more potent than **SirReal2**, however exhibits a slightly lower inhibitory effect than lead compound **Yang_24a**. Hybrids **FM345** (IC_{50} = 5.3 µM) and **FM368** (IC_{50} = 6.5 µM) have clearly lost inhibitory activity compared to the corresponding lead compounds and the replacement of the methylene bridge with the more flexible oxomethylene bridge results in a weakened interaction within the binding pocket of Sirt2. It is possible that the elongation associated with the

novel ether units leads to an unfavourable positioning of the benzene ring of **FM345** or the naphthalene ring of **FM368** and to an excessive space requirement. The superiority of the 1-methyl-*N*-phenyl-1*H*-pyrazole-4-carboxamide moiety compared to the *N*-phenylthiophene-2-carboxamide moiety of the lead compounds **Yang_24a** and **Yang_28e**, previously observed by Yang et al. [17] was confirmed, which can be directly transferred to the hybrid compounds **FM358** and **FM352**. Compound **FM358** benefits from the replacement of the benzene ring by the aminothiazole ring, thus the associated rearrangement leads to advantageous interactions, resulting in a 1.2 times stronger inhibition compared to lead compound **Yang_24a** and providing an excellent starting point for further modifications and optimization. Visualization of polar contacts of the docking pose of **FM358** within the binding pocket of Sirt2 reveals various interactions with the substrate channel residues, including hydrogen bonds of the amide-carbonyl with Arg97 and potentially with the ribose unit of cofactor NAD^+, as well as amide-nitrogen with the backbone carbonyl of Val233 (Figure 4).

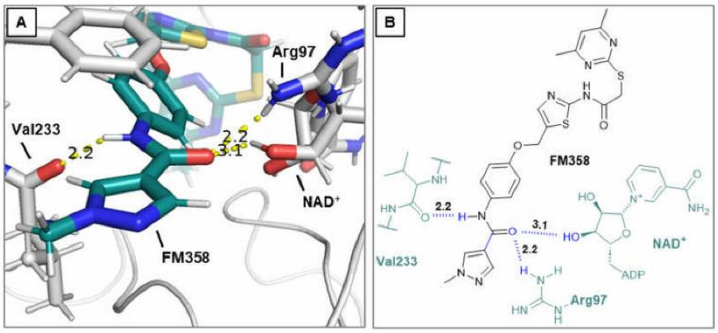

Figure 4. (**A**) Sirt2 docking pose of **FM358** (green) and predicted intermolecular polar contacts (distances in Ångström). Calculation based on PDB ID: 5YQO. The position of cofactor NAD^+ (grey) was copied from PDB ID: 4RMG for visualization, as not included in the co-crystal structure of **Yang_24a** (PDB ID: 5YQO). (**B**) Comprehensive structural formula representation of the calculated docking pose of **FM358** and Sirt2 with the relevant surrounding amino acids Val233 and Arg97, as well as the corresponding predicted intermolecular polar contacts (distances in Ångström).

2.4. Second Generation Targeted Halogenation Approach as a Follow-Up Strategy for Further Improvement of the Hybrid Candidate FM358

Concluding that the electrostatic interactions arising from the amide group (Figure 4) are significantly responsible for the superiority of **FM358** and **Yang_24a** over **FM345**, **FM368** and **SirReal2**, a further approach was applied that aimed to expand and intensify electrostatic interactions by targeted halogen substitution [21] (chlorine, bromine, iodine) of the neighboring benzene ring, close to the amide residue of the substrate channel residue with Val233 or Arg97 and NAD^+ (Figure 5).

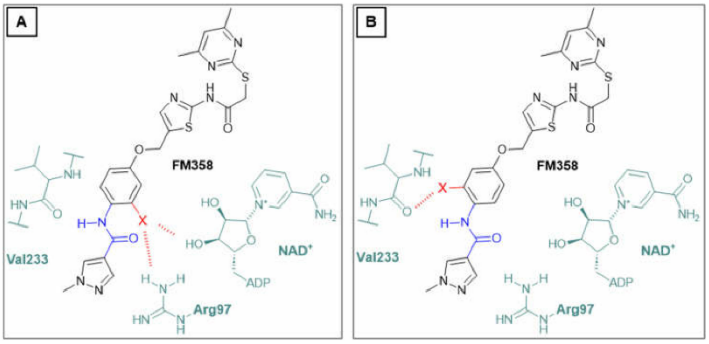

Figure 5. Schematic illustration of two rotameric forms of **FM358** in the Sirt2 binding pocket with the key amino acids identified in the previous docking study (Figure 4). Intended further structural optimization of **FM358** through the introduction of halogen atoms (residues X) to enable new potential electrostatic interactions with binding pocket and cofactor NAD^+. Abbreviations: X (halogen atom, Cl, Br or I). (**A**) Possible interactions of halogen atoms with NAD^+ and Arg97. (**B**) Possible interactions of the halogen atoms with Val233.

2.5. Synthesis of Second-Generation Hybrid Candidates

Amide couplings of *ortho*-halogenated hydroxyanilines with 1-methyl-1*H*-pyrazole-4-carboxylic acid showed initial difficulties with formation of the undesired phenol esters being preferred. Thus, the established synthetic route was slightly modified, and Williamson ether synthesis of the appropriate halogenated phenolates with the central chloromethylthiazole intermediate **5** (Scheme 2) was performed prior to the amide coupling. This circumvents the problem without any additional use of protecting groups for the phenol in the amide coupling (Scheme 3).

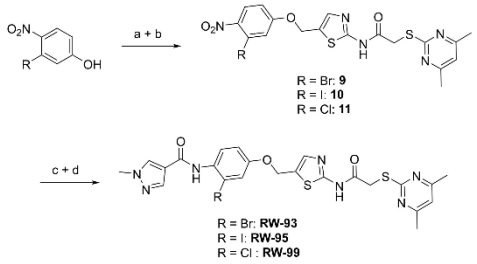

Scheme 3. (a) NaOMe 25% (*w*/*w*), DCM, rt, 2 min, crude, (b) **5**, DCM, rt, 3 h, 37% for **9**, 39% for **10**, 48% for **11**; (c) Fe, NH_4Cl, EtOH/H_2O (8:1 *v*/*v*), 90 °C, 2 h, crude; (d) 1-methyl-1*H*-pyrazole-4-carbonyl chloride, pyridine, DCM, rt, 1 h, 37% for **RW-93** (over two steps), 39% for **RW-95** (over two steps), 38% for **RW-99** (over two steps).

The Williamson ether synthesis was performed with initially prepared 3-halogen-4-nitrophenolates (obtained from corresponding phenols using sodium methoxide) and alkyl chloride **5**, based on the previously established general synthesis (Scheme 2). After reduction of the nitro group with Fe/NH_4Cl, the respective aniline was reacted without further purification with the 1-methyl-1*H*-pyrazole-4-carbonyl chloride, which was

previously prepared from the corresponding carboxylic acid by thionyl chloride, to yield the target compounds **RW-93**, **RW-95** and **RW-99**.

2.6. Biological Evaluation of Second-Generation Hybrid Candidates and Identification of the Bromine-Substituted Analog RW-93 as Top Inhibitor

The fluorescence-based assays to determine the inhibitory activity on Sirt2 and subtype selectivity of the halogenated derivatives of **FM358** (IC_{50} = 66 nM) revealed satisfactory results and confirmed the universal potency-enhancing impact of the halogen substituted chlorine (**RW-99**), bromine (**RW-93**) and iodine (**RW-95**) derivatives towards Sirt2 (see Table 2). Bromo compound **RW-93** (IC_{50} = 16 nM) shows an impressive 5-fold higher inhibitory activity than the original lead compounds **Yang_24a** (IC_{50} = 79 nM, Sirt2) and is more than 4 times more potent than the top hybrid precursor **FM358**.

Table 2. Inhibitory activity on Sirt2 and corresponding subtype selectivity towards Sirt1, Sirt3 and Sirt5 of respective inhibitors was determined by Reaction Biology Corporation (Malvern, PA, USA) using fluorescence-based assays. IC_{50} values were obtained for each serial dilution within the triplicate set through sigmoidal curve fitting, and the mean with standard deviation (SD) was calculated from these three values. Residual enzyme activity of Sirt1, Sirt3, and Sirt5 was measured as a percentage at a final inhibitor concentration of 50 µM, based on duplicate samples, and the mean with standard deviation (SD) was calculated thereof.

ID	Chemical Structure	IC_{50} [µM] ± SD Sirt2	Residual Enzyme Activity [%] ± SD		
			Sirt1	Sirt3	Sirt5
RW-99	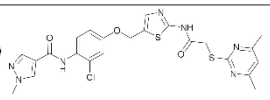	0.0250 ± 0.0026	53.9 ± 0.2	56.1 ± 0.1	55.1 ± 2.0
RW-93	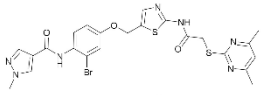	0.0155 ± 0.0007	58.2 ± 0.2	62.3 ± 1.2	53.0 ± 0.2
RW-95	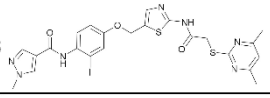	0.0485 ± 0.0056	60.9 ± 0.7	64.2 ± 1.2	48.2 ± 1.8

RW-99 (IC_{50} = 25 nM) and **RW-95** (IC_{50} = 49 nM) also demonstrate an improved inhibitory effect compared to **FM358**. Considering the pronounced inhibitory effect of the tested inhibitors, the inhibitory effect on other sirtuin subtypes (Sirt1, Sirt3 and Sirt5) is negligible. The halogen analogues can be ranked in descending order according to their determined inhibitory effect on Sirt2 as Br > Cl > I. An obvious explanation is that the extent of the polarizability and thus the strength of the possible halogen bridge correlates with the atom size and the associated space requirement. Bromine may have a sweet spot in terms of atomic radius and bond strength.

In the search for the exact cause of the potency-enhancing effect of the halogen substitution and to confirm a suspected halogen bridge, the bromo-substituted top compound **RW-93** was investigated in a further docking study (Figure 6). In principle, **FM358** and **RW-93** show a nearly congruent binding mode in the docking experiment, the only decisive difference being the bromine substitution. Interestingly, according to the predictions, the bromine atom does not orientate itself directly towards the position of NAD^+ and Arg97 (Figure 5A) but, as also additionally considered, to the side of Val233 and Phe235 (Figure 5B). Originating from the bromine atom, two polar contacts with the backbone

carbonyl of Val233 (3.2 Å) and backbone amide-nitrogen of Phe235 (3.1 Å) were predicted, which enable additional intermolecular interactions via halogen bonds. Interactions with Val233 were also described for the lead compounds **SirReal2** and **Yang_24a**, which, according to prediction, were further intensified by respective halogen substitution in the case of **RW-93.** Therefore, this specific binding region of Sirt2 can be considered as a potential attractive interaction target and serve as a key area for the design of further highly potent Sirt2 inhibitors. However, only a co-crystal structure of **RW-93** with Sirt2 can provide reliable information, and intensive efforts are currently being made to uncover the underlying structure-effect relationship, although limited solubility remains a significant barrier to successful co-crystallizations.

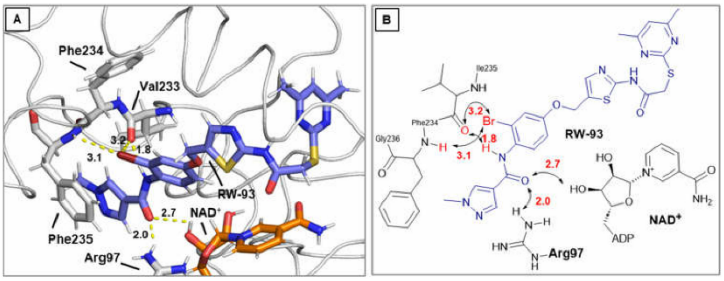

Figure 6. (**A**) Docking pose of **RW-93** (blue). Calculation based on PDB ID: 5YQO, with Sirt2. The position of NAD^+ (grey) was copied from PDB ID: 4RMG for visualization as not included in the crystal structure of **Yang_24a** (PDB ID: 5YQO). Polar contacts shown as dashed lines, distances in Ångström. (**B**) Schematic 2D illustration of **RW-93** and corresponding polar interaction with the key amino acids of the Sirt2 binding pocket. Non-scaled polar contacts represented with arrows, distances in Ångström.

2.7. Cell Viability Assay

The SirReal-based Sirt2 inhibitors (**FM345**, **FM352**, **FM358**, **FM368**, **RW-93**, **RW-95** and **RW-99**) were tested for potential acute cytotoxicity to human cells in an MTT-based cell viability assay. HL-60 cell line was selected based on literature report that showed that the lead structure **SirReal2** is not toxic in this particular cell line [22]. HL-60 cells were treated with the corresponding Sirt2 inhibitors at various concentrations and then incubated for 24 h. All investigated Sirt2 inhibitors showed no significant acute cytotoxicity with IC_{50} values above 50 µM. Representative cell viability results following treatment with **RW-93** are shown in Figure S1 of the Supplementary Materials.

2.8. Free Binding Energy Calculations and Validation Studies

The estimated docking scores and the free binding energies of the lead structures **SirReal2**, **Yang_24a** and **Yang_28e**, and the investigated Sirt2 inhibitors (**FM345**, **FM352**, **FM358**, **FM368**, **RW-93**, **RW-95** and **RW-99**) were calculated based on the PDB ID: 5YQO and compared with their respective IC_{50} values obtained from in vitro experiments. A comparative analysis showed a good degree of correlation between the estimated docking scores as well as the calculated free binding energies and the experimentally determined IC_{50} values with a Pearson correlation coefficient of 0.68 and 0.73, respectively. The most potent Sirt2 inhibitor **RW-93** displayed an estimated docking score of −14.63 kcal/mol and a calculated free binding energy (ΔG) of −110.82 kJ/mol (Table 3), which are among the most favourable values of the investigated Sirt2 inhibitors, aligning well with the in vitro determined IC_{50} data.

Table 3. Validation studies involving a comparative analysis of the estimated docking scores as well as the calculated free binding energies of the investigated Sirt2 inhibitors with their respective experimentally determined in vitro IC_{50} values. The correlation factor between the estimated docking scores and the IC_{50} values is 0.68, and the correlation factor between the calculated free binding energies (ΔG) and the IC_{50} values is 0.73.

ID	Chemical Structure	IC_{50} [μM] ± SD Sirt2	Docking Score [kcal/mol]	ΔG [kJ/mol]
SirReal2	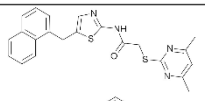	0.235 ± 0.008	−9.39	−81.59
Yang_24a	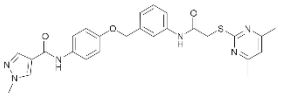	0.0790 ± 0.0030	−13.16	−130.59
Yang_28e	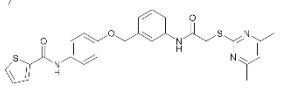	0.0867 ± 0.0085	−12.58	−126.99
FM345	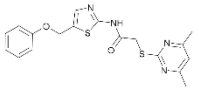	5.29 ± 0.73	−9.07	−77.87
FM352	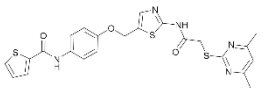	0.0935 ± 0.0064	−11.97	−111.29
FM358	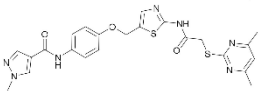	0.0656 ± 0.0044	−12.51	−110.30
FM368	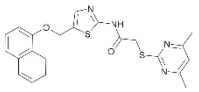	6.51 ± 0.84	−9.90	−79.76
RW-93	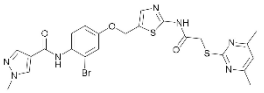	0.0155 ± 0.0007	−14.63	−110.82
RW-95	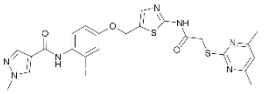	0.0485 ± 0.0056	−14.65	−104.97
RW-99	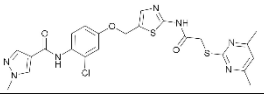	0.0250 ± 0.0026	−14.30	−115.51

2.9. In Silico ADME Profiling of Sirt2 Hybrid Inhibitors Calculated by QikProp

Selected synthesized Sirt2 hybrid inhibitors were evaluated for their drug-likeness by assessing their physicochemical properties (Table 4). Relevant parameters for the evaluation of the absorption and distribution of the Sirt2 inhibitors such as the predicted octanol/water partition coefficient (QPlogPo/w), brain/blood partition coefficient (QPlogBB) and cell permeability (QPPCaco) showed values within the recommended range. Furthermore, all four Sirt2 hybrid inhibitors showed high predicted oral absorption (HOA) of

over 80%. Drug-likeness of these inhibitors was additionally evaluated by their stars value (S) and their conformity to the Lipinski's rule of five (RO5) with values falling in the recommended range. Notably, these Sirt2 hybrid inhibitors showed poor predicted aqueous solubility with QPlogS values ranging from −8 to −8.5.

Table 4. ADME properties calculated by QikProp. S (Stars) = Number of property/descriptor values falling outside the 95% range of similar values for known drugs. Recommended values 0 to 5. MW = Molecular weight. QPlogPo/w = Predicted octanol/water partition coefficient. Recommended values −2.0 to 6.5. QPlogS = Predicted aqueous solubility. Recommended values −6.5 to 0.5. QPPCaco = Predicted apparent Caco-2 cell permeability in nm/sec. Recommended values < 25 poor, >500 great. QPlogBB = Predicted brain/blood partition coefficient. Recommended values −3.0 to 1.2. HOA = Predicted human oral absorption on 0 to 100% scale. Recommended values < 25% poor, >80% high. RO5 = Number of violations of Lipinski's rule of five. The rules are: mol. MW < 500, QPlogPo/w < 5, donorHB ≤ 5, accptHB ≤ 10. Recommended value < 4.

ID	S	MW	QPlogPo/w	QPlogS	QPP Caco	QPlogBB	HOA (%)	RO5
FM358	3	509.6	4.117	−7.991	232.950	−2.063	80.460	1
RW-93	3	588.5	4.557	−8.371	265.051	−1.808	84.039	1
RW-95	4	635.5	4.659	−8.529	264.457	−1.805	84.623	1
RW-99	3	544.0	4.506	−8.359	244.444	−1.872	83.112	1

3. Discussion

By successfully applying a lead structure-based hybridization strategy, highly potent and selective Sirt2 inhibitors were specifically developed, which provide a valuable extension of knowledge of structure–activity relationships of SirReal-type inhibitors. The development of a synthetic route to the previously unknown structural class of 5-(aryloxymethyl)thiazoles led to the identification of **FM358** (IC_{50} = 66 nM), an optimized hybrid compound whose inhibitory potency was further significantly enhanced through targeted ring halogenation. Docking calculations of bromo derivative **RW-93** suggest the formation of halogen bonds to Val233 or Phe235 within the Sirt2 binding pocket, which could contribute significantly to the observed increase in potency and thus could be an attractive target area for potential future design strategy of new Sirt2 inhibitors. With the bromo-substituted **RW-93** (IC_{50} = 16 nM) a highly potent and selective Sirt2 inhibitor was developed, which outperforms original lead compound **Yang_24a** (IC_{50} = 79 nM) by a factor of 5 and lead compound **SirReal2** by a factor of 15 and displays more than 3000-fold selectivity towards related subtypes Sirt1, Sirt3 and Sirt5. Furthermore, acute toxicity of **RW-93** to human cells was assessed and ruled out via MTT assay. Although the potential utility of **RW-93** at the cellular level remains an important objective, this study was still unable to demonstrate its effects in such biological contexts, primarily due to physicochemical limitations. In particular, solubility issues in various media remain a significant obstacle both in cellular assays and co-crystallization experiments. Within the framework of the in silico ADME investigation of the Sirt2 hybrid inhibitors, we showed that the predicted aqueous solubilities of these compounds were poor, aligning with the biological experimental challenges that we faced. However, the majority of relevant pharmacokinetic parameters reveal drug-likeness properties of these Sirt2 inhibitors, highlighting their potential use in further drug development. Our results showcase a novel and an effective strategy in the optimization and the development of highly potent Sirt2 inhibitors that can easily be transferred into the broader spectrum of SAR studies in other fields of medicinal chemistry. Together with computational validation, this strategy was executed with great success to deliver **RW-93**—the most potent low-molecular subtype selective Sirt2 inhibitor known to date.

4. Materials and Methods

4.1. Chemistry

Commercially available solvents and reagents were utilized as received without any additional purification. NMR spectra were recorded with an Avance III HD 400 MHz Bruker BioSpin (Bruker Corporation, Billerica, MA, USA) for ^{1}H-NMR (400 MHz) and ^{13}C-NMR (101 MHz) or an Avance III HD 500 MHz Bruker BioSpin (Bruker Corporation, Billerica, MA, USA) for ^{1}H-NMR (500 MHz) and 13C-NMR (126 MHz) MestreNova 14.3.0 (Mestrelab Research S.L., Santiago de Compostela, Spain) was utilized for data analysis and the respective chemical shifts (δ) were referenced to the deuterated solvent peak (DMSO-d_6: δH = 2.50 ppm, δC = 39.52 ppm; CD_2Cl_2: δH = 5.32 ppm, δC = 53.84 ppm; $CDCl_3$: δH = 7.26 ppm, δC = 77.16 ppm). Coupling constants (J) were reported in Hertz (Hz), and multiplicities were given as: s (singlet), d (doublet), t (triplet), q (quartet), or m (multiplet). While the compounds are numbered according to IUPAC guidelines, the respective hierarchy of NMR signal assignments (denoted with apostrophes) were simplified by following the sequence in which the compounds were synthesized. Thin-layer chromatography (TLC) was employed for reaction monitoring, using 0.2 mm silica gel coated POLYGRAM® SIL G/UV254 polyester plates (Macherey-Nagel, Düren, Germany), and visualized under UV light at 254 nm. Flash column chromatography was carried out using SiO_2 60 (0.040–0.063 mm, 230–400 mesh ASTM) from Merk (Darmstadt, Germany). Infrared spectroscopy (IR) was performed on a Perkin Elmer FT-IR BXII/1000 spectrometer (Waltham, USA), paired with a DuraSamp IR II Diamond ATR sensor (Smiths Detection, London, UK). The IR spectra were recorded over the range of 4000 to 650 cm^{-1}, and significant absorption bands were noted in cm^{-1}. High-resolution mass spectrometry (HR-MS) was conducted using either a Jeol Mstation 700 (Akishima, Japan) or a JMS GCmate II Jeol (Akishima, Japan) for electron impact ionization (EI). Electrospray ionization (ESI) HR-MS was performed using a Thermo Finnigan LTQ (Thermo Fisher Scientific, Waltham, MA, USA). Melting points were determined with a Büchi B-540 melting point meter (Fawil, Switzerland). The purity of compounds was assessed using an HP Agilent 1100 HPLC system (Agilent, Santa Clara, CA, USA) with a Zorbax Eclipse Plus® C18 5 µm (4.6 × 150 mm) column (Agilent, Santa Clara, CA, USA), using acetonitrile/water (method 1), or acetonitrile/phosphate buffer pH = 5 (method 2) as mobile phases.

General Procedure: Nitrobenzene reduction: To a stirred solution of the appropriate nitrobenzene derivative (1.0 equivalent) in EtOH with a concentration of 0.010 M were added iron powder (5.0 equivalents) and 0.30 M aq. NH_4Cl (5.0 equivalents) at 50 °C. The reaction mixture was refluxed at 90 °C for 2 h. Afterwards, the solids were removed by filtration and the filtrate was concentrated in vacuo. The crude product was used for the next step without further purification.

2-((4,6-Dimethylpyrimidin-2-yl)thio)acetic acid (2). 4,6-Dimethylpyrimidine-2-thiol (**1**) (3.80 g, 27.1 mmol, 1.00 eq) and chloroacetic acid (3.07 g, 32.5 mmol, 1.20 eq) were suspended in acetonitrile (25 mL) at room temperature. After addition of NEt_3 (15.1 mL, 108 mmol, 4.00 eq), the reaction mixture was stirred for 24 h. After evaporating the solvent, the crude product was purified via flash column chromatography (DCM/MeOH/AcOH 100:1:1) to yield thioether **2** as a light-beige solid (4.33 g, 21.8 mmol, 81%); m.p. 128 °C; IR (ATR) $\tilde{\nu}$/cm^{-1} 3474, 2942, 2534, 1924, 1716, 1584, 1538, 1309, 1267, 1208, 1172, 984, 862, 791, 661; δ_H (400 MHz; $(CD_3)_2SO$) 12.73 (s, 1H, COOH), 6.97 (s, 1H, 5-H), 3.90 (s, 2H, CH_2), 2.33 (s, 6H, 4-CH_3, 6-CH_3). δ_C (101 MHz; $(CD_3)_2SO$) 170.2 (COOH), 169.0 (C-2), 167.0 (C-4, C-6), 116.0 (C-5), 32.9 (CH_2), 23.3 (4-CH_3, 6-CH_3); HRMS (ESI): *m*/*z* = $[M-H]^-$ calculated for $C_8H_9N_2O_2S^-$: 197.0390; found: 197.0390.

2-((4,6-Dimethylpyrimidin-2-yl)thio)-*N*-(5-formylthiazol-2-yl)acetamide (3). Carboxylic acid **2** (1.55 g, 7.80 mmol, 1.00 eq) was dissolved in DMF (5 mL) and added to a

previously prepared solution of 2-aminothiazole-5-carbaldehyde (1.00 g, 7.80 mmol, 1.00 eq), DMAP (0.477 g, 3.90 mmol, 0.50 eq) and EDC·HCl (1.83 g, 9.36 mmol, 1.20 eq) in 5 mL DMF. After stirring for 16 h at room temperature, the reaction mixture was diluted with water (400 mL) and extracted with EtOAc (3 × 100 mL). The combined organic layers were dried over sodium sulfate. After evaporating the solvent, the crude product was purified via flash column chromatography (DCM/MeOH 100:1) to yield aldehyde **3** as a pale yellow solid (1.11 g, 3.61 mmol, 46%); m.p. 191–193 °C; IR (ATR) $\tilde{\nu}$/cm^{-1} 2924, 2137, 1688, 1664, 1586, 1555, 1516, 1427, 1385, 1311, 1268, 1234, 1173, 1123, 977, 872, 819, 733; δ_H (400 MHz; $(CD_3)_2SO$) 13.02 (s, 1H, NHCO), 9.96 (s, 1H, CHO), 8.44 (s, 1H, 4′-H), 6.97 (s, 1H, 5-H), 4.18 (s, 2H, CH_2), 2.28 (s, 6H, 4-CH_3, 6-CH_3). δ_C (101 MHz; $(CD_3)_2SO$) 184.1 (CHO), 168.7 (C-2), 168.4 (NHCO), 167.1 (C-4, C-6), 164.0 (C-2′), 150.7 (C-4′) 132.1 (C-5′), 116.2 (C-5), 34.4 (CH_2), 23.2 (4-CH_3, 6-CH_3); HRMS (ESI): *m*/*z* = $[M-H]^-$ calculated for $C_{12}H_{11}N_4O_2S_2^-$: 307.0329; found: 307.0330.

2-((4,6-Dimethylpyrimidin-2-yl)thio)-*N*-(5-(hydroxymethyl)thiazol-2-yl)acetamide (4). To a stirred solution of aldehyde **3** (550 mg, 1.78 mmol) in dry MeOH (20 mL) was added $NaBH_4$ (101 mg, 2.68 mmol) at 0 °C. The reaction mixture was stirred at 0 °C for 3 h under N_2 atmosphere. Water (15 mL) was then added, and the reaction mixture was stirred for another 10 min. The suspension was vacuum filtered, and the obtained solid washed with water (1 × 50 mL) and acetone (1 × 50 mL) to give alcohol **4** as a white solid (553 mg, 1.78 mmol, quantitative); m.p. 250–252 °C; IR (ATR) $\tilde{\nu}$/cm^{-1} 3284, 2917, 1696, 1588, 1537, 1323, 1273, 1262, 1161, 1037, 971, 843, 834, 788, 717; δ_H (400 MHz; $(CD_3)_2SO$) 12.22 (s, 1H, NHCO), 7.28 (d, *J* = 1.0 Hz, 1H, 4′-H), 6.96 (s, 1H, 5-H), 5.35 (t, *J* = 5.7 Hz, 1H, OH), 4.57 (dd, *J* = 5.7, 0.9 Hz, 2H, CH_2OH), 4.11 (s, 2H, CH_2S), 2.30 (s, 6H, 4-CH_3, 6-CH_3). δ_C (101 MHz; $(CD_3)_2SO$) 168.9 (C-2), 167.0 (C-4, C-6), 166.9 (NHCO), 157.5 (C-2′), 134.5 (C-4′) 133.1 (C-5′), 116.1 (C-5), 55.7 (CH_2OH), 34.1 (CH_2S), 23.3 (4-CH_3, 6-CH_3); HRMS (ESI): *m*/*z* = $[M-H]^-$ calculated for $C_{12}H_{13}N_4O_2S_2^-$: 309.0485; found: 309.0486.

***N*-(5-(Chloromethyl)thiazol-2-yl)-2-((4,6-dimethylpyrimidin-2-yl)thio)acetamide (5).** Primary alcohol **4** (358 mg, 1.15 mmol, 1.00 eq) was suspended in anhydrous DCM (15 mL) under nitrogen atmosphere and $SOCl_2$ (101 µL, 1.38 mmol, 1.20 eq) was added dropwise, while stirring at room temperature. After 18 h, *n*-hexane (5 mL) was added to the reaction mixture and the precipitate was collected by filtration. Subsequently the product was washed with *n*-hexane/DCM (1:1, 3 × 20 mL) to yield chloromethyl compound **5** as a white solid (378 mg, 1.15 mmol, quantitative yield); m.p. 226–233 °C (decomposition); IR (ATR) $\tilde{\nu}$/cm^{-1} 3270, 2421, 1720, 1624, 1602, 1582, 1540, 1417, 1370, 1333, 1307, 1268, 1158, 876, 849, 716, 703, 695; δ_H (400 MHz; $(CD_3)_2SO$) 12.46 (s, 1H, NHCO), 7.53 (s, 1H, 3′-H), 6.96 (s, 1H, 5-H), 5.03 (s, 2H, CH_2S), 4.13 (s, 2H, CH_2Cl), 2.29 (s, 6H, 4-CH_3, 6-CH_3). δ_C (101 MHz; $(CD_3)_2SO$) 168.8 (C-2), 167.4 (NHCO), 167.0 (C-4, C-6), 159.2 (C-2′), 138.2 (C-3′), 128.0 (C-4′), 116.2 (C-5), 38.7 (CH_2Cl), 34.1 (CH_2S), 23.2 (4-CH_3, 6-CH_3). HRMS (ESI): *m*/*z* = $[M-Cl+H_2O-2H]^-$ calculated for $C_{12}H_{13}N_4O_2S_2^-$: 309.0485; found: 309.0483.

2-((4,6-Dimethylpyrimidin-2-yl)thio)-*N*-(5-(phenoxymethyl)thiazol-2-yl)acetamide (FM345). Chloromethyl compound **5** (154 mg, 0.468 mmol, 1.00 eq) and sodium phenolate (54.4 mg, 0.468 mmol, 1.00 eq) were suspended in anhydrous DCM (20 mL) under nitrogen atmosphere and the reaction mixture was stirred for 24 h at room temperature. Following TLC monitoring, an additional equivalent of sodium phenolate (54.4 mg, 0.468 mmol, 1.00 eq) was added to complete the reaction. After 2 h, the solvent was evaporated under reduced pressure. NaOH solution (aq., 2 M, 50 mL) was added to the residue and the mixture was extracted with EtOAc (4 × 75 mL). The combined organic layers were dried over sodium sulfate. After evaporating the solvent, the crude product was purified by flash column chromatography (DCM/MeOH 100:1) to yield **FM345** as a white solid (33.0 mg, 0.0854 mmol, 18%); m.p. 160–163 °C; IR (ATR) $\tilde{\nu}$/cm^{-1} 2916, 2159, 1688, 1583, 1539, 1496, 1384, 1312, 1270, 1238, 1171, 1139, 1008, 966, 883, 803, 749, 733, 687; δ_H (500 MHz;

$(CD_3)_2SO$) 12.38 (s, 1H, NHCO), 7.54 (s, 1H, 4′-H), 7.33–7.25 (m, 2H, 3″-H, 5″-H), 7.03–6.98 (m, 2H, 2″-H, 5″-H), 6.98–6.91 (m, 2H, 4″-H, 5-H), 5.25 (s, 2H, CH_2O), 4.11 (s, 2H, CH_2S), 2.28 (s, 6H, 4-CH_3, 6-CH_3). δ_C (126 MHz; $(CD_3)_2SO$) 168.9 (C-2), 167.2 (NHCO), 167.0 (C-4, C-6), 158.6 (C-2′), 157.7 (C-1″), 137.7 (C-4′), 129.5 (C-3″, C-5″), 126.6 (C-5′), 121.0 (C-4′), 116.1 (C-5), 115.0 (C-2″, C-6″), 61.8 (CH_2O), 34.1 (CH_2S), 23.2 (4-CH_3, 6-CH_3). HRMS (ESI): *m*/*z* = $[M+H]^-$ calculated for $C_{18}H_{19}N_4O_2S_2^+$: 387.0944; found: 387.0944; Purity (HPLC): >99% (210 nm), >99% (254 nm), (method 1).

***N*-(4-Hydroxyphenyl)thiophene-2-carboxamide (7).** At room temperature, 4-aminophenol (**6**) (9.38 g, 86.0 mmol, 1.00 eq) was dissolved in DMF (30 mL) and pyridine (7.41 mL, 91.7 mmol, 1.07 eq) was added. The stirred mixture was cooled to 0 °C, and 2-thiophenecarbonyl chloride (9.78 mL, 91.4 mmol, 1.06 eq) was added dropwise. After 1.5 h the reaction mixture was diluted with water (300 mL) and extracted with EtOAc (4 × 100 mL). The combined organic layers were dried over sodium sulfate and concentrated in vacuo to obtain a viscous oil. The addition of DCM/hexanes (5 mL, 9:1) to the viscous oil induced the crystallization process. The obtained crystals were collected by filtration and washed with DCM/hexanes (9:1, 3 × 50 mL) to yield amide **7** as a white-pink solid (13.0 g, 59.1 mmol, 69%); m.p. 192–195 °C; IR (ATR) $\tilde{\nu}$/cm^{-1} 3109, 1620, 1598, 1539, 1505, 1438, 1355, 1314, 1264, 1245, 1221, 1173, 1095, 884, 8299, 765, 739, 712. δ_H (400 MHz; $(CD_3)_2SO$) 10.01 (s, 1H, NHCO), 9.27 (s, 1H, OH), 7.96 (dd, *J* = 3.8, 1.1 Hz, 1H, 3′-H), 7.81 (dd, *J* = 5.0, 1.2 Hz, 1H, 5′-H), 7.50–7.44 (m, 2H, 2-H, 6-H), 7.20 (dd, *J* = 5.0, 3.7 Hz, 1H, 4′-H), 6.77–6.72 (m, 2H, 3-H, 5-H). δ_C (101 MHz; $(CD_3)_2SO$) 159.4 (NHCO), 153.8 (C-4), 140.4 (C-2′), 131.3 (C-5′), 130.1 (C-1′), 128.5 (C-3′), 128.0 (C-4′), 122.4 (C-2, C-6), 115.0 (C-3, C-5). HRMS (ESI): *m*/*z* = $[M-H]^-$ calculated for $C_{11}H_8NO_2S^-$: 218.0281; found: 218.0280.

***N*-(4-Hydroxyphenyl)-1-methyl-1*H*-pyrazole-4-carboxamide (8).** DIPEA (3.80 mL, 22.0 mmol, 3.00 eq) and HATU (2.26 g, 5.95 mmol, 1.50 eq) were added to a solution of 1-methyl-1*H*-pyrazole-4-carboxylic acid (925 mg, 7.33 mmol, 1.00 eq) in anhydrous THF (15 mL) and the reaction mixture was stirred at room temperature for 1 h. 4-Aminophenol (**6**) (800 mg, 7.33 mmol, 1.00 eq) was added and the reaction mixture was stirred for another 3 h. Then the mixture was diluted with water (150 mL) and extracted with DCM (4 × 100 mL). The combined organic layers were dried over sodium sulfate. After evaporating the solvent, the crude product was purified by flash column chromatography (hexanes/EtOAc 2:8) to yield amide **8** as a white solid (171 mg, 0.787 mmol, 11%); m.p. 227–230 °C; IR (ATR) $\tilde{\nu}$/cm^{-1} 3347, 2926, 1641, 1601, 1558, 1509, 1430, 1388, 1308, 1273, 1201, 1151, 1099, 1005, 841, 812, 749, 703. δ_H (400 MHz; $(CD_3)_2SO$) 9.57 (s, 1H, NHCO), 9.18 (s, 1H, OH), 8.24 (s, 1H, 5′-H), 7.96 (s, 1H, 3′-H), 7.48–7.40 (m, 2H, 2-H, 6-H), 6.75–6.67 (m, 2H, 3-H, 5-H), 3.87 (s, 3H, CH_3). δ_C (101 MHz; $(CD_3)_2SO$) 160.0 (NHCO), 153.4 (C-4), 138.6 (C-3′), 132.3 (C-5′), 130.6 (C-1), 121.9 (C-2, C-6), 118.7 (C-4′), 114.0 (C-3, C-5), 38.8 (CH_3). HRMS (ESI): *m*/*z* = $[M+H]^+$ calculated for $C_{11}H_{12}N_3O_2^+$: 218.0924; found: 218.0928.

***N*-(4-((2-(2-((4,6-Dimethylpyrimidin-2-yl)thio)acetamido)thiazol-5-yl)methoxy)phenyl)thiophene-2-carboxamide (FM352).** Under nitrogen atmosphere, phenol **7** (268 mg, 1.22 mmol, 1.00 eq) was dissolved in anhydrous methanol (2 mL) and sodium methanolate (25% (*w*/*w*) in MeOH, 272 µL, 1.22 mmol, 1.00 eq) was added at room temperature. The reaction mixture was stirred for 2 min, subsequently the solvent was evaporated. The residue was dried under high vacuum to yield sodium 4-(thiophene-2-carboxamido)phenolate in quantitative yield, which was used without further purification for the next step. Chloromethyl compound **5** (123 mg, 0.374 mmol, 1.00 eq) and the previously prepared sodium 4-(thiophene-2-carboxamido)phenolate (90.2 mg, 0.374 mmol, 1.00 eq) were suspended in anhydrous DCM (15 mL) and the reaction mixture was stirred for 18 h at room temperature. Following TLC monitoring, an additional equivalent of sodium 4-(thiophene-2-carboxamido)phenolate (90.2 mg, 0.374 mmol, 1.00 eq) was added to complete the reaction. After 2 h, NaOH solution (aq., 2 M, 50 mL) was added, and the mixture

was extracted with DCM (3 × 50 mL). The combined organic layers were dried over sodium sulfate. After evaporating the solvent, the crude product was purified by flash column chromatography (DCM/MeOH 100:1) to yield **FM352** as a white solid (31.5 mg, 0.0616 mmol, 17%); m.p. 176–179 °C; IR (ATR) $\tilde{\nu}$/cm^{-1} 2923, 2164, 1700, 1635, 1578, 1512, 1422, 1323, 1265, 1229, 1159, 1010, 845, 734; δ_H (500 MHz; $(CD_3)_2SO$) 12.38 (s, 1H, 2′-NHCO), 10.11 (s, 1H, 4″-NHCO), 7.97 (d, *J* = 3.7 Hz, 1H, 3‴-H), 7.83 (d, *J* = 4.9 Hz, 1H, 5‴-H), 7.63–7.57 (m, 2H, 3″-H, 5″-H), 7.55 (s, 1H, 4′-H), 7.21 (t, *J* = 4.3 Hz, 1H, 4‴-H), 7.03–6.98 (m, 2H, 2″-H, 6″-H), 6.95 (s, 1H, 5-H), 5.25 (s, 2H, CH_2O), 4.12 (s, 2H, CH_2S), 2.28 (s, 6H, 4-CH_3, 6-CH_3). δ_C (126 MHz; $(CD_3)_2SO$) 168.9 (C-2) , 167.2 (2′-NHCO), 167.0 (C-4, C-6), 159.6 (4″-NHCO), 158.6 (C-2′), 154.0 (C-1″), 140.2 (C-2‴), 137.8 (C-4′), 132.2 (C-4″), 131.5 (C-5‴), 128.8 (C-3‴), 128.0 (C-4‴), 126.6 (C-5′), 121.9 (C-3″, C-5″), 116.1 (C-5), 115.1 (C-2″, C-6″), 62.1 (CH_2O), 34.1 (CH_2S), 23.2 (4-CH_3, 6-CH_3). HRMS (ESI): *m*/*z* = $[M-H]^-$ calculated for $C_{23}H_{20}N_8O_3S_3^-$: 510.0734; found: 510.0733. Purity (HPLC): >99% (210 nm), >99% (254 nm), (method 1).

***N*-(4-((2-((4,6-Dimethylpyrimidin-2-yl)thio)acetamido)thiazol-5-yl)methoxy)-phenyl)-1-methyl-1*H*-pyrazole-4-carboxamide (FM358).** Under nitrogen atmosphere, phenol 8 (294 mg, 1.35 mmol, 1.00 eq) was dissolved in anhydrous methanol (2 mL) and sodium methanolate (25% (*w*/*w*) in MeOH, 302 µL, 1.35 mmol, 1.00 eq) was added at room temperature. The reaction mixture was stirred for 2 min, subsequently the solvent was evaporated. The residue was dried under high vacuum to yield sodium 4-(1-methyl-1*H*-pyrazole-4-carboxamido)phenolate in quantitative yield, which was used without further purification for the next step. Under nitrogen atmosphere, chloromethyl compound 5 (150 mg, 0.456 mmol, 1.00 eq) and the previously prepared sodium 4-(1-methyl-1*H*-pyrazole-4-carboxamido)phenolate (109 mg, 0.456 mmol, 1.00 eq) were suspended in anhydrous DCM (15 mL) and the reaction mixture was stirred for 18 h at room temperature. Following TLC monitoring, an additional equivalent of sodium 4-(1-methyl-1*H*-pyrazole-4-carboxamido)phenolate (0.456 mmol, 109 mg, 1.00 eq) was added to complete the reaction. After 2 h, MeOH (1 mL) was added, and the reaction mixture was concentrated in vacuo. The crude product was purified by flash column chromatography (DCM/MeOH/AcOH 100:3:0.5) to yield FM358 as a white solid (87.1 mg, 0.171 mmol, 38%); m.p. 188–191 °C; IR (ATR) $\tilde{\nu}$/cm^{-1} 3285, 2923, 1692, 1640, 1578, 1559, 1512, 1489, 1438, 1413, 1378, 1325, 1268, 1226, 1172, 1158, 1007, 977, 870, 845, 820, 779, 757, 717; δ_H (500 MHz; $(CD_3)_2SO$) 12.37 (s, 1H, 2′-NHCO), 9.68 (s, 1H, 4″-NHCO), 8.26 (s, 1H, 4‴-H), 7.97 (s, 1H, 2‴-H), 7.60–7.58 (m, 2H, 3″-H, 5″-H), 7.53 (s, 1H, 4′-H), 6.98 (m, 2H, 2″-H), 6.95 (s, 1H, 5-H) 5.23 (s, 2H, CH_2O), 4.11 (s, 2H, CH_2S), 3.88 (s, 3H, NCH_3), 2.28 (s, 6H, 4-CH_3, 6-CH_3). δ_C (126 MHz; $(CD_3)_2SO$) 168.9 (C-2), 167.2 (2′-NHCO), 167.0 (C-4, C-6), 160.1 (4″-NHCO), 158.8 (C-2′), 153.6 (C-1″), 138.7 (C-2‴), 137.7 (C-4′), 132.7 (C-4″), 132.5 (C-4‴), 126.6 (C-5′), 121.4 (C-3″, C-5″), 118.6 (C-3‴), 116.1 (C-5‴), 115.1 (C-2‴, C-6‴), 62.2 (CH_2O), 38.8 (NCH_3), 34.2 (CH_2S), 23.2 (4-CH_3, 6-CH_3); HRMS (ESI): *m*/*z* = $[M-H]^-$ calculated for $C_{23}H_{22}N_7O_3S_2^-$: 508.1231; found: 508.1231; Purity (HPLC): >99% (210 nm), >99% (254 nm), (method 1).

2-((4,6-Dimethylpyrimidin-2-yl)thio)-*N*-(5-((naphthalen-1-yloxy)methyl)thiazol-2-yl)acetamide (FM368). Under nitrogen atmosphere, naphthalen-1-ol (377 mg, 2.61 mmol, 1.00 eq) was dissolved in anhydrous methanol (2 mL) and sodium methanolate (25% (*w*/*w*) in MeOH, 583 µL, 2.61 mmol, 1.00 eq) was added at room temperature. The reaction mixture was stirred for 2 min, subsequently the solvent was evaporated. The residue was dried under high vacuum to yield sodium 1-naphtholate in quantitative yield, which was used without further purification for the next step. Under nitrogen atmosphere chloromethyl compound **5** (150 mg, 0.456 mmol, 1.00 eq) and the previously prepared sodium 1-naphtholate (75.8 mg, 0.456 mmol, 1.00 eq) were suspended in anhydrous acetone (5 mL) and the reaction mixture was stirred for 3 h at room temperature. Following TLC monitoring, an additional equivalent of sodium 1-naptholate (75.8 mg, 0.456 mmol, 1.00 eq)

was added to complete the reaction. After 2 h, water (50 mL) was added to the reaction mixture and the mixture was extracted with EtOAc (3 × 100 mL). The combined organic layers were dried over sodium sulfate. After evaporating the solvent in vacuo, the crude product was purified by flash column chromatography (DCM/MeOH 100:0.5) to yield **FM368** as a white solid (28.0 mg, 0.0641 mmol, 14%); m.p. 181–183 °C; IR (ATR) $\tilde{\nu}$/cm^{-1} 2907, 1697, 1580, 1552, 1506, 1437, 1396, 1367, 1320, 1264, 1241, 1163, 1099, 1065, 1018, 975, 891, 874, 859, 834, 778, 768, 717; δ_H (500 MHz; $(CD_3)_2SO$) 12.42 (s, 1H; NHCO), 8.09 (d, *J* = 8.1 Hz, 1H, 8″-H), 7.87 (d, *J* = 8.0 Hz, 1H, 5″-H), 7.63 (s, 1H, 4′-H), 7.55–7.40 (m, 4H, 3″-H, 4″-H, 6″-H, 7″-H), 7.14 (d, *J* = 7.6 Hz, 1H, 2″-H), 6.95 (s, 1H, 5-H), 5.47 (s, 2H, CH_2O), 4.13 (s, 2H, CH_2S), 2.29 (s, 6H, 4-CH_3, 6-CH_3). δ_C (126 MHz; $(CD_3)_2SO$) 168.9 (C-2), 167.2 (NHCO), 167.0 (C-4, C-6), 158.7 (C-2′), 153.1 (C-1″), 137.6 (C-4′), 134.1 (C-4a″), 127.5 (C-5″), 126.7 (C-5′), 126.5 (C-3″), 126.1 (C-6″), 125.5 (C-7″), 125.0 (C-8a″), 121.4 (C-8″), 120.5 (C-4″), 116.1 (C-5), 106.1 (C-2″), 62.6 (CH_2O), 34.1 (CH_2S), 23.2 (4-CH_3, 6-CH_3); HRMS (EI): *m*/*z* = $[M]^{\bullet+}$ calculated for $C_{22}H_{20}N_4O_2S_2^{\bullet+}$: 436.1028; found: 436.1032; Purity (HPLC): >99% (210 nm), >99% (254 nm), (method 2).

***N*-(5-((3-Bromo-4-nitrophenoxy)methyl)thiazol-2-yl)-2-((4,6-dimethylpyrimidin-2-yl)thio)acetamide (9).** To a stirred solution of 3-bromo-4-nitrophenol (150 mg, 0.667 mmol) in dry MeOH (3 mL) was added sodium methanolate 25% (*w*/*w*) in MeOH (0.153 mL, 0.667 mmol). The solution was stirred at room temperature for 5 min, then concentrated in vacuo to give sodium 3-bromo-4-nitrophenolate as an orange solid, which was used for the next step without further purification. Chloromethyl compound **5** (80.0 mg, 0.243 mmol) and sodium 3-bromo-4-nitrophenolate (158 mg, 0.730 mmol) were dissolved in dry DCM (7 mL) and stirred at room temperature for 3 h under N_2 atmosphere. The reaction mixture was then diluted with DCM (50 mL) and washed with 2M NaOH (3 × 50 mL). The organic phase was then dried using a phase separation paper, concentrated in vacuo and purified by flash column chromatography (DCM/MeOH 98:2) to give ether **9** as a pale-yellow solid (45.9 mg, 0.0899 mmol, 37%); m.p. 175 °C; IR (ATR) $\tilde{\nu}$/cm^{-1} 2923, 1742, 1666, 1578, 1555, 1518, 1477, 1432, 1372, 1340, 1318, 1267, 1217, 1170, 1153, 1137, 1000, 979, 965, 809, 746, 721; δ_H (400 MHz; $(CD_3)_2SO$) 12.44 (s, 1H, CONH), 8.06 (d, *J* = 9.1 Hz, 1H, 5″-H), 7.61 (s, 1H, 4′-H), 7.55 (d, *J* = 2.6 Hz, 1H, 2″-H), 7.23 (dd, *J* = 9.1, 2.7 Hz, 1H, 6″-H), 6.95 (d, *J* = 0.6 Hz, 1H, 5-H), 5.46–5.43 (m, 2H, OCH_2), 4.12 (s, 2H, SCH_2), 2.28 (s, 6H, 4-CH_3 and 6-CH_3). δ_C (126 MHz; $(CD_3)_2SO$) 168.9 (C-2), 167.3 (CONH), 167.0 (C-4 and C-6), 161.0 (C-1″), 159.1 (C-2′), 142.6 (C-4″), 138.8 (C-4′), 127.9 (C-5″), 125.1 (C-5′), 120.6 (C-2″), 116.1 (C-5), 115.5 (C-3″), 115.2 (C-6″), 63.1 (OCH_2), 34.1 (SCH_2), 23.2 (4-CH_3 and 6-CH_3). HRMS (ESI): *m*/*z* = $[M+H]^+$ calculated for $C_{18}H_{17}BrN_5O_4S_2^+$: 509.9905; found: 509.9895.

2-((4,6-Dimethylpyrimidin-2-yl)thio)-*N*-(5-((3-iodo-4-nitrophenoxy)methyl)thiazol-2-yl)acetamide (10). To a stirred solution of 3-iodo-4-nitrophenol (220 mg, 0.805 mmol) in dry MeOH (3 mL) was added sodium methanolate 25% (*w*/*w*) in MeOH (0.179 mL, 0.805 mmol). The solution was stirred at room temperature for 5 min, then concentrated in vacuo to give sodium 3-iodo-4-nitrophenolate as an orange solid, which was used for the next step without further purification. Chloromethyl compound **5** (143 mg, 0.434 mmol) and sodium 3-iodo-4-nitrophenolate (177 mg, 0.650 mmol) were dissolved in dry DCM (7 mL) and stirred at room temperature for 3 h under N_2 atmosphere. The reaction mixture was then diluted with DCM (50 mL) and washed with 2M NaOH (3 × 50 mL). The organic phase was then dried using a phase separation paper, concentrated in vacuo and purified by flash column chromatography (DCM/MeOH 98:2) to give ether **10** as a pale-yellowsolid (93.3 mg, 0.167 mmol, 39%); m.p. 81 °C; IR (ATR) $\tilde{\nu}$/cm^{-1} 2920, 1688, 1574, 1515, 1337, 1315, 1265, 1222, 1165, 988, 868, 815, 747; δ_H (400 MHz; $(CD_3)_2SO$) 12.43 (s, 1H, CONH), 7.99 (d, *J* = 9.0 Hz, 1H, 5′-H), 7.72 (d, *J* = 2.7 Hz, 1H, 2′-H), 7.60 (s, 1H, 4-H), 7.23 (dd, *J* = 9.1, 2.7 Hz, 1H, 6′-H), 6.95 (s, 1H, 5″-H), 5.43–5.42 (m, 2H, OCH_2), 4.12 (s, 2H, SCH_2), 2.28 (s, 6H, 4″-CH_3 and 6″-CH_3). δ_C (101 MHz; $(CD_3)_2SO$) 168.9 (C-2″), 167.3 (CONH), 167.0

(C-4″ and C-6″), 160.6 (C-1′), 159.1 (C-2), 146.0 (C-4′), 138.7 (C-4), 127.3 (C-2′ or C-5′), 127.1 (C-2′ or C-5′), 125.2 (C-5), 116.1 (C-5″), 115.5 (C-6′), 90.2 (C-3′), 62.9 (OCH_2), 34.1 (SCH_2), 23.2 (4″-CH_3 and 6″-CH_3); HRMS (ESI): *m*/*z* = $[M+H]^+$ calculated for $C_{18}H_{17}IN_5O_4S_2^+$: 557.9761; found: 557.9755.

***N*-(5-((3-Chloro-4-nitrophenoxy)methyl)thiazol-2-yl)-2-((4,6-dimethylpyrimidin-2-yl)thio)acetamide (11).** To a stirred solution of 3-chloro-4-nitrophenol (141 mg, 0.805 mmol) in dry MeOH (3 mL) was added sodium methanolate 25% (*w*/*w*) in MeOH (0.179 mL, 0.805 mmol). The solution was stirred at room temperature for 5 min, then concentrated in vacuo to give sodium 3-chloro-4-nitrophenolate as an orange solid, which was used for the next step without further purification. Chloromethyl compound **5** (143 mg, 0.434 mmol) and sodium 3-chloro-4-nitrophenolate (116 mg, 0.652 mmol) were dissolved in dry DCM (7 mL) and stirred at room temperature for 3 h under N_2 atmosphere. The reaction mixture was then diluted with DCM (50 mL) and washed with 2M NaOH (3 × 50 mL). The organic phase was then dried using a phase separation paper, concentrated in vacuo and purified by flash column chromatography (DCM/MeOH 98:2) to give ether **11** as a pale-yellow solid (96.6 mg, 0.207 mmol, 48%); m.p. 225 °C; IR (ATR) $\tilde{\nu}$/cm^{-1} 2924, 1666, 1583, 1556, 1516, 1481, 1433, 1373, 1640, 1321, 1267, 1219, 1171, 1155, 1138, 1037, 985, 964, 891, 825, 808, 747, 721; δ_H (400 MHz; $(CD_3)_2SO$) 12.44 (s, 1H, CONH), 8.10 (d, *J* = 9.1 Hz, 1H, 5″-H), 7.62 (s, 1H, 4′-H), 7.43 (d, *J* = 2.7 Hz, 1H, 2″-H), 7.20 (dd, *J* = 9.2, 2.7 Hz, 1H, 6″-H), 6.95 (s, 1H, 5-H), 5.45 (d, *J* = 0.7 Hz, 2H, OCH_2), 4.12 (s, 2H, SCH_2), 2.28 (s, 6H, 4-CH_3 and 6-CH_3). δ_C (101 MHz; $(CD_3)_2SO$) 168.9 (C-2), 167.3 (CONH), 167.0 (C-4 and C-6), 161.3 (C-1″), 159.1 (C-2′), 140.6 (C-4″), 138.8 (C-4′), 128.1 (C-5″), 127.7 (C-3″), 125.0 (C-5′), 117.5 (C-2″), 116.1 (C-5), 114.9 (C-6″), 63.2 (OCH_2), 34.1 (SCH_2), 23.2 (4-CH_3 and 6-CH_3). HRMS (ESI): *m*/*z* = $[M+Na]^+$ calculated for $C_{18}H_{16}ClN_5O_4S_2Na^+$: 488.0230; found: 488.0218.

***N*-(2-Bromo-4-((2-(2-((4,6-dimethylpyrimidin-2-yl)thio)acetamido)thiazol-5-yl)-methoxy)phenyl)-1-methyl-1*H*-pyrazole-4-carboxamide (RW-93).** 1-Methyl-1*H*-pyrazole-4-carboxylic acid (3.00 g, 23.8 mmol) was treated with thionyl chloride (10 mL, 136 mmol) and the mixture stirred at 80 °C for 2 h. The excess thionyl chloride was then removed in vacuo to give 1-methyl-1*H*-pyrazole-4-carbonyl chloride as a thick white suspension which solidified to a white solid upon standing at room temperature. Reduction of nitrobenzene 9 (46.0 mg, 90.1 µmol) was performed according to General Procedure: Nitrobenzene reduction. The obtained crude amine was dissolved in dry DCM (1 mL). 1-Methyl-1*H*-pyrazole-4-carbonyl chloride (26.2 mg, 0.181 mmol) and pyridine (3.66 µL, 45.3 µmol) were added into the reaction mixture and the solution was stirred at room temperature for 1 h. The reaction mixture was then concentrated in vacuo and the crude product was purified by flash column chromatography (DCM/MeOH 98:2) to give RW-93 as a white solid (19.7 mg, 33.5 µmol, 37% over two steps); m.p. 185 °C; elemental analysis found: C, 46.9; H, 3.9; N, 16.1; S, 10.9%; calc. for $C_{23}H_{22}BrN_7O_3S_2$: C, 46.9; H, 3.8; N, 16.65; S, 10.9%; IR (ATR) $\tilde{\nu}$/cm^{-1} 3418, 2918, 1689, 1675, 1581, 1532, 1411, 1392, 1314, 1293, 1278, 1265, 1223, 1165, 1124, 1047, 1003, 982, 870, 845, 807, 743; δ_H (400 MHz; $(CD_3)_2SO$) 12.39 (s, 1H, 2″-NHCO), 9.49 (s, 1H, 4-CONH), 8.25 (s, 1H, 5-H), 7.96 (s, 1H, 3-H), 7.56 (s, 1H, 4″-H), 7.37–7.33 (m, 2H, 3′-H and 6′-H), 7.05 (dd, *J* = 8.8, 2.8 Hz, 1H, 5′-H), 6.96 (s, 1H, 5‴-H), 5.31 (s, 2H, OCH_2), 4.12 (s, 2H, SCH_2), 3.88 (s, 3H, NCH_3), 2.29 (s, 6H, 4‴-CH_3 and 6‴-CH_3). δ_C (101 MHz; $(CD_3)_2SO$) 168.9 (C-2‴), 167.0 (2″-NHCO, C-4‴ and C-6‴), 160.7 (4-CONH), 158.9 (C-2″) 156.2 (C-4′), 138.8 (C-3), 138.1 (C-4″), 132.6 (C-5), 129.8 (C-3′), 129.6 (C-1′), 126.0 (C-5″), 118.6 (C-6′), 117.9 (C-4), 116.1 (C-5‴), 115.0 (C-5′), 62.5 (OCH_2), 38.8 (NCH_3), 34.2 (SCH_2), 23.2 (4‴-CH_3 and 6‴-CH_3). HRMS (ESI): *m*/*z* = $[M+H]^+$ calculated for $C_{23}H_{23}BrN_7O_3S_2^+$: 588.0482; found: 588.0480.

***N*-(4-((2-(2-((4,6-Dimethylpyrimidin-2-yl)thio)acetamido)thiazol-5-yl)methoxy)-2-iodophenyl)-1-methyl-1*H*-pyrazole-4-carboxamide (RW-95).** 1-Methyl-1*H*-pyrazole-4-carboxylic acid (3.00 g, 23.8 mmol) was treated with thionyl chloride (10 mL, 136 mmol)

and the mixture stirred at 80 °C for 2 h. The excess thionyl chloride was then removed in vacuo to give 1-methyl-1*H*-pyrazole-4-carbonyl chloride as a thick white suspension which solidified to a white solid upon standing at room temperature. Reduction of nitrobenzene 10 (83.0 mg, 0.149 mmol) was performed according to General Procedure: Nitrobenzene reduction. The obtained crude primary amine was dissolved in dry DCM (1.5 mL). 1-Methyl-1*H*-pyrazole-4-carbonyl chloride (43.0 mg, 0.298 mmol) and pyridine (6.02 µL, 74.4 µmol) were added into the reaction mixture and the solution was stirred at room temperature for 1 h. The reaction mixture was then concentrated in vacuo and the crude product was purified via flash column chromatography (DCM/MeOH 98:2) to give RW-95 as a white solid (37.0 mg, 58.2 µmol, 39% over two steps); m.p. 202 °C; elemental analysis: found: C, 43.3; H, 3.5; N, 15.2; S, 10.1%; calc. for $C_{23}H_{22}IN_7O_3S_2$: C, 43.5; H, 3.5; N, 15.4; S, 10.1%; IR (ATR) $\tilde{\nu}$/cm^{-1} 3396, 3175, 3139, 2918, 1697, 1671, 1580, 1553, 1525, 1433, 1386, 1327, 1309, 1276, 1268, 1217, 1206, 1168, 1151, 991, 984, 855, 815, 777, 745, 732; δ_H (500 MHz; $(CD_3)_2SO$) 12.40 (s, 1H, 2″-NHCO), 9.48 (s, 1H, 4-CONH), 8.25 (s, 1H, 5-H), 7.96 (s, 1H, 3-H), 7.56 (s, 1H, 4″-H), 7.53 (d, *J* = 2.8 Hz, 1H, 3′-H), 7.25 (d, *J* = 8.8 Hz, 1H, 6′-H), 7.07 (dd, *J* = 8.7, 2.8 Hz, 1H, 5′-H), 6.96 (s, 1H, 5‴-H), 5.30 (s, 2H, OCH_2), 4.12 (s, 2H, SCH_2), 3.88 (s, 3H, NCH_3), 2.29 (s, 6H, 4‴-CH_3 and 6‴-CH_3). δ_C (126 MHz; $(CD_3)_2SO$) 168.9 (C-2‴), 167.2 (2″-NHCO), 167.0 (C-4‴ and C-6‴), 160.7 (4-CONH), 158.8 (C-2″), 156.2 (C-4′), 138.8 (C-3), 138.1 (C-4″), 133.0 (C-1′), 132.5 (C-5), 129.1 (C-6′), 126.1 (C-5″), 124.5 (C-3′), 118.1 (C-4), 116.1 (C-5‴), 115.6 (C-5′), 99.6 (C-2′), 62.4 (OCH_2), 38.8 (NCH_3), 34.1 (SCH_2), 23.2 (4‴-CH_3 and 6‴-CH_3); HRMS (ESI): *m*/*z* = $[M+H]^+$ calculated for $C_{23}H_{23}IN_7O_3S_2^+$: 636.0343; found: 636.0336.

***N*-(2-Chloro-4-((2-(2-((4,6-dimethylpyrimidin-2-yl)thio)acetamido)thiazol-5-yl)methoxy)phenyl)-1-methyl-1*H*-pyrazole-4-carboxamide (RW-99).** 1-Methyl-1*H*-pyrazole-4-carboxylic acid (3.00 g, 23.8 mmol) was treated with thionyl chloride (10 mL, 136 mmol) and the mixture stirred at 80 °C for 2 h. The excess thionyl chloride was then removed in vacuo to give 1-methyl-1*H*-pyrazole-4-carbonyl chloride as a thick white suspension which solidified to a white solid upon standing at room temperature. Reduction of nitrobenzene 9 (80.0 mg, 0.172 mmol) was performed according to General Procedure: Nitrobenzene reduction. The obtained crude amine was dissolved in dry DCM (1.5 mL). 1-methyl-1*H*-pyrazole-4-carbonyl chloride (49.7 mg, 0.344 mmol) and pyridine (6.96 µL, 86.0 µmol) were added into the reaction mixture and the solution was stirred at room temperature for 1 h. The reaction mixture was then concentrated in vacuo and the crude product was purified via flash column chromatography (DCM/MeOH 98:2) to give RW-99 as a white solid (35.8 mg, 65.8 µmol, 38% over two steps); m.p. 195 °C; elemental analysis: found: C, 50.5; H, 4.1; N, 17.6; S, 11.7; Cl, 6.9%; calc: for $C_{23}H_{22}ClN_7O_3S_2$: C, 50.8; H, 4.1; N, 18.0; S, 11.8; Cl, 6.5%; IR (ATR) $\tilde{\nu}$/cm^{-1} 2918, 1679, 1582, 1555, 1535, 1394, 1315, 1295, 1281, 1267, 1224, 1167, 1050, 1003, 900, 869, 845, 809, 743; δ_H (400 MHz; $(CD_3)_2SO$) 12.40 (s, 1H, 2″-NHCO), 9.51 (s, 1H, 4-CONH), 8.26 (s, 1H, 5-H), 7.96 (s, 1H, 3-H), 7.57 (s, 1H, 4″-H), 7.39 (d, *J* = 8.8 Hz, 1H, 6′-H), 7.22 (d, *J* = 2.8 Hz, 1H, 3′-H), 7.01 (dd, *J* = 8.8, 2.8 Hz, 1H, 5′-H), 6.96 (s, 1H, 5‴-H), 5.31 (s, 2H, OCH_2), 4.12 (s, 2H, SCH_2), 3.88 (s, 3H, NCH_3), 2.29 (s, 6H, 4‴-CH_3 and 6‴-CH_3). δ_C (101 MHz; $(CD_3)_2SO$) 168.9 (C-2‴), 167.2 (2″-NHCO), 167.0 (C-4‴ and C-6‴), 160.7 (4-CONH), 158.8 (C-2″), 156.0 (C-4′), 138.8 (C-3), 138.1 (C-4″), 132.6 (C-5), 130.4 (C-2′), 129.6 (C-6′), 128.1 (C-1′), 126.1 (C-5″), 117.8 (C-4), 116.1 (C-5‴), 115.6 (C-3′), 114.4 (C-5′), 62.5 (OCH_2), 38.8 (NCH_3), 34.1 (SCH_2), 23.2 (4‴-CH_3 and 6‴-CH_3). HRMS (ESI): *m*/*z* = $[M+Na]^+$ calculated for $C_{23}H_{22}ClN_7O_3S_2Na^+$: 566.0812; found: 566.0798.

4.2. Biological Investigations

Sirtuin assays. The biological activity of the test substances against the respective sirtuin enzymes was evaluated by means of a fluorescence-based assay performed by Reaction Biology Corporation (Malvern, PA, USA). The sirtuin enzymes used in the assays

were all obtained from in-house sources at Reaction Biology Corporation (Malvern, PA, USA). Sirt1, with accession number NM_012238, includes amino acids 1–747 (C-terminal) and is tagged with an N-terminal His-tag. Sirt1 was expressed in *E. coli* and purified to greater than 85% as confirmed by SDS-PAGE and is supplied as a solution in 50 mM Tris/HCl (pH 7.5), 100 mM NaCl, and 10% glycerol (*v*/*v*). Sirt2 (accession number NM_012237), comprising amino acids 50–389 (C-terminal), features an N-terminal His-tag and was expressed in *E. coli* and finally purified to over 90% by SDS-PAGE. Sirt2 is provided in a buffer containing 50 mM Tris/HCl (pH 7.5), 500 mM NaCl, 1 mM TCEP, and 10% glycerol (*v*/*v*). Sirt3, with accession number NM_012239.3, spans amino acids 101–399 and is tagged with an N-terminal GST and expressed in *E. coli* and purified to greater than 85% purity by SDS-PAGE. Sirt3 is supplied in 50 mM Tris/HCl (pH 7.5), 500 mM NaCl, and 10% glycerol (*v*/*v*). Sirt5 (accession number NM_012241), consisting of amino acids 37–310 (C-terminal) and tagged with an N-terminal His-tag, was expressed in *E. coli*, purified to greater than 95% purity by SDS-PAGE and delivered as a solution in 50 mM Tris/HCl (pH 7.5), 500 mM NaCl, 1 mM TCEP, and 10% glycerol (*v*/*v*). All proteins were provided in purified forms for use in the assays. The respective internal assay protocol is outlined in the following: After the test substances (dissolved in DMSO) were incubated with the desired sirtuin enzyme in assay buffer (Tris-HCl, pH = 8) for 10 min at 30 °C, a substrate mixture consisting of a 7-amino-4-methylcoumarin-linked fluorogenic peptide substrate (p53 residues 379–382) and the cofactor NAD^+ was added. After 2 h of incubation at 30 °C, the universal inhibitor nicotinamide was added in excess to completely stop the deacetylation reaction, followed by the addition of a protease-based developer to release 7-amino-4-methylcoumarin, resulting in characteristic fluorescence, which was measured after 1 h at 30 °C (excitation/emission = 360/460). A no-inhibitor control was implemented, serving as a reference for 100% enzyme activity. IC_{50} values for Sirt2 were determined in triplicate by performing a 10-point, 3-fold serial dilution starting at a final reaction concentration of 50 µM or 100 µM when needed). Three individual IC_{50} values per test compound were calculated from the corresponding three dilution series fluorescence data using sigmoidal curve fitting in Prism 8.0.2 (GraphPad Software, Boston, MA, USA), and these were averaged to determine the mean IC_{50} value along with the standard deviation. To assess the selectivity against Sirt1, Sirt3, and Sirt5, a 50 µM concentration of the test compound was tested in duplicate, and the inhibitory activity was expressed as the mean of the duplicates in percentage of enzyme activity, including standard deviation, relative to the no-inhibitor control (representative 100% enzyme activity).

Cell viability assay. The cytotoxicity of the Sirt2 inhibitors was determined using a colorimetric MTT assay following Mosmann's protocol [23]. HL-60 cells (purchased from DSMZ (German Collection of Microorganisms and Cell Cultures, Deutsche Sammlung von Mikroorganismen und Zellkulturen GmbH, Braunschweig, Germany) were cultivated in RPMI medium with 10% fetal bovine serum at 37 °C with 5% CO_2 atmosphere. The cells were then seeded in a 96-well plate with a concentration of 9 x 10^4 cells/well and a well volume of 99 µL. The cells were further incubated at 37 °C with 5% CO_2 atmosphere for 24 h. The cells were then treated with 1 µL solution of Sirt2 inhibitors in various concentrations, which were prepared from 10 mM or 20 mM DMSO stock solutions. Negative controls were treated with 1 µL DMSO and positive controls with 1 µL of 1% Triton-X solution. Three technical replicates were performed. After incubation for 24 h, 10 µL MTT (5.0 mg/mL in PBS) were added to each well and the cells were incubated at 37 °C with 5% CO_2 atmosphere for 2 h. Then 190 µL DMSO were added to each well and the plate shaken at room temperature at 600 rpm for 1 h with light exclusion. The absorbance of the MTT metabolite formazan was measured at 570 nm using the MRX Microplate Reader (Dynex Technologies, Chantilly, VA, USA). The means of the corresponding triplicates were calculated and set in relation to the 1% DMSO negative controls. The data was

processed using Prism 8.0.2 (GraphPad Software, Boston, MA, USA) software and a logarithmic sigmoidal curve fitting for the calculation of the respective IC_{50} values was performed. IC_{50} values above 50 μM were considered as non-cytotoxic.

4.3. Computational Methods

Docking simulations were performed utilizing Schrödinger software suite (Schrödinger Inc., New York, NY, USA, version 2020-3) [24] using crystal structures of Sirt2 and respective lead structures, imported from the Protein Data Bank (PDB) [25] (**SirReal2**: PDB ID: 4RMG [14]) (**Yang_24a:** PDB ID: 5YQO [19]) and prepared with the Protein Preparation Wizard (Schrödinger Inc. New York City, USA). Protonation and charge calculation were done using Epik and the respective ligands were prepared with Ligand Preparation Wizard (Schrödinger Inc., New York, NY, USA) [26]. The docking calculations were carried out using Glide in standard precision mode SP and all docking parameters left to their default values. Pymol 2.5.8 (Schrödinger Inc., New York, NY, USA) was used for visualization purposes. The top ranked poses were analysed, considering the favourable spatial orientation in relation to the crystal structures of the corresponding lead compounds. The docking grid center was located at coordinates x = −13.495516, y = −10.113182, and z = −18.406236. The dimensions for the INNERBOX were set to 10, while the OUTERBOX had a size of 30.6493 for all x, y, and z axes. A total of five poses per ligand were saved, with ligands being treated as flexible and subjected to 10 post-docking minimizations. All other parameters were left at their default settings. For redocking, the ligand L5C from the X-ray structure 5YQO was used, and the docking procedure yielded an exceptionally low RMSD value of 0.89, which suggests that this method is highly effective for calculating Sirt2 ligand interactions. Visualization of the results was performed using PyMOL 2.5.8 (Schrödinger Inc.). The poses with the most favourable docking scores were analysed, with particular attention paid to the orientation of the pyrimidine ring respectively the selectivity pocket binder moiety in general, ensuring it closely resembled the positioning found in the crystal structures of related lead compounds. The ligand binding energies were calculated using PRIME MM-GBSA [27]. The docking poses were taken as starting points, solvation model = VSDB, force field = OPLS4 and sampling method = minimize. All protein atoms surrounding the ligands were treated as flexible during the MM-GBSA calculations. ADMET calculations were performed utilizing QikProp, version 4.3 (Schrödinger Inc., New York, NY, USA).

Supplementary Materials: The following supporting information can be downloaded at: https://www.mdpi.com/article/10.3390/ijms26209855/s1.

Author Contributions: Conceptualization, F.B.; methodology, M.F., R.W., T.W. and F.B.; software, T.W.; validation, M.F., R.W., T.W. and F.B.; formal analysis, M.F., R.W., T.W. and F.B.; investigation, M.F., R.W. and T.W.; resources, F.B.; data curation, M.F., R.W., T.W. and F.B.; writing—original draft preparation, M.F., R.W., T.W. and F.B.; writing—review and editing, F.B.; visualization, T.W. and M.F.; supervision, F.B.; project administration, F.B.; funding acquisition, F.B. All authors have read and agreed to the published version of the manuscript.

Funding: This research was funded by Deutsche Forschungsgemeinschaft (DFG, German Research Foundation) with funds from SFB1309 (Chemical Biology of Epigenetic Modifications, project ID: 325871075–SFB1309) to F.B.

Institutional Review Board Statement: Not applicable.

Data Availability Statement: Experimental data and protocols are stored in the University's electronic lab journal at LMU Munich. The original contributions presented in this study are included in the article/supplementary material. Further inquiries can be directed to the corresponding author.

Acknowledgments: We thank Lars Allmendinger and Claudia Glas for NMR services, Werner Spahl and Sonja Kosak for MS services, and Anna Niedrig for HPLC services.

Conflicts of Interest: The authors declare no conflicts of interest.

Abbreviations

The following abbreviations are used in this manuscript:

AcOH	Acetic acid
ADP	Adenosine diphosphate
DCM	Dichloromethane
DMF	Dimethylformamide
DMSO	Dimethylsulfoxide
EtOAc	Ethyl acetate
MeOH	Methanol
NAD^+	Nicotinamide adenine dinucleotide
SAR	Structure–activity relationship
Sirt	Sirtuin
t-BuOK	Potassium tert-butoxide
Val	Valine

References

1. Arrowsmith, C.H.; Bountra, C.; Fish, P.V.; Lee, K.; Schapira, M. Epigenetic protein families: A new frontier for drug discovery. *Nat. Rev. Drug Discov.* **2012**, *11*, 384–400. https://doi.org/10.1038/nrd3674.
2. Miller, J.L.; Grant, P.A. The Role of DNA Methylation and Histone Modifications in Transcriptional Regulation in Humans. In *Epigenetics: Development and Disease*; Springer: Dordrecht, The Netherlands, 2013; pp. 289-317. https://doi.org/10.1007/978-94-007-4525-4_13.
3. Reid, M.A.; Dai, Z.; Locasale, J.W. The impact of cellular metabolism on chromatin dynamics and epigenetics. *Nat. Cell Biol.* **2017**, *19*, 1298–1306. https://doi.org/10.1038/ncb3629.
4. Milazzo, G.; Mercatelli, D.; Di Muzio, G.; Triboli, L.; De Rosa, P.; Perini, G.; Giorgi, F.M. Histone Deacetylases (HDACs): Evolution, Specificity, Role in Transcriptional Complexes, and Pharmacological Actionability. *Genes* **2020**, *11*, 556. https://doi.org/10.3390/genes11050556.
5. Park, S.-Y.; Kim, J.-S. A short guide to histone deacetylases including recent progress on class II enzymes. *Exp. Mol. Med.* **2020**, *52*, 204–212. https://doi.org/10.1038/s12276-020-0382-4.
6. Carafa, V.; Rotili, D.; Forgione, M.; Cuomo, F.; Serretiello, E.; Hailu, G.S.; Jarho, E.; Lahtela-Kakkonen, M.; Mai, A.; Altucci, L. Sirtuin functions and modulation: From chemistry to the clinic. *Clin. Epigenetics* **2016**, *8*, 61. https://doi.org/10.1186/s13148-016-0224-3.
7. Hamaidi, I.; Kim, S. Sirtuins are crucial regulators of T cell metabolism and functions. *Exp. Mol. Med.* **2022**, *54*, 207–215. https://doi.org/10.1038/s12276-022-00739-7.
8. Kaya, S.G.; Eren, G. Selective inhibition of SIRT2: A disputable therapeutic approach in cancer therapy. *Bioorganic Chem.* **2024**, *143*, 107038. https://doi.org/10.1016/j.bioorg.2023.107038.
9. Wang, Y.; He, J.; Liao, M.; Hu, M.; Li, W.; Ouyang, H.; Wang, X.; Ye, T.; Zhang, Y.; Ouyang, L. An overview of Sirtuins as potential therapeutic target: Structure, function and modulators. *Eur. J. Med. Chem.* **2019**, *161*, 48–77. https://doi.org/10.1016/j.ejmech.2018.10.028.
10. Zhu, C.; Dong, X.; Wang, X.; Zheng, Y.; Qiu, J.; Peng, Y.; Xu, J.; Chai, Z.; Liu, C. Multiple Roles of SIRT2 in Regulating Physiological and Pathological Signal Transduction. *Genet. Res.* **2022**, *2022*, 9282484. https://doi.org/10.1155/2022/9282484.
11. Penteado, A.B.; Hassanie, H.; Gomes, R.A.; Silva Emery, F.D.; Goulart Trossini, G.H. Human Sirtuin 2 inhibitors, Their Mechanisms and Binding Modes. *Future Med. Chem.* **2023**, *15*, 291–311. https://doi.org/10.4155/fmc-2022-0253.
12. Robaa, D.; Monaldi, D.; Wössner, N.; Kudo, N.; Rumpf, T.; Schiedel, M.; Yoshida, M.; Jung, M. Opening the Selectivity Pocket in the Human Lysine Deacetylase Sirtuin2–New Opportunities, New Questions. *Chem. Rec.* **2018**, *18*, 1701–1707. https://doi.org/10.1002/tcr.201800044.
13. Xue, J.; Hou, X.; Fang, H. Structure, functions, and recent advances in the development of SIRT2 inhibitors. *Pharm. Sci. Adv.* **2023**, *1*, 100010. https://doi.org/10.1016/j.pscia.2023.100010.

14. Rumpf, T.; Schiedel, M.; Karaman, B.; Roessler, C.; North, B.J.; Lehotzky, A.; Oláh, J.; Ladwein, K.I.; Schmidtkunz, K.; Gajer, M.; et al. Selective Sirt2 inhibition by ligand-induced rearrangement of the active site. *Nat. Commun.* **2015**, *6*, 6263. https://doi.org/10.1038/ncomms7263.
15. Schiedel, M.; Rumpf, T.; Karaman, B.; Lehotzky, A.; Olah, J.; Gerhardt, S.; Ovadi, J.; Sippl, W.; Einsle, O.; Jung, M. Aminothiazoles as Potent and Selective Sirt2 Inhibitors: A Structure-Activity Relationship Study. *J. Med. Chem.* **2016**, *59*, 1599–1612. https://doi.org/10.1021/acs.jmedchem.5b01517.
16. Schiedel, M.; Rumpf, T.; Karaman, B.; Lehotzky, A.; Gerhardt, S.; Ovádi, J.; Sippl, W.; Einsle, O.; Jung, M. Structure-Based Development of an Affinity Probe for Sirtuin 2. *Angew. Chem. Int. Ed.* **2016**, *55*, 2252–2256. https://doi.org/10.1002/anie.201509843.
17. Yang, L.; Ma, X.; Yuan, C.; He, Y.; Li, L.; Fang, S.; Xia, W.; He, T.; Qian, S.; Xu, Z.; et al. Discovery of 2-((4,6-dimethylpyrimidin-2-yl)thio)-N-phenylacetamide derivatives as new potent and selective human sirtuin 2 inhibitors. *Eur. J. Med. Chem.* **2017**, *134*, 230–241. https://doi.org/10.1016/j.ejmech.2017.04.010.
18. Yang, L.L.; Xu, W.; Yan, J.; Su, H.L.; Yuan, C.; Li, C.; Zhang, X.; Yu, Z.J.; Yan, Y.H.; Yu, Y.; et al. Crystallographic and SAR analyses reveal the high requirements needed to selectively and potently inhibit SIRT2 deacetylase and decanoylase. *MedChemComm* **2019**, *10*, 164–168. https://doi.org/10.1039/c8md00462e.
19. Yang, L.-L.; Wang, H.-L.; Zhong, L.; Yuan, C.; Liu, S.-Y.; Yu, Z.-J.; Liu, S.; Yan, Y.-H.; Wu, C.; Wang, Y.; et al. X-ray crystal structure guided discovery of new selective, substrate-mimicking sirtuin 2 inhibitors that exhibit activities against non-small cell lung cancer cells. *Eur. J. Med. Chem.* **2018**, *155*, 806–823. https://doi.org/10.1016/j.ejmech.2018.06.041.
20. Frei, M.; Wein, T.; Bracher, F. Lead-structure-based rigidization approach to optimize SirReal-Type Sirt2 inhibitors. *Molecules* **2025**, *30*, 1728. https://doi.org/10.3390/molecules30081728.
21. Wilcken, R.; Zimmermann, M.O.; Lange, A.; Joerger, A.C.; Boeckler, F.M. Principles and Applications of Halogen Bonding in Medicinal Chemistry and Chemical Biology. *J. Med. Chem.* **2013**, *56*, 1363–1388. https://doi.org/10.1021/jm3012068.
22. Vogelmann, A.; Schiedel, M.; Wössner, N.; Merz, A.; Herp, D.; Hammelmann, S.; Colcerasa, A.; Komaniecki, G.; Hong, J.Y.; Sum, M.; et al. Development of a NanoBRET assay to validate inhibitors of Sirt2-mediated lysine deacetylation and defatty-acylation that block prostate cancer cell migration. *RSC Chem. Biol.* **2022**, *3*, 468–485. https://doi.org/10.1039/d1cb00244a.
23. Mosmann, T. Rapid colorimetric assay for cellular growth and survival: Application to proliferation and cytotoxicity assays. *J. Immunol. Methods* **1983**, *65*, 55-63. https://doi.org/10.1016/0022-1759(83)90303-4.
24. Halgren, T.A.; Murphy, R.B.; Friesner, R.A.; Beard, H.S.; Frye, L.L.; Pollard, W.T.; Banks, J.L. Glide: A New Approach for Rapid, Accurate Docking and Scoring. 2. Enrichment Factors in Database Screening. *J. Med. Chem.* **2004**, *47*, 1750–1759. https://doi.org/10.1021/jm030644s.
25. Berman, H.M.; Westbrook, J.; Feng, Z.; Gilliland, G.; Bhat, T.N.; Weissig, H.; Shindyalov, I.N.; Bourne, P.E. The Protein Data Bank. *Nucleic Acids Res.* **2000**, *28*, 235–242. https://doi.org/10.1093/nar/28.1.235.
26. Shelley, J.C.; Cholleti, A.; Frye, L.L.; Greenwood, J.R.; Timlin, M.R.; Uchimaya, M. Epik: A software program for pKa prediction and protonation state generation for drug-like molecules. *J. Comput. Aided Mol. Des.* **2007**, *21*, 681–691. https://doi.org/10.1007/s10822-007-9133-z.
27. Knight, J.L.; Krilov, G.; Borrelli, K.W.; Williams, J.; Gunn, J.R.; Clowes, A.; Cheng, L.; Friesner, R.A.; Abel, R. Leveraging Data Fusion Strategies in Multireceptor Lead Optimization MM/GBSA End-Point Methods. *J. Chem. Theory Comput.* **2014**, *10*, 3207–3220. https://doi.org/10.1021/ct500189s.

Supplementary Information

Lead structure-based hybridization strategy reveals major potency enhancement of SirReal-type Sirt2 inhibitors

Matthias Frei*, Ricky Wirawan*, Thomas Wein and Franz Bracher **

Department of Pharmacy—Center for Drug Research, Ludwig-Maximilians University, Butenandtstr. 5–13, 81377 Munich, Germany;

matthias.frei@cup.uni-muenchen.de (M.F.); ricky.wirawan@cup.uni-muenchen.de (R.W.); thomas.wein@cup.uni-muenchen.de (T.W.).

* Equal contribution to this paper
** Correspondence: franz.bracher@cup.uni-muenchen.de; Tel.: +49-89-218077301

Table of Contents:

^{1}H (400 MHz; $(CD_3)_2SO$) and ^{13}C (101 MHz; $(CD_3)_2SO$) NMR spectra of compound **2**

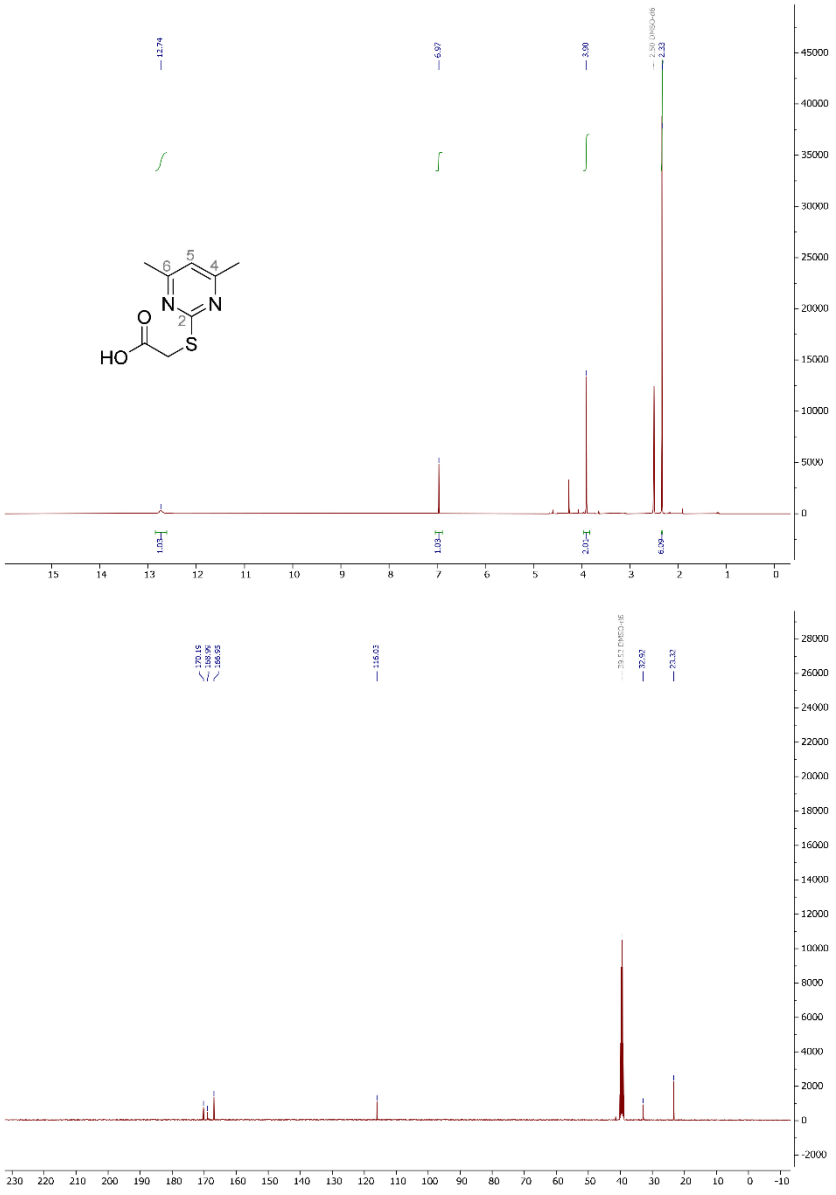

2

^{1}H (400 MHz; $(CD_3)_2SO$) and ^{13}C (101 MHz; $(CD_3)_2SO$) NMR spectra of compound **3**

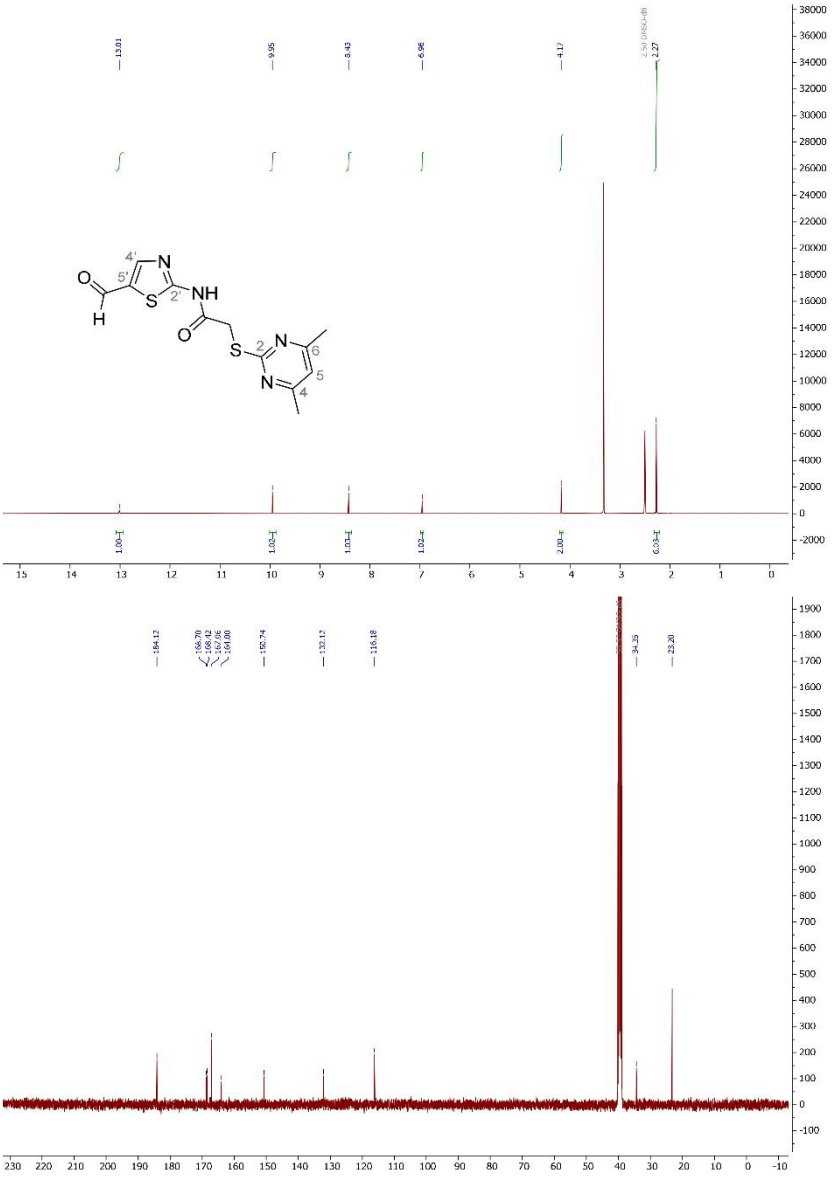

3

^{1}H (400 MHz; $(CD_3)_2SO$) and ^{13}C (101 MHz; $(CD_3)_2SO$) NMR spectra of compound **4**

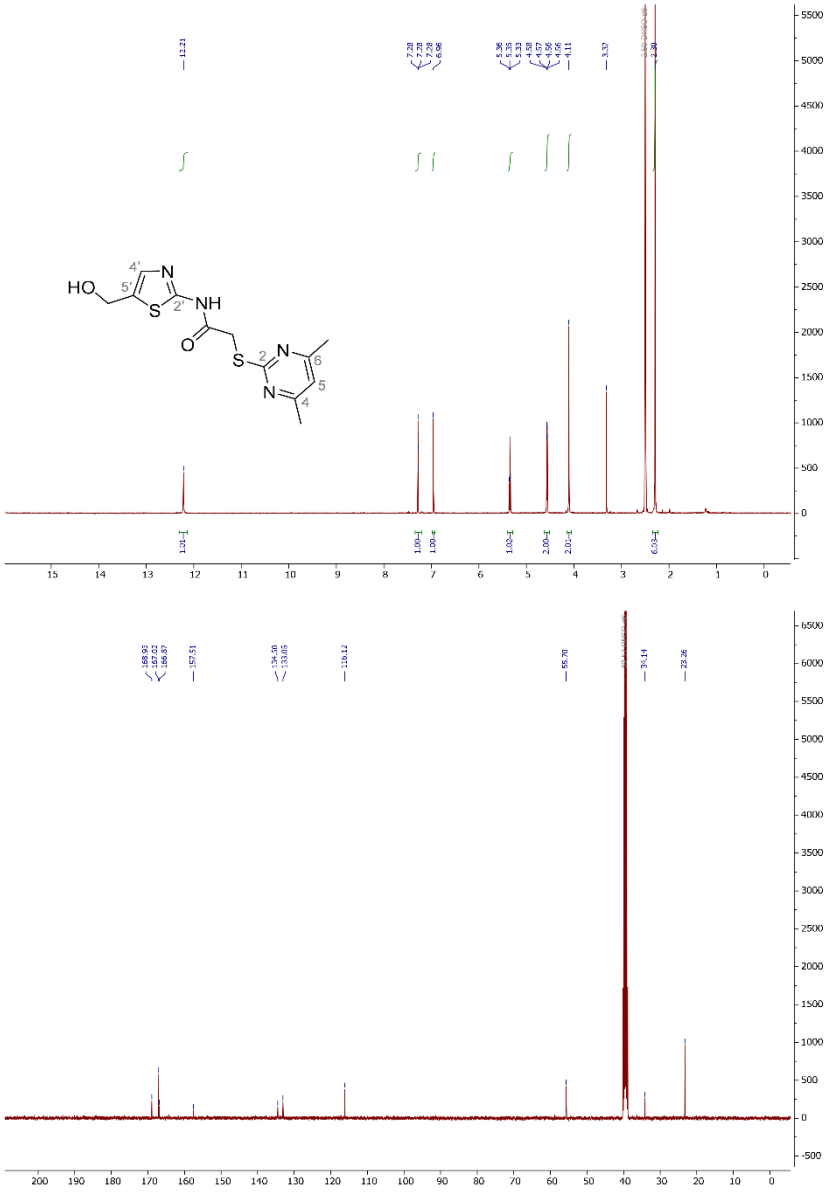

4

^{1}H (400 MHz; $(CD_3)_2SO$) and ^{13}C (101 MHz; $(CD_3)_2SO$) NMR spectra of compound **5**

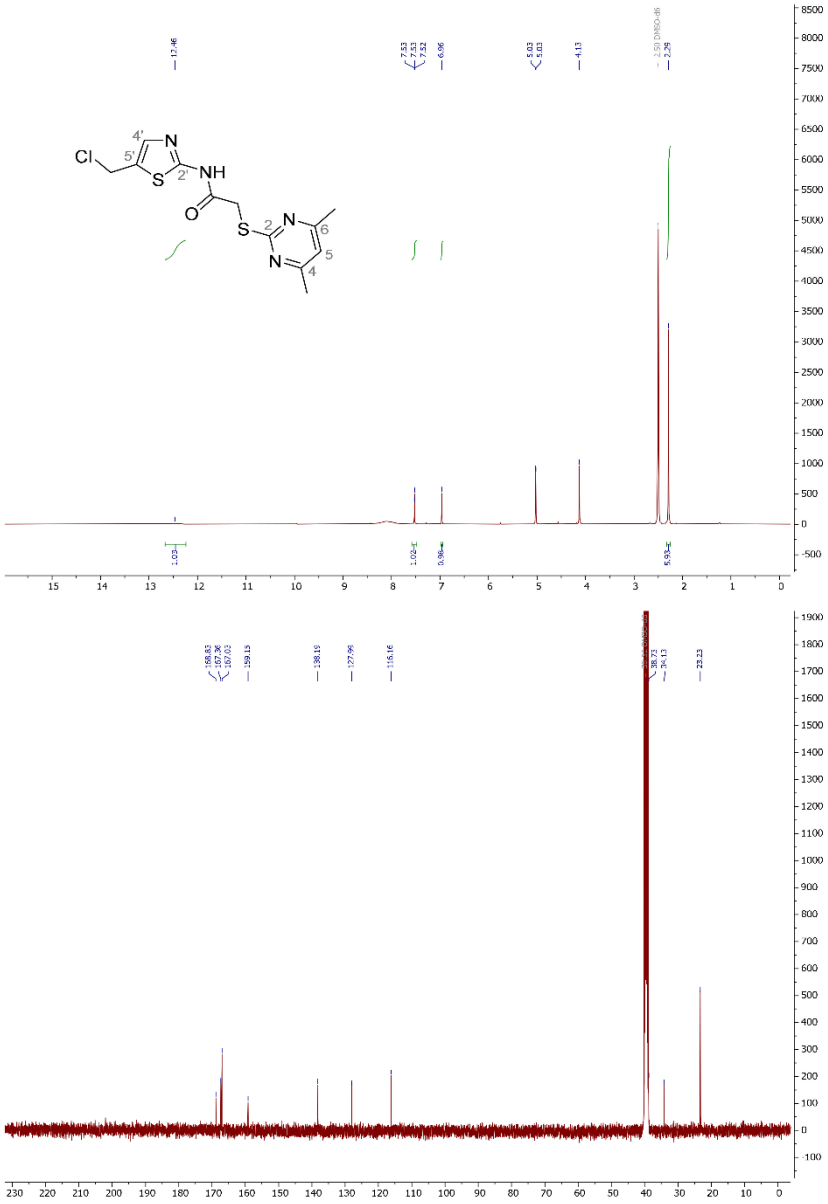

5

^{1}H (500 MHz; $(CD_3)_2SO$) and ^{13}C (126 MHz; $(CD_3)_2SO$) NMR spectra of **FM345**

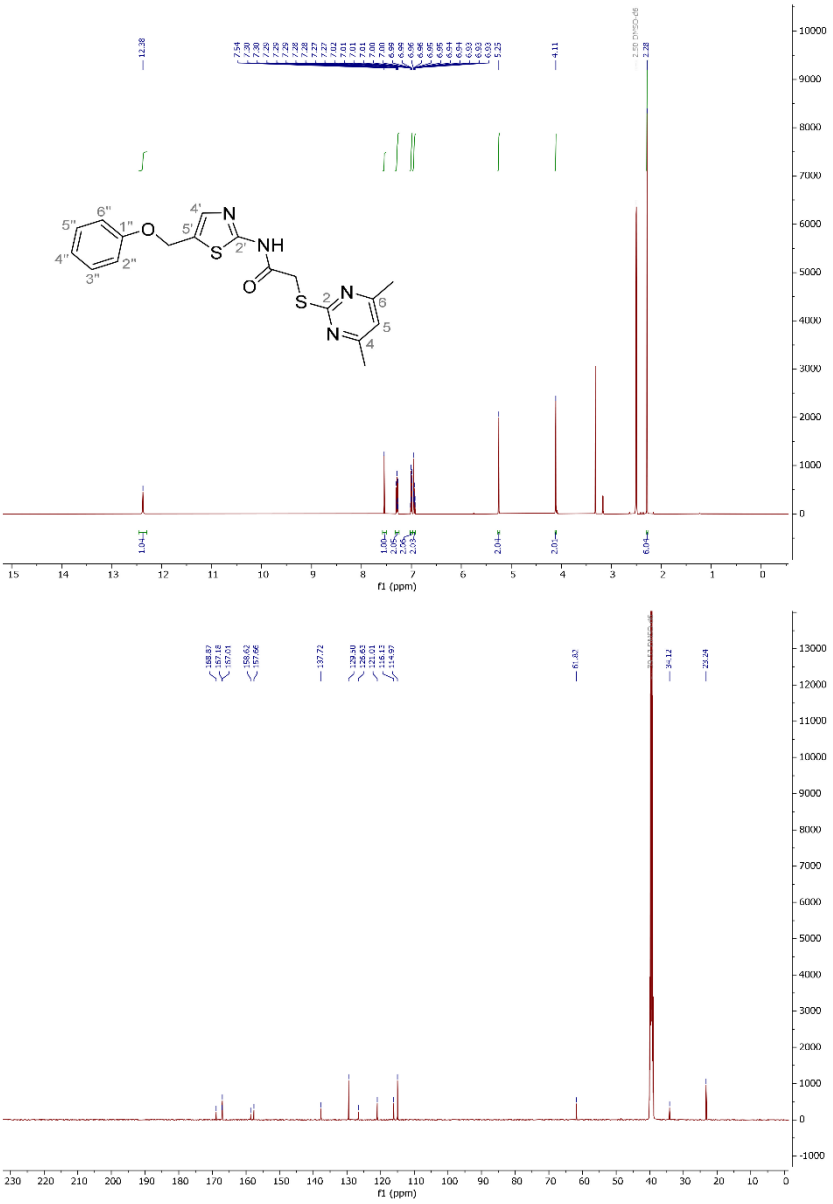

^{1}H (400 MHz; $(CD_3)_2SO$) and ^{13}C (101 MHz; $(CD_3)_2SO$) NMR spectra of compound **7**

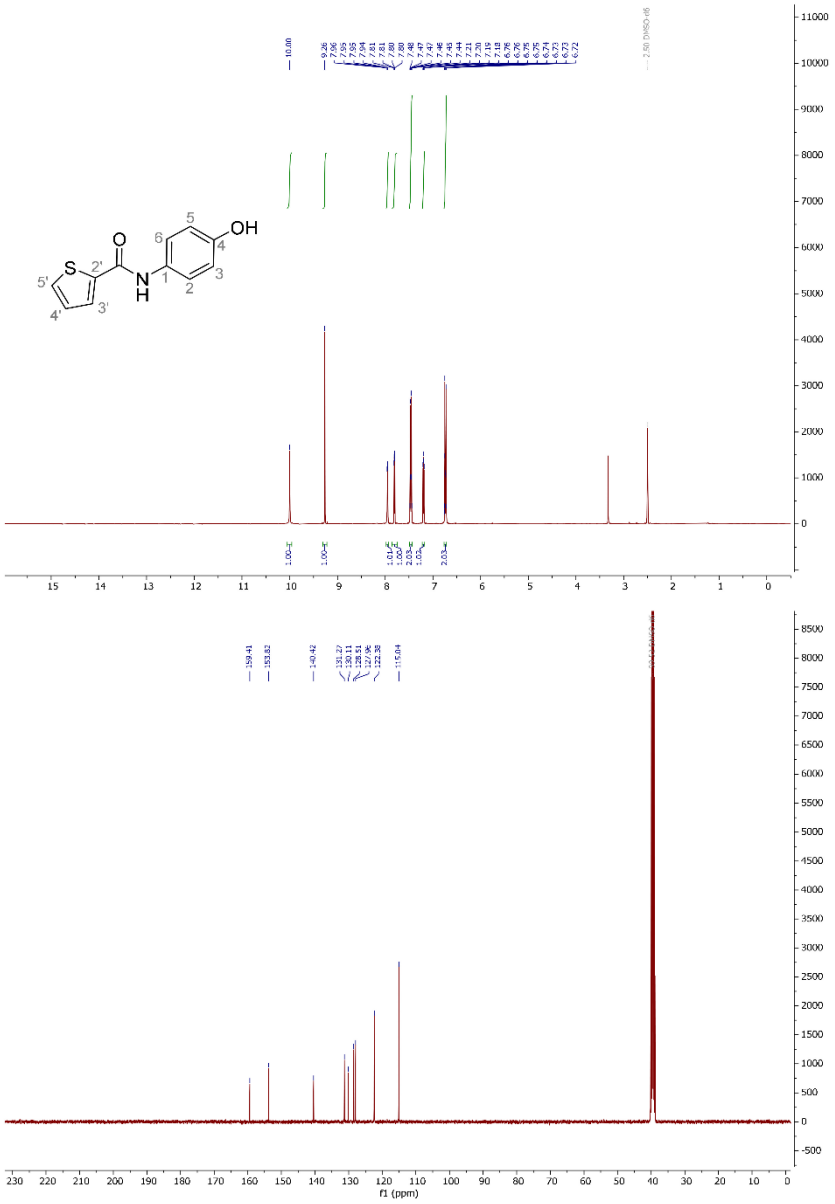

7

^{1}H (400 MHz; $(CD_3)_2SO$) and ^{13}C (101 MHz; $(CD_3)_2SO$) NMR spectra of compound **8**

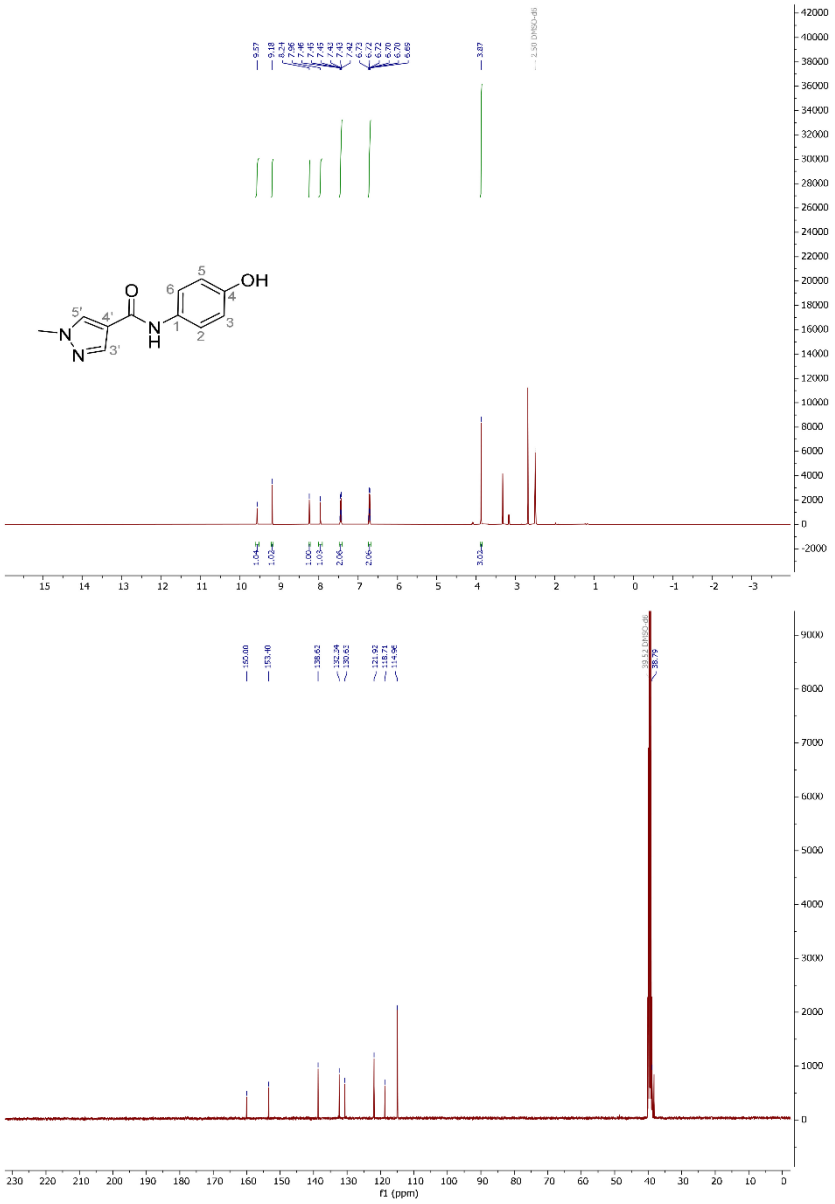

8

^{1}H (500 MHz; $(CD_3)_2SO$) and ^{13}C (126 MHz; $(CD_3)_2SO$) NMR spectra of **FM352**

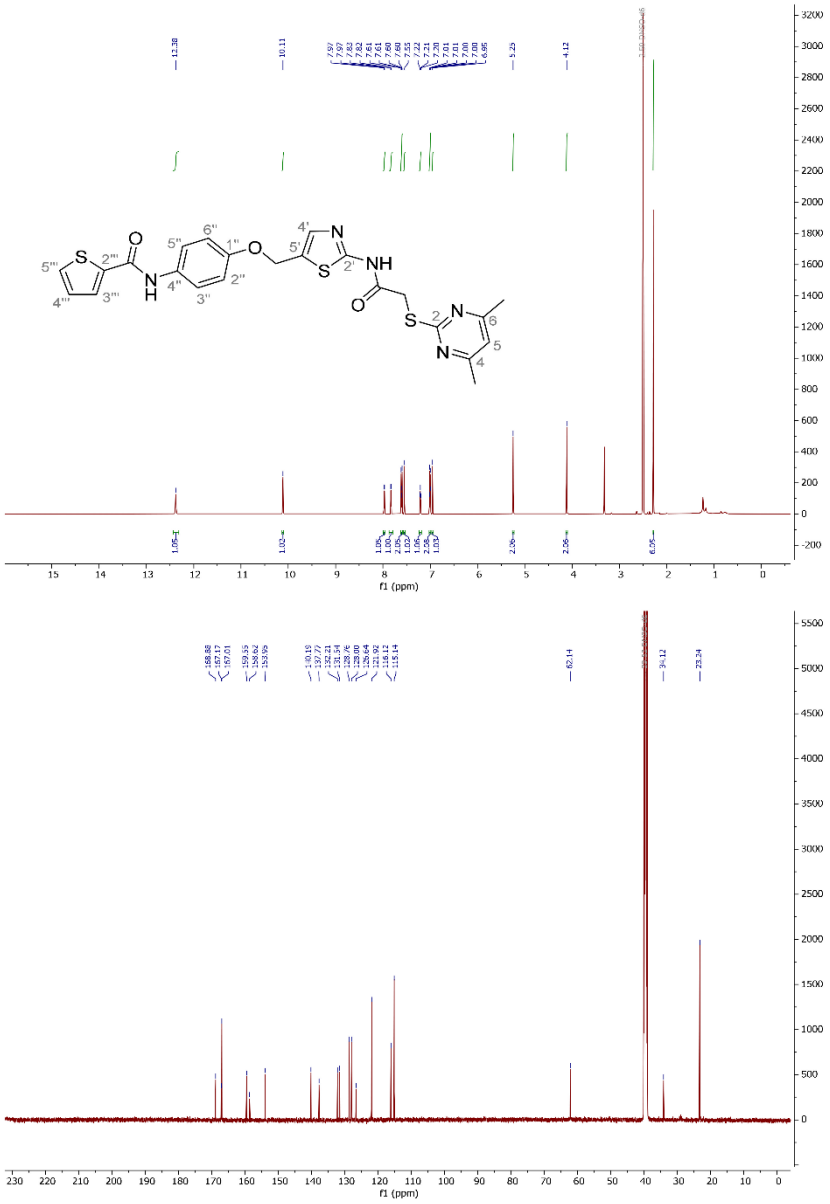

9

^{1}H (500 MHz; $(CD_3)_2SO$) and ^{13}C (126 MHz; $(CD_3)_2SO$) NMR spectra of **FM358**

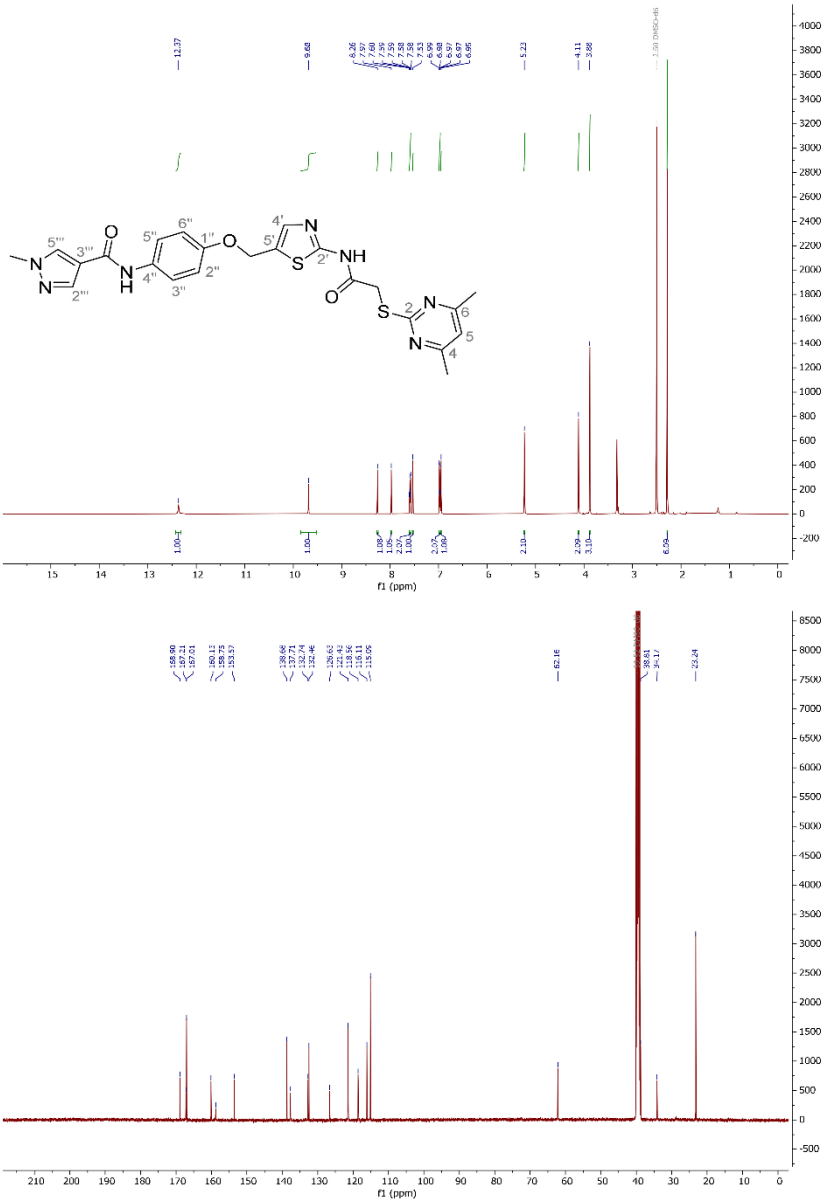

10

^{1}H (500 MHz; $(CD_3)_2SO$) and ^{13}C (126 MHz; $(CD_3)_2SO$) NMR spectra of **FM368**

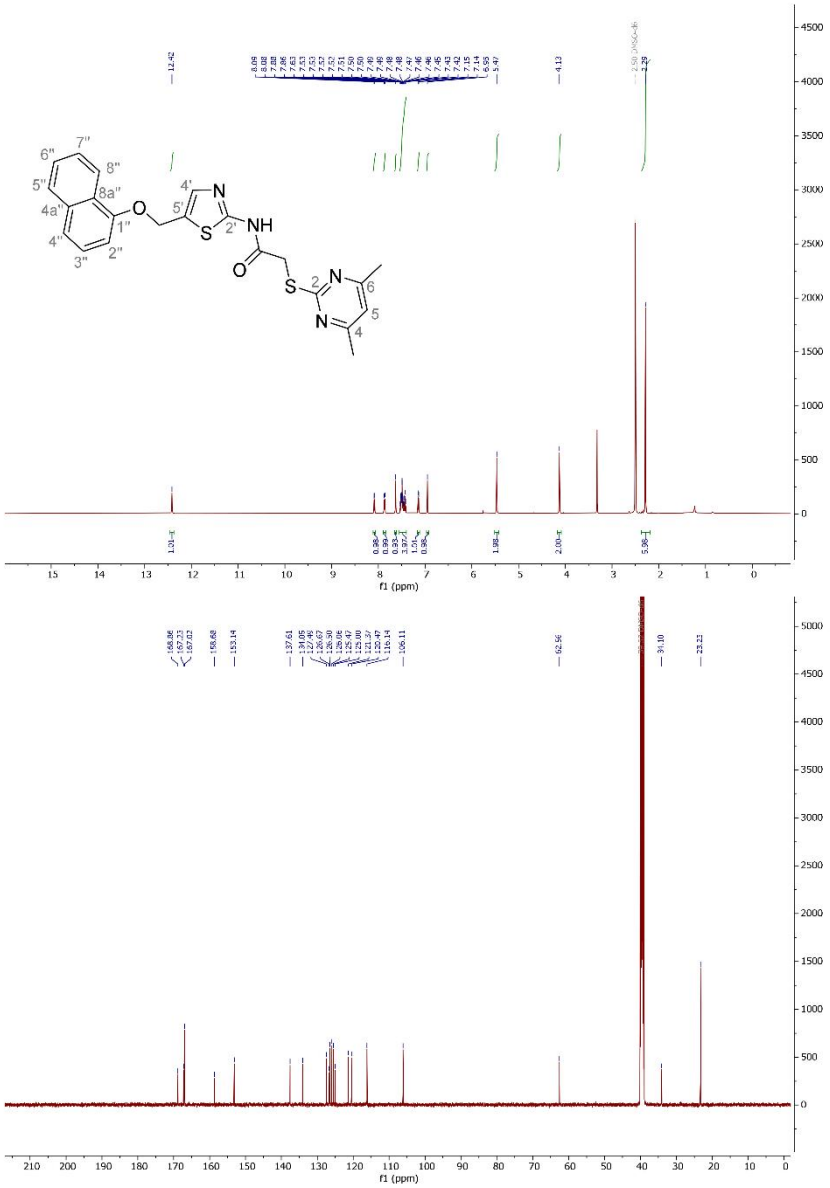

^{1}H (400 MHz; $(CD_3)_2SO$) and ^{13}C (126 MHz; $(CD_3)_2SO$) NMR spectra of compound **9**

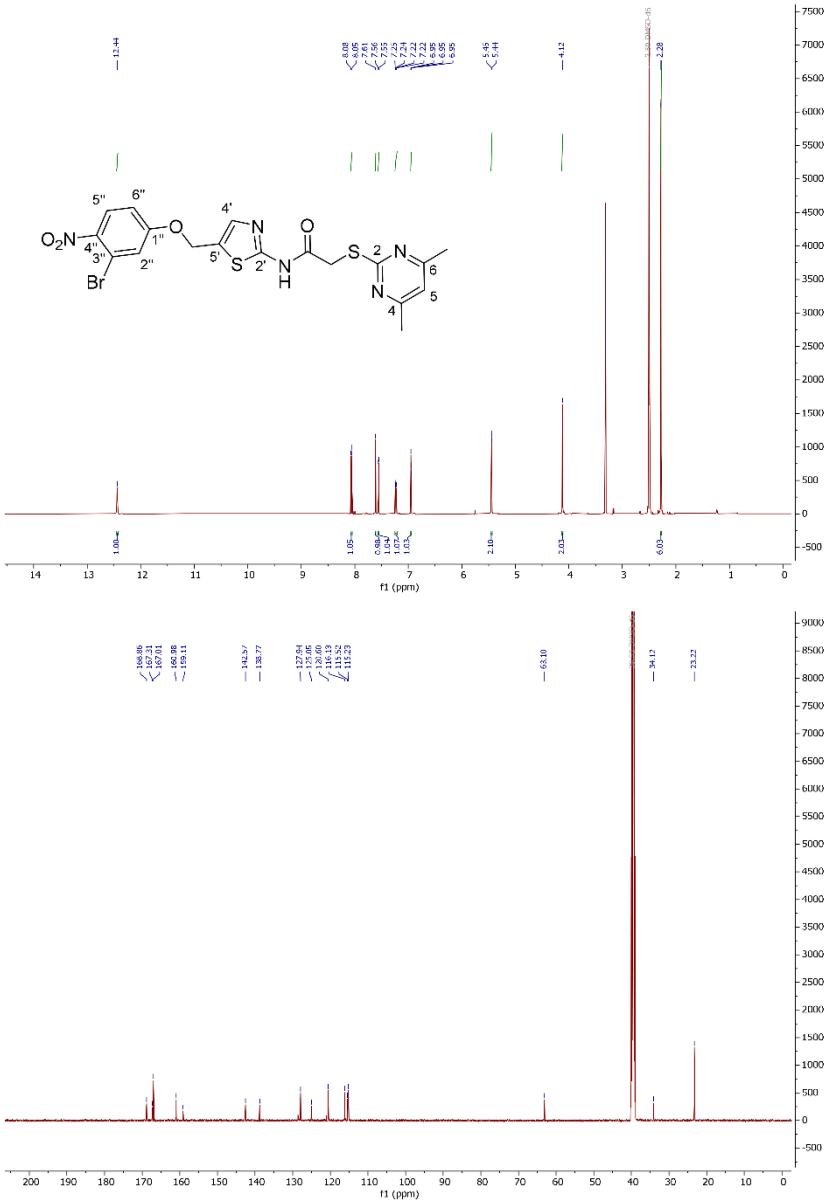

12

^{1}H (400 MHz; $(CD_3)_2SO$) and ^{13}C (101 MHz; $(CD_3)_2SO$) NMR spectra of compound **10**

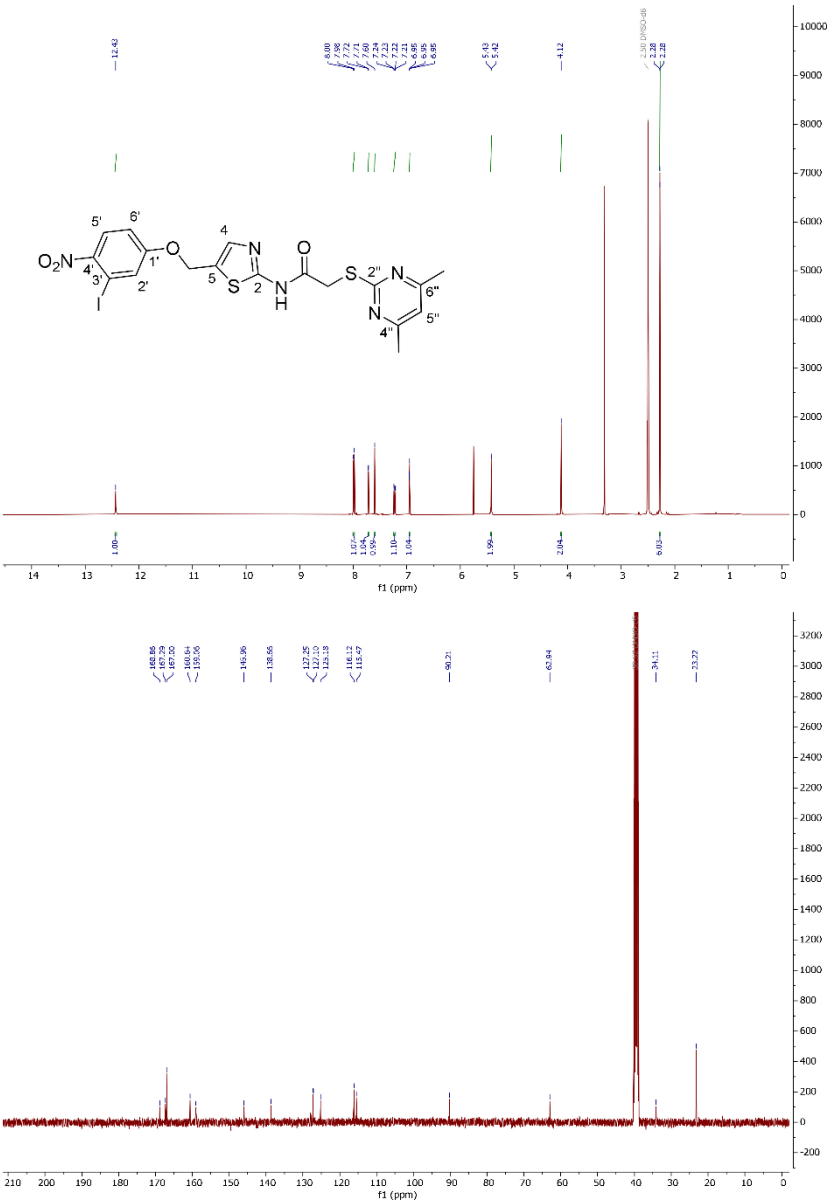

^{1}H (400 MHz; $(CD_3)_2SO$) and ^{13}C (101 MHz; $(CD_3)_2SO$) NMR spectra of compound **11**

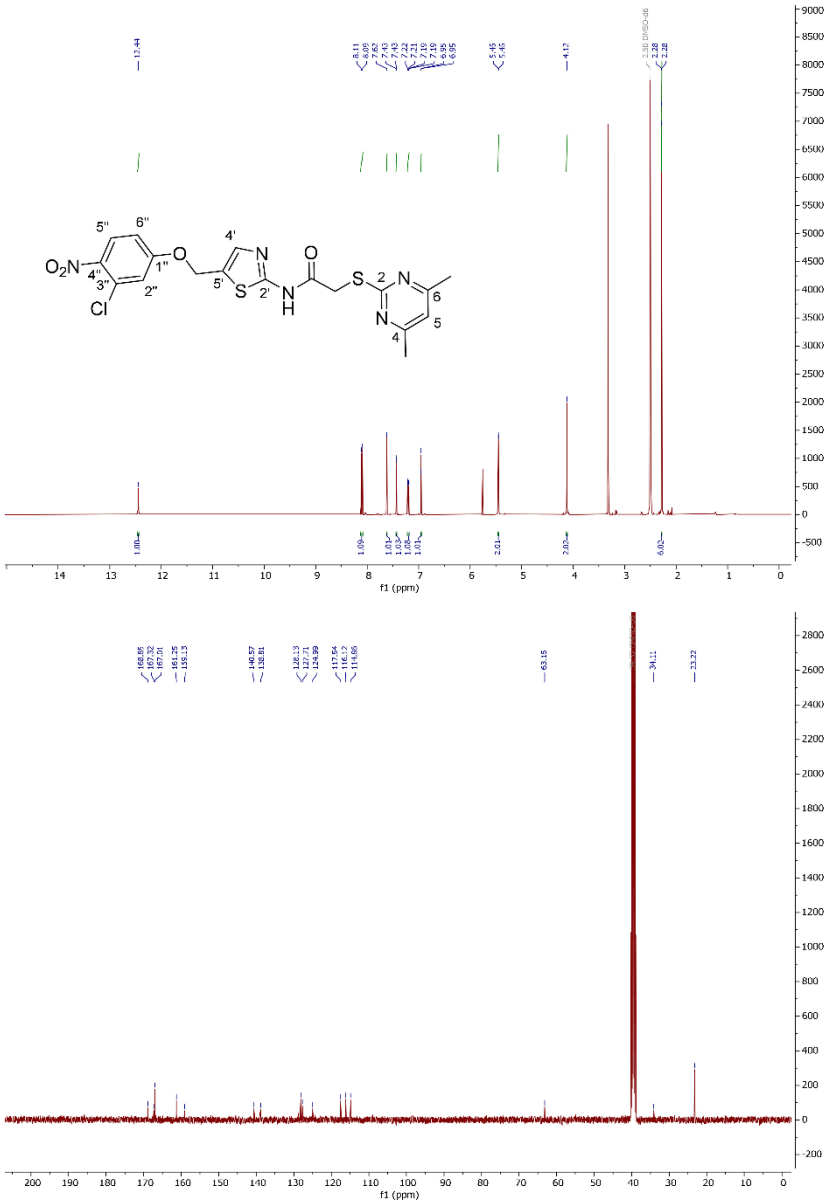

14

^{1}H (400 MHz; $(CD_3)_2SO$) and ^{13}C (101 MHz; $(CD_3)_2SO$) NMR spectra of **RW-93**

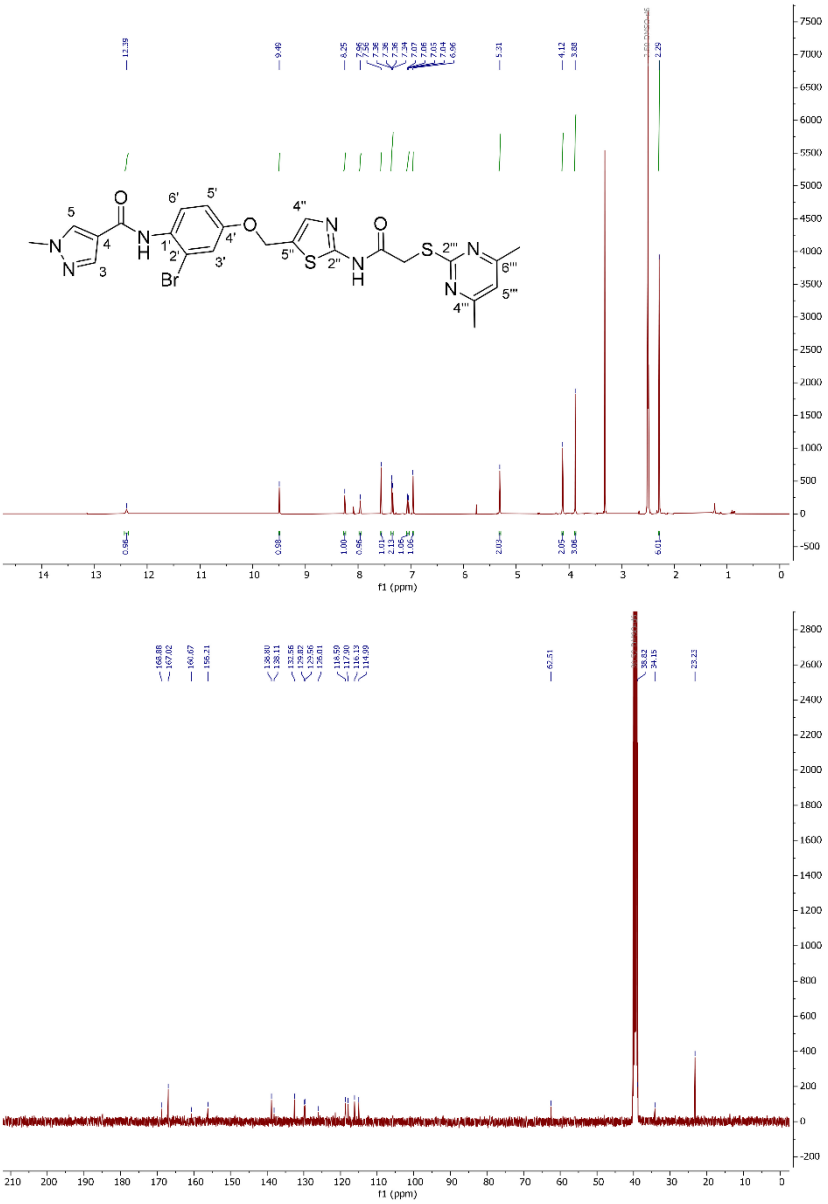

^{1}H (500 MHz; $(CD_3)_2SO$) and ^{13}C (126 MHz; $(CD_3)_2SO$) NMR spectra of **RW-95**

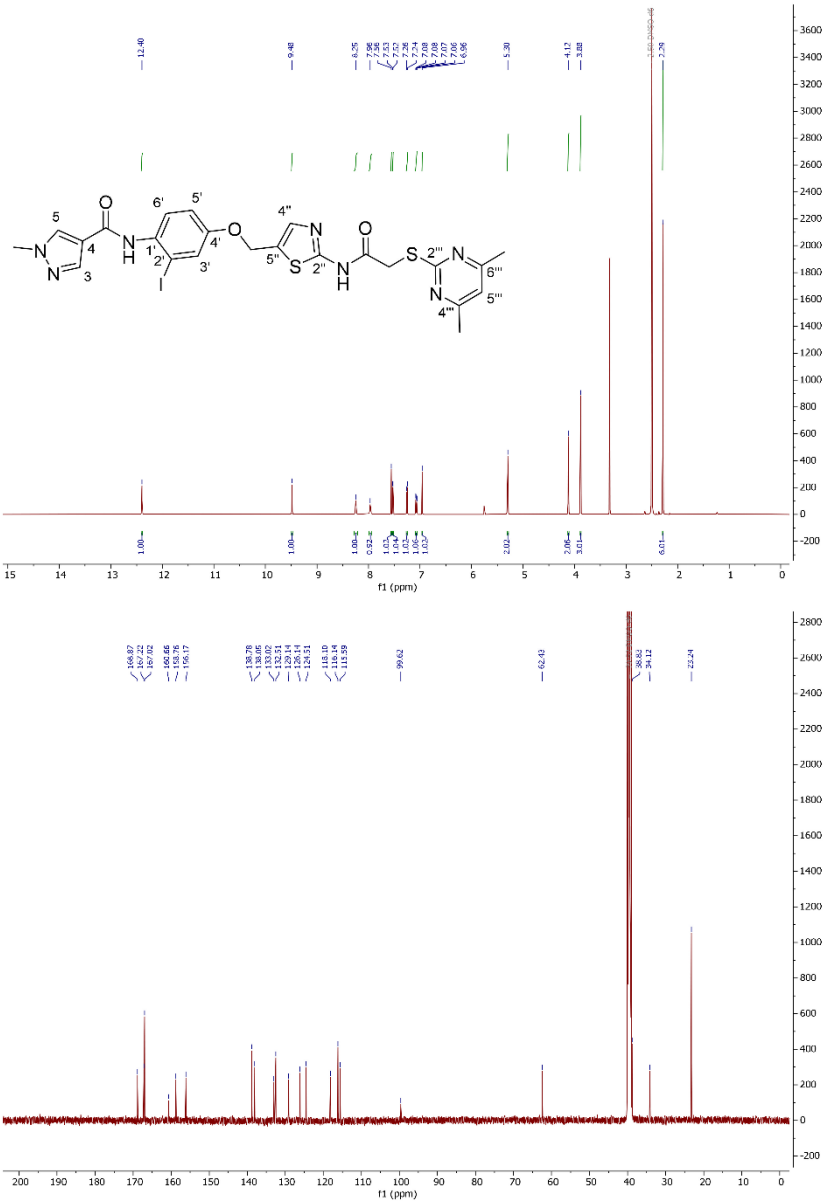

^{1}H (400 MHz; $(CD_3)_2SO$) and ^{13}C (101 MHz; $(CD_3)_2SO$) NMR spectra of **RW-99**

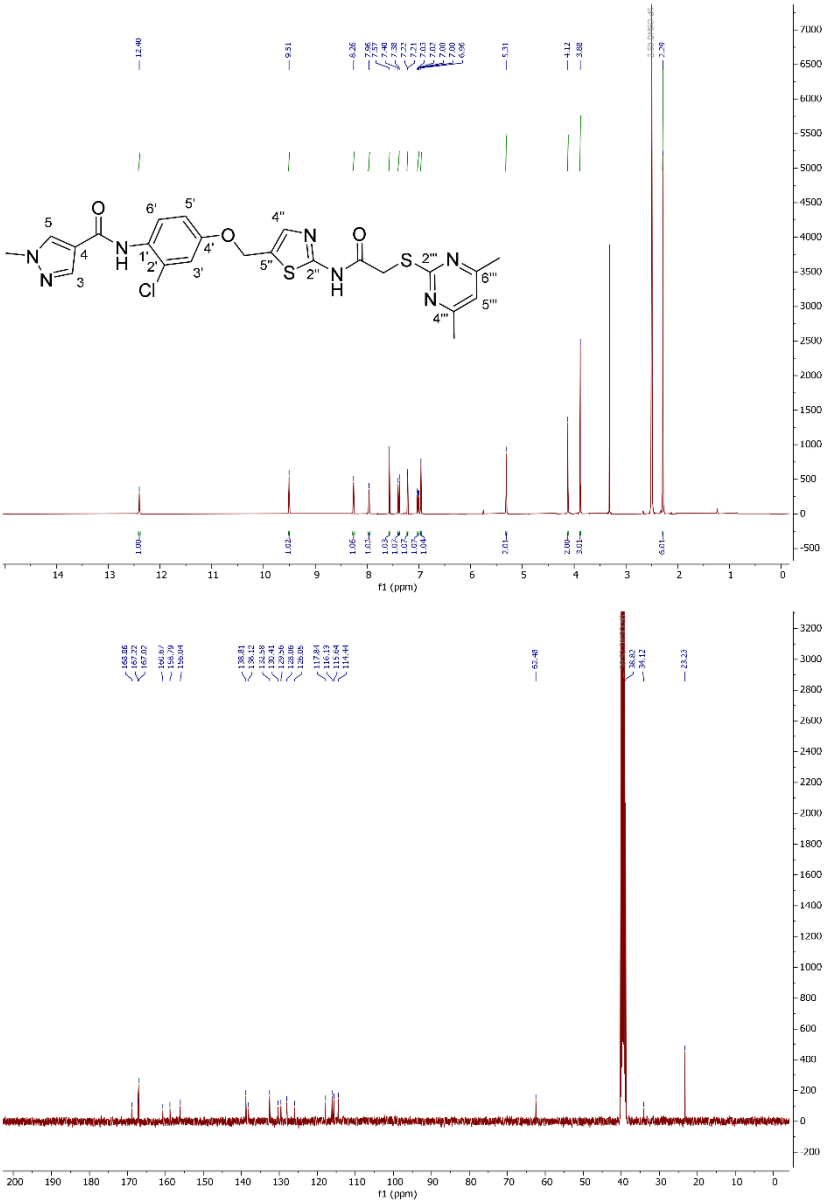

HPLC chromatogram of compound **Yang_28e**

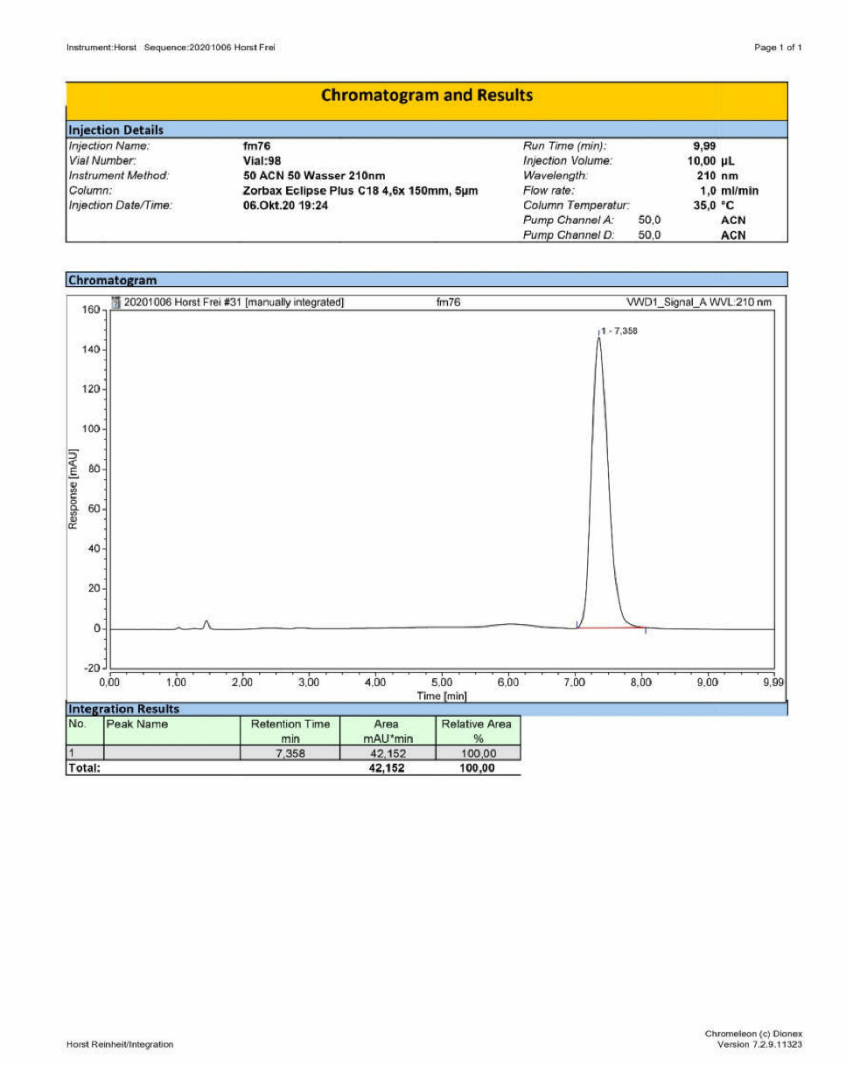

Instrument:Horst Sequence:20201006 Horst Frei Page 1 of 1

Chromatogram and Results

Injection Details

Injection Name:	**fm76**	*Run Time (min):*	**9,99**
Vial Number:	**Vial:98**	*Injection Volume:*	**10,00 µL**
Instrument Method:	**50 ACN 50 Wasser 210nm**	*Wavelength:*	**210 nm**
Column:	**Zorbax Eclipse Plus C18 4,6x 150mm, 5µm**	*Flow rate:*	**1,0 ml/min**
Injection Date/Time:	**06.Okt.20 19:24**	*Column Temperatur:*	**35,0 °C**
		Pump Channel A: 50,0	**ACN**
		Pump Channel D: 50,0	**ACN**

Chromatogram

Integration Results

No.	Peak Name	Retention Time min	Area mAU*min	Relative Area %
1		7,358	42,152	100,00
Total:			**42,152**	**100,00**

Horst Reinheit/Integration

Chromeleon (c) Dionex Version 7.2.9.11323

HPLC chromatogram of **FM345**

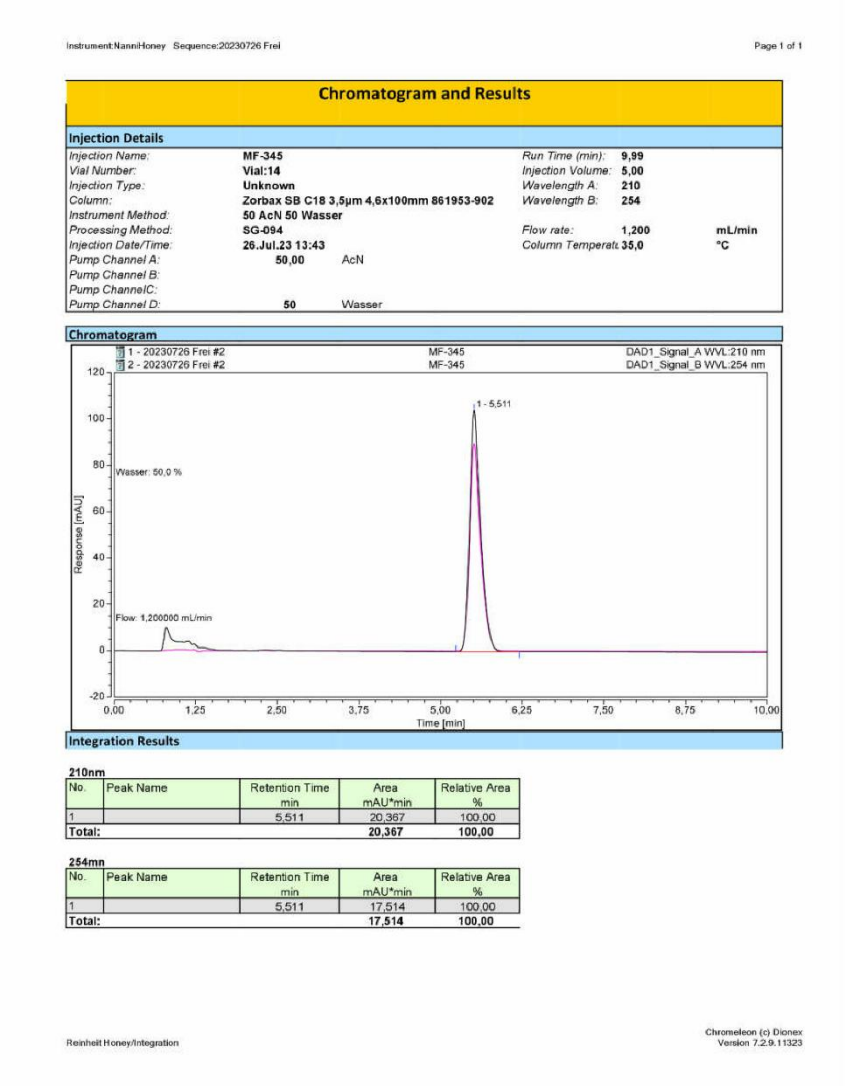

Instrument:NanniHoney Sequence:20230726 Frei Page 1 of 1

Chromatogram and Results

Injection Details

Injection Name:	**MF-345**		*Run Time (min):*	**9,99**	
Vial Number:	**Vial:14**		*Injection Volume:*	**5,00**	
Injection Type:	**Unknown**		*Wavelength A:*	**210**	
Column:	**Zorbax SB C18 3,5µm 4,6x100mm 861953-902**		*Wavelength B:*	**254**	
Instrument Method:	**50 AcN 50 Wasser**				
Processing Method:	**SG-094**		*Flow rate:*	**1,200**	**mL/min**
Injection Date/Time:	**26.Jul.23 13:43**		*Column Temperatu*	**35,0**	**°C**
Pump Channel A:	**50,00**	AcN			
Pump Channel B:					
Pump ChannelC:					
Pump Channel D:	**50**	Wasser			

Chromatogram

Integration Results

210nm

No.	Peak Name	Retention Time min	Area mAU*min	Relative Area %
1		5,511	20,367	100,00
Total:			**20,367**	**100,00**

254mn

No.	Peak Name	Retention Time min	Area mAU*min	Relative Area %
1		5,511	17,514	100,00
Total:			**17,514**	**100,00**

Reinheit Honey/Integration Chromeleon (c) Dionex Version 7.2.9.11323

HPLC chromatogram of **FM352**

19

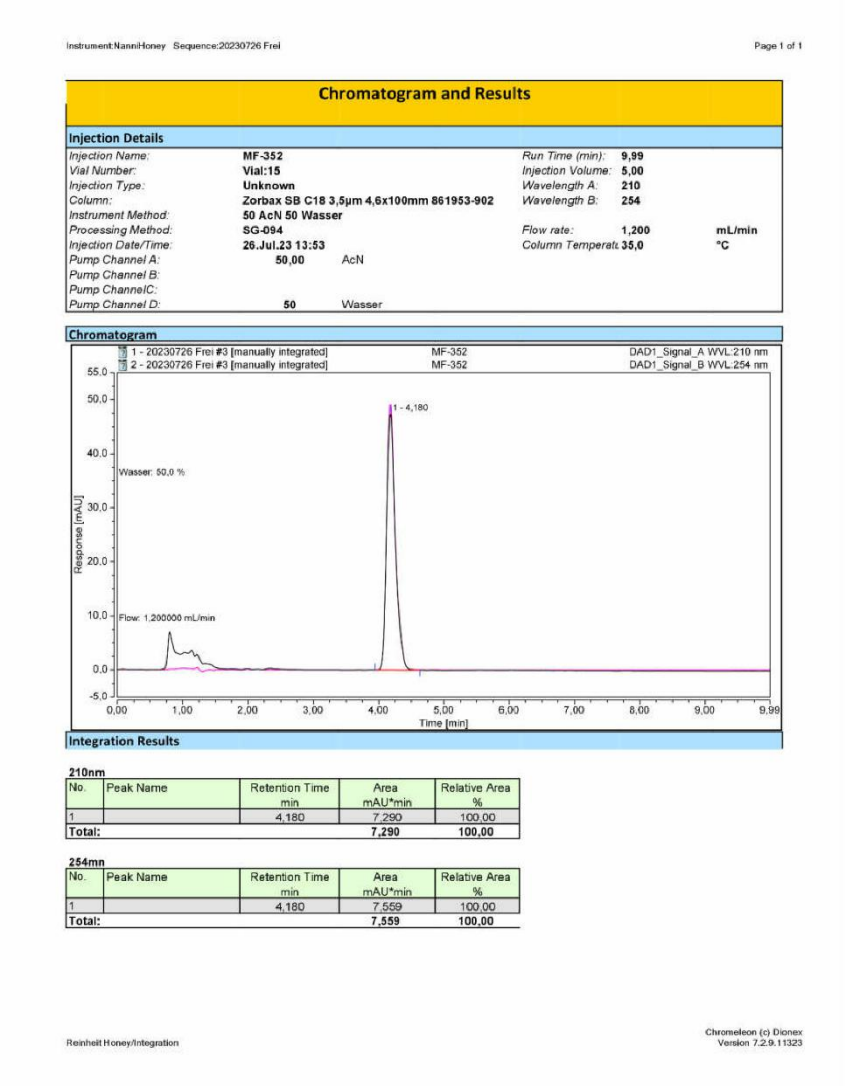

Instrument:NanniHoney Sequence:20230726 Frei Page 1 of 1

Chromatogram and Results

Injection Details

Injection Name:	**MF-352**		*Run Time (min):*	**9,99**	
Vial Number:	**Vial:15**		*Injection Volume:*	**5,00**	
Injection Type:	**Unknown**		*Wavelength A:*	**210**	
Column:	**Zorbax SB C18 3,5µm 4,6x100mm 861953-902**		*Wavelength B:*	**254**	
Instrument Method:	**50 AcN 50 Wasser**				
Processing Method:	**SG-094**		*Flow rate:*	**1,200**	**mL/min**
Injection Date/Time:	**26.Jul.23 13:53**		*Column Temperatu*	**35,0**	**°C**
Pump Channel A:	**50,00**	AcN			
Pump Channel B:					
Pump ChannelC:					
Pump Channel D:	**50**	Wasser			

Chromatogram

Integration Results

210nm

No.	Peak Name	Retention Time min	Area mAU*min	Relative Area %
1		4,180	7,290	100,00
Total:			**7,290**	**100,00**

254mn

No.	Peak Name	Retention Time min	Area mAU*min	Relative Area %
1		4,180	7,559	100,00
Total:			**7,559**	**100,00**

Reinheit Honey/Integration Chromeleon (c) Dionex Version 7.2.9.11323

HPLC chromatogram of **FM358**

20

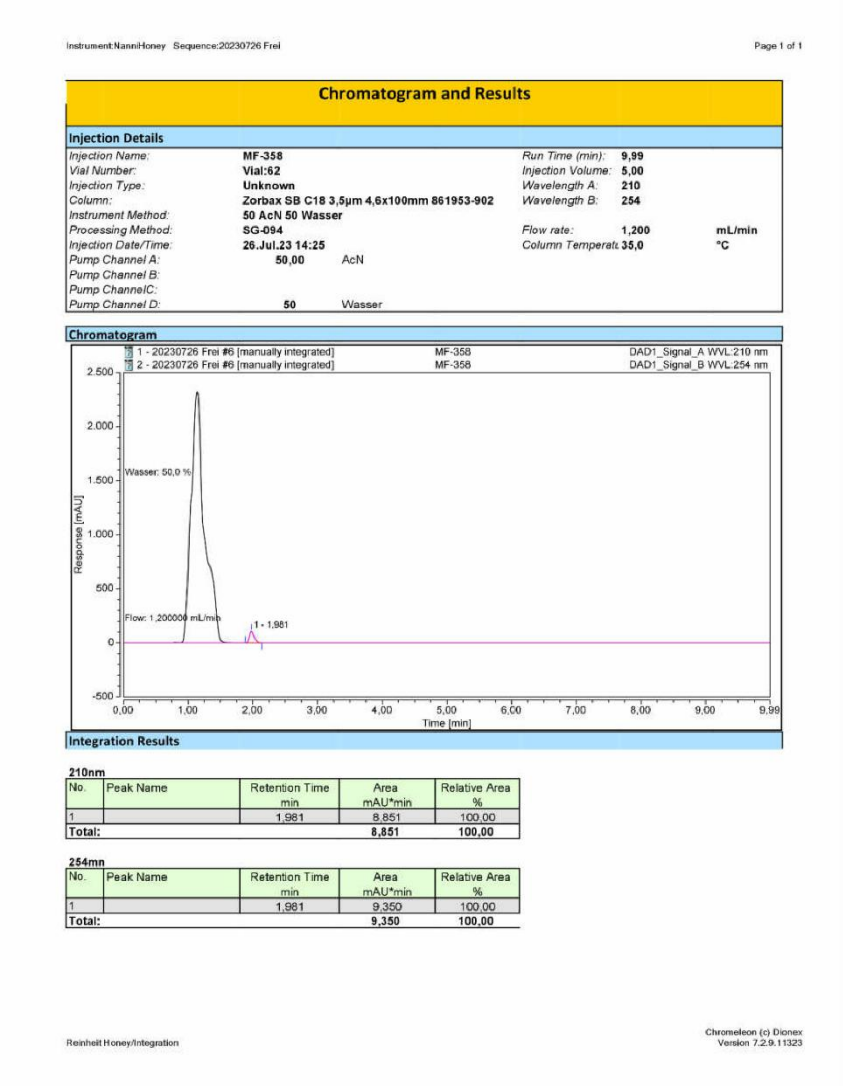

Instrument:NanniHoney Sequence:20230726 Frei Page 1 of 1

Chromatogram and Results

Injection Details

Injection Name:	**MF-358**		*Run Time (min):*	**9,99**	
Vial Number:	**Vial:62**		*Injection Volume:*	**5,00**	
Injection Type:	**Unknown**		*Wavelength A:*	**210**	
Column:	**Zorbax SB C18 3,5µm 4,6x100mm 861953-902**		*Wavelength B:*	**254**	
Instrument Method:	**50 AcN 50 Wasser**				
Processing Method:	**SG-094**		*Flow rate:*	**1,200**	**mL/min**
Injection Date/Time:	**26.Jul.23 14:25**		*Column Temperatu*	**35,0**	**°C**
Pump Channel A:	**50,00**	AcN			
Pump Channel B:					
Pump ChannelC:					
Pump Channel D:	**50**	Wasser			

Chromatogram

Integration Results

210nm

No.	Peak Name	Retention Time min	Area mAU*min	Relative Area %
1		1,981	8,851	100,00
Total:			**8,851**	**100,00**

254mn

No.	Peak Name	Retention Time min	Area mAU*min	Relative Area %
1		1,981	9,350	100,00
Total:			**9,350**	**100,00**

Reinheit Honey/Integration Chromeleon (c) Dionex Version 7.2.9.11323

HPLC chromatogram of **FM368**

21

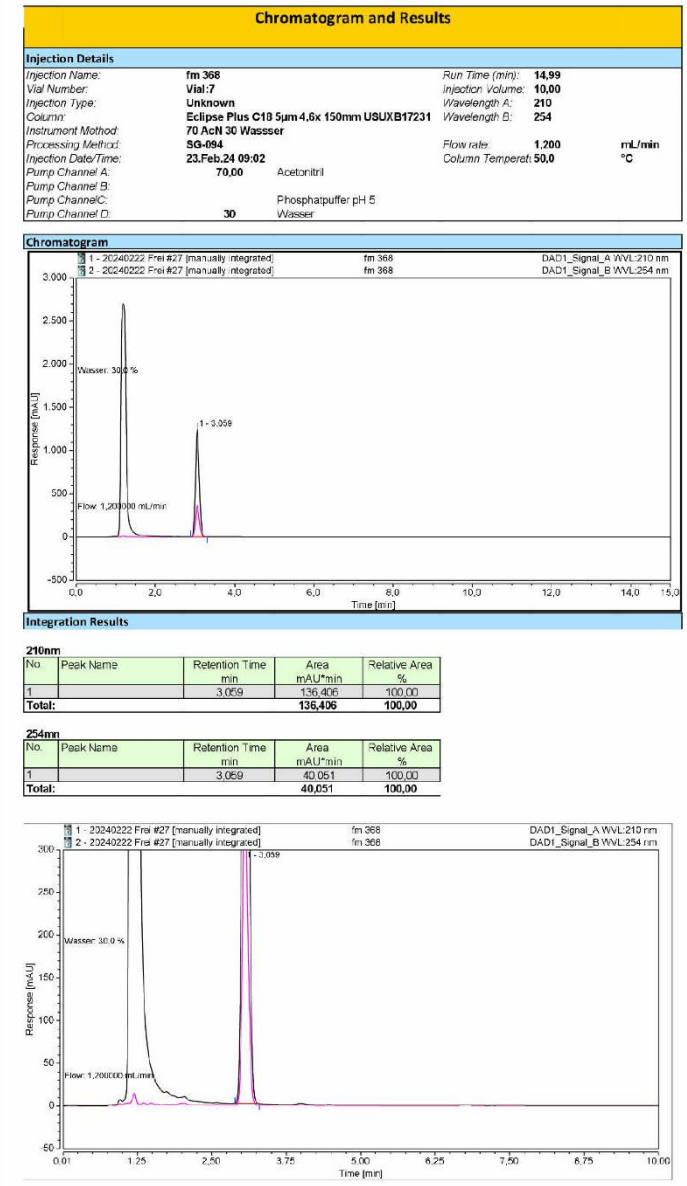

Chromatogram and Results

Injection Details

Injection Name:	**fm 368**		*Run Time (min):*	**14,99**	
Vial Number:	**Vial:7**		*Injection Volume:*	**10,00**	
Injection Type:	**Unknown**		*Wavelength A:*	**210**	
Column:	**Eclipse Plus C18 5µm 4,6x 150mm USUXB17231**		*Wavelength B:*	**254**	
Instrument Method:	**70 AcN 30 Wassser**				
Processing Method:	**SG-094**		*Flow rate:*	**1,200**	**mL/min**
Injection Date/Time:	**23.Feb.24 09:02**		*Column Temperat:*	**50,0**	**°C**
Pump Channel A:	**70,00**	Acetonitril			
Pump Channel B:					
Pump ChannelC:		Phosphatpuffer pH 5			
Pump Channel D:	**30**	Wasser			

Chromatogram

Integration Results

210nm

No.	Peak Name	Retention Time min	Area mAU*min	Relative Area %
1		3,059	136,406	100,00
Total:			**136,406**	**100,00**

254nm

No.	Peak Name	Retention Time min	Area mAU*min	Relative Area %
1		3,059	40,051	100,00
Total:			**40,051**	**100,00**

IR spectrum of lead compound **Yang_28e**

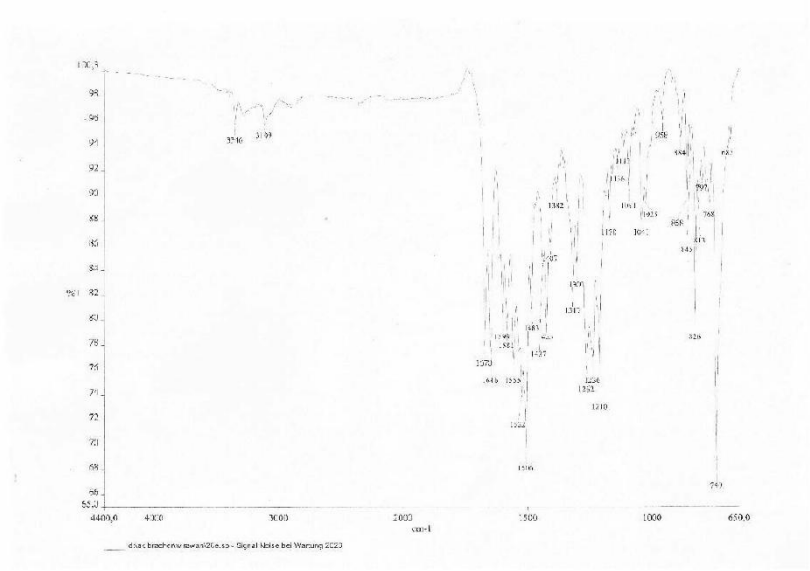

IR spectrum of lead compound **Yang_24a**

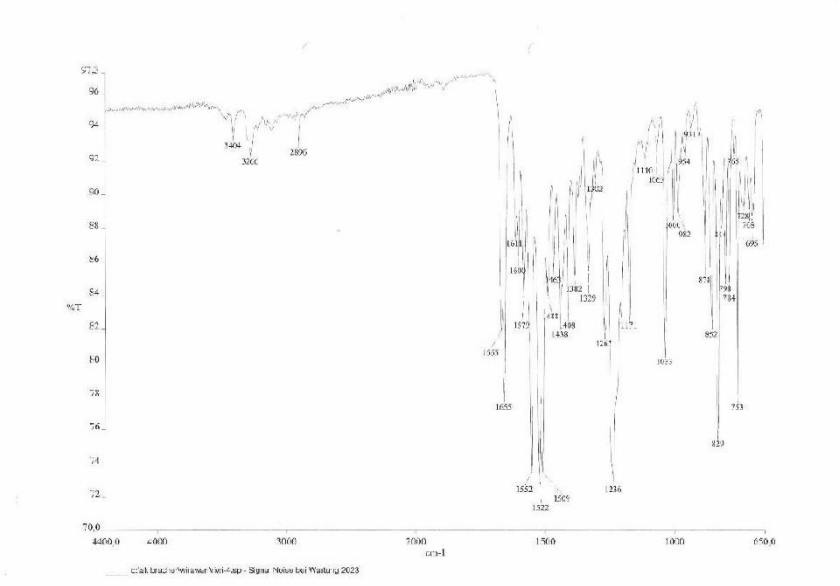

IR spectrum of **FM345**

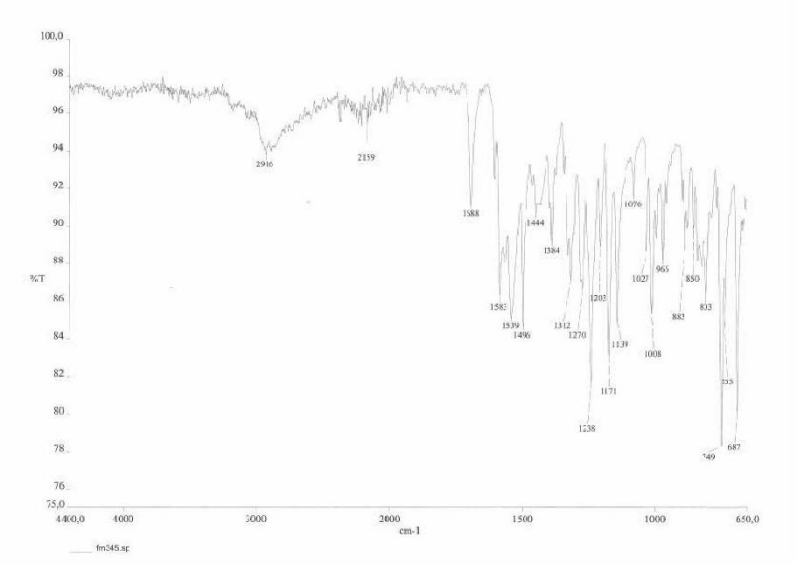

IR spectrum of **FM352**

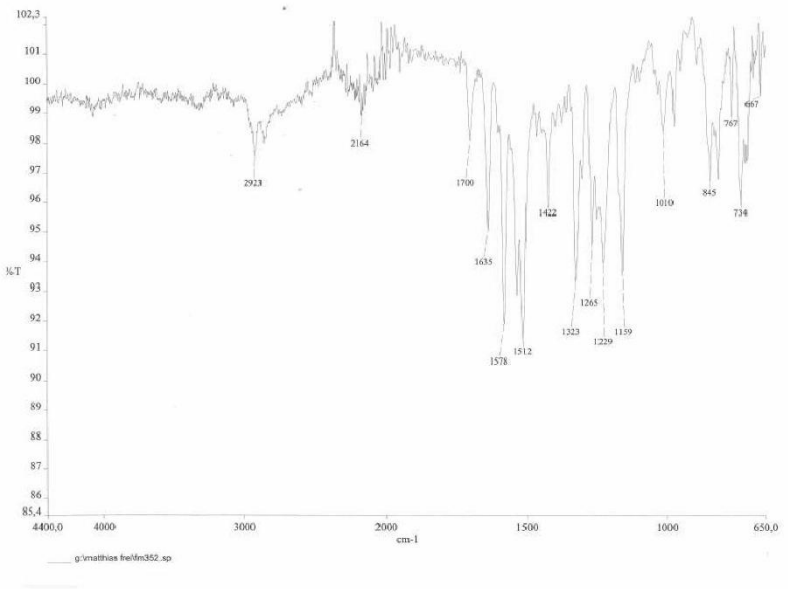

IR spectrum of **FM358**

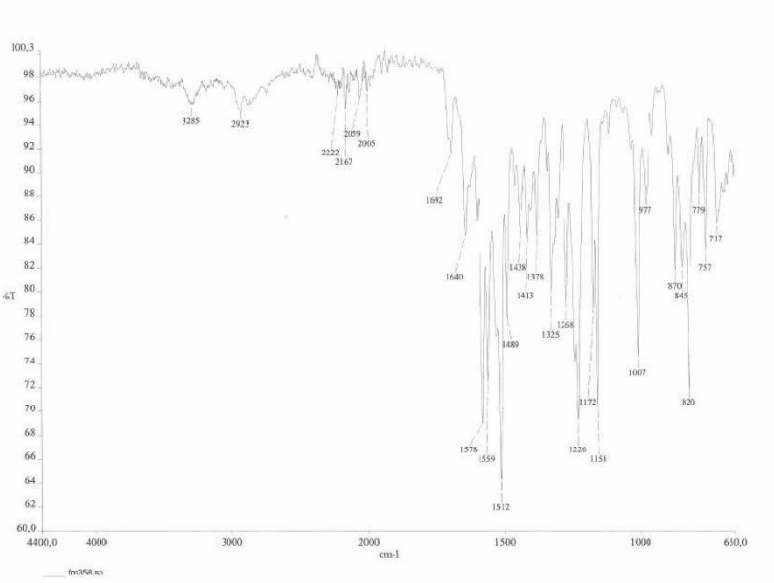

IR spectrum of **FM368**

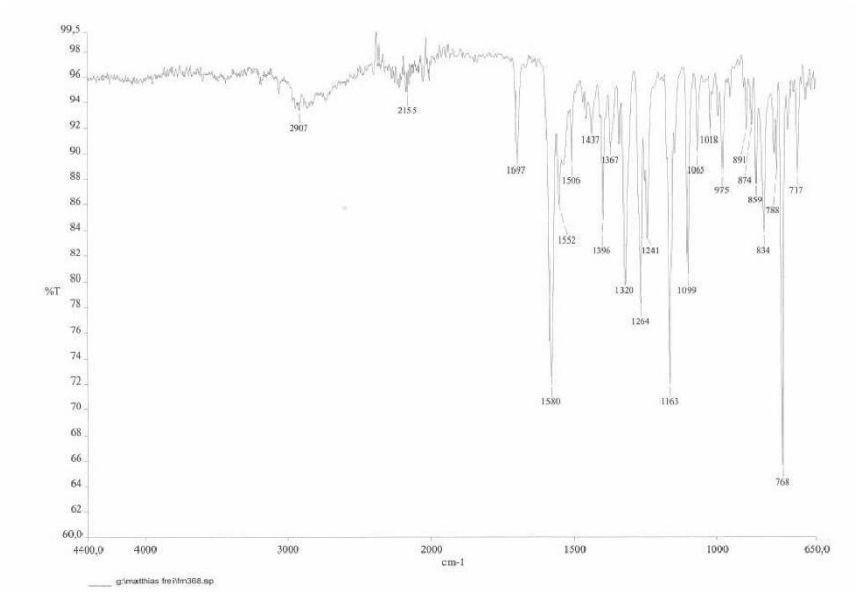

IR spectrum of **RW-93**

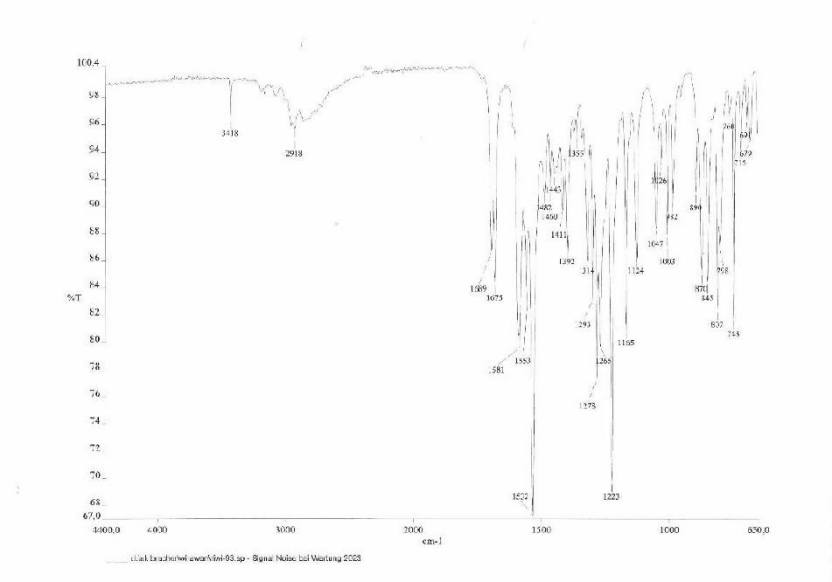

IR spectrum of **RW-95**

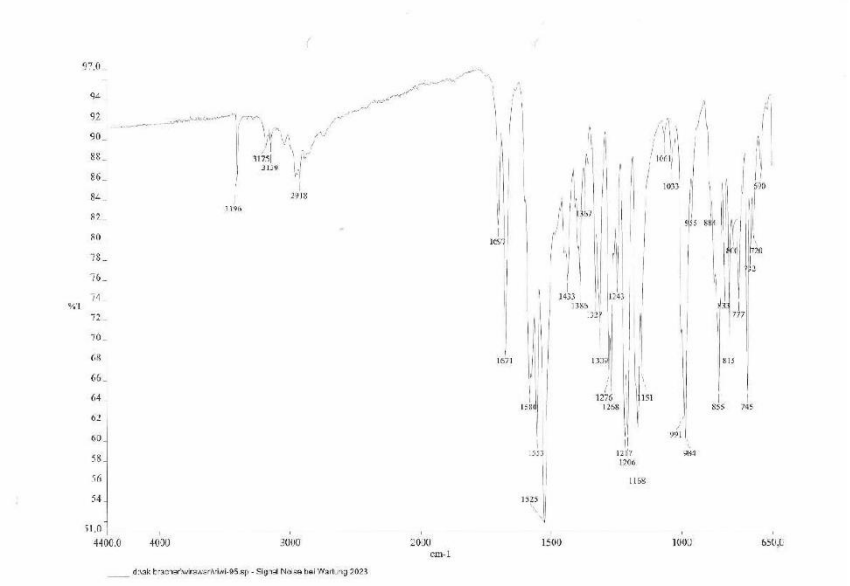

IR spectrum of **RW-99**

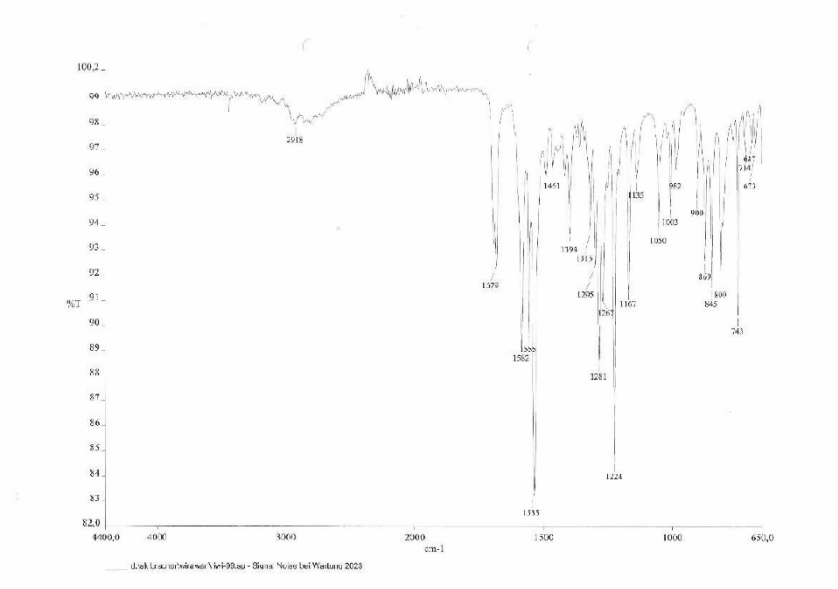

Cell viability data of **RW-93**

27

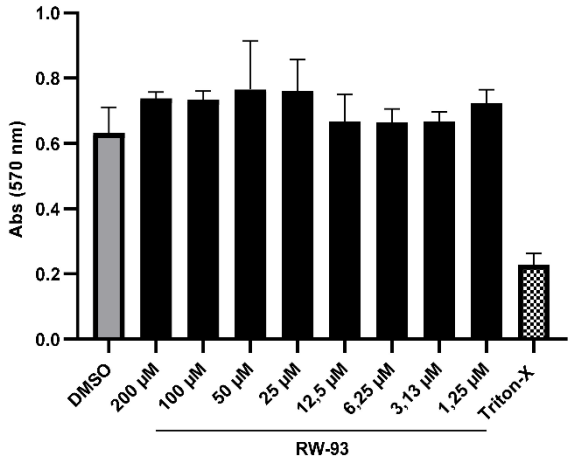

Figure S1: Cell viability data of RW-93. The acute cytotoxicity of **RW-93** was determined using a colorimetric MTT assay. HL-60 cells were treated with **RW-93** at various concentrations with three technical replicates. Triton-X was used as a positive control. No significant changes in the cell viability relative to DMSO control was determined following treatment with up to 200 µM of **RW-93**.

3.3. Project III: Balsalazide-derived heterotriaryls with reversible covalent warheads as Sirt5 inhibitors

Wirawan, R.; Huber, S. A.; Wein, T.; Bracher, F. Balsalazide-Derived Heterotriaryls as Sirtuin 5 Inhibitors: A Case Study of a Reversible Covalent Inhibition Strategy. *Molecules* **2025**, *30*, 3821.

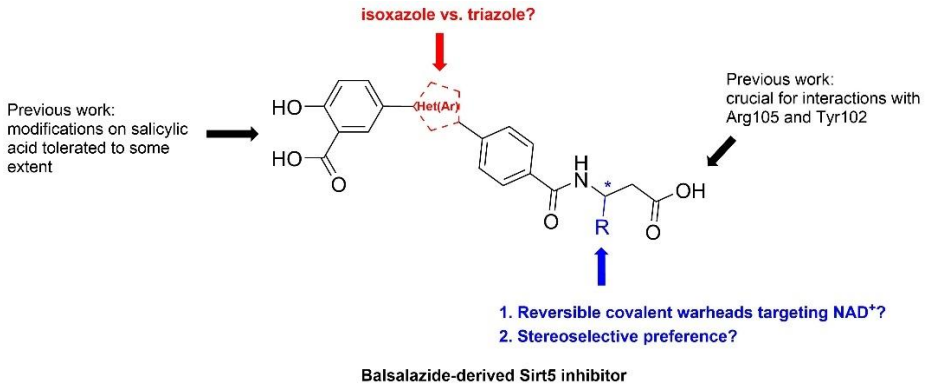

3.3.1. Summary

The pharmacokinetically optimised balsalazide-derived heterotriaryls **CG_209** and **CG_220** from a previous project in the Bracher group were selected as promising lead structures for the development of novel Sirt5 inhibitors. Building on these scaffolds, a diverse set of Sirt5 inhibitors possessing appropriate electrophilic functional groups such as boronic acids, nitriles and aldehydes were rationally designed following molecular docking studies to target the nicotinamide ribose vicinal diol unit of the co-factor NAD^+ *via* reversible covalent bonding. Challenges associated with the synthesis of enantiomerically pure Sirt5 inhibitors bearing these reversible covalent warheads were navigated through chiral-pool syntheses from commercially available amino acid derivatives. In total, 10 functionalized analogues were synthesised and investigated. Biological evaluation revealed superiority of the triazole-based inhibitors as well as stereo-selective preference of these functional group modifications, with all *S*-enantiomers showing higher potency compared to the corresponding *R*-enantiomers. From this library of Sirt5 inhibitors, the *S*-enantiomer triazole-based cyanomethyl **50** emerged as the top inhibitor with an IC_{50} of 27 µM, which lies in a similar potency range of other established Sirt5 inhibitors.

3.3.2. Personal Contributions

My personal contributions to this journal article include the synthesis and the characterization of all Sirt5 inhibitors and the precursors thereof, the supervision of Simon A. Huber's bachelor thesis, the management and coordination of this project, the writing of the original draft, the

reviewing and editing of the final manuscript, and the preparation of the graphical abstract and supplementary information.

Simon A. Huber synthesised and characterized both enantiomers of the isoxazole-based cyanomethyl Sirt5 inhibitors and the precursors thereof. Thomas Wein performed molecular docking experiments. Franz Bracher conceptualized and designed the study, managed and coordinated the project, supervised all synthetic work and Simon A. Huber's bachelor thesis, provided funding and resources, and reviewed and edited the final manuscript.

3.3.3. Article

molecules

MDPI

Article

Balsalazide-Derived Heterotriaryls as Sirtuin 5 Inhibitors: A Case Study of a Reversible Covalent Inhibition Strategy

Ricky Wirawan, Simon A. Huber, Thomas Wein and Franz Bracher *

Department of Pharmacy—Center for Drug Research, Ludwig-Maximilians University, Butenandtstr. 5-13, 81377 Munich, Germany; ricky.wirawan@cup.uni-muenchen.de (R.W.)
* Correspondence: franz.bracher@cup.uni-muenchen.de; Tel.: +49-89-218077301

Abstract

Sirtuin 5 is an NAD^+-dependent lysine deacylase that is involved in various biological processes and has emerged as a promising target for pharmaceutical therapies. The development of highly potent and subtype-selective sirtuin 5 inhibitors for their application as chemical tools and drug candidates still poses a significant challenge. Based on our own optimized balsalazide-derived sirtuin 5 inhibitors, this work presents a systematic investigation of the inhibitory effects of derivatives with moieties that were guided by docking experiments to target the nicotinamide ribose vicinal hydroxy groups of the essential co-factor NAD^+ via reversible covalent binding to potentially enhance their potency. Our results show that functionalizations with these moieties were tolerated to some extent and possessed a distinct stereo-selective preference. The (*S*)-configured cyanomethyl derivative **50** with an IC_{50} of 27 µM emerged from our synthesized library of compounds as the most potent functionalized inhibitor and lies in a similar potency range to other established sirtuin 5 inhibitors. Our findings offer a deeper insight into the structure–activity relationships of our balsalazide-derived heterotriaryl-based sirtuin 5 inhibitors and thus could provide an avenue for further optimizations in the future.

Keywords: histone deacetylases; sirtuin 5 inhibitor; Sirt5 inhibitor; balsalazide; structure–activity relationship; reversible covalent inhibitor; co-factor NAD^+

check for updates

Academic Editor: Spyridon Mourtas

Received: 22 August 2025
Revised: 16 September 2025
Accepted: 18 September 2025
Published: 20 September 2025

Citation: Wirawan, R.; Huber, S.A.; Wein, T.; Bracher, F. Balsalazide-Derived Heterotriaryls as Sirtuin 5 Inhibitors: A Case Study of a Reversible Covalent Inhibition Strategy. *Molecules* **2025**, *30*, 3821. https://doi.org/10.3390/molecules30183821

1. Introduction

Sirtuins, belonging to the unique class III histone deacetylases, represent highly conserved NAD^+-dependent enzymes [1]. In mammals, seven different sirtuin subtypes were identified, each with its own distinct function and subcellular localization [2]. As a protein that predominantly resides in the mitochondria, sirtuin 5 has gained significant interest over the years due to its governing role in various metabolic processes such as ammonia detoxification [3], ROS elimination [4], β-oxidation of fatty acids [5], glycolysis [6] and ketogenesis [7]. Dysregulation of sirtuin 5 has been implicated with the progression and exacerbation of numerous diseases, including metabolic disorders [8], neurodegeneration [9,10] and cancer [11–13]. Thus, sirtuin 5 presents itself as a promising biological target for pharmaceutical interventions. Extensive efforts were undertaken over the years to develop novel and effective Sirt5 inhibitors. However, most of them still suffer from subpar potency, lack of subtype selectivity and poor pharmacokinetic properties, signifying the challenges and obstacles associated with the development of drug-like sirtuin 5 inhibitors. Representative potent sirtuin 5 inhibitors include the indolinone GW5074 [14,15],

the β-naphthol-based cambinol [16] and Maurer et al. compound **2** [16] (Figure 1). However, these compounds also exhibit comparable inhibitory potency against other sirtuin subtypes such as sirtuin 2. Additionally, these inhibitors, as well as Liu et al. compound **37** [17], may exhibit promiscuity to other biological targets due to highly reactive motifs such as Michael acceptors and alkylidene thiobarbiturates that are typical in false-positive pan-assay interference compounds (PAINS) [18]. Although approved drugs such as anthralin, methacycline and balsalazide emerged as sirtuin 5 inhibitors in a high-throughput screening [19], their drug repurposing potential is limited due to significant liabilities associated with toxicity (anthralin), instability (anthralin), unwanted antimicrobial effects (methacycline) and suboptimal pharmacokinetic properties (balsalazide) [20,21]. For the latter, however, optimization efforts that involve the substitution of the gut-bacteria labile azo bond of balsalazide with metabolically more stable heteroaromatic rings such as isoxazole (**CG_209**) and triazole (**CG_220**) have been successfully conducted in our previous work [21,22].

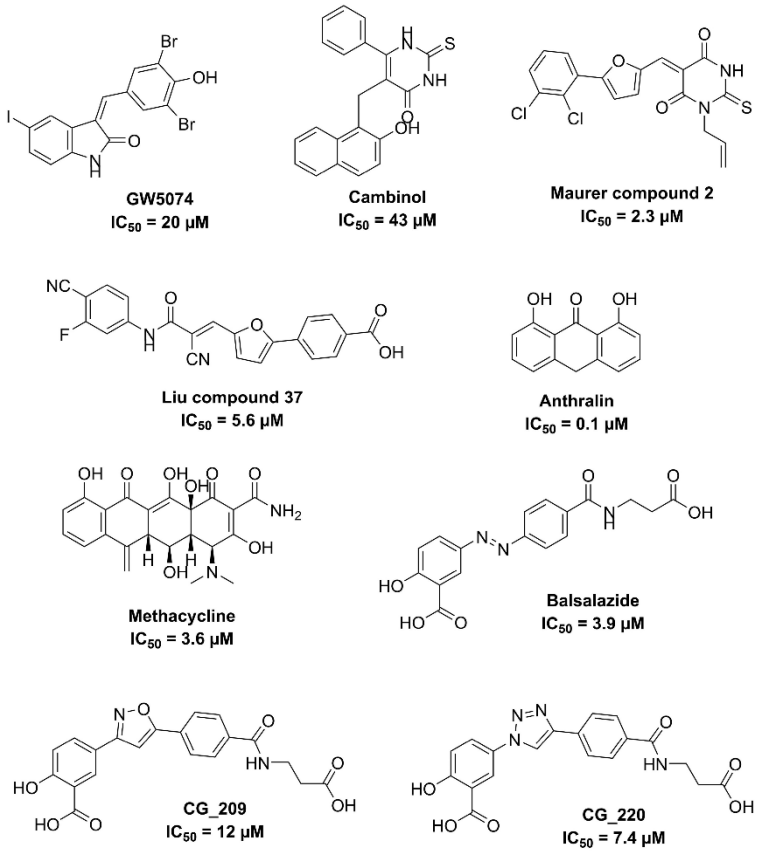

Figure 1. Selected examples of published sirtuin 5 inhibitors.

In continuation of our work on the optimization of balsalazide as a drug-like sirtuin 5 inhibitor through comprehensive SAR studies [21,22] and our work on developing reversible covalent sirtuin inhibitors [23], we sought to explore the potential of reversible

covalent inhibition as a tool to further improve the potency of our subtype selective sirtuin 5 inhibitors **CG_209** and **CG_220**. Reversible covalent inhibition with suitable functional groups has seen notable success in drug development as exemplified by the boronic acid-containing bortezomib in the treatment of multiple myeloma [24,25], the nitrile-based saxagliptin for the treatment of diabetes mellitus type II [26], and the aldehyde-containing sickle cell anemia drug voxelotor [27]. Nitriles can undergo reversible covalent bonding with the more reactive 2′-OH of the nicotinamide ribose based on the mechanistic insight of sirtuin catalysis [1], while boronic acids and aldehydes can additionally react with the 3′-OH nicotinamide ribose to form cyclic boronates and acetals (Figure 2). Reversible covalent inhibitors have the advantage of prolonged inhibition and thus potency compared to non-covalent inhibitors, yet at the same time reduced off-target toxicity and immunogenicity compared to irreversible covalent inhibitors, making them promising candidates for drug development [28]. Based on our previous docking experiments of balsalazide in sirtuin 5 [21], the position of balsalazide was shown to be in spatial proximity to the nicotinamide ribose ring of the co-factor NAD^+. These findings suggested the potential of the yet-unexploited co-factor NAD^+ as a site for additional binding interactions. A similar strategy has been executed to great success in the other sirtuin subtypes such as the development of mechanism-based sirtuin 2 inhibitors that yielded nanomolar potency [29]. However, to the best of our knowledge, this approach has never been investigated before in the field of sirtuin 5. Furthermore, the application of reversible covalent inhibition in the development of sirtuin 5 inhibitors remains unexplored. Thus, this work focuses on the systematic investigation of rational modifications of **CG_209** and **CG_220** that employ various functional groups such as boronic acids, nitriles and aldehydes at appropriate positions on the inhibitor scaffolds to not only give further insight into their structure–activity relationships, but to perhaps also potentially improve their potency through their engagement in reversible covalent bonding with the nicotinamide ribose hydroxy groups of NAD^+.

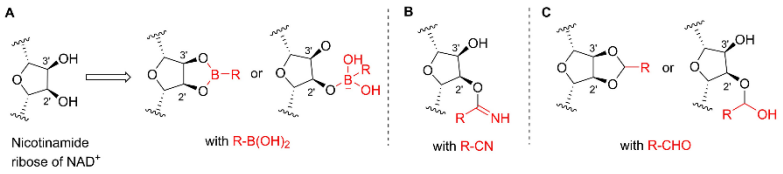

Figure 2. Proposed binding mode of the selected reversible covalent warheads with the nicotinamide ribose of the co-factor NAD^+. Boronic acids (**A**) and aldehydes (**C**) can react with one or both hydroxy groups to form (cyclic) boronates, and hemiacetals or cyclic acetals. Nitriles (**B**) can react with the more reactive 2′-OH to form iminoethers. Reversible covalent inhibition strategy blends the benefits of both irreversible covalent inhibition and non-covalent inhibition by prolonging inhibition and thus potency, while maintaining reversibility that reduces off-target toxicity.

2. Results & Discussion

2.1. Design Rationale of Inhibitors via Docking Experiments

Initial docking experiments with the envisaged boronic acid derivatives in sirtuin 5 were performed to give an insight into their potential binding poses (Figure 3). The results suggested the α-carbon atom to the essential terminal carboxylic acid as the appropriate position for functional group modifications to target the nicotinamide ribose hydroxy groups of the co-factor NAD^+. Notably, the docking calculations also predicted the requirement of an additional methylene group for optimal spacing of the modifications to allow reversible covalent bonding with the nicotinamide ribose hydroxy groups. Acknowledging the pres-

ence of a newly introduced chiral center involved in the functional group modifications, syntheses and subsequent biological evaluation of enantiomerically pure derivatives will additionally provide insight, if any, into the stereospecific preference of these moieties in the active site.

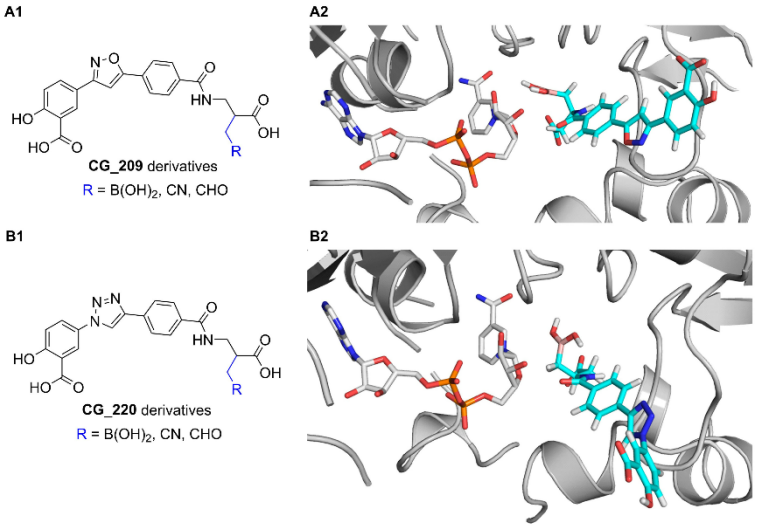

Figure 3. Target structures derived from **CG_209** (**A1**) and **CG_220** (**B1**). Docking experiments of the envisaged boronic acid derivatives of **CG_209** (cyan) (**A2**) and **CG_220** (cyan) (**B2**) in the presence of the co-factor NAD^+ (grey) (based on PDB ID: 3RIY [30]). Modifications with further functional groups such as nitriles and aldehydes were additionally chosen as suitable moieties for reversible covalent binding. Colors: oxygen (red), nitrogen (blue), phosphorus (orange).

2.2. Chemistry

The syntheses of lead structures **CG_209** and **CG_220** were generally performed following literature procedures [22] with slight modifications, particularly in the preparation of the benzamide **6** (Scheme 1). Instead of the reported three-step procedure [22], the amide **6** was synthesized directly from 4-ethynylbenzoic acid (**4**) and β-alanine ethyl ester hydrochloride (**5**) with CDI as an amide coupling reagent. For the preparation of the isoxazole **CG_209**, the salicylic acid moiety of 5-formylsalicylic acid (**1**) was first protected with acetone to give the acetonide **2**. Aldoxime **3** was then synthesized from acetonide **2** with hydroxylamine hydrochloride. PIFA-mediated oxidation of the aldoxime **3** to the nitrile oxide intermediate allowed the 1,3-dipolar cycloaddition with alkyne **6** to yield isoxazole **7**. Subsequent saponification of the acetonide and the ethyl ester gave lead structure **CG_209** in 73% yield. Similarly, the preparation of triazole **CG_220** involved the initial protection of 5-nitrosalicylic acid (**8**) to give acetonide **9**. The nitroarene **9** was then reduced to the aniline **10** and subsequently, after diazotation, converted to azide **11** with sodium azide. The copper catalyzed azide-alkyne cycloaddition (CuAAC) between azide **11** and alkyne **6** then afforded triazole **12**. Finally, dual protective group saponification led to the formation of lead structure **CG_220**.

The syntheses of the enantiomerically pure boronic acid and cyanomethyl derivatives were initiated by the reduction of 4-benzyl *N*-Boc-(*S*)- (**13**) and (*R*)- (**14**) aspartate to their corresponding primary alcohols **15** and **16** with ethyl chloroformate to initially generate the mixed anhydride intermediates and then sodium borohydride following procedures

from Isernia et al. [31] (Scheme 2). Conversion of the primary alcohol **15** to the alkyl iodide **17** via an Appel reaction was performed with triphenylphosphine and iodine following a published protocol [31]. Similarly, bromination of alcohols **15** and **16** via an Appel reaction afforded the alkyl bromides **18** and **19** according to published work by Röhrich et al. [32]. The borylation of the alkyl bromides **18** and **19** was then successfully performed with B_2pin_2, $Pd_2(dba)_3$ catalyst and *t*-$Bu_2MeP{\cdot}HBF_4$ ligand to give the boronic acid pinacol esters **20** and **21** in 60% and 51% yield, respectively.

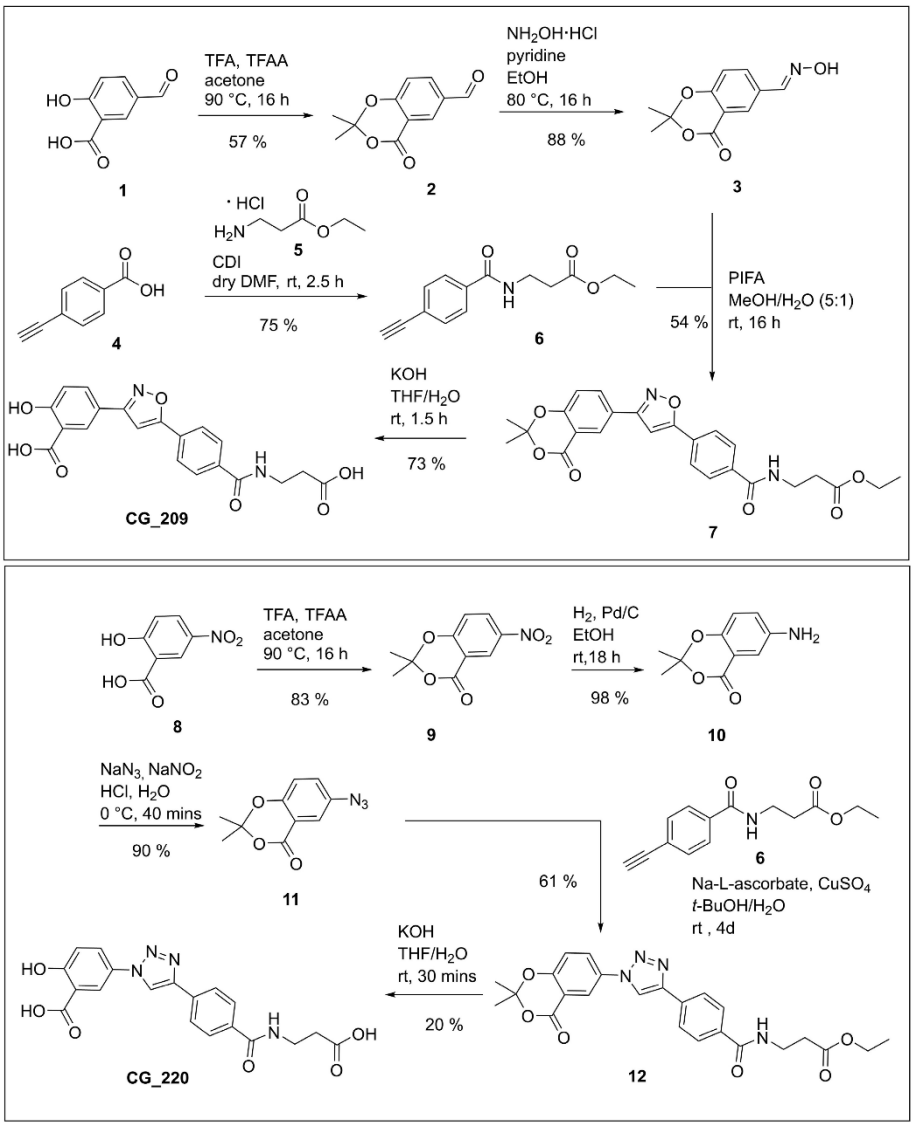

Scheme 1. Synthesis of lead structures **CG_209** and **CG_220** according to published literature with slight modifications, particularly in the preparation of the amide **6**.

Kolbe nitrile synthesis of the cyanomethyl compounds **22** and **23** from the alkyl bromides **18** and **19** was performed using Bu_4NCN, inspired by a method from Isernia et al. [31].

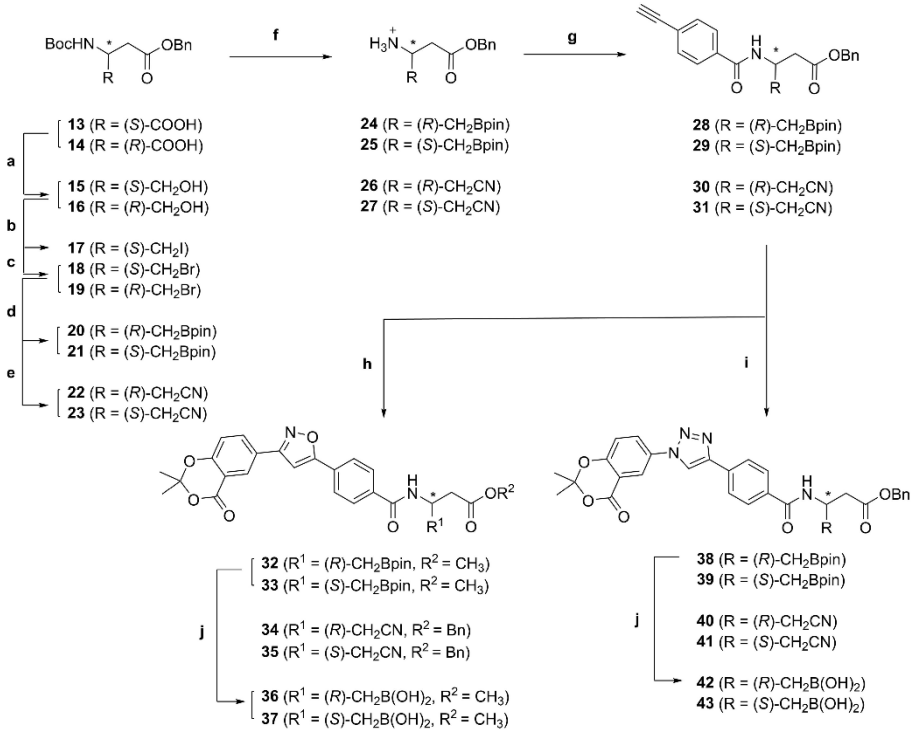

Scheme 2. Reagents, conditions and yields: (a) ethyl chloroformate, Et_3N, THF, 0 °C, 15 min, then $NaBH_4$, H_2O, rt, 1 h, 70% for **15** and 68% for **16**; (b) PPh_3, I_2, imidazole, DCM, rt, 2.5 h, 54%; (c) PPh_3, CBr_4, dry Et_2O, rt, 15 min, 60% for **18** and 58% for **19**; (d) B_2pin_2, $Pd_2(dba)_3$, *t*-$Bu_2MeP{\cdot}HBF_4$, K_2CO_3, *t*-BuOH/H_2O (12:1 *v*/*v*), 60 °C, 6 h, 60% for **20** and 51% for **21**; (e) Bu_4NCN, DCM, 55 °C, 17 h, 52% for **22** and 63% for **23**; (f) 4M HCl in dioxane, rt, 1 h, quant. for **24**, **25**, **26** and **27**; (g) 4-ethynylbenzoic acid (**4**), CDI, dry DMF, rt, 3 d, 80% for **28**, 64% for **29**, 58% for **30** and 71% for **31**; (h) aldoxime **3**, PIFA, MeOH/H_2O (5:1 *v*/*v*), rt, 16 h, 31% for **32**, 22% for **33**, 14% for **34** and 24% for **35**; (i) azide **11**, Na-L-ascorbate, $CuSO_4$, *t*-BuOH/H_2O (21:1 *v*/*v*), rt, 18 h, 17% for **38**, 8% for **39**, 41% for **40**, 53% for **41**, 24% for **42** and 33% for **43**; (j) $NaIO_4$, HCl, THF/H_2O (4:1 *v*/*v*), rt, 16 h, 73% for **36**, 64% for **37** and 68% for **42**. * = chiral center.

The *N*-Boc-protected derivatives **20**–**23** were then treated with HCl in dioxane following a procedure from Klein et al. [33] to give the primary amine hydrochlorides **24**–**27**, which were subsequently coupled with 4-ethynylbenzoic acid (**4**) utilizing CDI as an amide coupling reagent to give amides **28**–**31** in good yields. Of particular note was the formation of 2-oxazoline **45** as the main product when the bromo derivative **44** was subjected to amide coupling with 4-ethynylbenzoic acid (Scheme 3), suggesting that efficient introduction of the boronic acid pinacol ester and the nitrile moieties must be performed prior to the amide coupling as late-stage functionalization to the boronic acid pinacol esters or nitriles would no longer be possible with oxazoline **45**. Since the identity of the product was initially ambiguous, the X-ray crystal structure of compound **45** was solved to confirm its

molecular structure (see Supplementary Materials). The duality of CDI as both an amide coupling reagent and subsequently a source of base in the form of imidazole allows the facile base-mediated formation of 2-oxazoline in a single step.

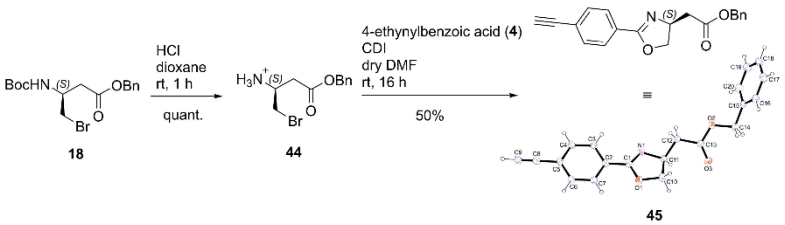

Scheme 3. Formation of the 2-oxazoline side product **45**, most likely via the imidazole-catalyzed deprotonation of the amide hydrogen atom that leads to nucleophilic attack of the amide at the reactive alkyl bromide.

1,3-Dipolar cycloaddition of the alkynes **28**–**31** and the previously synthesized aldoxime **3** in a methanol–water mixture then afforded the isoxazoles **32–35**. Notably, transesterification of the benzyl ester with the solvent methanol also occurred in this reaction but was only limited to the boronic acid pinacol esters derivatives **32** and **33**, presumably due to the strong Lewis acidity of the boronic acid pinacol ester in the neighboring position to the benzyl ester that promotes this transesterification process. Nonetheless, the next synthetic steps were carried on since the benzyl ester (or the methyl ester) only served as a protecting group for the terminal carboxylic acid and will have to be hydrolyzed in the following steps. The syntheses of triazoles **38**–**41** were performed via CuAAC of alkynes **28**–**31** and the previously prepared azide **11**. Remarkably, mixtures of both the boronic acid pinacol esters and the free boronic acids were generated. For example, CuAAC of alkyne **28** and azide **11** yielded 17% of the boronic acid pinacol ester **38** and 24% of the boronic acid **42**, while CuAAC of alkyne **29** and azide **11** yielded 8% of the boronic acid pinacol ester **39** and 33% of the boronic acid **43.** Subsequent oxidative cleavage of the boronic acid pinacol esters **32**, **33** and **38** with sodium periodate gave boronic acids **36**, **37** and **42** in satisfactory yields.

The borylation step involving the conversion of alkyl bromides **18** and **19** to the boronic acid pinacol esters **20** and **21** represents a pivotal segment in the syntheses of the envisaged boronic acid derivatives and required several rounds of optimizations in the reagents, reaction conditions and purification methods used (Table 1), all of which are listed here as entries in Table 1 and were inspired from published methods that were specifically developed for the preparation of alkyl boronic acids and esters thereof. Alkyl iodide **17** was initially subjected to borylation utilizing CuI as catalyst, triphenylphosphine as ligand and lithium methanolate as a base (entry 1 [34]), but this approach was unsuccessful. Replacement of the triphenylphosphine ligand with another phosphine-based ligand Xantphos and the base with potassium *tert*-butoxide with reactions performed both at room temperature (entry 2 [35]) and at elevated temperature (entry 3) likewise showed no success.

Substitution of the transition metal catalyst to Ni(II) in combination with a chiral pyridine bisoxazoline ligand led instead to the undesired dehalogenation of alkyl iodide **17** in 33% yield (entry 4). Such undesired dehalogenation was notably not observed in the original study where this method was developed [36]. Alternatively, utilization of $Pd_2(dba)_3$ catalyst and *t*-$Bu_2MeP{\cdot}HBF_4$ ligand with potassium carbonate as a base was performed in a solvent mixture of *tert*-butanol and water and gave trace amounts of the product (entry 5 [37]). Similarly, traces of the product were obtained when tetrabutylammonium iodide was additionally employed with the reagents listed in entry 1 (entry 6 [38]). However,

applying the exact same reagents and conditions from entry 6 with alkyl bromide **18** as the starting material, a significant increase in the yield was obtained, and the desired pinacol ester product **20** could be isolated in 10% yield (entry 7 [38]). When the reagents and the reaction conditions from entry 1 were repeated with alkyl bromide **18**, still no desired product **20** was formed (entry 8 [34]), highlighting the importance of tetrabutylammonium iodide in entry 7. Entry 5, which initially afforded only traces amount of the desired product **20**, was repeated using alkyl bromide **18**, yielding 16% of the desired boronic acid pinacol ester **20** (entry 9 [37]). This suggests that alkyl bromide **18** is better suited than iodide **17** in the borylation, likely due to the latter's lower stability in the given reaction conditions. The reaction time in entry 9 was then systematically varied to optimize the yield of product **20**, with 6 h identified as optimal despite incomplete consumption of starting material **18** (entry 10a). Finally, purification of the boronic acid pinacol ester **20** using boric acid-impregnated silica gel was performed, which was prepared as described by Hitosugi et al. [39]. This further improved the yield to 60% (entry 10b) due to the reduction of the Lewis basicity of the silica gel and thus the over-adsorption of the boronic acid pinacol ester **20** to the silica gel, a common problem in the purification of boronic acids and esters [39].

Table 1. Method development in the borylation of alkyl halides **17** and **18** for the preparation of boronic acid pinacol ester **20**.

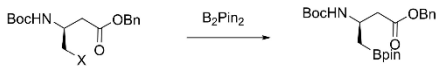

17 (X = I) or **18** (X = Br) **20**

Entry	X	Catalyst/Ligand	Base	Solvent	Temp.	Time	Yield
1	I	CuI, PPh_3	LiOMe	DMF	rt	16 h	-
2	I	CuCl, Xantphos	KO*t*Bu	THF	rt	16 h	-
3	I	CuCl, Xantphos	KO*t*Bu	THF	50 °C	16 h	-
4	I	$NiBr_2$·diglyme, *i*-Pr-PyBOX	KOEt	*i*-Pr_2O/DMA	60 °C	16 h	-/33% (**46**) [1]
5	I	$Pd_2(dba)_3$, *t*-Bu_2MeP·HBF_4	K_2CO_3	*t*-BuOH/H_2O	60 °C	16 h	traces
6	I	CuI, PPh_3, Bu_4NI	LiO*t*Bu	DMF	60 °C	18 h	traces
7	Br	CuI, PPh_3, Bu_4NI	LiO*t*Bu	DMF	60 °C	18 h	10%
8	Br	CuI, PPh_3	LiOMe	DMF	60 °C	16 h	-
9	Br	$Pd_2(dba)_3$, *t*-Bu_2MeP·HBF_4	K_2CO_3	*t*-BuOH/H_2O	60 °C	16 h	16%
10a	Br	$Pd_2(dba)_3$, *t*-Bu_2MeP·HBF_4	K_2CO_3	*t*-BuOH/H_2O	60 °C	6 h	42%
10b [2]	Br	$Pd_2(dba)_3$, *t*-Bu_2MeP·HBF_4	K_2CO_3	*t*-BuOH/H_2O	60 °C	6 h	60%

46: 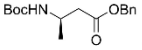

[1] Dehalogenated side product **46**. [2] Entry 10b differs from entry 10a in the purification method.

In the final step, the isoxazole cyanomethyl compounds **34** and **35** and the triazole cyanomethyl compounds **40** and **41** were subjected to saponification to afford the desired enantiomerically pure cyanomethylated isoxazoles **47** and **48** and triazoles **49** and **50** (Scheme 4). Similarly, the saponification of the boronic acids **36**, **37**, **42** and **43** was performed, albeit selective to the terminal methyl or benzyl ester to prevent the degradation of the boronic acids that stems from the inter- or intramolecular salicylic acid-boronic acid reactions. Selective saponification of the terminal methyl or benzyl ester was achieved by performing the reaction at 0 °C. Notably, in the presence of a base the boronic acids react intramolecularly with the neighboring amide moiety to form the cyclic boronates **51**–**54**. All attempts at deprotection of the acetonides to free salicylates led to very unstable products, and not even traces of the target products could be isolated.

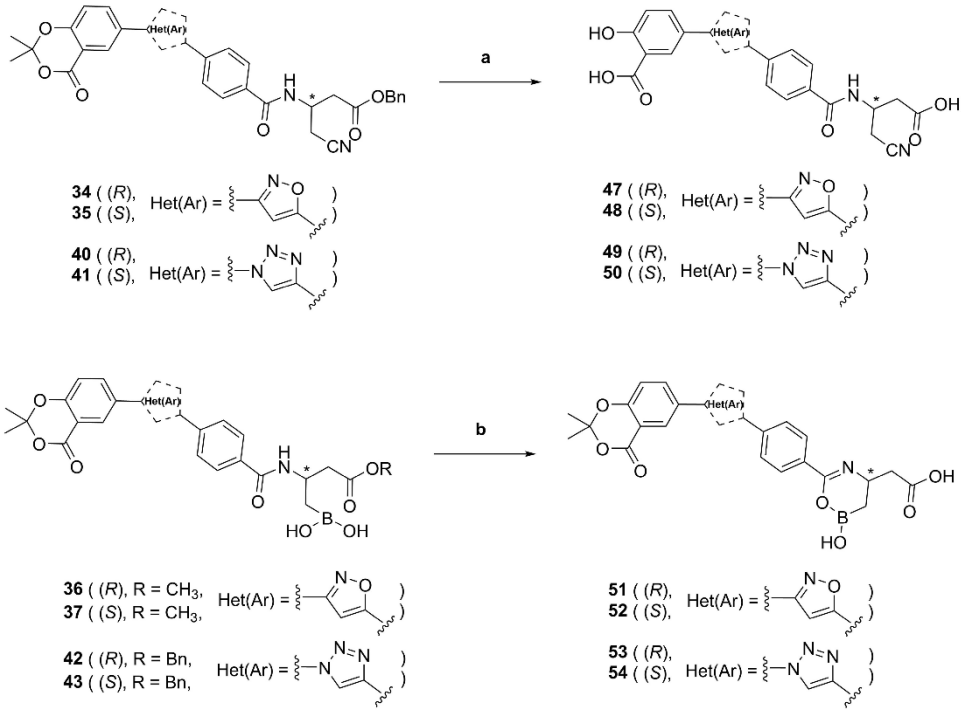

Scheme 4. Reagents, reactions conditions and yields: (a) KOH, THF, rt, 0.5–2.5 h, 50% for **47**, 55% for **48**, 39% for **49** and 58% for **50**; (b) KOH, THF, 0 °C, 0.5–1 h, 54% for **51**, 56% for **52**, 39% for **53** and 32% for **54**. * = chiral center.

The preparation of the corresponding aldehyde derivatives was initially attempted by chemoselective reduction of the nitrile intermediates (**34**, **35**, **40**, **41**), but disappointing results were obtained. So we moved to an alternative approach, which was initiated with the formation of the allyl ester **55** from carboxylic acid **13** with allyl bromide and diisopropylethylamine following published protocols [40]. Subsequent blue LED-mediated radical decarboxylation of allyl ester **55** to form a racemic mixture of the *N*-Boc-protected homoallylic amine **56** was accomplished with a combination of palladium and iridium-photoredox catalyst following a protocol published by Lang et al. [40]. *N*-Boc deprotection with HCl in dioxane gave primary amine **57**, and subsequent amide coupling with 4-ethynylbenzoic acid (**4**) then afforded amide **58** in 81% yield. 1,3-Dipolar cycloaddition of alkyne **58** with aldoxime **3** and CuAAC of alkyne **58** with azide **11** gave isoxazole **59** and triazole **62**, respectively. The saponification of the acetonide and benzyl ester moieties of isoxazole **59** and triazole **62** then yielded isoxazole **60** and triazole **63**. In the final step, ozonolysis was performed to oxidize the terminal vinyl groups of isoxazole **60** and triazole **63** to their corresponding racemic aldehydes **61** and **64** (Scheme 5).

2.3. Biological Evaluation

The synthesized cyclic boronate, cyanomethyl and formylmethyl derivatives of **CG_209** and **CG_220** were tested for their inhibitory effects against sirtuin 5 using a fluorescence-based assay utilizing a 7-amino-4-methyl coumarin-based succinylated lysine as its substrate. The IC_{50} values of these compounds were calculated as a mean of

three measurements (Table 2). The determined IC_{50} values of the literature-known lead structures **CG_209** and **CG_220** in this assay were in accordance with their published values of 12 μM and 7 μM, respectively [21,22]. In general, all the functionalized inhibitors showed micromolar inhibitory effects against sirtuin 5 but showed a loss in the potency compared to their lead structures. Among the three functional group modifications that were employed, cyanomethyl analogues showed the highest potency, followed by formyl and then boronate derivatives. Significant loss in the potency of the boronates **51–54** could be observed compared to their lead structures **CG_209** and **CG_220**.

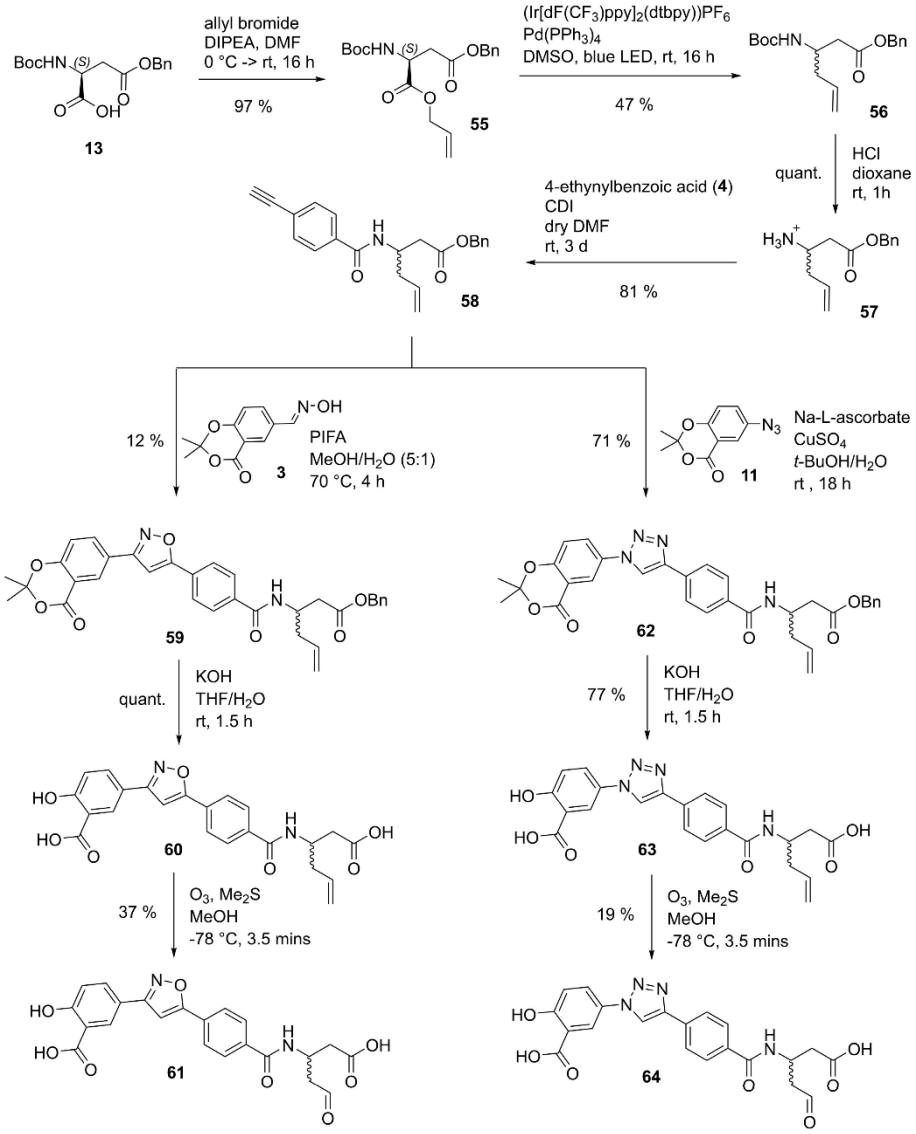

Scheme 5. Syntheses of aldehydes **61** and **64**.

Table 2. Inhibition of sirtuin 5 by **CG_209** and **CG_220** and the functionalized derivatives thereof. The IC_{50} values were calculated as a mean of three independent measurements with standard deviations shown. * = chiral center.

For Boronates **51-54**: 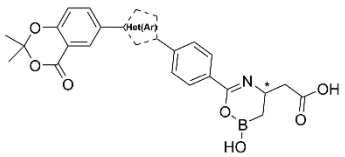

For Other Derivatives: 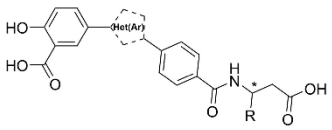

Compound ID	Configuration	Het(Ar)	R	IC_{50} (hSirt5) [µM] ± SD
CG_209	-		H	11 ± 1
CG_220	-		H	9 ± 2
47	*R*		CH_2CN	97 ± 22
48	*S*		CH_2CN	65 ± 15
49	*R*		CH_2CN	35 ± 6
50	*S*		CH_2CN	27 ± 9
51	*R*		-	203 ± 50
52	*S*		-	139 ± 18
53	*R*		-	137 ± 63
54	*S*		-	61 ± 9
61	*rac*		CH_2CHO	82 ± 3
64	*rac*		CH_2CHO	60 ± 15

We previously investigated the tolerance of several modifications in the salicylic acid moiety and found that a free salicylate is beneficial, but not mandatory, for affinity for Sirt5 [22]. So, although the acetonide protecting group may contribute to the loss in potency observed for **51**–**54** here, we believe that this observation is likely due to the introduction of the cyclic boronate moieties. The additional rigidization associated with the cyclic boronate may restrict the flexibility of the inhibitor that is required for optimal fitting in the active site of sirtuin 5. In contrast, functionalization with cyanomethyl groups was better

tolerated with cyanomethyl derivative **50** representing the most potent functionalized inhibitor in this library screening. With an IC_{50} of 27 μM, the potency of compound **50** thus lies in a similar range of other established sirtuin 5 inhibitors published in the literature. Additionally, a general trend of higher potency for the triazole derivatives (**49**, **50**, **53**, **54** and **64**) could be interpreted when they were compared with the isoxazole derivatives (**47**, **48**, **51**, **52** and **61**) of the corresponding functionalization. For example, the *S*-enantiomer of triazole boronate **54** displayed an IC_{50} of 61 μM, a doubling in the potency compared to its corresponding isoxazole derivative **52**. Furthermore, a stereoselective preference of these functional group modifications could be observed. In all cases, the *S*-enantiomers showed higher potency than the corresponding *R*-enantiomers. The *S*-enantiomer of the cyanomethyl isoxazole **48**, for instance, displayed an IC_{50} of 65 μM, whereas the corresponding *R*-enantiomer **47** had an IC_{50} of 97 μM. Based on these results, we concluded that modifications incorporating moieties such as boronic acids, cyanomethyl and formylmethyl groups were tolerated to a certain extent and retained micromolar inhibitory in vitro activities against sirtuin 5. Although these functionalized derivatives did not yield the anticipated enhancement in potency and thus reversible covalent inhibition of the functionalized inhibitors is not evident as their inhibitory activities would otherwise be significantly improved via reversible covalent binding with the co-factor NAD^+, our findings offer valuable insights into the SAR of balsalazide analogues as sirtuin 5 inhibitors. Importantly, these results highlight the triazole-based scaffold with potentially further modifications in the *S*-configuration as a promising platform for further structural elaborations. Future optimization efforts focusing on diverse functional group modifications that are not limited to reversible covalent inhibition may lead to the development of more potent sirtuin 5 inhibitors. Although the exact binding mechanism of these functionalized sirtuin 5 inhibitors could not yet be shown in this study due to significant challenges in obtaining stable co-crystals with these inhibitors, ongoing efforts are actively being made to elucidate its structural biology. Notably, the majority of the obtained sirtuin 5 co-crystals are in complex with macromolecules or peptide-based larger molecules [41,42], highlighting the challenges in obtaining sirtuin 5 co-crystals with low-molecular inhibitors.

3. Materials and Methods

3.1. Chemical Synthesis

All solvents and reagents were purchased from commercial sources and used without further purification. Standard vacuum line techniques were applied. Reactions were monitored via thin-layer silica gel chromatography (TLC) using polyester sheets POLYGRAM SIL G/UV254 coated with 0.2 mm silica gel (Macherey-Nagel, Düren, Germany). Plates were visualized using UV light (254 nm or 365 nm) or staining with $KMnO_4$, curcumin, CAM (ceric ammonium molybdate) or DNPH (dinitrophenylhydrazine). Products were purified by flash column chromatography (normal-phase silica gel chromatography or boric acid-impregnated normal-phase silica gel chromatography) using SiO_2 60 (0.040–0.063 mm, 230–400 mesh ASTM) from Merck (Darmstadt, Germany). NMR spectra were recorded with Avance III HD 400 MHz Bruker BioSpin and Avance III HD 500 MHz Bruker BioSpin (^{1}H-NMR: 400 MHz and 500 MHz, ^{13}C-NMR: 101 MHz and 126 MHz) (Bruker, Billerica, MA, USA) using the deuterated solvent stated. Chemical shifts (δ) are quoted in parts per million (ppm) and referenced to the residual solvent peak. Multiplicities are denoted as follows: s—singlet, d—doublet, t—triplet, q—quartet and quin—quintet. Coupling constants *J* are given in Hz and rounded to the nearest 0.1 Hz. Infrared spectra were recorded from 4000 to 650 cm^{-1} on a Perkin Elmer Spectrum BX-59343 FT-IR instrument (Perkin Elmer, Shelton, CT, USA). A Smiths Detection DuraSamp IR II Diamond ATR sensor (Smiths

Detection, Danbury, CT, USA) was used for detection. The absorption bands are reported in wavenumbers [cm^{-1}]. High-resolution mass spectra (HR-MS) were recorded using a Jeol Mstation 700 or JMS GCmate II Jeol instrument (Jeol, Tokyo, Japan) for electron impact ionization (EI). Thermo Finnigan LTQ (Thermo Finnigan, Somerset, NJ, USA) was used for electrospray ionization (ESI). Melting points were measured with a Büchi Schmelzpunktapparatur B-540 (Büchi, Flawil, Switzerland). HPLC analytical measurements at 210 nm and 254 nm for purities determination was performed with a Zorbax Eclipse Plus C18 column (Waters, Milford, MA, USA) with a diameter of 4.6 mm and a length of 150 mm and a particle size of 3.5 µm.

General Procedure A—*N*-Boc deprotection with HCl [33]**.** The appropriate *N*-Boc-protected amine (1.0 equivalent) was dissolved in 4.0 M HCl dioxane solution (3.2 equivalents) under N_2 atmosphere and stirred at room temperature for 1 h. The solvent was removed in vacuo and then co-evaporated with diethyl ether (4×). The obtained amine hydrochlorides could be used for the subsequent steps without further purification.

General Procedure B—Amide coupling with CDI. To a stirred solution of the appropriate carboxylic acid (1.0 equivalent) in DMF with a concentration of 0.20 M, CDI (1.1 equivalents) was added. The reaction mixture was stirred at room temperature for 15 min. Afterwards, the appropriate amine (1.0 equivalent) was added, and unless stated otherwise, the solution was stirred at room temperature for 3 d. The solution was diluted with EtOAc, and the organic phase was washed with brine (3×). The organic phase was dried using a phase separation paper, and the solvent was removed in vacuo. If necessary, the crude product was purified by FCC using the indicated eluent.

General Procedure C—PIFA-mediated isoxazole formation [43]**.** To a stirred solution of the appropriate alkyne (1.0 equivalent) in MeOH/H_2O (5:1 v/v) with a concentration of 0.10 M, the appropriate oxime (1.5 equivalents) was added. Then, 0.5 equivalents of PIFA were added every 2 h. After the addition of 1.5 equivalents PIFA, the reaction mixture was stirred at room temperature for another 16 h. The solvents were removed in vacuo, and the crude product was resuspended in EtOAc. Water was added, the resulting two phases were separated, and the aqueous phase was extracted with EtOAc (3×). The combined organic phases were dried using a phase separation paper and the solvent was removed in vacuo. The crude product was purified by FCC using the indicated eluent.

General Procedure D—Copper-catalyzed azide-alkyne cycloaddition. To a stirred solution of the appropriate azide (1.0 equivalent) in *t*-BuOH/DMSO (21:1 v/v) with a concentration of 0.13 M, we added a solution of the appropriate alkyne (1.2 equivalents) in *t*-BuOH with a concentration of 0.33 M. A 0.027 M aq. $CuSO_4$ solution (0.2 equivalents) and a 0.13 M aq. sodium ascorbate solution (1.0 equivalent) were added, and the reaction mixture was stirred at room temperature for 18 h. The reaction mixture was diluted with EtOAc, and the organic phase was washed sequentially with 1 M HCl (1×), aq. sat. $NaHCO_3$ (1×) and brine (1×). The organic phase was dried using a phase separation paper, and the solvent was removed in vacuo. The crude product was purified by the indicated method.

General Procedure E—Alkaline deprotection of acetonides and esters. To a stirred solution of the appropriate protected starting material (1.0 equivalent) in THF with a concentration of 0.15 M, an aq. KOH solution was added with the stated concentration and equivalents. The reaction mixture was stirred at the stated temperature for the stated time and then acidified to pH 1 with 2 M HCl. EtOAc was added to the suspension, the resulting two phases were separated, and the aqueous phase was extracted with EtOAc (3×). The combined organic phases were dried using a phase separation paper, and the solvent was removed in vacuo. The crude product was purified by the indicated method.

Ethyl 3-(4-ethynylbenzamido)propanoate (6). Prepared according to **General Procedure B** from ß-alanine ethyl ester hydrochloride (1.00 g, 6.51 mmol) and 4-ethynylbenzoic acid (1.00 g, 6.51 mmol). The reaction mixture was stirred at room temperature for 2.5 h. The amide **6** (1.20 g, 4.89 mmol, 75%) was obtained as a brownish-yellow solid. Analytical data are in alignment with literature [22].

Benzyl (*R*)-3-((*tert*-butoxycarbonyl)amino)-4-(4,4,5,5-tetramethyl-1,3,2-dioxaborolan-2-yl)butanoate (20). $Pd_2(dba)_3$ (31.9 mg, 0.0348 mmol), di-*tert*-butyl(methyl)phosphonium tetrafluoroborate (51.8 mg, 0.209 mmol), bis(pinacolato)diboron (2.12 g, 8.35 mmol), K_2CO_3 (1.92 g, 13.9 mmol) and alkyl bromide **18** (2.59 g, 6.96 mmol) were added to a 100 mL round-bottomed flask and evacuated and backfilled three times with N_2. 19 mL of a degassed *t*-BuOH/H_2O (12:1 *v*/*v*) solution were added. The reaction mixture was stirred at 65 °C for 6 h, then diluted with EtOAc (200 mL). The organic phase was washed with brine (2 × 200 mL), dried using a phase separation paper, concentrated in vacuo and purified by FCC with boric acid-impregnated silica gel (hexanes/EtOAc 89:11) to give boronic acid pinacol ester **20** (1.75 g, 4.17 mmol, 60%) as a yellow oil. ^{1}H-NMR (400 MHz, ($CDCl_3$): δ (ppm) = 7.37–7.29 (m, 5H, 2′-H, 3′-H, 4′-H, 5′-H and 6′-H), 5.12–5.09 (m, 2H, 1′-CH_2), 4.24–4.16 (m, 1H, 3-H), 2.69–2.52 (m, 2H, 2-H), 1.42 (s, 9H, $C(CH_3)_3$), 1.24–1.20 (m, 12H, $(C(CH_3)_2)_2$), 1.15 (d, *J* = 6.7 Hz, 2H, 4-H). ^{13}C-NMR (101 MHz, ($CDCl_3$): δ (ppm) = 171.59 (C-1), 155.13 (NHCOO), 136.05 (C-1′), 128.67–128.32 (C-2′, C-3′, C-4′, C-5′ and C-6′), 83.59 ($(\mathbf{C}(CH_3)_2)_2$), 79.22 ($\mathbf{C}(CH_3)_3$), 66.41 (1′-CH_2), 44.96 (C-3) 41.17 (C-2), 28.56 ($C(\mathbf{C}H_3)_3$), 24.97–24.86 ($(C(\mathbf{C}H_3)_2)_2$), 17.78 (C-4). IR (ATR): $\tilde{\nu}$ (cm^{-1}) = 3348, 2977, 1709, 1514, 1366, 1168, 1140, 1019, 965, 846, 697. HR-MS (ESI): *m*/*z* = $[M + Na]^+$ calcd for $C_{22}H_{34}BNO_6Na^+$: 442.2377; found: 442.2372. Specific rotation: $[\alpha]_D^{20}$ +3 (c 0.1 in DMSO).

Benzyl (*S*)-3-((*tert*-butoxycarbonyl)amino)-4-(4,4,5,5-tetramethyl-1,3,2-dioxaborolan-2-yl)butanoate (21). $Pd_2(dba)_3$ (49.2 mg, 0.0537 mmol), di-*tert*-butyl(methyl)phosphonium tetrafluoroborate (80.0 mg, 0.322 mmol), bis(pinacolato)diboron (3.27 g, 12.9 mmol), K_2CO_3 (2.97 g, 21.5 mmol) and alkyl bromide **19** (4.00 g, 10.7 mmol) were added to a 100 mL round-bottomed flask and evacuated and backfilled three times with N_2. 32 mL of a degassed *t*-BuOH/H_2O (12:1 *v*/*v*) solution were added. The reaction mixture was stirred at 65 °C for 6 h, then diluted with EtOAc (500 mL). The organic phase was washed with brine (2 × 400 mL), dried using a phase separation paper, concentrated in vacuo and purified by FCC with boric acid-impregnated silica gel (hexanes/EtOAc 89:11) to give boronic acid pinacol ester **21** (2.30 g, 5.48 mmol, 51%) as a yellow oil. ^{1}H-NMR (400 MHz, ($CDCl_3$): δ (ppm) = 7.38–7.29 (m, 5H, 2′-H, 3′-H, 4′-H, 5′-H and 6′-H), 5.13–5.08 (m, 2H, 1′-CH_2), 4.27–4.08 (m, 1H, 3-H), 2.75–2.52 (m, 2H, 2-H), 1.45–1.40 (m, 9H, $C(CH_3)_3$), 1.25–1.20 (m, 12H, $(C(CH_3)_2)_2$)), 1.15 (d, *J* = 6.7 Hz, 2H, 4-H). ^{13}C-NMR (101 MHz, ($CDCl_3$): δ (ppm) = 171.65 (C-1), 155.13 (NHCOO), 136.04 (C-1′), 128.68–128.34 (C-2′, C-3′, C-4′, C-5′ and C-6′), 83.59 ($(\mathbf{C}(CH_3)_2)_2$), 79.16 ($\mathbf{C}(CH_3)_3$), 66.42 (1′-CH_2), 44.87 (C-3), 41.13 (C-2), 28.56 ($C(\mathbf{C}H_3)_3$), 24.96–24.86 ($(C(\mathbf{C}H_3)_2)_2$)), 17.96 (C-4). IR (ATR): $\tilde{\nu}$ (cm^{-1}) = 3371, 2977, 1711, 1498, 1366, 1164, 1140, 1019, 967, 846, 696. HR-MS (ESI): *m*/*z* = $[M + Na]^+$ calcd for $C_{22}H_{34}BNO_6Na^+$: 442.2377; found: 442.2376. Specific rotation: $[\alpha]_D^{20}$ −5 (c 0.1 in DMSO).

(*R*)-4-(Benzyloxy)-4-oxo-1-(4,4,5,5-tetramethyl-1,3,2-dioxaborolan-2-yl)butan-2-aminium chloride (24). Prepared according to **General Procedure A** from *N*-Boc-protected amine **20** (3.20 g, 7.63 mmol). The amine hydrochloride **24** (2.45 g, 7.65 mmol, quant.) was obtained as a viscous yellow oil. ^{1}H-NMR (500 MHz, $(CD_3)_2SO$): δ (ppm) = 8.04 (s, 3H, NH_3^+), 7.40–7.32 (m, 5H, 2′-H, 3′-H, 4′-H, 5′-H and 6′-H), 5.14 (d, *J* = 6.9 Hz, 2H, 1′-CH_2), 3.63–3.53 (m, 1H, 2-H), 2.79–2.67 (m, 2H, 3-H), 1.27–1.22 (m, 1H, 1-H), 1.19 (d, *J* = 2.5 Hz, 12H, $(C(CH_3)_2)_2$), 1.16–1.13 (m, 1H, 1-H). ^{13}C-NMR (126 MHz, $(CD_3)_2SO$): δ (ppm) = 169.87 (C-4), 135.74 (C-1′), 128.45–128.05 (C-2′, C-3′, C-4′, C-5′ and C-6′), 83.51 ($(\mathbf{C}(CH_3)_2)_2$), 66.06 (1′-CH_2), 44.96 (C-2), 38.12 (C-3), 24.46 ($(C(\mathbf{C}H_3)_2)_2$), 16.03 (C-1). IR (ATR): $\tilde{\nu}$ (cm^{-1}) = 3263, 1978, 2883,

2828, 2109, 1727, 1382, 1322, 1204, 1163, 1140, 967, 844, 696. HR-MS (ESI): m/z = $[M]^+$ calcd for $C_{17}H_{27}BNO_4^+$: 320.2028; found: 320.2027. Specific rotation: $[\alpha]_D^{20}$ −6 (c 0.1 in DMSO).

(*S*)-4-(Benzyloxy)-4-oxo-1-(4,4,5,5-tetramethyl-1,3,2-dioxaborolan-2-yl)butan-2-aminium chloride (25). Prepared according to **General Procedure A** from *N*-Boc-protected amine **21** (2.80 g, 6.68 mmol). The amine hydrochloride **25** (2.14 g, 6.68 mmol, quant.) was obtained as a viscous yellow oil. ^{1}H-NMR (500 MHz, $(CD_3)_2SO$): δ (ppm) = 8.04 (s, 3H, NH_3^+), 7.40–7.33 (m, 5H, 2′-H, 3′-H, 4′-H, 5′-H and 6′-H), 5.14 (d, J = 6.9 Hz, 2H, 1′-CH_2), 3.64–3.51 (m, 1H, 2-H), 2.78–2.67 (m, 2H, 3-H), 1.27–1.22 (m, 1H, 1-H), 1.19 (d, J = 2.5 Hz, 12H, $C(CH_3)_2)_2$), 1.16–1.10 (m, 1H, 1-H). ^{13}C-NMR (101 MHz, $(CD_3)_2SO$): δ (ppm) = 169.86 (C-4), 135.74 (C-1′), 128.44–128.04 (C-2′, C-3′, C-4′, C-5′ and C-6′), 83.50 (($\mathbf{C}(CH_3)_2)_2$), 66.05 (1′-CH_2), 44.96 (C-2), 38.12 (C-3), 24.46 (($C(\mathbf{C}H_3)_2)_2$), 16.02 (C-1). IR (ATR): $\tilde{\nu}$ (cm^{-1}) = 2977, 2883, 2833, 2034, 1730, 1381, 1324, 1211, 1165, 1139, 966, 845, 696. HR-MS (ESI): m/z = $[M]^+$ calcd for $C_{17}H_{27}BNO_4^+$: 320.2028; found: 320.2038. Specific rotation: $[\alpha]_D^{20}$ +7 (c 0.1 in DMSO).

(*R*)-4-(Benzyloxy)-1-cyano-4-oxobutan-2-aminium chloride (26). Prepared according to **General Procedure A** from *N*-Boc-protected amine **22** (2.50 g, 7.85 mmol). The amine hydrochloride **26** (1.72 g, 7.84 mmol, quant.) was obtained as a purple-gray solid. m.p.: 107 °C. ^{1}H-NMR (400 MHz, $(CD_3)_2SO$): δ (ppm) = 8.59 (s, 3H, NH_3^+), 7.44–7.32 (m, 5H, 2′-H, 3′-H, 4′-H, 5′-H and 6′-H), 5.15 (s, 2H, 1′-CH_2), 3.84 (p, J = 6.3 Hz, 1H, 2-H), 3.06 (dd, J = 6.0, 1.4 Hz, 2H, 1-H), 2.96–2.81 (m, 2H, 3-H). ^{13}C-NMR (126 MHz, $(CD_3)_2SO$): δ (ppm) = 168.99 (C-4), 135.58 (C-1′), 128.47–128.16 (C-2′, C-3′, C-4′, C-5′ and C-6′), 116.74 (CN), 66.36 (1′-CH_2), 43.86 (C-2), 36.09 (C-3), 20.80 (C-1). IR (ATR): $\tilde{\nu}$ (cm^{-1}) = 3033, 2923, 2854, 2641, 2500, 2252, 1716, 1541, 1454, 1401, 1217, 1188, 1157, 1117, 972, 754, 696. HR-MS (ESI): m/z = $[M]^+$ calcd for $C_{12}H_{15}N_2O_2^+$: 219.1128; found: 219.1137. Specific rotation: $[\alpha]_D^{20}$ −8 (c 0.1 in DMSO).

(*S*)-4-(Benzyloxy)-1-cyano-4-oxobutan-2-aminium chloride (27). Prepared according to **General Procedure A** from *N*-Boc-protected amine **23** (1.30 g, 4.08 mmol). The amine hydrochloride **27** (895 g, 4.08 mmol, quant.) was obtained as a beige solid. m.p.: 109 °C. ^{1}H-NMR (400 MHz, $(CD_3)_2SO$): δ (ppm) = 8.59 (s, 3H, NH_3^+), 7.43–7.33 (m, 5H, 2′-H, 3′-H, 4′-H, 5′-H and 6′-H), 5.15 (s, 2H, 1′-CH_2), 3.84 (p, J = 6.3 Hz, 1H, 2-H), 3.06 (dd, J = 6.0, 1.4 Hz, 2H, 1-H), 2.95–2.80 (m, 2H, 3-H). ^{13}C-NMR (101 MHz, $(CD_3)_2SO$): δ (ppm) = 168.98 (C-4), 135.57 (C-1′), 128.46–128.15 (C-2′, C-3′, C-4′, C-5′ and C-6′), 116.74 (CN), 66.36 (1′-CH_2), 43.86 (C-2), 36.09 (C-3), 20.80 (C-1). IR (ATR): $\tilde{\nu}$ (cm^{-1}) = 3033, 2922, 2854, 2641, 2541, 2252, 1716, 1541, 1454, 1401, 1217, 1188, 1157, 1117, 972, 754, 696. HR-MS (ESI): m/z = $[M]^+$ calcd for $C_{12}H_{15}N_2O_2^+$: 219.1128; found: 219.1124. Specific rotation: $[\alpha]_D^{20}$ +8 (c 0.1 in DMSO).

Benzyl (*R*)-3-(4-ethynylbenzamido)-4-(4,4,5,5-tetramethyl-1,3,2-dioxaborolan-2-yl) butanoate (28). Prepared according to **General Procedure B** from amine hydrochloride **24** (2.45 g, 7.68 mmol) and 4-ethynylbenzoic acid (1.18 g, 7.68 mmol). The crude product was purified by FCC with boric acid-impregnated silica gel (hexanes/EtOAc 75:25) to give amide **28** (2.73 mg, 6.10 mmol, 80%) as a yellow oil. ^{1}H-NMR (400 MHz, $(CD_3)_2SO$): δ (ppm) = 8.38 (d, J = 8.2 Hz, 1H, CONH), 7.79–7.75 (m, 2H, 2′-H and 6′-H), 7.57–7.53 (m, 2H, 3′-H and 5′-H), 7.34–7.25 (m, 5H, 2″-H, 3″-H, 4″-H, 5″-H and 6″-H), 5.06–5.04 (m, 2H, 1″-CH_2), 4.50–4.43 (m, 1H, 3-H), 4.36 (s, 1H, C≡CH), 2.69–2.55 (m, 2H, 2-H), 1.14 (s, 12H, $C(CH_3)_2)_2$), 1.10–1.05 (m, 2H, 4-H). ^{13}C-NMR (101 MHz, $(CD_3)_2SO$): δ (ppm) = 170.65 (C-1), 164.56 (CONH), 136.12 (C-1″), 134.80 (C-1′), 131.49 (C-3′ and C-5′), 128.30–127.80 (C-2″, C-3″, C-4″, C-5″ and C-6″), 127.48 (C-2′ and C-6′), 124.19 (C-4′), 82.88 (($\mathbf{C}(CH_3)_2)_2$), 82.72 ($\mathbf{C}$≡CH and C≡$\mathbf{C}$H), 65.46 (1″-CH_2), 43.97 (C-3), 41.04 (C-2), 24.48 (($C(\mathbf{C}H_3)_2)_2$), 17.81 (C-4). IR (ATR): $\tilde{\nu}$ (cm^{-1}) = 3263, 2978, 2109, 1729, 1641, 1537, 1372, 1323, 1140, 967, 848, 696. HR-MS (ESI): m/z = $[M + H]^+$ calcd for $C_{26}H_{31}BNO_5^+$: 448.2290; found: 448.2288. Specific rotation: $[\alpha]_D^{20}$ +6 (c 0.1 in DMSO).

Benzyl (*S*)-3-(4-ethynylbenzamido)-4-(4,4,5,5-tetramethyl-1,3,2-dioxaborolan-2-yl) butanoate (29). Prepared according to **General Procedure B** from amine hydrochloride **25** (2.14 g, 6.68 mmol) and 4-ethynylbenzoic acid (1.03 g, 6.68 mmol). The crude product was purified by FCC with boric acid-impregnated silica gel (hexanes/EtOAc 75:25) to give amide **29** (1.92 g, 4.29 mmol, 64%) as a yellow oil. ^{1}H-NMR (500 MHz, $(CD_3)_2SO$): δ (ppm) = 8.38 (d, *J* = 8.2 Hz, 1H, CONH), 7.78–7.75 (m, 2H, 2′-H and 6′-H), 7.57–7.53 (m, 2H, 3′-H and 5′-H), 7.33–7.26 (m, 5H, 2″-H, 3″-H, 4″-H, 5″-H and 6″-H), 5.07–5.04 (m, 2H, 1″-CH_2), 4.50–4.43 (m, 1H, 3-H), 4.36 (s, 1H, C≡CH), 2.69–2.55 (m, 2H, 2-H), 1.14 (s, 12H, $C(CH_3)_2)_2$), 1.10–1.03 (m, 2H, 4-H). ^{13}C-NMR (101 MHz, $(CD_3)_2SO$): δ (ppm) = 170.65 (C-1), 164.56 (CONH), 136.12 (C-1′), 134.80 (C-1′), 131.49 (C-3′ and C-5′), 128.30–127.80 (C-2″, C-3″, C-4″, C-5″ and C-6″), 127.48 (C-2′ and C-6′), 124.20 (C-4′), 82.88 ((**C**$(CH_3)_2)_2$, **C**≡CH and C≡**C**H), 65.46 (1″-CH_2), 43.98 (C-3), 41.04 (C-2), 24.48 ((C(**C**$H_3)_2)_2$), 17.80 (C-4). IR (ATR): $\tilde{\nu}$ (cm^{-1}) = 3284, 2978, 2107, 1731, 1639, 1535, 1372, 1323, 1139, 966, 846, 696. HR-MS (ESI): *m*/*z* = $[M + H]^+$ calcd for $C_{26}H_{31}BNO_5^+$: 448.2290; found: 448.2295. Specific rotation: $[\alpha]_D^{20}$ −5 (c 0.1 in DMSO).

Benzyl (*R*)-4-cyano-3-(4-ethynylbenzamido)butanoate (30). Prepared according to **General Procedure B** from amine hydrochloride **26** (1.72 g, 7.84 mmol) and 4-ethynylbenzoic acid (1.21 g, 7.84 mmol). The crude product was purified by FCC (hexanes/EtOAc 80:20) to give amide **30** (1.58 g, 4.56 mmol, 58%) as a white solid. ^{1}H-NMR (500 MHz, $CDCl_3$): δ (ppm) = 7.66 (m, 2H, 2′-H and 6′-H), 7.53 (m, 2H, 3′-H and 5′-H), 7.36 (m, 5H, 2″-H, 3″-H, 4″-H, 5″-H and 6″-H), 7.00 (CONH), 5.18 (s, 2H, 1″-CH_2), 4.71 (m, 1H, 3-H), 3.22 (s, 1H, C≡CH), 2.90 (m, 4H, 2-H and 4-H). ^{13}C-NMR (126 MHz, $CDCl_3$): δ (ppm) = 170.69 (C-1), 166.31 (CONH), 135.06 (C-1″), 133.32 (C-1′), 132.54 (C-3′ and C-5′), 128.91–128.65 (C-2″, C-3″, C-4″, C-5″ and C-6″), 127.14 (C-2′ and C-6′), 126.16 (C-4′), 116.88 (CN), 82.73 (**C**≡CH), 80.05 (C≡**C**H), 67.51 (1″-CH_2), 43.67 (C-3), 36.92 (C-2), 22.68 (C-4). IR (ATR): $\tilde{\nu}$ (cm^{-1}) = 3366, 3337, 3295, 3263, 2938, 2248, 1731, 1717, 1650, 1607, 1585, 1525, 1426, 1385, 1290, 1272, 1165, 1084, 1001, 967, 900, 853, 766, 751, 699. HR-MS (ESI): *m*/*z* = $[M + Na]^+$ calcd for $C_{21}H_{18}O_3N_2Na^+$: 369.1215; found: 369.1208. Specific rotation: $[\alpha]_D^{20}$ −9 (c 0.1 in $CHCl_3$).

Benzyl (*S*)-4-cyano-3-(4-ethynylbenzamido)butanoate (31). Prepared according to **General Procedure B** from amine hydrochloride **27** (895 mg, 4.08 mmol) and 4-ethynylbenzoic acid (628 mg, 4.08 mmol). The crude product was purified by FCC (hexanes/EtOAc 70:30) to give amide **31** (998 mg, 2.88 mmol, 71%) as a beige solid. m.p.: 103 °C. ^{1}H-NMR (500 MHz, $CDCl_3$): δ (ppm) = 7.66 (m, 2H, 2′-H and 6′-H), 7.53 (m, 2H, 3′-H and 5′-H), 7.36 (m, 5H, 2″-H, 3″-H, 4″-H, 5″-H and 6″-H), 7.00 (CONH), 5.18 (s, 2H, 1″-CH_2), 4.71 (m, 1H, 3-H), 3.22 (s, 1H, C≡CH), 2.90 (m, 4H, 2-H and 4-H). ^{13}C-NMR (126 MHz, $CDCl_3$): δ (ppm) = 170.69 (C-1), 166.33 (CONH), 135.07 (C-1″), 133.32 (C-1′), 132.54 (C-3′ and C-5′), 128.91–128.64 (C-2″, C-3″, C-4″, C-5″ and C-6″), 127.15 (C-2′ and C-6′), 126.16 (C-4′), 116.89 (CN), 82.73 (**C**≡CH), 80.05 (C≡**C**H), 67.51 (1″-CH_2), 43.68 (C-3), 36.93 (C-2), 22.68 (C-4). IR (ATR): $\tilde{\nu}$ (cm^{-1}) = 3366, 3294, 3263, 2962, 2938, 2248, 1729, 1717, 1649, 1607, 1525, 1495, 1454, 1384, 1322, 1273, 1166, 1082, 1012, 967, 900, 853, 766, 750, 730, 699. HR-MS (ESI): *m*/*z* = $[M + Na]^+$ calcd for $C_{21}H_{18}O_3N_2Na^+$: 369.1215; found: 369.1210. Specific rotation: $[\alpha]_D^{20}$ +10 (c 0.1 in $CHCl_3$).

Methyl (*R*)-3-(4-(3-(2,2-dimethyl-4-oxo-4*H*-benzo[*d*][1,3]dioxin-6-yl)isoxazol-5-yl) benzamido)-4-(4,4,5,5-tetramethyl-1,3,2-dioxaborolan-2-yl)butanoate (32). Prepared according to **General Procedure C** from alkyne **28** (350 mg, 0.782 mmol) and aldoxime **3** (260 mg, 1.17 mmol). The crude product was purified by FCC with boric acid-impregnated silica gel (hexanes/EtOAc 60:40) to give isoxazole **32** (141 mg, 0.239 mmol, 31%) as a pale yellow oil. ^{1}H-NMR (500 MHz, $(CD_3)_2SO$): δ (ppm) = 8.44 (d, *J* = 8.2 Hz, 1H, CONH), 8.39 (d, *J* = 2.2 Hz, 1H, 5‴-H), 8.24 (dd, *J* = 8.6, 2.2 Hz, 1H, 7‴-H), 8.04–8.00 (m, 2H,

3′-H and 5′-H), 7.99–7.95 (m, 2H, 2′-H and 6′-H), 7.87 (s, 1H, 4″-H), 7.34 (d, *J* = 8.6 Hz, 1H, 8‴-H), 4.50–4.41 (m, 1H, 3-H), 3.57 (s, 3H, OCH_3), 2.66–2.54 (m, 2H, 2-H), 1.75 (s, 6H, 2‴-$(CH_3)_2$), 1.16–1.15 (m, 12H, $(C(CH_3)_2)_2$), 1.13–1.08 (m, 2H, 4-H). ^{13}C-NMR (126 MHz, $(CD_3)_2SO$): δ (ppm) = 171.22 (C-1), 169.26 (C-5″), 164.50 (CONH), 161.38 (C-3″), 159.75 (C-4‴), 156.78 (C-8a‴), 136.25 (C-1′), 134.79 (C-7‴), 128.74 (C-4′), 128.18 (C-2′ and C-6′), 127.33 (C-5‴), 125.41 (C-3′ and C-5′), 123.34 (C-6‴), 118.54 (C-8‴), 113.56 (C-4a‴), 107.01 (C-2‴), 99.67 (C-4″), 82.90 (**C**$(CH_3)_2)_2$), 51.32 (OCH_3), 43.96 (C-3), 40.95 (C-2), 25.32 (2‴-$(CH_3)_2$), 24.95–24.48 (C(**C**$H_3)_2)_2$), 17.76 (C-4). IR (ATR): $\tilde{\nu}$ (cm^{-1}) = 3324, 2979, 1732, 1626, 1498, 1378, 1286, 1200, 1141, 1046, 846, 826, 673. HR-MS (ESI): m/z = $[M + H]^+$ calcd for $C_{31}H_{36}BN_2O_9^+$: 591.2514; found: 591.2500. Specific rotation: $[\alpha]_D^{20}$ +3 (c 0.1 in DMSO).

Methyl (*S*)-3-(4-(3-(2,2-dimethyl-4-oxo-4*H*-benzo[*d*][1,3]dioxin-6-yl)isoxazol-5-yl) benzamido)-4-(4,4,5,5-tetramethyl-1,3,2-dioxaborolan-2-yl)butanoate (33). Prepared according to **General Procedure C** from alkyne **29** (650 mg, 1.45 mmol) and aldoxime **3** (482 mg, 2.18 mmol). The crude product was purified by FCC with boric acid-impregnated silica gel (hexanes/EtOAc 60:40) to give isoxazole **33** (187 mg, 0.316 mmol, 22%) as a pale yellow oil. ^{1}H-NMR (400 MHz, $(CD_3)_2SO$): δ (ppm) = 8.44 (d, *J* = 8.2 Hz, 1H, CONH), 8.39 (d, *J* = 2.2 Hz, 1H, 5‴-H), 8.24 (dd, *J* = 8.6, 2.2 Hz, 1H, 7‴-H), 8.04–8.00 (m, 2H, 3′-H and 5′-H), 7.98–7.95 (m, 2H, 2′-H and 6′-H), 7.87 (s, 1H, 4″-H), 7.34 (d, *J* = 8.6 Hz, 1H, 8‴-H), 4.50–4.41 (m, 1H, 3-H), 3.57 (s, 3H, OCH_3), 2.65–2.54 (m, 2H, 2-H), 1.75 (s, 6H, 2‴-$(CH_3)_2$), 1.16–1.15 (m, 12H, $(C(CH_3)_2)_2$), 1.13–1.09 (m, 2H, 4-H). ^{13}C-NMR (126 MHz, $(CD_3)_2SO$): δ (ppm) = 171.22 (C-1), 169.26 (C-5″), 164.51 (CONH), 161.38 (C-3″), 159.75 (C-4‴), 156.78 (C-8a‴), 136.26 (C-1′), 134.79 (C-7‴), 128.74 (C-4′), 128.18 (C-2′ and C-6′), 127.34 (C-5‴), 125.41 (C-3′ and C-5′), 123.33 (C-6‴), 118.54 (C-8‴), 113.56 (C-4a‴), 107.01 (C-2‴), 99.68 (C-4″), 82.90 (**C**$(CH_3)_2)_2$), 51.33 (OCH_3), 43.96 (C-3), 40.95 (C-2), 25.32 (2‴-$(CH_3)_2$), 24.95–24.48 (C(**C**$H_3)_2)_2$), 17.73 (C-4). IR (ATR): $\tilde{\nu}$ (cm^{-1}) = 3388, 2980, 1735, 1624, 1498, 1379, 1288, 1200, 1139, 1052, 847, 828, 673. HR-MS (ESI): m/z = $[M + H]^+$ calcd for $C_{31}H_{36}BN_2O_9^+$: 591.2514; found: 591.2510. Specific rotation: $[\alpha]_D^{20}$ −3 (c 0.1 in DMSO).

Benzyl (*R*)-4-cyano-3-(4-(3-(2,2-dimethyl-4-oxo-4*H*-benzo[*d*][1,3]dioxin-6-yl)isoxazol-5-yl)benzamido)butanoate (34). Prepared according to **General Procedure C** from alkyne **30** (50.0 mg, 0.144 mmol) and aldoxime **3** (47.9 mg, 0.217 mmol). The crude product was purified by FCC (hexanes/EtOAc 60:40) to give isoxazole **34** (11.5 mg, 0.0203 mmol, 14%) as a white solid. m.p.: 161 °C. ^{1}H-NMR (400 MHz, $(CD_3)_2SO$): δ (ppm) = 8.88 (d, *J* = 7.9 Hz, 1H, CONH), 8.40 (d, *J* = 2.3 Hz, 1H, 5″-H), 8.25 (dd, *J* = 8.6, 2.3 Hz, 1H, 7‴-H), 8.02 (m, 4H, 2′-H, 3′-H, 5′-H and 6′-H), 7.90 (s, 1H, 4″-H), 7.35 (d, *J* = 3.7 Hz, 1H, 8‴-H), 7.32 (m, 5H, 2⁗-H, 3⁗-H, 4⁗-H, 5⁗-H and 6⁗-H), 5.11 (s, 2H,1⁗-CH_2), 4.63 (d, *J* = 6.9 Hz, 1H, 3-H), 2.93 (d, *J* = 11.9 Hz, 2H, 4-H), 2.83 (d, *J* = 9.5 Hz, 2H, 2-H), 1.75 (s, 6H, $C(CH_3)_2$). ^{13}C-NMR (126 MHz, $(CD_3)_2SO$): δ (ppm) = 169.84 (C-1), 169.15 (C-5″), 165.29 (CONH), 161.43 (C-3″), 159.76 (C-4‴), 156.79 (C-8a‴), 135.92 (C-1⁗), 135.30 (C-1′), 134.81 (C-7‴), 129.17 (C-4′), 128.35 (C-2′ and C-6′), 128.00 -127.88, (C-2⁗, C-3⁗, C-4⁗, C-5⁗ and C-6⁗), 127.36 (C-5‴), 125.54 (C-3′ and C-5′), 123.31 (C-4a‴), 118.55 (C-8‴), 118.28 (CN), 107.02 (C-2‴), 99.89 (C-4″), 65.82 (1⁗-CH_2), 43.67 (C-3), 37.71 (C-2), 25.32 (C(**C**$H_3)_2$), 22.43 (C-4). IR (ATR): $\tilde{\nu}$ (cm^{-1}) = 3354, 1735, 1642, 1620, 1598, 1534, 1500, 1417, 1389, 1312, 1291, 1194, 1144, 1059, 981, 925, 855, 816, 774, 745, 697, 672. HR-MS (ESI): m/z = $[M - H]^-$ calcd for $C_{32}H_{26}O_7N_3^-$: 564.1771; found: 564.1770. Specific rotation: $[\alpha]_D^{20}$ −25 (c 0.1 in $CHCl_3$).

Benzyl (*S*)-4-cyano-3-(4-(3-(2,2-dimethyl-4-oxo-4*H*-benzo[*d*][1,3]dioxin-6-yl)isoxazol -5-yl)benzamido)butanoate (35). Prepared according to **General Procedure C** from alkyne **31** (620 mg, 1.79 mmol) and aldoxime **3** (594 mg, 2.68 mmol). The crude product was purified by FCC (hexanes/EtOAc 60:40) to give isoxazole **35** (239 mg, 0.423 mmol, 24%) as a white solid. m.p.: 162 °C. ^{1}H-NMR (400 MHz, $(CD_3)_2SO$): δ (ppm) = 8.88 (d, *J* = 7.9 Hz, 1H, CONH), 8.40 (d, *J* = 2.3 Hz, 1H, 5″-H), 8.25 (dd, *J* = 8.6, 2.3 Hz, 1H, 7‴-H), 8.02 (m,

4H, 2′-H, 3′-H, 5′-H and 6′-H), 7.90 (s, 1H, 4″-H), 7.35 (d, *J* = 3.7 Hz, 1H, 8‴-H), 7.32 (m, 5H, 2⁗-H, 3⁗-H, 4⁗-H, 5⁗-H and 6⁗-H), 5.11 (s, 2H, 1⁗-CH_2), 4.63 (d, *J* = 6.9 Hz, 1H, 3-H), 2.93 (d, *J* = 11.9 Hz, 2H, 4-H), 2.83 (d, *J* = 9.5 Hz, 2H, 2-H), 1.75 (s, 6H, C(CH_3)$_2$). ^{13}C-NMR (126 MHz, $(CD_3)_2SO$): δ (ppm) = 169.84 (C-1), 169.15 (C-5″), 165.29 (CONH), 161.43 (C-3″), 159.75 (C-4‴), 156.79 (C-8a‴), 135.92 (C-1⁗), 135.30 (C-1′), 134.81 (C-7‴), 129.17 (C-4′), 128.35 (C-2′ and C-6′), 128.00 -127.88 (C-2⁗, C-3⁗, C-4⁗, C-5⁗ and C-6⁗), 127.36 (C-5‴), 125.54 (C-3′ and C-5′), 123.31 (C-4a‴), 118.54 (C-8‴), 118.28 (CN), 107.01 (C-2‴), 99.88 (C-4″), 65.82 (C-7⁗), 43.67 (C-3), 37.71 (C-2), 25.32 (C(**C**H_3)$_2$), 22.43 (C-4). IR (ATR): $\tilde{\nu}$ (cm^{-1}) = 3354, 1732, 1642, 1620, 1598, 1533, 1499, 1441, 1389, 1312, 1290, 1193, 1144, 1059, 962, 924, 855, 816, 774, 745, 697, 672. HR-MS (ESI): m/z = $[M + Na]^+$ calcd for $C_{32}H_{27}O_7N_3Na^+$: 588.1747; found: 588.1737. Specific rotation: $[\alpha]_D^{20}$ +13 (c 0.1 in $CHCl_3$).

(*R*)-(2-(4-(3-(2,2-Dimethyl-4-oxo-4*H*-benzo[*d*][1,3]dioxin-6-yl)isoxazol-5-yl)benzamido)-4-methoxy-4-oxobutyl)boronic acid (36). To a stirred solution of boronic acid pinacol ester **32** (50 mg, 0.0847 mmol) in 3.5 mL THF/water (4:1 *v*/*v*), sodium periodate (90.6 mg, 0.423 mmol) was added, and the reaction mixture was stirred vigorously for 45 min at room temperature. 1M HCl (0.102 mmol, 0.102 mL) was then added to the resulting suspension, and the mixture stirred for another 16 h. The suspension was diluted with EtOAc (50 mL) and water (50 mL), the phases were separated, and the aqueous phase was extracted with EtOAc (2 × 50 mL). The combined organic phases were dried with Na_2SO_4, concentrated in vacuo and purified by FCC with boric acid-impregnated silica gel (DCM/MeOH 97:3 -> 95:5) to give boronic acid **36** (31.2 mg, 0.0614 mmol, 73%) as a white solid. m.p.: 152 °C. ^{1}H-NMR (500 MHz, $(CD_3)_2SO$): δ (ppm) = 8.39 (d, *J* = 2.2 Hz, 1H, 5‴-H), 8.37 (d, *J* = 8.1 Hz, 1H, CONH), 8.25 (dd, *J* = 8.6, 2.2 Hz, 1H, 7‴-H), 8.03–8.00 (m, 2H, 3′-H and 5′-H), 7.98–7.96 (m, 2H, 2′-H and 6′-H), 7.87 (s, 1H, 4″-H), 7.66 (s, 2H, $B(OH)_2$), 7.34 (d, *J* = 8.6 Hz, 1H, 8‴-H), 4.50–4.43 (m, 1H, 2-H), 3.56 (s, 3H, OCH_3), 2.62–2.55 (m, 2H, 3-H), 1.75 (s, 6H, 2‴-(CH_3)$_2$), 1.07–1.01 (m, 2H, 1-H). ^{13}C-NMR (126 MHz, $(CD_3)_2SO$): 171.47 (C-4), 169.28 (C-5″), 164.65 (CONH), 161.40 (C-3″), 159.76 (C-4‴), 156.78 (C-8a‴), 136.32 (C-1′), 134.81 (C-7⁗), 128.73 (C-4′), 128.20 (C-2′ and C-6′), 127.34 (C-5⁗), 125.43 (C-3′ and C-5′), 123.34 (C-6‴), 118.54 (C-8‴), 113.56 (C-4a‴), 107.01 (C-2‴), 99.68 (C-4″), 51.21 (OCH_3), 44.57 (C-2), 40.81 (C-3), 25.32 (2‴-(CH_3)$_2$), 22.16 (C-1). IR (ATR): $\tilde{\nu}$ (cm^{-1}) = 3323, 2952, 1731, 1623, 1498, 1286, 1200, 927, 764. HR-MS (ESI): m/z = $[M - H]^-$ calcd for $C_{25}H_{24}BN_2O_9^-$: 507.1575; found: 507.1579. Specific rotation: $[\alpha]_D^{20}$ −11 (c 0.1 in DMSO).

(*S*)-(2-(4-(3-(2,2-Dimethyl-4-oxo-4*H*-benzo[*d*][1,3]dioxin-6-yl)isoxazol-5-yl)benzamido)-4-methoxy-4-oxobutyl)boronic acid (37). To a stirred solution of boronic acid pinacol ester **33** (170 mg, 0.288 mmol) in 12 mL THF/water (4:1 *v*/*v*), sodium periodate (308 mg, 1.44 mmol) was added, and the reaction mixture was stirred vigorously for 45 min at room temperature. 1M HCl (0.346 mmol, 0.346 mL) was then added to the resulting suspension, and the mixture stirred for another 16 h. The suspension was diluted with EtOAc (100 mL) and water (100 mL), the phases were separated, and the aqueous phase was extracted with EtOAc (2 × 100 mL). The combined organic phases were dried with Na_2SO_4, concentrated in vacuo and purified by FCC with boric acid-impregnated silica gel (DCM/MeOH 97:3 -> 95:5) to give boronic acid **37** (93.1 mg, 0.183 mmol, 64%) as a white solid. m.p.: 157 °C. ^{1}H-NMR (500 MHz, $(CD_3)_2SO$): δ (ppm) = 8.39 (d, *J* = 2.2 Hz, 1H, 5‴-H), 8.37 (d, *J* = 8.2 Hz, 1H), 8.25 (dd, *J* = 8.6, 2.2 Hz, 1H, 7‴-H), 8.03–8.00 (m, 2H, 3′-H and 5′-H), 7.99–7.96 (m, 2H, 2′-H and 6′-H), 7.87 (s, 1H, 4″-H), 7.66 (s, 2H, $B(OH)_2$), 7.34 (d, *J* = 8.6 Hz, 1H, 8‴-H), 4.51–4.41 (m, 1H, 2-H), 3.56 (s, 3H, OCH_3), 2.64–2.55 (m, 2H, 3-H), 1.75 (s, 6H, 2‴-(CH_3)$_2$), 1.08–0.99 (m, 2H, 1-H). ^{13}C-NMR (126 MHz, $(CD_3)_2SO$): δ (ppm) = 171.47 (C-4), 169.28 (C-5″), 164.65 (CONH), 161.40 (C-3″), 159.76 (C-4‴), 156.78 (C-8a‴), 136.32 (C-1′), 134.81 (C-7⁗), 128.73 (C-4′), 128.20 (C-2′ and C-6′), 127.34 (C-5‴), 125.43 (C-3′ and C-5′), 123.34 (C-6‴), 118.54 (C-8‴), 113.56 (C-4a‴), 107.01 (C-2‴), 99.68 (C-4″), 51.22 (OCH_3), 44.56 (C-2), 40.82 (C-3), 25.32

(2‴-(CH_3)$_2$), 22.09 (C-1). IR (ATR): $\tilde{\nu}$ (cm^{-1}) = 3364, 2997, 1730, 1622, 1498, 1287, 1200, 927, 764. HR-MS (ESI): m/z = $[M - H]^-$ calcd for $C_{25}H_{24}BN_2O_9^-$: 507.1575; found: 507.1568. Specific rotation: $[\alpha]_D^{20}$ +10 (c 0.1 in DMSO).

Benzyl (*R*)-3-(4-(1-(2,2-dimethyl-4-oxo-4*H*-benzo[*d*][1,3]dioxin-6-yl)-1*H*-1,2,3-triazol-4-yl)benzamido)-4-(4,4,5,5-tetramethyl-1,3,2-dioxaborolan-2-yl)butanoate (38). Prepared according to **General Procedure D** from azide **11** (300 mg, 1.37 mmol) and alkyne **28** (735 mg, 1.64 mmol). The crude product was purified by FCC with boric acid-impregnated silica gel (hexanes/EtOAc 50:50) to give triazole **38** (153 mg, 0.230 mmol, 17%) as a pale yellow solid. m.p.: 140 °C. ^{1}H-NMR (500 MHz, $(CD_3)_2SO$): δ (ppm) = 9.54 (s, 1H, 5″-H), 8.42 (d, *J* = 2.7 Hz, 1H, 5‴-H), 8.37 (d, *J* = 8.2 Hz, 1H, CONH), 8.32 (dd, *J* = 8.9, 2.7 Hz, 1H, 7‴-H), 8.05–8.00 (m, 2H, 3′-H and 5′-H), 7.95–7.89 (m, 2H, 2′-H and 6′-H), 7.44 (d, *J* = 8.9 Hz, 1H, 8‴-H), 7.37–7.27 (m, 5H, 2⁗-H, 3⁗-H, 4⁗-H, 5⁗-H and 6⁗-H), 5.09–5.07 (m, 2H, 1⁗-CH_2), 4.55–4.48 (m, 1H, 3-H), 2.73–2.67 (m, 1H, 2-H), 2.65–2.58 (m, 1H, 2-H), 1.78 (s, 6H, 2‴-(CH_3)$_2$), 1.17 (s, 12H, (C(CH_3)$_2$)$_2$), 1.16–1.06 (m, 2H, 4-H). ^{13}C-NMR (126 MHz, $(CD_3)_2SO$): δ (ppm) = 170.71 (C-1), 164.88 (CONH), 159.48 (C-4‴), 155.21 (C-8a‴), 146.69 (C-4″), 136.16 (C-1⁗), 134.27 (C-1′), 132.54 (C-4′), 131.70 (C-6‴), 128.66 (C-7‴), 128.31 (C-2⁗, C-3⁗, C-4⁗, C-5⁗ and C-6⁗), 128.03 (C-2′ and C-6′), 127.90–127.81 (C-2⁗, C-3⁗, C-4⁗, C-5⁗ and C-6⁗), 124.90 (C-3′ and C-5′), 120.66 (C-5″), 120.18 (C-5‴), 119.26 (C-8‴), 113.77 (C-4a‴), 107.23 (C-2‴), 82.90 ((**C**(CH_3)$_2$)$_2$), 65.47 (1⁗-CH_2), 43.97 (C-3), 41.10 (C-2), 25.27 (2‴-(CH_3)$_2$), 24.66–24.51 ((C(**C**H_3)$_2$)$_2$), 17.85 (C-4). IR (ATR): $\tilde{\nu}$ (cm^{-1}) = 3316, 2977, 1736, 1628, 1509, 1378, 1295, 1139, 1047, 853, 697. HR-MS (ESI): m/z = $[M + H]^+$ calcd for $C_{36}H_{40}BN_4O_8^+$: 667.2939; found: 667.2961. Specific rotation: $[\alpha]_D^{20}$ +4 (c 0.1 in DMSO).

Benzyl (*S*)-3-(4-(1-(2,2-dimethyl-4-oxo-4*H*-benzo[*d*][1,3]dioxin-6-yl)-1*H*-1,2,3-triazol-4-yl)benzamido)-4-(4,4,5,5-tetramethyl-1,3,2-dioxaborolan-2-yl)butanoate (39). Prepared according to **General Procedure D** from azide **11** (300 mg, 1.37 mmol) and alkyne **29** (735 mg, 1.64 mmol). The crude product was purified by FCC with boric acid-impregnated silica gel (hexanes/EtOAc 50:50) to give triazole **39** (76.8 mg, 0.115 mmol, 8%) as a pale yellow solid. m.p.: 129 °C. ^{1}H-NMR (400 MHz, $(CD_3)_2SO$): δ (ppm) = 9.53 (s, 1H, 5″-H), 8.41 (d, *J* = 2.7 Hz, 1H, 5‴-H), 8.36 (d, *J* = 8.2 Hz, 1H, CONH), 8.31 (dd, *J* = 8.9, 2.7 Hz, 1H, 7‴-H), 8.05–7.98 (m, 2H, 3′-H and 5′-H), 7.95–7.87 (m, 2H, 2′-H and 6′-H), 7.43 (d, *J* = 8.9 Hz, 1H, 8‴-H), 7.35–7.26 (m, 5H, 2⁗-H, 3⁗-H, 4⁗-H, 5⁗-H and 6⁗-H), 5.08–5.06 (m, 2H, 1⁗-CH_2), 4.55–4.44 (m, 1H, 3-H), 2.72–2.65 (m, 1H, 2-H), 2.64–2.57 (m, 1H, 2-H), 1.77 (s, 6H, 2‴-(CH_3)$_2$), 1.16 (s, 12H, (C(CH_3)$_2$)$_2$), 1.16–1.04 (m, 1H, 4-H). ^{13}C-NMR (101 MHz, $(CD_3)_2SO$): δ (ppm) = 170.71 (C-1), 164.87 (CONH), 159.48 (C-4‴), 155.21 (C-8a‴), 146.69 (C-4″), 136.15 (C-1⁗), 134.27 (C-1′), 132.53 (C-4′), 131.70 (C-6‴), 128.65 (C-7‴), 128.31 (C-2⁗, C-3⁗, C-4⁗, C-5⁗ and C-6⁗), 128.02 (C-2′ and C-6′), 127.89–127.80 (C-2⁗, C-3⁗, C-4⁗, C-5⁗ and C-6⁗), 124.90 (C-3′ and C-5′), 120.66 (C-5″), 120.18 (C-5‴), 119.25 (C-8‴), 113.77 (C-4a‴), 107.23 (C-2‴), 82.89 ((**C**(CH_3)$_2$)$_2$), 65.47 (1⁗-CH_2), 43.97 (C-3), 41.09 (C-2), 25.27 (2‴-(CH_3)$_2$), 24.66–24.50 ((C(**C**H_3)$_2$)$_2$), 17.87 (C-4). IR (ATR): $\tilde{\nu}$ (cm^{-1}) = 3316, 2977, 1734, 1627, 1509, 1377, 1295, 1139, 1046, 847, 697. HR-MS (ESI): m/z = $[M + H]^+$ calcd for $C_{36}H_{40}BN_4O_8^+$: 667.2939; found: 667.2949. Specific rotation: $[\alpha]_D^{20}$ −3 (c 0.1 in DMSO).

Benzyl (*R*)-4-cyano-3-(4-(1-(2,2-dimethyl-4-oxo-4*H*-benzo[*d*][1,3]dioxin-6-yl)-1*H*-1,2,3-triazol-4-yl)benzamido)butanoate (40). Prepared according to **General Procedure D** from azide **11** (150 mg, 0.684 mmol) and alkyne **30** (284 mg, 0.821 mmol). The crude product was resuspended in EtOAc (20 mL), filtered and the solid residue collected to give triazole **40** (157 mg, 0.278 mmol, 41%) as a pale yellow solid. m.p.: 196 °C. ^{1}H-NMR (400 MHz, $(CD_3)_2SO$): δ (ppm) = 9.55 (s, 1H, 5″-H), 8.79 (d, *J* = 7.9 Hz, 1H, CONH), 8.41 (d, *J* = 2.7 Hz, 1H, 5‴-H), 8.31 (dd, *J* = 8.9, 2.8 Hz, 1H, 7‴-H), 8.08–8.04 (m, 2H, 3′-H and 5′-H), 7.98–7.94

(m, 2H, 2′-H and 6′-H), 7.44 (d, *J* = 8.9 Hz, 1H, 8‴-H), 7.36–7.28 (m, 5H, 2⁗-H, 3⁗-H, 4⁗-H, 5⁗-H and 6⁗-H), 5.11 (s, 2H, 1⁗-CH_2), 4.68–4.57 (m, 1H, 3-H), 2.99–2.75 (m, 4H, 2-H and 4-H), 1.77 (s, 6H, $(CH_3)_2$). ^{13}C-NMR (101 MHz, $(CD_3)_2SO$): δ (ppm) = 169.88 (C-1), 165.63 (CONH), 159.48 (C-4‴), 155.23 (C-8a‴), 146.59 (C-4″), 135.94 (C-1⁗), 133.35 (C-1′), 133.04 (C-4′), 131.69 (C-6‴), 128.69 (C-7‴), 128.35 (C-2⁗, C-3⁗, C-4⁗, C-5⁗ and C-6⁗), 128.17 (C-2′ and C-6′), 127.99–127.86 (C-2⁗, C-3⁗, C-4⁗, C-5⁗ and C-6⁗), 125.04 (C-3′ and C-5′), 120.81 (C-5″), 120.22 (C-5‴), 119.26 (C-8‴), 118.32 (CN), 113.77 (C-4a‴), 107.23 (C-2‴), 65.81 (1⁗-CH_2), 43.61 (C-3), 37.77 (C-2), 25.27 ($(CH_3)_2$), 22.45 (C-4). IR (ATR): $\tilde{\nu}$ (cm^{-1}) = 3330, 1735, 1721, 1645, 1524, 1506, 1296, 1040. HR-MS (ESI): m/z = $[M + H]^+$ calcd for $C_{31}H_{28}N_5O_6^+$: 566.2040; found: 566.2034. Specific rotation: $[\alpha]_D^{20}$ −9 (c 0.1 in DMSO).

Benzyl (*S*)-4-cyano-3-(4-(1-(2,2-dimethyl-4-oxo-4*H*-benzo[*d*][1,3]dioxin-6-yl)-1*H*-1,2,3-triazol-4-yl)benzamido)butanoate (41). Prepared according to **General Procedure D** from azide **11** (200 mg, 0.912 mmol) and alkyne **31** (379 mg, 1.09 mmol). The crude product was resuspended in EtOAc (20 mL), filtered and the solid residue collected to give triazole **41** (275 mg, 0.487 mmol, 53%) as a yellow solid. m.p.: 198 °C. ^{1}H-NMR (400 MHz, $(CD_3)_2SO$): δ (ppm) = 9.55 (s, 1H, 5″-H), 8.80 (d, *J* = 7.9 Hz, 1H, CONH), 8.41 (d, *J* = 2.7 Hz, 1H, 5‴-H), 8.31 (dd, *J* = 8.9, 2.7 Hz, 1H, 7‴-H), 8.10–8.03 (m, 2H, 3′-H and 5′-H), 8.00–7.93 (m, 2H, 2′-H and 6′-H), 7.44 (d, *J* = 9.0 Hz, 1H, 8‴-H), 7.37–7.28 (m, 5H, 2⁗-H, 3⁗-H, 4⁗-H, 5⁗-H and 6⁗-H), 5.11 (s, 2H, 1⁗-CH_2), 4.67–4.57 (m, 1H, 3-H), 2.99–2.76 (m, 4H, 2-H and 4-H), 1.77 (s, 6H, $(CH_3)_2$). ^{13}C-NMR (126 MHz, $(CD_3)_2SO$): δ (ppm) = 169.89 (C-1), 165.62 (CONH), 159.48 (C-4‴), 155.23 (C-8a‴), 146.59 (C-4″), 135.94 (C-1⁗), 133.35 (C-1′), 133.04 (C-4′), 131.69 (C-6‴), 128.69 (C-7‴), 128.35 (C-2⁗, C-3⁗, C-4⁗, C-5⁗ and C-6⁗), 128.17 (C-2′ and C-6′), 127.99–127.87 (C-2⁗, C-3⁗, C-4⁗, C-5⁗ and C-6⁗), 125.05 (C-3′ and C-5′), 120.82 (C-5″), 120.22 (C-5‴), 119.26 (C-8‴), 118.33 (CN), 113.77 (C-4a‴), 107.24 (C-2‴), 65.81 (1⁗-CH_2), 43.61 (C-3), 37.77 (C-2), 25.27 ($(CH_3)_2$), 22.45 (C-4). IR (ATR): $\tilde{\nu}$ (cm^{-1}) = 3325, 1734, 1720, 1636, 1523, 1506, 1295, 1039. HR-MS (ESI): m/z = $[M + Na]^+$ calcd for $C_{31}H_{27}N_5O_6Na^+$: 588.1859; found: 588.1864. Specific rotation: $[\alpha]_D^{20}$ +7 (c 0.1 in DMSO).

(*R*)-(4-(Benzyloxy)-2-(4-(1-(2,2-dimethyl-4-oxo-4*H*-benzo[*d*][1,3]dioxin-6-yl)-1*H*-1,2,3-triazol-4-yl)benzamido)-4-oxobutyl)boronic acid (42). Method A: Prepared according to **General Procedure D** from azide **11** (300 mg, 1.37 mmol) and alkyne **28** (735 mg, 1.64 mmol). The crude product was purified by FCC with boric acid-impregnated silica gel (DCM/MeOH 95:5) to give triazole **42** (193 mg, 0.331 mmol, 24%) as a yellow solid. **Method B**: To a stirred solution of boronic acid pinacol ester 38 (70 mg, 0.105 mmol) in 5 mL THF/water (4:1 *v*/*v*), sodium periodate (112 mg, 0.525 mmol) was added, and the reaction mixture was stirred vigorously for 45 min at room temperature. 1 M HCl (0.126 mmol, 0.126 mL) was added to the resulting suspension, and the mixture stirred for another 16 h. The suspension was then filtered and the filtrate concentrated in vacuo. The crude product was purified by FCC with boric acid-impregnated silica gel (DCM/MeOH 95:5) to give triazole **42** (41.9 mg, 0.0717 mmol, 68%) as a yellow solid. m.p.: 138 °C. ^{1}H-NMR (400 MHz, $(CD_3)_2SO$): δ (ppm) = 9.53 (s, 1H, 5″-H), 8.41 (d, *J* = 2.7 Hz, 1H, 5‴-H), 8.31 (dd, *J* = 8.8, 2.5 Hz, 2H, CONH and 7‴-H), 8.05–8.00 (m, 2H, 3′-H and 5′-H), 7.94–7.88 (m, 2H, 2′-H and 6′-H), 7.67 (s, 2H, $B(OH)_2$), 7.44 (d, *J* = 8.9 Hz, 1H, 8‴-H), 7.35–7.26 (m, 5H, 2⁗-H, 3⁗-H, 4⁗-H, 5⁗-H and 6⁗-H), 5.05 (s, 2H, 1⁗-CH_2), 4.47–4.55 (m, 1H, 2-H), 2.69–2.62 (m, 2H, 3-H), 1.77 (s, 6H, $(CH_3)_2$), 1.08–1.01 (m, 2H, 1-H). ^{13}C-NMR (126 MHz, $(CD_3)_2SO$): δ (ppm) = 170.97 (C-4), 165.07 (CONH), 159.49 (C-4‴), 155.22 (C-8a‴), 146.69 (C-4″), 136.21 (C-1⁗), 134.28 (C-1′), 132.55 (C-4′), 131.71 (C-6‴), 128.69 (C-7‴), 128.30–128.04 (C-2⁗, C-3⁗, C-4⁗, C-5⁗ and C-6⁗), 127.85 (C-2′ and C-6′), 127.81 (C-2⁗, C-3⁗, C-4⁗, C-5⁗ and C-6⁗), 124.92 (C-3′ and C-5′), 120.68 (C-5″), 120.20 (C-5‴), 119.26 (C-8‴), 113.77 (C-4a‴), 107.24

(C-2‴), 65.40 (1⁗-CH_2), 44.53 (C-2), 41.01 (C-3), 25.27 ((CH_3)$_2$), 22.49 (C-1). IR (ATR): $\tilde{\nu}$ (cm^{-1}) = 3307, 1735, 1624, 1509, 1295, 1202, 1047, 932, 697. HR-MS (ESI): m/z = $[M + Na]^+$ calcd for $C_{30}H_{29}BN_4O_8Na^+$: 607.1976; found: 607.1970. Specific rotation: $[\alpha]_D^{20}$ −15 (c 0.1 in DMSO).

(*S*)-(4-(Benzyloxy)-2-(4-(1-(2,2-dimethyl-4-oxo-4*H*-benzo[*d*][1,3]dioxin-6-yl)-1*H*-1,2,3-triazol-4-yl)benzamido)-4-oxobutyl)boronic acid (43). Prepared according to **General Procedure D** from azide **11** (300 mg, 1.37 mmol) and alkyne **29** (735 mg, 1.64 mmol). The crude product was purified by FCC with boric acid-impregnated silica gel (DCM/MeOH 95:5) to give triazole **43** (263 mg, 0.450 mmol, 33%) as a yellow solid. m.p.: 141 °C. ^{1}H-NMR (500 MHz, (CD_3)$_2$SO): δ (ppm) = 9.53 (s, 1H, 5″-H), 8.41 (d, *J* = 2.7 Hz, 1H, 5‴-H), 8.31 (dd, *J* = 9.0, 2.5 Hz, 2H, CONH and 7‴-H), 8.05–7.99 (m, 2H, 3′-H and 5′-H), 7.93–7.90 (m, 2H, 2′-H and 6′-H), 7.67 (s, 2H, $B(OH)_2$), 7.44 (d, *J* = 8.9 Hz, 1H, 8‴-H), 7.35–7.26 (m, 5H, 2⁗-H, 3⁗-H, 4⁗-H, 5⁗-H and 6⁗-H), 5.05 (s, 2H, 1⁗-CH_2), 4.47–4.55 (m, 1H, 2-H), 2.67–2.63 (m, 2H, 3-H), 1.77 (s, 6H, (CH_3)$_2$), 1.10–1.00 (m, 2H, 1-H). ^{13}C-NMR (126 MHz, (CD_3)$_2$SO): δ (ppm) = 170.98 (C-4), 165.09 (CONH), 159.50 (C-4‴), 155.23 (C-8a‴), 146.70 (C-4″), 136.21 (C-1⁗), 134.28 (C-1′), 132.57 (C-4′), 131.72 (C-6‴), 128.70 (C-7‴), 128.31–128.05 (C-2⁗, C-3⁗, C-4⁗, C-5⁗ and C-6⁗), 127.87 (C-2′ and C-6′), 127.82 (C-2⁗, C-3⁗, C-4⁗, C-5⁗ and C-6⁗), 124.93 (C-3′ and C-5′), 120.69 (C-5″), 120.22 (C-5‴), 119.27 (C-8‴), 113.78 (C-4a‴), 107.25 (C-2‴), 65.41 (1⁗-CH_2), 44.54 (C-2), 41.02 (C-3), 25.28 ((CH_3)$_2$), 22.63 (C-1). IR (ATR): $\tilde{\nu}$ (cm^{-1}) = 3307, 1733, 1617, 1506, 1296, 1199, 1036, 929, 697. HR-MS (ESI): m/z = $[M + Na]^+$ calcd for $C_{30}H_{29}BN_4O_8Na^+$: 607.1976; found: 607.1970. Specific rotation: [$[\alpha]_D^{20}$ +14 (c 0.1 in DMSO).

(*S*)-4-(Benzyloxy)-1-bromo-4-oxobutan-2-aminium (44). Prepared according to **General Procedure A** from *N*-Boc-protected amine **18** (520 mg, 1.40 mmol). The aminium **44** (380 mg, 1.39 mmol, quant.) was obtained as a white solid. m.p.: 109 °C. ^{1}H-NMR (400 MHz, (CD_3)$_2$SO): δ (ppm) = 8.49 (s, 3H, NH_3^+), 7.45–7.29 (m, 5H, 2′-H, 3′-H, 4′-H, 5′-H and 6′-H), 5.15 (s, 2H, 1′-CH_2), 3.88–3.72 (m, 3H, 1-H and 2-H), 2.87 (dd, *J* = 6.4, 1.4 Hz, 2H, 3-H). ^{13}C-NMR (101 MHz, (CD_3)$_2$SO): δ (ppm) = 169.19 (C-4), 135.62 (C-1′), 128.47–128.13 (C-2′, C-3′, C-4′, C-5′ and C-6′), 66.30 (1′-CH_2), 47.67 (C-2), 35.66 (C-3), 33.90 (C-1). IR (ATR): $\tilde{\nu}$ (cm^{-1}) = 3203, 2866, 2812, 2590, 1720, 1708, 1501, 1395, 1348, 1227, 1154, 1138, 1082, 944, 739, 697. HR-MS (ESI): m/z = $[M]^+$ calcd for $C_{11}H_{15}BrNO_2^+$: 272.0281; found: 272.0279. Specific rotation: $[\alpha]_D^{20}$ −4 (c 0.1 in DMSO).

Benzyl (*S*)-2-(2-(4-ethynylphenyl)-4,5-dihydrooxazol-4-yl)acetate (45). Prepared according to **General Procedure B** from aminium **44** (459 mg, 1.68 mmol) and 4-ethynylbenzoic acid (284 mg, 1.85 mmol). The reaction mixture was stirred at room temperature for 16 h. The crude product was purified by FCC (hexanes/EtOAc 75:25) to give oxazoline **45** (269 mg, 0.842 mmol, 50%) as a yellow solid. m.p.: 82 °C. ^{1}H-NMR (400 MHz, (CD_3)$_2$SO): δ (ppm) = 7.86–7.82 (m, 2H, 2″-H and 6″-H), 7.60–7.55 (m, 2H, 3″-H and 5″-H), 7.39–7.28 (m, 5H, 2‴-H, 3‴-H, 4‴-H, 5‴-H and 6‴-H), 5.13 (d, *J* = 2.0 Hz, 2H, 1‴-CH_2), 4.63–4.55 (m, 2H, 4′-H and 5′-H), 4.41 (s, 1H, C≡CH), 4.20–4.11 (m, 1H, 5′-H), 2.78–2.73 (m, 2H, 2-H). ^{13}C-NMR (101 MHz, (CD_3)$_2$SO): δ (ppm) = 170.65 (C-1), 162.29 (C-2′), 136.08 (C-1‴), 131.94 (C-3″ and C-5″), 128.40–127.97 (C-2‴, C-3‴, C-4‴, C-5‴ and C-6‴), 127.84 (C-2″ and C-6″), 127.41 (C-1″), 124.73 (C-4″), 83.24 (**C**≡CH or C≡**C**H), 82.80 (**C**≡CH or C≡**C**H), 72.12 (C-5′), 65.53 (1‴-CH_2), 62.91 (C-4′), 39.50 (C-2). IR (ATR): $\tilde{\nu}$ (cm^{-1}) = 3212, 2812, 2590, 1719, 1710, 1645, 1500, 1348, 1227, 1167, 1082, 954, 739, 697, 679. HR-MS (ESI): m/z = $[M + H]^+$ calcd for $C_{20}H_{18}NO_3^+$: 320.1287; found: 320.1280. Specific rotation: $[\alpha]_D^{20}$ −42 (c 0.1 in DMSO).

(*R*)-5-(5-(4-((1-Carboxy-3-cyanopropan-2-yl)carbamoyl)phenyl)isoxazol-3-yl)-2-hydroxybenzoic acid (47). Prepared according to **General Procedure E** from isoxazole **34** (12.0 mg, 0.0212 mmol) and 0.70 M aq. KOH solution (5.95 mg, 0.106 mmol). The reaction mixture was stirred at room temperature for 2.5 h. The crude product was puri-

fied by FCC (hexanes/EtOAc 30:70 + 1% AcOH) to give isoxazole **47** (4.60 mg, 0.0106 mmol, 50%) as a white solid. m.p.: 228 °C. ^{1}H-NMR (400 MHz, $(CD_3)_2SO$): δ (ppm) = 12.41 (s, 1H, 1-COOH or 1‴-COOH), 8.85 (d, *J* = 7.8 Hz, 1H, CONH), 8.33 (d, *J* = 2.3 Hz, 1H, 6-H), 8.07 (s, 1H, 4-H), 8.03 (m, 4H, 2″-H, 3″-H, 5″-H and 6″-H), 7.77 (s, 1H, 4′-H), 7.11 (d, *J* = 8.6 Hz, 1H, 3-H), 4.54 (d, *J* = 7.2 Hz, 1H, 2‴-H), 2.89 (d, *J* = 5.0 Hz, 2H, 3‴-H), 2.67 (d, *J* = 7.9 Hz, 2H, 1‴-H). ^{13}C-NMR (126 MHz, $(CD_3)_2SO$): δ (ppm) = 171.53 (1‴-COOH), 171.21 (1-COOH), 168.73 (C-5′), 165.27 (CONH), 163.49 (C-2), 161.95 (C-3′), 135.23 (C-4″), 132.99 (C-4), 129.32 (C-1″), 128.65 (C-6), 128.28 (C-3″ and C-5″), 125.51 (C-2″ and C-6″), 119.09 (C-5), 118.38 (CN), 118.09 (C-3), 114.62 (C-1), 99.62 (C-4′), 43.61 (C-2‴), 37.66 (C-1″), 22.34 (C-3″). IR (ATR): $\tilde{\nu}$ (cm^{-1}) = 2922, 1653, 1598, 1540, 1497, 1423, 1291, 1207, 1074, 948, 798, 768, 686. HR-MS (ESI): m/z = $[M - H]^-$ calcd for $C_{22}H_{16}O_7N_3^-$: 434.0988; found: 434.0986. Specific rotation: $[\alpha]_D^{20}$ −28 (c 0.1 in DMSO). Purity (HPLC): 210 nm: >95%; 254 nm: >95%.

(*S*)-5-(5-(4-((1-Carboxy-3-cyanopropan-2-yl)carbamoyl)phenyl)isoxazol-3-yl)-2-hydroxybenzoic acid (48). Prepared according to **General Procedure E** from isoxazole **35** (228 mg, 0.403 mmol) and 0.70 M aq. KOH solution (113 mg, 2.02 mmol). The reaction mixture was stirred at room temperature for 2.5 h. The crude product was purified by FCC (hexanes/EtOAc 30:70 + 1% AcOH) to give isoxazole **48** (95.6 mg, 0.220 mmol, 55%) as a white solid. m.p.: 231 °C. ^{1}H-NMR (400 MHz, $(CD_3)_2SO$): δ (ppm) = 12.41 (s, 1H, 1-COOH or 1‴-COOH), 8.85 (d, *J* = 7.8 Hz, 1H, CONH), 8.33 (d, *J* = 2.3 Hz, 1H, 6-H), 8.07 (s, 1H, 4-H), 8.03 (m, 4H, 2″-H, 3″-H, 5″-H and 6″-H), 7.77 (s, 1H, 4′-H), 7.11 (d, *J* = 8.6 Hz, 1H, 3-H), 4.54 (d, *J* = 7.2 Hz, 1H, 2‴-H), 2.89 (d, *J* = 5.0 Hz, 2H, 3‴-H), 2.67 (d, *J* = 7.9 Hz, 2H, 1‴-H). ^{13}C-NMR (126 MHz, $(CD_3)_2SO$): δ (ppm) = 171.53 (1‴-COOH), 171.31 (1-COOH), 168.81 (C-5′), 165.26 (CONH), 162.53 (C-2), 161.82 (C-3′), 135.26 (C-4″), 133.35 (C-4), 129.28 (C-1″), 128.65 (C-6), 128.29 (C-3″ and C-5″), 125.52 (C-2″ and C-6″), 119.47 (C-5), 118.38 (CN), 118.22 (C-3), 113.88 (C-1), 99.64 (C-4′), 43.61 (C-2‴), 37.66 (C-1″), 22.34 (C-3″). IR (ATR): $\tilde{\nu}$ (cm^{-1}) = 2922, 1664, 1597, 1533, 1496, 1421, 1287, 1197, 797, 768, 686. HR-MS (ESI): m/z = $[M - H]^-$ calcd for $C_{22}H_{16}O_7N_3^-$: 434.0988; found: 434.0986. Specific rotation: $[\alpha]_D^{20}$ +28 (c 0.1 in DMSO). Purity (HPLC): 210 nm: >95%; 254 nm: >95%.

(*R*)-5-(4-(4-((1-Carboxy-3-cyanopropan-2-yl)carbamoyl)phenyl)-1*H*-1,2,3-triazol-1-yl)-2-hydroxybenzoic acid (49). Prepared according to **General Procedure E** from triazole **40** (60.0 mg, 0.106 mmol) and 0.70 M aq. KOH solution (29.8 mg, 0.530 mmol). The reaction mixture was stirred at room temperature for 30 min. The crude product was resuspended in EtOAc (10 mL), filtered and the solid residue collected to give cyanomethyl **49** (18.0 mg, 0.0413 mmol, 39%) as a white solid. m.p.: 290 °C. ^{1}H-NMR (400 MHz, $(CD_3)_2SO$): δ (ppm) = 12.43 (s, 1H, 1-COOH or 1‴-COOH), 9.42 (s, 1H, 5′-H), 8.74 (d, *J* = 7.7 Hz, 1H, CONH), 8.30 (d, *J* = 2.8 Hz, 1H, 6-H), 8.12–8.06 (m, 1H, 4-H), 8.08–8.04 (m, 2H, 2″-H and 6″-H), 8.01–7.94 (m, 2H, 3″-H and 5″-H), 7.22 (d, *J* = 9.0 Hz, 1H, 3-H), 4.58–4.48 (m, 1H, 2‴-H), 2.98–2.80 (m, 2H, 3‴-H), 2.77–2.60 (m, 2H, 1‴-H). ^{13}C-NMR (101 MHz, $(CD_3)_2SO$): δ (ppm) = 171.58 (1‴-COOH), 170.84 (1-COOH), 165.60 (CONH), 160.93 (C-2), 146.40 (C-4′), 133.30 (C-4″), 133.19 (C-1″), 128.48 (C-5), 128.13 (C-3″ and C-5″), 127.37 (C-4), 125.01 (C-2″ and C-6″), 121.67 (C-6), 120.62 (C-5′), 118.68 (C-3), 118.42 (CN), 114.03 (C-1), 43.55 (C-2‴), 37.71 (C-3‴), 22.36 (C-1‴). IR (ATR): $\tilde{\nu}$ (cm^{-1}) = 3364, 3116, 1728, 1673, 1521, 1291, 1184, 1042, 829, 772, 691. HR-MS (ESI): m/z = $[M + H]^+$ calcd for $C_{21}H_{18}N_5O_6^+$: 436.1257; found: 436.1250. Specific rotation: $[\alpha]_D^{20}$ −18 (c 0.1 in DMSO). Purity (HPLC): 210 nm: >95%; 254 nm: >95%.

(*S*)-5-(4-(4-((1-Carboxy-3-cyanopropan-2-yl)carbamoyl)phenyl)-1*H*-1,2,3-triazol-1-yl)-2-hydroxybenzoic acid (50). Prepared according to **General Procedure E** from triazole **41** (120 mg, 0.212 mmol) and 0.70 M aq. KOH solution (59.5 mg, 1.06 mmol). The reaction mixture was stirred at room temperature for 30 min. The crude product was resuspended in EtOAc (10 mL), filtered and the solid residue collected to give cyanomethyl **50**

(53.7 mg, 0.123 mmol, 58%) as a white solid. m.p.: 292 °C. ^{1}H-NMR (400 MHz, $(CD_3)_2SO$): δ (ppm) = 12.44 (s, 1H, 1-COOH or 1′-COOH), 9.42 (s, 1H, 5′-H), 8.74 (d, *J* = 7.7 Hz, 1H, CONH), 8.30 (d, *J* = 2.8 Hz, 1H, 6-H), 8.11–8.08 (m, 1H, 4-H), 8.10–8.03 (m, 2H, 2″-H and 6″-H), 8.01–7.94 (m, 2H, 3″-H and 5″-H), 7.22 (d, *J* = 8.9 Hz, 1H, 3-H), 4.58–4.48 (m, 1H, 2‴′-H), 2.97–2.81 (m, 2H, 3‴′-H), 2.77–2.61 (m, 2H, 1‴′-H). ^{13}C-NMR (101 MHz, $(CD_3)_2SO$): δ (ppm) = 171.58 (1‴′-COOH), 170.85 (1-COOH), 165.60 (CONH), 160.91 (C-2), 146.40 (C-4′), 133.31 (C-4″), 133.19 (C-1″), 128.50 (C-5), 128.13 (C-3″ and C-5″), 127.40 (C-4), 125.01 (C-2″ and C-6″), 121.67 (C-6), 120.62 (C-5′), 118.69 (C-3), 118.42 (CN), 113.99 (C-1), 43.55 (C-2‴′), 37.71 (C-3‴′), 22.36 (C-1‴′). IR (ATR): $\tilde{\nu}$ (cm^{-1}) = 3364, 3116, 1716, 1675, 1546, 1292, 1194, 1045, 828, 768, 691. HR-MS (ESI): *m*/*z* = $[M - H]^-$ calcd for $C_{21}H_{16}N_5O_6^-$: 434.1101; found: 434.1102. Specific rotation: $[\alpha]_D^{20}$ +12 (c 0.1 in DMSO). Purity (HPLC): 210 nm: >95%; 254 nm: >95%.

(*R*)-2-(6-(4-(3-(2,2-Dimethyl-4-oxo-4*H*-benzo[*d*][1,3]dioxin-6-yl)isoxazol-5-yl)phenyl)-2-hydroxy-3,4-dihydro-2*H*-1,5,2-oxazaborinin-4-yl)acetic acid (51). Prepared according to **General Procedure E** from isoxazole **36** (30.0 mg, 0.0590 mmol) and 0.40 M aq. KOH solution (4.97 mg, 0.0885 mmol). The reaction mixture was stirred at 0 °C for 30 min. The crude product was resuspended in DCM (10 mL), filtered and the solid residue collected to give cyclic boronic acid **51** (15.1 mg, 0.0317 mmol, 54%) as an off-white solid. m.p.: 233 °C. ^{1}H-NMR at 90 °C (400 MHz, $(CD_3)_2SO$): δ (ppm) = 8.41–8.37 (m, 1H, 5‴′-H), 8.25–8.19 (m, 1H, 7‴′-H), 8.09–7.97 (m, 4H, 2″-H, 3″-H, 5″-H and 6″-H), 7.77–7.68 (m, 1H, 4‴-H), 7.29 (d, *J* = 8.6 Hz, 1H, 8‴′-H), 4.27–4.10 (m, 1H, 4′-H), 3.78–3.53 (m, 2H, 2-H or 3′-H), 2.69–2.54 (m, 2H, 2-H or 3′-H), 1.76 (s, 6H, $(CH_3)_2$). ^{13}C-NMR (126 MHz, $(CD_3)_2SO$): δ (ppm) = 172.68 (C-1), 169.16 (C-5‴′), 166.79 (C-6′), 161.45 (C-3‴′), 159.75 (C-4‴′), 156.81 (C-8a‴′), 134.79 (C-1″ and C-7‴′), 128.75 (C-4″), 128.37 (C-2″ and C-6″ or C-3″ and C-5″), 127.36 (C-5‴′), 125.87–125.51 (C-2″ and C-6″ or C-3″ and C-5″), 123.23 (C-6‴′), 118.56 (C-8‴′), 113.56 (C-4a‴′), 107.02 (C-2‴′), 99.66 (C-4‴′), 64.03 (C-2 or C-3′), 48.18 (C-4′), 25.33 ($(CH_3)_2$). IR (ATR): $\tilde{\nu}$ (cm^{-1}) = 3122, 2995, 1736, 1619, 1287, 1199, 1016, 927, 763, 674. HR-MS (ESI): *m*/*z* = $[M + H]^+$ calcd for $C_{24}H_{22}BN_2O_8^+$: 477.1469; found: 477.1427. Specific rotation: $[\alpha]_D^{20}$ −6 (c 0.1 in DMSO). Purity (HPLC): 210 nm: 94%; 254 nm: >95%.

(*S*)-2-(6-(4-(3-(2,2-Dimethyl-4-oxo-4*H*-benzo[*d*][1,3]dioxin-6-yl)isoxazol-5-yl)phenyl)-2-hydroxy-3,4-dihydro-2*H*-1,5,2-oxazaborinin-4-yl)acetic acid (52). Prepared according to **General Procedure E** from isoxazole **37** (20.0 mg, 0.0393 mmol) and 0.40 M aq. KOH solution (3.31 mg, 0.0590 mmol). The reaction mixture was stirred at 0 °C for 30 min. The crude product was resuspended in DCM (10 mL), filtered and the solid residue collected to give cyclic boronic acid **52** (10.4 mg, 0.0218 mmol, 56%) as an off-white solid. m.p.: 188 °C. ^{1}H-NMR at 90 °C (400 MHz, $(CD_3)_2SO$): δ (ppm) = 8.41–8.37 (m, 1H, 5‴′-H), 8.22 (dd, *J* = 8.6, 2.2 Hz, 1H, 7‴′-H), 8.08–7.95 (m, 4H, 2″-H, 3″-H, 5″-H and 6″-H), 7.75–7.69 (m, 1H, 4‴-H), 7.29 (d, *J* = 8.7 Hz, 1H, 8‴′-H), 4.41–4.00 (m, 1H, 4′-H), 3.70–3.41 (m, 2H, 2-H or 3′-H), 2.63–2.56 (m, 1H, 2-H or 3′-H), 2.41–2.31 (m, 1H, 2-H or 3′-H), 1.76 (s, 6H, $(CH_3)_2$). ^{13}C-NMR (101 MHz, $(CD_3)_2SO$): δ (ppm) = 161.07 (C-3″), 159.11 (C-4‴′), 156.42 (C-8a‴′), 134.33 (C-7‴′ and C-1″), 127.92 (C-2″ and C-6″ or C-3″ and C-5″), 126.91 (C-5‴′), 125.28 (C-2″ and C-6″ or C-3″ and C-5″), 123.05 (C-6‴′), 117.93 (C-8‴′), 113.27 (C-4a‴′), 106.50 (C-2‴′), 25.01 ($(CH_3)_2$). IR (ATR): $\tilde{\nu}$ (cm^{-1}) = 3118, 2918, 1738, 1619, 1287, 1199, 1018, 926, 762, 674. HR-MS (ESI): *m*/*z* = $[M - H]^-$ calcd for $C_{24}H_{20}BN_2O_8^-$: 475.1313; found: 475.1294. Specific rotation: $[\alpha]_D^{20}$ +4 (c 0.1 in DMSO). Purity (HPLC): 210 nm: >95%; 254 nm: >95%.

(*R*)-2-(6-(4-(1-(2,2-Dimethyl-4-oxo-4*H*-benzo[*d*][1,3]dioxin-6-yl)-1*H*-1,2,3-triazol-4-yl)phenyl)-2-hydroxy-3,4-dihydro-2*H*-1,5,2-oxazaborinin-4-yl)acetic acid (53). Prepared according to **General Procedure E** from triazole **42** (180 mg, 0.308 mmol) and 0.40 M aq. KOH solution (25.9 mg, 0.462 mmol). The reaction mixture was stirred at 0 °C for 1 h. The

crude product was purified by FCC with boric acid-impregnated silica gel (DCM/MeOH 90:10 + 1% AcOH) to give cyclic boronic acid **53** (56.5 mg, 0.119 mmol, 39%) as a white solid. m.p.: 292 °C (decomposition). ^{1}H-NMR (400 MHz, CD_3OD): δ (ppm) = 9.08 (s, 1H, 5″-H), 8.42 (d, *J* = 2.7 Hz, 1H, 5‴′-H), 8.22 (dd, *J* = 8.9, 2.7 Hz, 1H, 7‴′-H), 8.07–8.02 (m, 2H, 3″-H and 5″-H), 7.97–7.92 (m, 2H, 2″-H and 6″-H), 7.31 (d, *J* = 8.9 Hz, 1H, 8‴′-H), 4.38–4.29 (m, 1H, 4′-H), 2.74–2.66 (m, 1H, 2-H), 2.56–2.47 (m, 1H, 2-H), 1.80 (s, 6H, $(CH_3)_2$), 0.92–0.83 (m, 1H, 3′-H), 0.77–0.68 (m, 1H, 3′-H). ^{13}C-NMR (101 MHz, CD_3OD): δ (ppm) = 174.68 (C-1), 168.94 (C-6′), 161.47 (C-4‴′), 157.46 (C-8a‴′), 148.62 (C-4‴), 136.12 (C-1′ and C-4″), 133.45 (C-6‴′), 129.95 (C-7‴′), 129.18 (C-2″ and C-6″), 126.84 (C-3″ and C-5″), 121.99 (C-5‴′), 121.34 (C-5‴), 120.35 (C-8‴′), 115.55 (C-4a‴′), 108.66 (C-2‴′), 47.39 (C-4′), 40.50 (C-2), 25.86 ($(CH_3)_2$). IR (ATR): $\tilde{\nu}$ (cm^{-1}) = 3343, 1733, 1618, 1509, 1379, 1299, 1044, 828, 767. HR-MS (ESI): *m*/*z* = $[M + H]^+$ calcd for $C_{23}H_{22}BN_4O_7^+$: 477.1582; found: 477.1564. Specific rotation: $[\alpha]_D^{20}$ −12 (c 0.1 in DMSO). Purity (HPLC): 210 nm: >95%; 254 nm: >95%.

(*S*)-2-(6-(4-(1-(2,2-Dimethyl-4-oxo-4*H*-benzo[*d*][1,3]dioxin-6-yl)-1*H*-1,2,3-triazol-4-yl) phenyl)-2-hydroxy-3,4-dihydro-2*H*-1,5,2-oxazaborinin-4-yl)acetic acid (54). Prepared according to **General Procedure E** from triazole **43** (205 mg, 0.351 mmol) and 0.40 M aq. KOH solution (29.5 mg, 0.526 mmol). The reaction mixture was stirred at 0 °C for 1 h. The crude product was purified by FCC with boric acid-impregnated silica gel (DCM/MeOH 90:10 + 1% AcOH) to give cyclic boronic acid **54** (53.0 mg, 0.111 mmol, 32%) as a pale yellow solid. m.p.: 304 °C (decomposition). ^{1}H-NMR (500 MHz, CD_3OD): δ (ppm) = 9.10 (s, 1H, 5‴-H), 8.42 (d, *J* = 2.7 Hz, 1H, 5‴′-H), 8.23 (dd, *J* = 8.9, 2.7 Hz, 1H, 7‴′-H), 8.10–8.05 (m, 2H, 3″-H and 5″-H), 8.00–7.95 (m, 2H, 2″-H and 6″-H), 7.31 (d, *J* = 9.0 Hz, 1H, 8‴′-H), 4.36–4.26 (m, 1H, 4′-H), 2.76–2.67 (m, 1H, 2-H), 2.64–2.50 (m, 1H, 2-H), 1.80 (s, 6H, $(CH_3)_2$), 0.92–0.86 (m, 1H, 3′-H), 0.82–0.73 (m, 1H, 3′-H). ^{13}C-NMR (126 MHz, CD_3OD): δ (ppm) = 175.06 (C-1), 169.18 (C-6′), 161.46 (C-4‴′), 157.48 (C-8a‴′), 148.51 (C-4‴), 135.11 (C-1″ and C-4″), 133.43 (C-6‴′), 129.95 (C-7‴′), 129.33 (C-2″ and C-6″), 126.91 (C-3″ and C-5″), 121.99 (C-5‴′), 121.46 (C-5‴), 120.36 (C-8‴′), 115.56 (C-4a‴′), 108.66 (C-2‴′), 45.77 (C-4′), 40.53 (C-2), 25.86 ($(CH_3)_2$). IR (ATR): $\tilde{\nu}$ (cm^{-1}) = 3343, 1733, 1616, 1508, 1378, 1298, 1041, 826, 766. HR-MS (ESI): *m*/*z* = $[M + H]^+$ calcd for $C_{23}H_{22}BN_4O_7^+$: 477.1582; found: 477.1583. Specific rotation: $[\alpha]_D^{20}$ +8 (c 0.1 in DMSO). Purity (HPLC): 210 nm: >95%; 254 nm: >95%.

1-(Benzyloxy)-1-oxohex-5-en-3-aminium (57). Prepared according to **General Procedure A** from *N*-Boc-protected homoallyl amine **56** (1.37 g, 4.29 mmol). The aminium **57** (945 mg, 4.31 mmol, quant.) was obtained as a viscous yellow oil. ^{1}H-NMR (400 MHz, $(CD_3)_2SO$): δ (ppm) = 8.22 (s, 3H, NH_3^+), 7.40–7.32 (m, 5H, 2′-H, 3′-H, 4′-H, 5′-H and 6′-H), 5.83–5.71 (m, 1H, 5-H), 5.17–5.10 (m, 4H, 6-H and 1′-CH_2), 3.58–3.48 (m, 1H, 3-H), 2.81–2.64 (m, 2H, 2-H), 2.47–2.30 (m, 2H, 4-H). ^{13}C-NMR (101 MHz, $(CD_3)_2SO$): δ (ppm) = 169.74 (C-1), 135.71 (C-1′), 132.41 (C-5), 128.45 -128.18 (2′-H, 3′-H, 4′-H, 5′-H and 6′-H), 119.51 (C-6), 66.10 (1′-CH_2), 46.86 (C-3), 36.42 (C-4), 36.09 (C-2). IR (ATR): $\tilde{\nu}$ (cm^{-1}) = 2977, 2880, 2834, 1998, 1728, 1601, 1497, 1395, 1216, 1190, 1128, 923, 738, 696. HR-MS (ESI): *m*/*z* = $[M]^+$ calcd for $C_{13}H_{18}NO_2^+$: 220.1332; found: 220.1353.

Benzyl 3-(4-ethynylbenzamido)hex-5-enoate (58). Prepared according to **General Procedure B** from aminium **57** (490 mg, 2.23 mmol) and 4-ethynylbenzoic acid (344 mg, 2.23 mmol). The crude product was purified by FCC (hexanes/EtOAc 80:20) to give amide **58** (629 mg, 1.81 mmol, 81%) as a pale yellow solid. m.p.: 104 °C. ^{1}H-NMR (400 MHz, $(CD_3)_2SO$): δ (ppm) = 8.42 (d, *J* = 8.4 Hz, 1H, CONH), 7.81–7.77 (m, 2H, 2′-H and 6′-H), 7.57–7.54 (m, 2H, 3′-H and 5′-H), 7.33–7.27 (m, 5H, 2″-H, 3″-H, 4″-H, 5″-H and 6″-H), 5.77 (ddt, *J* = 17.2, 10.2, 7.0 Hz, 1H, 5-H), 5.10–4.99 (m, 4H, 6-H and 1″-CH_2), 4.45–4.38 (m, 1H, 3-H), 4.37 (s, 1H, C≡CH), 2.66–2.61 (m, 2H, 2-H), 2.33–2.28 (m, 2H, 4-H). ^{13}C-NMR (101 MHz, $(CD_3)_2SO$): δ (ppm) = 170.67 (C-1), 164.98 (CONH), 136.08 (C-1″), 134.92 (C-5), 134.62 (C-1′), 131.55 (C-3′ and C-5′), 128.31–127.86 (C-2″, C-3″, C-4″, C-5″ and C-6″), 127.50

(C-2′ and C-6′), 124.32 (C-4′), 117.42 (C-6), 82.90 (**C**≡CH and C≡**C**H), 65.54 (1″-CH_2), 46.34 (C-3), 38.63 (C-2), 38.46 (C-4). IR (ATR): $\tilde{\nu}$ (cm^{-1}) = 3317, 3271, 1737, 1716, 1638, 1543, 1536, 1495, 1301, 1258, 1164, 1116, 854, 757, 698, 675. HR-MS (ESI): m/z = $[M + H]^+$ calcd for $C_{22}H_{22}NO_3^+$: 348.1600; found: 348.1607.

Benzyl 3-(4-(3-(2,2-dimethyl-4-oxo-4*H*-benzo[*d*][1,3]dioxin-6-yl)isoxazol-5-yl)benzamido) hex-5-enoate (59). To a stirred solution of alkyne **58** (844 mg, 2.43 mmol) in 24 mL MeOH/H_2O (5:1 *v*/*v*), aldoxime **3** (806 mg, 3.64 mmol) and PIFA (403 mg, 1.82 mmol) were added. The reaction mixture was stirred at 70 °C for 2 h. Another equivalent of PIFA (403 mg, 1.82 mmol) was added, and the reaction mixture was stirred at 70 °C for another 2 h. The solvents were removed in vacuo, and the crude product was redissolved in EtOAc (150 mL). Water (150 mL) was added, the resulting two phases were separated, and the aqueous phase was extracted with EtOAc (3 × 150 mL). The combined organic phases were dried using a phase separation paper, and the solvent was removed in vacuo. The crude product was purified by FCC (hexanes/EtOAc 70:30) to give isoxazole **59** (163.2 mg, 0.290 mmol, 12%) as a white solid. m.p.: 173 °C. ^{1}H-NMR (500 MHz, $CDCl_3$): δ (ppm) = 8.37 (d, *J* = 2.2 Hz, 1H, 5‴-H), 8.19 (dd, *J* = 8.6, 2.2 Hz, 1H, 7‴-H), 7.89–7.86 (m, 2H, 3′-H and 5′-H), 7.84–7.81 (m, 2H, 2′-H and 6′-H), 7.39–7.31 (m, 5H, 2⁗-H, 3⁗-H, 4⁗-H, 5⁗-H and 6⁗-H), 7.11 (d, *J* = 8.6 Hz, 1H, 8‴-H), 6.97 (d, *J* = 8.7 Hz, 1H, CONH), 6.94 (s, 1H, 4″-H), 5.81 (ddt, *J* = 19.5, 9.6, 7.1 Hz, 1H, 5-H), 5.20–5.09 (m, 4H, 6-H and 1⁗-CH_2), 4.60–4.52 (m, 1H, 3-H), 2.74 (d, *J* = 5.0 Hz, 2H, 2-H), 2.54–2.38 (m, 2H, 4-H), 1.79 (s, 6H, $(CH_3)_2$). ^{13}C-NMR (126 MHz, $CDCl_3$): δ (ppm) = 171.98 (C-1), 169.88 (C-5″), 165.75 (CONH), 161.72 (C-3″), 160.74 (C-4‴), 157.46 (C-8a‴), 136.06 (C-1′), 135.57 (C-1⁗), 134.69 (C-7‴), 133.95 (C-5), 129.88 (C-4′), 128.85–128.57 (C-2⁗, C-3⁗, C-4⁗, C-5⁗ and C-6⁗), 128.35 (C-5‴), 127.89 (C-2′ and C-6′), 126.12 (C-3′ and C-5′), 123.97 (C-6‴), 118.77 (C-6), 118.39 (C-8‴), 113.90 (C-4a‴), 107.10 (C-2‴), 98.46 (C-4″), 66.91 (1⁗-CH_2), 46.21 (C-3), 38.59 (C-4), 37.59 (C-2), 26.04 ($(CH_3)_2$). IR (ATR): $\tilde{\nu}$ (cm^{-1}) = 3300, 2922, 2851, 1748, 1720, 1634, 1627, 1534, 1429, 1284, 1200, 1050, 922, 914, 822, 763, 688. HR-MS (ESI): m/z = $[M + H]^+$ calcd for $C_{33}H_{31}N_2O_7^+$: 567.2131; found: 567.2117.

5-(5-(4-((1-Carboxypent-4-en-2-yl)carbamoyl)phenyl)isoxazol-3-yl)-2-hydroxybenzoic acid (60). Prepared according to **General Procedure E** from isoxazole **59** (165 mg, 0.291 mmol) and 0.70 M aq. KOH solution (81.4 mg, 1.45 mmol). The reaction mixture was stirred at room temperature for 1.5 h. The crude product was resuspended in EtOAc (20 mL), filtered and the solid residue collected to give vinyl **60** (127 mg, 0.291 mmol, quant.) as a white solid. m.p.: 225 °C. ^{1}H-NMR (500 MHz, $(CD_3)_2SO$): δ (ppm) = 12.19 (s, 1H, 1-COOH or 1‴-COOH), 8.45 (d, *J* = 8.4 Hz, 1H, CONH), 8.34 (d, *J* = 2.3 Hz, 1H, 6-H), 8.06 (dd, *J* = 8.7, 2.3 Hz, 1H, 4-H), 8.05–7.99 (m, 2H, 2″-H and 6″-H), 8.01–7.95 (m, 2H, 3″-H and 5″-H), 7.76 (s, 1H, 4′-H), 7.14 (d, *J* = 8.6 Hz, 1H, 3-H), 5.81 (ddt, *J* = 17.1, 10.2, 7.0 Hz, 1H, 4‴-H), 5.11–5.01 (m, 2H, 5‴-H), 4.43–4.34 (m, 1H, 2‴-H), 2.57–2.51 (m, 2H, 1‴-H), 2.37–2.30 (m, 2H, 3‴-H). ^{13}C-NMR (126 MHz, $(CD_3)_2SO$): δ (ppm) = 172.42 (1‴-COOH), 171.32 (1-COOH), 168.91 (C-5′), 164.84 (CONH), 162.53 (C-2), 161.80 (C-3′), 136.02 (C-4″), 135.10 (C-4‴), 133.35 (C-4), 128.94 (C-1″), 128.65 (C-6), 128.16 (C-3″ and C-5″), 125.42 (C-2″ and C-6″), 119.50 (C-5), 118.22 (C-3), 117.31 (C-5‴), 113.88 (C-1), 99.48 (C-4′), 46.26 (C-2‴), 38.71 (C-1‴), 38.45 (C-3‴). IR (ATR): $\tilde{\nu}$ (cm^{-1}) = 3315, 2916, 1729, 1688, 1632, 1589, 1531, 1499, 1421, 1290, 1212, 926, 796, 769, 695. HR-MS (ESI): m/z = $[M - H]^-$ calcd for $C_{23}H_{19}N_2O_7^-$: 435.1192; found: 435.1192.

5-(5-(4-((1-Carboxy-4-oxobutan-2-yl)carbamoyl)phenyl)isoxazol-3-yl)-2-hydroxybenzoic acid (61). A solution of vinyl **60** (85 mg, 0.195 mmol) in 7 mL MeOH was flushed with N_2 and cooled to -78 °C. O_3 (flowrate: 25–30, power: 35%) was then bubbled into the solution for 3.5 min. Me_2S (21.7 µL, 0.292 mmol) was added and the solution stirred at room temperature for 1 h. The solvent was removed in vacuo and the crude product purified by

PTLC (DCM/MeOH 88:12 + 1% AcOH) to give formylmethyl **61** (31.4 mg, 0.0716 mmol, 37%) as a beige solid. m.p.: 275 °C. ^{1}H-NMR (500 MHz, $(CD_3)_2SO$): δ (ppm) = 9.73 (s, 1H, CONH), 9.68 (s, 1H, 4‴-H), 8.23 (d, *J* = 2.4 Hz, 1H, 6-H), 8.04–8.00 (m, 2H, 2″-H and 6″-H), 7.94–7.90 (m, 2H, 3″-H and 5″-H), 7.71 (dd, *J* = 8.5, 2.4 Hz, 1H, 4-H), 7.61 (s, 1H, 4′-H), 6.74 (d, *J* = 8.4 Hz, 1H, 3-H), 4.63–4.53 (m, 1H, 2‴-H), 2.76–2.55 (m, 2H, 3‴-H), 2.32–2.22 (m, 2H, 1‴-H). ^{13}C-NMR (126 MHz, $(CD_3)_2SO$): δ (ppm) = 202.04 (C-4‴), 174.07 (1‴-COOH), 170.65 (1-COOH), 168.14 (C-5′), 166.02 (C-2), 164.19 (CONH), 162.94 (C-3′), 135.74 (C-4″), 129.76 (C-4), 129.28 (C-1″), 128.61 (C-6), 127.76 (C-3″ and C-5″), 125.50 (C-2″ and C-6″), 120.44 (C-5), 116.97 (C-3), 115.53 (C-1), 99.33 (C-4′), 48.90 (C-3‴), 43.15 (C-2‴), 41.28 (C-1‴). IR (ATR): $\tilde{\nu}$ (cm^{-1}) = 3300, 2925, 1715, 1635, 1560, 1497, 1392, 1257, 1077, 948, 834, 768, 700. HR-MS (ESI): *m*/*z* = $[M - H]^-$ calcd for $C_{22}H_{17}N_2O_8^-$: 437.0985; found: 437.0988. Purity (HPLC): 210 nm: 90%; 254 nm: 91%.

Benzyl 3-(4-(1-(2,2-dimethyl-4-oxo-4*H*-benzo[*d*][1,3]dioxin-6-yl)-1*H*-1,2,3-triazol-4-yl)benzamido)hex-5-enoate (62). Prepared according to **General Procedure D** from azide **11** (300 mg, 1.37 mmol) and alkyne **58** (571 mg, 1.64 mmol). The crude product was resuspended in EtOAc (20 mL), filtered and the solid residue collected to give triazole **62** (550 mg, 0.971 mmol, 71%) as a white solid. m.p.: 173 °C. ^{1}H-NMR (400 MHz, $(CD_3)_2SO$): δ (ppm) = 9.53 (s, 1H, 5″-H), 8.42–8.38 (m, 2H, CONH and 5‴-H), 8.31 (dd, *J* = 8.9, 2.7 Hz, 1H, 7‴-H), 8.06–8.00 (m, 2H, 3′-H and 5′-H), 7.96–7.90 (m, 2H, 2′-H and 6′-H), 7.43 (d, *J* = 8.9 Hz, 1H, 8‴-H), 7.35–7.27 (m, 5H, 2⁗-H, 3⁗-H, 4⁗-H, 5⁗-H and 6⁗-H), 5.87–5.74 (m, 1H, 5-H), 5.13–5.01 (m, 4H, 6-H and 1⁗-CH_2), 4.50–4.40 (m, 1H, 3-H), 2.69–2.64 (m, 2H, 2-H), 2.34 (t, *J* = 6.9 Hz, 2H, 4-H), 1.77 (s, 6H, $(CH_3)_2$). ^{13}C-NMR (101 MHz, $(CD_3)_2SO$): δ (ppm) = 170.73 (C-1), 165.27 (CONH), 159.48 (C-4‴), 155.22 (C-8a‴), 146.67 (C-4″), 136.11 (C-1⁗), 134.99 (C-5), 134.08 (C-1′), 132.66 (C-4′), 131.70 (C-6‴), 128.67 (C-7‴), 128.33 (C-2⁗, C-3⁗, C-4⁗, C-5⁗ and C-6⁗), 128.04 (C-2′ and C-6′), 127.92–127.87 (C-2‴, C-3‴, C-4‴, C-5‴ and C-6‴), 124.95 (C-3′ and C-5′), 120.69 (C-5″), 120.20 (C-5‴), 119.25 (C-8‴), 117.41 (C-6), 113.77 (C-4a‴), 107.23 (C-2‴), 65.55 (1⁗-CH_2), 46.33 (C-3), 38.71 (C-2 or C-4), 38.53 (C-2 or C-4), 25.27 ($(CH_3)_2$). IR (ATR): $\tilde{\nu}$ (cm^{-1}) = 3313, 1735, 1630, 1507, 1295, 1170, 1047, 932, 851, 697. HR-MS (ESI): *m*/*z* = $[M + H]^+$ calcd for $C_{32}H_{31}N_4O_6^+$: 567.2244; found: 567.2259.

5-(4-(4-((1-Carboxypent-4-en-2-yl)carbamoyl)phenyl)-1*H*-1,2,3-triazol-1-yl)-2-hydroxybenzoic acid (63). Prepared according to **General Procedure E** from triazole **62** (422 mg, 0.745 mmol) and 0.70 M aq. KOH solution (208 mg, 3.71 mmol). The reaction mixture was stirred at room temperature for 1.5 h. The crude product was resuspended in EtOAc (50 mL), filtered and the solid residue collected to give vinyl **63** (249 mg, 0.570 mmol, 77%) as a white solid. m.p.: 223 °C. ^{1}H-NMR (400 MHz, $(CD_3)_2SO$): δ (ppm) = 12.12 (s, 1H, 1-COOH or 1‴-COOH), 9.40 (s, 1H, 5′-H), 8.34 (d, *J* = 8.4 Hz, 1H, CONH), 8.30 (d, *J* = 2.8 Hz, 1H, 6-H), 8.09 (dd, *J* = 8.9, 2.8 Hz, 1H, 4-H), 8.06–7.99 (m, 2H, 2″-H and 6″-H), 7.98–7.90 (m, 2H, 3″-H and 5″-H), 7.22 (d, *J* = 8.9 Hz, 1H, 3-H), 5.87–5.75 (m, 1H, 4‴-H), 5.13–5.00 (m, 2H, 5‴-H), 4.44–4.34 (m, 1H, 2‴-H), 2.52–2.48 (m, 2-H, 1‴-H), 2.33 (t, *J* = 6.9 Hz, 2H, 3‴-H). ^{13}C-NMR (126 MHz, $(CD_3)_2SO$): δ (ppm) = 172.47 (1‴-COOH), 170.87 (1-COOH), 165.19 (CONH), 160.89 (C-2), 146.49 (C-4′), 135.17 (C-4‴), 134.06 (C-4″), 132.80 (C-1″), 128.52 (C-5), 128.00 (C-3″ and C-5″), 127.40 (C-4), 124.93 (C-2″ and C-6″), 121.65 (C-6), 120.50 (C-5′), 118.70 (C-3), 117.26 (C-5‴), 113.96 (C-1), 46.18 (C-2‴), 38.77 (C-1‴), 38.49 (C-3‴). IR (ATR): $\tilde{\nu}$ (cm^{-1}) = 3119, 1723, 1669, 1593, 1546, 1492, 1288, 1209, 1182, 1046, 828, 689. HR-MS (ESI): *m*/*z* = $[M + H]^+$ calcd for $C_{22}H_{21}N_4O_6^+$: 437.1461; found: 437.1471.

5-(4-(4-((1-Carboxy-4-oxobutan-2-yl)carbamoyl)phenyl)-1*H*-1,2,3-triazol-1-yl)-2-hydroxybenzoic acid (64). A solution of vinyl **63** (100 mg, 0.229 mmol) in 8 mL MeOH was flushed with N_2 and cooled to −78 °C. O_3 (flowrate: 25–30, power: 35%) was then bubbled into the solution for 3.5 min. Me_2S (25.5 µL, 0.344 mmol) was added and the

solution stirred at room temperature for 1 h. The solvent was removed in vacuo and the crude product purified by PTLC (DCM/MeOH 85:15 + 1% AcOH) to give aldehyde **64** (18.9 mg, 0.0431 mmol, 19%) as a beige solid. m.p.: 151 °C (decomposition). ^{1}H-NMR (500 MHz, $(CD_3)_2SO$): δ (ppm) = 9.69 (s, 1H, 4‴-H), 9.65 (s, 1H, CONH), 9.27 (s, 1H, 5′-H), 8.13 (d, *J* = 2.9 Hz, 1H, 6-H), 8.06–8.01 (m, 2H, 2″-H and 6″-H), 7.89–7.85 (m, 2H, 3″-H and 5″-H), 7.69 (dd, *J* = 8.7, 2.9 Hz, 1H, 4-H), 6.82 (d, *J* = 8.7 Hz, 1H, 3-H), 4.61–4.55 (m, 1H, 2‴-H), 2.76–2.55 (m, 2H, 3‴-H), 2.30–2.20 (m, 2H, 1‴-H). ^{13}C-NMR (126 MHz, $(CD_3)_2SO$): δ (ppm) = 202.17 (C-4‴), 174.34 (1‴-COOH), 170.08 (1-COOH), 164.53 (CONH), 164.03 (C-2), 146.09 (C-4′), 133.81 (C-4″), 133.18 (C-1″), 127.57 (C-3″ and C-5″), 125.87 (C-5), 125.00 (C-2″ and C-6″), 123.76 (C-4), 121.70 (C-6), 120.71 (C-1), 120.23 (C-5′), 117.03 (C-3), 49.01 (C-3‴), 43.08 (C-2‴), 41.44 (C-1‴). IR (ATR): $\tilde{\nu}$ (cm^{-1}) = 3300, 2918, 1716, 1636, 1576, 1487, 1374, 1252, 1043, 829, 769, 706. HR-MS (ESI): m/z = $[M\text{-}H]^-$ calcd for $C_{21}H_{17}N_4O_7^-$: 437.1097; found: 437.1102. Purity (HPLC): 210 nm: 94%; 254 nm: 92%.

3.2. Sirtuin 5 Assay

The inhibitory activities of the synthesized target compounds were determined by Reaction Biology Corporation (Malvern, PA, USA) using a fluorescence-based assay. The sirtuin 5 enzyme utilized in this assay was produced in-house by Reaction Biology. The enzyme construct (accession number: NM_012241) comprised amino acids 37–310 (C-terminal region), carried an *N*-terminal His-tag and was expressed in *Escherichia coli*. The recombinant protein was purified to >95% purity, as confirmed by SDS-PAGE, and supplied in a solution containing 50 mM Tris-HCl (pH 8.0), 137 mM NaCl, 2.7 mM KCl, 1 mM $MgCl_2$, 1 mg/mL BSA, and 1% DMSO with a protein concentration of 19 nM. Test compounds were prepared at a concentration of 10 mM in DMSO and incubated with 5 µL sirtuin 5 in the assay buffer per well at 30 °C for 10 min in a concentration range between 5 nM and 0.1 mM. 5 µL assay buffer without sirtuin 5 were used for control wells. The deacylation reaction was initiated by the addition of 5 µL substrate mixture comprising 50 µM fluorogenic substrate Ac-Lys-succ-AMC and the co-factor NAD^+. After a 2 h incubation at 30 °C, the reaction was terminated by adding 10 µL protease-based developer with 4 mM nicotinamide, which cleaves 7-amino-4-methylcoumarin to yield a fluorescent signal. Fluorescence was measured after an additional 1 h incubation at 30 °C, with excitation/emission wavelengths of 360/460 nm with EnVision® Plate Reader (Revvity, Waltham, MA, USA). To standardize results, a no-inhibitor control representing 100% enzyme activity was included in all assays. IC_{50} values for sirtuin 5 inhibition were determined in triplicate using a 10-dose, 3-fold serial dilution series. For each replicate, individual IC_{50} values were calculated by fitting sigmoidal dose–response curves using Prism 8.0.2 software (GraphPad Software, Boston, MA, USA). The final IC_{50} values are reported as the mean ± standard deviation of the triplicate measurements.

3.3. Computational Methods

Molecular docking studies were performed using the Schrödinger software suite (version 2020-3, Schrödinger Inc., New York, NY, USA) [44]. X-ray crystal structure of sirtuin 5 in complex with its reference succinyl peptide substrate (PDB ID: 3RIY [30]) was obtained from the Protein Data Bank [45] and prepared using the Protein Preparation Wizard. Ligands were prepared with the Ligand Preparation Wizard, employing Epik for protonation state and charge assignments with a pH value of 7.4 assumed [46]. The protein was prepared without the ligand in the active site. The center of mass of ligand 2 in Chain A of 3RIY was set as center of the docking grid (x = −12.8, y = 2.41 and z = −6.59). Docking was conducted using Glide in standard precision (SP) mode with default parameters. OPLS4 force field was applied for structural optimization and docking. The resulting poses

were analyzed and visualized using PyMOL 2.5.8 (Schrödinger Inc., New York, NY, USA). Top-ranked docking poses (5 poses) were evaluated based on their spatial alignment and interactions relative to the co-crystallized succinyl peptide substrate.

4. Conclusions

A growing body of literature implicating sirtuin 5 with the development and exacerbation of various diseases has solidified this NAD^+-dependent lysine deacylase as a promising biological target for pharmaceutical interventions. However, the accessibility to potent sirtuin 5 inhibitors with satisfactory pharmacokinetic properties remains limited. Through a comprehensive SAR analysis of balsalazide, we previously generated a series of derivatives with optimized pharmacokinetic properties and further attempted to optimize their potency through various inhibitor–enzyme interactions. Herein, we continued this endeavor by employing the principles of reversible covalent bonding, a well-established optimization method in drug development, to potentially enhance the binding affinity and potency of these sirtuin 5 inhibitors. Guided by initial docking experiments, the introduction of boronic acid, cyanomethyl and formylmethyl groups was rationally employed at the most optimal position for reversible covalent bonding with the nicotinamide ribose vicinal hydroxy groups of the essential co-factor NAD^+. Challenges associated with the syntheses and purification of alkyl boronic acids, as well as the syntheses of enantiomerically pure derivatives, were addressed and navigated through method developments and optimizations, and chiral-pool syntheses from commercially available amino acid derivatives. Biological evaluation of the synthesized functionalized inhibitors showed that these modifications were tolerated to some extent, but did not show any significant improvement in inhibitory potency compared to their lead structures. Additionally, triazole-based inhibitors demonstrated superior potency compared to their corresponding isoxazole-based inhibitors. Furthermore, a stereo-selective preference of these functional group modifications was observed with *S*-enantiomers showing higher potency compared to their corresponding *R*-enantiomers. Among the functional group modifications, the cyanomethyl derivatives emerged as the most potent inhibitors, highlighted by the *S*-enantiomer of the triazole-based cyanomethyl derivative **50** with an IC_{50} of 27 μM, which lies in a similar potency range to current established sirtuin 5 inhibitors. The exact binding mechanisms of the functionalized sirtuin 5 inhibitors could not yet be proven in this work due to the lack of co-crystal structures, but we are still actively pursuing this area of research. Nevertheless, our findings offer valuable insight into the SAR of balsalazide analogues as sirtuin 5 inhibitors and thus a viable foundation for the design and development of more potent balsalazide-based sirtuin 5 inhibitors in the future.

Supplementary Materials: The following supporting information can be downloaded at: https://www.mdpi.com/article/10.3390/molecules30183821/s1: S1. ^1H and ^{13}C NMR spectra of synthesized compounds; S2. HPLC chromatograms of tested compounds; S3. Crystal structure data of compound **45** (including relevant references no. [47–50]).

Author Contributions: Conceptualization, F.B.; methodology, R.W., S.A.H., T.W. and F.B.; software, T.W.; validation, R.W., T.W. and F.B.; formal analysis, R.W., T.W. and F.B.; investigation, R.W., S.A.H. and T.W.; resources, F.B.; data curation, R.W., T.W. and F.B.; writing—original draft preparation, R.W.; writing—review and editing, T.W. and F.B.; visualization, R.W. and T.W.; supervision, F.B.; project administration, F.B.; funding acquisition, F.B. All authors have read and agreed to the published version of the manuscript.

Funding: This research was funded by Deutsche Forschungsgemeinschaft (DFG, German Research Foundation) with funds from SFB1309 (Chemical Biology of Epigenetic Modifications, project ID: 325871075–SFB1309) to F.B.

Institutional Review Board Statement: Not applicable.

Informed Consent Statement: Not applicable.

Data Availability Statement: The entirety of the experimental data and protocols are stored in the university's electronic lab journal at LMU Munich.

Acknowledgments: We thank Lars Allmendinger and Claudia Glas for NMR services, Werner Spahl and Sonja Kosak for MS services, Anna Niedrig for HPLC services and Peter Mayer for X-ray crystallographic services.

Conflicts of Interest: The authors declare no conflicts of interest.

Abbreviations

The following abbreviations are used in this manuscript:

NAD^+	Nicotinamide adenine dinucleotide
IC_{50}	Half maximal inhibitory concentration
CDI	1,1′-Carbonyldiimidazole
PIFA	(Bis(trifluoroacetoxy)iodo)benzene
CuAAC	Copper-catalyzed azide-alkyne cycoladdition
LED	Light-emitting diode
FCC	Flash column chromatography
PTLC	Preparative thin-layer chromatography

References

1. Schiedel, M.; Robaa, D.; Rumpf, T.; Sippl, W.; Jung, M. The Current State of NAD+-Dependent Histone Deacetylases (Sirtuins) as Novel Therapeutic Targets. *Med. Res. Rev.* **2018**, *38*, 147–200. [CrossRef]
2. Giblin, W.; Lombard, D.B. Chapter 3—Sirtuins, Healthspan, and Longevity in Mammals. In *Handbook of the Biology of Aging*, 8th ed.; Kaeberlein, M.R., Martin, G.M., Eds.; Academic Press: Cambridge, MA, USA, 2016; pp. 83–132.
3. Nakagawa, T.; Lomb, D.J.; Haigis, M.C.; Guarente, L. SIRT5 Deacetylates carbamoyl phosphate synthetase 1 and regulates the urea cycle. *Cell* **2009**, *137*, 560–570. [CrossRef] [PubMed]
4. Lin, Z.-F.; Xu, H.-B.; Wang, J.-Y.; Lin, Q.; Ruan, Z.; Liu, F.-B.; Jin, W.; Huang, H.-H.; Chen, X. SIRT5 desuccinylates and activates SOD1 to eliminate ROS. *Biochem. Biophys. Res. Commun.* **2013**, *441*, 191–195. [CrossRef]
5. Zhang, Y.; Bharathi, S.S.; Rardin, M.J.; Uppala, R.; Verdin, E.; Gibson, B.W.; Goetzman, E.S. SIRT3 and SIRT5 regulate the enzyme activity and cardiolipin binding of very long-chain acyl-CoA dehydrogenase. *PLoS ONE* **2015**, *10*, e0122297. [CrossRef]
6. Wang, T.; Tan, G.; Jiang, M.; Liu, G.; Li, W.; Qing, X. SIRT5 inhibits glycolysis and nasal type extranodal NK/T cell lymphoma cell proliferation by catalyzing the desuccinylation of glucose-6-phosphate isomerase. *Transl. Oncol.* **2025**, *51*, 102215. [CrossRef] [PubMed]
7. Rardin, M.J.; He, W.; Nishida, Y.; Newman, J.C.; Carrico, C.; Danielson, S.R.; Guo, A.; Gut, P.; Sahu, A.K.; Li, B.; et al. SIRT5 regulates the mitochondrial lysine succinylome and metabolic networks. *Cell Metab.* **2013**, *18*, 920–933. [CrossRef]
8. Fabbrizi, E.; Fiorentino, F.; Carafa, V.; Altucci, L.; Mai, A.; Rotili, D. Emerging Roles of SIRT5 in Metabolism, Cancer, and SARS-CoV-2 Infection. *Cells* **2023**, *12*, 852. [CrossRef]
9. Liu, L.; Peritore, C.; Ginsberg, J.; Shih, J.; Arun, S.; Donmez, G. Protective role of SIRT5 against motor deficit and dopaminergic degeneration in MPTP-induced mice model of Parkinson's disease. *Behav. Brain Res.* **2015**, *281*, 215–221. [CrossRef]
10. Lutz, M.I.; Milenkovic, I.; Regelsberger, G.; Kovacs, G.G. Distinct patterns of sirtuin expression during progression of Alzheimer's disease. *Neuromol Med.* **2014**, *16*, 405–414. [CrossRef]
11. Greene, K.S.; Lukey, M.J.; Wang, X.; Blank, B.; Druso, J.E.; Lin, M.J.; Stalnecker, C.A.; Zhang, C.; Negrón Abril, Y.; Erickson, J.W.; et al. SIRT5 stabilizes mitochondrial glutaminase and supports breast cancer tumorigenesis. *Proc. Natl. Acad. Sci. USA* **2019**, *116*, 26625–26632. [CrossRef] [PubMed]
12. Wang, Y.Q.; Wang, H.L.; Xu, J.; Tan, J.; Fu, L.N.; Wang, J.L.; Zou, T.H.; Sun, D.F.; Gao, Q.Y.; Chen, Y.X.; et al. Sirtuin5 contributes to colorectal carcinogenesis by enhancing glutaminolysis in a deglutarylation-dependent manner. *Nat. Commun.* **2018**, *9*, 545. [CrossRef] [PubMed]
13. Lu, W.; Zuo, Y.; Feng, Y.; Zhang, M. SIRT5 facilitates cancer cell growth and drug resistance in non-small cell lung cancer. *Tumour Biol.* **2014**, *35*, 10699–10705. [CrossRef] [PubMed]

14. Suenkel, B.; Fischer, F.; Steegborn, C. Inhibition of the human deacylase Sirtuin 5 by the indole GW5074. *Bioorg Med. Chem. Lett.* **2013**, *23*, 143–146. [CrossRef]
15. Trapp, J.; Jochum, A.; Meier, R.; Saunders, L.; Marshall, B.; Kunick, C.; Verdin, E.; Goekjian, P.; Sippl, W.; Jung, M. Adenosine Mimetics as Inhibitors of NAD+-Dependent Histone Deacetylases, from Kinase to Sirtuin Inhibition. *J. Med. Chem.* **2006**, *49*, 7307–7316. [CrossRef]
16. Maurer, B.; Rumpf, T.; Scharfe, M.; Stolfa, D.A.; Schmitt, M.L.; He, W.; Verdin, E.; Sippl, W.; Jung, M. Inhibitors of the NAD(+)-Dependent Protein Desuccinylase and Demalonylase Sirt5. *ACS Med. Chem. Lett.* **2012**, *3*, 1050–1053. [CrossRef]
17. Liu, S.; Ji, S.; Yu, Z.J.; Wang, H.L.; Cheng, X.; Li, W.J.; Jing, L.; Yu, Y.; Chen, Q.; Yang, L.L.; et al. Structure-based discovery of new selective small-molecule sirtuin 5 inhibitors. *Chem. Biol. Drug Des.* **2018**, *91*, 257–268. [CrossRef]
18. Baell, J.B.; Holloway, G.A. New Substructure Filters for Removal of Pan Assay Interference Compounds (PAINS) from Screening Libraries and for Their Exclusion in Bioassays. *J. Med. Chem.* **2010**, *53*, 2719–2740. [CrossRef]
19. Guetschow, E.D.; Kumar, S.; Lombard, D.B.; Kennedy, R.T. Identification of sirtuin 5 inhibitors by ultrafast microchip electrophoresis using nanoliter volume samples. *Anal. Bioanal. Chem.* **2016**, *408*, 721–731. [CrossRef]
20. Muijsers, R.B.R.; Goa, K.L. Balsalazide. *Drugs* **2002**, *62*, 1689–1705. [CrossRef] [PubMed]
21. Glas, C.; Dietschreit, J.C.B.; Wössner, N.; Urban, L.; Ghazy, E.; Sippl, W.; Jung, M.; Ochsenfeld, C.; Bracher, F. Identification of the subtype-selective Sirt5 inhibitor balsalazide through systematic SAR analysis and rationalization via theoretical investigations. *Eur. J. Med. Chem.* **2020**, *206*, 112676. [CrossRef] [PubMed]
22. Glas, C.; Naydenova, E.; Lechner, S.; Wössner, N.; Yang, L.; Dietschreit, J.C.B.; Sun, H.; Jung, M.; Kuster, B.; Ochsenfeld, C.; et al. Development of hetero-triaryls as a new chemotype for subtype-selective and potent Sirt5 inhibition. *Eur. J. Med. Chem.* **2022**, *240*, 114594. [CrossRef]
23. Wirawan, R.; Frei, M.; Heider, A.; Papenkordt, N.; Friedrich, F.; Wein, T.; Jung, M.; Groll, M.; Huber, E.M.; Bracher, F. Tailored SirReal-type inhibitors enhance SIRT2 inhibition through ligand stabilization and disruption of NAD+ co-factor binding. *RSC Med. Chem.* **2025**. *online ahead of print*. [CrossRef]
24. Groll, M.; Berkers, C.R.; Ploegh, H.L.; Ovaa, H. Crystal structure of the boronic acid-based proteasome inhibitor bortezomib in complex with the yeast 20S proteasome. *Structure* **2006**, *14*, 451–456. [CrossRef]
25. Beck, P.; Dubiella, C.; Groll, M. Covalent and non-covalent reversible proteasome inhibition. *Biol. Chem.* **2012**, *393*, 1101–1120. [CrossRef] [PubMed]
26. Wang, Y.-H.; Zhang, F.; Diao, H.; Wu, R. Covalent Inhibition Mechanism of Antidiabetic Drugs—Vildagliptin vs. Saxagliptin. *ACS Catal.* **2019**, *9*, 2292–2302. [CrossRef]
27. Oksenberg, D.; Dufu, K.; Patel, M.P.; Chuang, C.; Li, Z.; Xu, Q.; Silva-Garcia, A.; Zhou, C.; Hutchaleelaha, A.; Patskovska, L.; et al. GBT440 increases haemoglobin oxygen affinity, reduces sickling and prolongs RBC half-life in a murine model of sickle cell disease. *Br. J. Haematol.* **2016**, *175*, 141–153. [CrossRef] [PubMed]
28. Boike, L.; Henning, N.J.; Nomura, D.K. Advances in covalent drug discovery. *Nat. Rev. Drug Discov.* **2022**, *21*, 881–898. [CrossRef] [PubMed]
29. Farooqi, A.S.; Hong, J.Y.; Cao, J.; Lu, X.; Price, I.R.; Zhao, Q.; Kosciuk, T.; Yang, M.; Bai, J.J.; Lin, H. Novel Lysine-Based Thioureas as Mechanism-Based Inhibitors of Sirtuin 2 (SIRT2) with Anticancer Activity in a Colorectal Cancer Murine Model. *J. Med. Chem.* **2019**, *62*, 4131–4141. [CrossRef]
30. Du, J.; Zhou, Y.; Su, X.; Yu, J.J.; Khan, S.; Jiang, H.; Kim, J.; Woo, J.; Kim, J.H.; Choi, B.H.; et al. Sirt5 Is a NAD-Dependent Protein Lysine Demalonylase and Desuccinylase. *Science* **2011**, *334*, 806–809. [CrossRef]
31. Isernia, C.; Bucci, E.M.; Napoli, L.d.; Lello, P.D.; Iacovino, R.; Montesarchio, D.; Piccialli, G.; Rossi, F.; Saviano, M.; Benedetti, E. Synthesis and conformation of dipeptide taste ligands containing homo-β-amino acid residues. *J. Phys. Org. Chem.* **1999**, *12*, 577–587. [CrossRef]
32. Röhrich, T.; Abu Thaher, B.; Manicone, N.; Otto, H.-H. Substituted 1,2-Thiazetidine 1,1-Dioxides. Synthesis of (RS)- and (S)-1,2-Thiazetidine-3-acetic Acid 1,1-Dioxide and its Reactions with Amino Acids and Dipeptides. *Monatsh Chem.* **2004**, *135*, 979–999. [CrossRef]
33. Klein, P.; Barthels, F.; Johe, P.; Wagner, A.; Tenzer, S.; Distler, U.; Le, T.A.; Schmid, P.; Engel, V.; Engels, B.; et al. Naphthoquinones as Covalent Reversible Inhibitors of Cysteine Proteases-Studies on Inhibition Mechanism and Kinetics. *Molecules* **2020**, *25*, 2064. [CrossRef]
34. Yang, C.-T.; Zhang, Z.-Q.; Tajuddin, H.; Wu, C.-C.; Liang, J.; Liu, J.-H.; Fu, Y.; Czyzewska, M.; Steel, P.G.; Marder, T.B.; et al. Alkylboronic Esters from Copper-Catalyzed Borylation of Primary and Secondary Alkyl Halides and Pseudohalides. *Angew. Chem. Int. Ed.* **2012**, *51*, 528–532. [CrossRef] [PubMed]
35. Ito, H.; Kubota, K. Copper(I)-Catalyzed Boryl Substitution of Unactivated Alkyl Halides. *Org. Lett.* **2012**, *14*, 890–893. [CrossRef]
36. Dudnik, A.S.; Fu, G.C. Nickel-Catalyzed Coupling Reactions of Alkyl Electrophiles, Including Unactivated Tertiary Halides, To Generate Carbon–Boron Bonds. *J. Am. Chem. Soc.* **2012**, *134*, 10693–10697. [CrossRef] [PubMed]

37. Joshi-Pangu, A.; Ma, X.; Diane, M.; Iqbal, S.; Kribs, R.J.; Huang, R.; Wang, C.-Y.; Biscoe, M.R. Palladium-Catalyzed Borylation of Primary Alkyl Bromides. *J. Org. Chem.* **2012**, *77*, 6629–6633. [CrossRef]
38. Ursinyova, N.; Bedford, R.B.; Gallagher, T. Copper-Catalyzed Borylation of Cyclic Sulfamidates: Access to Enantiomerically Pure (β-and γ-Aminoalkyl)boronic Esters. *Eur. J. Org. Chem.* **2016**, *2016*, 673–677. [CrossRef]
39. Hitosugi, S.; Tanimoto, D.; Nakanishi, W.; Isobe, H. A Facile Chromatographic Method for Purification of Pinacol Boronic Esters. *Chem. Lett.* **2012**, *41*, 972–973. [CrossRef]
40. Lang, S.B.; O'Nele, K.M.; Douglas, J.T.; Tunge, J.A. Dual Catalytic Decarboxylative Allylations of α-Amino Acids and Their Divergent Mechanisms. *Chem. Eur. J.* **2015**, *21*, 18589–18593. [CrossRef]
41. Schuetz, A.; Min, J.; Antoshenko, T.; Wang, C.L.; Allali-Hassani, A.; Dong, A.; Loppnau, P.; Vedadi, M.; Bochkarev, A.; Sternglanz, R.; et al. Structural basis of inhibition of the human NAD+-dependent deacetylase SIRT5 by suramin. *Structure* **2007**, *15*, 377–389. [CrossRef]
42. Yang, L.-L.; Wang, H.-L.; Yan, Y.-H.; Liu, S.; Yu, Z.-J.; Huang, M.-Y.; Luo, Y.; Zheng, X.; Yu, Y.; Li, G.-B. Sensitive fluorogenic substrates for sirtuin deacylase inhibitor discovery. *Eur. J. Med. Chem.* **2020**, *192*, 112201. [CrossRef] [PubMed]
43. Jawalekar, A.M.; Reubsaet, E.; Rutjes, F.P.J.T.; van Delft, F.L. Synthesis of isoxazoles by hypervalent iodine-induced cycloaddition of nitrile oxides to alkynes. *Chem. Commun.* **2011**, *47*, 3198–3200. [CrossRef]
44. Friesner, R.A.; Banks, J.L.; Murphy, R.B.; Halgren, T.A.; Klicic, J.J.; Mainz, D.T.; Repasky, M.P.; Knoll, E.H.; Shelley, M.; Perry, J.K.; et al. Glide: A new approach for rapid, accurate docking and scoring. 1. Method and assessment of docking accuracy. *J. Med. Chem.* **2004**, *47*, 1739–1749. [CrossRef]
45. Berman, H.M.; Westbrook, J.; Feng, Z.; Gilliland, G.; Bhat, T.N.; Weissig, H.; Shindyalov, I.N.; Bourne, P.E. The Protein Data Bank. *Nucleic Acids Res.* **2000**, *28*, 235–242. [CrossRef]
46. Shelley, J.C.; Cholleti, A.; Frye, L.L.; Greenwood, J.R.; Timlin, M.R.; Uchimaya, M. Epik: A software program for pK(a) prediction and protonation state generation for drug-like molecules. *J. Comput. Aided Mol. Des.* **2007**, *21*, 681–691. [CrossRef]
47. Bruker. *SAINT*; Bruker AXS Inc.: Madison, WI, USA, 2012.
48. Sheldrick, G.M. *SADABS*; University of Göttingen: Göttingen, Germany, 1996.
49. Sheldrick, G.M. SHELXT—Integrated space-group and crystal-structure determination. *Acta Cryst. A* **2015**, *A71*, 3–8. [CrossRef] [PubMed]
50. Farrugia, L.J. WinGX and ORTEP for Windows: An update. *J. Appl. Cryst.* **2012**, *45*, 849–854. [CrossRef]

Supporting Information

Balsalazide-Derived Heterotriaryls as Sirtuin 5 Inhibitors: A Case Study of a Reversible Covalent Inhibition Strategy

Ricky Wirawan, Simon A. Huber, Thomas Wein and Franz Bracher *

Department of Pharmacy—Center for Drug Research, Ludwig-Maximilians University, Butenandtstr. 5-13, 81377 Munich, Germany; ricky.wirawan@cup.uni-muenchen.de (R.W.); simon.huber@campus.lmu.de (S.A.H.); thomas.wein@cup.uni-muenchen.de (T.W.)
* Correspondence: franz.bracher@cup.uni-muenchen.de; Tel.: +49-89-218077301

Contents:

S1. ^{1}H and ^{13}C NMR spectra of synthesized compounds

^{1}H and ^{13}C NMR spectra of benzyl (*R*)-3-((*tert*-butoxycarbonyl)amino)-4-(4,4,5,5-tetramethyl-1,3,2-dioxaborolan-2-yl)butanoate (**20**).

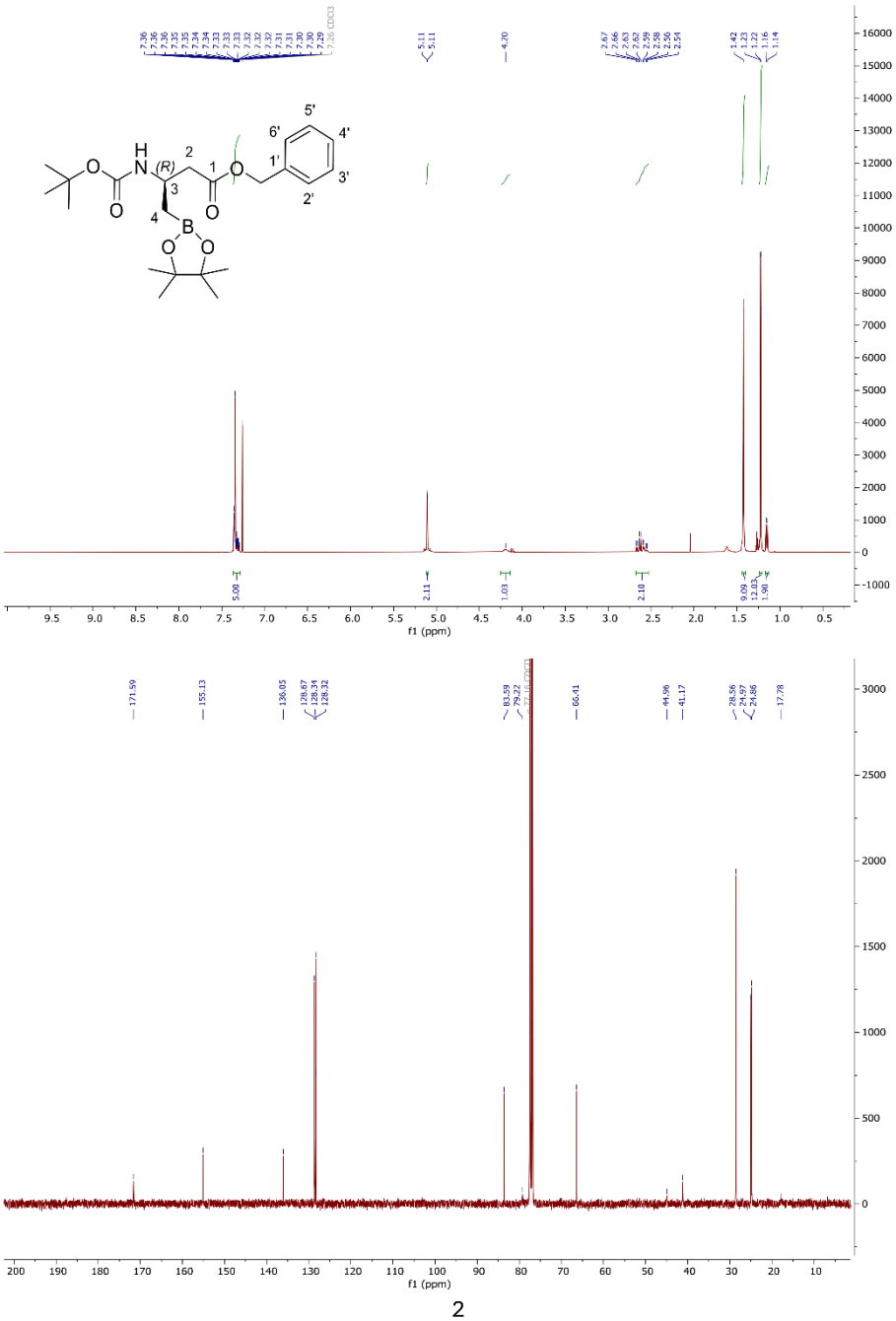

2

^{1}H and ^{13}C NMR spectra of benzyl (*S*)-3-((*tert*-butoxycarbonyl)amino)-4-(4,4,5,5-tetramethyl-1,3,2-dioxaborolan-2-yl)butanoate (**21**).

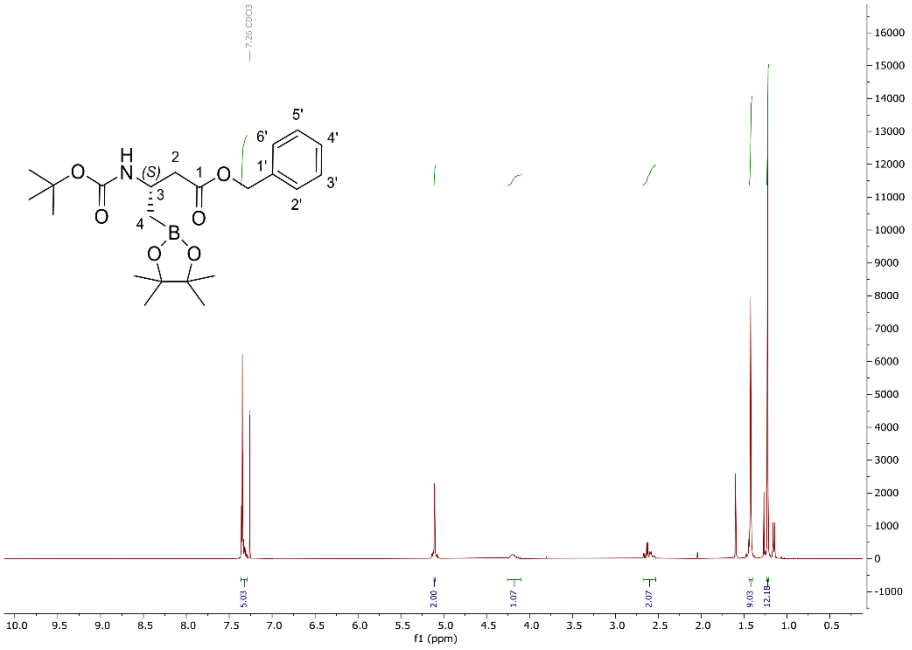

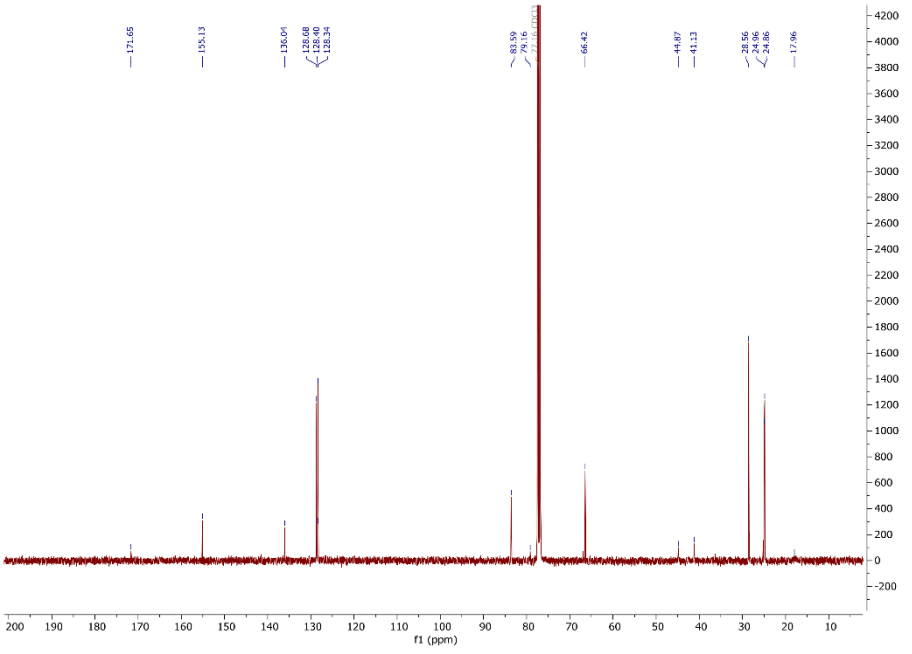

^{1}H and ^{13}C NMR spectra of (*R*)-4-(benzyloxy)-4-oxo-1-(4,4,5,5-tetramethyl-1,3,2-dioxaborolan-2-yl)butan-2-aminium (**24**).

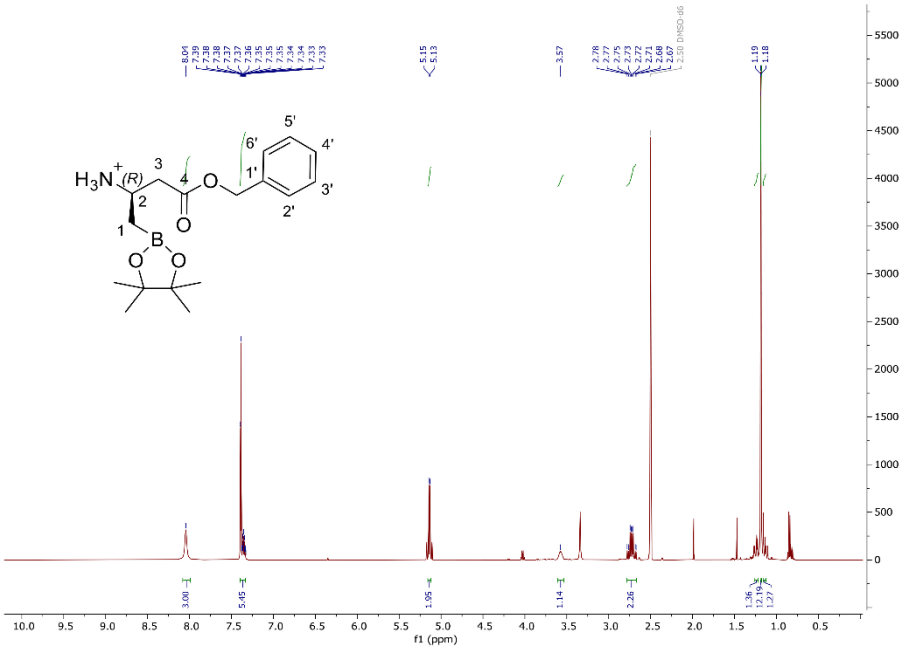

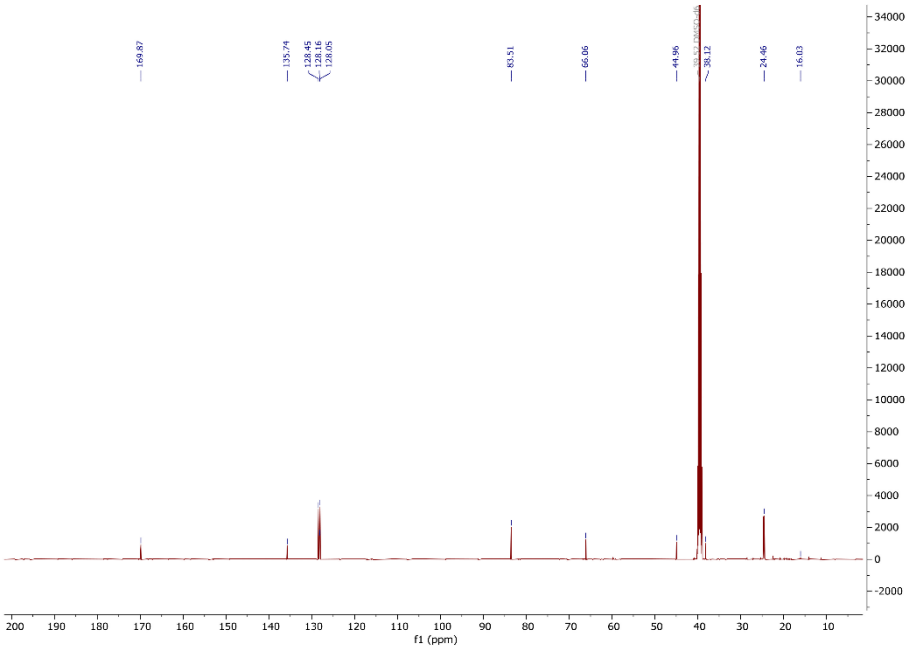

^{1}H and ^{13}C NMR spectra of (*S*)-4-(benzyloxy)-4-oxo-1-(4,4,5,5-tetramethyl-1,3,2-dioxaborolan-2-yl)butan-2-aminium (**25**).

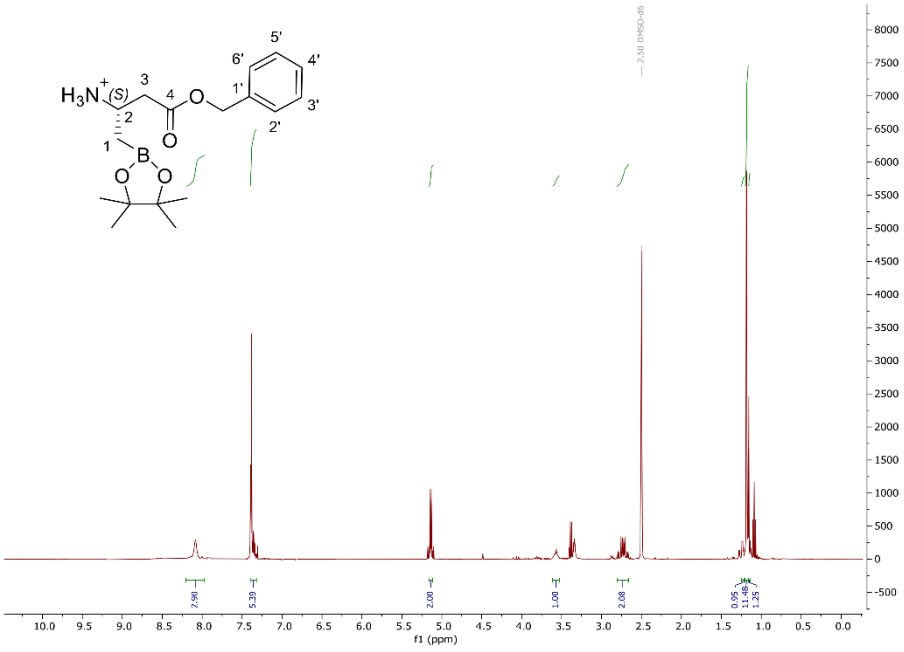

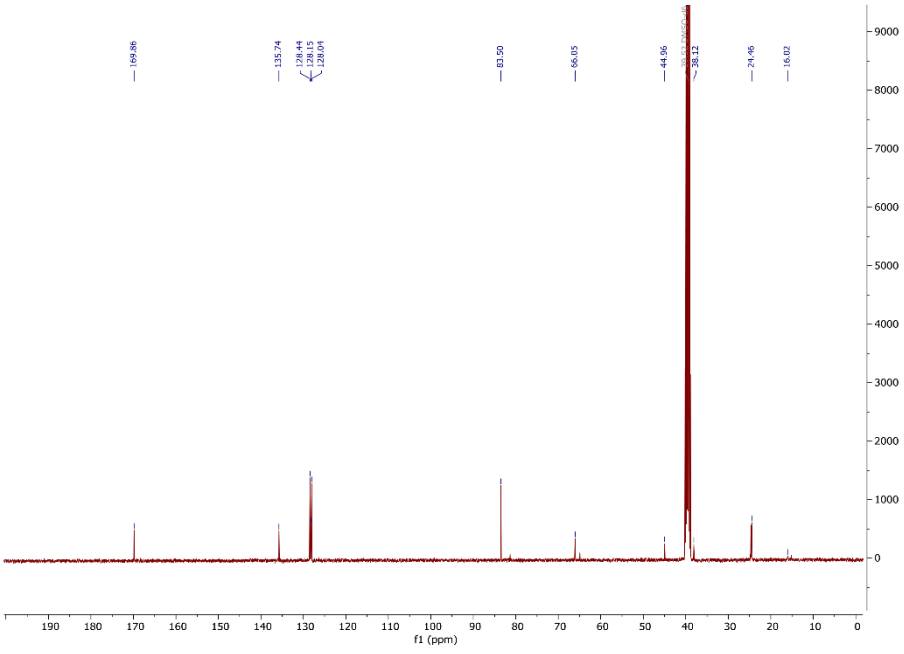

^{1}H and ^{13}C NMR spectra of (*R*)-4-(benzyloxy)-1-cyano-4-oxobutan-2-aminium (**26**).

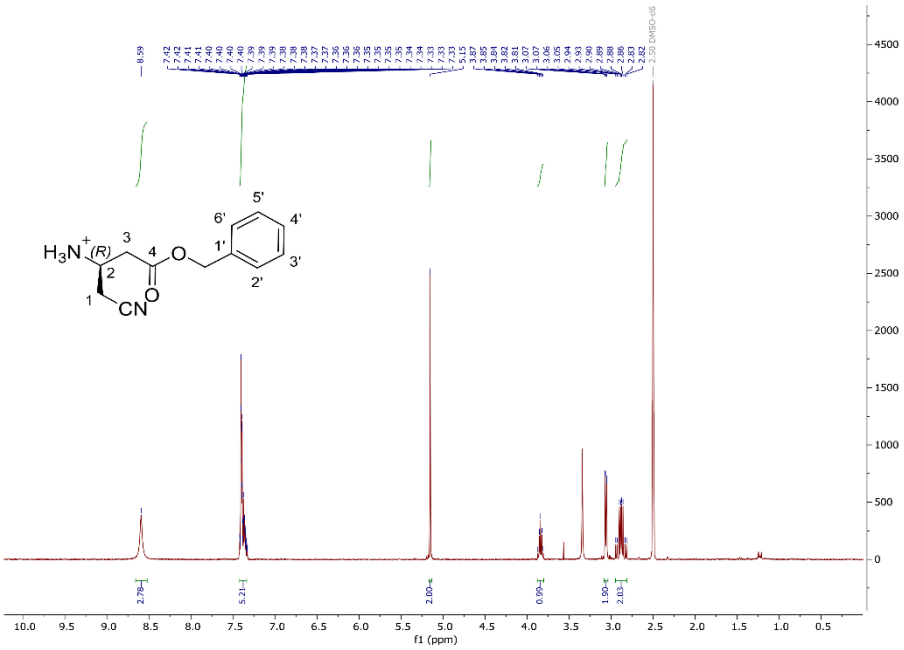

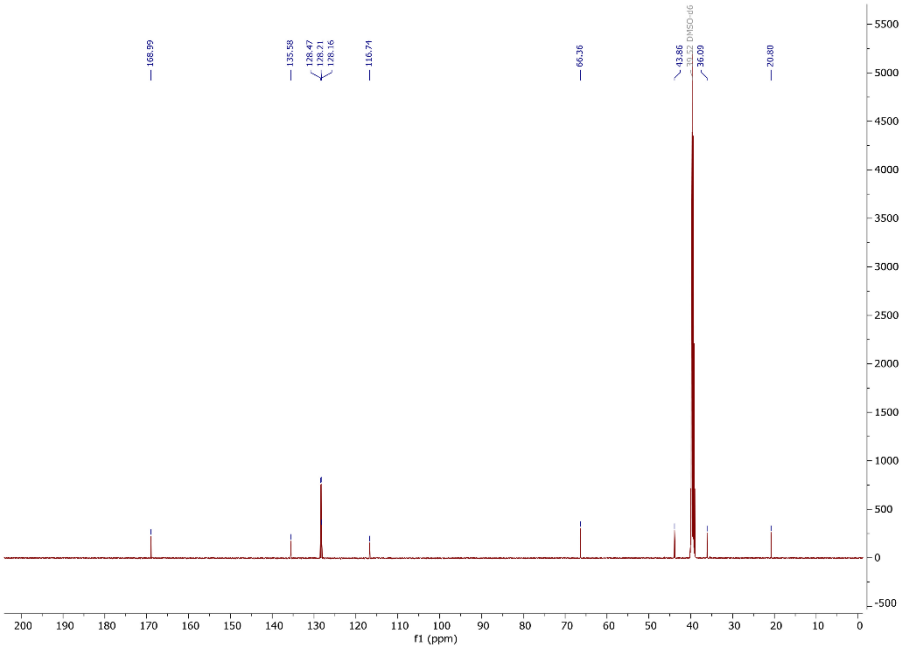

^{1}H and ^{13}C NMR spectra of (*S*)-4-(benzyloxy)-1-cyano-4-oxobutan-2-aminium (**27**).

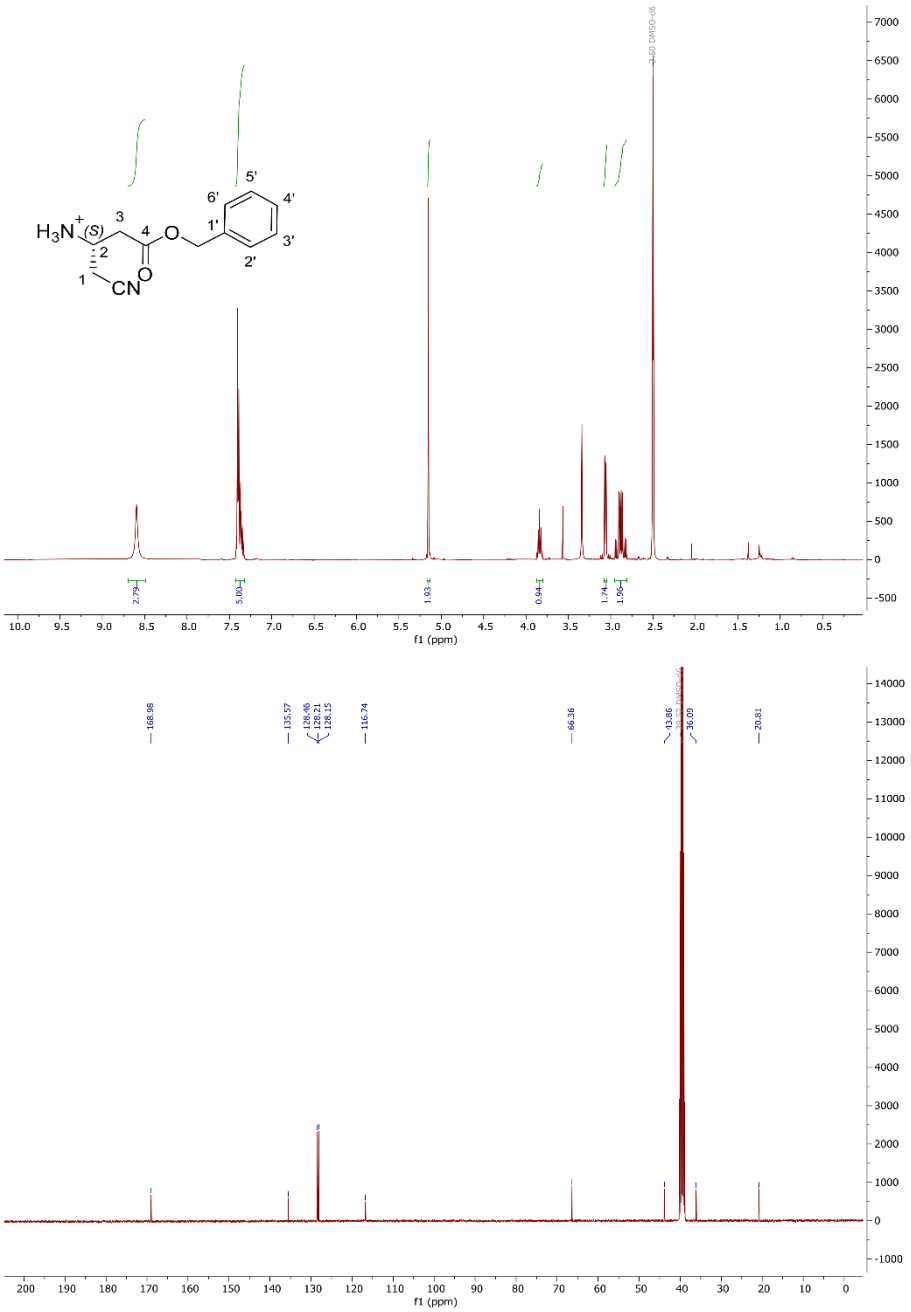

^{1}H and ^{13}C NMR spectra of benzyl (*R*)-3-(4-ethynylbenzamido)-4-(4,4,5,5-tetramethyl-1,3,2-dioxaborolan-2-yl)butanoate (**28**).

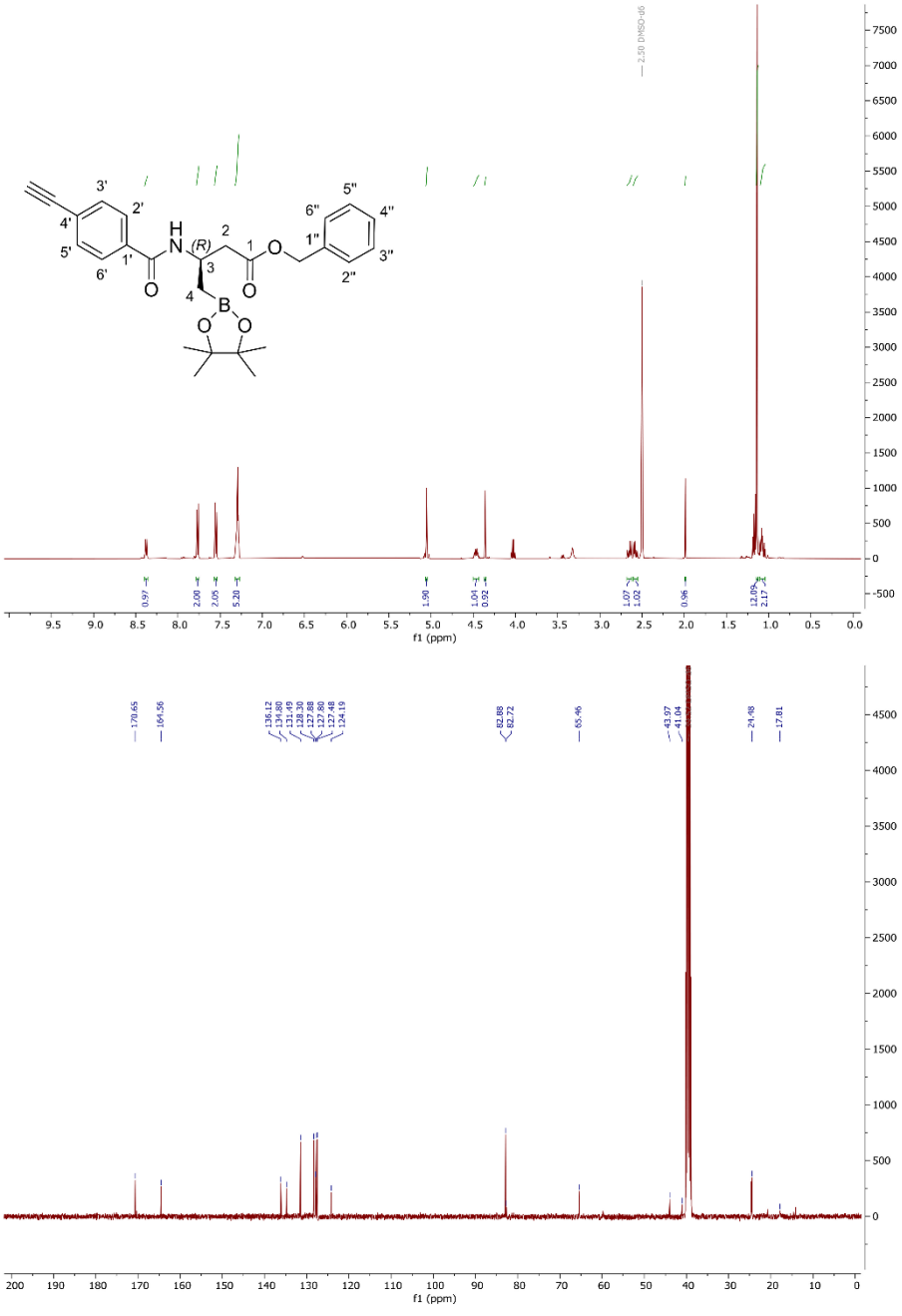

^{1}H and ^{13}C NMR spectra of benzyl (*S*)-3-(4-ethynylbenzamido)-4-(4,4,5,5-tetramethyl-1,3,2-dioxaborolan-2-yl)butanoate (**29**).

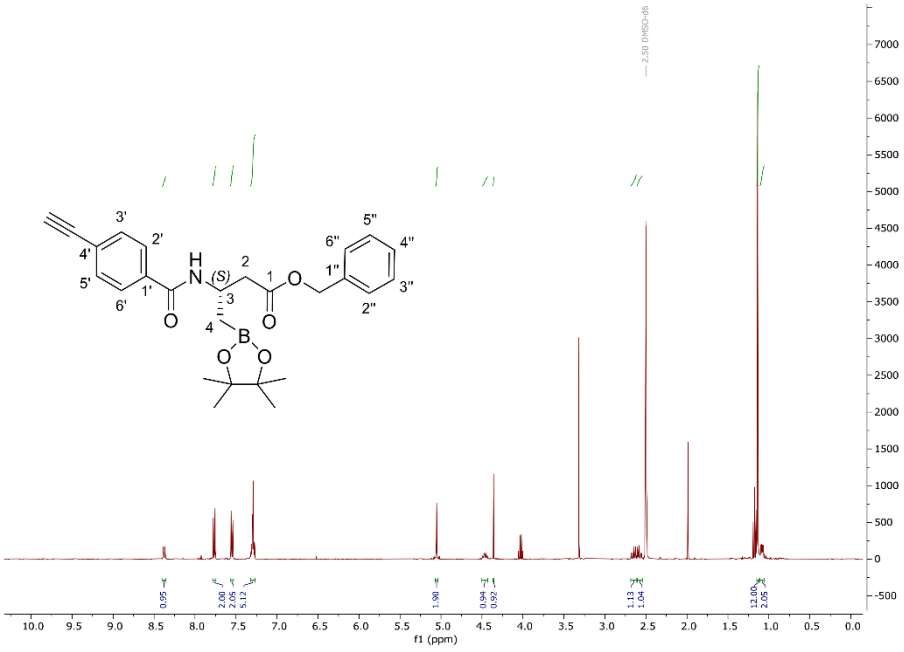

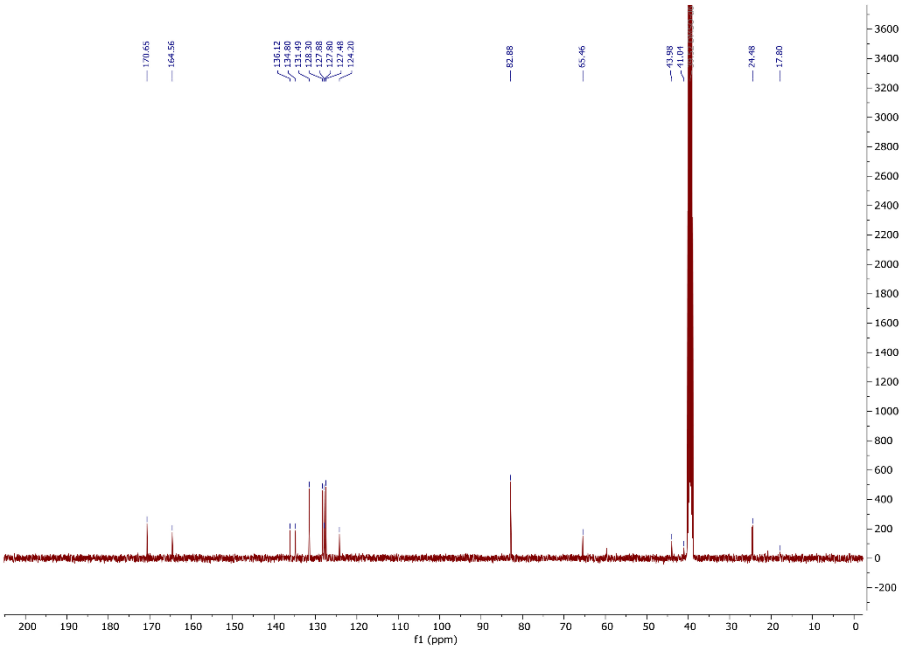

^{1}H and ^{13}C NMR spectra of benzyl (*R*)-4-cyano-3-(4-ethynylbenzamido)butanoate (**30**).

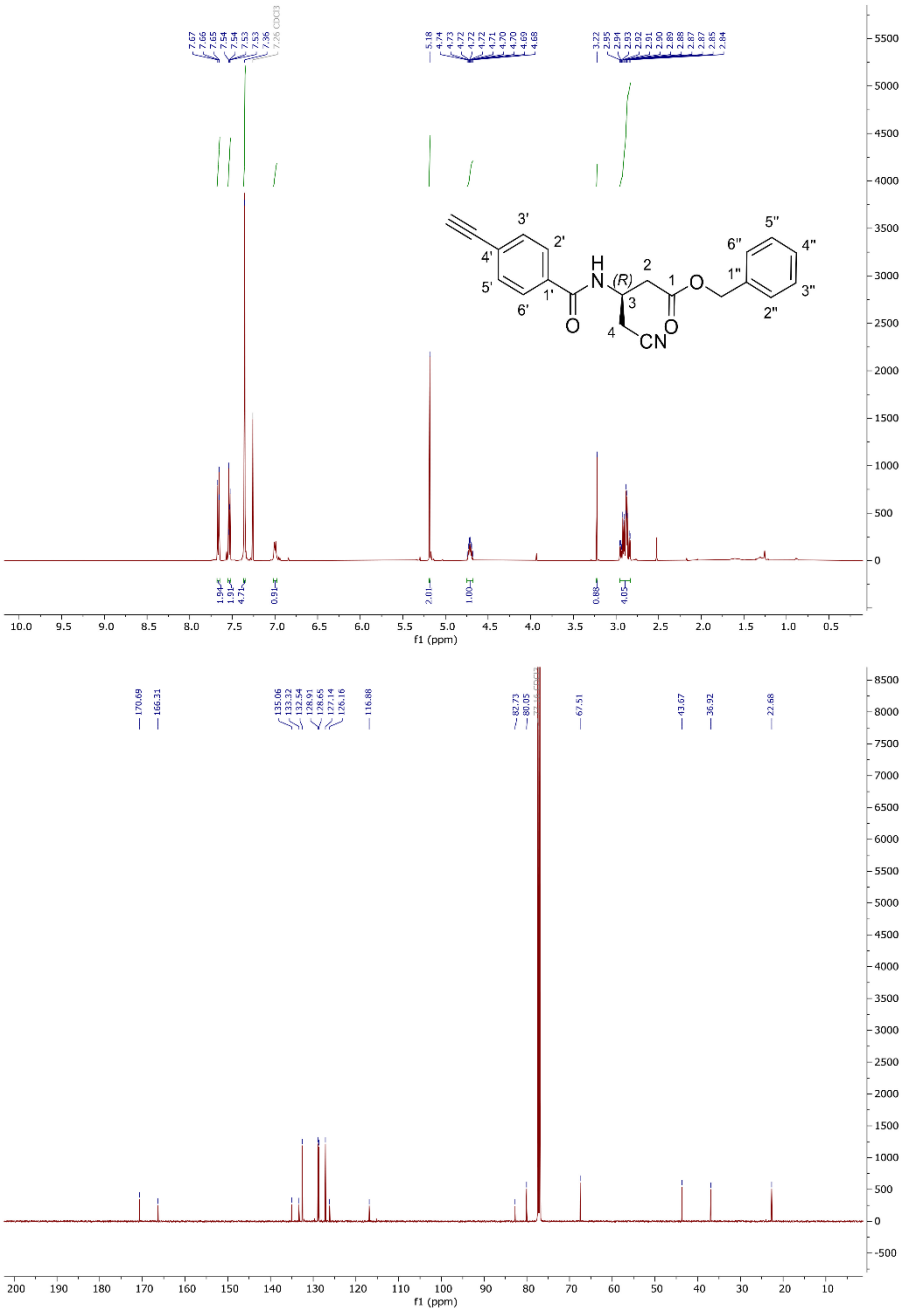

^{1}H and ^{13}C NMR spectra of benzyl (*S*)-4-cyano-3-(4-ethynylbenzamido)butanoate (**31**).

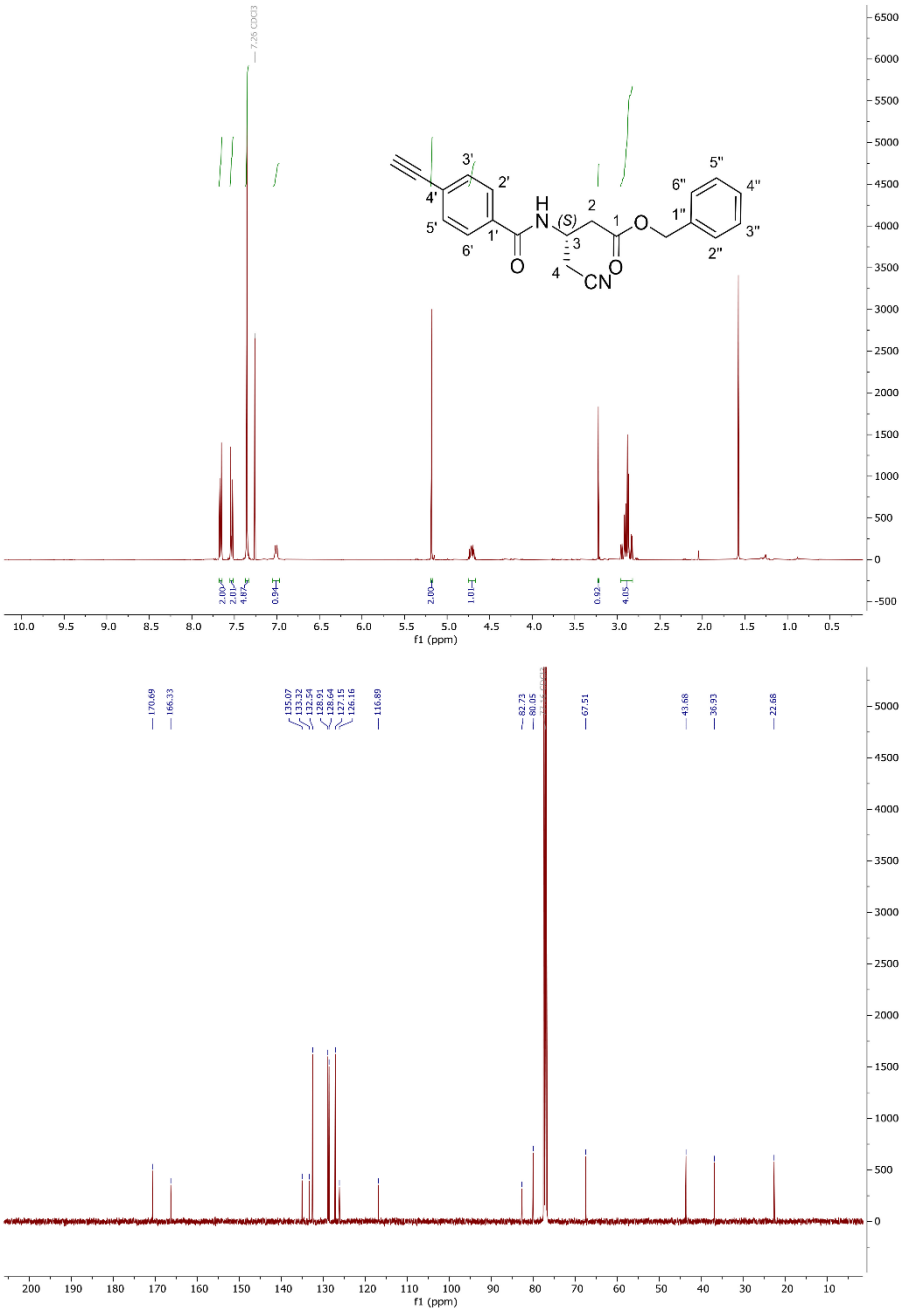

^{1}H and ^{13}C NMR spectra of methyl (*R*)-3-(4-(3-(2,2-dimethyl-4-oxo-4*H*-benzo[*d*][1,3]dioxin-6-yl)isoxazol-5-yl)benzamido)-4-(4,4,5,5-tetramethyl-1,3,2-dioxaborolan-2-yl)butanoate (**32**).

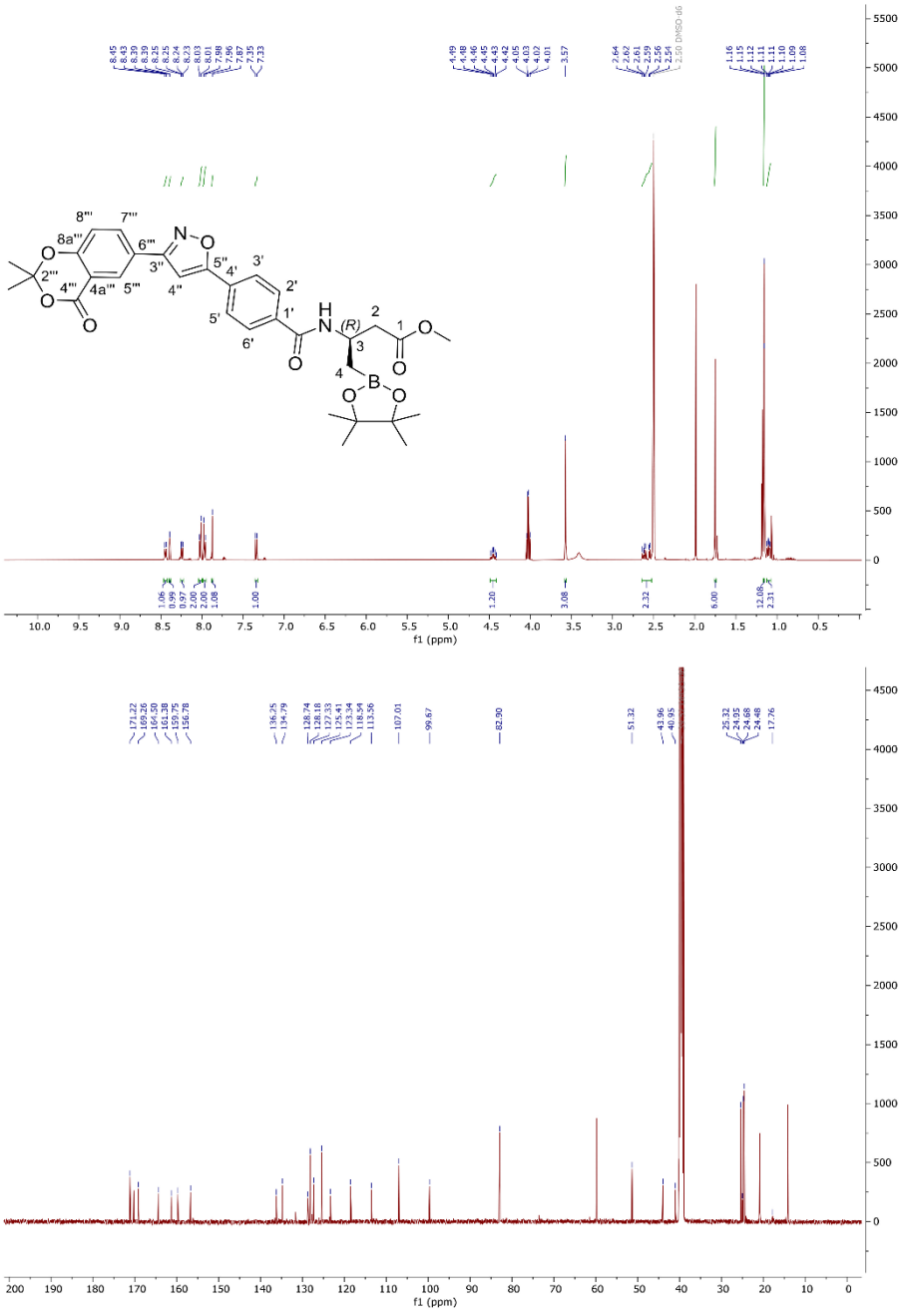

^{1}H and ^{13}C NMR spectra of methyl (*S*)-3-(4-(3-(2,2-dimethyl-4-oxo-4*H*-benzo[*d*][1,3]dioxin-6-yl)isoxazol-5-yl)benzamido)-4-(4,4,5,5-tetramethyl-1,3,2-dioxaborolan-2-yl)butanoate (**33**).

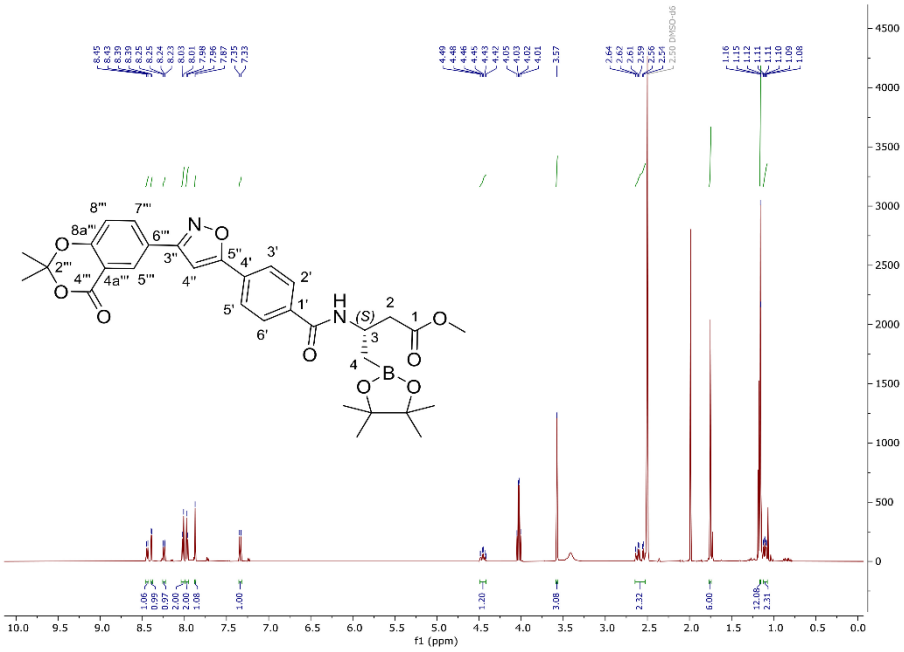

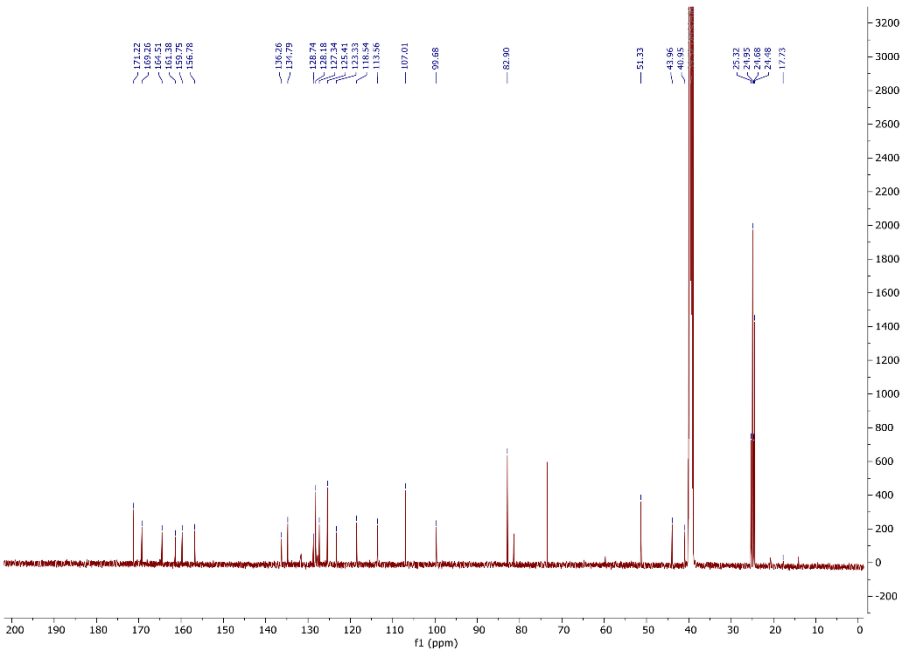

^{1}H and ^{13}C NMR spectra of benzyl (*R*)-4-cyano-3-(4-(3-(2,2-dimethyl-4-oxo-4*H*-benzo[*d*][1,3]dioxin-6-yl)isoxazol-5-yl)benzamido)butanoate (**34**).

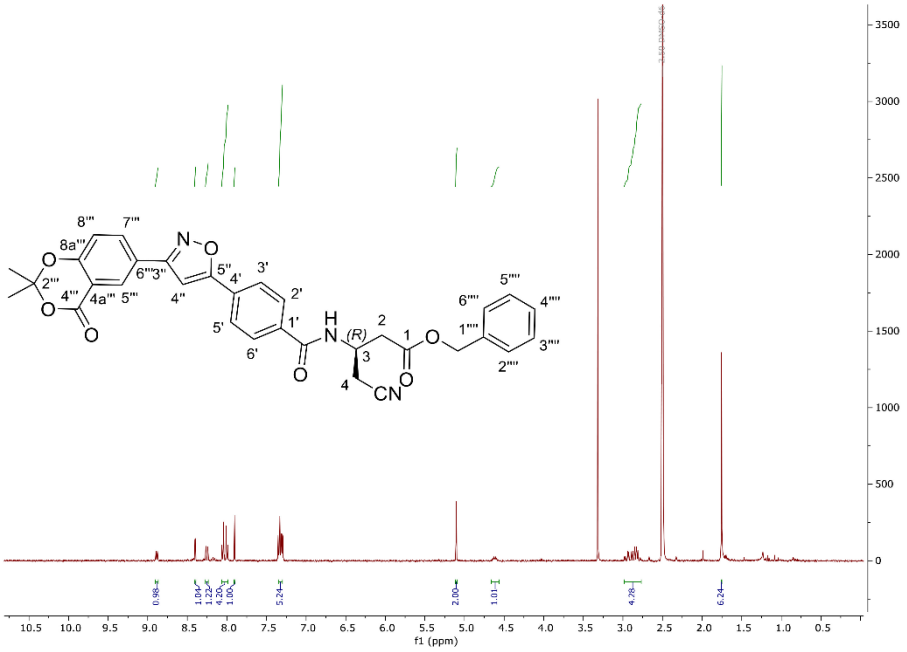

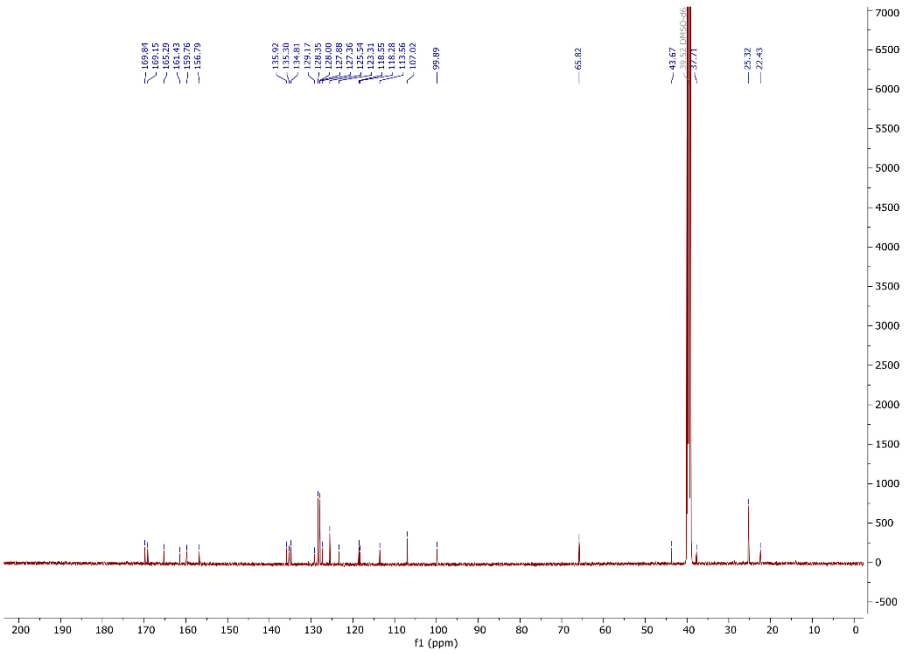

^{1}H and ^{13}C NMR spectra of benzyl (*S*)-4-cyano-3-(4-(3-(2,2-dimethyl-4-oxo-4*H*-benzo[*d*][1,3]dioxin-6-yl)isoxazol-5-yl)benzamido)butanoate (**35**).

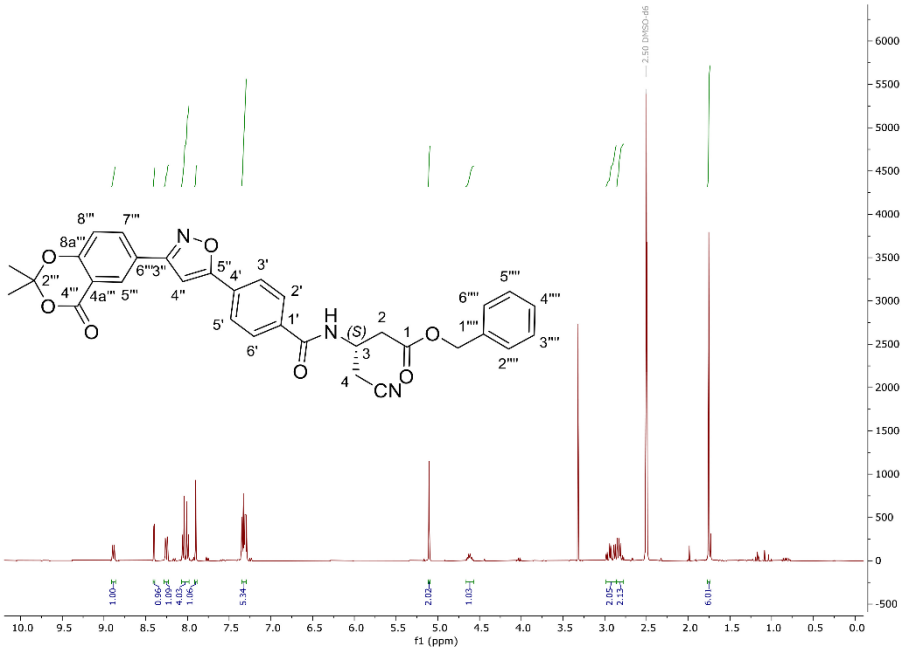

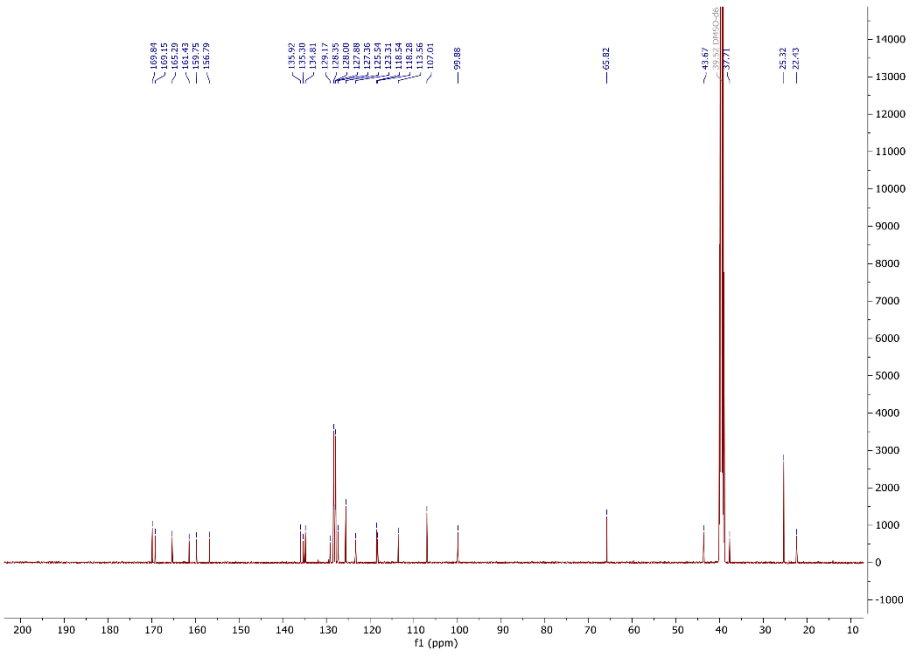

^{1}H and ^{13}C NMR spectra of (*R*)-(2-(4-(3-(2,2-dimethyl-4-oxo-4*H*-benzo[*d*][1,3]dioxin-6-yl)isoxazol-5-yl)benzamido)-4-methoxy-4-oxobutyl)boronic acid (**36**).

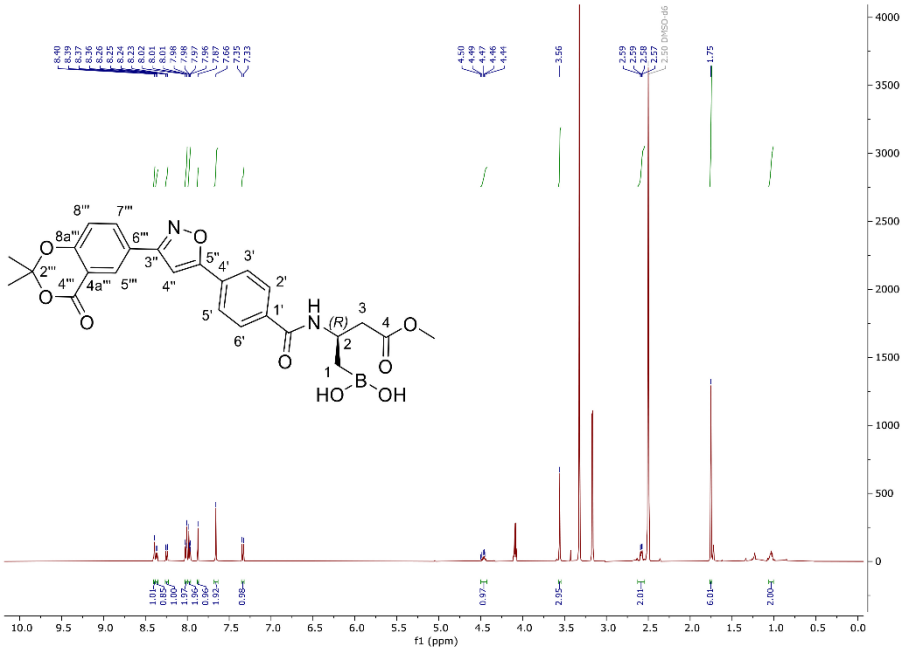

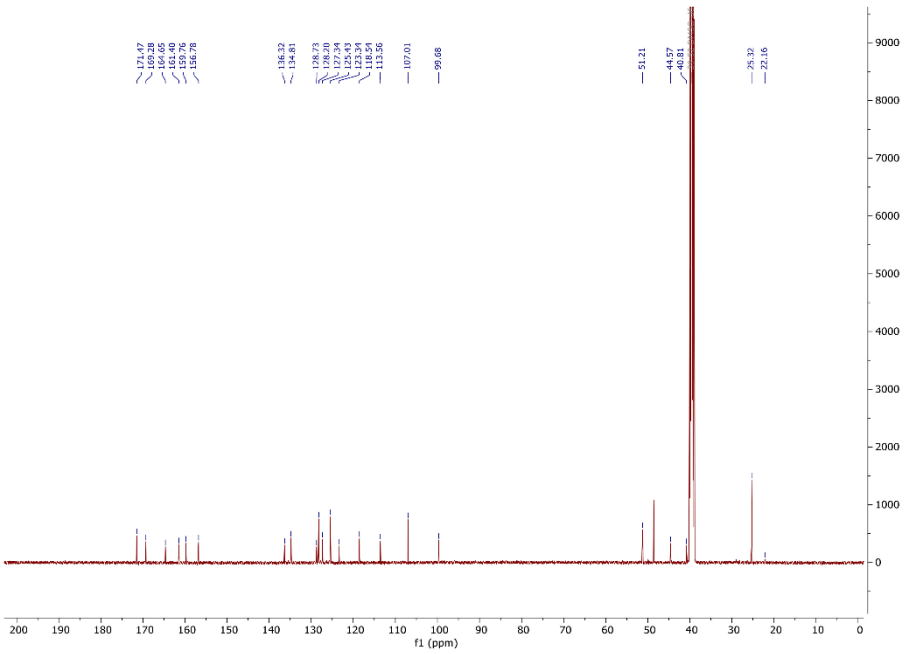

^{1}H and ^{13}C NMR spectra of (*S*)-(2-(4-(3-(2,2-Dimethyl-4-oxo-4*H*-benzo[*d*][1,3]dioxin-6-yl)isoxazol-5-yl)benzamido)-4-methoxy-4-oxobutyl)boronic acid (**37**).

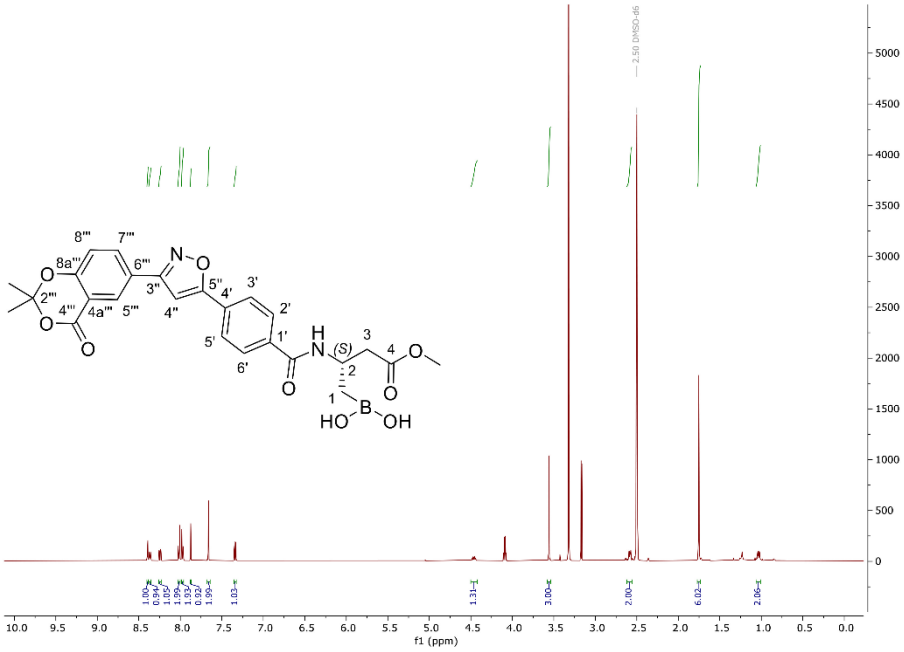

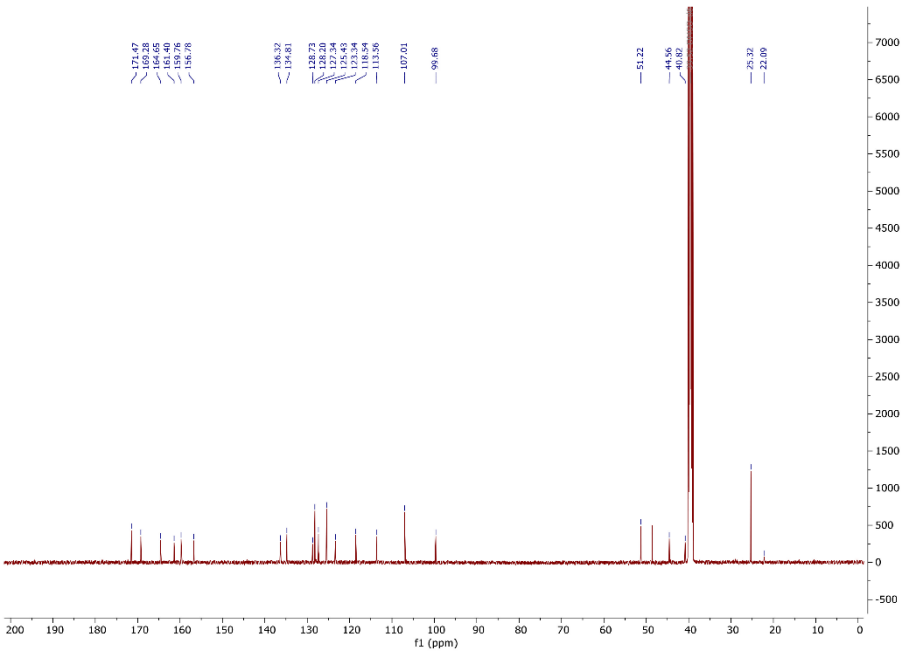

^{1}H and ^{13}C NMR spectra of benzyl (*R*)-3-(4-(1-(2,2-dimethyl-4-oxo-4*H*-benzo[*d*][1,3]dioxin-6-yl)-1*H*-1,2,3-triazol-4-yl)benzamido)-4-(4,4,5,5-tetramethyl-1,3,2-dioxaborolan-2-yl)butanoate (**38**).

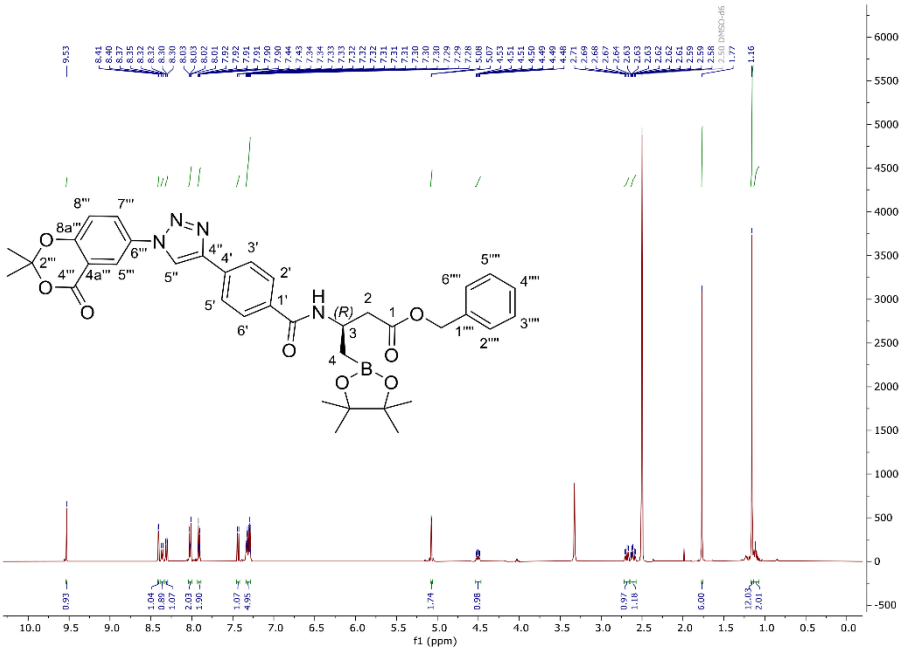

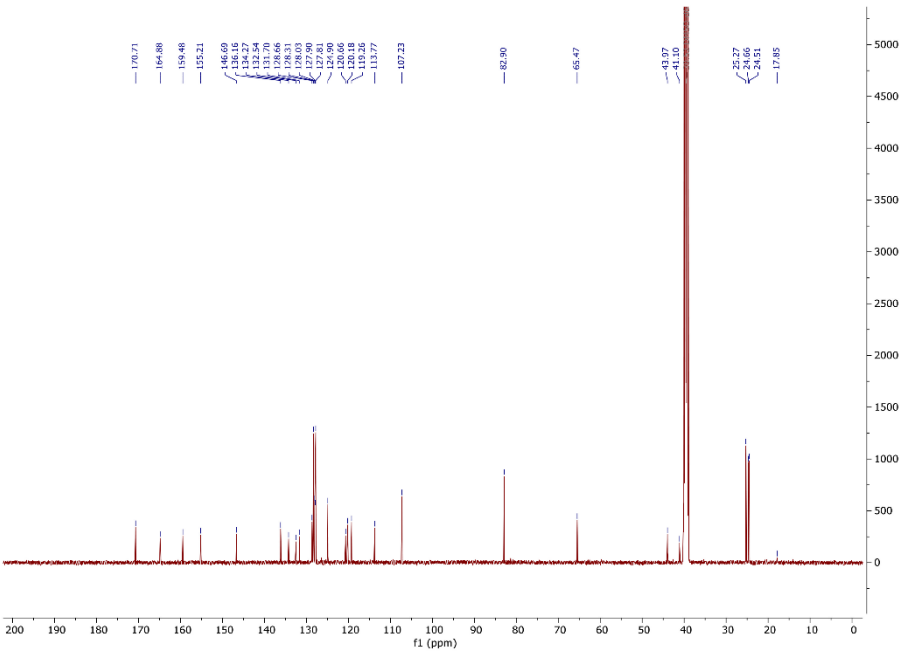

^{1}H and ^{13}C NMR spectra of benzyl (*S*)-3-(4-(1-(2,2-dimethyl-4-oxo-4*H*-benzo[*d*][1,3]dioxin-6-yl)-1*H*-1,2,3-triazol-4-yl)benzamido)-4-(4,4,5,5-tetramethyl-1,3,2-dioxaborolan-2-yl)butanoate (**39**).

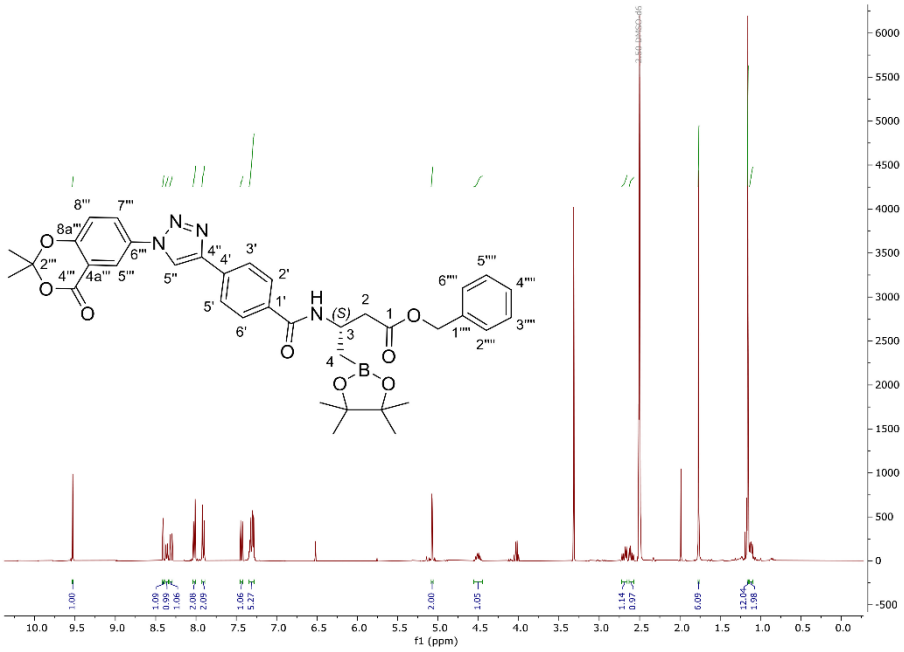

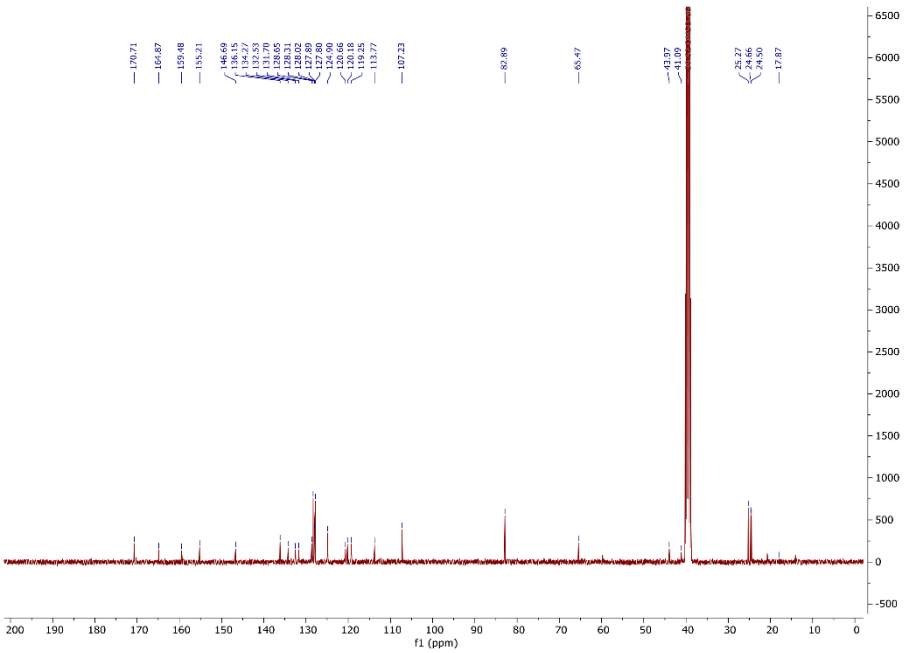

^{1}H and ^{13}C NMR spectra of benzyl (*R*)-4-cyano-3-(4-(1-(2,2-dimethyl-4-oxo-4*H*-benzo[*d*][1,3]dioxin-6-yl)-1*H*-1,2,3-triazol-4-yl)benzamido)butanoate (**40**).

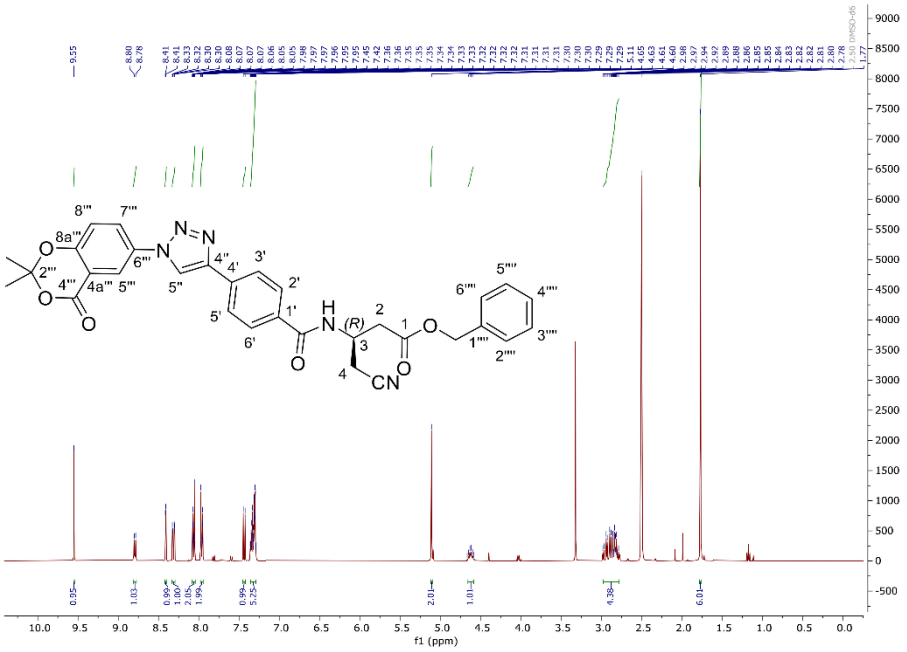

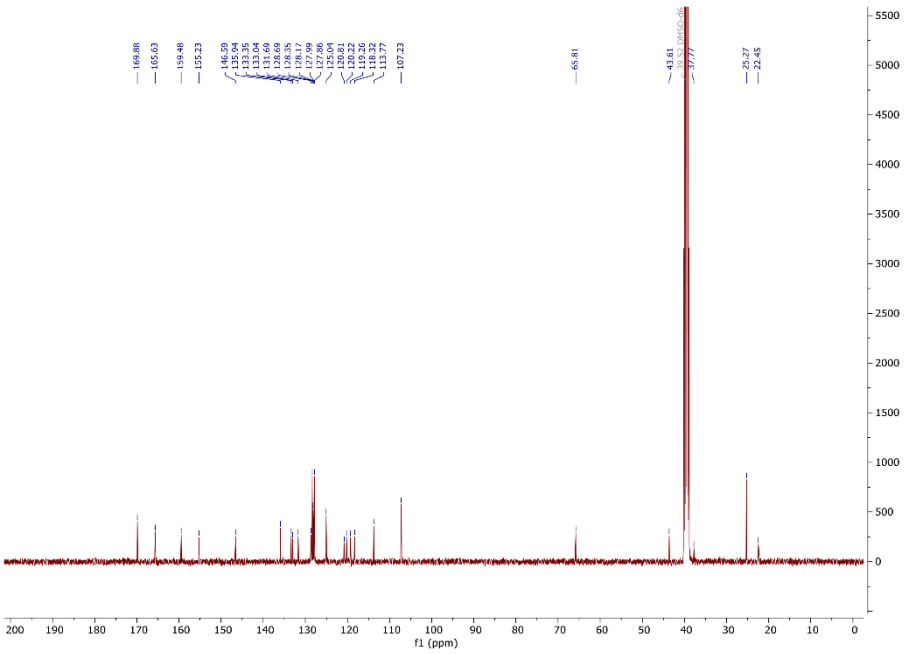

^{1}H and ^{13}C NMR spectra of benzyl (*S*)-4-cyano-3-(4-(1-(2,2-dimethyl-4-oxo-4*H*-benzo[*d*][1,3]dioxin-6-yl)-1*H*-1,2,3-triazol-4-yl)benzamido)butanoate (**41**).

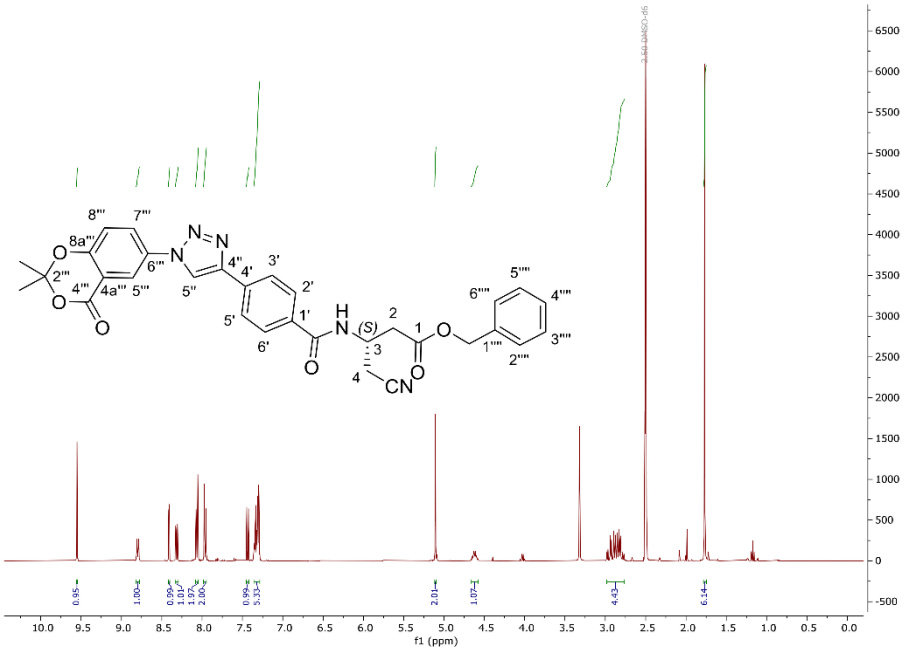

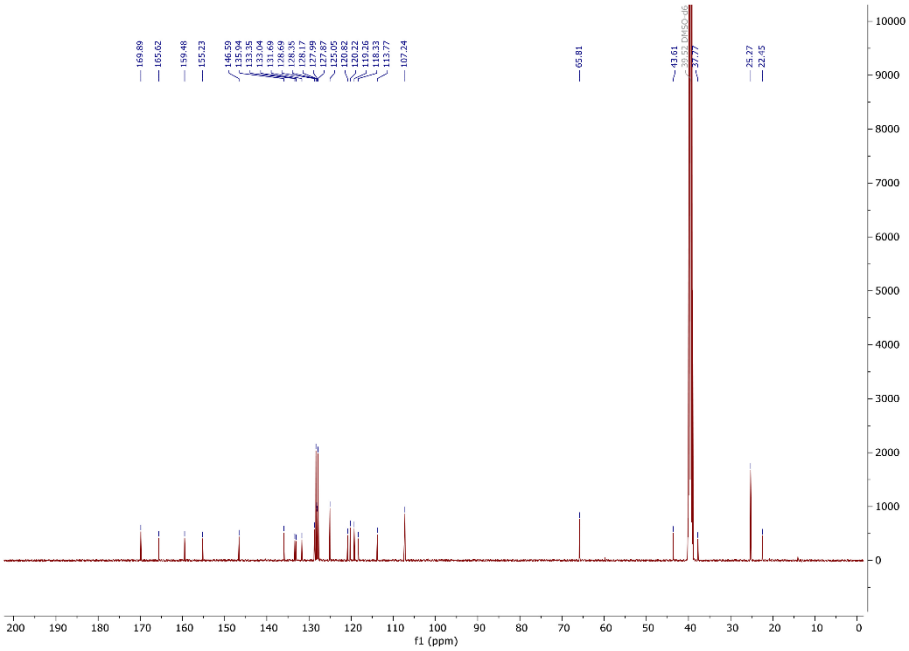

^{1}H and ^{13}C NMR spectra of (*R*)-(4-(benzyloxy)-2-(4-(1-(2,2-dimethyl-4-oxo-4*H*-benzo[*d*][1,3]dioxin-6-yl)-1*H*-1,2,3-triazol-4-yl)benzamido)-4-oxobutyl)boronic acid (**42**).

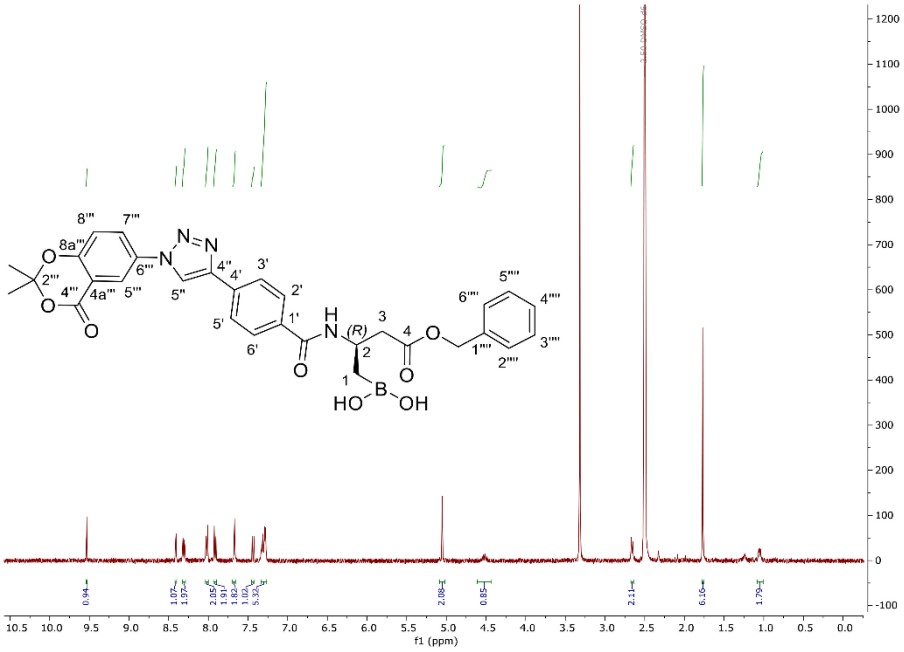

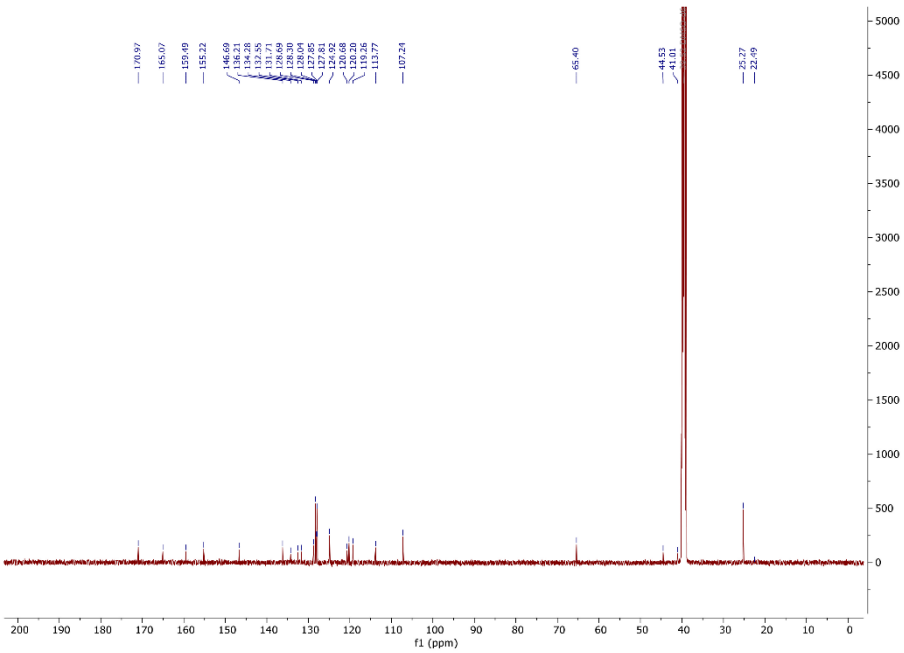

^{1}H and ^{13}C NMR spectra of (*S*)-(4-(benzyloxy)-2-(4-(1-(2,2-dimethyl-4-oxo-4*H*-benzo[*d*][1,3]dioxin-6-yl)-1*H*-1,2,3-triazol-4-yl)benzamido)-4-oxobutyl)boronic acid (**43**).

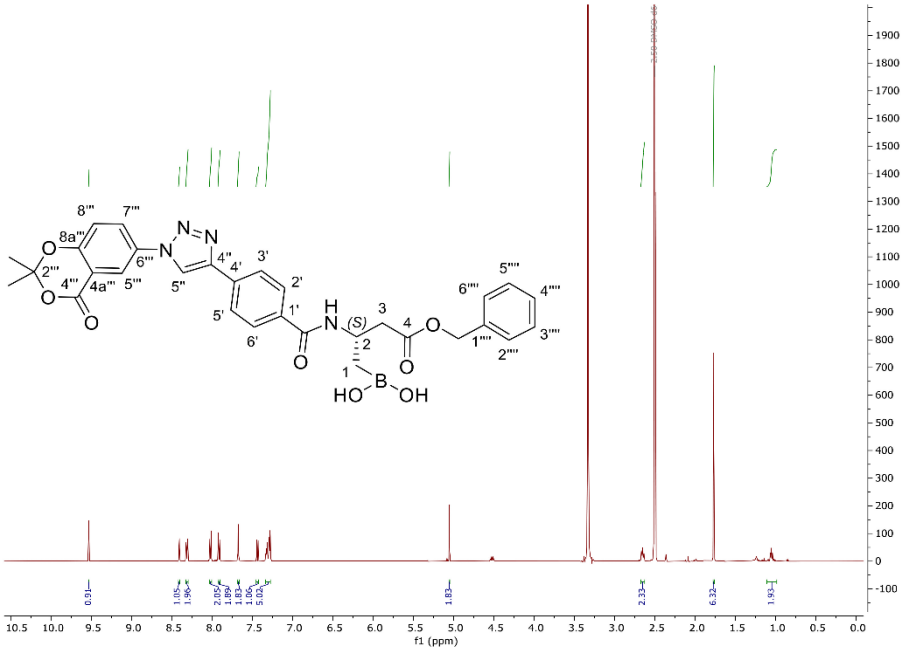

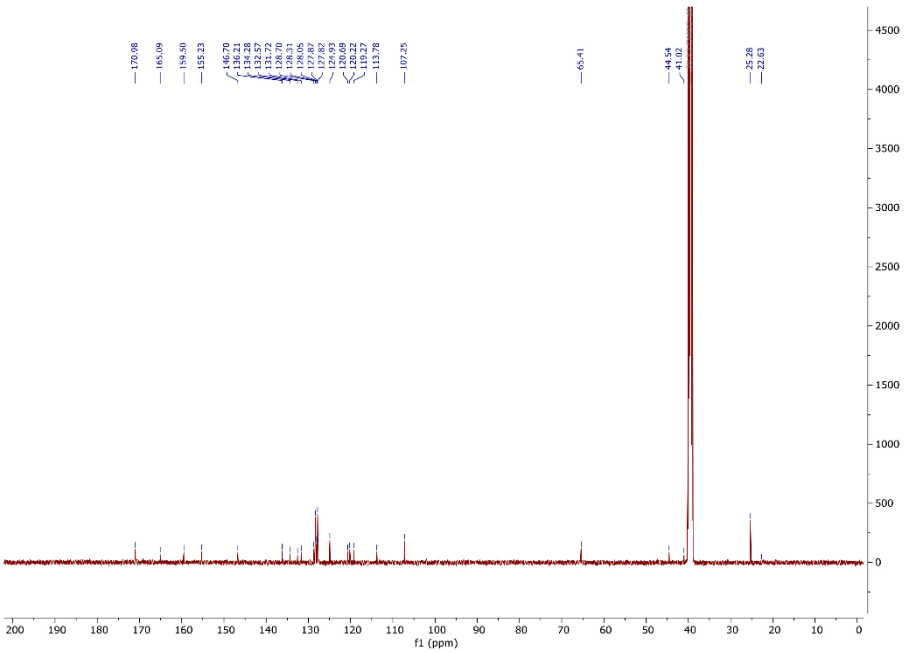

^{1}H and ^{13}C NMR spectra of (*S*)-4-(benzyloxy)-1-bromo-4-oxobutan-2-aminium (**44**).

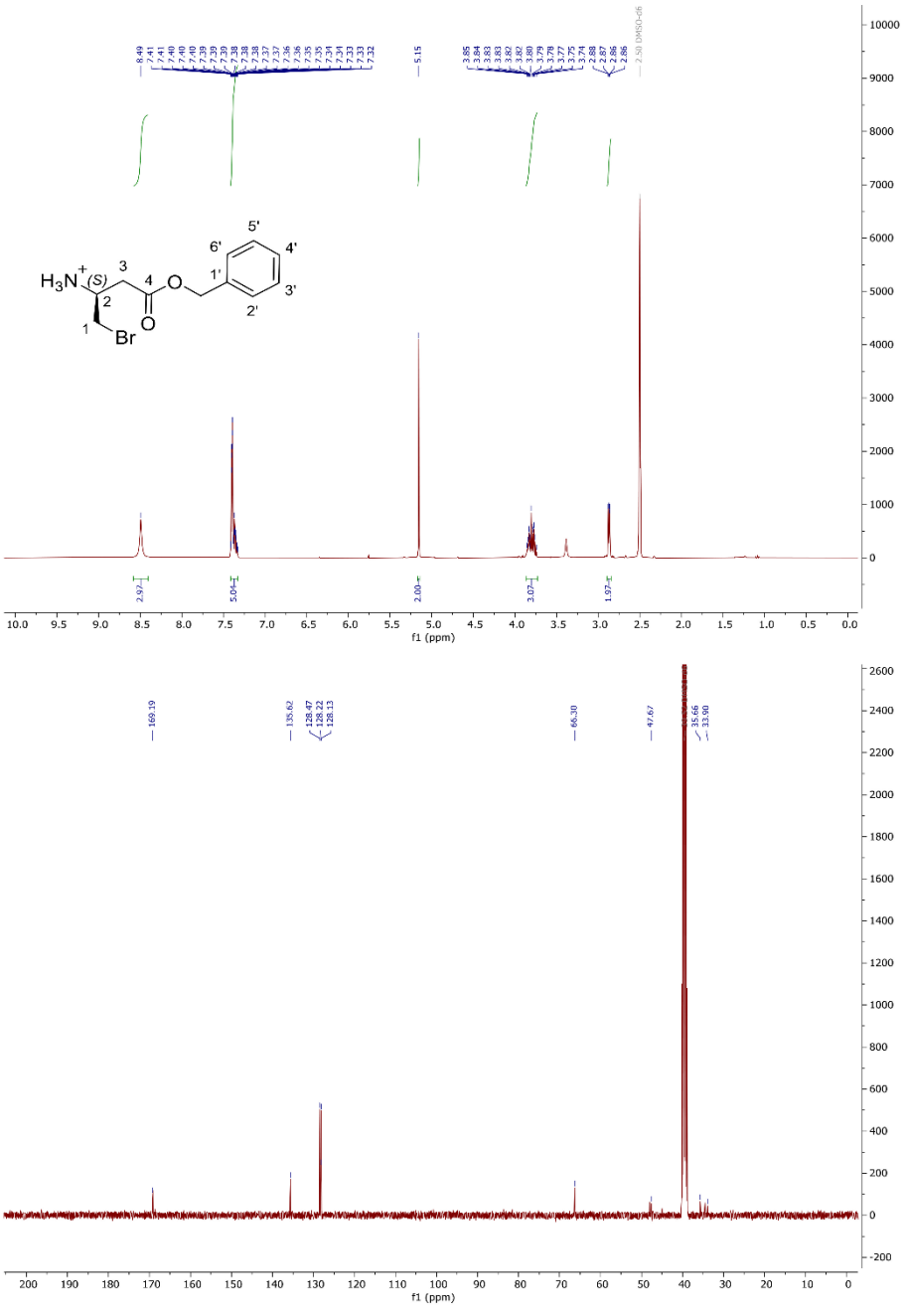

^{1}H and ^{13}C NMR spectra of benzyl (*S*)-2-(2-(4-ethynylphenyl)-4,5-dihydrooxazol-4-yl)acetate (**45**).

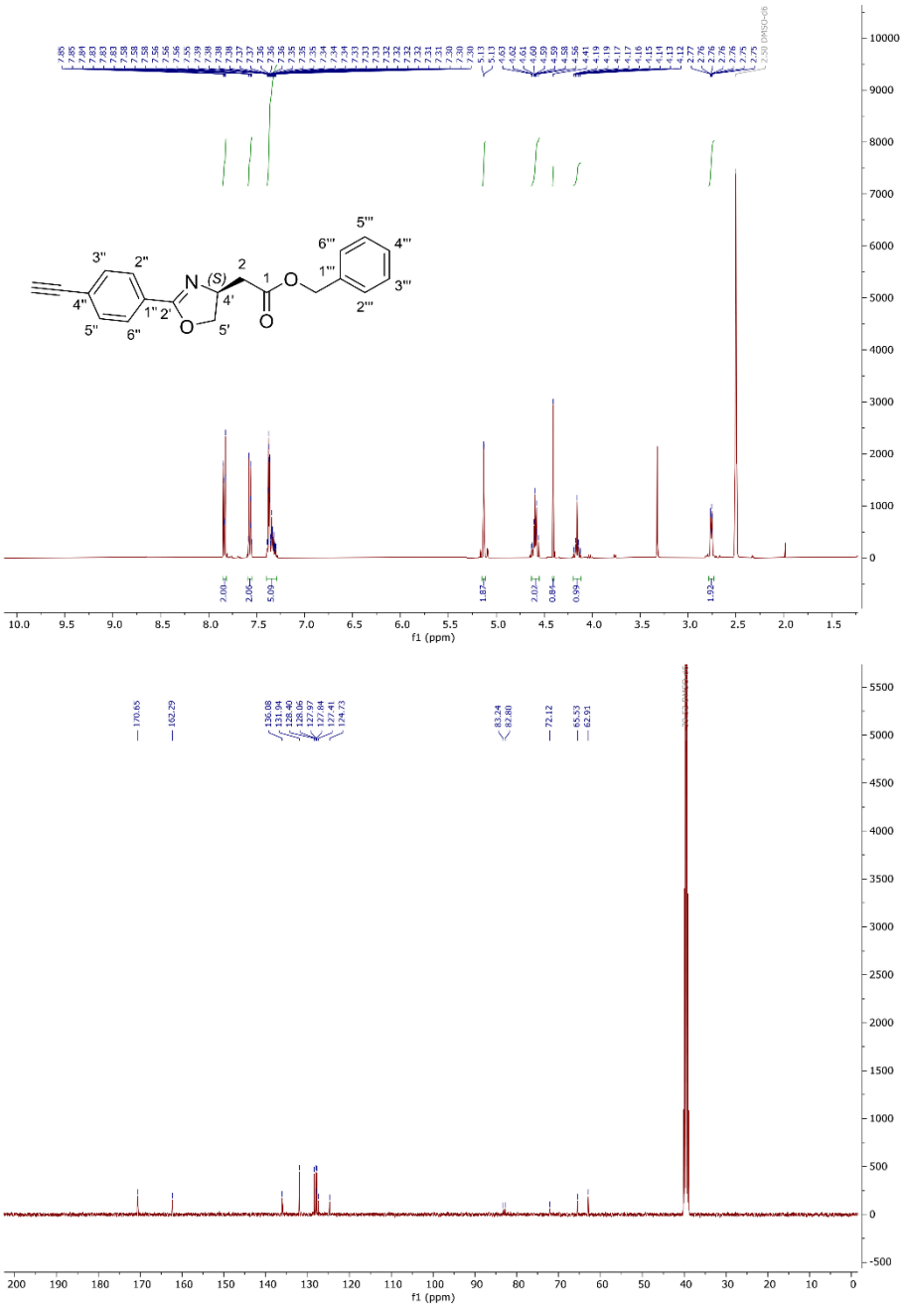

^{1}H and ^{13}C NMR spectra of (*R*)-5-(5-(4-((1-carboxy-3-cyanopropan-2-yl)carbamoyl)phenyl)isoxazol-3-yl)-2-hydroxybenzoic acid (**47**).

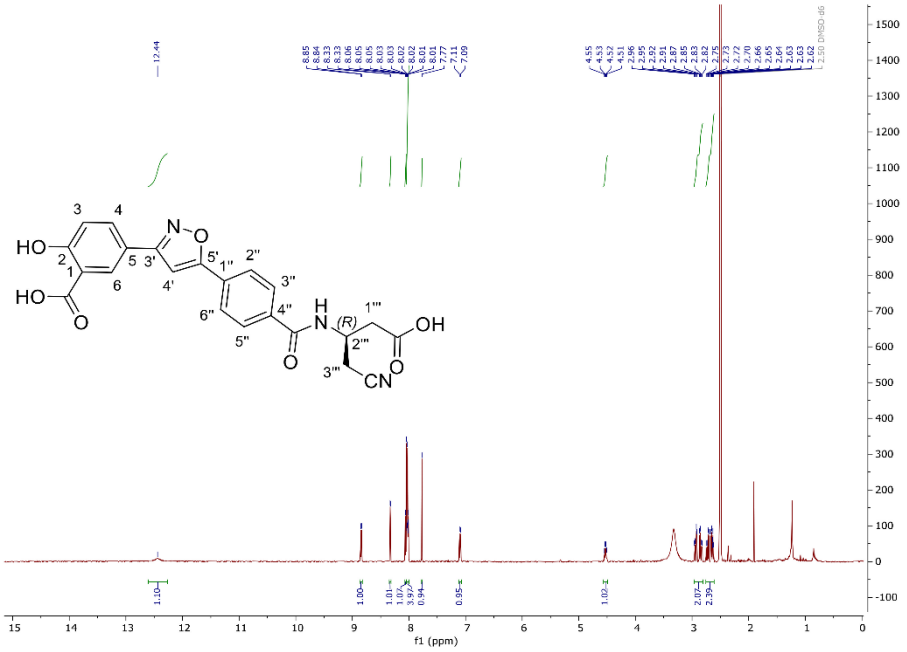

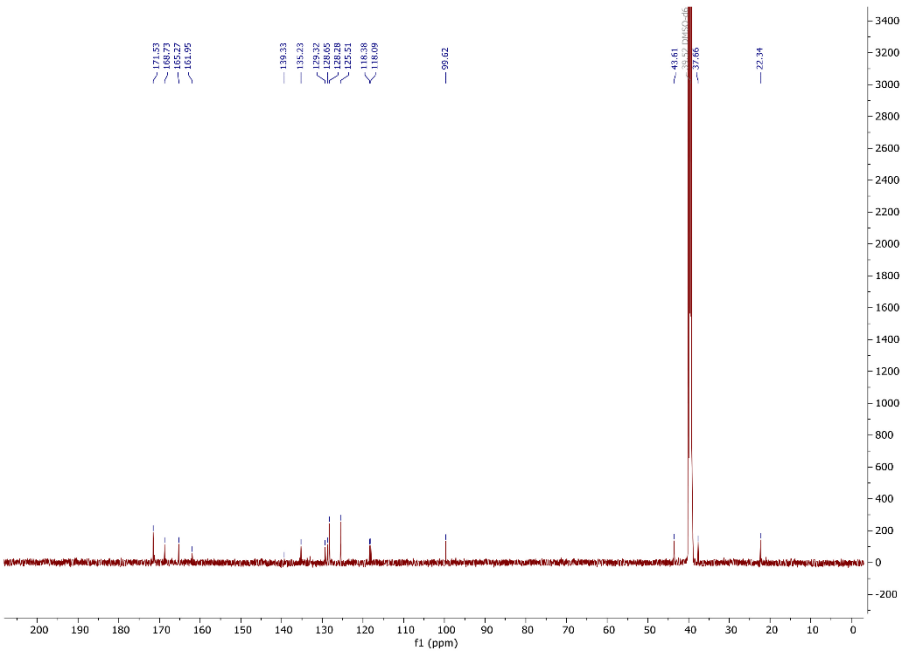

^{1}H and ^{13}C NMR spectra of (*S*)-5-(5-(4-((1-carboxy-3-cyanopropan-2-yl)carbamoyl)phenyl)isoxazol-3-yl)-2-hydroxybenzoic acid (**48**).

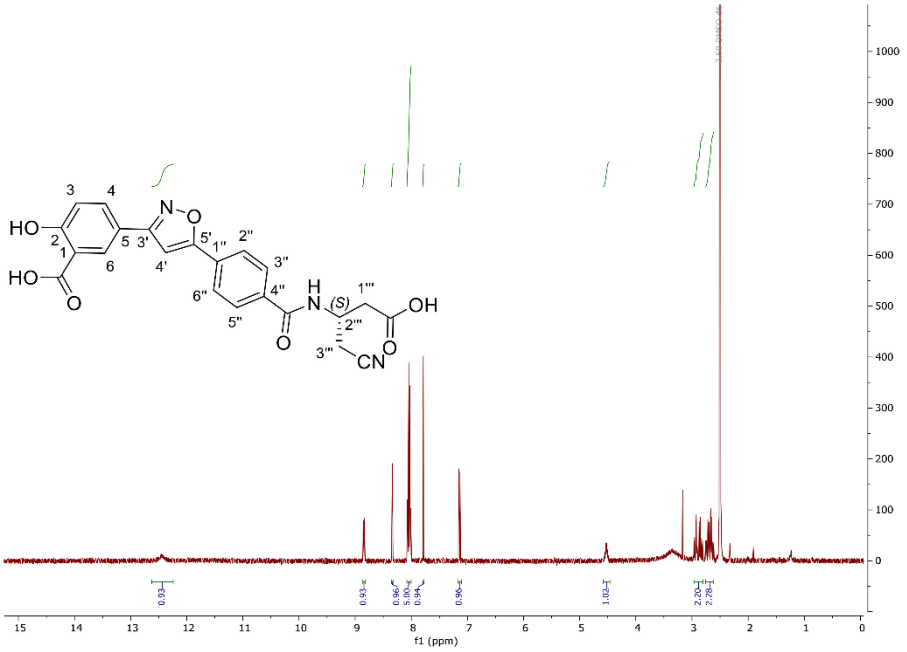

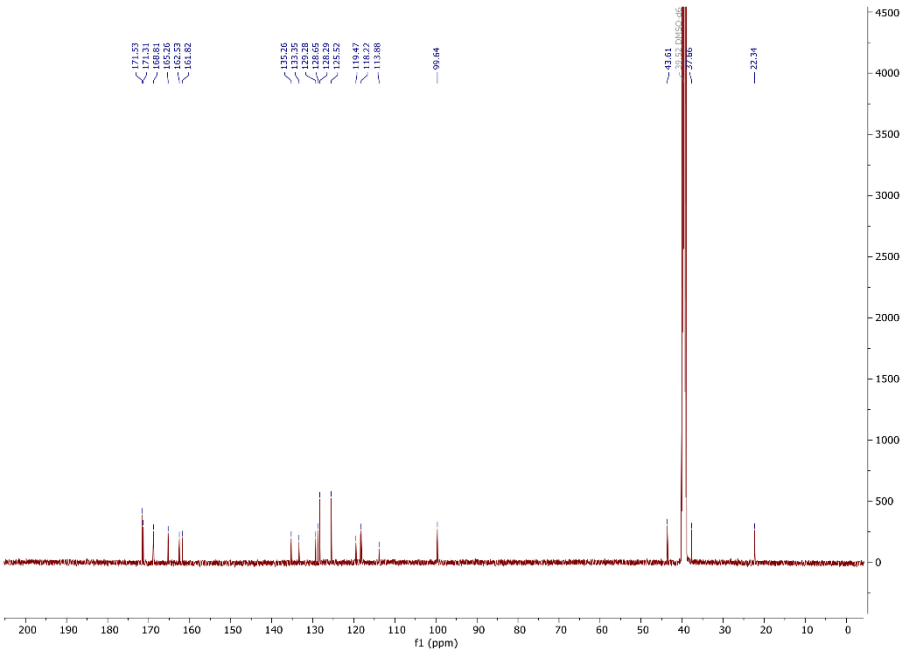

^{1}H and ^{13}C NMR spectra of (*R*)-5-(4-(4-((1-carboxy-3-cyanopropan-2-yl)carbamoyl)phenyl)-1*H*-1,2,3-triazol-1-yl)-2-hydroxybenzoic acid (**49**).

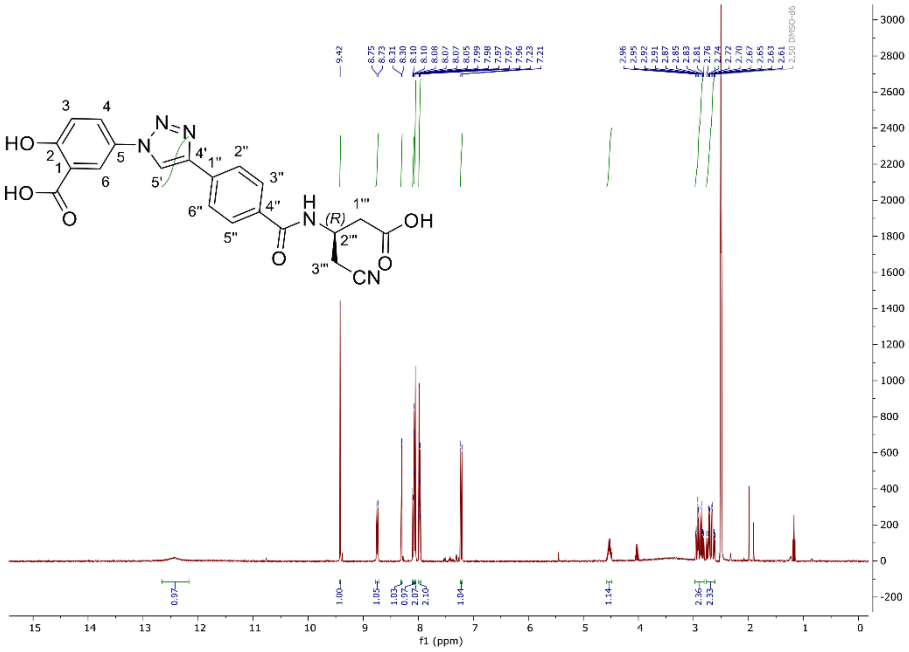

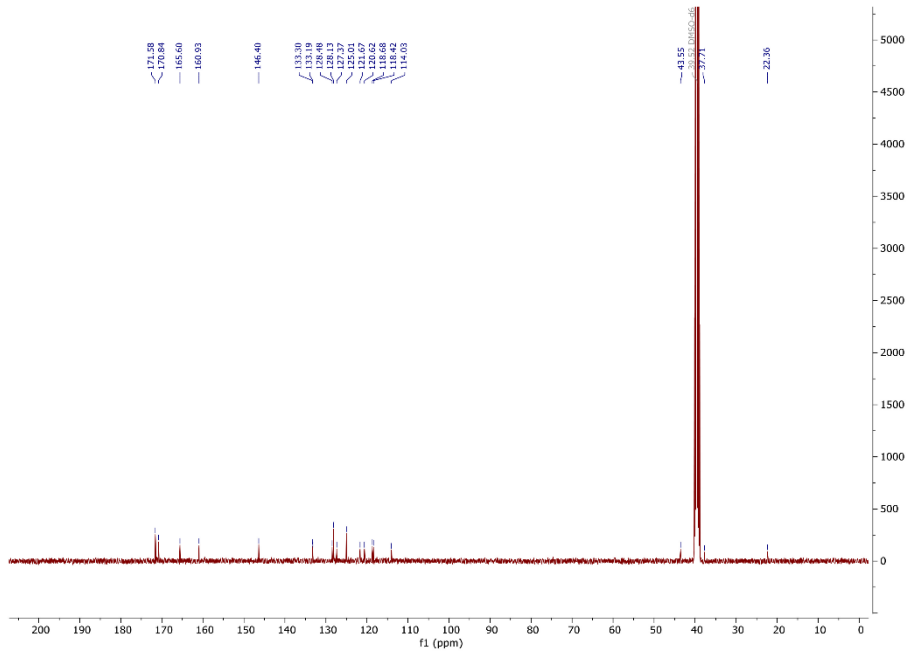

^{1}H and ^{13}C NMR spectra of (*S*)-5-(4-(4-((1-carboxy-3-cyanopropan-2-yl)carbamoyl)phenyl)-1*H*-1,2,3-triazol-1-yl)-2-hydroxybenzoic acid (**50**).

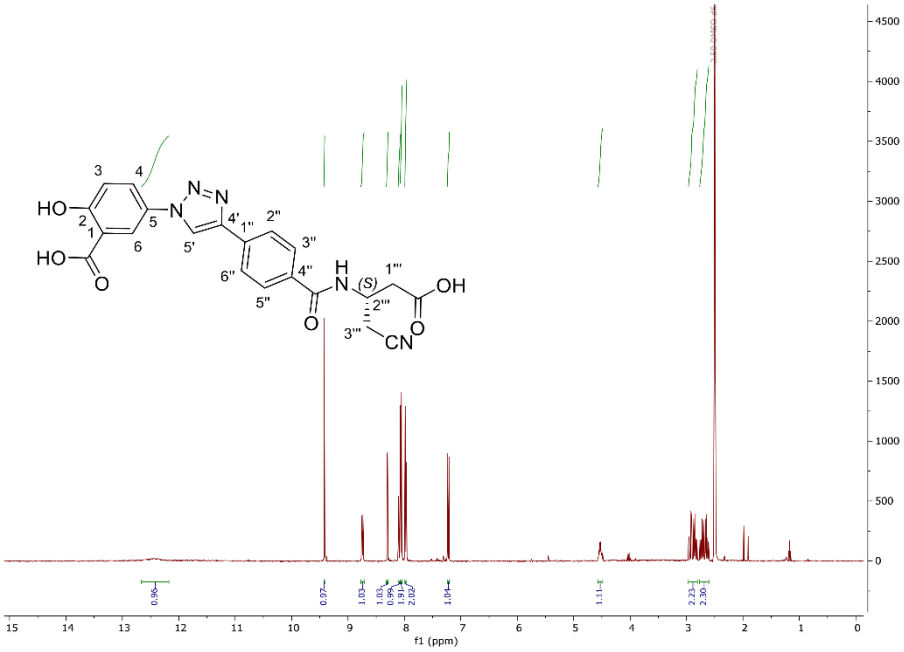

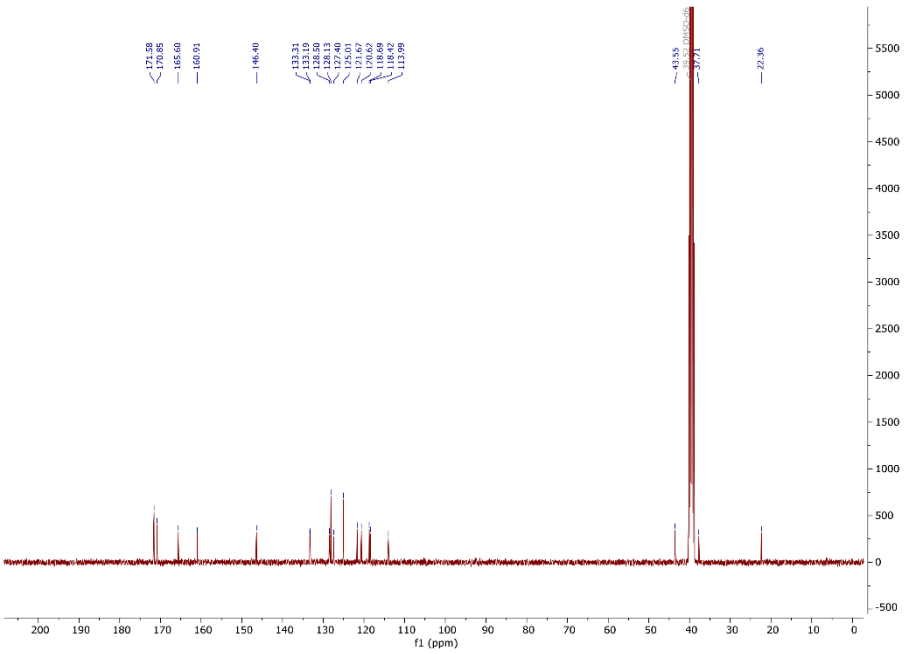

^{1}H and ^{13}C NMR spectra of (*R*)-2-(6-(4-(3-(2,2-dimethyl-4-oxo-4*H*-benzo[*d*][1,3]dioxin-6-yl)isoxazol-5-yl)phenyl)-2-hydroxy-3,4-dihydro-2*H*-1,5,2-oxazaborinin-4-yl)acetic acid (**51**).

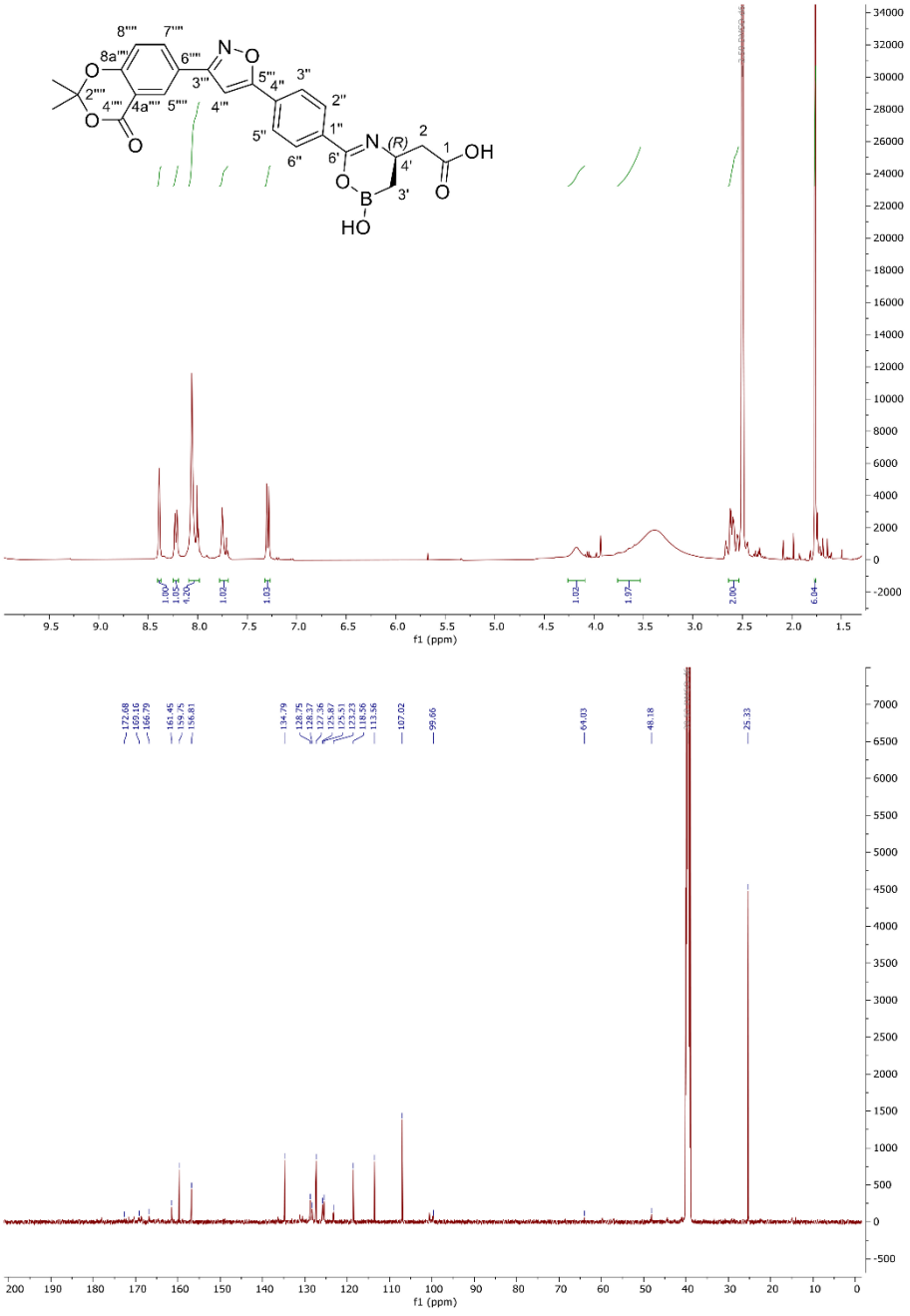

^{1}H and ^{13}C NMR spectra of (*S*)-2-(6-(4-(3-(2,2-dimethyl-4-oxo-4*H*-benzo[*d*][1,3]dioxin-6-yl)isoxazol-5-yl)phenyl)-2-hydroxy-3,4-dihydro-2*H*-1,5,2-oxazaborinin-4-yl)acetic acid (**52**).

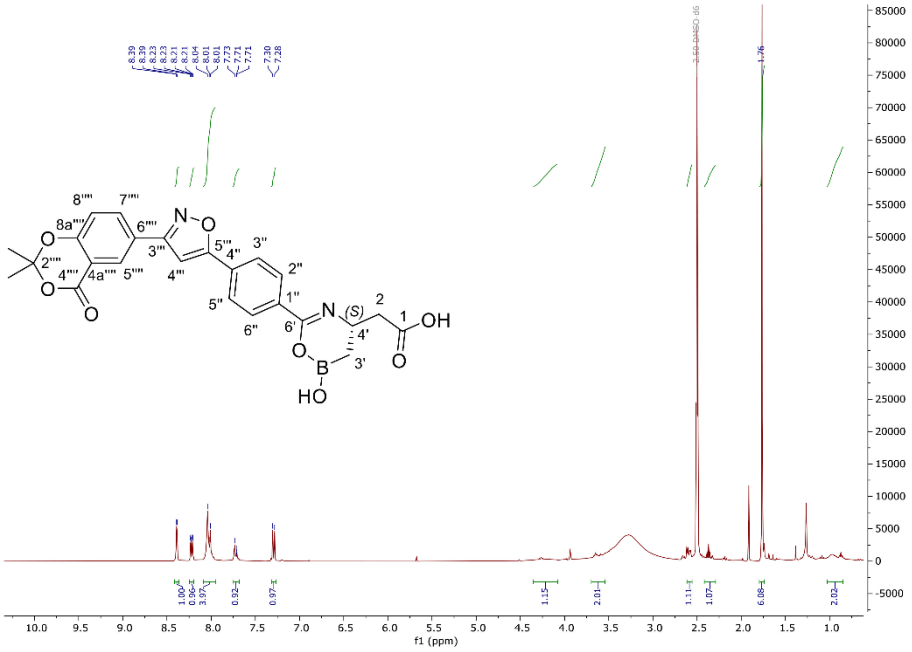

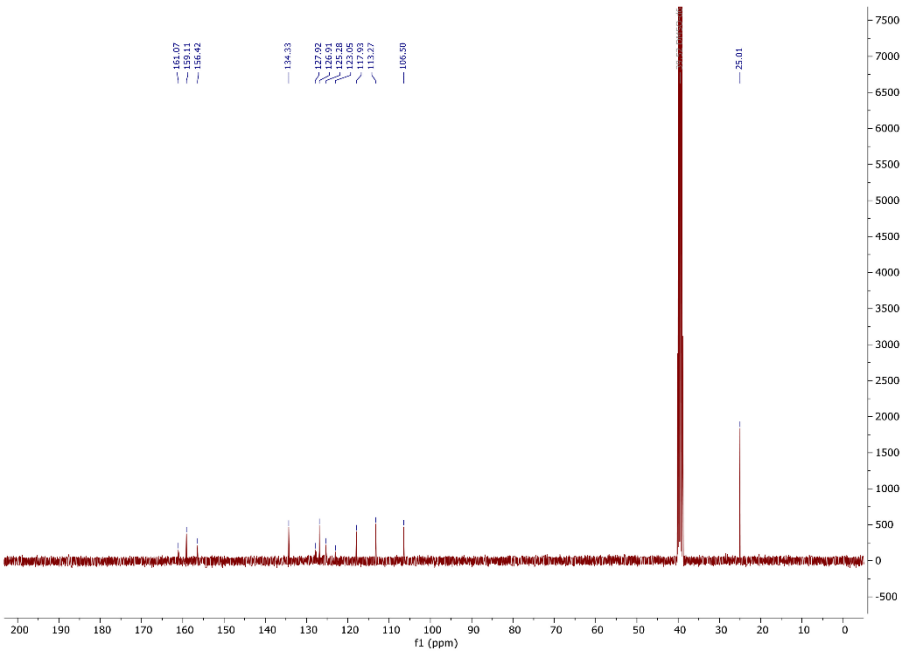

^{1}H and ^{13}C NMR spectra of (*R*)-2-(6-(4-(1-(2,2-dimethyl-4-oxo-4*H*-benzo[*d*][1,3]dioxin-6-yl)-1*H*-1,2,3-triazol-4-yl)phenyl)-2-hydroxy-3,4-dihydro-2*H*-1,5,2-oxazaborinin-4-yl)acetic acid (**53**).

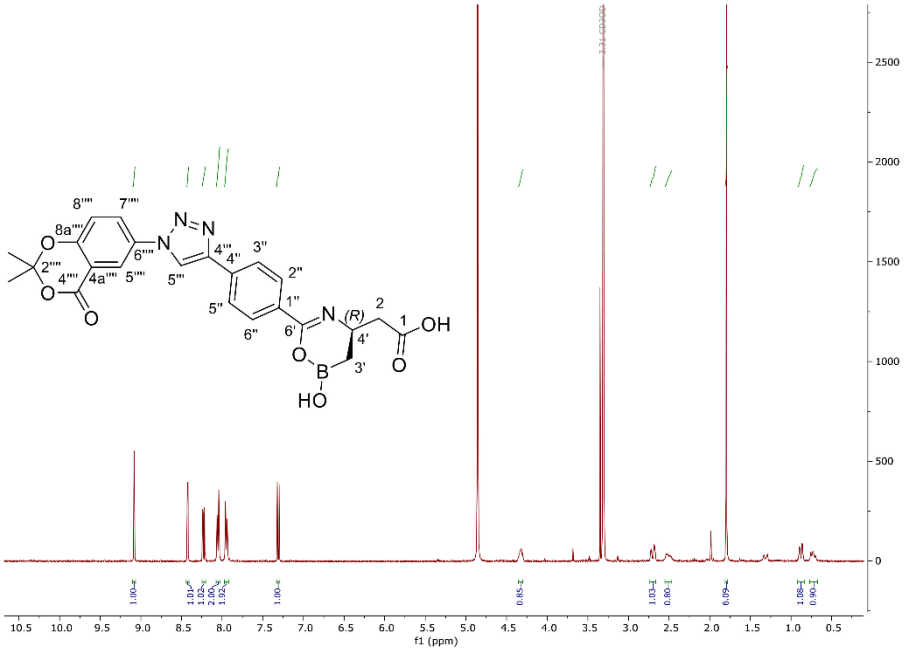

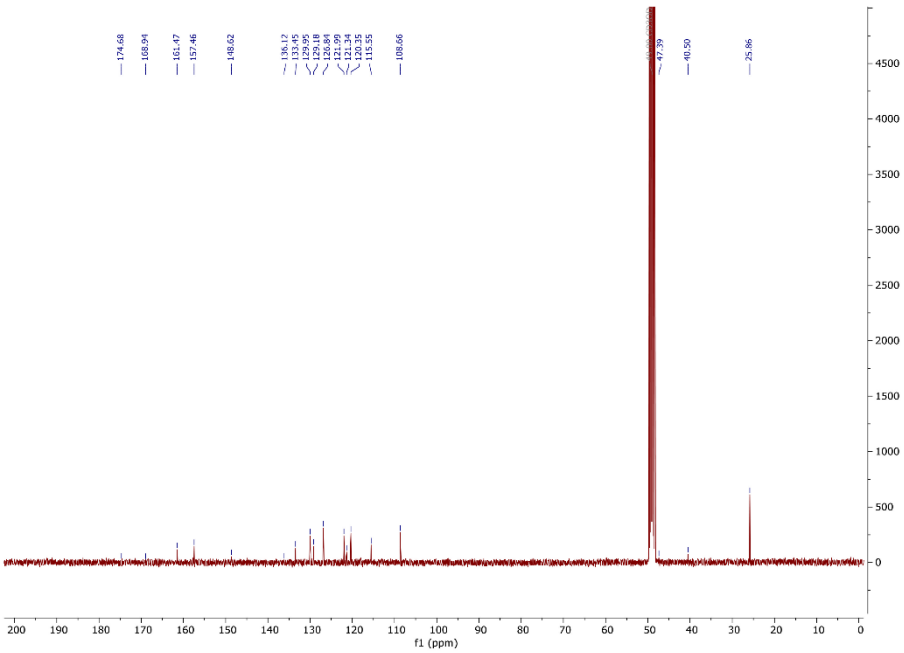

^{1}H and ^{13}C NMR spectra of (*S*)-2-(6-(4-(1-(2,2-dimethyl-4-oxo-4*H*-benzo[*d*][1,3]dioxin-6-yl)-1*H*-1,2,3-triazol-4-yl)phenyl)-2-hydroxy-3,4-dihydro-2*H*-1,5,2-oxazaborinin-4-yl)acetic acid (**54**).

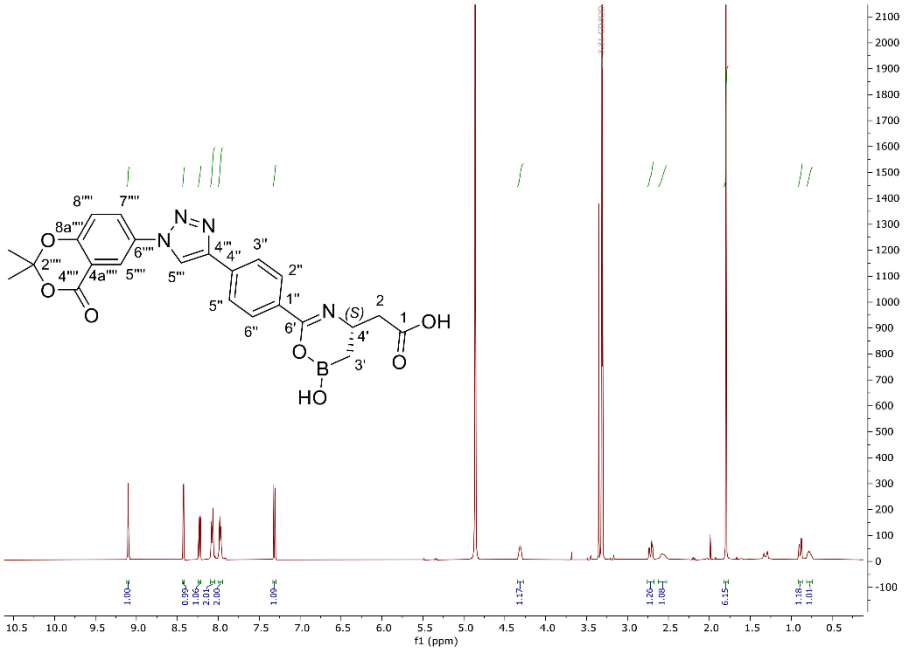

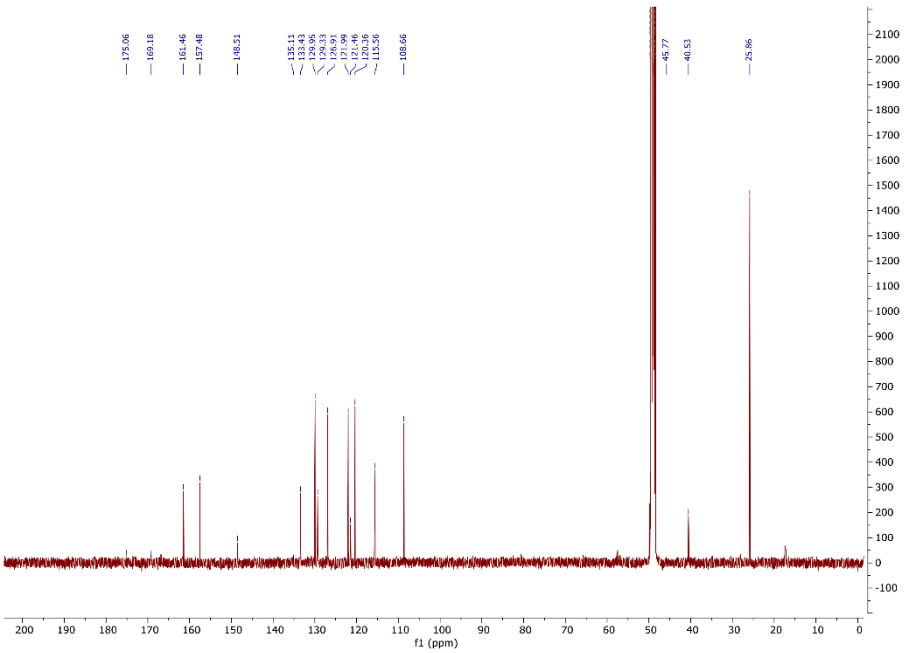

^{1}H and ^{13}C NMR spectra of 1-(benzyloxy)-1-oxohex-5-en-3-aminium (**57**).

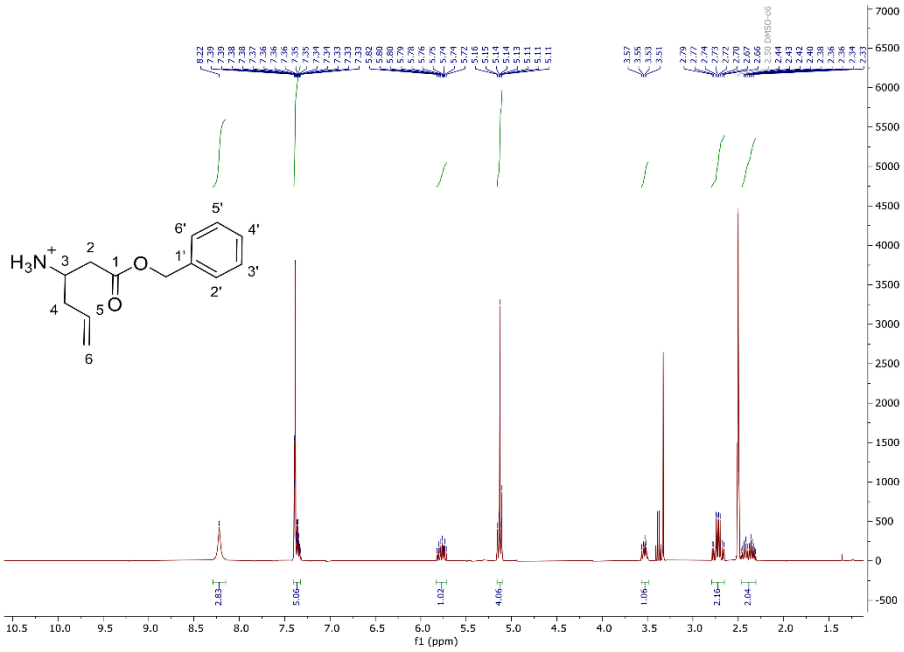

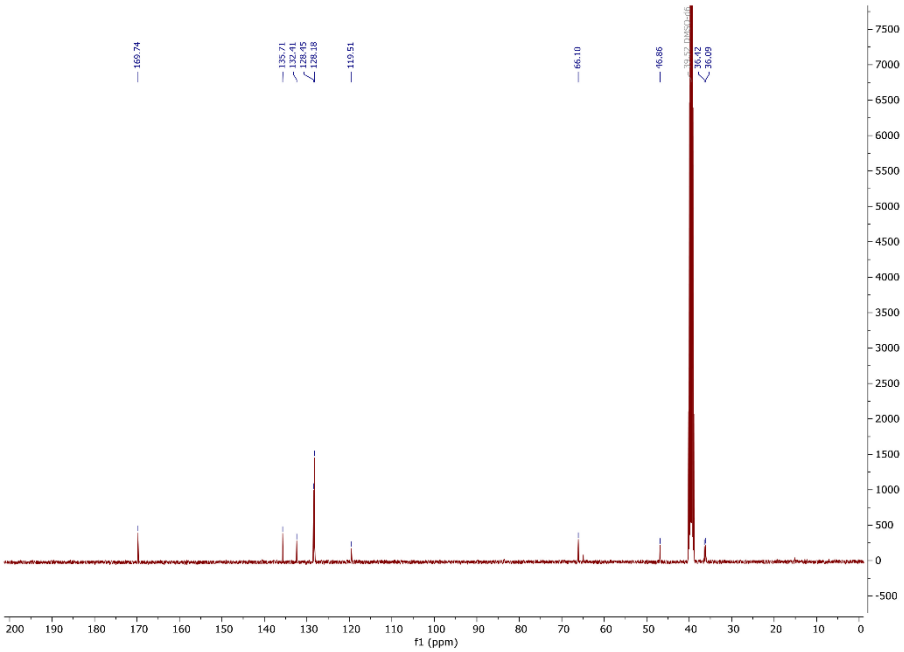

^{1}H and ^{13}C NMR spectra of benzyl 3-(4-ethynylbenzamido)hex-5-enoate (**58**).

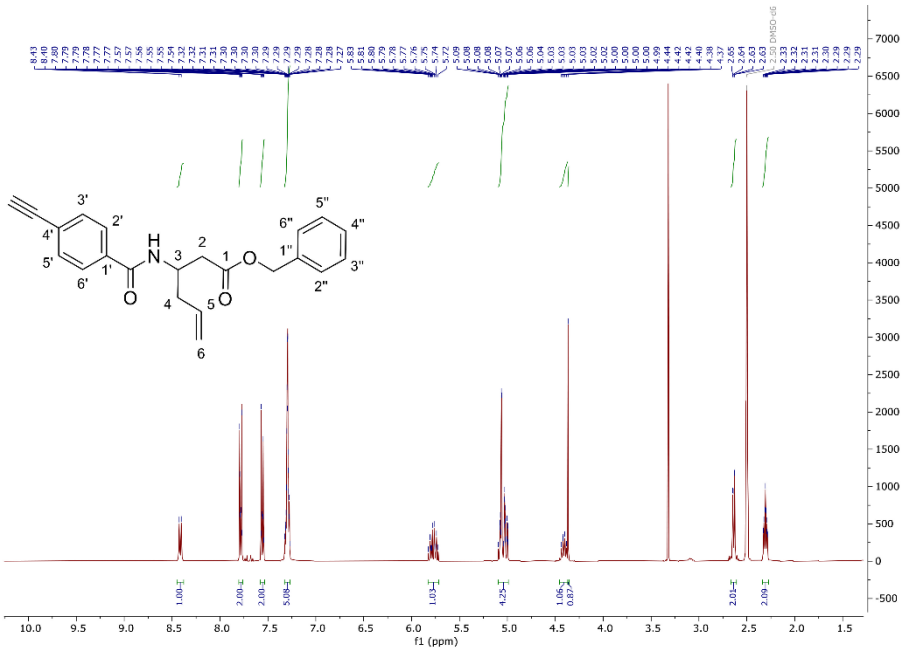

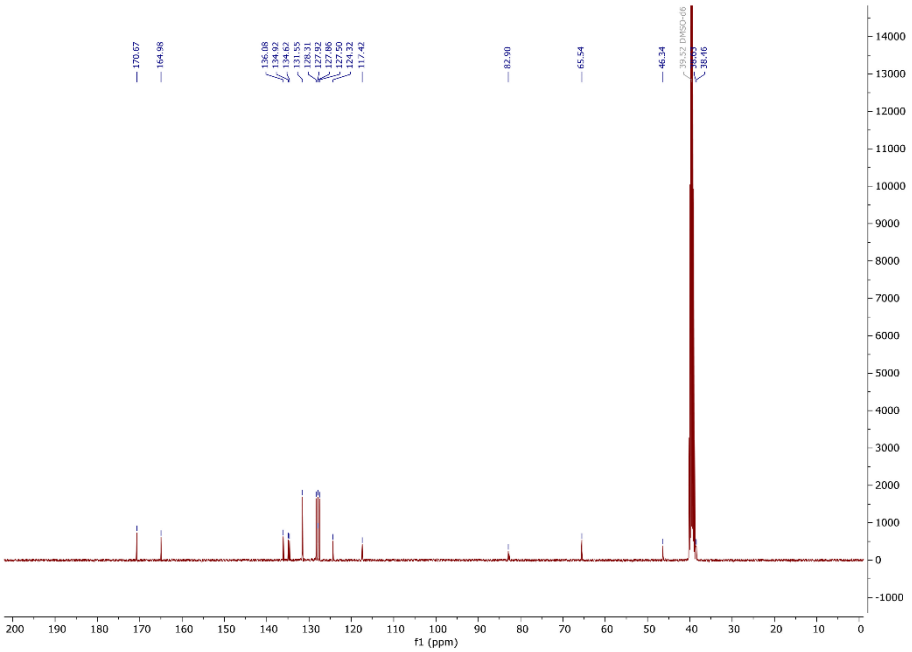

^{1}H and ^{13}C NMR spectra of benzyl 3-(4-(3-(2,2-dimethyl-4-oxo-4*H*-benzo[*d*][1,3]dioxin-6-yl)isoxazol-5-yl)benzamido)hex-5-enoate (**59**).

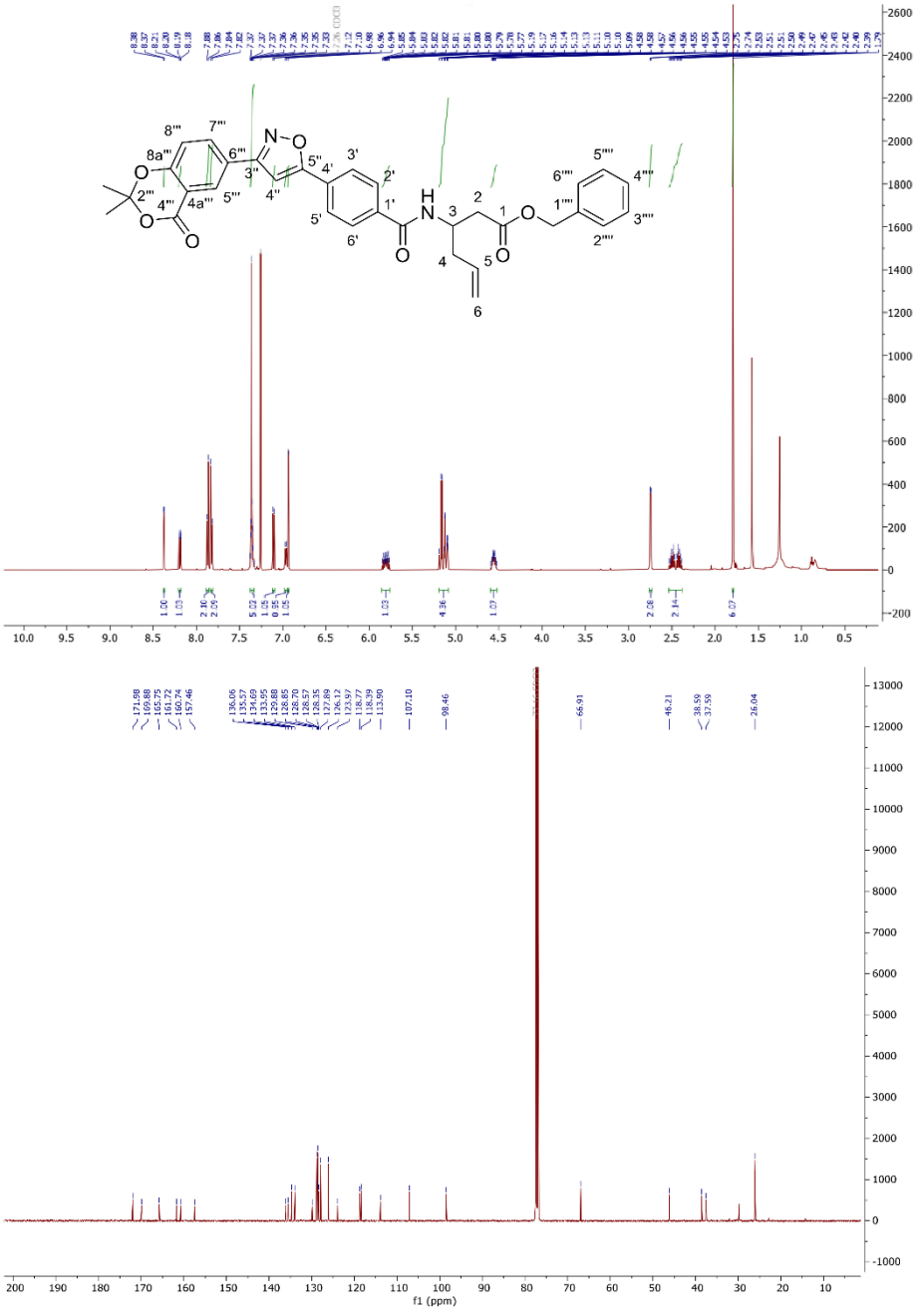

^{1}H and ^{13}C NMR spectra of 5-(5-(4-((1-carboxypent-4-en-2-yl)carbamoyl)phenyl)isoxazol-3-yl)-2-hydroxybenzoic acid (**60**).

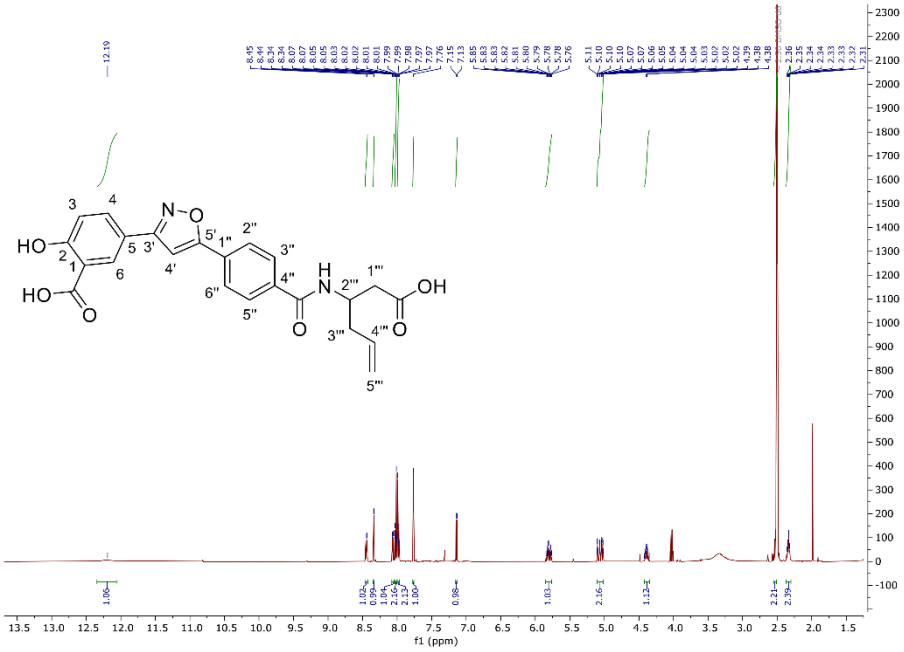

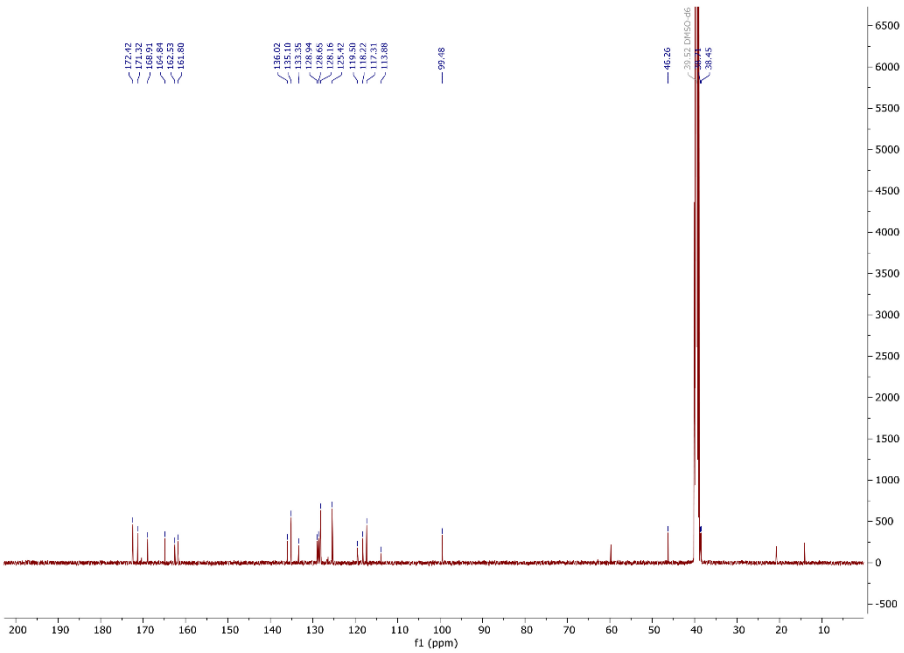

^{1}H and ^{13}C NMR spectra of 5-(5-(4-((1-carboxy-4-oxobutan-2-yl)carbamoyl)phenyl)isoxazol-3-yl)-2-hydroxybenzoic acid (**61**).

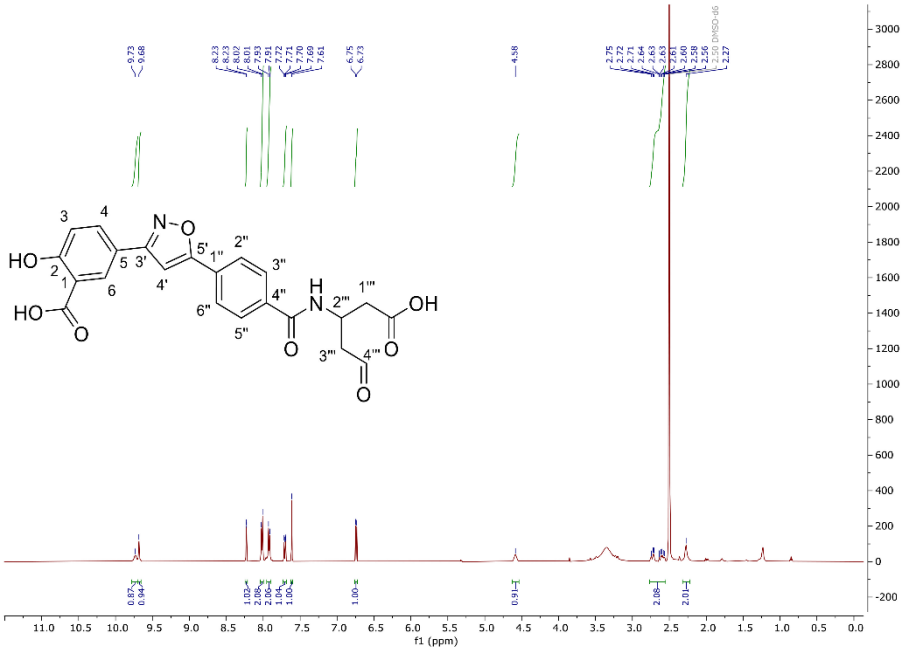

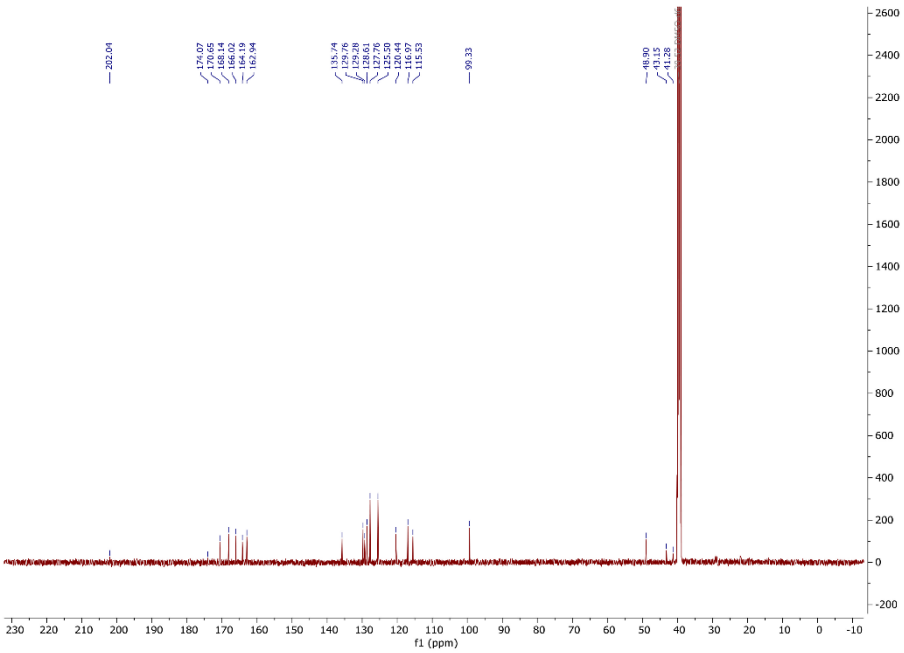

^{1}H and ^{13}C NMR spectra of benzyl 3-(4-(1-(2,2-dimethyl-4-oxo-4*H*-benzo[*d*][1,3]dioxin-6-yl)-1*H*-1,2,3-triazol-4-yl)benzamido)hex-5-enoate (**62**).

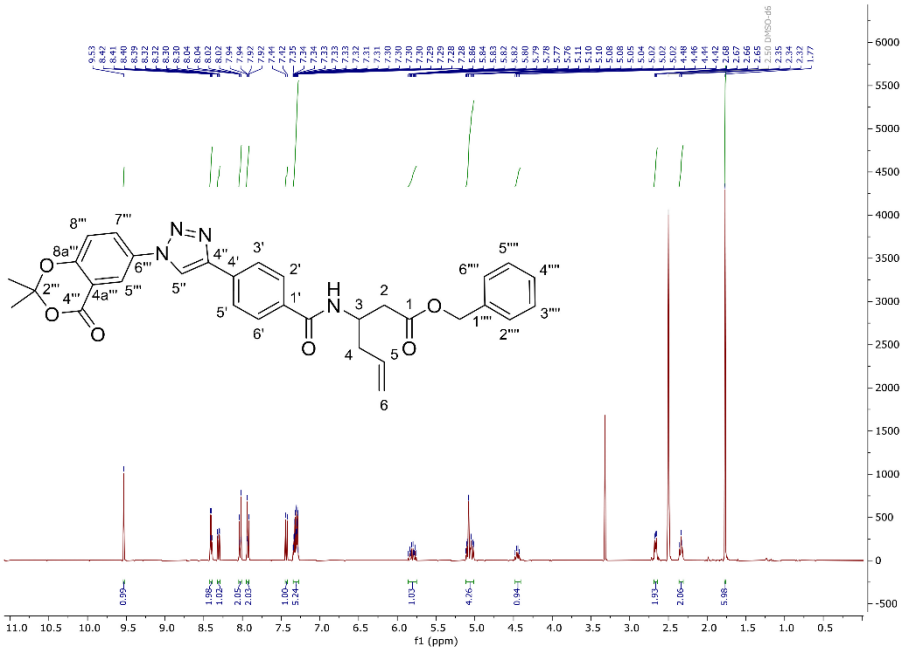

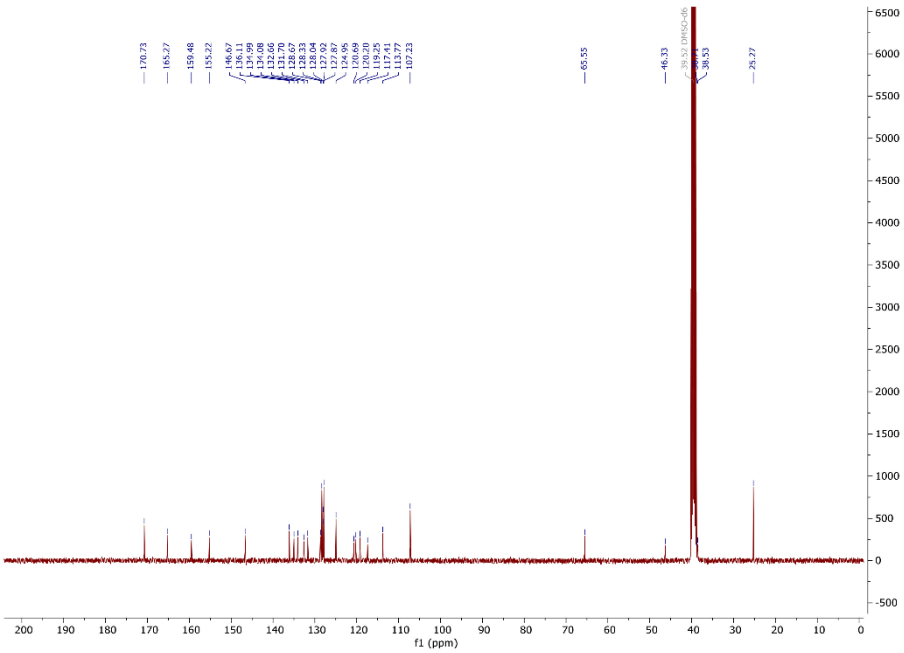

^{1}H and ^{13}C NMR spectra of 5-(4-(4-((1-carboxypent-4-en-2-yl)carbamoyl)phenyl)-1*H*-1,2,3-triazol-1-yl)-2-hydroxybenzoic acid (**63**).

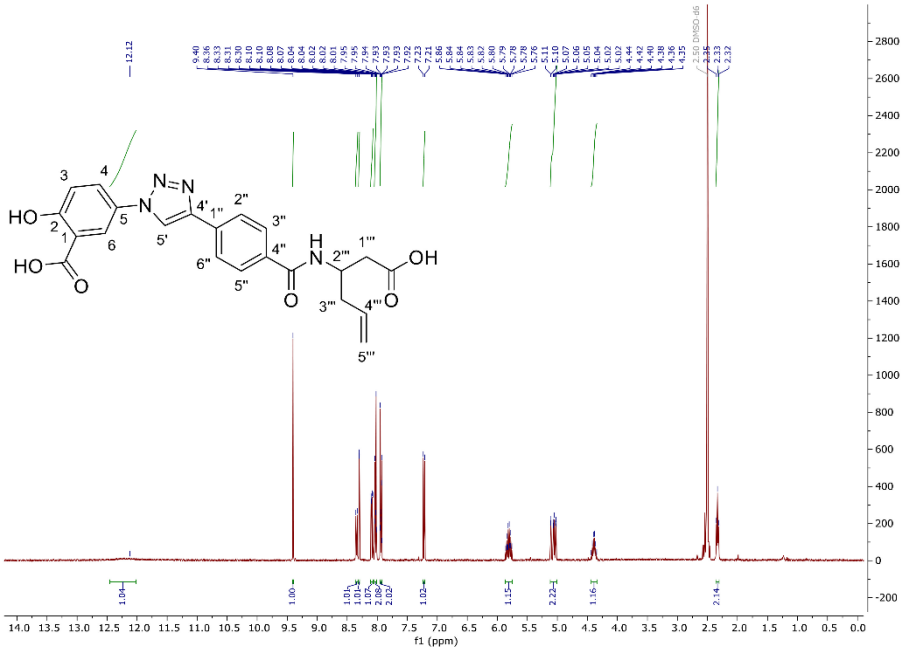

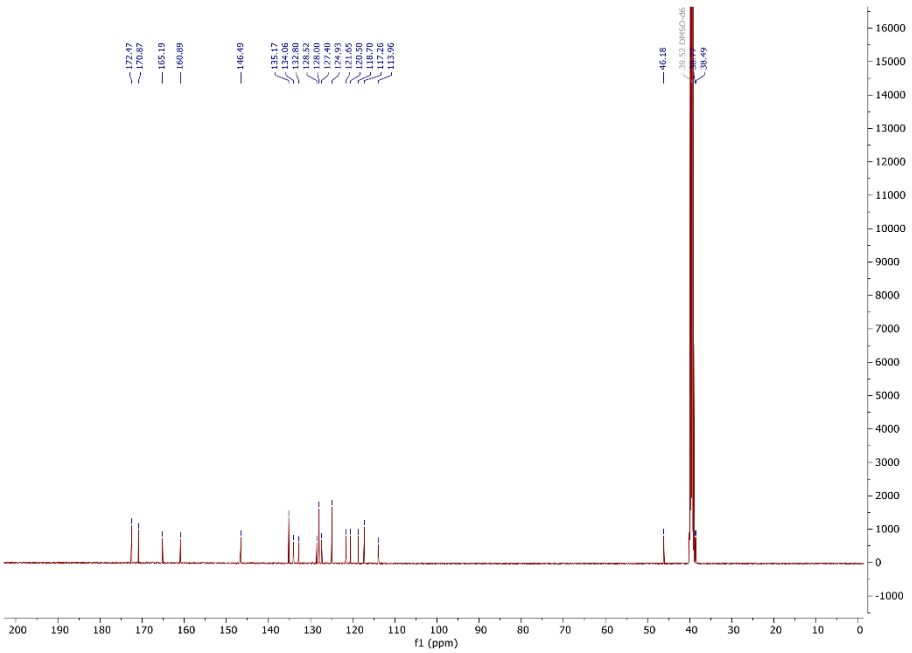

^{1}H and ^{13}C NMR spectra of 5-(4-(4-((1-carboxy-4-oxobutan-2-yl)carbamoyl)phenyl)-1*H*-1,2,3-triazol-1-yl)-2-hydroxybenzoic acid (**64**).

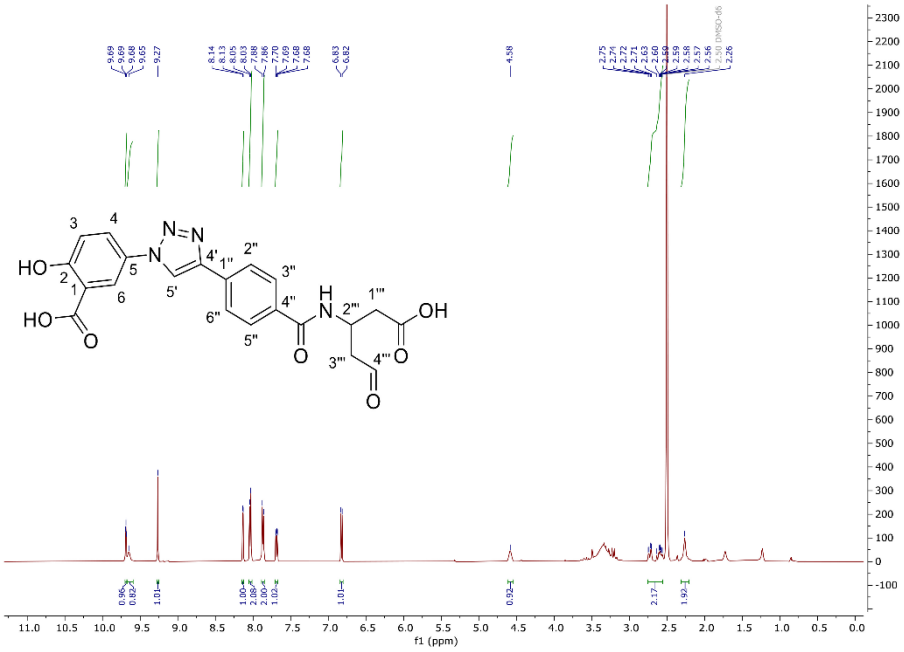

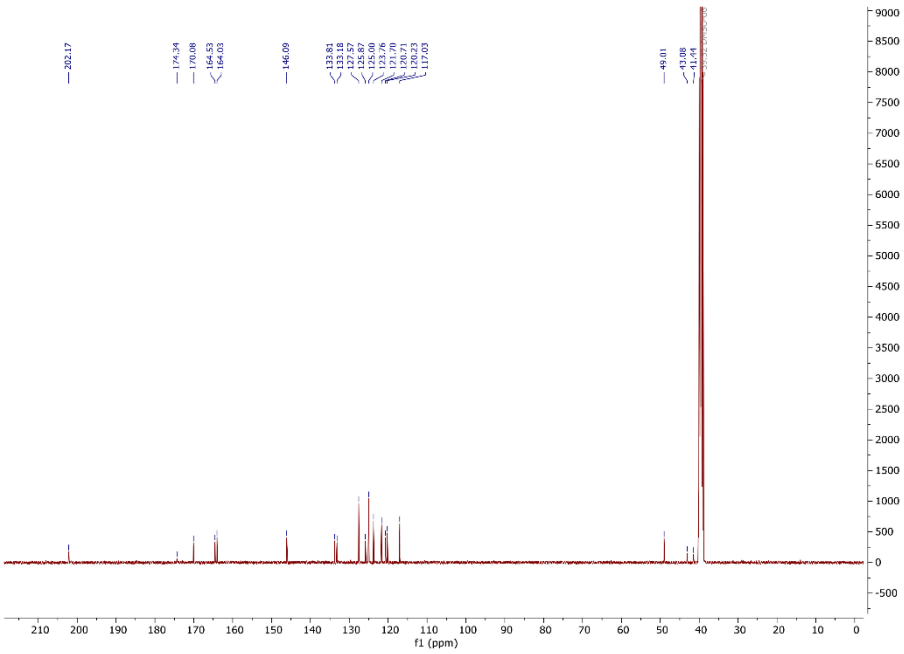

S2. HPLC chromatograms of tested compounds

HPLC chromatrogram of (*R*)-5-(5-(4-((1-carboxy-3-cyanopropan-2-yl)carbamoyl)phenyl)isoxazol-3-yl)-2-hydroxybenzoic acid (**47**).

Instrument:Trudel Sequence:20250121 Wirawan Page 1 of 2

Chromatogram and Results

Injection Details

Injection Name:	**RW-SAH-11**	*Run Time (min):*	**14,99**
Vial Number:	**Vial:13**	*Injection Volume:*	**5 µL**
Injection Type:	**Unknown**	*Wavelength:*	**210 nm**
		Wavelength:	**254 nm**
Instrument Method:	**Trudel Gradient MeOH Phosphatpuffer pH 5**	*Flow rate:*	**1,0 ml/min**
Column:	**Zorbax Eclipe Plus C18 4,6 x 150mm 3,5µm**	*Column Temperatur:*	**50 °C**
Injection Date/Time:	**21.Jan.25 12:15**	*Pump Channel A:*	**5**
		Pump Channel B:	**95,0 Puffer pH 5**

Chromatogram

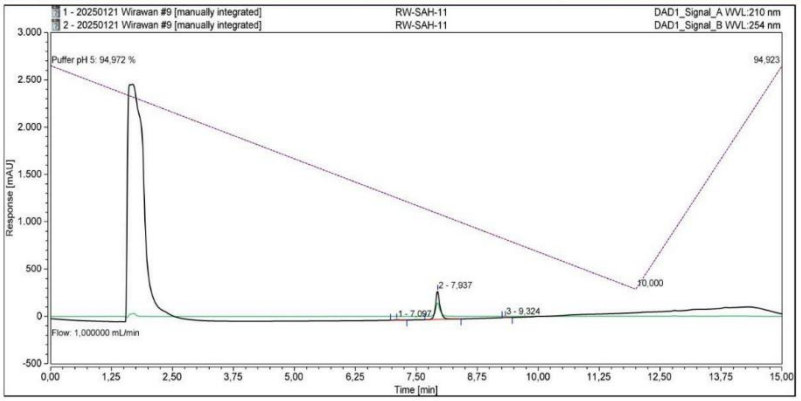

DAD1_Signal_A

No.	Retention Time min	Area mAU*min	Relative Area %
1	7,097	0,410	1,24
2	7,937	32,389	98,15
3	9,324	0,200	0,61
Total:		**32,999**	**100**

DAD1_Signal_B

No.	Retention Time min	Area mAU*min	Relative Area %
1	7,097	0,201	1,28
2	7,937	15,089	96,13
3	9,317	0,113	0,72
4	12,791	0,294	1,87
Total:		**15,697**	**100**

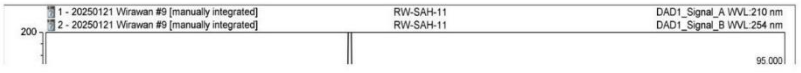

Reinheit Trudel/Integration

Chromeleon (c) Dionex Version 7.2.9.11323

HPLC chromatrogram of (*S*)-5-(5-(4-((1-carboxy-3-cyanopropan-2-yl)carbamoyl)phenyl)isoxazol-3-yl)-2-hydroxybenzoic acid (**48**).

Instrument:Trudel Sequence:20250121 Wirawan Page 1 of 2

Chromatogram and Results

Injection Details

Injection Name:	**RW-SAH-18**	*Run Time (min):*	**14,99**
Vial Number:	**Vial:14**	*Injection Volume:*	**5 µL**
Injection Type:	**Unknown**	*Wavelength:*	**210 nm**
		Wavelength:	**254 nm**
Instrument Method:	**Trudel Gradient MeOH Phosphatpuffer pH 5**	*Flow rate:*	**1,0 ml/min**
Column:	**Zorbax Eclipe Plus C18 4,6 x 150mm 3,5µm**	*Column Temperatur:*	**50 °C**
Injection Date/Time:	**21.Jan.25 12:31**	*Pump Channel A:*	**5**
		Pump Channel B:	**95,0 Puffer pH 5**

Chromatogram

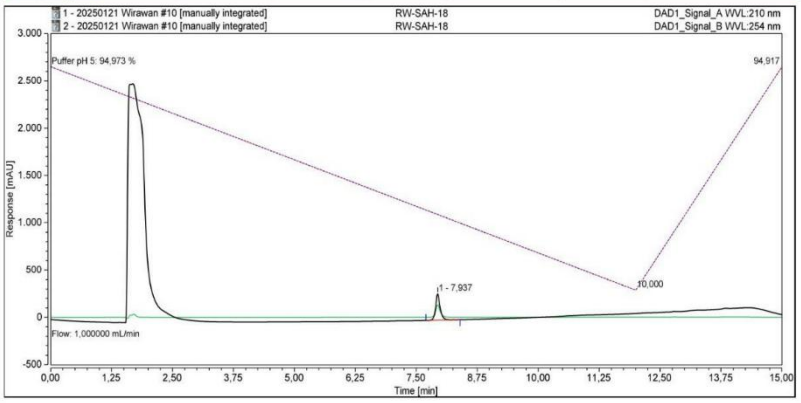

DAD1_Signal_A

No.	Retention Time min	Area mAU*min	Relative Area %
1	7,937	29,993	100,00
Total:		**29,993**	**100**

DAD1_Signal_B

No.	Retention Time min	Area mAU*min	Relative Area %
1	7,937	14,336	98,77
2	12,784	0,179	1,23
Total:		**14,515**	**100**

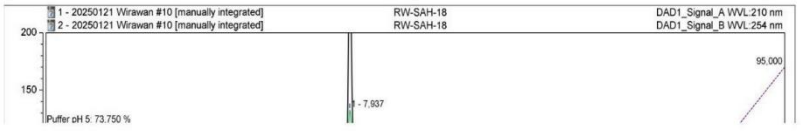

Reinheit Trudel/Integration

Chromeleon (c) Dionex Version 7.2.9.11323

HPLC chromatrogram of (*R*)-5-(4-(4-((1-carboxy-3-cyanopropan-2-yl)carbamoyl)phenyl)-1*H*-1,2,3-triazol-1-yl)-2-hydroxybenzoic acid (**49**).

Instrument:Trudel Sequence:20250121 Wirawan Page 1 of 2

Chromatogram and Results

Injection Details

Injection Name:	**RW-183**	*Run Time (min):*	**14,99**
Vial Number:	**Vial:19**	*Injection Volume:*	**5 µL**
Injection Type:	**Unknown**	*Wavelength:*	**210 nm**
		Wavelength:	**254 nm**
Instrument Method:	**Trudel Gradient MeOH Phosphatpuffer pH 5**	*Flow rate:*	**1,0 ml/min**
Column:	**Zorbax Eclipe Pius C18 4,6 x 150mm 3,5µm**	*Column Temperatur:*	**50 °C**
Injection Date/Time:	**21.Jan.25 13:49**	*Pump Channel A:*	**5**
		Pump Channel B:	**95,0 Puffer pH 5**

Chromatogram

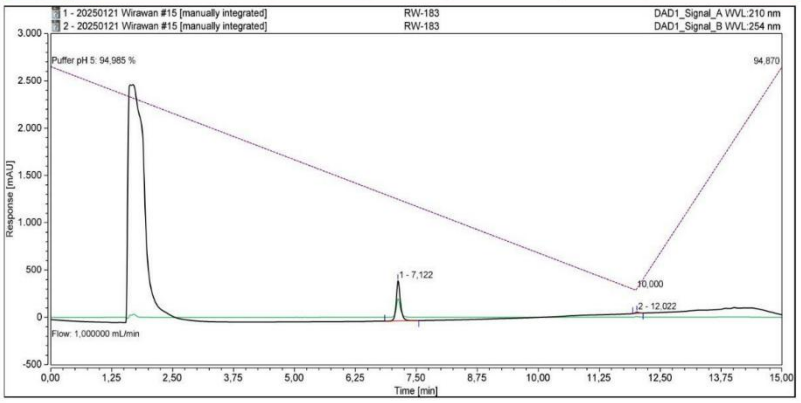

DAD1_Signal_A

No.	Retention Time min	Area mAU*min	Relative Area %
1	7,122	41,887	97,52
2	12,022	1,067	2,48
Total:		**42,953**	**100**

DAD1_Signal_B

No.	Retention Time min	Area mAU*min	Relative Area %
1	7,122	19,353	97,14
2	12,022	0,569	2,86
Total:		**19,922**	**100**

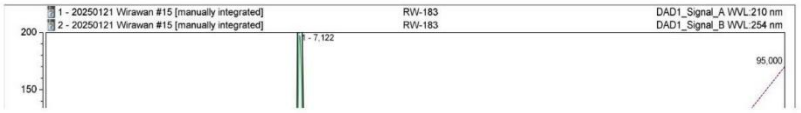

Reinheit Trudel/Integration

Chromeleon (c) Dionex Version 7.2.9.11323

HPLC chromatrogram of (*S*)-5-(4-(4-((1-carboxy-3-cyanopropan-2-yl)carbamoyl)phenyl)-1*H*-1,2,3-triazol-1-yl)-2-hydroxybenzoic acid (**50**).

Instrument:Trudel Sequence:20250121 Wirawan Page 1 of 2

Chromatogram and Results

Injection Details

Injection Name:	**RW-191**	*Run Time (min):*	**14,99**
Vial Number:	**Vial:20**	*Injection Volume:*	**5 µL**
Injection Type:	**Unknown**	*Wavelength:*	**210 nm**
		Wavelength:	**254 nm**
Instrument Method:	**Trudel Gradient MeOH Phosphatpuffer pH 5**	*Flow rate:*	**1,0 ml/min**
Column:	**Zorbax Eclipe Pius C18 4,6 x 150mm 3,5µm**	*Column Temperatur:*	**50 °C**
Injection Date/Time:	**21.Jan.25 14:05**	*Pump Channel A:*	**5**
		Pump Channel B:	**95,0 Puffer pH 5**

Chromatogram

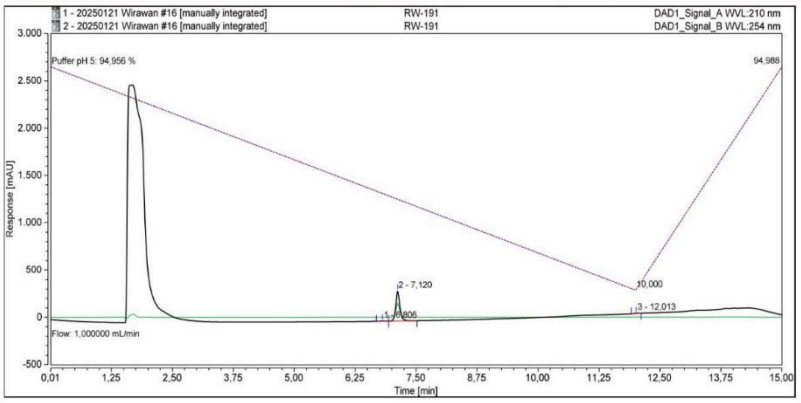

DAD1_Signal_A

No.	Retention Time min	Area mAU*min	Relative Area %
1	6,806	0,292	0,91
2	7,120	31,161	97,67
3	12,013	0,453	1,42
Total:		**31,906**	**100**

DAD1_Signal_B

No.	Retention Time min	Area mAU*min	Relative Area %
1	6,800	0,148	1,00
2	7,120	14,461	97,00
3	12,013	0,298	2,00
Total:		**14,907**	**100**

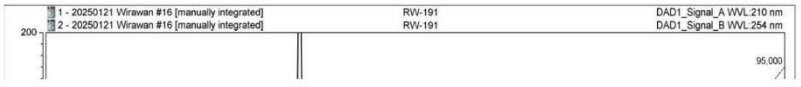

Reinheit Trudel/Integration

Chromeleon (c) Dionex Version 7.2.9.11323

HPLC chromatrogram of (*R*)-2-(6-(4-(3-(2,2-dimethyl-4-oxo-4*H*-benzo[*d*][1,3]dioxin-6-yl)isoxazol-5-yl)phenyl)-2-hydroxy-3,4-dihydro-2*H*-1,5,2-oxazaborinin-4-yl)acetic acid (**51**).

Instrument:Trudel Sequence:20250122 Wirawan 3 Page 1 of 2

Chromatogram and Results

Injection Details

Injection Name:	**RW-136 Stock mit Wasser**	*Run Time (min):*	**11,99**	
Vial Number:	**Vial:31**	*Injection Volume:*	**5 µL**	
Injection Type:	**Unknown**	*Wavelength:*	**210 nm**	
		Wavelength:	**254 nm**	
Instrument Method:	**MeOH Wasser +0,1% TFA Gradient 2**	*Flow rate:*	**1,0 ml/min**	
Column:	**Zorbax Eclipe Pius C18 4,6 x 150mm 3,5µm**	*Column Temperatur:*	**50 °C**	
Injection Date/Time:	**24.Jan.25 11:08**	*Pump Channel A:*	**10**	
		Pump Channel B:	**90,0**	**Wasser + 0,1% TFA**

Chromatogram

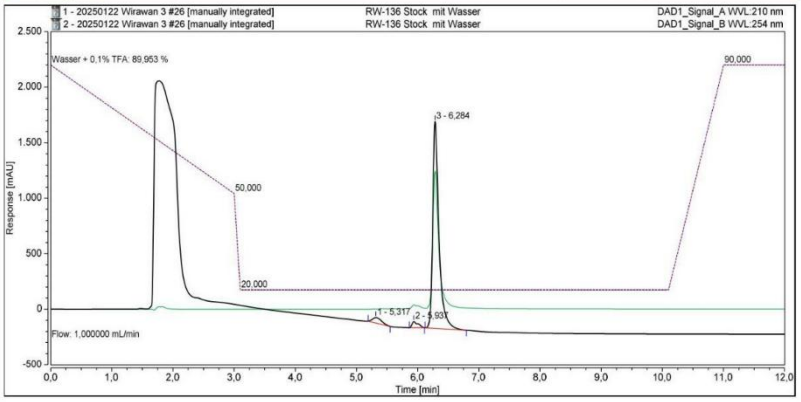

DAD1_Signal_A

No.	Retention Time min	Area mAU*min	Relative Area %
1	5,317	8,482	3,60
2	5,937	6,420	2,72
3	6,284	220,737	93,68
Total:		**235,639**	**100**

DAD1_Signal_B

No.	Retention Time min	Area mAU*min	Relative Area %
1	5,937	4,144	2,82
2	6,284	142,868	97,18
Total:		**147,012**	**100**

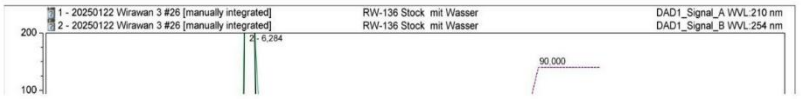

Reinheit Trudel/Integration

Chromeleon (c) Dionex Version 7.2.9.11323

HPLC chromatrogram of (*S*)-2-(6-(4-(3-(2,2-dimethyl-4-oxo-4*H*-benzo[*d*][1,3]dioxin-6-yl)isoxazol-5-yl)phenyl)-2-hydroxy-3,4-dihydro-2*H*-1,5,2-oxazaborinin-4-yl)acetic acid (**52**).

Instrument:NanniHoney Sequence:20250130 Wirawan Page 1 of 1

Chromatogram and Results

Injection Details

Injection Name:	**RW-155-2**		*Run Time (min):*	**11,09**	
Vial Number:	**Vial:92**		*Injection Volume:*	**2,00**	
Injection Type:	**Unknown**		*Wavelength A:*	**210**	
Column:	**Eclipse Plus C18 3,5µm 4,6x 150mm 959963-902**		*Wavelength B:*	**254**	
Instrument Method:	**Methanol Wassser 0,1% TFA Gradient 2**				
Processing Method:	**SG-094**		*Flow rate:*	**1,000**	**mL/min**
Injection Date/Time:	**30.Jan.25 15:05**		*Column Temperatı*	**50,0**	**°C**
Pump Channel A:	**0,00**	Acetonitril			
Pump Channel B:	**10**	Methanol			
Pump ChannelC:	**90**	Wasser 0,1% TFA			
Pump Channel D:		Wasser			

Chromatogram

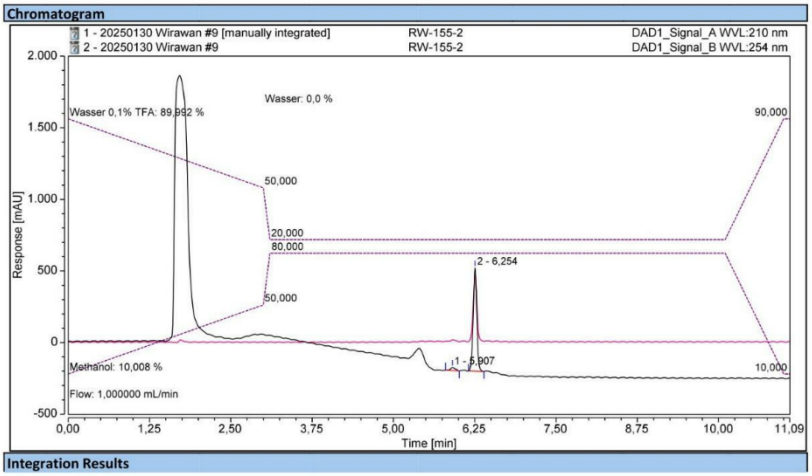

Integration Results

210nm

No.	Peak Name	Retention Time min	Area mAU*min	Relative Area %
1		5,907	1,753	3,6
2		6,254	47,468	96,4
Total:			**49,221**	**100,00**

254mn

No.	Peak Name	Retention Time min	Area mAU*min	Relative Area %
n.a.	n.a.	n.a.	n.a.	n.a.
1		6,254	31,159	100,0
Total:			**31,159**	**100,00**

Reinheit Honey/Integration Chromeleon (c) Dionex Version 7.2.9.11323

HPLC chromatrogram of (*R*)-2-(6-(4-(1-(2,2-dimethyl-4-oxo-4*H*-benzo[*d*][1,3]dioxin-6-yl)-1*H*-1,2,3-triazol-4-yl)phenyl)-2-hydroxy-3,4-dihydro-2*H*-1,5,2-oxazaborinin-4-yl)acetic acid (**53**).

Instrument:Trudel Sequence:20250122 Wirawan 3 Page 1 of 2

Chromatogram and Results

Injection Details

Injection Name:	**RW-186 mit Wasser**	*Run Time (min):*	**11,99**
Vial Number:	**Vial:21**	*Injection Volume:*	**5 µL**
Injection Type:	**Unknown**	*Wavelength:*	**210 nm**
		Wavelength:	**254 nm**
Instrument Method:	**50 MeOH 50 Wasser +0,1% TFA**	*Flow rate:*	**1,0 ml/min**
Column:	**Zorbax Eclipe Pius C18 4,6 x 150mm 3,5µm**	*Column Temperatur:*	**50 °C**
Injection Date/Time:	**23.Jan.25 13:30**	*Pump Channel A:* **50**	
		Pump Channel B: **50,0**	**Wasser + 0,1% TFA**

Chromatogram

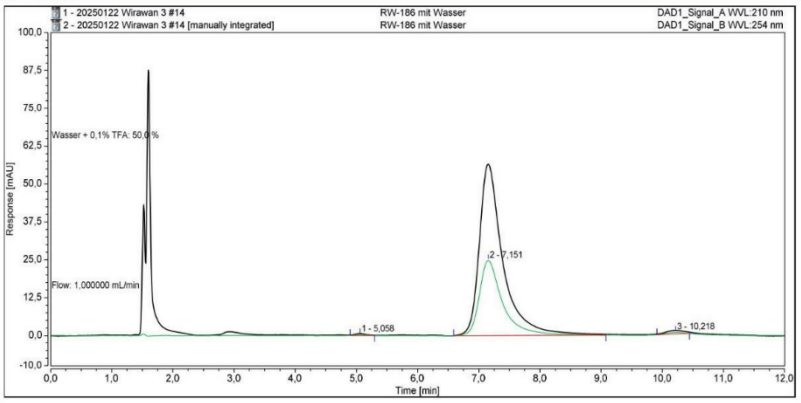

DAD1_Signal_A

No.	Retention Time min	Area mAU*min	Relative Area %
1	7,151	25,012	100,00
Total:		**25,012**	**100**

DAD1_Signal_B

No.	Retention Time min	Area mAU*min	Relative Area %
1	5,058	0,054	0,48
2	7,151	10,905	97,99
3	10,218	0,170	1,53
Total:		**11,129**	**100**

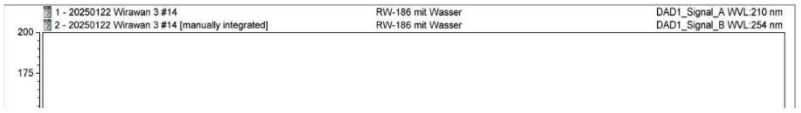

Reinheit Trudel/Integration

Chromeleon (c) Dionex
Version 7.2.9.11323

HPLC chromatrogram of (*S*)-2-(6-(4-(1-(2,2-dimethyl-4-oxo-4*H*-benzo[*d*][1,3]dioxin-6-yl)-1*H*-1,2,3-triazol-4-yl)phenyl)-2-hydroxy-3,4-dihydro-2*H*-1,5,2-oxazaborinin-4-yl)acetic acid (**54**).

Instrument:Trudel Sequence:20250122 Wirawan 3 Page 1 of 2

Chromatogram and Results

Injection Details

Injection Name:	**RW-193 mit Wasser**	*Run Time (min):*	**11,99**
Vial Number:	**Vial:22**	*Injection Volume:*	**5 µL**
Injection Type:	**Unknown**	*Wavelength:*	**210 nm**
		Wavelength:	**254 nm**
Instrument Method:	**50 MeOH 50 Wasser +0,1% TFA**	*Flow rate:*	**1,0 ml/min**
Column:	**Zorbax Eclipe Plus C18 4,6 x 150mm 3,5µm**	*Column Temperatur:*	**50 °C**
Injection Date/Time:	**23.Jan.25 13:42**	*Pump Channel A:*	**50**
		Pump Channel B:	**50,0** **Wasser + 0,1% TFA**

Chromatogram

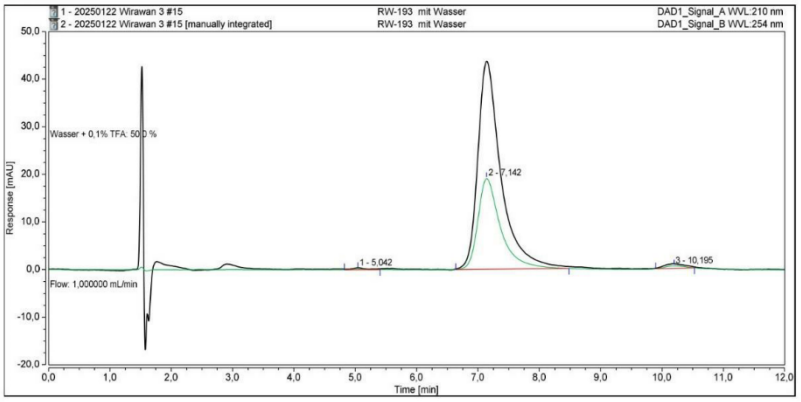

DAD1_Signal_A

No.	Retention Time min	Area mAU*min	Relative Area %
1	7,142	19,382	100,00
Total:		**19,382**	**100**

DAD1_Signal_B

No.	Retention Time min	Area mAU*min	Relative Area %
1	5,042	0,042	0,50
2	7,142	8,183	97,33
3	10,195	0,182	2,17
Total:		**8,407**	**100**

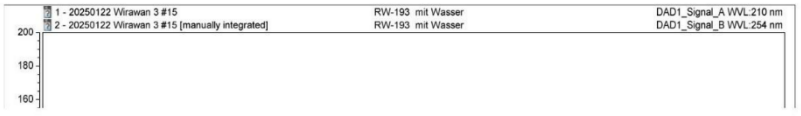

Reinheit Trudel/Integration

Chromeleon (c) Dionex
Version 7.2.9.11323

HPLC chromatrogram of 5-(5-(4-((1-carboxy-4-oxobutan-2-yl)carbamoyl)phenyl)isoxazol-3-yl)-2-hydroxybenzoic acid (**61**).

Instrument:Trudel Sequence:20250121 Wirawan Page 1 of 2

Chromatogram and Results

Injection Details

Injection Name:	**RW-170**	*Run Time (min):*	**14,99**
Vial Number:	**Vial:17**	*Injection Volume:*	**5 µL**
Injection Type:	**Unknown**	*Wavelength:*	**210 nm**
		Wavelength:	**254 nm**
Instrument Method:	**Trudel Gradient MeOH Phosphatpuffer pH 5**	*Flow rate:*	**1,0 ml/min**
Column:	**Zorbax Eclipse Plus C18 4,6 x 150mm 3,5µm**	*Column Temperatur:*	**50 °C**
Injection Date/Time:	**21.Jan.25 13:18**	*Pump Channel A:*	**5**
		Pump Channel B:	**95,0 Puffer pH 5**

Chromatogram

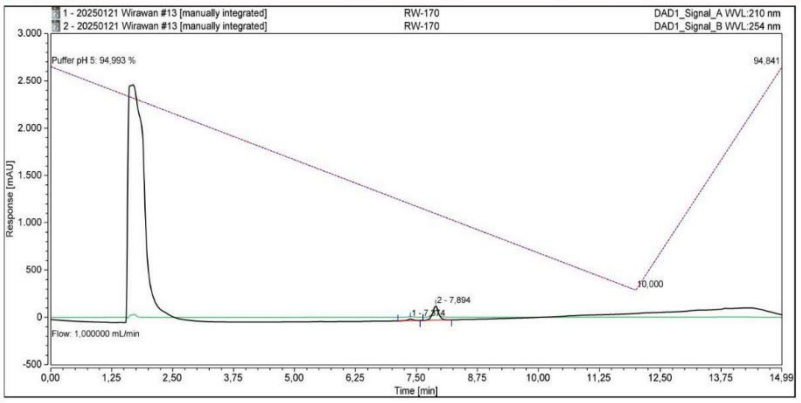

DAD1_Signal_A

No.	Retention Time min	Area mAU*min	Relative Area %
1	7,374	2,295	9,65
2	7,894	21,497	90,35
Total:		**23,792**	**100**

DAD1_Signal_B

No.	Retention Time min	Area mAU*min	Relative Area %
1	7,374	1,005	8,71
2	7,894	10,539	91,29
Total:		**11,544**	**100**

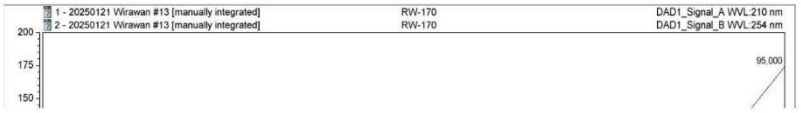

Reinheit Trudel/Integration

Chromeleon (c) Dionex
Version 7.2.9.11323

HPLC chromatrogram of 5-(4-(4-((1-carboxy-4-oxobutan-2-yl)carbamoyl)phenyl)-1*H*-1,2,3-triazol-1-yl)-2-hydroxybenzoic acid (**64**).

Instrument:Trudel Sequence:20250121 Wirawan Page 1 of 2

Chromatogram and Results

Injection Details

Injection Name:	**RW-196**	*Run Time (min):*	**14,99**
Vial Number:	**Vial:21**	*Injection Volume:*	**5 µL**
Injection Type:	**Unknown**	*Wavelength:*	**210 nm**
		Wavelength:	**254 nm**
Instrument Method:	**Trudel Gradient MeOH Phosphatpuffer pH 5**	*Flow rate:*	**1,0 ml/min**
Column:	**Zorbax Eclipe Pius C18 4,6 x 150mm 3,5µm**	*Column Temperatur:*	**50 °C**
Injection Date/Time:	**21.Jan.25 14:21**	*Pump Channel A:*	**5**
		Pump Channel B:	**95,0 Puffer pH 5**

Chromatogram

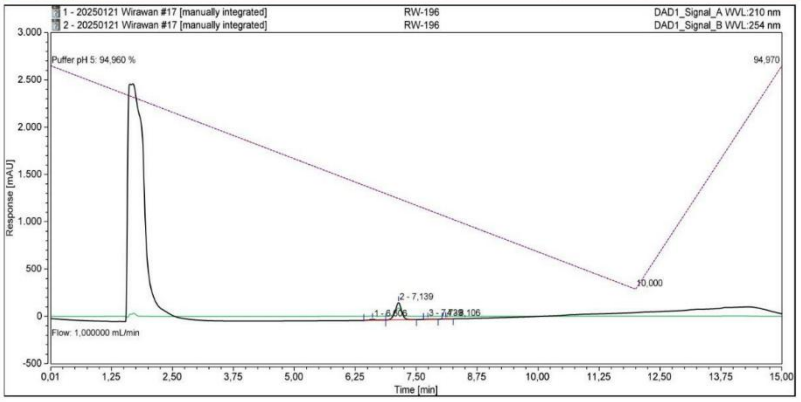

DAD1_Signal_A

No.	Retention Time min	Area mAU*min	Relative Area %
1	6,606	1,309	4,49
2	7,139	27,468	94,27
3	7,739	0,209	0,72
4	8,106	0,153	0,52
Total:		**29,138**	**100**

DAD1_Signal_B

No.	Retention Time min	Area mAU*min	Relative Area %
1	6,599	0,676	4,69
2	7,139	13,201	91,63
3	7,732	0,121	0,84
4	8,106	0,144	1,00
5	8,312	0,125	0,87
6	8,719	0,139	0,97
Total:		**14,407**	**100**

1 - 20250121 Wirawan #17 [manually integrated] RW-196 DAD1_Signal_A WVL:210 nm

Reinheit Trudel/Integration

Chromeleon (c) Dionex Version 7.2.9.11323

S3. Crystal structure data of oxazoline 45

X-ray experimental details and crystal structure of benzyl (*S*)-2-(2-(4-ethynylphenyl)-4,5-dihydrooxazol-4-yl)acetate (**45**).

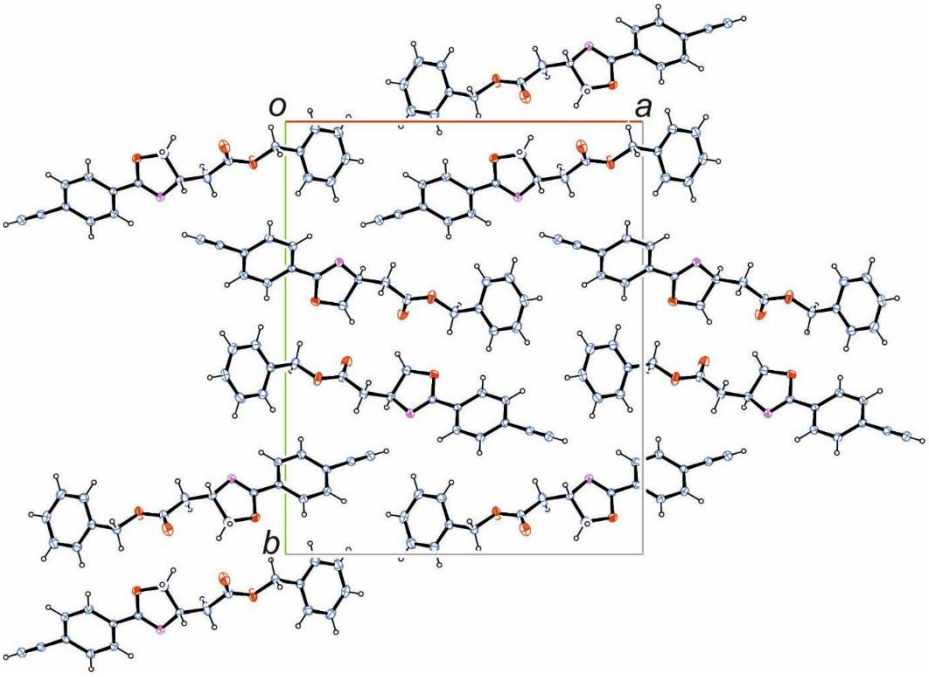

Experimental details

The X-ray intensity data of cv088 were measured on a Bruker D8 Venture TXS system equipped with a multilayer mirror monochromator and a Mo Kα rotating anode X-ray tube (λ = 0.71073 Å). The frames were integrated with the Bruker SAINT software package [47]. Data were corrected for absorption effects using the Multi-Scan method (SADABS) [48]. The structure was solved and refined using the Bruker SHELXTL Software Package [49]. All hydrogen atoms have been calculated in ideal geometry riding on their parent atoms. The figures have been drawn at the 25% ellipsoid probability level [50].

References:

47. Bruker. Bruker AXS Inc., Madison, Wisconsin, USA. SAINT (**2012**).

48. Sheldrick, G.M. University of Göttingen, Germany. SADABS (**1996**).

49. Sheldrick, G.M. SHELXT – Integrated space-group and crystal-structure determination. *Acta Cryst. A* **2015,** *A71, 3–8*. https://doi.org/10.1107/S2053273314026370.

50. Farrugia, L.J. WinGX and ORTEP for Windows: An update. *J. Appl. Cryst.* **2012**, *45, 849–854*. http://dx.doi.org/10.1107/S0021889812029111

net formula	$C_{20}H_{17}NO_3$	parameters	217
Mr/*g mol−1*	319.35	restraints	0
crystal size/mm	0.180 × 0.130 × 0.060	$R(F_{obs})$	0.0345
T/*K*	173.(2)	$Rw(F^2)$	0.0854
radiation	MoKα	*S*	1.105
diffractometer	'Bruker D8 Venture TXS'	shift/errormax	0.001
crystal system	orthorhombic	max electron density/e Å^{-3}	0.106
space group	'P 21 21 21'	min electron density/e Å^{-3}	−0.131
a/*Å*	17.2267(8)		
b/*Å*	20.8646(10)		
c/*Å*	4.5968(2)		
α/°	90		
β/°	90		
γ/°	90		
V/*Å*^{3}	1652.22(13)		
Z	4		
calc. density/g cm^{-3}	1.284		
μ/mm^{-1}	0.087		
absorption correction	Multi-Scan		
transmission factor range	0.95–0.99		
refls. measured	30396		
Rint	0.0420		
mean σ(I)/I	0.0202		
θ range	3.067–25.349		
observed refls.	2861		
x, *y* (weighting scheme)	0.0284, 0.4773		
hydrogen refinement	constr		
Flack parameter	0.0(4)		

refls in refinement	3037

3.4. Project IV: Sirt2 bisubstrate analogues

Wirawan, R.; Ungar, F.; Bracher, F., Substrate- and NAD$^+$ cofactor-mimicking bisubstrate analogues as highly potent SIRT2 inhibitors. *Final manuscript in preparation.*

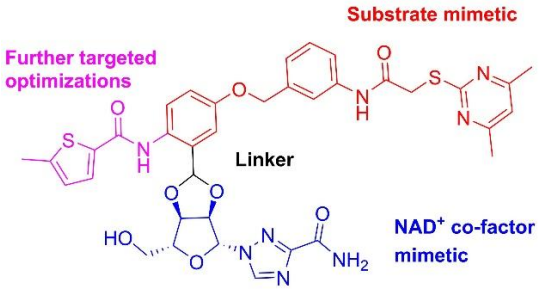

3.4.1. Summary

The application of bisubstrate analogues in the development of highly potent and subtype selective inhibitors has seen notable success in medicinal chemistry. Herein, Sirt2 bisubstrate analogues were rationally designed to concurrently mimic the natural peptide substrate and the essential co-factor NAD$^+$. These preassembled bisubstrate analogues comprise two functional fragments, each targeting a distinct binding site on the enzyme, and are connected *via* an appropriate linker. This dual engagement strategy enables additional interactions with the enzyme, potentially leading to synergistic binding effects. As a result, bisubstrate analogues may exhibit enhanced binding affinity and improved selectivity compared to their monosubstrate counterparts. Ribavirin was selected as a non-ionic low-molecular NAD$^+$ co-factor mimetic with superior pharmacokinetic properties compared to nicotinamide riboside. By connecting ribavirin to the SirReal-type lead compound substrate mimetic **28a** *via* an acetal linker to form the envisaged proof-of-concept Sirt2 bisubstrate analogue **8**, a 20-fold potency increase compared to **28a** was achieved. Further optimisations targeting additional interactions in the acetyl-lysine binding channel of Sirt2 with a methyl-thiophene carboxamide motif led to the development of the bisubstrate analogue **17** that displayed a 30-fold potency increase compared to **28a**. The proposed binding mode of bisubstrate analogue **17** is currently being investigated through co-crystallization experiments by collaborative partners.

3.4.2. Personal Contributions

My personal contributions to this manuscript include the synthesis and the characterization of the optimised bisubstrate analogue **17** and all precursors thereof, the supervision of Florian Ungar's master thesis, the management and coordination of this project, the writing of the original draft and the preparation of the graphical abstract and supplementary information.

Florian Ungar synthesised and characterized the proof-of-concept bisubstrate analogue **8** and all precursors thereof. Franz Bracher conceptualized and designed the study, managed and

coordinated the project, supervised all synthetic work and Florian Ungar's master thesis, provided funding and resources, and reviewed the manuscript.

3.4.3. Manuscript

Substrate- and NAD$^+$ cofactor-mimicking bisubstrate analogues as highly potent SIRT2 inhibitors

Ricky Wirawan[a], Florian Ungar[a], Franz Bracher*[a]

[a]Department of Pharmacy, Ludwig-Maximilians University Munich, Butenandtstraße 5-13, 81377 Munich, Germany. *E-mail: franz.bracher@cup.uni-muenchen.de

Abstract

Sirtuin 2 (SIRT2) has been implicated with the development and exacerbation of various diseases. Significant interest has gained over the past few years in developing highly potent and subtype selective SIRT2 inhibitors. Herein, we applied the principles of bisubstrate analogues that mimic both the natural substrate and the essential co-factor NAD$^+$ in the development of novel and potent SIRT2 inhibitors. Furthermore, the utilization of the antiviral agent ribavirin as an NAD$^+$ co-factor mimetic was implemented in this investigation. Our results revealed a 20-fold increase in the potency of the envisaged bisubstrate analogue **8** compared to its lead structure **28a**, highlighting this effective strategy as a viable option for the development of SIRT2 inhibitors. Further optimizations led to the identification of the bisubstrate analogue **17** with an IC_{50} of 0.27 µM that showed a 30-fold increase in the potency compared to **28a**. Our findings offer a novel and an effective strategy in the development and optimization of SIRT2 inhibitors.

Introduction

Sirtuins (SIRTs) are NAD$^+$-dependent enzymes that belong to the unique class III histone deacetylases[1, 2]. Seven distinct SIRT subtypes have been identified in humans, each characterized by its unique biological roles and subcellular localizations[3]. The predominantly nuclear and cytoplasmic SIRT2 has gained significant interest through the years due to its involvement in the pathogenesis of various diseases such as cancer[4], neurodegeneration[5, 6] and viral infections[7]. Extensive efforts in recent years have focused on the development of highly potent and subtype-selective drug-like SIRT2 inhibitors to advance their utilization as not only practical chemical tools in studying biological processes but also potentially for effective pharmaceutical interventions. However, these rigorous attempts still pose a significant challenge. Notable progress in the development of SIRT2 inhibitors was made through the

identification of the selectivity pocket of SIRT2, which emerges upon the binding of a particular class of inhibitors called SirReals (sirtuin rearranging ligands)[8]. This selectivity pocket can be exploited *via* the binding of the 4,6-dimethylmercaptopyrimidine scaffold of SirReals that confers high subtype-selectivity towards SIRT2[8, 9]. Independent related studies were conducted and have led to the development of further highly potent and subtype-selective SIRT2 inhibitors (Fig.1A)[10, 11].

Although unexplored thus far in the field of SIRTs, the application of bisubstrate analogues as highly potent inhibitors has been established as a promising strategy in medicinal chemistry as exemplified by the development of protein methyltransferase inhibitors[12], DNA methyltransferase inhibitors[13], glycosyltransferase inhibitors[14] and kinase inhibitors[15-17]. Pre-formed bisubstrate analogues consist of two fragments that are tethered to one another *via* a suitable linker, each targeting a distinct binding site of the target protein. Consequently, bisubstrate analogues may facilitate additional ligand-protein interactions, leading to synergistic effects that enhance binding affinities and sometimes also selectivity relative to their monosubstrate counterparts[18]. Herein with this design rationale, we continued our efforts in developing highly potent and subtype-selective SIRT inhibitors[19-21]. The envisaged pre-formed SIRT2 bisubstrate analogues were designed to mimic both the natural peptide substrate and the essential cofactor NAD^+. The SirReal-type inhibitor **28a**[11] was selected as a suitable proof-of-concept lead structure to inhibit the active site of SIRT2 selectively. Furthermore, the selection of a suitable NAD^+ cofactor mimetic is of paramount importance. Although the endogenous co-factor NAD^+ itself can in principle be utilized, the substantial size and potential instability of the pyrophosphates would introduce significant pharmacokinetic challenges. Thus, we considered only the essential motif of the cofactor that is involved in the enzymatic reaction of SIRT2, that is nicotinamide riboside[2]. For this purpose, we selected the antiviral agent ribavirin (**1**) as a low-molecular, drug-like compound that structurally mimics nicotinamide riboside. Sharing the ribosyl scaffold with nicotinamide riboside, ribavirin additionally features a heteroarylamide that is structurally aligned with that of nicotinamide riboside. Furthermore, the nitrogen-containing, aromatic triazole ring of ribavirin that lacks a positive charge even under physiological conditions conveniently offers a pharmacokinetically more favorable motif compared to the pyridinium ring of nicotinamide riboside (Fig.1B).

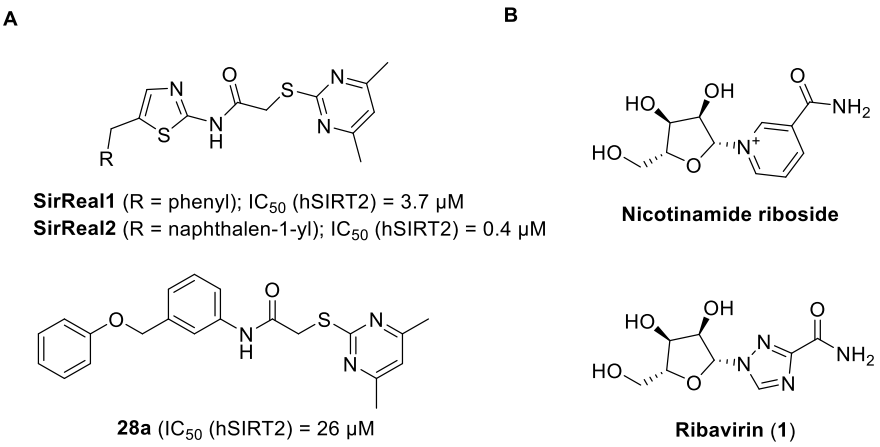

Fig. 1: (**A**) **SirReal**s[8, 9] and the SirReal-type inhibitor **28a**[11] inhibit SIRT2 selectively through binding to the selectivity pocket of SIRT2. (**B**) Chemical structures of the essential part of the co-factor NAD^+ nicotinamide riboside and the structurally aligned antiviral agent ribavirin (**1**).

Based on the co-crystal structure of SirReal2 with SIRT2 (PDB ID: 4RMG)[8] and prior docking experiments of SirReal-type derivatives in our previous work[19], we determined that the vicinal diol unit of the nicotinamide riboside lies in close proximity to the inhibitor and thus offers a suitable site for potential linkage with the inhibitor *via* a short and compact linker. Appropriate electrophilic functional groups at the proper position on the substrate-mimetic inhibitor can form a stable covalent linkage with the vicinal diol unit of the nicotinamide riboside mimetic ribavirin to form the envisaged SIRT2 bisubstrate analogues. Although several electrophilic functional groups such as boronic acids (with the formation of cyclic boronates) can be employed[22], we selected aldehydes with the formation of cyclic acetals as a suitable linker due to their higher stability compared to cyclic boronates[23]. Due to the stability issues of aliphatic and aromatic aldehydes that we encountered in our previous works[19, 24], we decided to initiate the synthesis of the envisaged bisubstrate analogues by first performing the acetalization of ribavirin (**1**) with commercially available functionalized benzaldehydes by applying published acetalization protocols of ribavirin with benzaldehyde by Dong *et al*[25]. The more stable cyclic acetals will serve as key intermediates for subsequent steps in the synthesis of the envisaged bisubstrate analogues.

Results & Discussion

Chemistry

The synthesis of the envisaged bisubstrate analogue consisting of the SIRT2 inhibitor **28a** and ribavirin (**1**) was initiated by the formation of the cyclic acetal **3** from ribavirin (**1**) and 3-hydroxybenzaldehyde (**2**) with zinc chloride (Scheme 1). This procedure was applied from a published acetalization protocol[25] of ribavirin (**1**) with benzaldehyde. Phenol **3** was then subjected to Williamson ether synthesis with 3-nitrobenzyl bromide (**4**) and potassium

carbonate as a base to give aryl-benzyl ether **5** in a relatively low 20% yield, possibly due to steric hindrance attributed from the ribavirin moiety. In the final step, nitroarene **5** was reduced to the corresponding aniline **6** *via* palladium-catalyzed hydrogenation and subsequently coupled with the commercially available carboxylic acid **7** in the presence of the amide coupling reagent EDC-HCl to give the SIRT2 bisubstrate analogue **8** in 49% yield over 2 steps.

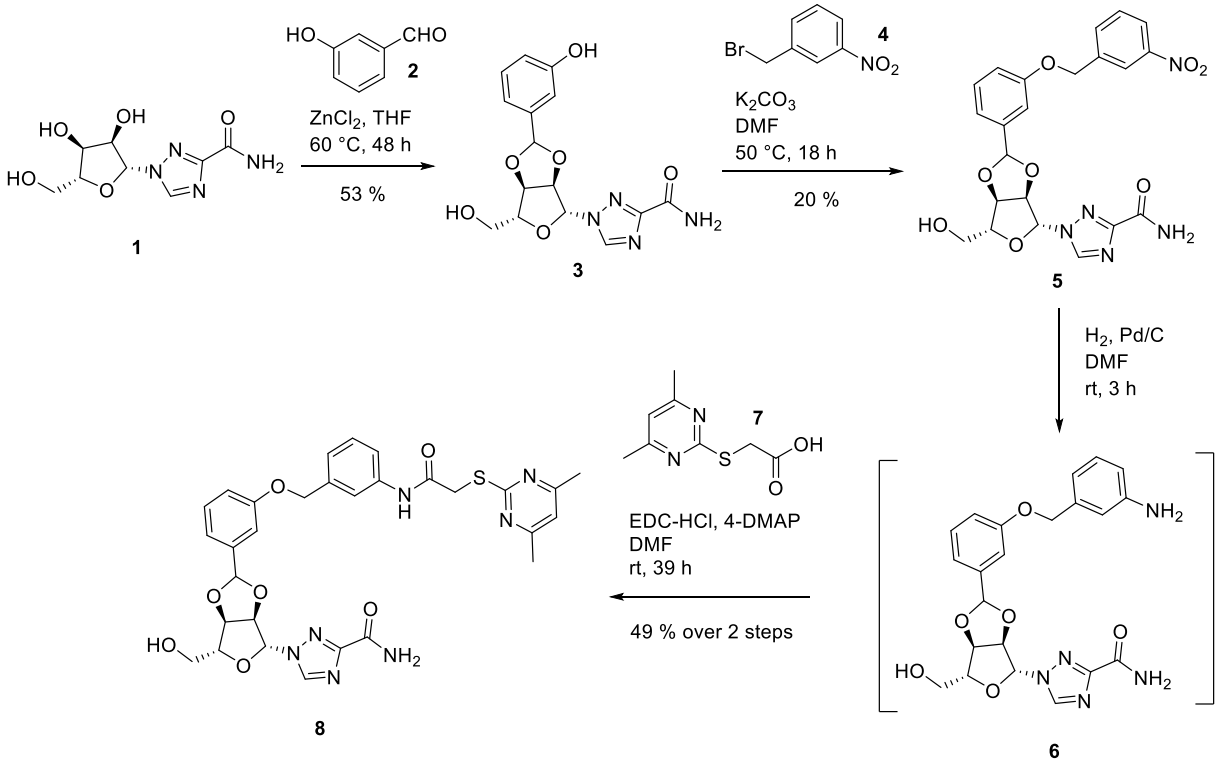

Scheme 1: Synthesis of the envisaged SIRT2 bisubstrate analogue **8** consisting of the SirReal-type inhibitor **28a** and ribavirin (**1**).

Following our previous work on the optimization of SirReal-type inhibitors[20], we determined that 5-methylthiophene-2-carboxamide motifs at the *para*-position to the aryl ether proved to be particularly favorable. Thus, we extended our investigation by optimizing bisubstrate analogue **8** through the incorporation of 5-methylthiophene-2-carboxamide motif to potentially enhance its potency. For this purpose, the cyclic acetal **13** was first synthesized from ribavirin (**1**) and 5-hydroxy-2-nitrobenzaldehyde (**12**) with TFA applying published acetalization protocols[26] for nucleosides with benzaldehyde (Scheme 2). Notably, the previous acetalization conditions with zinc chloride were unsuccessful in yielding the cyclic acetal **13**. Williamson ether synthesis was then performed with phenol **13** and, as opposed to the original route, not benzyl bromide **4**, but rather benzyl bromide **11** to afford aryl ether **14**. Benzyl bromide **4** is not suitable in this case as the product formed would contain two aromatic nitro groups that would simultaneously be reduced with iron in the subsequent step to their corresponding aromatic amines. Thus, selective amide coupling in the final step would not be possible due to the

presence of the two aromatic amines. Benzyl bromide **11** was synthesized from benzyl alcohol **10** with PPh_3 and CBr_4 applying a general Appel reaction protocol[27] , which was prepared by amide coupling of aniline **9** and carboxylic acid **7**. Nitroarene **14** was then reduced to the corresponding aniline **15** with iron and ammonium chloride in a mixture of ethanol and water. Notably, the acetal group remained stable in these aqueous acidic conditions. Reduction of nitroarene **14** *via* palladium-catalyzed hydrogenation showed no success, most likely due to poisoning of the catalyst by the thioether-containing starting material. In the final step, aniline **15** was coupled with 5-methylthiophene-2-carbonyl chloride (**16**) in the presence of pyridine to give the optimized SIRT2 bisubstrate analogue **17.**

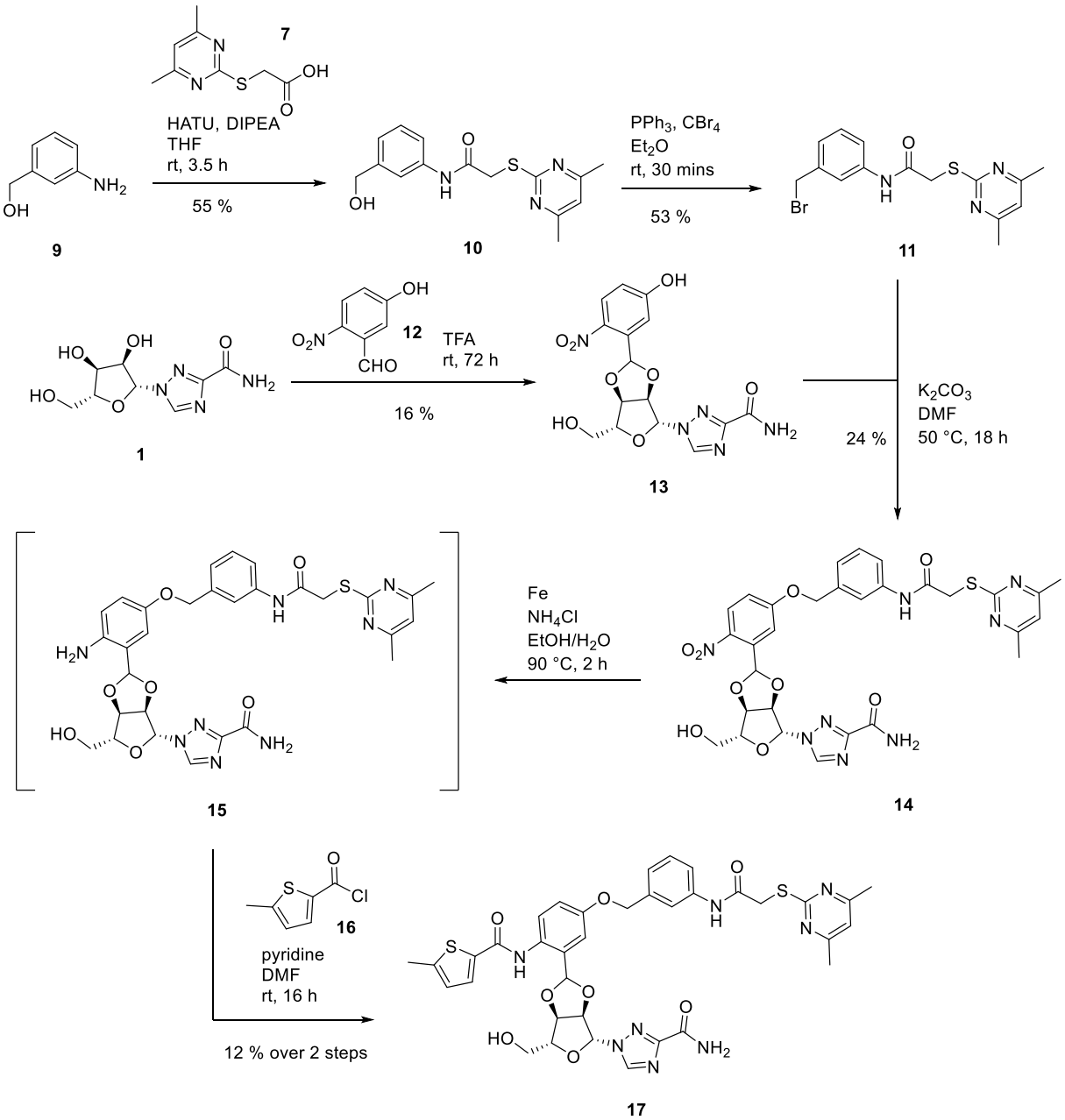

Scheme 2: Synthesis of the optimized SIRT2 bisubstrate analogue **17** incorporating 5-methylthiophene-2-carboxamide motif.

In vitro SIRT inhibitory activities

The SIRT2 inhibitory activities were determined by Reaction Biology Corporation (Malvern, PA, USA) using a fluorescence-based assay using the fluorogenic peptide of p53 residues 379-382 (RHKK(Ac) -FI). In addition, the subtype selectivity of the synthesized compounds was investigated by measuring the residual activity of SIRT1, 3 and 5 after treatment with 50 µM inhibitor. The IC_{50} value of the published SirReal-type lead structure **28a** against SIRT2 was determined to be 8 µM, which is slightly lower than its literature value of 26 µM[11] (Table 1). Ribavirin (**1**), on the other hand, showed very weak SIRT2 inhibition with 12% inhibition at 1 mM. However, even linking ribavirin (**1**) to a phenyl ring with a cyclic acetal linker to form compound **3** resulted in a significant increase in the SIRT2 inhibition with an IC_{50} of 43 µM. However, subtype selectivity was not observed with compound **3** showing similar potency against SIRT1 with 87% inhibition at 50 µM, presumably due to the promiscuity of ribavirin (**1**) to other NAD^+-dependent enzymes. Extending the length of the substrate mimetic with the addition of a 3-nitrobenzyl ether motif to form compound **5** led to a further increase in the SIRT2 inhibition with an IC_{50} of 26 µM. Furthermore, subtype selectivity was also improved with a decrease in the SIRT1 inhibition from 87% to 15% at 50 µM inhibitor concentration. Further increasing the length of the substrate mimetic to utilize the complete molecular structure of **28a** to form the envisaged bisubstrate analogue **8** resulted in a significant increase in the potency against SIRT2 inhibition with an IC_{50} of 0.45 µM. Thus, the conjugation of the substrate mimetic SIRT2 inhibitor **28a** with the putative co-factor mimetic ribavirin (**1**) led to an approximately 20-fold increase in the potency compared to the SirReal-type inhibitor **28a** alone. Furthermore, selectivity against other related SIRT subtypes 1,3 and 5 was observed. Similar results were obtained with an additional nitro group at the *para*-position to the aryl ether of **28a** with an IC_{50} of 0.50 µM identified for bisubstrate analogue **14**. Further optimization of bisubstrate analogue **8** with the incorporation of 5-methylthiophene-2-carboxamide motif to form compound **17** led to an additional increase in the potency with an IC_{50} of 0.27 µM against SIRT2 observed, making bisubstrate analogue **17** around 30-fold more potent than the lead structure **28a**. Bisubstrate analogue **17** showed slight inhibition of SIRT3 with 58% at 50 µM. However, considering the low IC_{50} value of 0.27 µM for the desired target SIRT2, subtype selectivity can be concluded for bisubstrate analogue **17**.

Table 1: *In vitro* inhibition of SIRT1, 2, 3 and 5 by lead structures **1** (ribavirin) and **28a** and the synthesized bisubstrate analogues thereof. IC_{50} values against SIRT2 are shown as a mean of three independent measurements with standard deviations. Inhibitory activity against SIRT2 by compound **1** (ribavirin) was measured at 1 mM and given as mean percentage from three independent measurements. Inhibition percentages at 50 µM for SIRT1, 3

and 5 are given as mean from two independent measurements. n.d. (not determined), n.i. (no inhibition). *Literature-known compound **28a** published by Yang *et al.* with an IC_{50} value for SIRT2 of 26 μM[11].

Compound ID	IC_{50} (μM)	Inhibition of SIRT1/3/5 in % at 50 μM		
	SIRT2	SIRT1	SIRT3	SIRT5
1 (ribavirin)	12% inhibition at 1 mM	n.d.	n.d.	n.d.
28a*	8 ± 1	n.i.	14	n.i.
3	43 ± 3	87	13	22
5	26 ± 1	15	27	6
8	0.45 ± 0.08	11	30	11
14	0.50 ± 0.11	76	35	16
17	0.27 ± 0.02	3	58	8

Conclusions

The development of bisubstrate analogues is a well-established methodology in medicinal chemistry and represents a promising approach in modern drug discovery. Herein, we applied this effective strategy to develop highly potent SIRT2 inhibitors based on the SirReal-type substrate mimetic **28a**. Furthermore, we rationally selected the antiviral agent ribavirin as a suitable NAD^+ co-factor mimetic. Systematic investigation of the synthesized cyclic acetal-linked bisubstrate analogues revealed a positive correlation in terms of potency and subtype selectivity towards SIRT2 by increasing the length of the substrate mimetic. The proof-of-concept bisubstrate analogue **8** that is made up of ribavirin and **28a** resulted in a 20-fold increase in potency compared to **28a** alone. Further targeted optimization led to the identification of the highly potent bisubstrate analogue **17** (IC_{50} = 0.27 μM) that showed a 30-fold increase in potency compared to the lead structure **28a**. Our findings offer a novel insight into the utility of ribavirin as an NAD^+ co-factor mimetic and the application of bisubstrate analogues as a viable strategy in the development of highly potent SIRT2 inhibitors.

Experimental

Chemistry

Materials and instruments. All reagents and solvents were purchased from commercial sources and used without further purification. Standard Schlenk line techniques were employed. Reactions were monitored by thin-layer chromatography (TLC) using POLYGRAM SIL G/UV254 polyester sheets (Macherey-Nagel, Düren, Germany) coated with 0.2 mm silica gel and visualized under UV light (254 or 365 nm) or by staining with $KMnO_4$ and ceric ammonium molybdate (CAM). Flash column chromatography was performed using normal-

phase silica gel (SiO_2 60, 0.040–0.063 mm, 230–400 mesh) (Merck, Darmstadt, Germany) as the stationary phase. NMR spectra were recorded on Bruker Avance III HD 400 MHz and 500 MHz spectrometers (^{1}H: 400/500 MHz; ^{13}C: 101/126 MHz) (Bruker, Billerica, MA, USA) in the indicated deuterated solvents. Chemical shifts (δ) are reported in ppm relative to residual solvent peaks. Signal multiplicities are denoted as s (singlet), d (doublet), t (triplet), q (quartet), and quin (quintet). Coupling constants (J) are given in Hz and rounded to the nearest 0.1 Hz. Infrared spectra were recorded using a PerkinElmer Spectrum BX-59343 FT-IR spectrometer (Perkin Elmer, Shelton, CT, USA) equipped with a Smiths Detection DuraSamplIR II diamond ATR sensor (Smiths Detection, Danbury, CT, USA) over the range of 4000–650 cm^{-1}. Absorption bands are reported in wavenumbers (cm^{-1}). High-resolution mass spectrometry (HRMS) was performed on a JEOL Mstation 700 or JMS GCmate II (EI) (Jeol, Tokyo, Japan) and a Thermo Finnigan LTQ (ESI) (Thermo Finnigan, Somerset, NJ, USA). Melting points were determined using a Büchi Schmelzpunktapparatur B-540 (Büchi, Flawil, Switzerland). Analytical HPLC was conducted at 210 and 254 nm using a Zorbax Eclipse Plus C18 column (4.6 mm × 150 mm, 3.5 µm particle size) (Waters, Milford, MA, USA) for purity determination.

Synthetic Procedures

1-((3*aR*,4*R*,6*R*,6*aR*)-6-(Hydroxymethyl)-2-(3-hydroxyphenyl)tetrahydrofuro[3,4-*d*][1,3]dioxol-4-yl)-1*H*-1,2,4-triazole-3-carboxamide (**3**). To a stirred solution of ribavirin (**1**) (300 mg, 1.23 mmol) in dry THF (3 mL) was added 3-hydroxybenzaldehyde (**2**) (1.21 mg, 9.92 mmol). The reaction mixture was stirred at 60 °C for 45 h. The crude product was poured into cold diethyl ether and the white precipitate formed filtered off and washed with diethyl ether (3x). The filter residue was collected and further purified by FCC (DCM/MeOH 96:4) to give cyclic acetal **3** (227 mg, 0.651 mmol, 53 %) as a white solid. m.p.: 118 °C. ^{1}H-NMR (400 MHz, DMF-d_7): δ (ppm) = 9.79 (s, 1H, 3''-OH), 8.94 (s, 1H, 5-H), 7.95 (s, 1H, $CONH_2$), 7.70 (s, 1H, $CONH_2$), 7.28 (m, 1H, 5''-H), 7.12 – 7.07 (m, 1H, 2''-H), 7.03 (m, 1H, 4''-H), 6.93 – 6.91 (m, 1H, 6''-H), 6.46 (d, *J* = 1.5 Hz, 4'-H), 5.96 (s, 1H, 1''-CHO_2), 5.45 – 5.34 (m, 1H, 3a'-H), 5.23 – 5.11 (m, 2H, 6a'-H and OH), 4.52 (m, 1H, 6'-H), 3.76 – 3.56 (m, 2H, 6'-CH_2). ^{13}C-NMR (101 MHz, DMF-d_7): δ (ppm) = 163.34 ($CONH_2$), 161.61 (C-3''), 159.12 (C-3), 146.54 (C-5), 139.09 (C-1''), 130.52 (C-5''), 118.85 (C-6''), 117.84 (C-4''), 114.80 (C-2''), 107.59 (1''-CHO_2), 94.33 (C-4'), 89.99 (C-6'), 86.49 (C-3a'), 84.41 (C-6a'), 63.13 (6'-CH_2). IR (ATR): $\tilde{\nu}$ (cm^{-1}) = 3317, 2359, 1681, 1594, 1464, 1403, 1285, 1175, 1095, 1072, 869, 786, 696. HRMS (ESI): *m*/*z* = $[M-H]^-$ calcd for $C_{15}H_{15}N_4O_6^-$: 347.0997; found: 347.0993. Specific rotation: $[\alpha]^{20}_D$ +102 (c 0.1 in EtOAc).

1-((3*aR*,4*R*,6*R*,6*aR*)-6-(Hydroxymethyl)-2-(3-((3-nitrobenzyl)oxy)phenyl) tetrahydrofuro[3,4-*d*][1,3]dioxol-4-yl)-1*H*-1,2,4-triazole-3-carboxamide (**5**). To a stirred

solution of phenol **3** (588 mg, 1.69 mmol) in DMF (16 mL) was added 1-(bromomethyl)-3-nitrobenzene (**4**) (304 mg, 1.41 mmol) and the reaction mixture stirred at room temperature for 30 minutes. K_2CO_3 (583 mg, 4.22 mmol) was added and the reaction mixture was stirred at 50 °C for 21 h. The reaction mixture was diluted with EtOAc and the organic phase was washed with 2 M NaOH (3 x 100 mL). The combined organic phase was dried using a phase separation paper and concentrated *in vacuo.* The crude residue was purified by FCC (DCM/MeOH 94:6) to give aryl ether **5** (171 mg, 0.354 mmol, 20 %) as a white solid. m.p.: 92 °C. ^{1}H-NMR (500 MHz, DMF-d_7): δ (ppm) = 8.92 (s, 1H, 5-H), 8.45 (s, 1H, 2‘‘‘-H), 8.27 (ddd, *J* = 8.2, 2.4, 1.0 Hz, 1H, 4‘‘‘-H), 8.05 (d, *J* = 1.3 Hz, 1H, 6‘‘‘-H), 7.95 (s, 1H, $CONH_2$), 7.79 (t, *J* = 7.9 Hz, 1H, 5‘‘‘-H), 7.70 (s, 1H, $CONH_2$), 7.48 – 7.39 (m, 1H, 5‘‘-H), 7.32 (dd, *J* = 2.6, 1.5 Hz, 1H, 2‘‘-H), 7.27 – 7.16 (m, 2H, 4‘‘-H and 6‘‘-H), 6.49 (d, *J* = 1.6 Hz, 1H, 4‘-H), 6.04 (s, 1H, 1‘‘-CHO_2), 5.45 (dd, *J* = 6.3, 1.6 Hz, 1H, 3a‘-H), 5.41 (s, 2H, 1‘‘‘-CH_2), 5.21 – 5.15 (m, 1H, OH), 5.16 – 5.13 (m, 1H, 6a‘-H), 4.52 (td, *J* = 6.1, 1.7 Hz, 1H, 6‘-H), 3.76 – 3.57 (m, 2H, 2‘-CH_2). ^{13}C-NMR (126 MHz, DMF-d_7): δ (ppm) = 160.84 ($CONH_2$), 158.86 (C-3’’), 158.37 (C-3), 148.68 (C-3’’’), 145.76 (C-5), 140.23 (C-1’’’), 138.64 (C-1’’), 134.42 (C-6’’’), 130.44 (C-5’’), 130.11 (C-5’’’), 123.12 (C-4’’’), 122.48 (C-2’’’), 120.16 (C-6’’), 116.43 (C-4’’), 113.86 (C-2’’), 106.55 (1’’-CHO_2), 93.55 (C-4’), 89.11 (C-6’), 85.79 (C-3a’), 83.77 (C-6a’), 68.76 (1’’’-CH_2), 62.31 (6’-CH_2). IR (ATR): $\tilde{\nu}$ (cm^{-1}) = 3367, 3154, 1699, 1663, 1594, 1529, 1353, 1260, 1183, 1126, 1095, 1077, 1021, 790, 733. HRMS (ESI): *m*/*z* = $[M+Na]^+$ calcd for $C_{22}H_{21}N_5O_8Na^+$: 506.1283; found: 506.1277. Purity (HPLC): 210 nm: >95 %; 254 nm: >95 %. Specific rotation: $[\alpha]^{20}_D$ +38 (c 0.1 in acetone).

1-((3*aR*,4*R*,6*R*,6*aR*)-2-(3-((3-(2-((4,6-Dimethylpyrimidin-2-yl)thio)acetamido)benzyl)oxy)phenyl)-6-(hydroxymethyl)tetrahydrofuro[3,4-*d*][1,3]dioxol-4-yl)-1*H*-1,2,4-triazole-3-carboxamide (**8**). Nitroarene **5** (100 mg, 0.207 mmol) was dissolved in DMF (6 mL) and 10 % Pd/C (10.0 mg, 0.094 mmol) was added under N_2 atmosphere. Hydrogenation was performed under atmospheric H_2 pressure at room temperature for 3 h. Upon reaction completion, the reaction mixture was filtered through a pad of celite. The pad was washed with EtOAc and the solvent removed *in vacuo*. The crude product **6** was then used without further purification in the next step. To a stirred solution of 2-((4,6-dimethylpyrimidin-2-yl)thio)acetic acid (**7**) (126 mg, 0.622 mmol) in DMF (3 mL) were added EDC-HCl (122 mg, 0.622 mmol) and 4-DMAP (101 mg, 0.829 mmol) and the reaction mixture was stirred for 10 minutes. Crude product **6** in DMF (6 mL) was then added into the reaction mixture and stirred at room temperature for 39 h. EtOAc (50 mL) and water (50 mL) were added and the organic phase was washed with brine (3 x 50 mL). The collected organic phase was dried using a phase separation paper and concentrated *in vacuo*. The crude product was purified by FCC (DCM/MeOH 96:4) to give amide **8** (63.7 mg, 0.101 mmol, 49 % over 2 steps) as a light orange solid. m.p.: 113 °C. ^{1}H-NMR (500 MHz, $(CD_3)_2SO$): δ (ppm) =

10.29 (s, 1H, CONH), 8.84 (s, 1H, 5-H), 7.87 (s, 1H, $CONH_2$), 7.72 (s, 1H, 2'''-H), 7.69 (s, 1H, $CONH_2$), 7.53 (d, *J* = 8.1 Hz, 1H, 4'''-H), 7.41 – 7.30 (m, 2H, 2''-H and 4''-H), 7.21 – 7.05 (m, 4H, 2''-H, 5''-H, 6''-H and 6'''-H), 6.95 (s, 1H, 5''''-H), 6.54 – 6.43 (m, 1H, 4'-H), 5.92 (s, 1H, 1''-CHO_2), 5.32 (dd, *J* = 6.3, 1.4 Hz, 1H, 6a'-H), 5.12 (s, 2H, OH and 1'''-CH_2), 5.07 (dd, *J* = 6.2, 2.1 Hz, 1H, 3a'-H), 4.98 (s, 1H, 1'''-CH_2), 4.55 (t, *J* = 6.5 Hz, 1H, 6'-H), 4.37 – 4.12 (m, 2H, 6'-CH_2), 3.93 (d, *J* = 1.6 Hz, 2H, SCH_2), 2.26 (s, 6H, 4''''-CH_3 and 6''''-CH_3). ^{13}C-NMR (126 MHz, $(CD_3)_2SO$): δ (ppm) = 169.30 (CONH), 168.81 (C-2''''), 167.10 – 166.97 (C-4'''' and C-6''''), 160.09 ($CONH_2$), 158.47 (C-1'''), 158.31 (C-3''), 157.73 (C-3), 145.81 (C-5), 137.44 (C-1''), 129.70 (C-4''), 128.91 (C-5'''), 122.53 (C-5''), 119.31 (C-6''), 118.61 (C-4'''), 118.12 (C-2'''), 116.07 (C-6''' and C-5''''), 113.32 (C-2''), 105.83 (1''-CHO_2), 91.61 (C-4'), 85.21 (C-6'), 84.86 (C-6a'), 82.24 (C-3a'), 69.72 (1'''-CH_2), 64.72 (6'-CH_2), 32.65 (SCH_2), 23.26 (4''''-CH_3 and 6''''-CH_3). IR (ATR): $\tilde{\nu}$ (cm^{-1}) = 3339, 1690, 1583, 1532, 1441, 1370, 1266, 1100, 1031, 878, 785, 693. HRMS (ESI): *m*/*z* = $[M+H]^+$ calcd for $C_{30}H_{32}N_7O_7S^+$: 634.2084; found: 634.2071. Purity (HPLC): 210 nm: >95 %; 254 nm: >95 %. Specific rotation: $[\alpha]^{20}_D$ +48 (c 0.1 in EtOAc).

2-((4,6-Dimethylpyrimidin-2-yl)thio)-*N*-(3-(hydroxymethyl)phenyl)acetamide (**10**). To a stirred solution of 2-((4,6-dimethylpyrimidin-2-yl)thio)acetic acid (**7**) (500 mg, 2.47 mmol) in THF (32 mL) was added DIPEA (1.3 mL, 7.42 mmol) and HATU (1.41 g, 3.71 mmol) and the reaction mixture was stirred at room temperature for 1 h. (3-Aminophenyl)methanol (**9**) (304 mg, 2.47 mmol) was added and the reaction mixture was stirred at room temperature for 3.5 h. Water (100 mL) was added and the aqueous phase was extracted with DCM (3 x 150 mL). The collected organic phase was dried using a phase separation paper, concentrated *in vacuo* and purified by FCC (DCM/MeOH 97:3) to give alcohol **10** (414 mg, 1.37 mmol, 55 %) as a pale yellow solid. m.p.: 135 °C. ^{1}H-NMR (400 MHz, $(CD_3)_2SO$): δ (ppm) = 10.20 (s, 1H, CONH), 7.56 (t, *J* = 1.8 Hz, 1H, 4-H), 7.47 – 7.41 (m, 1H, 5-H), 7.24 (t, *J* = 7.8 Hz, 1H, 2-H), 7.00 – 6.97 (m, 1H, 6-H), 6.97 – 6.96 (m, 1H, 5'-H), 5.18 (t, *J* = 5.7 Hz, 1H, OH), 4.45 (d, *J* = 5.7 Hz, 2H, 3-CH_2), 4.03 (s, 2H, SCH_2), 2.33 (s, 6H, 4'-CH_3 and 6'-CH_3). ^{13}C-NMR (101 MHz, $(CD_3)_2SO$): δ (ppm) = 169.34 (CONH), 166.95 (C-2'), 166.43 (C-4' and C-6'), 143.25 (C-3), 138.89 (C-1), 128.39 (C-2), 121.33 (C-6), 117.45 (C-4), 117.16 (C-5), 116.05 (C-5'), 62.80 (3-CH_2), 35.47 (SCH_2), 23.33 (4'-CH_3 and 6'-CH_3). IR (ATR): $\tilde{\nu}$ (cm^{-1}) = 3260, 1667, 1580, 1555, 1491, 1428, 1333, 1264, 1199, 880, 850, 794, 729. HRMS (ESI): *m*/*z* = $[M+Na]^+$ calcd for $C_{15}H_{17}N_3O_2NaS^+$: 326.0934; found: 326.0933.

***N*-(3-(Bromomethyl)phenyl)-2-((4,6-dimethylpyrimidin-2-yl)thio)acetamide** (**11**). To a stirred solution of alcohol **10** (540 mg, 1.78 mmol) and CBr_4 (1.18 g, 3.56 mmol) in THF (15 mL) was added PPh_3 (943 mg, 3.56 mmol) and the reaction mixture was stirred for 40 minutes. The reaction mixture was diluted with EtOAc (400 mL) and water (100 mL). The organic phase was washed with water (3 x 100 mL) and dried using a phase separation paper and

concentrated *in vacuo.* The crude residue was purified by FCC (hexanes/EtOAc 65:35) to give alkyl bromide **11** (346 mg, 0.945 mmol, 53 %) as a white solid. m.p.: 120 °C. ^{1}H-NMR (400 MHz, $CDCl_3$): δ (ppm) = 9.57 (s, 1H, CONH), 7.56 (t, *J* = 2.0 Hz, 1H, 4'-H), 7.35 (ddd, *J* = 8.1, 2.2, 1.1 Hz, 1H, 5'-H), 7.30 – 7.21 (m, 1H, 6'-H), 7.10 (dt, *J* = 7.6, 1.4 Hz, 1H, 2'-H), 6.84 (s, 1H, 5-H), 4.45 (s, 2H, CH_2Br), 3.88 (s, 2H, SCH_2), 2.50 (s, 6H, 4-CH_3 and 6-CH_3). ^{13}C-NMR (101 MHz, $CDCl_3$): δ (ppm) = 170.31 (CONH), 167.97 (C-2), 167.78 (C-4 and C-6), 138.81 (C-3'), 138.62 (C-1'), 129.55 (C-6'), 124.79 (C-2'), 120.33 (C-4'), 119.71 (C-5'), 116.89 (C-4), 35.65 (SCH_2), 33.36 (CH_2Br), 24.10 (4-CH_3 and 6-CH_3). IR (ATR): ṽ (cm^{-1}) = 3327, 2920, 1667, 1587, 1554, 1432, 1387, 1271, 1069, 843, 788, 989. HRMS (ESI): *m*/*z* = $[M+H]^+$ calcd for $C_{15}H_{16}BrN_3NaOS^+$: 388.0090; found: 388.0092.

1-((3a*R*,4*R*,6*R*,6a*R*)-2-(5-Hydroxy-2-nitrophenyl)-6-(hydroxymethyl)tetrahydrofuro[3,4-*d*][1,3]dioxol-4-yl)-1*H*-1,2,4-triazole-3-carboxamide (**13**)**.** To a stirred solution of ribavirin (**1**) (3.00 g, 12.3 mmol) in TFA (30 mL) was added 5-hydroxy-2-nitrobenzaldehyde (**12**) (4.10 g, 24.6 mmol) at 0 °C. The reaction was allowed to warm gradually to room temperature while stirring for 72 h. TFA was removed in *vacuo* and the crude product purified by FCC (DCM/MeOH 97:3 -> 95:5) to give cyclic acetal **13** (779 mg, 1.98 mmol, 16 %) as a brown solid. m.p.: 163 °C. ^{1}H-NMR (400 MHz, $(CD_3)_2SO$): δ (ppm) = 11.20 (s, 1H, 5''-OH), 8.82 (s, 1H, 5-H), 8.03 (d, *J* = 9.0 Hz, 1H, 3''-H), 7.87 (s, 1H, $CONH_2$), 7.66 (s, 1H, $CONH_2$), 7.36 (d, *J* = 2.7 Hz, 1H, 6''-H), 6.99 (dd, *J* = 9.0, 2.8 Hz, 1H, 4''-H), 6.54 (s, 1H, 1''-CHO_2), 6.33 – 6.31 (m, 1H, 4'-H), 5.36 (dd, *J* = 6.1, 1.4 Hz, 1H, 3a'-H), 5.08 (dd, *J* = 6.3, 1.8 Hz, 1H, 6a'-H), 5.04 (t, *J* = 5.3 Hz, 1H, OH), 4.34 (dt, *J* = 5.7, 5.7 Hz, 1H, 6'-H), 3.55 – 3.39 (m, 2H, 6'-CH_2). ^{13}C-NMR (101 MHz, $(CD_3)_2SO$): δ (ppm) = 162.58 (C-5''), 160.22 ($CONH_2$), 157.46 (C-3), 145.35 (C-5), 139.71 (C-2''), 133.86 (C-1''), 127.95 (C-3''), 116.51 (C-4''), 113.87 (C-6''), 101.21 (1''-CHO_2), 92.07 (C-4'), 87.96 (C-6'), 84.92 (C-3a'), 82.84 (C-6a'), 61.23 (6'-CH_2). IR (ATR): ṽ (cm^{-1}) = 3319, 2953, 1667, 1597, 1520, 1497, 1449, 1337, 1307, 1189, 1135, 1066, 1027, 849, 798, 721. HRMS (ESI): *m*/*z* = $[M+Na]^+$ calcd for $C_{15}H_{15}N_5O_8Na^+$: 416.0818; found: 416.0810. Purity (HPLC): 210 nm: >95 %; 254 nm: >95 %. Specific rotation: $[\alpha]^{20}_D$ -27 (c 0.1 in DMSO).

1-((3a*R*,4*R*,6*R*,6a*R*)-2-(5-((3-(2-((4,6-Dimethylpyrimidin-2-yl)thio)acetamido)benzyl)oxy)-2-nitrophenyl)-6-(hydroxymethyl)tetrahydrofuro[3,4-*d*][1,3]dioxol-4-yl)-1*H*-1,2,4-triazole-3-carboxamide (**14**). To a stirred solution of phenol **13** (1.10 g, 2.80 mmol) in DMF (25 mL) was added alkyl bromide **11** (1.23 g, 3.36 mmol) and the reaction mixture stirred at room temperature for 30 minutes. K_2CO_3 (1.16 g, 8.39 mmol) was added and the reaction mixture was stirred at 50 °C for 21 h. The reaction mixture was diluted with EtOAc and the organic phase was washed with 2 M NaOH (3 x 200 mL). The combined organic phase was dried using a phase separation paper and concentrated *in vacuo.* The crude product was purified by FCC (DCM/MeOH 95:5) to give aryl ether **14** (453 mg, 0.667 mmol, 24 %) as a

white solid. m.p.: 199 °C. ^{1}H-NMR (500 MHz, $(CD_3)_2SO$): δ (ppm) = 10.31 (s, 1H, CONH), 8.80 (s, 1H, 5-H), 8.13 (d, *J* = 9.1 Hz, 1H, 3‘‘-H), 7.88 – 7.85 (m, 1H, $CONH_2$), 7.75 – 7.71 (m, 1H, 2‘‘‘-H), 7.68 – 7.65 (m, 1H, $CONH_2$), 7.56 – 7.51 (m, 1H, 4‘‘‘-H), 7.48 (d, *J* = 2.8 Hz, 1H, 6‘‘-H), 7.38 – 7.33 (m, 1H, 5‘‘‘-H), 7.30 (dd, *J* = 9.1, 2.9 Hz, 1H, 4‘‘-H), 7.21 – 7.17 (m, 1H, 6‘‘‘-H), 6.95 (s, 1H, 5‘‘‘‘-H), 6.55 (s, 1H, 1‘‘-CHO_2), 6.35 (s, 1H, 4‘-H), 5.37 (dd, *J* = 6.1, 1.5 Hz, 1H, 3a‘-H), 5.28 (s, 2H, 5‘‘-OCH_2), 5.10 – 5.07 (m, 1H, 6a‘-H), 5.03 – 4.99 (m, 1H, OH), 4.31 (t, *J* = 6.0 Hz, 1H, 6‘-H), 4.03 (s, 2H, SCH_2), 3.53 – 3.38 (m, 2H, 6‘-CH_2), 2.31 (s, 6H, 4‘‘‘‘-CH_3 and 6‘‘‘‘-CH_3). ^{13}C-NMR (126 MHz, $(CD_3)_2SO$): δ (ppm) = 169.29 (C-2‘‘‘‘), 166.95 (C-4‘‘‘‘ and C-6’‘’‘), 166.70 (CONH), 162.12 (C-5’‘), 160.22 ($CONH_2$), 157.45 (C-3), 145.34 (C-5), 141.18 (C-2’‘), 139.32 (C-3’‘’), 136.58 (C-1’‘’), 133.53 (C-1’‘), 129.06 (C-5’‘’), 127.71 (C-3’‘), 122.75 (C-6’‘’), 118.93 (C-4’‘’), 118.26 (C-2’‘’), 116.06 (C-5’‘’‘), 115.47 (C-4’‘), 113.86 (C-6’‘), 101.09 (1’‘-CHO_2), 92.03 (C-4’), 87.80 (C-6’), 84.95 (C-3a’), 82.94 (C-6a’), 70.18 (5’‘-OCH_2), 61.15 (6’-CH_2), 35.47 (SCH_2), 23.31 (4’‘’‘-CH_3 and 6’‘’‘-CH_3). IR (ATR): $\tilde{\nu}$ (cm^{-1}) = 3623, 3359, 2931, 1682, 1613, 1582, 1487, 1324, 1287, 1230, 1178, 1105, 1066, 979, 849. HRMS (ESI): *m*/*z* = $[M+Na]^+$ calcd for $C_{30}H_{30}N_8O_9SNa^+$: 701.1754; found: 701.1740. Purity (HPLC): 210 nm: >95 %; 254 nm: >95 %. Specific rotation: $[\alpha]^{20}_D$ -37 (c 0.1 in DMSO).

1-((3a*R*,4*R*,6*R*,6a*R*)-2-(5-((3-(2-((4,6-Dimethylpyrimidin-2-yl)thio)acetamido)benzyl)oxy)-2-(5-methylthiophene-2-carboxamido)phenyl)-6-(hydroxymethyl)tetrahydrofuro[3,4-*d*][1,3]dioxol-4-yl)-1*H*-1,2,4-triazole-3-carboxamide (**17**). To a stirred solution of nitroarene **14** (150 mg, 0.221 mmol) in EtOH (45 mL) was added iron powder (61.7 mg, 1.11 mmol) at 50 °C. 0.3 M ammonium chloride solution (3.75 mL) was added and the reaction mixture was refluxed at 90 °C for 2 h. The iron powder was filtered and the filtrate concentrated *in vacuo*. The crude residue was redissolved in EtOAc, sat. aq. $NaHCO_3$ was added and the aqueous phase extracted with EtOAc (3 x 100 mL). The organic phase was dried using a phase separation paper, concentrated *in vacuo* to give crude aniline **15**, which was taken up for the next step without further purification. To a stirred solution of the obtained crude aniline **15** in DMF (5 mL) was added acid chloride **16** (43.1 mg, 0.268 mmol) and pyridine (9.04 µL, 0.112 mmol). The reaction was stirred at room temperature for 1 h before adding another equivalent of acid chloride **16** (43.1 mg, 0.268 mmol). The reaction was stirred at room temperature for 16 h. EtOAc (100 mL) was added and the organic phase was washed with 2M NaOH (2 x 100 mL) and brine (2 x 100 mL). The organic phase was dried using a phase separation paper, concentrated in vacuo and purified by FCC (DCM/MeOH 96:4) to give amide **17** (20.0 mg, 0.026 mmol, 12 % over 2 steps) as a pale yellow solid.

Sirtuin Assays. Sirtuin inhibitory activity was assessed using a fluorescence-based assay performed by Reaction Biology Corporation (Malvern, PA, USA) following standard internal protocols. Test compounds, prepared in DMSO, were added to enzyme solutions in Tris-HCl

buffer (pH 8.0) and incubated for 10 min at 30 °C. The reaction was initiated by the addition of NAD^+ and a 7-amino-4-methylcoumarin (AMC)-labeled fluorogenic peptide substrate. After 2 h at 30 °C, the reaction was terminated with 2 mM nicotinamide, followed by a protease-based developer to release AMC. Fluorescence was recorded 1 h later at 30 °C (excitation/emission: 360/460 nm). Enzyme activity was measured relative to a no-inhibitor control (set as 100%). IC_{50} values for each test compound were determined in triplicate using 10-point, 3-fold serial dilutions starting at 10 µM, 50 µM, 100 µM or 1 mM. Individual IC_{50} values were calculated by nonlinear regression using a sigmoidal dose–response model (GraphPad Prism 8.0.2) (GraphPad Software, Boston, MA, USA) and the mean ± standard deviation was reported. Selectivity against SIRT1, 3, and 5 was evaluated in duplicate at a single 50 µM concentration, with residual enzyme activity expressed as a percentage of the no-inhibitor control.

Author contributions

Conceptualization, F.B.; methodology, R.W., F.U. and F.B.; formal analysis, R.W. and F.B.; investigation, R.W., F.U. and F.B.; resources, F.B.; data curation, R.W., F.U. and F.B.; writing—original draft preparation, R.W.; writing—review and editing, F.B.; visualization, R.W.; supervision, R.W. and F.B.; project administration, F.B.; funding acquisition, F.B.

Conflicts of interest

There are no conflicts to declare.

Data availability

^1H and ^{13}C NMR spectra of synthesized compounds and the HPLC chromatograms of tested compounds have been included as part of the Supplementary Information.

Acknowledgements

This research was funded by the Deutsche Forschungsgemeinschaft (DFG, German Research Foundation) with funds from SFB1309 (Chemical Biology of Epigenetic Modifications, project ID: 325871075‑SFB1309) to F.B.

We thank Lars Allmendinger and Claudia Glas for NMR services, Werner Spahl and Sonja Kosak for MS services, Anna Niedrig for HPLC services.

References

(1) Behnisch-Cornwell, S.; Grathwol, C. W.; Schulig, L.; Voigt, A.; Baecker, D.; Link, A.; Bednarski, P. J. Correlation Analysis of Protein Expression of 10 HDAC/Sirtuin Isoenzymes with Sensitivities of 23 Anticancer Drugs in 17 Cancer Cell Lines and Potentiation of Drug Activity by Co-Treatment with HDAC Inhibitors. *Cancers (Basel)* **2021**, *14* (1).

(2) Schiedel, M.; Robaa, D.; Rumpf, T.; Sippl, W.; Jung, M. The Current State of NAD+-Dependent Histone Deacetylases (Sirtuins) as Novel Therapeutic Targets. *Med Res Rev* **2018**, *38* (1), 147-200.
(3) Giblin, W.; Lombard, D. B. Chapter 3 - Sirtuins, Healthspan, and Longevity in Mammals. In *Handbook of the Biology of Aging (Eighth Edition)*, Kaeberlein, M. R., Martin, G. M. Eds.; Academic Press, **2016**; pp 83-132.
(4) Jing, H.; Hu, J.; He, B.; Negrón Abril, Y. L.; Stupinski, J.; Weiser, K.; Carbonaro, M.; Chiang, Y. L.; Southard, T.; Giannakakou, P.; et al. A SIRT2-Selective Inhibitor Promotes c-Myc Oncoprotein Degradation and Exhibits Broad Anticancer Activity. *Cancer Cell* **2016**, *29* (3), 297-310.
(5) Sola-Sevilla, N.; Mesa-Lombardo, A.; Aleixo, M.; Expósito, S.; Diaz-Perdigón, T.; Azqueta, A.; Zamani, F.; Suzuki, T.; Maioli, S.; Eroli, F.; et al. SIRT2 Inhibition Rescues Neurodegenerative Pathology but Increases Systemic Inflammation in a Transgenic Mouse Model of Alzheimer's Disease. *J Neuroimmune Pharmacol* **2023**, *18* (3), 529-550.
(6) de Oliveira, R. M.; Vicente Miranda, H.; Francelle, L.; Pinho, R.; Szegö É, M.; Martinho, R.; Munari, F.; Lázaro, D. F.; Moniot, S.; Guerreiro, P.; et al. The mechanism of sirtuin 2-mediated exacerbation of alpha-synuclein toxicity in models of Parkinson disease. *PLoS Biol* **2017**, *15* (3), e2000374.
(7) Duran-Castells, C.; Llano, A.; Kawana-Tachikawa, A.; Prats, A.; Martinez-Zalacain, I.; Kobayashi-Ishihara, M.; Oriol-Tordera, B.; Peña, R.; Gálvez, C.; Silva-Arrieta, S.; et al. Sirtuin-2, NAD-Dependent Deacetylase, Is a New Potential Therapeutic Target for HIV-1 Infection and HIV-Related Neurological Dysfunction. *J Virol* **2023**, *97* (2), e0165522.
(8) Rumpf, T.; Schiedel, M.; Karaman, B.; Roessler, C.; North, B. J.; Lehotzky, A.; Oláh, J.; Ladwein, K. I.; Schmidtkunz, K.; Gajer, M.; et al. Selective Sirt2 inhibition by ligand-induced rearrangement of the active site. *Nat Commun* **2015**, *6*, 6263.
(9) Schiedel, M.; Rumpf, T.; Karaman, B.; Lehotzky, A.; Oláh, J.; Gerhardt, S.; Ovádi, J.; Sippl, W.; Einsle, O.; Jung, M. Aminothiazoles as Potent and Selective Sirt2 Inhibitors: A Structure-Activity Relationship Study. *J Med Chem* **2016**, *59* (4), 1599-1612.
(10) Yang, L.; Ma, X.; Yuan, C.; He, Y.; Li, L.; Fang, S.; Xia, W.; He, T.; Qian, S.; Xu, Z.; et al. Discovery of 2-((4,6-dimethylpyrimidin-2-yl)thio)-N-phenylacetamide derivatives as new potent and selective human sirtuin 2 inhibitors. *Eur J Med Chem* **2017**, *134*, 230-241.
(11) Yang, L. L.; Wang, H. L.; Zhong, L.; Yuan, C.; Liu, S. Y.; Yu, Z. J.; Liu, S.; Yan, Y. H.; Wu, C.; Wang, Y.; et al. X-ray crystal structure guided discovery of new selective, substrate-mimicking sirtuin 2 inhibitors that exhibit activities against non-small cell lung cancer cells. *Eur J Med Chem* **2018**, *155*, 806-823.

(12) Chen, D.; Dong, C.; Dong, G.; Srinivasan, K.; Min, J.; Noinaj, N.; Huang, R. Probing the Plasticity in the Active Site of Protein N-terminal Methyltransferase 1 Using Bisubstrate Analogues. *J Med Chem* **2020**, *63* (15), 8419-8431.

(13) Halby, L.; Menon, Y.; Rilova, E.; Pechalrieu, D.; Masson, V.; Faux, C.; Bouhlel, M. A.; David-Cordonnier, M. H.; Novosad, N.; Aussagues, Y.; et al. Rational Design of Bisubstrate-Type Analogues as Inhibitors of DNA Methyltransferases in Cancer Cells. *J Med Chem* **2017**, *60* (11), 4665-4679.

(14) Izumi, M.; Yuasa, H.; Hashimoto, H. Bisubstrate analogues as glycosyltransferase inhibitors. *Curr Top Med Chem* **2009**, *9* (1), 87-105.

(15) Parang, K.; Till, J. H.; Ablooglu, A. J.; Kohanski, R. A.; Hubbard, S. R.; Cole, P. A. Mechanism-based design of a protein kinase inhibitor. *Nat Struct Biol* **2001**, *8* (1), 37-41.

(16) Ricouart, A.; Gesquiere, J. C.; Tartar, A.; Sergheraert, C. Design of potent protein kinases inhibitors using the bisubstrate approach. *J Med Chem* **1991**, *34* (1), 73-78.

(17) Kumar, A.; Wang, Y.; Lin, X.; Sun, G.; Parang, K. Synthesis and Evaluation of 3-Phenylpyrazolo[3,4-d]pyrimidine-Peptide Conjugates as Src Kinase Inhibitors. *ChemMedChem* **2007**, *2* (9), 1346-1360.

(18) Lavogina, D.; Enkvist, E.; Uri, A. Bisubstrate Inhibitors of Protein Kinases: from Principle to Practical Applications. *ChemMedChem* **2010**, *5* (1), 23-34.

(19) Wirawan, R.; Frei, M.; Heider, A.; Papenkordt, N.; Friedrich, F.; Wein, T.; Jung, M.; Groll, M.; Huber, E. M.; Bracher, F. Tailored SirReal-type inhibitors enhance SIRT2 inhibition through ligand stabilization and disruption of NAD+ co-factor binding. *RSC Med Chem* **2025**, *16* (11), 5419-5440.

(20) Frei, M.; Wein, T.; Bracher, F. Lead-Structure-Based Rigidization Approach to Optimize SirReal-Type Sirt2 Inhibitors. *Molecules* **2025**, *30* (8).

(21) Frei, M.; Wirawan, R.; Wein, T.; Bracher, F. Lead Structure-Based Hybridization Strategy Reveals Major Potency Enhancement of SirReal-Type Sirt2 Inhibitors. *Int J Mol Sci* **2025**, Vol. 26, p 9855.

(22) Deore, B. A.; Freund, M. S. Reactivity of Poly(anilineboronic acid) with NAD+ and NADH. *Chem Mater* **2005**, *17* (11), 2918-2923.

(23) Bernardini, R.; Oliva, A.; Paganelli, A.; Menta, E.; Grugni, M.; Munari, S. D.; Goldoni, L. Stability of Boronic Esters to Hydrolysis: A Comparative Study. *Chem Lett* **2009**, *38* (7), 750-751.

(24) Wirawan, R.; Huber, S. A.; Wein, T.; Bracher, F. Balsalazide-Derived Heterotriaryls as Sirtuin 5 Inhibitors: A Case Study of a Reversible Covalent Inhibition Strategy. *Molecules* **2025**, Vol. 30, p 3821.

(25) Dong, Z.; Li, Q.; Guo, D.; Shu, Y.; Polli, J. E. Synthesis and Evaluation of Bile Acid-Ribavirin Conjugates as Prodrugs to Target the Liver. *J Pharm Sci* **2015**, *104* (9), 2864-2876.

(26) Douglass, J. G.; Patel, R. I.; Yerxa, B. R.; Shaver, S. R.; Watson, P. S.; Bednarski, K.; Plourde, R.; Redick, C. C.; Brubaker, K.; Jones, A. C.; et al. Lipophilic Modifications to Dinucleoside Polyphosphates and Nucleotides that Confer Antagonist Properties at the Platelet P2Y12 Receptor. *J Med Chem* **2008**, *51* (4), 1007-1025.
(27) Röhrich, T.; Abu Thaher, B.; Manicone, N.; Otto, H.-H. Substituted 1,2-Thiazetidine 1,1-Dioxides. Synthesis of (RS)- and (S)-1,2-Thiazetidine-3-acetic Acid 1,1-Dioxide and its Reactions with Amino Acids and Dipeptides. *Monatsh Chem* **2004**, *135* (8), 979-999.

Supplementary Information

Substrate- and NAD$^+$ cofactor-mimicking bisubstrate analogues as highly potent SIRT2 inhibitors

Ricky Wirawan[a], Florian Ungar[a], Franz Bracher*[a]

[a]Department of Pharmacy, Ludwig-Maximilians University Munich, Butenandtstraße 5-13, 81377 Munich, Germany. *E-mail: franz.bracher@cup.uni-muenchen.de

Table of Contents:

^{1}H and ^{13}C NMR spectra of compound **3**

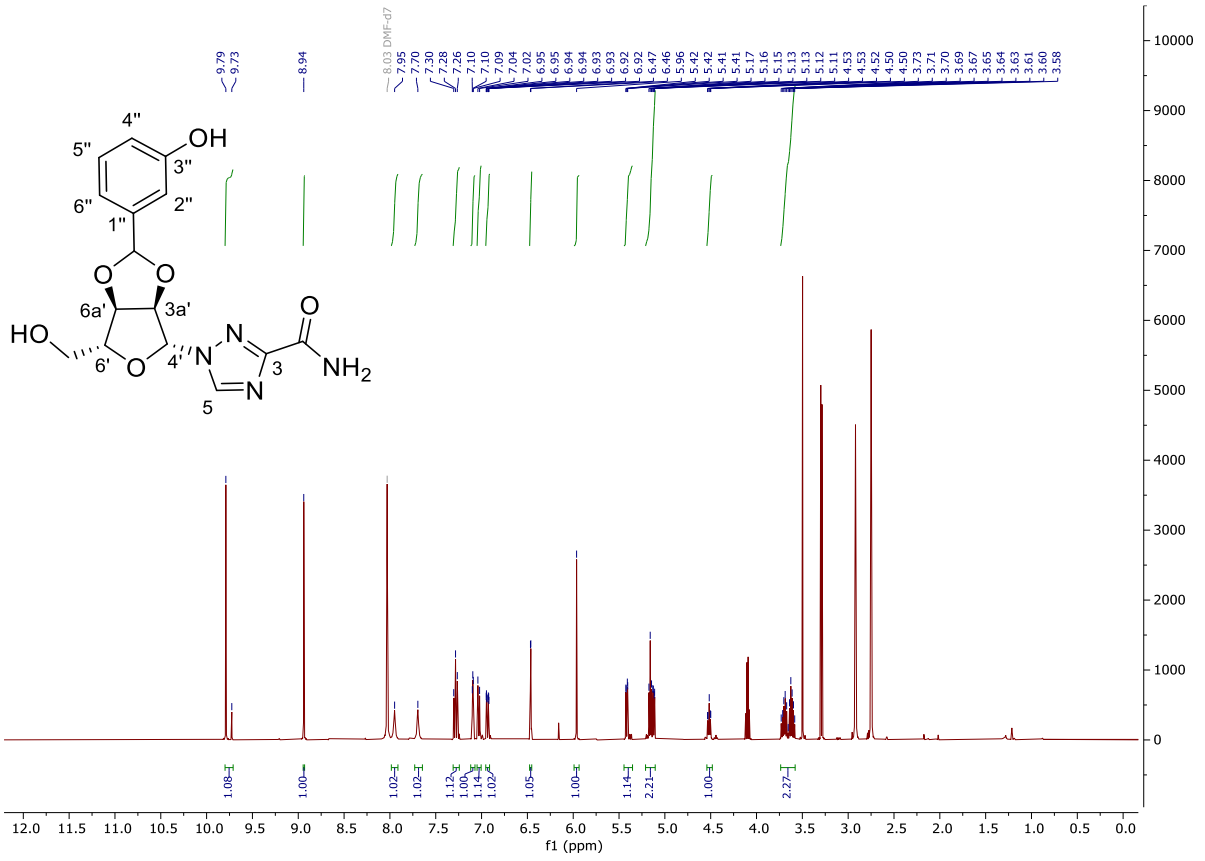

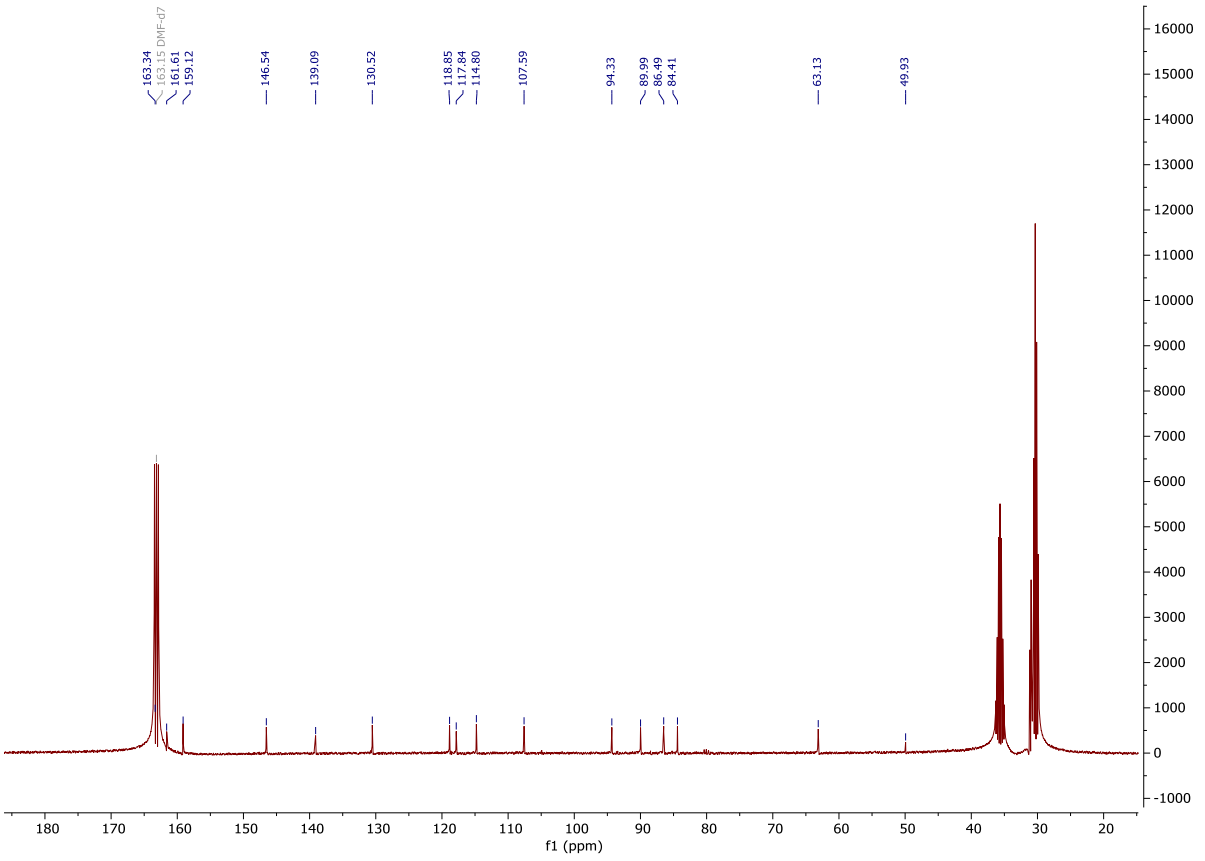

^{1}H and ^{13}C NMR spectra of compound **5**

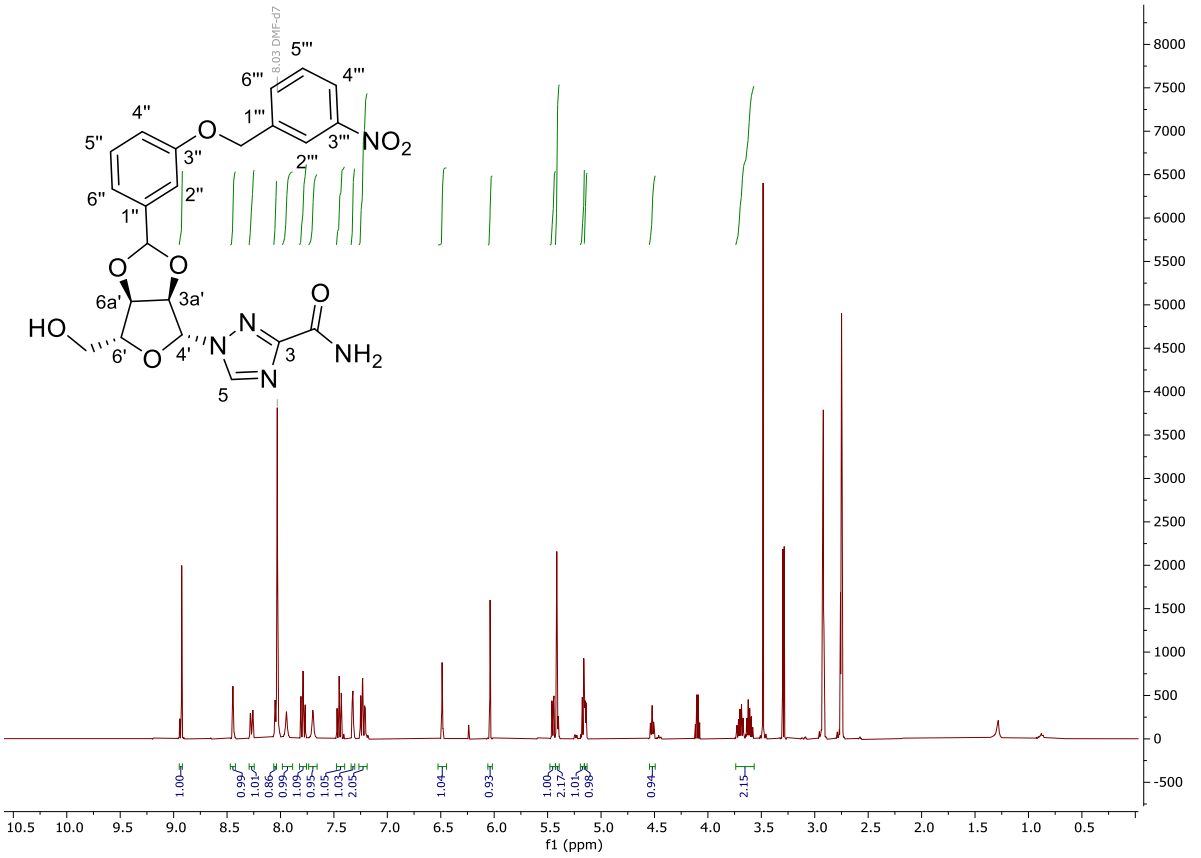

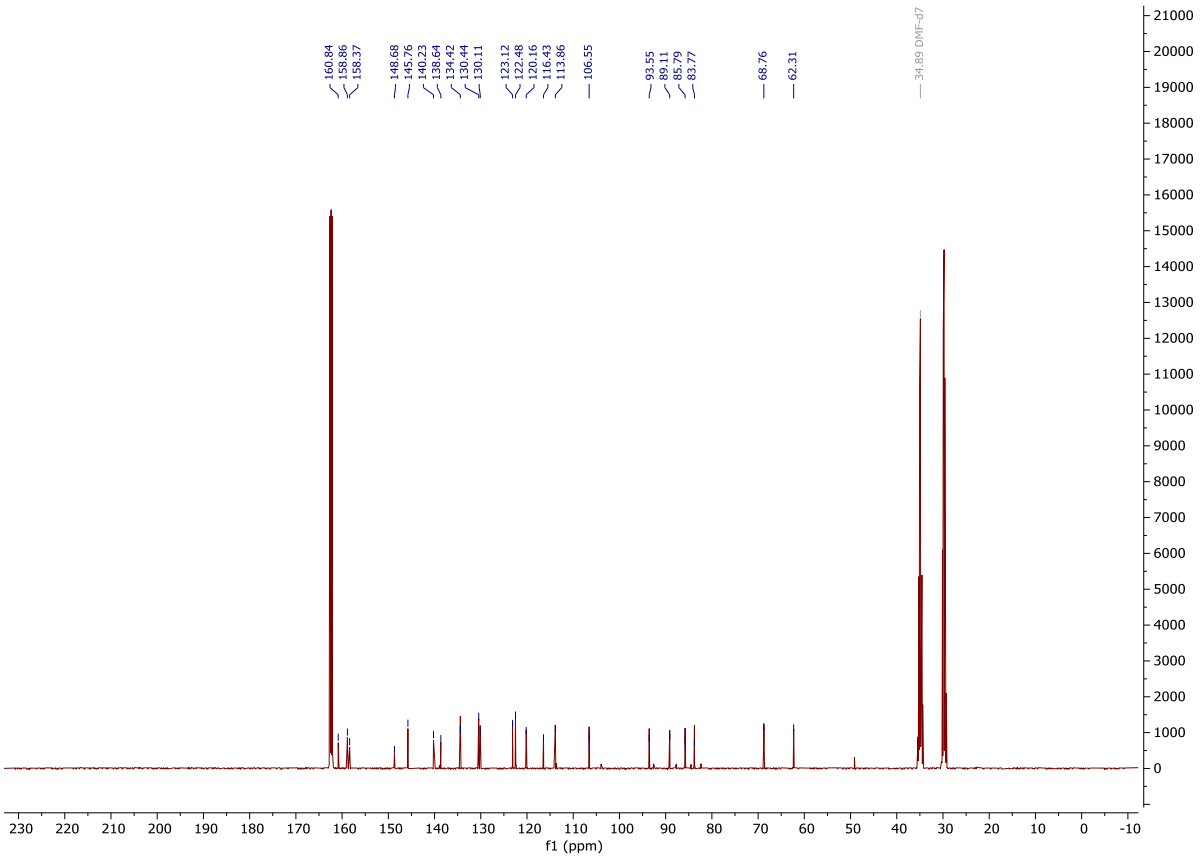

^{1}H and ^{13}C NMR spectra of compound **8**

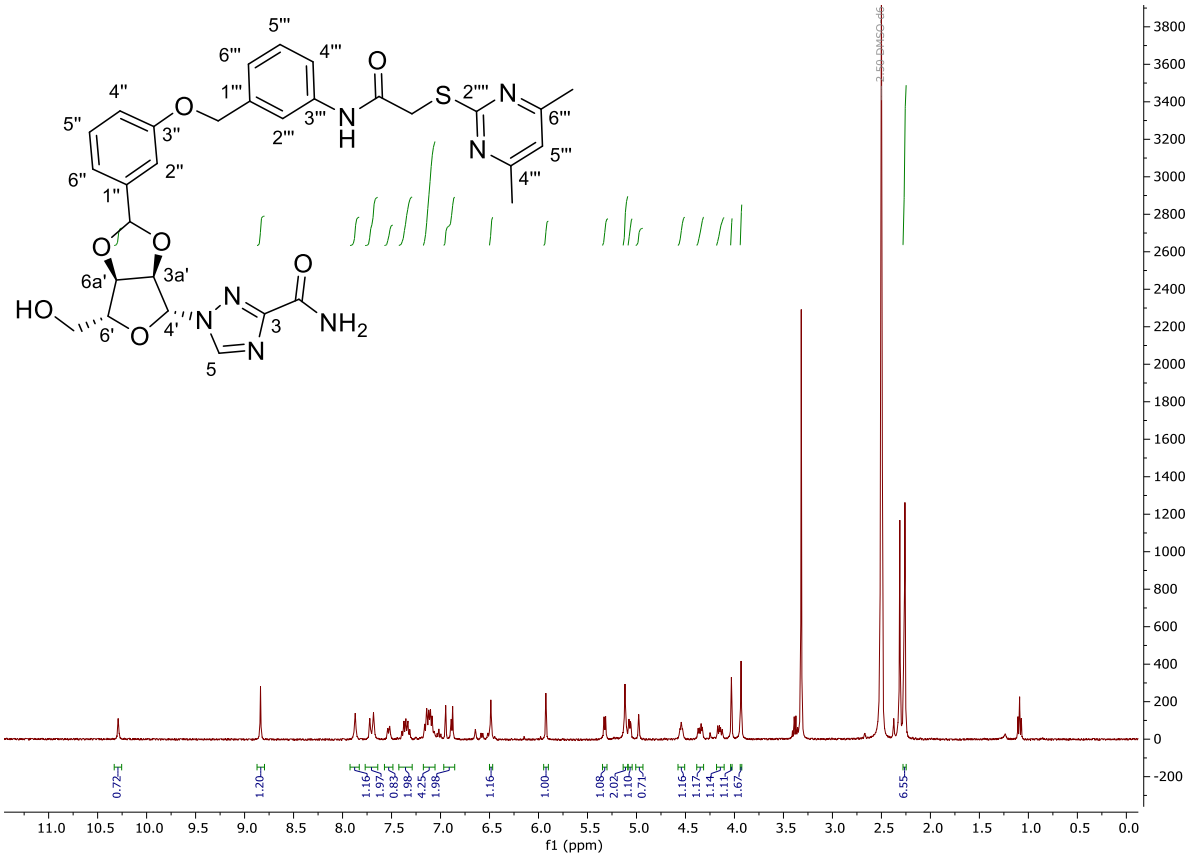

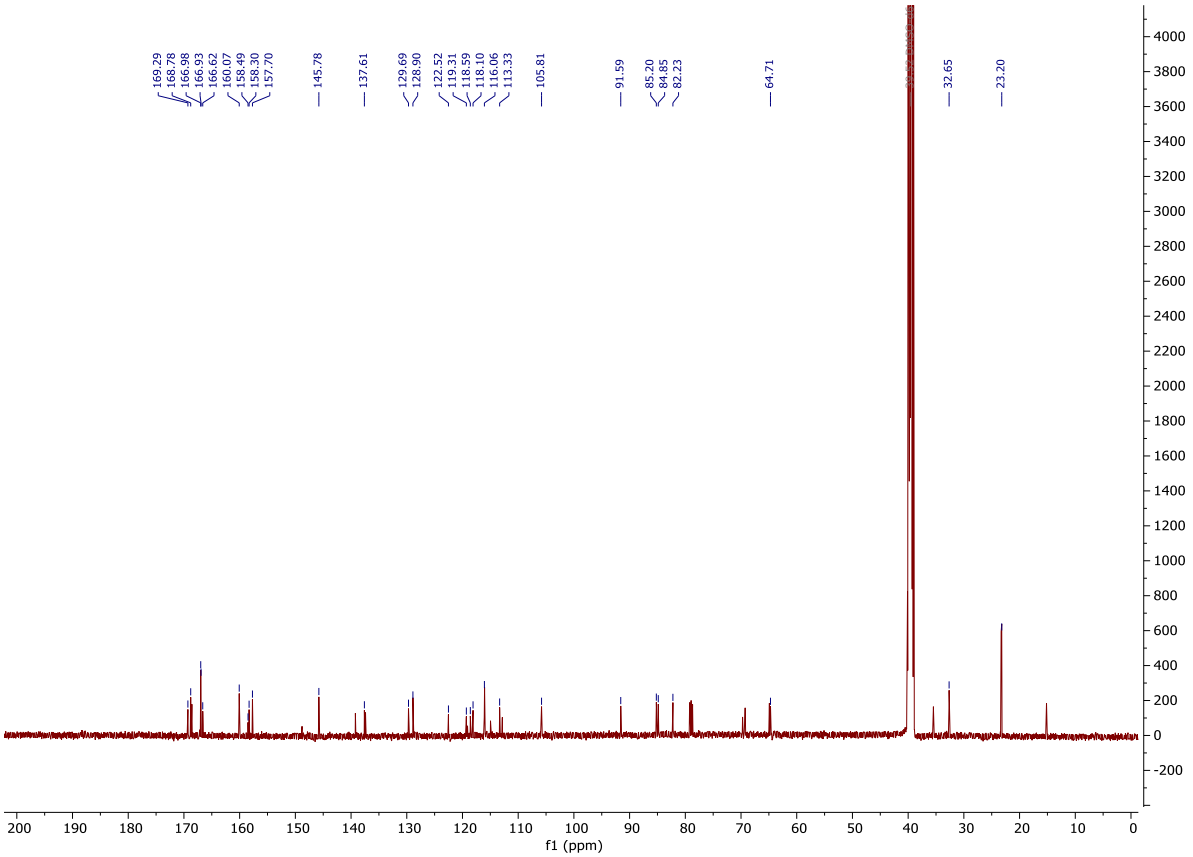

^{1}H and ^{13}C NMR spectra of compound **10**

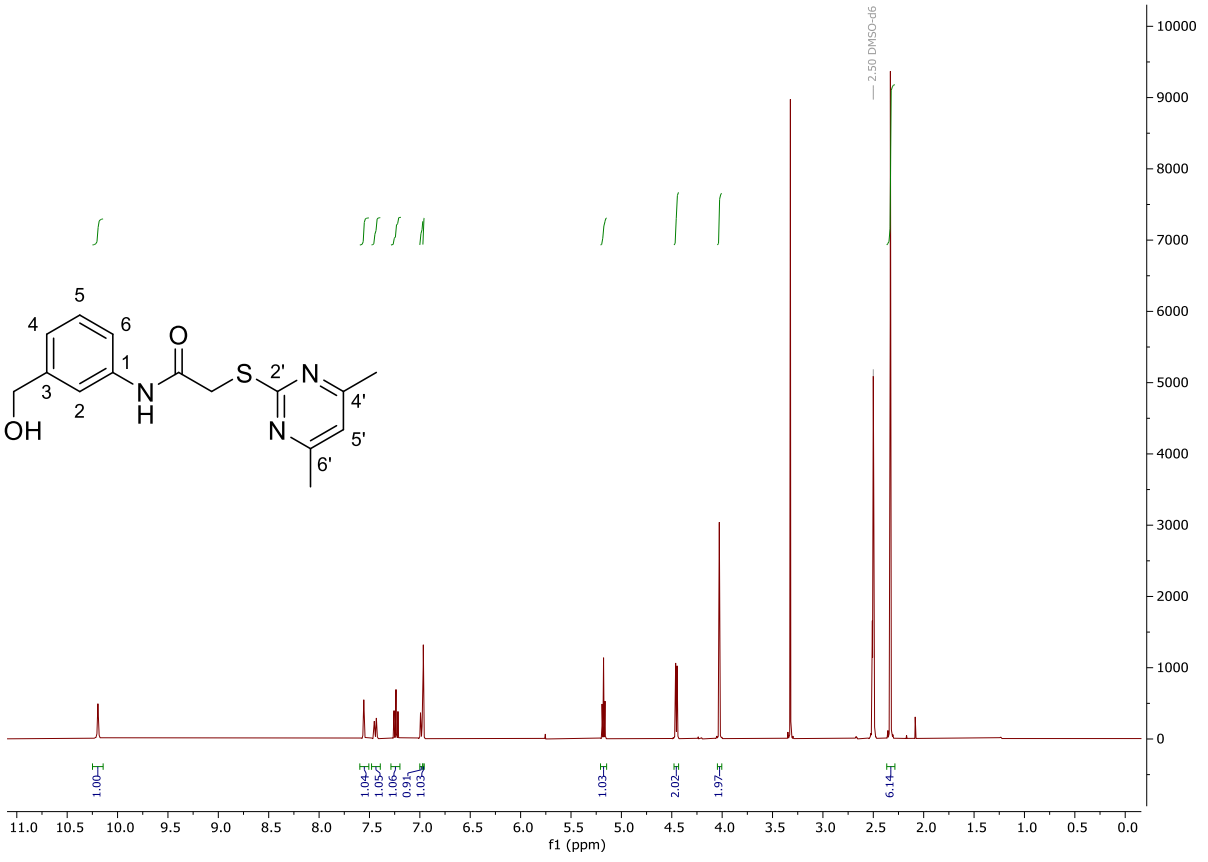

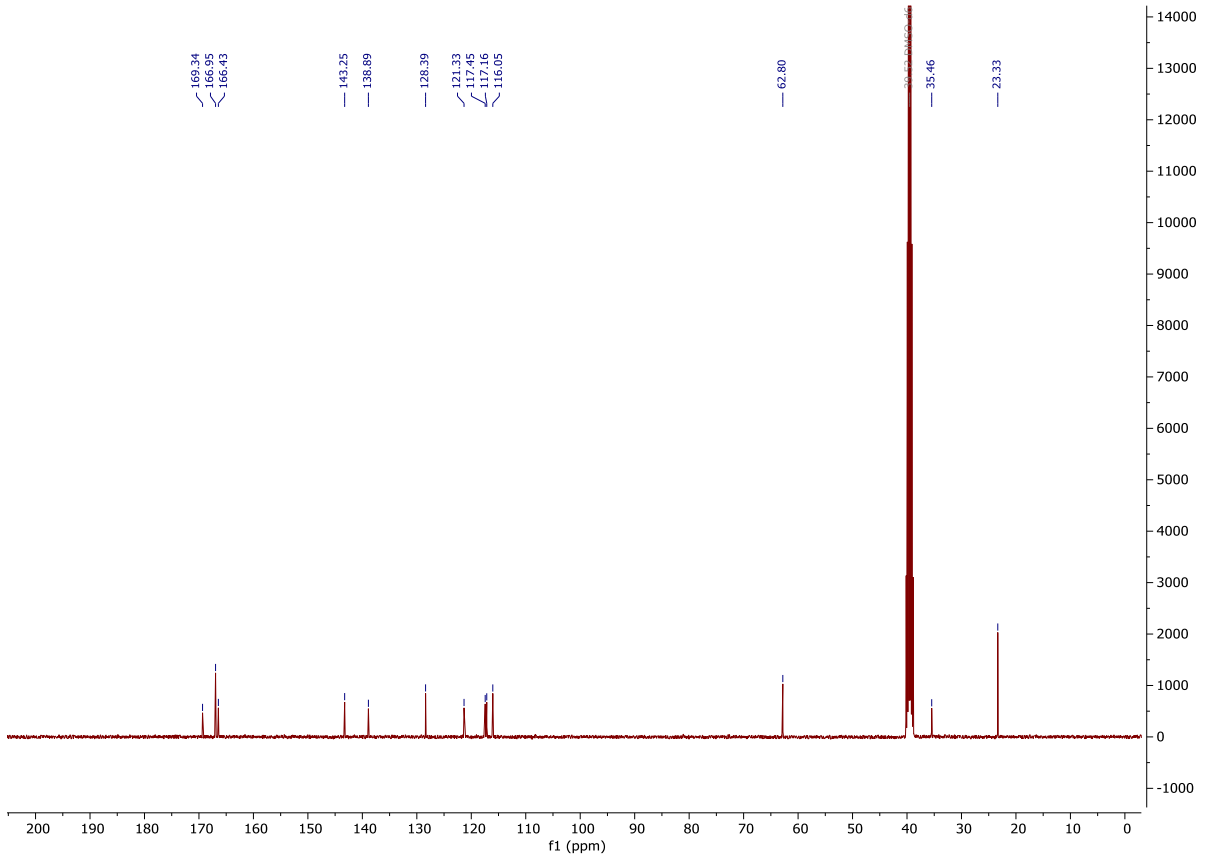

^{1}H and ^{13}C NMR spectra of compound **11**

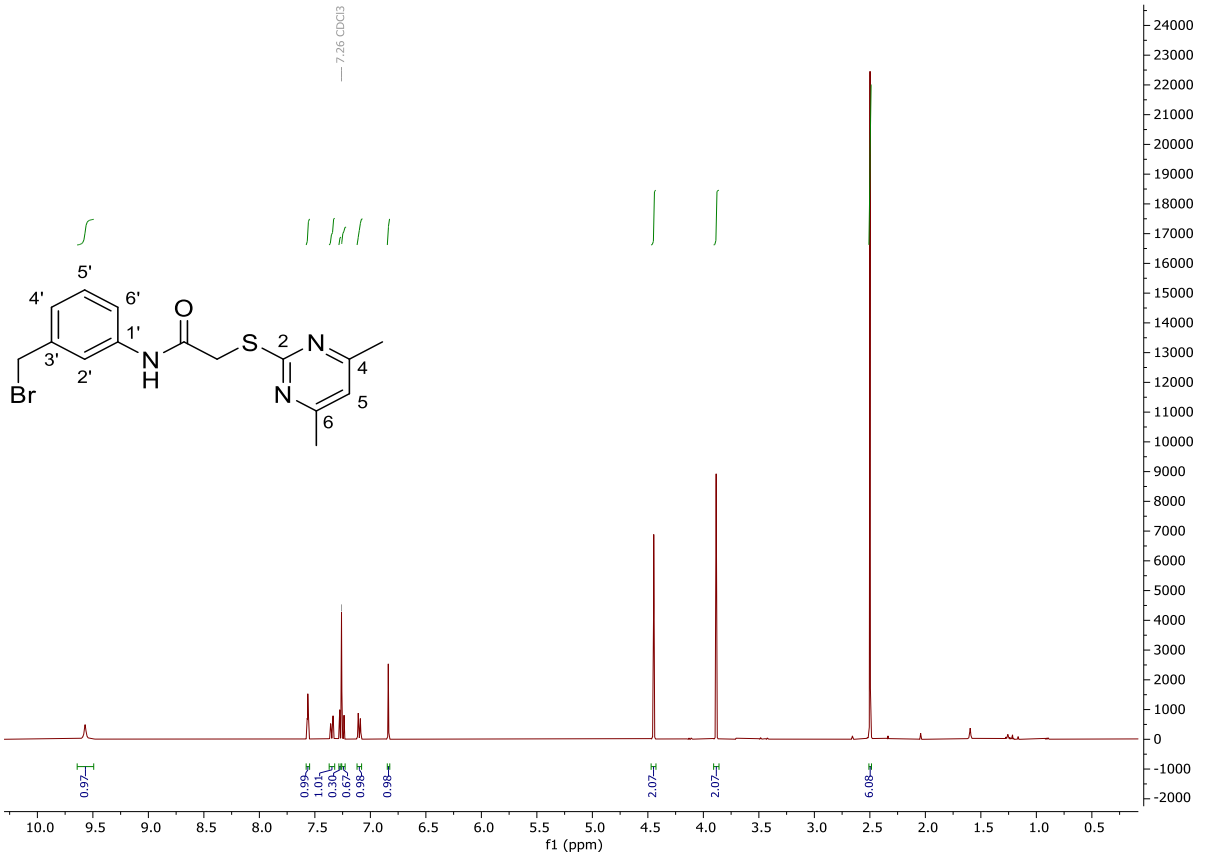

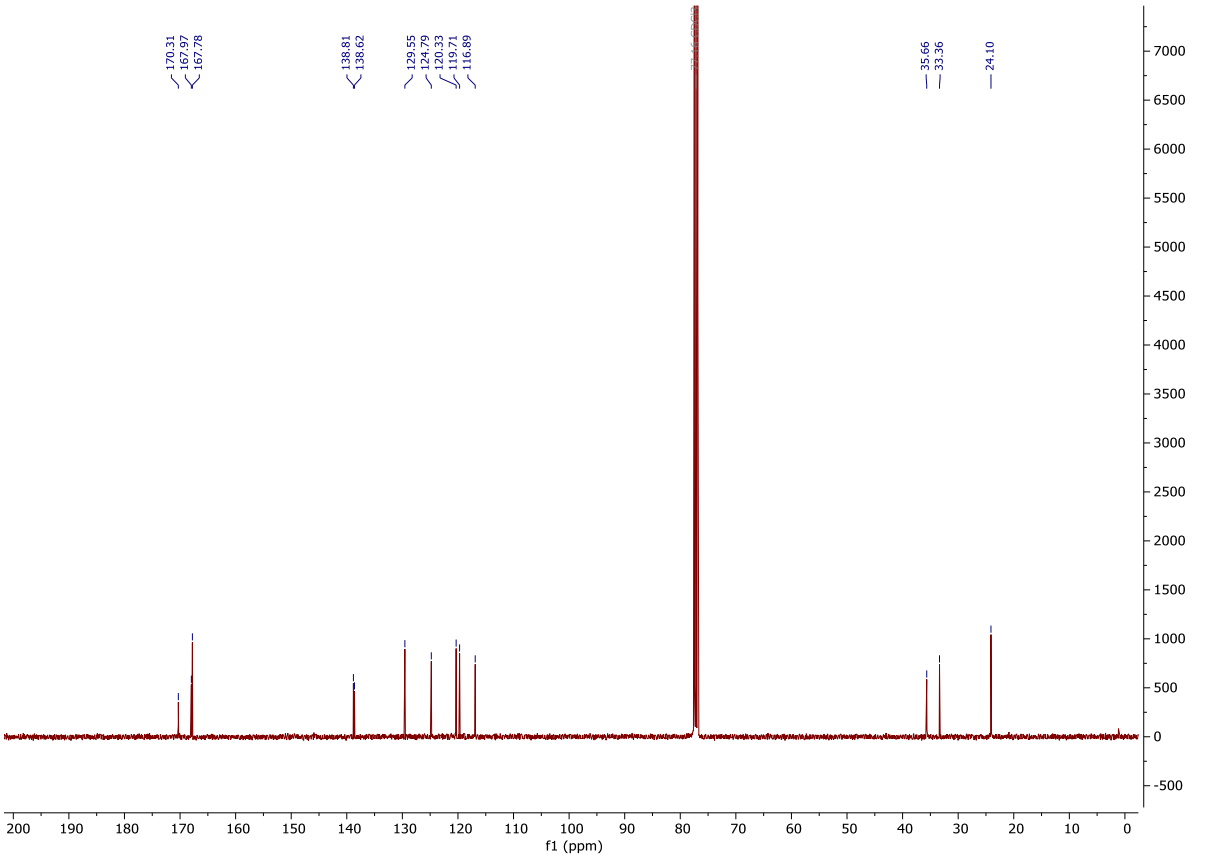

^{1}H and ^{13}C NMR spectra of compound **13**

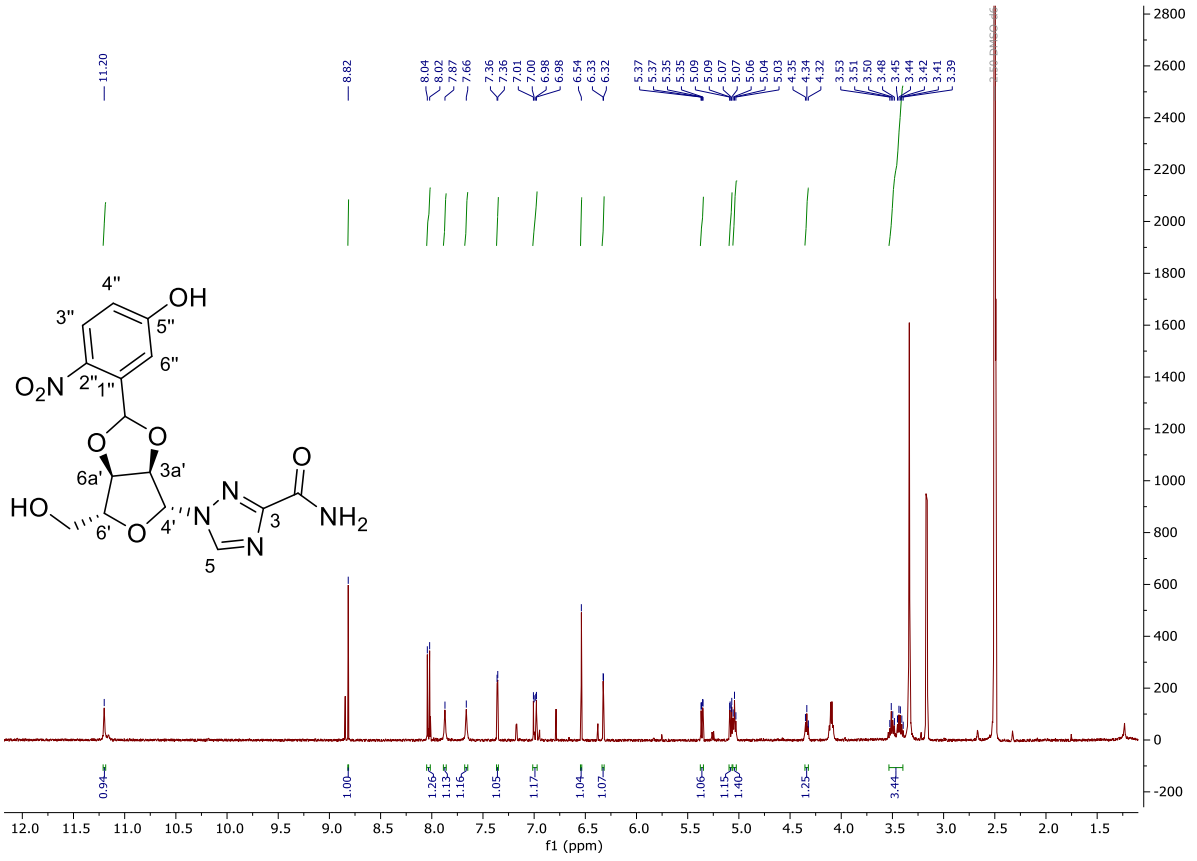

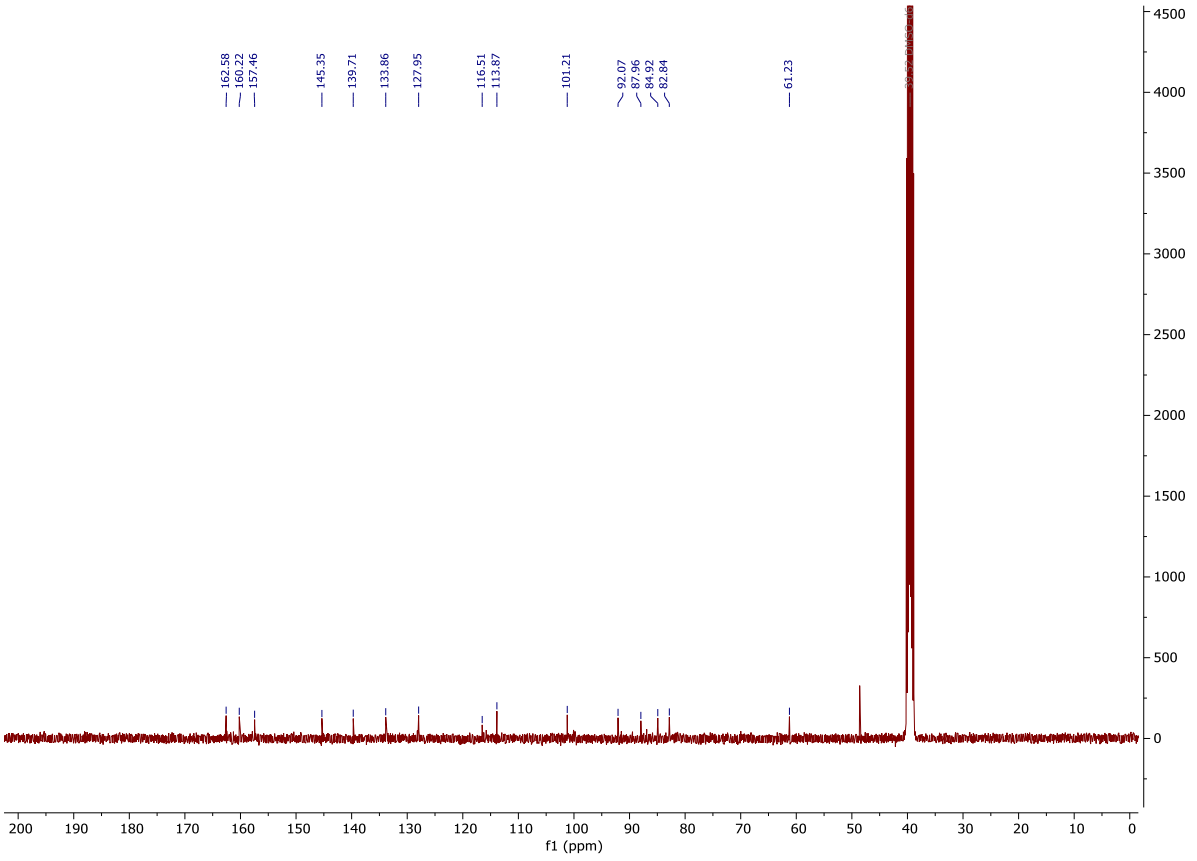

^{1}H and ^{13}C NMR spectra of compound **14**

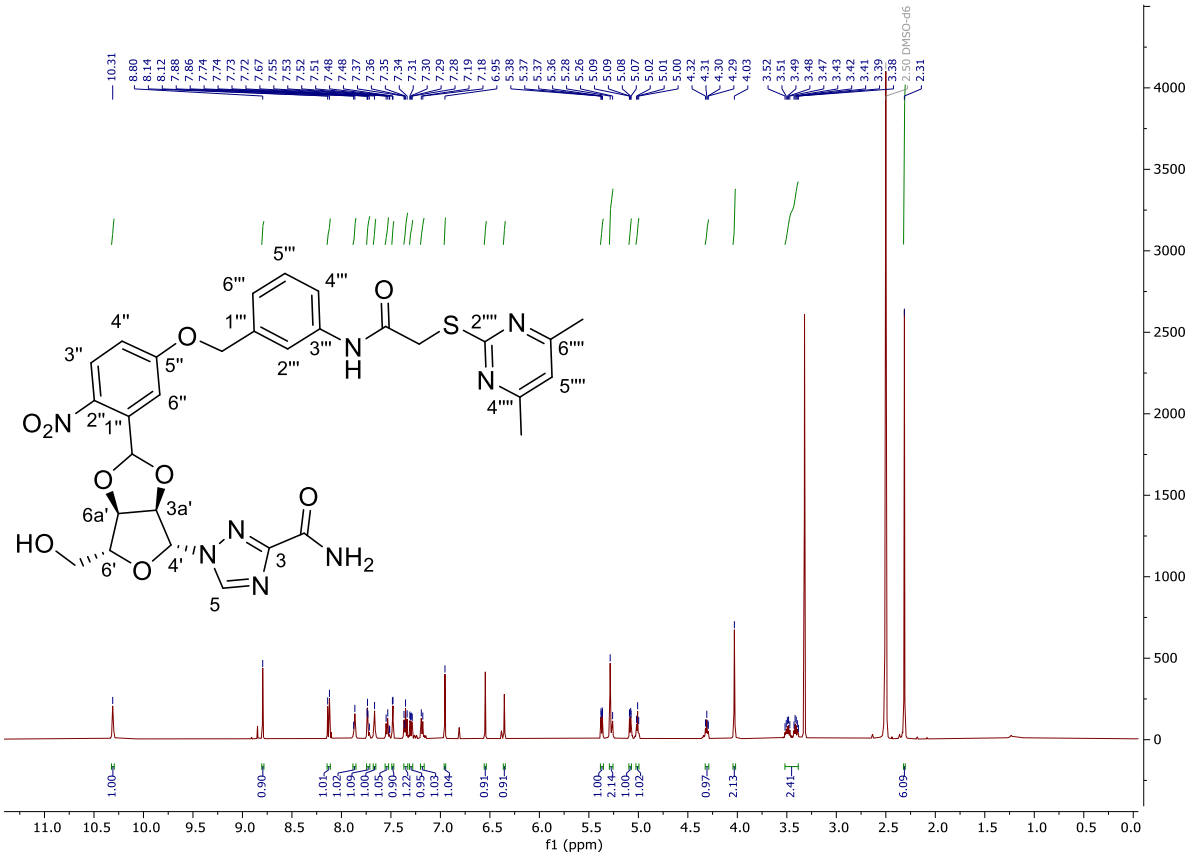

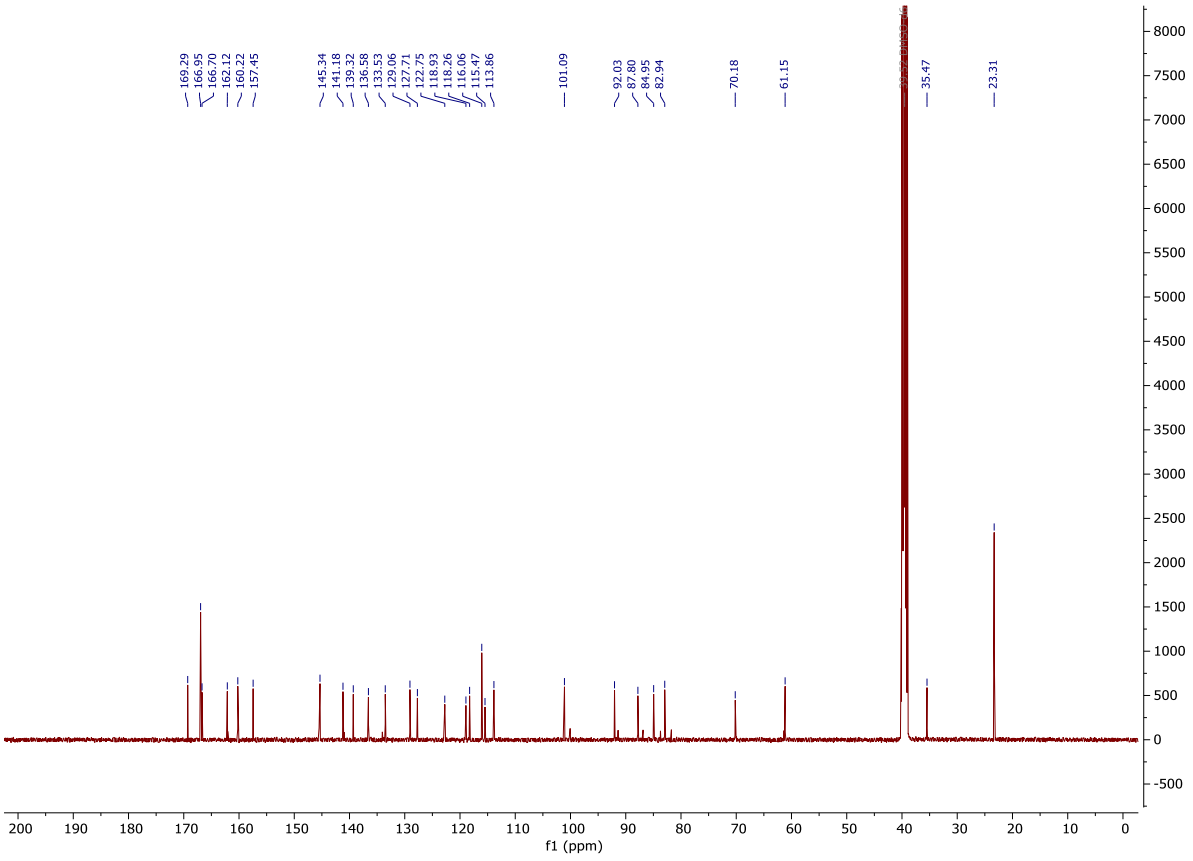

^{1}H and ^{13}C NMR spectra of compound **17**

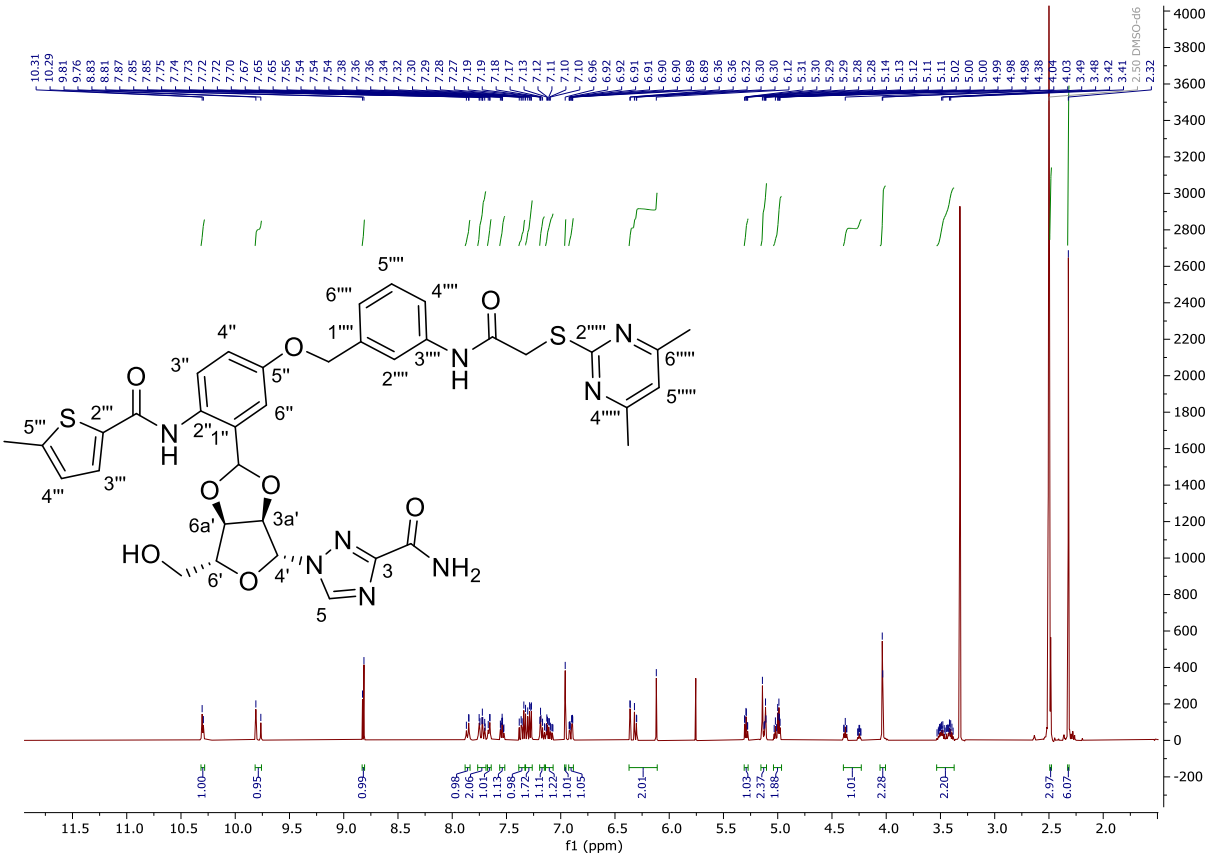

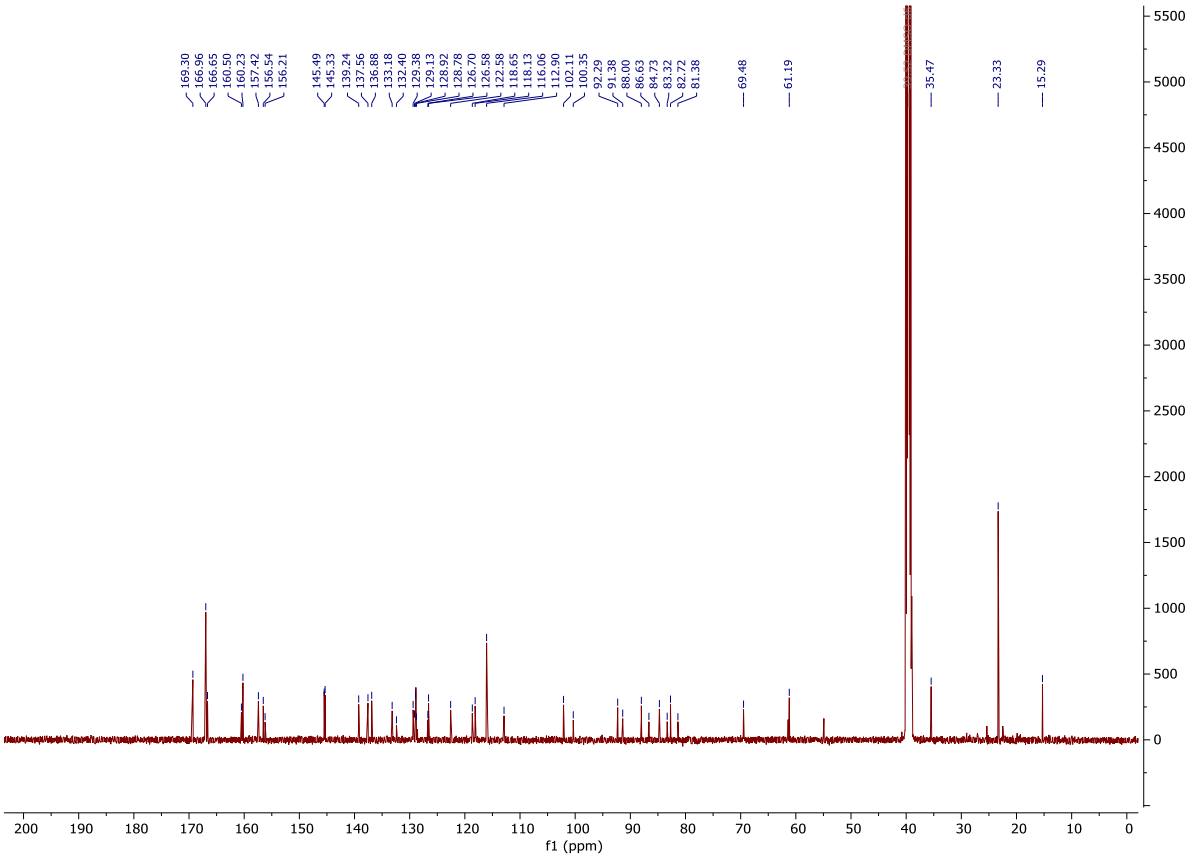

HPLC chromatogram of compound **5**

Instrument:NanniHoney Sequence:20240124 Unger Page 1 of 1

Chromatogram and Results

Injection Details

Injection Name:	**FLUN 23**		*Run Time (min):*	**34,99**	
Vial Number:	**Vial:32**		*Injection Volume:*	**10,00**	
Injection Type:	**Unknown**		*Wavelength A:*	**210**	
Column:	**Eclipse Plus C18 5µm 4,6x 150mm USUXB17231**		*Wavelength B:*	**254**	
Instrument Method:	**Methanol Wasser Gradient 2**				
Processing Method:	**Quantitative**		*Flow rate:*	**1,000**	**mL/min**
Injection Date/Time:	**30.Jan.24 10:10**		*Column Temperatu*	**15,0**	**°C**
Pump Channel A:	**0,00**	Acetonitril			
Pump Channel B:	**40**	Methanol			
Pump ChannelC:		Wasser 0,1% TFA			
Pump Channel D:	**60**	Wasser			

Chromatogram

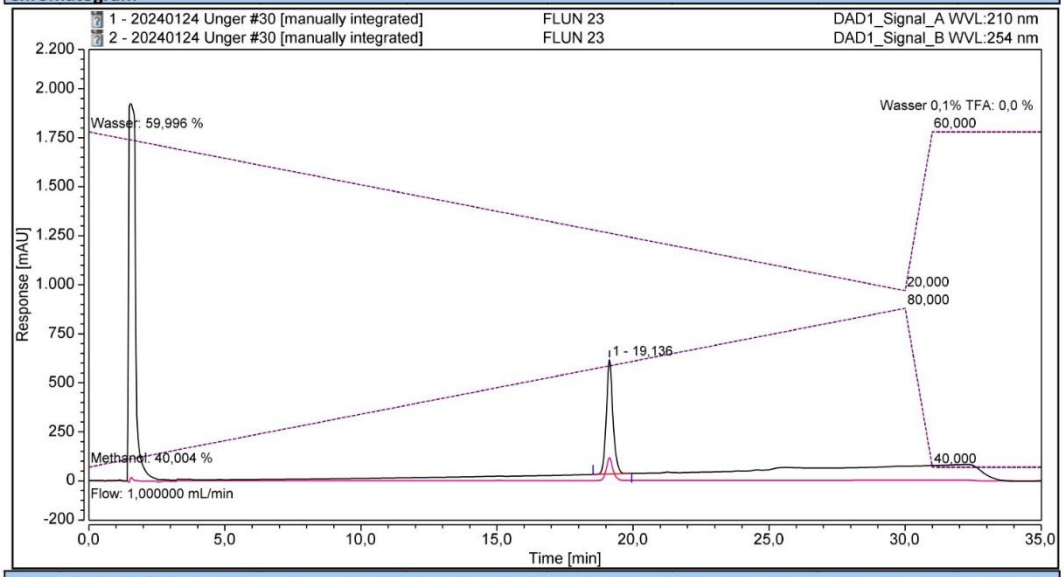

Integration Results

210nm

No.	Peak Name	Retention Time min	Area mAU*min	Relative Area %
1		19,136	163,658	100,00
Total:			**163,658**	**100,00**

254mn

No.	Peak Name	Retention Time min	Area mAU*min	Relative Area %
2		19,136	32,749	99,27
Total:			**32,749**	**99,27**

Reinheit Honey/Integration

Chromeleon (c) Dionex
Version 7.2.9.11323

HPLC chromatogram of compound **8**

Instrument:NanniHoney Sequence:20240124 Unger Page 1 of 1

Chromatogram and Results

Injection Details

Injection Name:	**FLUN 32**		*Run Time (min):*	**34,99**	
Vial Number:	**Vial:23**		*Injection Volume:*	**10,00**	
Injection Type:	**Unknown**		*Wavelength A:*	**210**	
Column:	**Eclipse Plus C18 5µm 4,6x 150mm USUXB17231**		*Wavelength B:*	**254**	
Instrument Method:	**Methanol Wasser Gradient**				
Processing Method:	**Quantitative**		*Flow rate:*	**1,000**	**mL/min**
Injection Date/Time:	**25.Jan.24 13:31**		*Column Temperatu*	**15,0**	**°C**
Pump Channel A:	**0,00**	Acetonitril			
Pump Channel B:	**10**	Methanol			
Pump ChannelC:		Wasser 0,1% TFA			
Pump Channel D:	**90**	Wasser			

Chromatogram

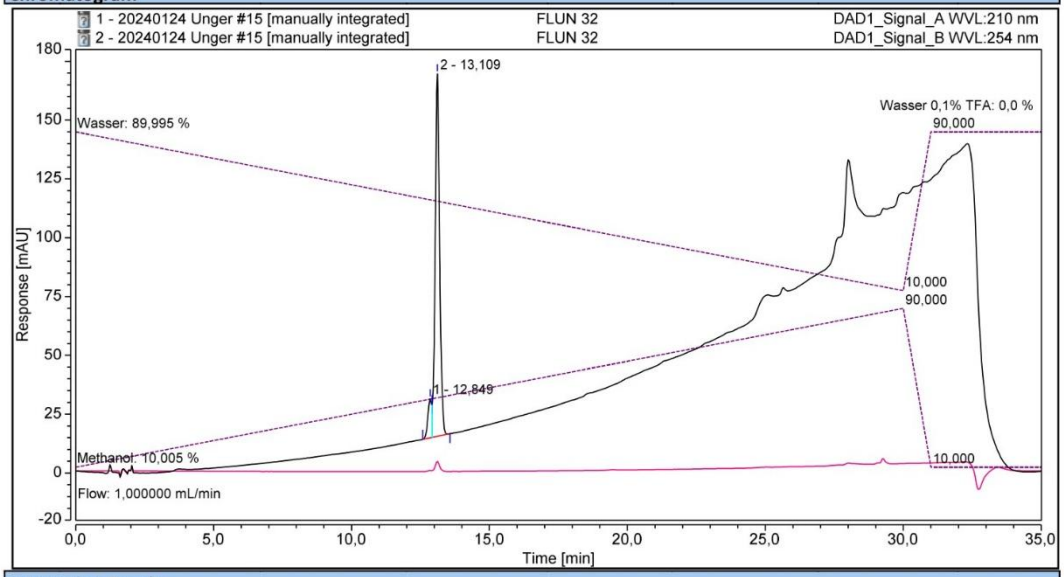

Integration Results

210nm

No.	Peak Name	Retention Time min	Area mAU*min	Relative Area %
1		12,849	2,629	8,39
2		13,109	28,711	91,61
Total:			**31,339**	**100,00**

254mn

No.	Peak Name	Retention Time min	Area mAU*min	Relative Area %
1		12,842	0,080	9,13
2		13,109	0,799	90,87
Total:			**0,880**	**100,00**

Reinheit Honey/Integration

Chromeleon (c) Dionex
Version 7.2.9.11323

HPLC chromatogram of compound **13**

Instrument:Trudel Sequence:20250430 Wirawan Page 1 of 1

Chromatogram and Results

Injection Details

Injection Name:	**RW-199**	*Run Time (min):*	**10,99**
Vial Number:	**Vial:52**	*Injection Volume:*	**5 µL**
Injection Type:	**Unknown**	*Wavelength:*	**210 nm**
		Wavelength:	**254 nm**
Instrument Method:	**MeOH Wasser +0,1% TFA Gradient 4**	*Flow rate:*	**0,8 ml/min**
Column:	**Zorbax Eclipe Plus C18 4,6 x 150mm 3,5µm**	*Column Temperatur:*	**50 °C**
Injection Date/Time:	**30.Apr.25 13:13**	*Pump Channel A:* **50**	Methanol
		Pump Channel B: **20,0**	**Wasser TFA 0,1%**

Trudel:
HPLC-DAD using an Agilent Series 1200 HPLC system (Waldbronn, Germany) consisting of a binary pump system (G1312 B BinPump SL), an autosampler (G1367D HiP ALS SL +), a column oven (G1316B TCC SL) and a DAD detector (G1315C DAD SL)
Data analysis and instrument control was carried out with Thermo Scientific™ Dionex™ Chromeleon™ 7.2 Chromatography Data System (Dreieich, Germany)

Chromatogram

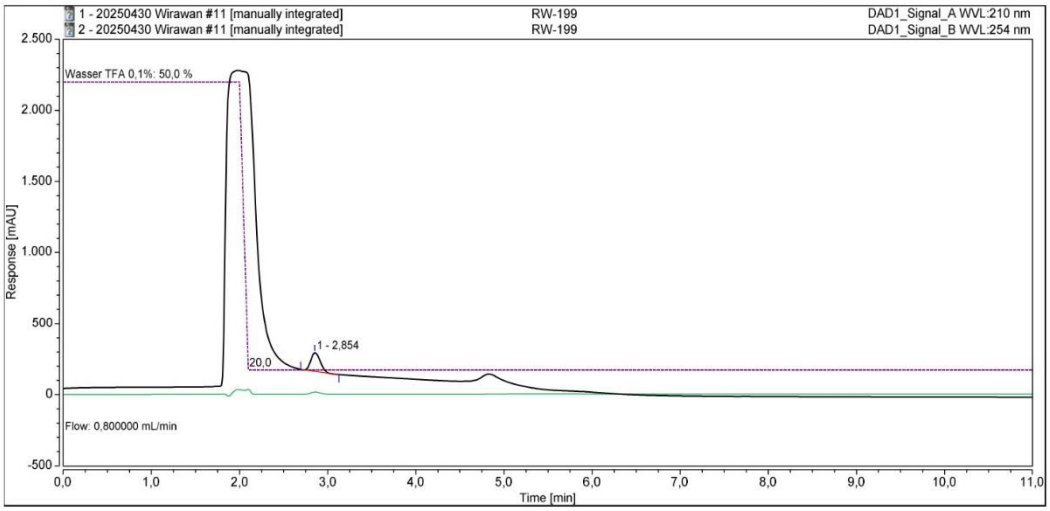

DAD1_Signal_A

No.	Retention Time min	Area mAU*min	Relative Area %
1	2,854	16,013	100,00
Total:		**16,013**	**100**

DAD1_Signal_B

No.	Retention Time min	Area mAU*min	Relative Area %
1	2,860	2,211	100,00
Total:		**2,211**	**100**

Reinheit Trudel/Integration

Chromeleon (c) Dionex
Version 7.2.9.11323

HPLC chromatogram of compound **14**

Instrument:Trudel Sequence:20250430 Wirawan

Page 1 of 1

Chromatogram and Results

Injection Details

Injection Name:	**RW-200**	*Run Time (min):*	**10,99**
Vial Number:	**Vial:53**	*Injection Volume:*	**5 µL**
Injection Type:	**Unknown**	*Wavelength:*	**210 nm**
		Wavelength:	**254 nm**
Instrument Method:	**MeOH Wasser +0,1% TFA Gradient 4**	*Flow rate:*	**0,8 ml/min**
Column:	**Zorbax Eclipe Plus C18 4,6 x 150mm 3,5µm**	*Column Temperatur:*	**50 °C**
Injection Date/Time:	**30.Apr.25 13:28**	*Pump Channel A:* **50**	Methanol
		Pump Channel B: **20,0**	**Wasser TFA 0,1%**

Trudel:
HPLC-DAD using an Agilent Series 1200 HPLC system (Waldbronn, Germany) consisting of a binary pump system (G1312 B BinPump SL), an autosampler (G1367D HiP ALS SL +), a column oven (G1316B TCC SL) and a DAD detector (G1315C DAD SL)
Data analysis and instrument control was carried out with Thermo Scientific™ Dionex™ Chromeleon™ 7.2 Chromatography Data System (Dreieich, Germany)

Chromatogram

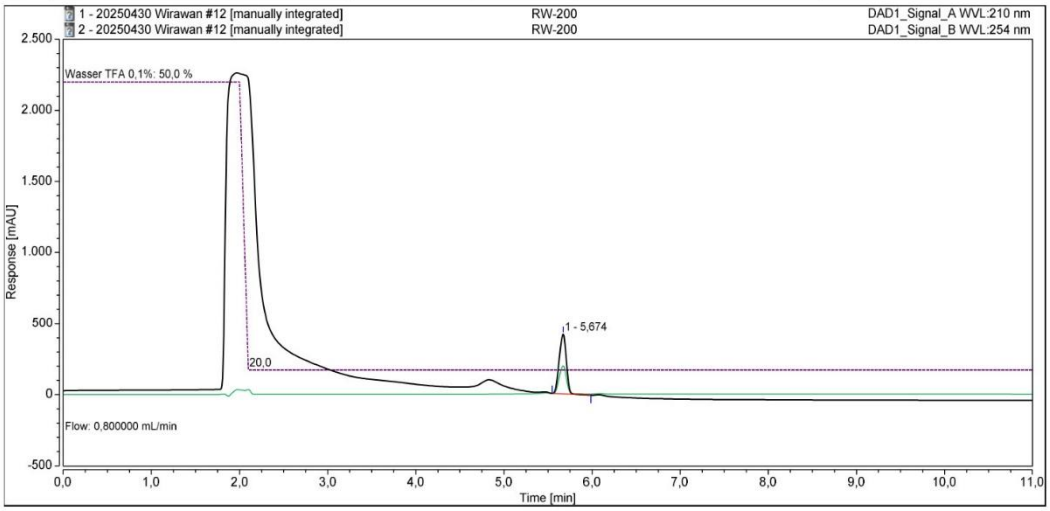

DAD1_Signal_A

No.	Retention Time min	Area mAU*min	Relative Area %
1	5,674	39,878	100,00
Total:		**39,878**	**100**

DAD1_Signal_B

No.	Retention Time min	Area mAU*min	Relative Area %
1	5,474	0,520	2,67
2	5,674	18,688	95,79
3	6,087	0,301	1,54
Total:		**19,510**	**100**

Reinheit Trudel/Integration

Chromeleon (c) Dionex
Version 7.2.9.11323

HPLC chromatogram of compound **17**

Instrument:Trudel Sequence:20250430 Wirawan

Chromatogram and Results

Injection Details

Injection Name:	**RW-207**	*Run Time (min):*		**10,99**	
Vial Number:	**Vial:55**	*Injection Volume:*		**5**	**µL**
Injection Type:	**Unknown**	*Wavelength:*		**210**	**nm**
		Wavelength:		**254**	**nm**
Instrument Method:	**MeOH Wasser +0,1% TFA Gradient 4**	*Flow rate:*		**0,8**	**ml/min**
Column:	**Zorbax Eclipe Plus C18 4,6 x 150mm 3,5µm**	*Column Temperatur:*		**50**	**°C**
Injection Date/Time:	**30.Apr.25 13:57**	*Pump Channel A:*	**50**		Methanol
		Pump Channel B:	**20,0**		**Wasser TFA 0,1%**

Trudel:
HPLC-DAD using an Agilent Series 1200 HPLC system (Waldbronn, Germany) consisting of a binary pump system (G1312 B BinPump SL), an autosampler (G1367D HiP ALS SL +), a column oven (G1316B TCC SL) and a DAD detector (G1315C DAD SL)
Data analysis and instrument control was carried out with Thermo Scientific™ Dionex™ Chromeleon™ 7.2 Chromatography Data System (Dreieich, Germany)

Chromatogram

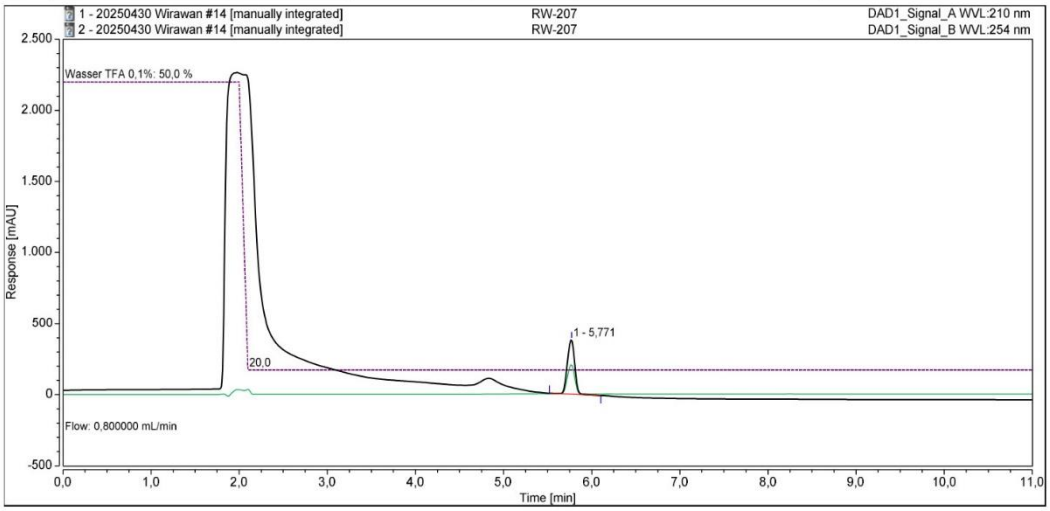

DAD1_Signal_A

No.	Retention Time min	Area mAU*min	Relative Area %
1	5,771	36,694	100,00
Total:		**36,694**	**100**

DAD1_Signal_B

No.	Retention Time min	Area mAU*min	Relative Area %
1	5,771	19,391	100,00
Total:		**19,391**	**100**

Reinheit Trudel/Integration

Chromeleon (c) Dionex
Version 7.2.9.11323

4. Summary

The epigenome of an organism represents a complex regulatory network that takes a governing role in genome function and integrity, which controls heritable changes in gene expression without any alterations in the DNA sequence. The development and exacerbation of several major pathological conditions such as cancer, cardiovascular diseases, neurological and metabolic disorders have been associated with aberrant epigenetic changes. Thus, epigenetic regulation through novel chemical entities represents a prospective approach, not only as practical diagnostic tools (chemical probes) but also as effective therapeutical options (pharmaceutical drugs). Sirtuins are protein deacylases that belong to the unique class III histone deacetylases, which utilise NAD^+ as their co-factor in their enzymatic activity for epigenetic regulation. Seven different sirtuin subtypes were identified in mammalian cells to date with diverse cellular functions and various subcellular localisations. This thesis covers the development and optimisation of inhibitors of the two subtypes Sirt2 and Sirt5 by employing various drug design strategies that to the best of current knowledge has yet to be investigated in the field of sirtuins.

In the first project, a series of functionalised derivatives of the SirReal-type Sirt2 inhibitor **24a** was rationally designed and synthesised with the aid of molecular docking experiments to target the vicinal diol unit of the nicotinamide ribose of NAD^+. Appropriate electrophilic functional groups that have been established as effective reversible covalent warheads and halogen bond mediators were employed at the most optimal position on the inhibitor scaffold to allow reversible covalent bonding or halogen bonding with the co-factor NAD^+. A systematic investigation of these synthesised inhibitors revealed halogen derivatives to be the most favourable. In particular, the chloro-derivative **RW-78** demonstrated a 3-fold increase in potency compared to the lead compound **24a**, displaying an IC_{50} of 26 nM against Sirt2. In addition, high target engagement of **RW-78** with an EC_{50} of 15 nM was determined *via* NanoBRET assays in HEK293T cells. Further in-depth investigation to its binding mode through x-ray crystallography revealed, on the contrary to the initial inhibitors design, halogen-π interactions with F235. This induces a structural rearrangement of the active site that disrupts the binding of the co-factor NAD^+. This novel insight highlights the interference of co-factor binding as a viable option in the development of highly potent Sirt2 inhibitors.

In the second project, a series of Sirt2 hybrid inhibitors that incorporate relevant pharmacophoric structural motifs from both **SirReal2** and **24a** were designed and synthesised. Further targeted optimisations with halogens that were inspired from the first project were carried out. This strategy was executed to deliver the most potent low-molecular Sirt2 inhibitor known to date – the bromo-derivative Sirt2 hybrid inhibitor **RW-93** with an IC_{50} of 16 nM.

Molecular docking studies indicate possible potency enhancement *via* halogen bonding with Val233 or Arg97 and a hydroxy group of the nicotinamide ribose of the co-factor NAD^+, though disruption of co-factor binding following active site structural rearrangement *via* π-halogen interactions with F235 as shown in the first project should not be disregarded due to the lack of actual binding insights. The *in vitro* results that were obtained were well validated by MM-GBSA ∆G calculations. In addition, ADME profiling of the Sirt2 hybrid inhibitors showed favourable pharmacokinetic and drug-likeness properties.

In the third project, the focus centred on the development and optimisations of Sirt5 inhibitors derived from the anti-inflammatory drug balsalazide. By applying the principles of reversible covalent inhibition targeting the vicinal diol unit of the nicotinamide ribose of the co-factor NAD^+ similar to the first project, a series of functionalised derivatives from lead compounds **CG_209** and **CG_220** were designed and synthesised following insights from molecular docking experiments. Synthetic obstacles in obtaining enantiomerically pure functionalised inhibitors were overcome through chiral-pool syntheses from commercially available amino acids. Moreover, challenges in the preparation and purification of alkyl boronic acids were mitigated through several rounds of method optimisations. SAR analysis revealed the superiority of the triazole-based inhibitors and a stereoselective preference of functional group modifications at the (*S*)-configuration with the (*S*)-configured triazole-based cyanomethyl derivative **RW-191** identified as the most potent from this study with an IC_{50} of 27 µM.

In the fourth project, the application of bisubstrate analogues that simultaneously mimic both the natural peptide substrate and the co-factor NAD^+ as Sirt2 inhibitors was explored. Bisubstrate analogues have gained significant traction in drug design over the years, offering the potential for enhanced potency and selectivity by the concurrent engagement of multiple enzymatic binding sites. Ribavirin was investigated as a low-molecular NAD^+ mimetic that offers superior pharmacokinetic properties relative to nicotinamide riboside. The Sirt2 proof-of-concept bisubstrate analogue **FU-32**, which was constructed by covalently linking ribavirin with the SirReal-type lead compound **28a** *via* a tailored acetal-based linker, demonstrated a 20-fold increase in potency. Further optimisations involving the incorporation of a methyl thiopheneamide motif designed to exploit further interactions in the acetyl-lysine binding binding site led to the development of the Sirt2 bisubstrate analogue **RW-207**, which exhibited a 30-fold potency enhancement relative to **28a**, highlighting the synergistic potential of bisubstrate engagement. These findings underscore the successful application of bisubstrate analogues in the rational design of highly potent Sirt2 inhibitors, and the potential utility of ribavirin as an NAD^+ mimetic that may perhaps extend to the inhibitor design of other NAD^+ dependent enzymes.

Based on the drug design rationale of utilising the co-factor NAD^+ as a target for inhibitor interactions and mimetics, a total of 34 Sirt2 and Sirt5 inhibitors were investigated in this thesis (Figure 15). These novel strategies in the field of sirtuins were implemented successfully, leading to significant advancement in the development of more potent sirtuin inhibitors. The first three projects of this thesis were completed with results published in peer-reviewed scientific journals including *RSC Med. Chem.*, *Int. J. Mol. Sci.* and *Molecules*, while the fourth project is still awaiting further results from collaborative partners prior to submission in a peer-reviewed journal. In addition to the identification of several highly potent and subtype selective Sirt2 inhibitors with potential utility, comprehensive SAR studies and novel binding insights of these inhibitors were also demonstrated in this thesis, which provide a promising methodological framework and a solid foundation for the future development of further novel sirtuin inhibitors.

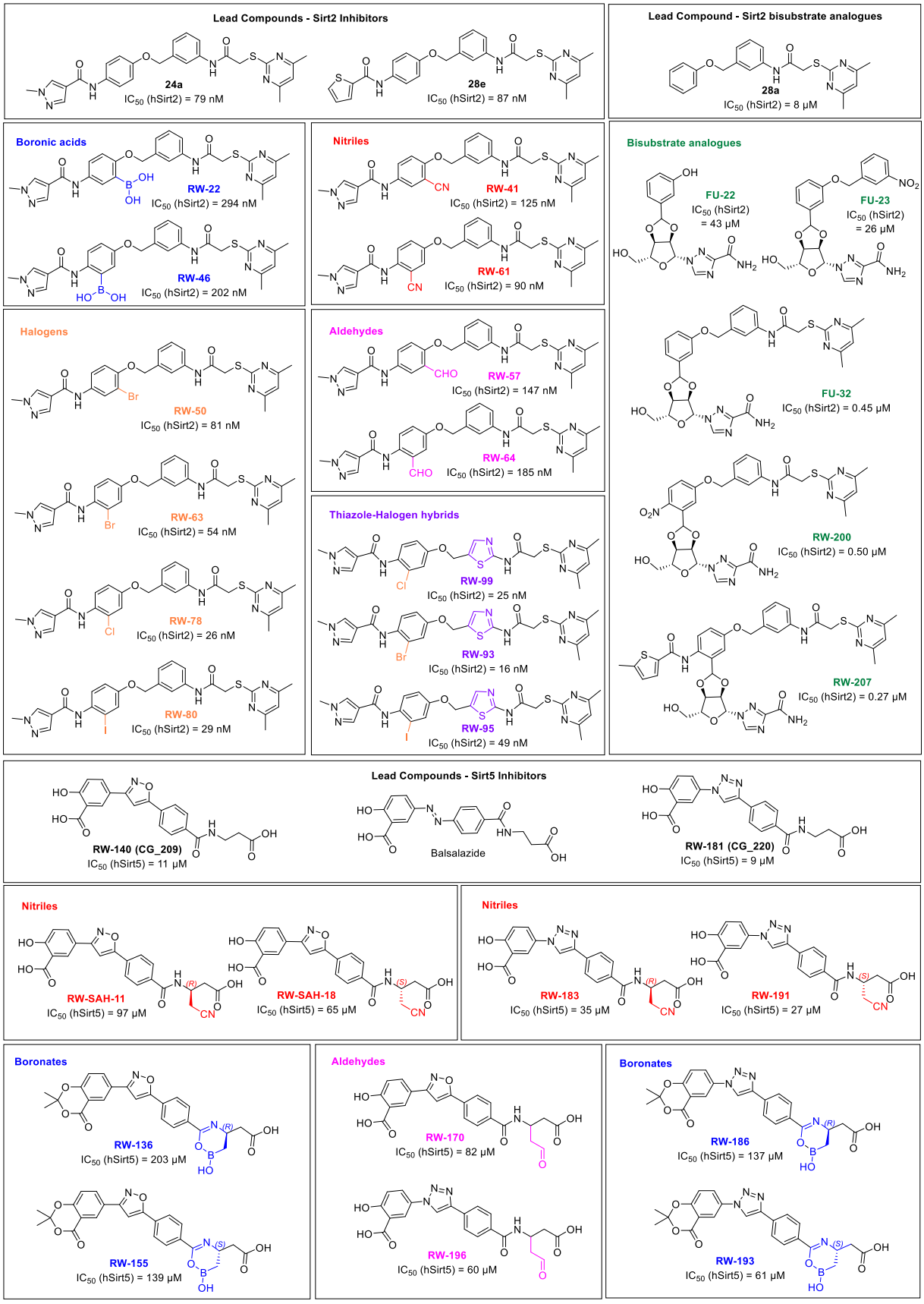

Figure 15: Overview of all Sirt2 and Sirt5 inhibitors investigated in this thesis.

5. Abbreviations

ADME	Absorption, distribution, metabolism and excretion
ADP	Adenosine diphosphate
c-Myc	Cellular myelocytomatosis oncogene
CoA	Coenzyme A
CpG	Cytosine phosphate guanine dinucleotide
DNA	Deoxyribonucleic acid
DPP4	Dipeptidyl peptidase 4
EC_{50}	Half maximal effective concentration
G2/M	Gap2/mitosis
HIV	Human immunodeficiency virus
IC_{50}	Half maximal inhibitory concentration
MM-GBSA	Molecular mechanics - generalized Born surface area
NAD^+	Nicotinamide adenine dinucleotide
PDB	Protein data bank
PDE5	Phosphodiesterase type 5
ROS	Reactive oxygen species
RNA	Ribonucleic acid
Sir2	Silent information regulator 2
Sirt	Sirtuin
S_N2	Bimolecular nucleophilic substitution

6. References

1. G. Egger, G. Liang, A. Aparicio and P. A. Jones, *Nature*, 2004, **429**, 457-463.
2. D. L. Prado-Romero and J. L. Medina-Franco, *ACS Omega*, 2021, **6**, 22478-22486.
3. M. Wang and E. M. Ibeagha-Awemu, *Front Genet*, 2020, **11**, 613636.
4. C. H. Waddington, *Int J Epidemol*, 2012, **41**, 10-13.
5. S. U. Devaskar and S. Raychaudhuri, *Pediatr Res*, 2007, **61**, 1-4.
6. A. Petronis, *Nature*, 2010, **465**, 721-727.
7. A. Farsetti, B. Illi and C. Gaetano, *Eur J Intern Med*, 2023, **114**, 15-22.
8. S. J. Serrano-Gomez, M. Maziveyi and S. K. Alahari, *Mol Cancer*, 2016, **15**, 18.
9. S. Götze, M. Wolter, G. Reifenberger, O. Müller and S. Sievers, *Int J Cancer*, 2010, **126**, 2584-2593.
10. T. Milde, I. Oehme, A. Korshunov, A. Kopp-Schneider, M. Remke, P. Northcott, H. E. Deubzer, M. Lodrini, M. D. Taylor, A. von Deimling, S. Pfister and O. Witt, *Clin Cancer Res*, 2010, **16**, 3240-3252.
11. R. Barrès, M. E. Osler, J. Yan, A. Rune, T. Fritz, K. Caidahl, A. Krook and J. R. Zierath, *Cell Metab*, 2009, **10**, 189-198.
12. C. Ling, S. Del Guerra, R. Lupi, T. Rönn, C. Granhall, H. Luthman, P. Masiello, P. Marchetti, L. Groop and S. Del Prato, *Diabetologia*, 2008, **51**, 615-622.
13. Y. P. Liu, R. Wen, C. F. Liu, T. N. Zhang and N. Yang, *Biomed Pharmacother*, 2023, **164**, 114931.
14. Y. Z. Jiang, E. Manduchi, C. J. Stoeckert, Jr. and P. F. Davies, *BMC Genomics*, 2015, **16**, 506.
15. S. Zaina, H. Heyn, F. J. Carmona, N. Varol, S. Sayols, E. Condom, J. Ramírez-Ruz, A. Gomez, I. Gonçalves, S. Moran and M. Esteller, *Circ Cardiovasc Genet*, 2014, **7**, 692-700.
16. P. Desplats, B. Spencer, E. Coffee, P. Patel, S. Michael, C. Patrick, A. Adame, E. Rockenstein and E. Masliah, *J Biol Chem*, 2011, **286**, 9031-9037.
17. F. Soldner, Y. Stelzer, C. S. Shivalila, B. J. Abraham, J. C. Latourelle, M. I. Barrasa, J. Goldmann, R. H. Myers, R. A. Young and R. Jaenisch, *Nature*, 2016, **533**, 95-99.
18. Z. Zhao and A. Shilatifard, *Genome Biol*, 2019, **20**, 245.
19. A. J. Bannister and T. Kouzarides, *Cell Res*, 2011, **21**, 381-395.
20. C. D. Allis and T. Jenuwein, *Nat Rev Genet*, 2016, **17**, 487-500.
21. R. R. Kanherkar, N. Bhatia-Dey and A. B. Csoka, *Front Cell Dev Biol*, 2014, **2**, 49.
22. S. Biswas and C. M. Rao, *Eur J Pharmacol*, 2018, **837**, 8-24.
23. L. Simó-Riudalbas and M. Esteller, *Br J Pharmacol*, 2015, **172**, 2716-2732.
24. A. P. Bird, *Nature*, 1986, **321**, 209-213.

25. F. van Leeuwen, P. R. Gafken and D. E. Gottschling, *Cell*, 2002, **109**, 745-756.
26. L. Zhang, E. E. Eugeni, M. R. Parthun and M. A. Freitas, *Chromosoma*, 2003, **112**, 77-86.
27. E. L. Mersfelder and M. R. Parthun, *Nucleic Acids Research*, 2006, **34**, 2653-2662.
28. G. Millán-Zambrano, A. Burton, A. J. Bannister and R. Schneider, *Nat Rev Genet*, 2022, **23**, 563-580.
29. E. L. Greer and Y. Shi, *Nat Rev Genet*, 2012, **13**, 343-357.
30. P. Gallinari, S. Di Marco, P. Jones, M. Pallaoro and C. Steinkühler, *Cell Res*, 2007, **17**, 195-211.
31. A. J. de Ruijter, A. H. van Gennip, H. N. Caron, S. Kemp and A. B. van Kuilenburg, *Biochem J*, 2003, **370**, 737-749.
32. J. M. Wagner, B. Hackanson, M. Lübbert and M. Jung, *Clin Epigenetics*, 2010, **1**, 117-136.
33. A. Budillon, E. Di Gennaro, F. Bruzzese, M. Rocco, G. Manzo and M. Caraglia, *Recent Pat Anticancer Drug Discov*, 2007, **2**, 119-134.
34. J. Li, L. Lu, L. Liu, X. Ren, J. Chen, X. Yin, Y. Xiao, J. Li, G. Wei, H. Huang, W. Wei and J. Wong, *Cell Discov*, 2023, **9**, 85.
35. C. Wei, M. Shi, S. Dong, Z. Li, B. Zhao, D. Liu, G. Li, J. Cen, L. Yu, X. Liang and L. Shi, *Int J Biol Sci*, 2024, **20**, 585-605.
36. C. Moreno-Yruela, I. Galleano, A. S. Madsen and C. A. Olsen, *Cell Chem Biol*, 2018, **25**, 849-856.
37. B. C. Valdez, Y. Nieto, B. Yuan, D. Murray and B. S. Andersson, *Oncotarget*, 2022, **13**, 1122-1135.
38. S. Behnisch-Cornwell, C. W. Grathwol, L. Schulig, A. Voigt, D. Baecker, A. Link and P. J. Bednarski, *Cancers (Basel)*, 2022, **14**, 187.
39. M. Braunstein, A. B. Rose, S. G. Holmes, C. D. Allis and J. R. Broach, *Genes Dev*, 1993, **7**, 592-604.
40. W. Dang, *Drug Discov Today Technol*, 2014, **12**, e9-e17.
41. J. Rine and I. Herskowitz, *Genetics*, 1987, **116**, 9-22.
42. C. B. Brachmann, J. M. Sherman, S. E. Devine, E. E. Cameron, L. Pillus and J. D. Boeke, *Genes Dev*, 1995, **9**, 2888-2902.
43. W. Giblin and D. B. Lombard, in *Handbook of the Biology of Aging (Eighth Edition)*, eds. M. R. Kaeberlein and G. M. Martin, Academic Press, San Diego, 2016, pp. 83-132.
44. B. D. Sanders, B. Jackson and R. Marmorstein, *Biochim Biophys Acta*, 2010, **1804**, 1604-1616.
45. M. S. Finnin, J. R. Donigian and N. P. Pavletich, *Nature Structural Biology*, 2001, **8**, 621-625.

46. J. R. Min, T. Antoshenko, A. Dong, A. Schuetz, P. Loppnau, J. Weigelt, M. Sundstrom, C. H. Arrowsmith, A. M. Edwards, A. Bochkarev and A. N. Plotnikov, *PDB,* 2006. PDB DOI: 10.2210/pdb2B4Y/pdb.
47. J. Min, J. Landry, R. Sternglanz and R. M. Xu, *Cell*, 2001, **105**, 269-279.
48. K. Zhao, X. Chai and R. Marmorstein, *J Mol Biol*, 2004, **337**, 731-741.
49. M. Schiedel, D. Robaa, T. Rumpf, W. Sippl and M. Jung, *Med Res Rev*, 2018, **38**, 147-200.
50. A. A. Sauve and D. Y. Youn, *Curr Opin Chem Biol*, 2012, **16**, 535-543.
51. Y. Wang, Y. M. E. Fung, W. Zhang, B. He, M. W. H. Chung, J. Jin, J. Hu, H. Lin and Q. Hao, *Cell Chem Biol*, 2017, **24**, 339-345.
52. M. M. Maxwell, E. M. Tomkinson, J. Nobles, J. W. Wizeman, A. M. Amore, L. Quinti, V. Chopra, S. M. Hersch and A. G. Kazantsev, *Hum Mol Genet*, 2011, **20**, 3986-3996.
53. N. Sola-Sevilla, A. Mesa-Lombardo, M. Aleixo, S. Expósito, T. Diaz-Perdigón, A. Azqueta, F. Zamani, T. Suzuki, S. Maioli, F. Eroli, A. Matton, M. J. Ramírez, M. Solas, R. M. Tordera, E. D. Martín and E. Puerta, *J Neuroimmune Pharmacol*, 2023, **18**, 529-550.
54. R. M. de Oliveira, H. Vicente Miranda, L. Francelle, R. Pinho, M. Szegö É, R. Martinho, F. Munari, D. F. Lázaro, S. Moniot, P. Guerreiro, L. Fonseca-Ornelas, Z. Marijanovic, P. Antas, E. Gerhardt, F. J. Enguita, B. Fauvet, D. Penque, T. F. Pais, Q. Tong, S. Becker, S. Kügler, H. A. Lashuel, C. Steegborn, M. Zweckstetter and T. F. Outeiro, *PLoS Biol*, 2017, **15**, e2000374.
55. H. Jing, J. Hu, B. He, Y. L. Negrón Abril, J. Stupinski, K. Weiser, M. Carbonaro, Y. L. Chiang, T. Southard, P. Giannakakou, R. S. Weiss and H. Lin, *Cancer Cell*, 2016, **29**, 297-310.
56. V. K. Singh, A. Mishra, K. Truong, J. A. Bohorquez, S. Sharma, A. Khan, F. Bracher, K. Zhang, J. Endsley, M. Endsley, A. P. Rice, J. T. Kimata, G. Yi and C. Jagannath, *bioRxiv*, 2024. DOI: 10.1101/2024.10.27.620499.
57. C. Duran-Castells, A. Llano, A. Kawana-Tachikawa, A. Prats, I. Martinez-Zalacain, M. Kobayashi-Ishihara, B. Oriol-Tordera, R. Peña, C. Gálvez, S. Silva-Arrieta, B. Clotet, E. Riveira-Muñoz, E. Ballana, J. G. Prado, J. Martinez-Picado, J. Sanchez, B. Mothe, D. Hartigan-O'Connor, T. Wyss-Coray, A. Meyerhans, M. Gisslén, R. W. Price, C. Soriano-Mas, J. A. Muñoz-Moreno, C. Brander and M. Ruiz-Riol, *J Virol*, 2023, **97**, e0165522.
58. K. L. Roche, S. Remiszewski, M. J. Todd, J. L. Kulp, III, L. Tang, A. V. Welsh, A. P. Barry, C. De, W. W. Reiley, A. Wahl, J. V. Garcia, M. A. Luftig, T. Shenk, J. R. Tonra, E. A. Murphy and L. W. Chiang, *J Clin Invest*, 2023, **133**, e158978.

59. P. Mellini, Y. Itoh, H. Tsumoto, Y. Li, M. Suzuki, N. Tokuda, T. Kakizawa, Y. Miura, J. Takeuchi, M. Lahtela-Kakkonen and T. Suzuki, *Chem Sci*, 2017, **8**, 6400-6408.
60. A. S. Farooqi, J. Y. Hong, J. Cao, X. Lu, I. R. Price, Q. Zhao, T. Kosciuk, M. Yang, J. J. Bai and H. Lin, *J Med Chem*, 2019, **62**, 4131-4141.
61. S. Moniot, M. Forgione, A. Lucidi, G. S. Hailu, A. Nebbioso, V. Carafa, F. Baratta, L. Altucci, N. Giacché, D. Passeri, R. Pellicciari, A. Mai, C. Steegborn and D. Rotili, *J Med Chem*, 2017, **60**, 2344-2360.
62. T. Seifert, M. Malo, T. Kokkola, K. Engen, M. Fridén-Saxin, E. A. Wallén, M. Lahtela-Kakkonen, E. M. Jarho and K. Luthman, *J Med Chem*, 2014, **57**, 9870-9888.
63. N. Kudo, A. Ito, M. Arata, A. Nakata and M. Yoshida, *Philos Trans R Soc Lond B Biol Sci*, 2018, **373**, 20170070.
64. N. Walker, C. Howe, M. Glover, H. McRobbie, J. Barnes, V. Nosa, V. Parag, B. Bassett and C. Bullen, *N Engl J Med*, 2014, **371**, 2353-2362.
65. T. F. Outeiro, E. Kontopoulos, S. M. Altmann, I. Kufareva, K. E. Strathearn, A. M. Amore, C. B. Volk, M. M. Maxwell, J. C. Rochet, P. J. McLean, A. B. Young, R. Abagyan, M. B. Feany, B. T. Hyman and A. G. Kazantsev, *Science*, 2007, **317**, 516-519.
66. R. Wirawan, M. Frei, A. Heider, N. Papenkordt, F. Friedrich, T. Wein, M. Jung, M. Groll, E. M. Huber and F. Bracher, *RSC Med Chem*, 2025, **16**, 5419-5440.
67. M. Schiedel, T. Rumpf, B. Karaman, A. Lehotzky, J. Oláh, S. Gerhardt, J. Ovádi, W. Sippl, O. Einsle and M. Jung, *J Med Chem*, 2016, **59**, 1599-1612.
68. T. Rumpf, M. Schiedel, B. Karaman, C. Roessler, B. J. North, A. Lehotzky, J. Oláh, K. I. Ladwein, K. Schmidtkunz, M. Gajer, M. Pannek, C. Steegborn, D. A. Sinclair, S. Gerhardt, J. Ovádi, M. Schutkowski, W. Sippl, O. Einsle and M. Jung, *Nat Commun*, 2015, **6**, 6263.
69. M. Schiedel, T. Rumpf, B. Karaman, A. Lehotzky, S. Gerhardt, J. Ovádi, W. Sippl, O. Einsle and M. Jung, *Angew Chem Int Ed Engl*, 2016, **55**, 2252-2256.
70. L. L. Yang, H. L. Wang, L. Zhong, C. Yuan, S. Y. Liu, Z. J. Yu, S. Liu, Y. H. Yan, C. Wu, Y. Wang, Z. Wang, Y. Yu, Q. Chen and G. B. Li, *Eur J Med Chem*, 2018, **155**, 806-823.
71. L. Yang, X. Ma, C. Yuan, Y. He, L. Li, S. Fang, W. Xia, T. He, S. Qian, Z. Xu, G. Li and Z. Wang, *Eur J Med Chem*, 2017, **134**, 230-241.
72. E. Fabbrizi, F. Fiorentino, V. Carafa, L. Altucci, A. Mai and D. Rotili, *Cells*, 2023, **12**, 852.
73. T. Nakagawa, D. J. Lomb, M. C. Haigis and L. Guarente, *Cell*, 2009, **137**, 560-570.
74. Z.-F. Lin, H.-B. Xu, J.-Y. Wang, Q. Lin, Z. Ruan, F.-B. Liu, W. Jin, H.-H. Huang and X. Chen, *Biochem Biophys Res Commun*, 2013, **441**, 191-195.
75. Y. Zhang, S. S. Bharathi, M. J. Rardin, R. Uppala, E. Verdin, B. W. Gibson and E. S. Goetzman, *PLoS One*, 2015, **10**, e0122297.

76. T. Wang, G. Tan, M. Jiang, G. Liu, W. Li and X. Qing, *Transl Oncol*, 2025, **51**, 102215.
77. M. J. Rardin, W. He, Y. Nishida, J. C. Newman, C. Carrico, S. R. Danielson, A. Guo, P. Gut, A. K. Sahu, B. Li, R. Uppala, M. Fitch, T. Riiff, L. Zhu, J. Zhou, D. Mulhern, R. D. Stevens, O. R. Ilkayeva, C. B. Newgard, M. P. Jacobson, M. Hellerstein, E. S. Goetzman, B. W. Gibson and E. Verdin, *Cell Metab*, 2013, **18**, 920-933.
78. L. Liu, C. Peritore, J. Ginsberg, J. Shih, S. Arun and G. Donmez, *Behav Brain Res*, 2015, **281**, 215-221.
79. M. I. Lutz, I. Milenkovic, G. Regelsberger and G. G. Kovacs, *Neuromolecular Med*, 2014, **16**, 405-414.
80. K. S. Greene, M. J. Lukey, X. Wang, B. Blank, J. E. Druso, M. J. Lin, C. A. Stalnecker, C. Zhang, Y. Negrón Abril, J. W. Erickson, K. F. Wilson, H. Lin, R. S. Weiss and R. A. Cerione, *Proc Natl Acad Sci USA*, 2019, **116**, 26625-26632.
81. Y. Q. Wang, H. L. Wang, J. Xu, J. Tan, L. N. Fu, J. L. Wang, T. H. Zou, D. F. Sun, Q. Y. Gao, Y. X. Chen and J. Y. Fang, *Nat Commun*, 2018, **9**, 545.
82. W. Lu, Y. Zuo, Y. Feng and M. Zhang, *Tumour Biol*, 2014, **35**,10699-10705.
83. B. Suenkel, F. Fischer and C. Steegborn, *Bioorg Med Chem Lett*, 2013, **23**, 143-146.
84. J. Trapp, A. Jochum, R. Meier, L. Saunders, B. Marshall, C. Kunick, E. Verdin, P. Goekjian, W. Sippl and M. Jung, *J Med Chem*, 2006, **49**, 7307-7316.
85. B. Maurer, T. Rumpf, M. Scharfe, D. A. Stolfa, M. L. Schmitt, W. He, E. Verdin, W. Sippl and M. Jung, *ACS Med Chem Lett*, 2012, **3**, 1050-1053.
86. S. Liu, S. Ji, Z. J. Yu, H. L. Wang, X. Cheng, W. J. Li, L. Jing, Y. Yu, Q. Chen, L. L. Yang, G. B. Li and Y. Wu, *Chem Biol Drug Des*, 2018, **91**, 257-268.
87. J. B. Baell and G. A. Holloway, *J Med Chem*, 2010, **53**, 2719-2740.
88. R. Wirawan, S. A. Huber, T. Wein and F. Bracher, *Molecules*, 2025, **30**, 3821.
89. E. D. Guetschow, S. Kumar, D. B. Lombard and R. T. Kennedy, *Anal Bioanal Chem*, 2016, **408**, 721-731.
90. C. Glas, J. C. B. Dietschreit, N. Wössner, L. Urban, E. Ghazy, W. Sippl, M. Jung, C. Ochsenfeld and F. Bracher, *Eur J Med Chem*, 2020, **206**, 112676.
91. R. B. R. Muijsers and K. L. Goa, *Drugs*, 2002, **62**, 1689-1705.
92. C. Glas, E. Naydenova, S. Lechner, N. Wössner, L. Yang, J. C. B. Dietschreit, H. Sun, M. Jung, B. Kuster, C. Ochsenfeld and F. Bracher, *Eur J Med Chem*, 2022, **240**, 114594.
93. M. Frei, T. Wein and F. Bracher, *Molecules*, 2025, **30**, 1728.
94. J. Du, Y. Zhou, X. Su, J. J. Yu, S. Khan, H. Jiang, J. Kim, J. Woo, J. H. Kim, B. H. Choi, B. He, W. Chen, S. Zhang, R. A. Cerione, J. Auwerx, Q. Hao and H. Lin, *Science*, 2011, **334**, 806-809.
95. M. Gehringer and S. A. Laufer, *J Med Chem*, 2019, **62**, 5673-5724.

96. R. A. M. Serafim, L. Haarer, J. G. B. Pedreira and M. Gehringer, *Curr Res Chem Biol*, 2023, **3**, 100040.
97. L. Zheng, Y. Li, D. Wu, H. Xiao, S. Zheng, G. Wang and Q. Sun, *MedComm – Oncol*, 2023, **2**, e56.
98. L. Boike, N. J. Henning and D. K. Nomura, *Nat Rev Drug Discov*, 2022, **21**, 881-898.
99. M. Groll, C. R. Berkers, H. L. Ploegh and H. Ovaa, *Structure*, 2006, **14**, 451-456.
100. P. Beck, C. Dubiella and M. Groll, *Biol Chem*, 2012, **393**, 1101-1120.
101. Y.-H. Wang, F. Zhang, H. Diao and R. Wu, *ACS Catalysis*, 2019, **9**, 2292-2302.
102. D. Oksenberg, K. Dufu, M. P. Patel, C. Chuang, Z. Li, Q. Xu, A. Silva-Garcia, C. Zhou, A. Hutchaleelaha, L. Patskovska, Y. Patskovsky, S. C. Almo, U. Sinha, B. W. Metcalf and D. R. Archer, *Br J Haematol*, 2016, **175**, 141-153.
103. A. Priimagi, G. Cavallo, P. Metrangolo and G. Resnati, *Acc Chem Res*, 2013, **46**, 2686-2695.
104. Z. Xu, Z. Liu, T. Chen, T. Chen, Z. Wang, G. Tian, J. Shi, X. Wang, Y. Lu, X. Yan, G. Wang, H. Jiang, K. Chen, S. Wang, Y. Xu, J. Shen and W. Zhu, *J Med Chem*, 2011, **54**, 5607-5611.
105. A. Benjahad, J. Guillemont, K. Andries, C. H. Nguyen and D. S. Grierson, *Bioorg Med Chem Lett*, 2003, **13**, 4309-4312.
106. D. M. Himmel, K. Das, A. D. Clark, S. H. Hughes, A. Benjahad, S. Oumouch, J. Guillemont, S. Coupa, A. Poncelet, I. Csoka, C. Meyer, K. Andries, C. H. Nguyen, D. S. Grierson and E. Arnold, *J Med Chem*, 2005, **48**, 7582-7591.
107. G. Cavallo, P. Metrangolo, R. Milani, T. Pilati, A. Priimagi, G. Resnati and G. Terraneo, *Chem Rev*, 2016, **116**, 2478-2601.
108. Y. Lu, Y. Liu, Z. Xu, H. Li, H. Liu and W. Zhu, *Expert Opin Drug Discov*, 2012, **7**, 375-383.
109. Z. Xu, Z. Yang, Y. Liu, Y. Lu, K. Chen and W. Zhu, *J Chem Inf and Model*, 2014, **54**, 69-78.
110. R. Wilcken, M. O. Zimmermann, A. Lange, A. C. Joerger and F. M. Boeckler, *J Med Chem*, 2013, **56**, 1363-1388.
111. D. Lavogina, E. Enkvist and A. Uri, *ChemMedChem*, 2010, **5**, 23-34.
112. N. C. Garbett and J. B. Chaires, *Expert Opin Drug Discov*, 2012, **7**, 299-314.
113. D. Chen, C. Dong, G. Dong, K. Srinivasan, J. Min, N. Noinaj and R. Huang, *J Med Chem*, 2020, **63**, 8419-8431.
114. L. Halby, Y. Menon, E. Rilova, D. Pechalrieu, V. Masson, C. Faux, M. A. Bouhlel, M. H. David-Cordonnier, N. Novosad, Y. Aussagues, A. Samson, L. Lacroix, F. Ausseil, L. Fleury, D. Guianvarc'h, C. Ferroud and P. B. Arimondo, *J Med Chem*, 2017, **60**, 4665-4679.

115. M. Izumi, H. Yuasa and H. Hashimoto, *Curr Top Med Chem*, 2009, **9**, 87-105.
116. K. Parang, J. H. Till, A. J. Ablooglu, R. A. Kohanski, S. R. Hubbard and P. A. Cole, *Nat Struct Biol*, 2001, **8**, 37-41.
117. A. Ricouart, J. C. Gesquiere, A. Tartar and C. Sergheraert, *J Med Chem*, 1991, **34**, 73-78.
118. A. Kumar, Y. Wang, X. Lin, G. Sun and K. Parang, *ChemMedChem*, 2007, **2**, 1346-1360.
119. A. D. Napper, J. Hixon, T. McDonagh, K. Keavey, J.-F. Pons, J. Barker, W. T. Yau, P. Amouzegh, A. Flegg, E. Hamelin, R. J. Thomas, M. Kates, S. Jones, M. A. Navia, J. O. Saunders, P. S. DiStefano and R. Curtis, *J Med Chem*, 2005, **48**, 8045-8054.
120. M. Gertz, F. Fischer, G. T. T. Nguyen, M. Lakshminarasimhan, M. Schutkowski, M. Weyand and C. Steegborn, *PNAS,* 2013, **110**, E2772-E2781.
121. H. Cui, Z. Kamal, T. Ai, Y. Xu, S. S. More, D. J. Wilson and L. Chen, *J Med Chem*, 2014, **57**, 8340-8357.
122. T. Ai, D. J. Wilson, S. S. More, J. Xie and L. Chen, *J Med Chem*, 2016, **59**, 2928-2941.
123. T. Ai, D. J. Wilson and L. Chen, *Molecules*, 2023, **28**, 7655.
124. C. S. Rye and J. B. Baell, *Curr Med Chem*, 2005, **12**, 3127-3141.
125. M. V. Makarov, F. Hayat, B. Graves, M. Sonavane, E. A. Salter, A. Wierzbicki, N. R. Gassman and M. E. Migaud, *ACS Chem Biol*, 2021, **16**, 604-614.
126. G. Gebeyehu, V. E. Marquez, A. Van Cott, D. A. Cooney, J. A. Kelley, H. N. Jayaram, G. S. Ahluwalia, R. L. Dion, Y. A. Wilson and D. G. Johns, *J Med Chem*, 1985, **28**, 99-105.
127. K. Pankiewicz and K. Felczak, *Heterocycl Commun*, 2015, **21**, 249-257.
128. C. M. Hadi, A. Goba, S. H. Khan, J. Bangura, M. Sankoh, S. Koroma, B. Juana, A. Bah, M. Coulibaly and D. G. Bausch, *Emerg Infect Dis*, 2010, **16**, 2009-2011.